THE UNIVERSITY *of* EDINBURGH

Assessing the potential for gene therapy in a mouse model of *SYNGAP1* haploinsufficiency-associated disorder

Sarah Giachetti

Principal supervisor:

Professor Stuart Cobb

Second supervisor:

Professor Peter Kind

Submitted for the degree of Doctor of Philosophy

at The University of Edinburgh

2022

DECLARATION

I declare that this thesis and the work presented here are entirely my own with the following exceptions:

- Ms Stephanie L. Mearns carried out part of the genotyping.
- Ms Amanda Morris carried out the viral vector DNA sequencing and whole plasmid sequencing while the data analysis was performed by Dr Paul Ross.
- Dr Ralph D. Hector performed the therapeutic cassettes design.
- Dr Jorge M. Royo performed the Motion Sequencing data analysis.
- Ms Marie Bowers, Ms Jessica Rodda and Mr Scott Noble contributed to the acquisition of part of the behavioural data, and Mr Scott Noble and Dr Kamal K. E. Gadalla assisted during part of the tissue collection procedures.

The work presented in this thesis has not been submitted for any other degree or professional qualification.

Signed …….. Date……

ACKNOWLEDGEMENTS

I would like to start by thanking my supervisor, Prof. Stuart Cobb, for his help and guidance during these years and for allowing me to pursue my ideas, good or bad. My gratitude goes also to my second supervisor, Prof. Peter Kind, for the support, help and advice during these long years of PhD and to Prof. Emily Osterweil.

In addition, I would like to thank the SIDB for funding this work and to have gone above and beyond to support me and all the SIDB students during the COVID years.

I would like to thank Dr Kamal Gadalla who, by reminding me that very very few students are “good students”, pushed me to improve my skills and critical thinking, and for all the help during these years. Dr Jim Selfridge for the many advice during our always delayed Friday meetings and Dr Sophie Thomson for being the western blotting master and helping me with the experimental setup. Last but not least, I would like to thank Dr Ralph Hector and Dr Paul Ross for their help with the viral vector design and expert opinion during the thesis writing.

A special thank goes to Steph, Amanda, Gwen, Scott, Marie and Noha for the help around the lab (which I have hopefully repaid with enough chocolate).

Finally, I would like to thank my family, friends, my fellow siblings-in-pain SIDB students Costantinos and Raven, at least we got to be miserable together, Sarah who got to read a very long and boring thesis and Giulia. If it wasn’t for them I would not be here today.

SCIENTIFIC ABSTRACT

SYNGAP1 (Synaptic Ras GTPase activating protein 1) haploinsufficiency-associated disorder or intellectual developmental disorder, autosomal dominant 5 (MRD5) is caused by autosomal dominant loss-of-function mutations in the *SYNGAP1* gene. *De novo SYNGAP1* mutations represent one of the most common causes of non-syndromic intellectual disability (NSID) (OMIM #603384). The most common symptoms include moderate-to-severe intellectual disability (ID), epilepsy and autism spectrum phenotypes.

SYNGAP1 protein is a component of the postsynaptic density complex where it acts as one of the key effectors of N-methyl-D-aspartate (NMDA) receptor downstream pathways. It is involved in regulatory pathways such as the trafficking of the α-amino-3-hydroxy-5-mehyl-4-isoxazolepropionic acid (AMPA) receptors, regulation of AMPA receptor translation and the regulation of several forms of synaptic plasticity.

With the aim to study SYNGAP1 protein function and its involvement in the pathophysiology of the disease, several rodent models have been created and extensively characterised. These studies revealed phenotypes which partially resemble the symptomatology observed in humans such as seizure susceptibility, hyperactivity and impulsivity. It has been shown that early restoration of normal SYNGAP1 protein levels prevents the onset of haploinsufficiency-associated phenotypes in the mouse. This, and the monogenic origin of the disorder, makes *SYNGAP1* a candidate target for gene replacement therapeutic approaches.

I hypothesised that restoration of SYNGAP1 levels via Adeno Associated Virus (AAV)-mediated gene transfer during early postnatal development, will prevent the appearance or ameliorate the severity of behavioural phenotypes observed in the mouse model of *SYNGAP1* haploinsufficiency. Therefore, the aim of this project was to evaluate molecular therapies to test this hypothesis.

To this end, I first defined a robust battery of behavioural tests in order to confirm and identify deficits to use as endpoints to evaluate the efficacy of gene therapy products. Well-established and novel phenotypes were evaluated in wild-type and *Syngap1*$^{+/-}$ mice at different postnatal developmental time points. *Syngap1*$^{+/-}$ mice showed increased locomotor activity, anxiety-like phenotype and a risk-taking like behaviour. No genotype effect was observed in tests assessing compulsive behaviour, working memory, motor function and general well-being and depth perception.

For the first generation of candidate therapeutic constructs two different promoters were used, the minimal murine *Mecp2* promoter (MeP) 229 and the synthetic JeT promoter. MeP229 regulated constructs were expressing three different Myc-tagged human *SYNGAP1* isoforms, Aα2, Aα1 and Bα2 while the JeT regulated construct the Myc-tagged human *SYNGAP1* isoform Aα1. *In vitro* evaluation of protein expression revealed low levels of plasmid-derived SYNGAP1 produced from the MeP229 regulated constructs while a higher amount of Myc-tagged SYNGAP1 protein was detectable from the JeT regulated cassette via both fluorescence immunocytochemistry and immunoblotting.

Protein expression from the vectorised ssAAV9/JeT-*hSYNGAP1_Aα1-Myc* was confirmed in the brain *in vivo* at 5 weeks post intracerebroventricular injection. A therapeutic dose escalation efficacy study assessing ssAAV9/JeT-*hSYNGAP1_Aα1-Myc* was then conducted in *Syngap1*$^{+/-}$ mice (1E10, 5E10 and 1E11 vg/mouse). Overall, these data revealed no amelioration of hyperactivity or anxiety phenotypes, but a modest trend toward the amelioration of the risk-taking behaviour was observed in a platform departure test. Post-hoc immunoblot analysis confirmed a dose-dependent expression of the vector-derived SYNGAP1. However absolute levels of SYNGAP1 protein measured in different brain areas were below physiological levels of the native protein. Subcellular localisation analysis in whole hippocampal synaptosomal preparation showed that the vector-derived protein was correctly translocated to the synaptic compartment, mimicking endogenous patterns of protein localisation.

With the aim to improve the previous generation construct, a new therapeutic cassette was designed that expressed a codon-optimised FLAG-tagged version of the human SYNGAP1 Aα1 isoform, under the control of the human SYNAPSIN1 (hSYN1) promoter. *In vitro* expression of the hSYN1-*FLAG-hSYNGAP1(opt)_Aα1* cassette was verified by immunostaining of transfected HEK293A cells and *in vivo* expression of ssAAV9/hSYN1-*hSYNGAP1(opt)_Aα1* was verified in the brain at 5 weeks post intracerebroventricular injection. Behavioural analysis, at 7 and 15 weeks of mice treated with 5E10 and 1E11 vg/mouse, delivered via intracerebroventricular injections, recapitulated what was observed with the JeT-*hSYNGAP1_Aα1* expressing vector. There was no treatment effect on hyperactivity or the anxiety phenotype, but an improvement in the platform departure test was observed. Moreover, I showed the utility of the Motion Sequence test, a novel machine learning system that allows analysing 3D modular elements of mouse behaviour in an ethologically conserved manner. The test identified a clear genotype effect between wild-type and *Syngap1*$^{+/-}$ vehicle-treated mice however, there was no treatment effect observed in the vector-treated *Syngap1*$^{+/-}$ group. Post-hoc analysis showed expression of the transgene in the hippocampus and cortex, however, vector-derived SYNGAP1 protein accounted only for a small portion of the total SYNGAP1. Whole hippocampus synaptosomal preparation showed correct localisation of the FLAG-tagged protein.

In conclusion, I identified a series of robust disease relevant genotype effects to utilise as outcome measures in preclinical gene therapy trials. I have also shown the many challenges to overcome to develop an effective gene replacement treatment of *SYNGAP1* haploinsufficiency-associated disorder. The very limited therapeutic effect observed in these studies could be due to the low expression level of the vector-derived protein, the unequal distribution of AAV9 across the brain and the exclusion of other SYNGAP1 isoforms which could be necessary for a therapeutic effect. The identification of the most important isoform is mandatory for the further development of the next generation vectors.

LAY SUMMARY

Neurons are one of the many cell types that compose the brain. Their primary function is to transmit messages which occur via intercellular connection points called synapses. In several cases, neurodevelopmental diseases are caused by mutations, deleterious changes in the DNA sequence, in key genes involved in the regulation of synaptic function.

One of these genes is Synaptic GTPase Activating Protein 1 (SYNGAP1). Detrimental mutations in this gene are one of the most common causes of intellectual disability which is associated with epilepsy and autism spectrum disorder.

SYNGAP1 functions have been extensively studied using mice in which the gene has been disrupted to model the human disease and we now know that, if normal levels are restored early in life, the development of the disease-associated phenotypes can be prevented. Moreover, this disease is caused by mutations in a single gene making it easy to replace. Altogether, these factors suggest that a gene therapy approach could be a potential strategy to treat this disorder. Gene therapy is a therapeutic approach where the coding sequence of a gene of interest, in this case *SYNGAP1,* is inserted in an engineered virus, defined as viral vector, which is then delivered to patients. In the case of *SYNGAP1,* I hypothesised that the normalisation of the SYNGAP1 protein levels would then help to restore synaptic function and ameliorate the disease related phenotypes.

In the first part of my project, I investigated the behaviour of mice modelling SYNGAP1 disease, identifying a robust behavioural battery of tests. Phenotypes identified in mutant mice were hyperactivity, anxiety-like phenotype and an increase in risk taking-like behaviour.

Subsequently, I tested the capacity of SYNGAP1 gene therapy molecules, to rescue the phenotypes observed in mutant mice. To this end, after verifying that these molecules had the ability to produce the SYNGAP1 protein in cells grown in a dish, they were injected into mutant mouse brains to test for efficacy. Data showed a trend toward the amelioration of some aspects of the mutant mice behaviour.

I confirmed that the therapeutic SYNGAP1 protein produced by the virus was produced and correctly delivered to the synapses. However, the level of the therapeutic protein was very low compared to the normal level of SYNGAP1 protein in healthy mice which could explain the modest effect of the treatment.

Overall, my work showed the potential of the gene transfer approach as a treatment for the disorder associated with mutations in the *SYNGAP1* gene. However, it also highlighted the necessity for a better understanding of the protein and its function in order to be able to design better and more efficient therapeutic approaches.

TABLE OF CONTENTS

LIST OF ABBREVIATIONS

6BIO	6-bromoindirubin-3’-oxime
AAP	Assembly-activating protein
AAV	Adeno-associated virus
Actb	Actin
Ad	Adeno virus
ADHD	Attention deficit hyperactivity disorder
Amp	Ampicillin
AMPAR	α-amino-3-hydroxy-5-methyl-4-isoxazolepropionic acid receptor
ASD	Autism spectrum disorders
ASO	Antisense oligonucleotides
BBB	Blood brain barrier
bp	Base pair
BSA	Bovine serum albumin
CAI	Codon adaptation index
CaMKII	Ca^{2+}/calmodulin-dependent protein kinase II
CBA	Chicken beta actin
CBD	Cannabidiol
CC	Coiled-coil domain
CDK5	Cyclin-dependent Kinase 5
CDMS	Charge detection mass spectrometry
CI	Confidence interval
CMV	Cytomegalovirus
CNS	Central nervous system
Ct	Cycle threshold
DAPI	4’,6-diamidino-2-phenylindole
ddPCR	Digital droplets PCR
DMEM	Dulbecco's modified eagle medium
DMSO	Dimethyl sulfoxide
DNA	Deoxyribonucleic acid
dNTP	Deoxyribonucleotide triphosphate
dsDNA	Double strand DNA
E_{AMP}	Efficiency of amplification
E_{AMP}%	Percent efficiency of amplification
EDTA	Ethylenediaminetetraacetic acid
EEG	Electroencephalography

EPM	Elevated plus maze
ER	Estrogen receptor
ERK	Extracellular signal-regulated kinase
FMR1	Fragile messenger ribonucleoprotein 1
HSV	Herpes simplex virus
ID	Intellectual disability
IQ	Intelligence quotient
IR	Infrared
ITR	Inverted terminal repeats
Kan	Kanamycin
kb	Kilobase
KO	Knockout
LB	Luria-Bertani medium
LTP	Long term potentiation
MeCP2	Methyl-CpG binding protein 2
MeP	*Mecp2* endogenous core promoter
mEPSCs	Miniature excitatory postsynaptic currents
MoSeq	Motion sequencing
MRD5	Intellectual developmental disorder, autosomal dominant 5
MRI	Magnetic resonance imaging
mRNA	Messenger ribonucleic acid
NDD	Neurodevelopmental disorders
NMDAR	N-methyl-D-aspartate receptor
NSID	Non syndromic intellectual disability
OF	Open field
PBM	PDZ binding motif
PBS	Phosphate buffer saline
PCR	Polymerase chain reaction
PD	Platform departure
PH	Pleckstrin homology domain
PLK2	Polo-like kinase 2
PLO-FN	Ploy-L-ornithine/fibronectin
PND	Postnatal day
PolyA	Polyadenylation signal
PPI	Prepulse inhibition
PSD	Post synaptic density
PSD95	Postsynaptic density protein 95
qPCR	Quantitative real time PCR

RM	Repeated measure
RNA	Ribonucleic acid
rpm	Revolutions per minute
RT-PCR	Reverse transcription PCR
SDS	Sodium dodecyl sulphate
SEM	Standard error of the mean
SID	Syndromic intellectual disabilities
SOC	Super optimal broth with catabolite repression
SpA	Synthetic polyA signal
ssAAV	Single stranded AAV
SSC	Somatosensory cortex
ssDNA	Single strand DNA
(h)SYN1	(human) Synapsin 1
SYNGAP1	Synaptic Ras GTPase activating protein 1
TAE	Tris-acetate-EDTA
TSC1	Tuberous sclerosis complex 1
TSC2	Tuberous sclerosis complex 2
UBE3A	Ubiquitin-protein ligase E3A
vg	Viral vector genome
Vh	Vehicle
VP1	Viral capsid protein1
VP2	Viral capsid protein2
VP3	Viral capsid protein 3
WT	Wild-type

LIST OF FIGURES

LIST OF TABLES

CHAPTER 1: INTRODUCTION

Intellectual disability (ID), which affects 1 to 3% of the total population, is the most frequent disorder diagnosed in children. ID is characterised by an intelligence quotient (IQ) 2 standard deviations below the mean of the general population (<70) and is associated with deficits in functional and adaptive skills. Historically, ID severity has been classified as follows: IQ <20, profound; 20-34, severe; 35-49, moderate; 50-69, mild. More recently, criteria used for severity classification have been updated to include several other aspects, like communication, language and basic skills (Patel *et al.*, 2018).

In a high percentage of patients with neurodevelopmental disorders (NDDs) ID shows co-morbidity with autism spectrum disorders (ASD), schizophrenia, depression, anxiety, sleep disorders and epilepsy (Lord *et al.*, 2018; Munir, 2018; Simonoff *et al.*, 2008). For this reason, it has been hypothesized that there is convergence in the developmental mechanisms of behavioural and cognitive symptoms that define these disorders. Altered neuronal circuitry and synaptic function are believed to be the causative common mechanisms of ID and ASD (Kroon *et al.*, 2013). Indeed, among the vast number of candidate genes identified for this form of NDDs, many are involved in the regulation of synaptic functions or morphology, or themselves regulated by synaptic activity (Bear, 2005; Gauthier *et al.*, 2011; Moyses-Oliveira *et al.*, 2020; Willsey *et al.*, 2022; Zoghbi *et al.*, 2012). Most genes associated with syndromic ID (SID) in combination with other forms of NDD are X-linked or autosomal with recessive inheritance. For example: *FMR1* (Fragile Messenger Ribonucleoprotein 1, Fragile X Syndrome), *TSC1* and *TSC2* (Tuberous Sclerosis Complex, Tuberous Sclerosis), *UBE3A* (Ubiquitin-protein ligase E3A, Angelman Syndrome) and *MECP2* (Methyl-CpG binding protein 2, Rett Syndrome). Autosomal dominant inheritance is not frequent, and when present it is caused by *de novo* mutations, as is found for mutations identified in *SYNGAP1* (Synaptic Ras GTPase Activating Protein 1).

SYNGAP1 is the most abundant protein in the postsynaptic density (PSD) complex (Chen *et al.*, 1998; Kim *et al.*, 1998). It is the principal effector of N-methyl-D-aspartate receptor (NMDAR) signalling pathways (Chen *et al.*, 1998; Kim *et al.*, 1998) and it is involved in several regulatory pathways via the direct negative regulation of small G proteins, such as trafficking regulation of α-amino-3-hydroxy-5-methyl-4-isoxazolepropionic acid receptors (AMPAR) to the postsynaptic membrane (Kim *et al.*, 2003; Rumbaugh *et al.*, 2006; Walkup *et al.*, 2015), local regulation of AMPAR translation (Wang *et al.*, 2013) and modulation of dendritic spine morphology and synaptic plasticity during development (Llamosas *et al.*, 2020, 2021; Vazquez *et al.*, 2004).

SYNGAP1 haploinsufficiency is caused by *de novo* pathological loss-of-function mutations in the *SYNGAP1* gene (Hamdan *et al.*, 2009) (OMIM #603384). Affected individuals present a defined set of symptoms referred to as intellectual developmental disorder, autosomal dominant 5 (MRD5) (Berryer *et al.*, 2013; Hamdan *et al.*, 2011; Jimenez-Gomez *et al.*, 2019; Krepischi *et al.*, 2010; Martín-Jiménez *et al.*, 2018; Mignot *et al.*, 2016; Parker *et al.*, 2015; Vlaskamp *et al.*, 2019).

1.1 SYNGAP1 FUNCTIONS, PROTEIN DOMAINS AND ISOFORMS

1.1.1 Structure and functional domains

SYNGAP1 is located on the short arm of human chromosome 6 (6p21.32), the full gene has a total length of 33620 base pair (bp) (GRCh37/hg19), and it encodes for the Synaptic Ras GTPase-activating protein 1 which presents multiple isoforms (Chen *et al.*, 1998; Kim *et al.*, 1998; McMahon *et al.*, 2012). The full-length protein contains an N-terminal Pleckstrin Homology (PH) domain, while the core of the protein is composed of the C2 and GAP domains as well as a stretch of serine-threonine phosphorylation sites (Chen *et al.*, 1998; Walkup *et al.*, 2015, 2018). The C-terminus of SYNGAP1 contains a coiled-coil (CC) domain (Zeng *et al.*, 2016) and some isoforms contain a PDZ binding motif (PBM) (Kim *et al.*, 1998) (Figure 1-1).

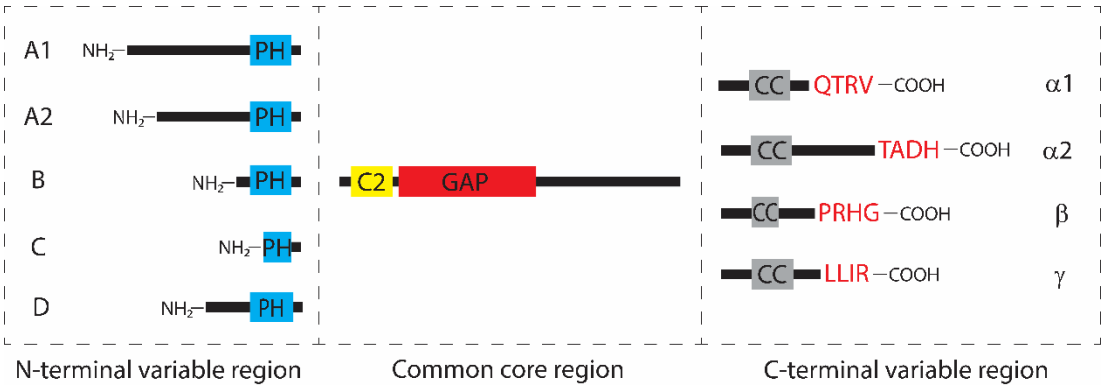

Figure 1-1. Schematic representation of SYNGAP1 domains and composition of the isoforms.

N- and C-terminal variable regions, that give rise to different isoforms, are represented respectively in the left and right panels. The central panel illustrates the core region, common to all isoforms. Protein domains are represented in different colours, letters in red represent the different C-terminals. PH: Pleckstrin Homology. CC: coiled-coil. Data from McMahon *et al.* 2012, Araki *et al.* 2020, Gou *et al.* 2020.

PH domains are among the most abundant class of domains. They are known to regulate enzymatic activity through inter and intra-molecular binding events mediating protein-protein and protein-lipid interaction (Lemmon, 2004). It is reported that a small portion of PH domains interact with phosphatidylinositol lipids in membranes (Cash *et al.*, 2019; Le Huray *et al.*, 2022; Lemmon, 2008).

C2 domains are Ca^{2+}-dependent membrane binding domains (Clark *et al.*, 1991; Davletov *et al.*, 1993; Kishimoto *et al.*, 1989; Nishizuka, 1988; Yamaguchi *et al.*, 1993). Several C2-containing proteins are part of signal transduction and membrane trafficking pathways and a subset of them have been described as Ca^{2+} effectors due to their function as Ca^{2+}-dependent membrane binding protein (Cho *et al.*, 2006).
The C2 domain of SYNGAP1 is required for the modulation of the Rap activity of the GAP domain (Pena *et al.*, 2008).

The GAP domain is a functional domain able to catalyse the intrinsic GTPase activity of G proteins. The GAP domain of SYNGAP1 is described as a bifunctional GAP able to stimulate the GTPase activity of two small G proteins, Ras and Rap (Kim *et al.*, 1998; Krapivinsky *et al.*, 2004; Pena *et al.*, 2008). Analysis of the crystallographic structure

suggests that the intrinsic motility showed by the C2 domain could modulate the access to catalytic residues of Rap or Ras (Pena *et al.*, 2008).

Downstream to the GAP domain a stretch of serine and threonine has been identified which can be subjected to phosphorylation (Oh *et al.*, 2004; Walkup *et al.*, 2015, 2016, 2018). Three kinases have been described to phosphorylate residues in this region, events that are involved in the modulation of the GAP domain affinity for small G proteins: Ca^{2+}/calmodulin-dependent protein kinase II (CaMKII), induces an increased affinity of the GAP domain for Rap and regulates SYNGAP1 localisation (Araki *et al.*, 2015; Walkup *et al.*, 2015; Yang *et al.*, 2013); Polo-like Kinase 2 (PLK2), increases the affinity of GAP for Ras (Walkup *et al.*, 2015, 2018); Cyclin-dependent Kinase 5 (CDK5), shows the same effect on GAP caused by PLK2 (Walkup *et al.*, 2015, 2018).

At the C-terminal region of SYNGAP1, is a CC domain that, together with the PBM present only in the α1 type of C-terminus, is involved in the interaction with the postsynaptic density protein 95 (PSD95). Zeng *et al.* (Zeng *et al.*, 2016) resolved the crystallographic structure of SYNGAP1-CC-PBM and showed that SYNGAP1, interacting via the CC, forms trimers and binds to two molecules of PSD95 in a ratio of 3:2. Moreover, they showed that this protein complex, undergoing liquid-to-liquid phase separation, is implicated in PSD functioning (Araki *et al.*, 2015; Zeng *et al.*, 2016).

1.1.2 Isoforms: how they arise, localisation and developmental expression pattern

Although it can be detected at the mRNA levels in low amounts in lungs, kidneys and other tissues (Chen *et al.*, 1998), SYNGAP1 is primarily expressed in the brain, in particular in glutamatergic excitatory and GABAergic inhibitory neurons (Berryer *et al.*, 2016; Chen *et al.*, 1998; Kim *et al.*, 1998; Moon *et al.*, 2008; Ozkan *et al.*, 2014). During early stages of development (embryonic day 8.5 to 16.5) SYNGAP1 is detected in cortex, hippocampus, hypothalamus and basal ganglia. It is also detected in other

regions of the embryo such as somites, heart and the neuronal tube (Porter *et al.*, 2005). Postnatally, SYNGAP1 is detected in hippocampus, cortex and striatum and to a lesser extent, in the olfactory bulb, thalamus, cerebellum, and brainstem (Gou *et al.*, 2020; Kim *et al.*, 2003; Knuesel *et al.*, 2005; Moon *et al.*, 2008; Porter *et al.*, 2005; Tomoda *et al.*, 2004). In adulthood, SYNGAP1 is highly expressed in the cortex, hippocampus and striatum while traces are detected in the olfactory bulb and cerebellum (Gou *et al.*, 2020; Porter *et al.*, 2005)

SYNGAP1 isoforms expression patterns are temporally regulated and change across brain regions (Araki *et al.*, 2020; Gou *et al.*, 2020). *Syngap1* expression peaks are temporally correlated with synaptogenesis (McMahon *et al.*, 2012).

1.1.2.1 Isoforms generation

As previously mentioned, SYNGAP1 protein has multiple isoforms that are generated from multiple transcription start sites and alternative splicing events. Five N-termini (A1, A2, B, C and D) and four C-termini (α1, α2, β, and γ) (Figure 1-2) have been identified (Chen *et al.*, 1998; Gou *et al.*, 2020; Kim *et al.*, 1998; Li *et al.*, 2001; McMahon *et al.*, 2012).

A1/2 isoforms present the earliest transcription start site, and together with isoform B, which exhibits unique exons, encode the full-length PH domain. The transcription start site for isoform C is contained in the exon that encodes for the N-terminus of the PH domain, therefore the resulting protein presents a truncated version of the PH domain (Chen *et al.*, 1998; Gou *et al.*, 2020; Li *et al.*, 2001; McMahon *et al.*, 2012). The D isoform's transcription start site is localized in exon 3 and presents a full-length PH domain (Gou *et al.*, 2020; Li *et al.*, 2001).

The skipping of exon 19 and the selective splicing of exon 20 produces isoforms α1, containing the PBM QTRV, and α2 which presents an additional stretch of amino acids at the carboxy terminal. Isoform β, which presents a truncated CC domain, is produced by the frameshift extension of exon 18 that causes premature termination.

The inclusion of exon 19, which contains a stop codon, leads to the production of isoform γ (Araki *et al.*, 2020).

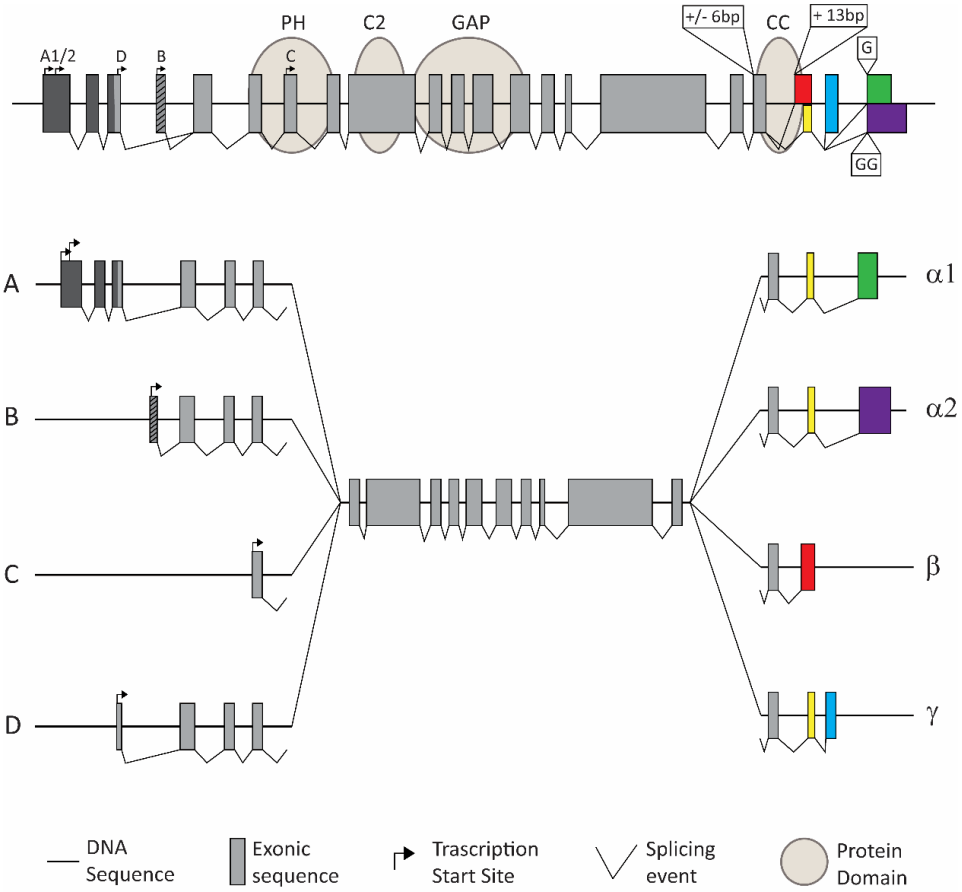

Figure 1-2. Syngap1 gene gives rise to multiple isoforms generated by different transcription start sites and alternative splicing events.
Schematic representation of the exonic composition of *Syngap1* with transcription start sites and alternative splicing events for each isoform. The upper panel shows the exonic and intronic composition of the full-length gene. The bottom panel shows the intronic and exonic composition of each N- and C-terminal isoform. In grey are reported exonic sequences common to all isoforms while isoform-specific exons are reported with different colours. The intronic sequence is reported as a straight thin line. Splicing events are indicated with "V" shaped lines. PH: Pleckstrin Homology, CC: coiled-coil. Data from McMahon *et al.* 2012, Araki *et al.* 2020, Gou *et al.* 2020.

1.1.2.2 Developmental expression pattern and subcellular localization

Gou *et al.* (Gou *et al.*, 2020) investigated the temporal expression of α1, α2, and β C-termini. They observed that each C-terminus is spatially and temporally regulated during development. Moreover, they observed that at each time point considered

each C- can be associated with two different N-termini. This suggests that isoform expression is regulated at the level of the C-terminus, while the association with different N-termini is not temporally regulated.

With only the exception of the cerebellum, where stable low levels of SYNGAP1 expression were observed throughout development, an isoform specific temporal regulation was observed in the other considered brain regions: cortex, hippocampus, striatum and olfactory bulb. In all considered brain regions, $\alpha 1$ expression increases with age reaching the maximum at postnatal day (PND) 56. A similar pattern is observed for the $\alpha 2$ isoform in the striatum, however, in all other regions, maximum level of expression is achieved at PND21 to then be maintained at a constant high level. The analysis of the expression profile of the β isoform showed that, in the cortex, the peak of expression is achieved at PND21, after which expression levels decrease. In the hippocampus and striatum, expression peaks at PND21 and plateaus, while in the olfactory bulb β has a stable level of expression throughout development (Gou *et al.*, 2020).

Subcellular fractionation studies showed that SYNGAP1 is majorly localised at the PSD but it is detectable also in the cytosol (Gou *et al.*, 2020). Of the total SYNGAP1 protein detected in these compartments, single isoforms contribute to a different extent. β isoform is the most enriched in the cytosolic compartment while $\alpha 1$, $\alpha 2$ and γ are detectable only in traces. At the PSD, $\alpha 1$ and $\alpha 2$ show the highest enrichment while β and γ are present at lower levels. γ is primarily detected at the synaptosomal plasma membrane (Araki *et al.*, 2020; Gou *et al.*, 2020).

While $\alpha 1$ isoform has been detected only in excitatory neurons in homogenates and cell culture, β isoform has been detected in excitatory and inhibitory neurons (Kim *et al.*, 1998; Moon *et al.*, 2008).

1.1.3 SYNGAP1 is a key effector of synaptic transmission regulation

1.1.3.1 SYNGAP1 role in synaptic function

The proposed model for SYNGAP1 function in wild-type tissue is schematically illustrated in Figure 1-3a. During pre-stimulation, unphosphorylated SYNGAP1 is associated with the PSD proteins (PSD95, Dlg1 and zo-1) via the PDZ domain preventing the clustering of AMPARs on the membrane (Walkup *et al.*, 2016). PSD-bound SYNGAP1 negatively regulates Ras while Rap is upregulated. This induces the removal of AMPAR from the membrane via the p38 mitogen-activated protein kinases (MAPK) pathway (Zhu *et al.*, 2002).

NMDAR activation and Ca^{2+} flux lead to SYNGAP1 phosphorylation by CaMKII (Araki *et al.*, 2015; Walkup *et al.*, 2015). Phosphorylated SYNGAP1 dissociates from the PSD (Yang *et al.*, 2013), freeing the PBM. In this condition the GAP domain affinity changes, shifting towards Rap, resulting in the inhibition of the p38-MAPK pathway and activation of the Extracellular signal-Regulated Kinases (ERK) pathway that leads to the active translocation of the AMPAR to the synaptic membrane (Araki *et al.*, 2015; Kim *et al.*, 1998; Komiyama *et al.*, 2002; Walkup *et al.*, 2015, 2018). SYNGAP1 is also involved in the modulation of AMPAR concentration via the mTOR-dependent protein synthesis pathway (Wang *et al.*, 2013; Zhu *et al.*, 2002).

SYNGAP1 is an essential element during NMDAR-mediated long-term potentiation (LTP). During the early phases of development, glutamatergic synapses present only one type of receptor, the NMDAR, and are defined as silent synapses as they are non-conducting elements. LTP is the mechanism for which the synapses are unsilenced in an activity-dependent manner, due to the incorporation of AMPARs in the membrane (Isaac *et al.*, 1995). SYNGAP1, in silent synapses, is involved in the prevention of early dendritic spine maturation, thanks to the negative regulation of the cofilin regulatory pathway via Ras (Carlisle *et al.*, 2008). Cofilin is an F-actin severing molecule that regulates the cytoskeleton remodelling system. After synaptic unsilencing, the shifted activity of SYNGAP1 induces cytoskeleton remodelling and therefore changes in spine structure (Carlisle *et al.*, 2008).

In animal models of *SYNGAP1* haploinsufficiency we observe a major disruption of the synaptic function (Figure 1-3b). In basal conditions, when the synapse is not stimulated and it is silent, the absence of negative regulation of Ras induces constitutive activation of the ERK pathways that causes a premature, non-activity dependent unsilencing of the synapse. Due to the activation of Ras, early cytoskeleton remodelling is also observed, leading to an aberrant spine morphology which leads to the early development of mushroom-like spines (Aceti *et al.*, 2015; Clement *et al.*, 2013; Vazquez *et al.*, 2004). The increased concentration of AMPAR on the membrane causes excitation/inhibition imbalance, leading to circuital alteration and seizures, while the absence of LTP-induced maturation causes a lack of experience-related spine maturation.

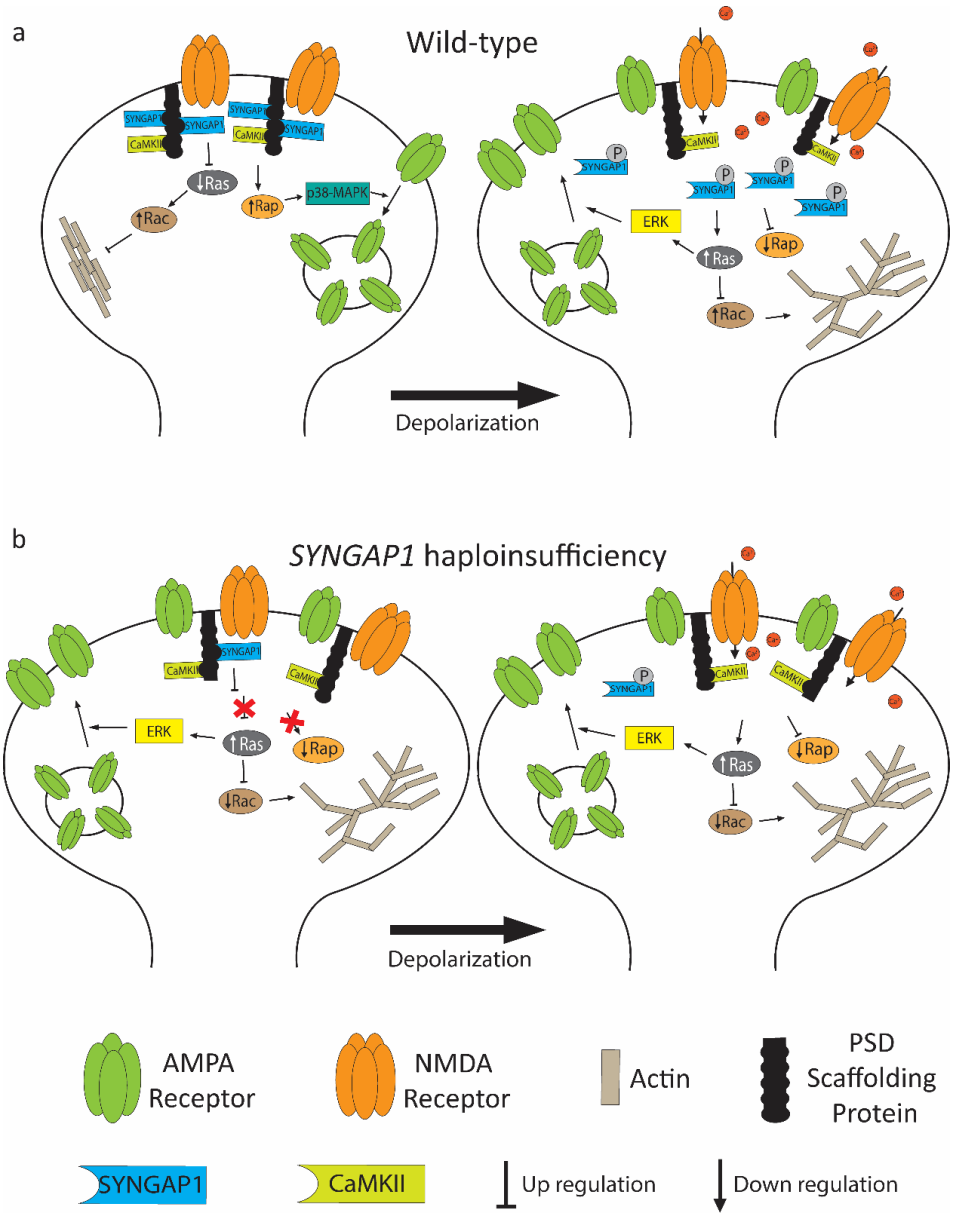

Figure 1-3. SYNGAP1 is involved in the activity-dependent regulation of AMPAR insertion in the synaptic membrane and cytoskeleton remodelling.
Schematic diagram of SYNGAP1 regulated synaptic pathways in wild-type (a) and haploinsufficiency (b) conditions before and after stimulation. Red "X" indicates disrupted pathways. AMPAR: α-amino-3-hydroxy-5-methyl-4-isoxazolepropionic acid receptor. NMDAR: N-methyl-D-aspartate receptor. CaMKII: Ca^{2+}/calmodulin-dependent protein kinase II. PSD: post-synaptic density. ERK: Extracellular signal-Regulated Kinase. p38-MAPK: p38 mitogen-activated protein kinases.

1.1.3.2 Functions of individual SYNGAP1 isoforms

McMahon *et al.* (McMahon *et al.*, 2012), using neurons derived from *Syngap1*$^{-/-}$ mice, showed that different N- and C-termini have distinct effects on neuronal cell

functions (presence or absence of miniature excitatory synaptic currents (mEPSCs), amplitude, frequency) and that each combination has a different overall effect on synaptic strength (McMahon *et al.*, 2012). N-terminal A1/2, as well as C-terminal α1 were observed to strongly decrease synaptic strength. Expression of the Aα1 isoform led to an increased percentage of non-firing neurons, around 70% of transfected cells, and to an overall decrease in the amplitude and frequency of mEPSCs. N-terminal B and C-terminal α2 combination caused an increase in synaptic strength that was characterised by an overall effect opposite to the one caused by Aα1. Finally, the expression of the Aα2 combination led to a neutral effect. These results suggest that each N- and C-terminal can independently regulate synaptic function and strength.

As mentioned before, SYNGAP1, upon phosphorylation, dissociates from the PSD during LTP events. It has been shown that different isoforms have different rates of dispersion following LTP (Araki *et al.*, 2020). α1 has the most rapid dispersion, followed by α2, while β, which is the least enriched at the PSD, shows no dispersion after LTP. Interestingly, Araki *et al.* (Araki *et al.*, 2020) showed, in cultured neurons where *Syngap1* expression was suppressed using small hairpin RNA-mediated knockdown, that re-expression of α1 and α2, even if to a smaller degree, rescued spine enlargement and AMPAR accumulation phenotype while β did not. They also observed that in the absence of SYNGAP1, the number of proximal neurite extensions is increased while the distal branch number is decreased. Only β and α1 isoform carrying mutations in the CC domain, which prevent the formation of trimers, can rescue the distal branches phenotype.

More recent work from Kilinc *et al.* (Kilinc *et al.*, 2022) investigated the C-terminal isoform-specific functions *in vivo* using three novel mouse lines.
In the attempt to generate a reporter line, an IRES-TdTomato cassette was inserted between stop codons for the generation of isoforms α1 and α2 (Figure 1-2). Kilinc *et al.* (Kilinc *et al.*, 2022) observed that *Syngap1*$^{td/td}$ mice, which expressed about 50% of absolute levels of SYNGAP1 protein, presented a reduced life span, similar to what

was observed for *Syngap1*$^{-/-}$ mice. Interestingly, they observed that different isoforms were contributing in different percentages to the total amount of SYNGAP1. In *Syngap1*$^{+/td}$ mice, which express an absolute level of SYNGAP1 around 70% of the wild-type, α1 and α2 levels were about 50% of wild-type protein levels, while β levels were comparable to wild-type. In *Syngap1*$^{td/td}$ mice the difference in isoforms abundance was more drastic, with α1 and α2 almost undetectable and β levels doubled compared to wild-type. Behaviourally, *Syngap1*$^{+/td}$ mice presented increased horizontal activity, reduced seizure threshold, reduced freezing time in remote contextual fear memory test and increased excitatory synaptic function. These results suggest that α C-termini are fundamental for survival and their loss, or loss-of-function, might be the most prominent cause of the abnormal behaviours observed in *Syngap1*$^{+/-}$ mice.

Kilinc *et al.* (Kilinc *et al.*, 2022) also demonstrated that mice carrying mutations in the PBM present a normal life span but showed cellular and behavioural abnormalities similar to what is seen in germline *Syngap1*$^{+/-}$ mice. Moreover, they also investigated the effect of α1 and α2 isoform overexpression. For this, *Syngap1*$^{+/\beta*}$ mice were designed with a point mutation preventing the expression of β C-terminal isoforms while α1 and α2 levels increased. *Syngap1*$^{\beta*/\beta*}$ mice had a normal life span, decreased horizontal activity, normal freezing time, improved Morris water maze performance and higher seizure threshold compared to *Syngap1*$^{+/-}$ mice.

1.2 *SYNGAP1* HAPLOINSUFFICIENCY-ASSOCIATED DISORDER

1.2.1 Mutations

Mutations in *SYNAGP1* have been estimated to be one of the most common causes of ID with an incidence of *SYNGAP1* loss-of-function mutations in around 1-4/10000 individuals (Weldon *et al.*, 2018).

Mutations in *SYNGAP1* were first identified by Hamdan *et al.* in 2009 (Hamdan *et al.*, 2009). In this study, three *de novo* mutations were identified, two nonsense and one

frameshift. Since then, an increasing number of mutations have been reported with the majority of them being nonsense or frameshift mutations (Hamdan *et al.*, 2011; Mignot *et al.*, 2016; Parker *et al.*, 2015; Rauch *et al.*, 2012; Vissers *et al.*, 2010; Vlaskamp *et al.*, 2019) while missense mutations, together with splicing variants, account for about 30% of the total (Berryer *et al.*, 2013; Chevarin *et al.*, 2020; Hamdan *et al.*, 2009; Iossifov *et al.*, 2012; Kimura *et al.*, 2017; Lee *et al.*, 2020; De Rubeis *et al.*, 2014; Vlaskamp *et al.*, 2019). Variants affecting splicing (Carvill *et al.*, 2013; Hamdan *et al.*, 2011; de Ligt *et al.*, 2012; Vissers *et al.*, 2017; Vlaskamp *et al.*, 2019) as well as copy number loss (Krepischi *et al.*, 2010; Mignot *et al.*, 2016; Parker *et al.*, 2015; Pinto *et al.*, 2010; Vlaskamp *et al.*, 2019) have also been reported. Other identified mutations affecting *SYNGAP1* were microdeletions of chromosome 6 (6p21.3), reported by three separate studies (Krepischi *et al.*, 2010; Writzl *et al.*, 2013; Zollino *et al.*, 2011), and a balanced translocation between chromosome 6 and 22 (Klitten *et al.*, 2011) (Figure 1-4).

Given the wide spectrum of symptoms that characterise MRD5 patients, the phenotype-genotype association is not well defined except for epilepsy, where an association has been observed. In general, severe phenotypes and pharmacoresistant epilepsy occur more often with mutations in exons 8 to 15, while mutations between exons 1 to 4 result in a less severe phenotype (Mignot *et al.*, 2016; Vlaskamp *et al.*, 2019)**.**

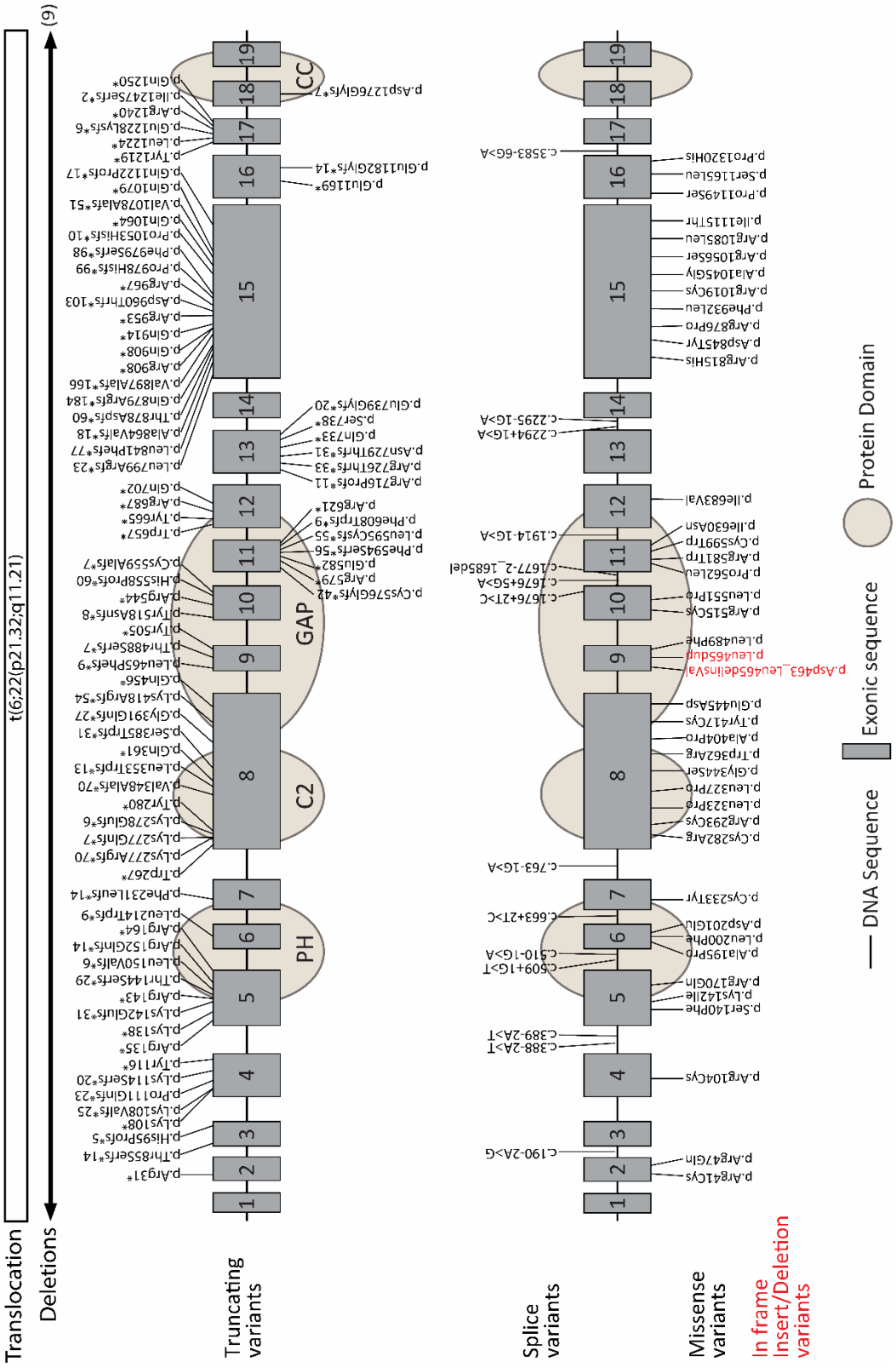

Figure 1-4. Schematic representation of SYNGAP1 mutations described in patients.
(Figure caption in the subsequent page)

Pathological *SYNGAP1* mutations present in the SFARI gene database. Mutations are mapped on their relative position on the exons or introns. If changes occur in an exon, mutations are reported following this nomenclature: p. (protein), three-letter code of the amino acid present in the wild-type protein, number (amino acid position affected by the change), three-letter code of the amino acid present in the mutated protein followed by either "*" (formation of a stop codon) or "fs*" (frameshift mutation with the downstream formation of a stop codon). Intronic mutations are reported as: c. (transcript), number indicating the position of the mutated base on the reference *SYNGAP1* sequence, letter indicating the wild-type base, >, letter indicating the mutated base. Exons, introns and protein domains' size are not drawn to scale. Based on the human transcript NM_006772.3.

1.2.2 Clinical manifestations

1.2.2.1 Behavioural characteristics

The totality of MRD5 patients present moderate-to-severe ID, with general developmental delays that manifest at 1-2 years of age, such as sitting around 12 months and walking at the age of 3 (Lo Barco *et al.*, 2022; Holder *et al.*, 2018; Vlaskamp *et al.*, 2019).

An association between ASD and mutations or ASD and level of ID has not been found, but more than half of *SYNGAP1* affected individuals present autistic behaviour. Language impairment is common; about one-third of individuals older than 5 years are nonverbal. Among those that are verbal, language development is generally delayed with the usage of single words or very short sentences. General verbal communication comprehension is also impaired (Lo Barco *et al.*, 2022; Berryer *et al.*, 2013; Holder *et al.*, 2018; Jimenez-Gomez *et al.*, 2019; Mignot *et al.*, 2016; Vlaskamp *et al.*, 2019).

Around 60-75% of patients present sleep difficulties and behavioural problems ranging from aggression and self-injury to hyperexcitability (Berryer *et al.*, 2013; Hamdan *et al.*, 2011; Mignot *et al.*, 2016; Parker *et al.*, 2015; Smith-Hicks *et al.*, 2021; Vlaskamp *et al.*, 2019).

SYNGAP1 mutations have also been identified as risk factors for schizophrenia (Funk *et al.*, 2009; Niu *et al.*, 2019; Purcell *et al.*, 2014).

1.2.2.2 Physical features

Although *SYNGAP1* haploinsufficiency was first, and is today, classified as NSID, a portion of affected individuals present physical features such as facial dysmorphisms, skeletal abnormalities, strabismus and microcephaly (Hamdan *et al.*, 2011; Krepischi *et al.*, 2010; Parker *et al.*, 2015; Writzl *et al.*, 2013; Zollino *et al.*, 2011). Moreover, patients can show axial or facial hypotonia, ataxia or gait instability and high pain threshold (Hamdan *et al.*, 2011; Mignot *et al.*, 2016; Parker *et al.*, 2015; Vlaskamp *et al.*, 2019).

1.2.2.3 Epilepsy

Epilepsy is the second most common symptom, with more than 85% of MRD5 patients showing generalised seizures (Vlaskamp *et al.*, 2019). Several types of seizures have been observed in patients (Berryer *et al.*, 2013; Mignot *et al.*, 2016; Parker *et al.*, 2015; Vlaskamp *et al.*, 2019) and given this, 85% might be an underestimation of the actual portion of patients manifesting epilepsy that is instead believed to be close to 100% (Weldon *et al.*, 2018).

The onset of seizures, with average onset at 2-3 years old, is usually preceded by developmental delays followed by a developmental plateau and regression (Lo Barco *et al.*, 2021; Berryer *et al.*, 2013; Mignot *et al.*, 2016; Vlaskamp *et al.*, 2019). In about 50% of cases, epilepsy is resistant to treatment while the other half tends to respond to various drugs. In many cases seizures are caused by activity or specific stimuli such as eating (Stülpnagel *et al.*, 2018; Vlaskamp *et al.*, 2019), photostimulation (Klitten *et al.*, 2011; Mignot *et al.*, 2016; Vlaskamp *et al.*, 2019) and vision elimination by darkness or eye closure (Chérot *et al.*, 2018; Stülpnagel *et al.*, 2018).

1.2.3 Treatments

As of today, no treatment has been developed for *SYNGAP1* haploinsufficiency-associated disorder. Patients receive treatments targeted at ameliorating specific symptoms and in general to reduce pain and distress (Holder *et al.*, 2018).

Clonidine, melatonin or trazodone have been prescribed to MRD5 patients for the treatment of sleep problems (Parker *et al.*, 2015; Vlaskamp *et al.*, 2019).
Lovastatin, a hydroxymethyl glutaryl-Coenzyme A Reductase Inhibitor that, at high dosage, increases Ras GTP loading and leads to activation of the Ras-p38-MAPK pathway (Cho *et al.*, 2011), has been used to treat a patient carrying a *de novo* truncating mutation. Amelioration of hyperactivity, improved concentration and increased range of interest was observed (Cook *et al.*, 2019).

Epilepsy is treated with a wide range of antiepileptic drugs such as valproic acid, clobazam, topiramate and others. In a few reports, patients showing pharmacoresistance have been treated with cannabidiol (CBD) (Kuchenbuch *et al.*, 2020; Vlaskamp *et al.*, 2019), which led to a considerable reduction in epileptic events. CBD has also been used to treat sleep abnormalities in *SYNGAP1* patients (Smith-Hicks *et al.*, 2021). Rosuvastatin, another statin, has been used in one case report to treat epilepsy, with the patient showing a reduction in the total number and severity of epileptic events (Kluger *et al.*, 2019).

1.3 *SYNGAP1* HAPLOINSUFFICIENCY ANIMAL MODELS

Since the first description of SYNGAP1 (Chen *et al.*, 1998; Kim *et al.*, 1998), several animal models have been created, including knock-out mice (Kim *et al.*, 2003; Komiyama *et al.*, 2002; Vazquez *et al.*, 2004), conditional ON or OFF mice (Clement *et al.*, 2012; Knuesel *et al.*, 2005; Muhia *et al.*, 2012; Ozkan *et al.*, 2014) and null or with GAP deletion rats (Katsanevaki *et al.*, 2020; Mastro *et al.*, 2020). A summary of the published behavioural phenotype present in the various deletion model developed to date is reported in Table 1-1.

***Table 1-1. Syngap1* animal models phenotypic behaviour comparison.**

Publication	Mutation	Species	Genetic background	Sex	Body Weight	Body Temperature	Grip Strength	Wire Hang
Kilinc et al,. 2022	*Syngap1*$^{PBM/PBM}$	Mouse	C57BL/6J	Not indicated	-	-	-	-
	Syngap1$^{+/Td}$				-	-	-	-
	Syngap1$^{\beta+/\beta+}$				-	-	-	-
Katsanevaki et al., 2020	*Syngap1*$^{+/\Delta GAP}$	Rat	Long Evans	Male and Female	-	-	-	-
Nakajima et al., 2019	*Syngap1*$^{+/-}$	Mouse	C57BL/6J	Male	n.s.	n.s.	n.s.	n.s.
Kilinc et al., 2018	*Syngap1*$^{+/-}$	Mouse	C57BL/6	Male and Female	-	-	-	-
Berryer et al., 2016	*Syngap1*$^{+/-}$	Mouse	C57BL/6	Not indicated	-	-	-	-
	Nkx2.1-Cre:Syngap1 cKO				-	-	-	-
Ozkan et al., 2014	*Emx1-Cre:Syngap1* cKO	Mouse	C57BL/6J 129sv/ev	Not indicated	-	-	-	-
	Gad2-Cre:Syngap1 cKO				-	-	-	-
	Syngap1 global inducible KO (Syngap1$^{+/-}$)				-	-	-	-
Clement et al., 2012	*Syngap1*$^{+/-}$	Mouse	C57BL/6J 129sv/ev	Male and Female	-	-	-	-
Muhia et al., 2012	*Syngap1*cKO (rAAV-Cre; hippocampus-specific)	Mouse	C57BL/6	Male and Female	-	-	-	-
Duarte et al., 2011	*Syngap1*$^{+/-}$	Mouse	C57BL/6J	Not indicated	-	-	-	-
Muhia et al., 2010	*Syngap1*$^{+/-}$	Mouse	C57BL/6	Male and Female	-	n.s.	-	n.s.
Guo et al., 2009	*Syngap1*$^{+/-}$	Mouse	C57BL/6J 129sv/ev	Male and Female	-	-	-	-
Komiyama et al., 2002	*Syngap1*$^{+/-}$	Mouse	ES 129/Ola, blast B6, exp F2 MF1	Male and Female	-	-	-	-

EPM-Time on Open Arms	EPM-Distance Travelled	EPM-Entries into Open Arms	EPM-Entries	OF-Stereotypic Counts	OF-Centre Time	OF-Vertical Activity	OF-Total Distance	Hot Plate-Latency	Seizure	Rotarod-Latency to Fall
-	-	-	-	-	-	-	↑	-	↓ threshold	-
-	-	-	-	-	-	-	↑	-	↓ threshold	-
-	-	-	-	-	-	-	↓	-	↑ threshold	-
n.s.	n.s.	n.s.	-	-	-	-	↑ only in first 20 min	-	Present	n.s.
↑	↑	n.s.	↑	↑	↑	↑	↑	↑	-	↓
↑	-	↑	-	-	-	-	-	-	-	-
↑	-	-	-	-	-	-	↑	-	-	-
n.s.	-	-	-	-	-	-	n.s.	-	-	-
↑	-	-	-	-	-	-	↑	-	↓ threshold	-
n.s.	-	-	-	-	-	-	n.s.	-	n.s.	-
n.s.	-	-	-	-	-	-	n.s.	-	-	-
	-	-	-	-	-	-	↑	-	↓ threshold	-
-	-	-	-	-	-	-	↑	-	-	-
-	-	-	-	-	-	-	-	n.s.	-	-
↑	↑	↑	-	-	↑	-	↑	n.s.	-	n.s. in male, ↓ in female
↑		n.s.	n.s.	↑	↑	-	↑	-	-	-
-	-	-	-	-	-	-	-	-	-	-

TM-Correct Responses	-	-	-	-	→	-	→	→	→	n.s.	n.s.		-	-	→	-	-
TM-Latency	-	-	-	-	n.s.	-	-	-	-	-	-	-	-	-	-	-	-
TM-Distance	-	-	-	-	←	-	-	-	-	-	-	-	-	-	-	-	-
YM-Entries	-	-	-	-	←	-	-	-	-	-	-	-	-	-	-	-	-
YM-Alternations	-	-	-	-	←	-	-	-	-	-	-	-	-	-	-	-	-
YM-Alternation (%)	-	-	-	-	n.s.	-	-	-	-	-	-	-	→	-	-	-	-
YM-Total Distance	-	-	-	-	←	-	-	-	-	-	-	-	-	-	-	-	-
BM-Error to 1st	-	-	-	-	←	-	-	-	-	-	-	-	-	-	-	-	-
BM-Latency to 1st	-	-	-	-	←	-	-	-	-	-	-	-	-	-	-	-	-
BM-Distance to 1st	-	-	-	-	←	-	-	-	-	-	-	-	-	-	-	-	-
BM-Omission Error	-	-	-	-	←	-	-	-	-	-	-	-	-	-	-	-	-
BM-PT (24 hr retention)	-	-	-	-	→	-	-	-	-	-	-	-	-	-	-	-	-
BM-PT (4 wks retention)	-	-	-	-	→	-	-	-	-	-	-	-	-	-	-	-	-
LD-Stay Time in Light	-	-	-	-	n.s.	-	-	-	-	-	-	-	-	-	-	-	-

PS-Immobility	PPI	PPI-Startle Response	CSI-Time Spent Around Cage (Stranger2 side)	CSI-Time Spent Around Cage (Stranger1 side)	SI-Distance Travelled	SI-Mean Duration/Contact	SI-Contacts	SI-Total Duration of Contact	CA-Edge departures	LD-Distance Traveled
-	-	-	-	-	-	-	-	-	-	-
-	-	-	-	-	-	-	-	-	-	-
-	-	-	-	-	-	-	-	-	-	-
-	-	-	n.s., ↓ exploration time	n.s., ↓ exploration time	-	-	n.s.	n.s.	-	-
↓	↓	n.s.	↓	↓	↑	↓	n.s.	↓		n.s.
-	-	-	-	-	-	-	-	-	↑	-
-	-	-	↓	-	-	-	-	-	-	-
-	-	-	↓	-	-	-	-	-	-	-
-	-	-	-	-	-	-	-	-	-	-
-	-	-	-	-	-	-	-	-	-	-
-	-	-	-	-	-	-	-	-	-	-
-	-	-	-	-	-	-	-	-	-	-
-	-	-	-	-	-	-	-	-	-	-
-	-	-	-	-	-	-	-	-	-	-
-	↓	↑	Social recognition impaired, social	n.s.	-	-	-	-	-	-
-	-	-	-	-	-	-	-	-	-	-

HCSI-Activity Level	HCSI-Particles	CCFC-Retention-Distance	CCFC-Retention-Cued	CCFC-Retention-Context	CCFC-Distance Travelled	CCFC-Freezing-Cued	CCFC-Freezing-Context	CCFC-Freezing-conditioning	TS-Immobility
-	-	-	-	-	-	-	↓	-	-
-	-	-	-	-	-	-	↓	-	-
-	-	-	-	-	-	-	n.s.	-	-
-	-	-	-	-	-	-	-	-	-
↑ at night	↑ at night	n.s.	n.s.	n.s.	n.s.	↓	n.s.	↓	↓
-	-	-	-	-	-	n.s.	↑	-	-
-	-	-	-	-	-	-	-	-	-
-	-	-	-	-	-	-	-	-	-
-	-	-	-	-	-	-	Impaired	-	-
-	-	-	-	-	-	-	n.s.	-	-
-	-	-	-	-	-	-	n.s.	-	-
-	-	-	-	-	-	-	Context discrimination impaired	n.s.	-
-	-	-	-	-	-	-	-	-	-
-	-	-	-	-	-	-	-	-	-
-	-	-	-	-	-	-	-	-	-
-	-	-	-	-	-	↓, activity ↑ during tone	n.s.	n.s.	
-	-	-	-	-	-	-	-	-	-

HC-Activity Level	-	-	-	-	↑ at night	-	-	-	-	-	-	-	-	-	-	-	-
MWM-visible	-	-	-	-	-	-	-	-	-	-	-	-	n.s.	-	n.s.	-	n.s.
MWM-hidden	-	-	-	n.s.	-	-	-	-	-	-	-	-	n.s.	-	n.s.	-	Path length ↓
MWM-Probe test	↓	n.s.	-	n.s.	-	-	-	-	-	-	-	-	↓	-	↓	-	↓
RM	-	-	-	-	-	-	-	-	-	-	-	-	-	-		correct choice ↓	-
RM-error	-	-	-	-	-	-	-	-	-	-	-	-	-	-	↓	-	-
Object Recognition	-	-	-	-	-	-	-	-	-	-	-	-	-	-	n.s.	-	-

BM=Barnes maze, CCFC=Contextual and cued fear conditioning, CSI=Crawley's sociability and social Novelty preference test, EPM=Elevated plus maze, HC=Home cage locomotor activity, HCSI=Home cage social interaction, LD=Light/dark transition, MWM=Morris water maze, OF=Open field, PPI=Prepulse inhibition, PS=Porsolt forced swim, PT=Probe test, RM=Radial maze, SI=Social interaction, TM=T-Maze, TS=Tail suspension, YM=Y-Maze. ↑ = Increased, ↓= Decreased. n.s.=not statistically significant. "-"=not tested.

Table adapted from Nakajima et at., 2019.

1.3.1 The behavioural and physiological phenotype of the *SYNGAP1* haploinsufficiency-associated disorder mouse model

1.3.1.1 General condition

Syngap1$^{+/-}$ mice present a normal life span and reduced brain volume, but they appear in general healthy (Kilinc *et al.*, 2018; Kim *et al.*, 2003; Komiyama *et al.*, 2002; Vazquez *et al.*, 2004). *Syngap1*$^{-/-}$ mice are normal at birth, but their growth is reduced beyond PND2 and they die before PND7 (Kim *et al.*, 2003; Komiyama *et al.*, 2002; Vazquez *et al.*, 2004). *Syngap1*$^{+/-}$ mice show an increase in GABAergic neuron apoptosis and a similar mechanism has been proposed to explain the premature death of *Syngap1*$^{-/-}$ mice. The model hypothesises that due to the reduction of SYNGAP1 in neurons, an increase in caspase-3 activation levels occurs leading to neuronal death via apoptosis (Knuesel *et al.*, 2005).

1.3.1.2 Hyperactivity, anxiety, and risk-taking behaviour

Associated with ID, MRD5 patients present also behavioural abnormalities such as attention deficit hyperactivity disorder (ADHD). Hyperactivity is a strong feature observed in all the *Syngap1*$^{+/-}$ mice lines which present higher distance travelled compared to wild-type littermates (Berryer *et al.*, 2016; Guo *et al.*, 2009; Muhia *et al.*, 2009, 2010; Nakajima *et al.*, 2019). Increased time in the open arms of the elevated plus maze is another widely reproduced phenotype (Berryer *et al.*, 2016; Guo *et al.*, 2009; Muhia *et al.*, 2010; Nakajima *et al.*, 2019). Moreover, they present an increased tendency to jump from an elevated platform during a cliff avoidance test (Kilinc *et al.*, 2018), which has been interpreted as increased impulsivity, lack of anxiety or risk-taking behaviour.

1.3.1.3 Sensory processing and sleep abnormalities

It has been reported that, although some cases show sensory hypersensitivity, MRD5 individuals present a high pain threshold which could be associated with reduced sensitivity (Parker *et al.*, 2015; Vlaskamp *et al.*, 2019). Muhia *et al.* (Muhia *et al.*, 2010) reported that, when *Syngap1*$^{+/-}$ mice and wild-type controls are exposed to acute

thermal stimulation, no genotype effect emerges. In contrast, Nakajima *et al.* (Nakajima *et al.*, 2019) described an increased latency to respond to heat shock. Michaelson *et al.* (Michaelson *et al.*, 2018) showed that *Syngap1*$^{+/-}$ mice are not able to discriminate novel objects using tactile stimuli during an object recognition task. Similarly, *Syngap1*$^{+/-}$ mice were unable to perform a Go/NoGo task when the presented cue was a whisker stimulation.

When tested with the prepulse inhibition (PPI) test and exposed to an acoustic startle response, *Syngap1*$^{+/-}$ mice presented a reduced PPI and increased startle reactivity (Guo *et al.*, 2009; Nakajima *et al.*, 2019). PPI is used to evaluate sensorimotor gating. The concept is based on the supposition that when an individual is exposed to a low-level acoustic stimulus, this will decrease the response to a high-level stimulus.

A large portion of patients bearing mutations in *SYNGAP1* also manifest sleep problems (Berryer *et al.*, 2013; Hamdan *et al.*, 2011; Mignot *et al.*, 2016; Parker *et al.*, 2015; Smith-Hicks *et al.*, 2021; Vlaskamp *et al.*, 2019). Sullivan *et al.* (Sullivan *et al.*, 2020) showed that adult *Syngap1*$^{+/-}$ mice tend to spend more time asleep during the light phase compared to the wild-type controls and vice versa during the dark phase. Moreover, *Syngap1*$^{+/-}$ mice present a higher number of sleep/wake cycles during the dark phase. Similar results have been reported by Aten *et al.* (Aten *et al.*, 2021).

1.3.1.4 Seizures

Clement *et al.* (Clement *et al.*, 2012) and Ozkan *et al.* (Ozkan *et al.*, 2014) reported that, although *Syngap1*$^{+/-}$ mice do not show spontaneous seizures, they present a reduced seizure threshold when exposed to flurothyl and that young *Syngap1*$^{+/-}$ mice experience audiogenic seizures when exposed to a 126 dB alarm.

Spontaneous seizures have been observed in adult mice by Sullivan *et al.* (Sullivan *et al.*, 2020) after 24h video and electroencephalography (EEG) monitoring.

1.3.1.5 Memory and social interaction

Syngap1$^{+/-}$ mice show deficits in spatial learning, social memory, consolidation of contextual memory and spatial working memory (Guo *et al.*, 2009; Komiyama *et al.*, 2002; Muhia *et al.*, 2010; Ozkan *et al.*, 2014). SYNGAP1 is a key effector of LTP-induced plasticity, therefore experience-dependent memory processes are heavily impaired in *Syngap1*$^{+/-}$ animals (Clement *et al.*, 2012; Kim *et al.*, 2003; Ozkan *et al.*, 2014).

Syngap1$^{+/-}$ mice presented a clear phenotype for reference memory and working memory when tested using the radial maze (Muhia *et al.*, 2010) and in working memory when tested on a spontaneous alternation test (Berryer *et al.*, 2016; Guo *et al.*, 2009; Muhia *et al.*, 2010; Nakajima *et al.*, 2019).

It was shown by Komiyama and colleagues (Komiyama *et al.*, 2002) first and by Muhia *et al.* (Muhia *et al.*, 2010) later, that *Syngap1*$^{+/-}$ mice present a mild deficit in spatial reference memory when tested using the Morris water maze.

Syngap1$^{+/-}$ mice showed an overall decreased freezing time when tested using cued and contextual fear conditioning (Clement *et al.*, 2012; Nakajima *et al.*, 2019). However, Guo *et al.* (Guo *et al.*, 2009) showed no genotype difference in a contextual fear conditioning paradigm.

Syngap1$^{+/-}$ mice display a reduction in social recognition and enhanced social isolation when tested in the three-chamber task (Berryer *et al.*, 2016; Guo *et al.*, 2009).

1.3.2 Behavioural phenotype in rat models of *SYNGAP1* haploinsufficiency-associated disorder

To date, two rat models have been generated for the study of SYNGAP1, a *Syngap1*$^{+/-}$ line (Mastro *et al.*, 2020), used to study the SYNGAP1 interactome, and a Δ-GAP model (Katsanevaki *et al.*, 2020) which carries a deletion of the GAP domain. *Syngap1*$^{+/\Delta\text{-}GAP}$ rats, as observed for *Syngap1*$^{+/-}$mice, have a normal life span and are overall healthy. Homozygosity of the GAP deletion is lethal, with a life span of 7 postnatal days on average. *Syngap1*$^{+/\Delta\text{-}GAP}$ rats show impairment in memory

extinction but normal spatial memory. When tested on the three chamber test, wild-type and *Syngap1*$^{+/\Delta\text{-}GAP}$ rats spend more time with a social cue compared to an inanimate object, but *Syngap1*$^{+/\Delta\text{-}GAP}$ rats display a reduction in time spent exploring. In contrast to what was observed in mice, *Syngap1*$^{+/\Delta\text{-}GAP}$ habituate to an open field and do not show hyperactivity (Katsanevaki *et al.*, 2020).

1.3.3 Circuit and cellular phenotype

As in MDR5 patients, it has been observed that *Syngap1*$^{+/-}$ mice present a reduction in total absolute brain volume when analysed via magnetic resonance imaging (MRI) scan (Kilinc *et al.*, 2018). The reduction affects specific regions of the brain, among which are areas of the visual and somatosensory cortex (SSC). Associated with these structural changes, circuit dysfunctions have also been observed in both the visual and SSC (Carreño-Muñoz *et al.*, 2021; Michaelson *et al.*, 2018) suggesting their implication in the development of behavioural abnormalities.

In *Syngap1*$^{+/-}$ mice, impaired synaptogenesis associated with premature spine maturation is observed (Aceti *et al.*, 2015; Vazquez *et al.*, 2004) suggesting that SYNGAP1 deficiency leads to an early spine maturation.
Abnormal long-range connectivity in layers 2/3 and 5 has been observed in *Syngap1*$^{+/-}$ mice (Aceti *et al.*, 2015; Michaelson *et al.*, 2018). Moreover, Barnett *et al.* (Barnett *et al.*, 2006) showed abnormal cellular barrel segregation. Impaired experience-induced plasticity has been observed in layer 2/3 of the SSC (Michaelson *et al.*, 2018).

Syngap1 haploinsufficiency in mice leads to abnormal neuronal excitability causing EEG abnormality with a lowered threshold for fluoroethyl-induced seizures (Clement *et al.*, 2012; Guo *et al.*, 2009; Ozkan *et al.*, 2014).
Seizure susceptibility is reflected by the presence of interictal spikes, abnormal electrical events that are caused by a hyperexcitable population of neurons that fire in synchrony (Ayala *et al.*, 1973; Karoly *et al.*, 2016). *Syngap1*$^{+/-}$ mice show electrical abnormalities (Carreño-Muñoz *et al.*, 2021; Sullivan *et al.*, 2020) similar to what is

observed in human patients (Kuchenbuch *et al.*, 2020; Mignot *et al.*, 2016; Vlaskamp *et al.*, 2019; Zollino *et al.*, 2011).

It has been shown that *Syngap1*$^{+/\Delta\text{-}GAP}$ rats present seizure-like events (Katsanevaki *et al.*, 2020). During these events head bobbing and absence of locomotion were observed. Moreover, EEG abnormalities during sleep have also been described in this model (Buller-peralta *et al.*, 2022).

1.4 DEFINITION OF RESCUE CRITICAL PERIOD AND EVIDENCE OF TREATMENT FEASIBILITY

The identification of a critical period for the rescue of *SYNGAP1* haploinsufficiency-associated disorder is crucially important for the rational design of a gene therapy approach. Several studies have been conducted with conditional knockout or conditional rescue models and pharmacological intervention.

1.4.1 Inactivation studies

Clement *et al.* (Clement *et al.*, 2012) used a *Syngap1*$^{+/fl}$ mouse line (*Syngap1*, which is normally expressed, is flanked by two LoxP sites). Injection of a Cre-expressing virus in the dentate gyrus induced localised haploinsufficiency at two different developmental stages, at PND1 or PND60. When haploinsufficiency was induced at early stages (PND1), an increase in AMPAR/NMDAR ratio was observed, in agreement with the findings in constitutive *Syngap1*$^{+/-}$ mice (Clement *et al.*, 2012). At PND60, AMPAR/NMDAR ratio was unaffected, but increased excitability of dentate gyrus granulate neurons was recorded.

Muhia *et al.* (Muhia *et al.*, 2012) used a floxed model (Knuesel *et al.*, 2005; Vazquez *et al.*, 2004) to study the behavioural effect of the total absence of *Syngap1* expression from the hippocampus. *Syngap1*$^{fl/fl}$ were injected intrahippocampally with a Cre expressing Adeno-associated virus (AAV) at 8-10 weeks of age and tested for

hyperactivity and anxiety 4 weeks after. They observed decreased hippocampal neurogenesis and electrophysiological abnormalities. Behaviourally, AAV-Cre treated, and control mice were equally able to locate the platform during the Morris water maze test and the anxiety levels, tested using the elevated plus maze, were not different between treatments. On the other hand, AAV-Cre treated mice showed a clear hyperactivity phenotype when tested in the open field. Another study showed that when heterozygosity was induced brain-wide at 8 weeks of age in *Syngap1*$^{+/fl}$ mice, no behavioural alterations were observed (Ozkan *et al.*, 2014).

1.4.2 Reactivation studies

Adulthood reactivation studies showed that the behavioural rescue window is likely to close early in life for core phenotypes. On the other hand, electrophysiological properties of the hippocampus show higher plasticity compared to other regions.
After brain-wide reactivation of *Syngap1* expression in a *Syngap1*$^{+/lox\text{-}stop}$ line crossed with a Cre-ERt2 driver line, in which the migration to the nucleus of the fusion protein Cre-estrogen receptor (ER) is pharmacologically controlled, Clement *et al.* (Clement *et al.*, 2012) showed that induction of *Syngap1* expression at 9 weeks of age was not able to revert behavioural abnormalities, such as reduced anxiety, hyperactivity and working memory impairments. Only impairments in NMDAR-dependent LTP in the hippocampus were improved after treatment.

More recent work suggests that different behavioural and cellular phenotypes present different rescue windows. Aceti *et al.* (Aceti *et al.*, 2015) showed that genetic rescue in a *Syngap1*$^{+/lox\text{-}stop}$ mouse model at PND1 prevents the development of hyperactivity, reduced anxiety and altered fear response while when induced at PND21 only fear conditioning behaviour was rescued. Late rescue of fear conditioning has been also shown by Creson *et al.* (Creson *et al.*, 2019) in 8 weeks old mice while Llamosas *et al.* (Llamosas *et al.*, 2021) showed restoration of SSC plasticity after genetic rescue at PND60.

1.4.3 Pharmacological rescue

Reversibility and identification of a critical window have also been studied via pharmacological treatment.

Ozkan *et al.* (Ozkan *et al.*, 2014) showed that reducing expression or restoring normal *SYNGAP1* levels only in GABAergic cells do not induce behavioural abnormalities. In opposition to this, a study aimed to pharmacologically restore GABA reversal potential (E_{GABA}), plasticity and LTP via the usage of 6-bromoindirubin-3'-oxime (6BIO), a potent inhibitor of Glycogen synthase kinase 3 beta, showed partial phenotypic rescue in *Syngap1*$^{+/-}$ mice (Verma *et al.*, 2022). Daily administration of 6BIO from PND10 was able to restore E_{GABA} and LTP. For all treatment regimens (daily administration of 6BIO from PND10 to PND16, from PND10 to PND80 and from PND30 to PND80), they observed a total or partial rescue of social interaction and novel object recognition. Social preference was not rescued in the PND10-16 group while hyperactivity was not rescued in the PND30-80 group. Seizures were tested only in the PND30-80 treatment group and were rescued.

Altogether, these results suggest that different phenotypes present different windows of intervention. Hyperactivity appeared to be fully rescuable only early in life (Aceti *et al.*, 2015; Verma *et al.*, 2022), while other phenotypes, such as fear conditioning, plasticity and seizures, appeared to have a wider window of intervention (Creson *et al.*, 2019; Llamosas *et al.*, 2021; Verma *et al.*, 2022).

1.5 BRAIN REGIONS ASSOCIATED WITH THE DEVELOPMENT OF BEHAVIOURAL ABNORMALITIES

As mentioned before, the work presented by Muhia *et al.* (Muhia *et al.*, 2012) suggested the involvement of the hippocampus in the development of the hyperactive phenotype.

Ozkan *et al.* (Ozkan *et al.*, 2014), using a *Syngap1*$^{+/fl}$ mouse line (Clement *et al.*, 2012) crossed with two different Cre lines, tried to understand the contribution of a specific cellular population to the definition of the haploinsufficient phenotype. When haploinsufficiency was confined to glutamatergic neurons of hippocampus and forebrain areas, excluding striatum, a behavioural phenotype similar to what was seen in germline *Syngap1*$^{+/-}$ mice was observed: increased horizontal activity in the open field, increased percentage of time spent in the open arms of the elevated plus maze, reduced freezing time in a fear conditioning tests and reduced flurothyl-induced seizure threshold. The same experiment was repeated in *Syngap1*$^{+/fl}$ mice crossed with Gad2-Cre, where haploinsufficiency was confined only to GABAergic neurons. No behavioural abnormalities were recorded. Interestingly restricting *Syngap1* expression to only forebrain glutamatergic neurons did not rescue the hyperactive and seizure phenotype, although anxiety and working memory were comparable to wild-type mice (Ozkan *et al.*, 2014).

The involvement of inhibitory neurons in the pathophysiology of the disorder was further investigated by Berryer *et al.* (Berryer *et al.*, 2016). They showed that a weak effect on behaviour was observed when haploinsufficiency is induced in parvalbumin and somatostatin interneuron precursors. Although mice did not show hyperactivity and reduced anxiety, they presented impairment in working and social memory.

These results suggest that haploinsufficiency in forebrain glutamatergic neurons contributes to the development of hyperactivity and to the anxiety reduction but also other areas, such as SSC and visual cortex, are likely to be involved in the pathophysiology of the disease (Carreño-Muñoz *et al.*, 2021; Llamosas *et al.*, 2021; Michaelson *et al.*, 2018).

1.6 GENE THERAPY

Gene therapy is a therapeutic approach that delivers DNA to cells of patients with genetic disorders and aims to correct diseases caused by the malfunctioning of a gene. Different types of gene therapy have been developed to respond to specific needs, for example a gene silencing therapy involves the silencing of a gene that has acquired a toxic function while in a gene replacement approach a functional gene is introduced to replace an existing non-working gene (Blömer *et al.*, 1996; Bulcha *et al.*, 2021; Ingusci *et al.*, 2019; Shahryari *et al.*, 2019).

Gene therapy can be performed *in vivo* when the therapeutic gene is delivered to patient cells; or *ex vivo,* when patient-derived cells, or cells from an allogenic source (derived from a universal donor (Farid *et al.*, 2018)), are modified *in vitro* and then re-introduced in the patient. In both cases, the therapeutic DNA can be delivered using viral or non-viral vectors (Bouard *et al.*, 2009; Gardlík *et al.*, 2005).

1.6.1 Non-viral vectors

Non-viral methods of delivery can be categorised as physical or chemical. Physical methods involve the direct delivery of naked DNA in combination with mechanical methods such as gene gun, electroporation or sonoporation (Chellappan *et al.*, 2018; Dutta *et al.*, 2021; Harris *et al.*, 2021; Mizuno *et al.*, 2009; Mukhopadhyay *et al.*, 2019; Rinaldi *et al.*, 2018). Chemical methods of non-viral gene delivery involve the encapsulation of DNA in lipid nanoparticles (liposomes) or synthetic polymers (Lin *et al.*, 2018). The strengths of this approach over virally mediated methods are the ability to deliver long DNA sequences and its low immunogenicity. However, the transfection efficiency of these methods is very low, limited to easily accessible tissues such as skin and muscle, and predominantly leads to short-term expression of the transgene, requiring multiple, regular dosing (Lin *et al.*, 2018; Wang *et al.*, 2019).

1.6.2 Viral vectors

Viruses evolved to efficiently infect eukaryotic cells by delivering their genomic DNA and replicating. The ability to transfect a specific cell type and induce a sustained expression of their genome in host cells is the basis of their use for gene therapy applications. Viral vectors used for gene therapy are recombinant replication-defective vectors which are able to deliver the transgene into the target cells, but they do not possess the ability to replicate (Bouard *et al.*, 2009). To generate replication-defective viruses, the wild-type viral genome is modified, eliminating the genes necessary for replication and the completion of the lytic cycles and replacing them with the gene of interest and required regulatory elements.

While viral vectors have many useful characteristics, a major downside is their immunogenicity, the ability to elicit an immune response in the host. For example, the vast majority of the human population has been infected by Adenovirus (Ad), therefore the delivery of this type of vector in a subject that expresses neutralising antibodies could induce a very strong immune reaction that could potentially be fatal. While the inflammation caused by the vector per se might not cause damage to the system, the immune response can decrease the efficiency of the therapy by decreasing the circulating viral particles (Shirley *et al.*, 2020).

The range of available vectors for gene therapy is continuously expanding, but the most widely used for the treatment of central nervous system (CNS) pathology is AAV. Other species of viruses are also used such as Ad, retrovirus and Herpes Simplex virus (HSV) (Robbins *et al.*, 1998). Each class of vector has different positive and negative properties.

Retroviruses are integrating RNA viruses that, except for lentiviruses, can infect only proliferating cells. They can carry a transgene cassette up to 9000 bp. Integration can result in long and stable expression of the transgene; however, such therapy carries the intrinsic risk of insertional mutagenesis that could lead to the development of

other pathologies, including cancer (Bulcha *et al.*, 2021; Cooray *et al.*, 2012; Sakuma *et al.*, 2012).

HSV is a dsDNA enveloped virus, with the capsid covered by a lipid membrane. HSV gene therapy vectors are based on serotype 1. HSVs have the ability of retrograde transport, which means that they can infect neurons at the periphery and then translocate to the CNS. HSV can infect dividing cells and remain in a latent state in quiescent cells. Moreover, it has a large cloning capacity, approximately 50 kilobases (kb). Negative aspects are the risk of toxicity for the host cells and the achievement of only transient expression of the transgene (Gardlík *et al.*, 2005; Goverdhana *et al.*, 2005; Lee *et al.*, 2017; Palella *et al.*, 1988; Simonato *et al.*, 2000).

Ad is a double-stranded (ds) DNA virus that can carry transgene cassettes of ~35 kb and can transduce both dividing and non-dividing cells. The fact that Ad virus infection is common in humans means that the use of these viruses as gene therapy vectors can cause a significant immunogenic reaction. Ad does not integrate into the host genome and results in only a transient transgene expression (Gardlík *et al.*, 2005; Lee *et al.*, 2017; Ritter *et al.*, 2002).

AAV is a single-stranded (ss) DNA virus with a wide range of naturally occurring serotypes and cell tropisms. Cloning capacity is limited to approximately 4700 to 5000 bp, but they are able to transduce both dividing and non-dividing cells and lead to stable, long-lasting transgene expression, making them a promising vector for gene therapy, and the current gold standard for gene therapy (Bouard *et al.*, 2009; Penaud-Budloo *et al.*, 2018).

1.6.2.1 AAV

AAVs are ssDNA viruses belonging to the family of Parvovirus and were isolated for the first time by Atchison *et al.* (Atchison *et al.*, 1965) from an Ad preparation. AAVs are defined dependoviruses because they are unable to replicate and express their genome without the presence of a helper virus, such as Ad or HSV (Daya *et al.*, 2008). AAVs are small, non-enveloped viruses with an icosahedral capsid composed of 60

subunits of three structural proteins, viral capsid protein (VP) 1, 2 and 3, organised in the ratio 1:1:10. So far, twelve wild-type serotypes have been identified, which differ in capsid structure and tissue tropism (Li *et al.*, 2020).

1.6.2.1.1 AAV genome, infection pathway and serotypes

The AAV genome, of approximately 4700 bp, contains two Open Reading Frames (ORFs) which encode for genes necessary for replication and packaging. The ORFs are flanked by Inverted Terminal Repeats (ITRs) necessary for replication and packaging (Figure 1-5). Transcription is driven by three promoters P5, P19 and P40 (Figure 1-5) (Haggerty *et al.*, 2020; Srivastava *et al.*, 1983). The first ORF is *rep,* which encodes for four proteins: Rep78 and Rep68, under the control of the promoter P5 and necessary for viral replication; Rep52 and Rep40, under the control of promoter P19 and necessary for the accumulation of the replicated ssDNA for packaging (Ni *et al.*, 1992). The *cap* ORF encodes the three viral capsid proteins VP1, VP2 and VP3 and its expression is driven by the P40 promoter (Agbandje-McKenna *et al.*, 2011). Within the *cap* gene is localised a third ORF, which encodes for the Assembly-activating protein (AAP) necessary for the capsid assembly (Li *et al.*, 2020; D. Wang *et al.*, 2019).

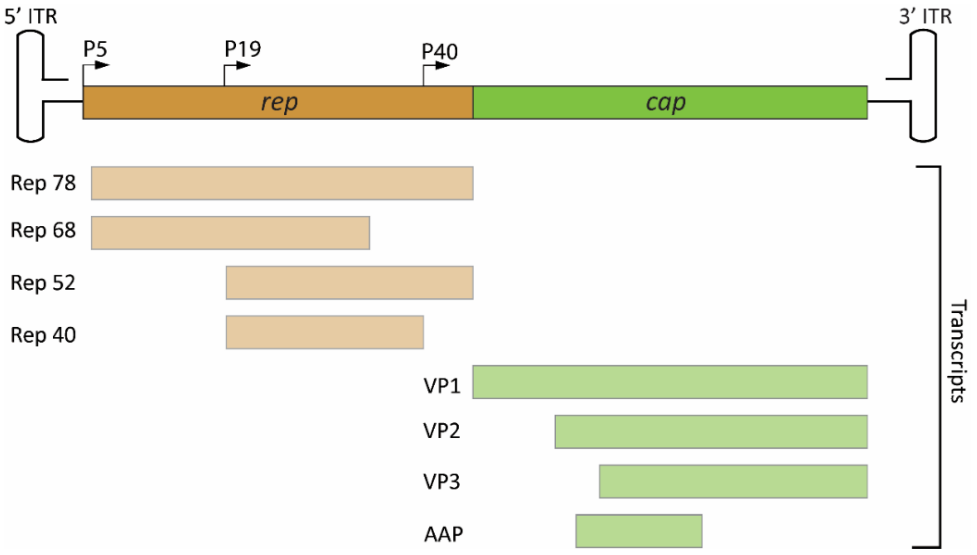

Figure 1-5. AAV genome contains two ORFs, rep and cap, encoding the proteins necessary for replication and packaging.
Schematic representation of AAV genome and relative transcripts. VP: Viral capsid Protein, AAP: Assembly-Activating Protein.

AAV particles enter cells via receptor-mediated endocytosis (Figure 1-6.1), the type of receptor depends on the stereotype. AAVs are then trafficked inside the cell via the endosomal system (Figure 1-6.2) (Ding *et al.*, 2005). Once in the endosome two events can occur: the viral particles remain in the endosome vesicles and are degraded (Figure 1-6.3), or they escape the endosome and are translocated to the nucleus via microtubules (Figure 1-6.4 and 5), achieving infection. Once in the nucleus, the virus is uncoated, releasing the ssDNA that is transformed into dsDNA by the host replication system (Wu *et al.*, 2006) (Figure 1-6.6 and 7). dsDNA can also be formed by annealing with a complementary strand derived from a second virus that is co-infecting the cell (Nakai *et al.*, 2000). However, in both cases, to complete the replication cycle, AAV requires the presence of helper viruses. In the absence of a helper, the AAV viral genome remains latent in an epichromosomal state in the nucleus. Integration events are rare but possible (Kotin *et al.*, 1991).

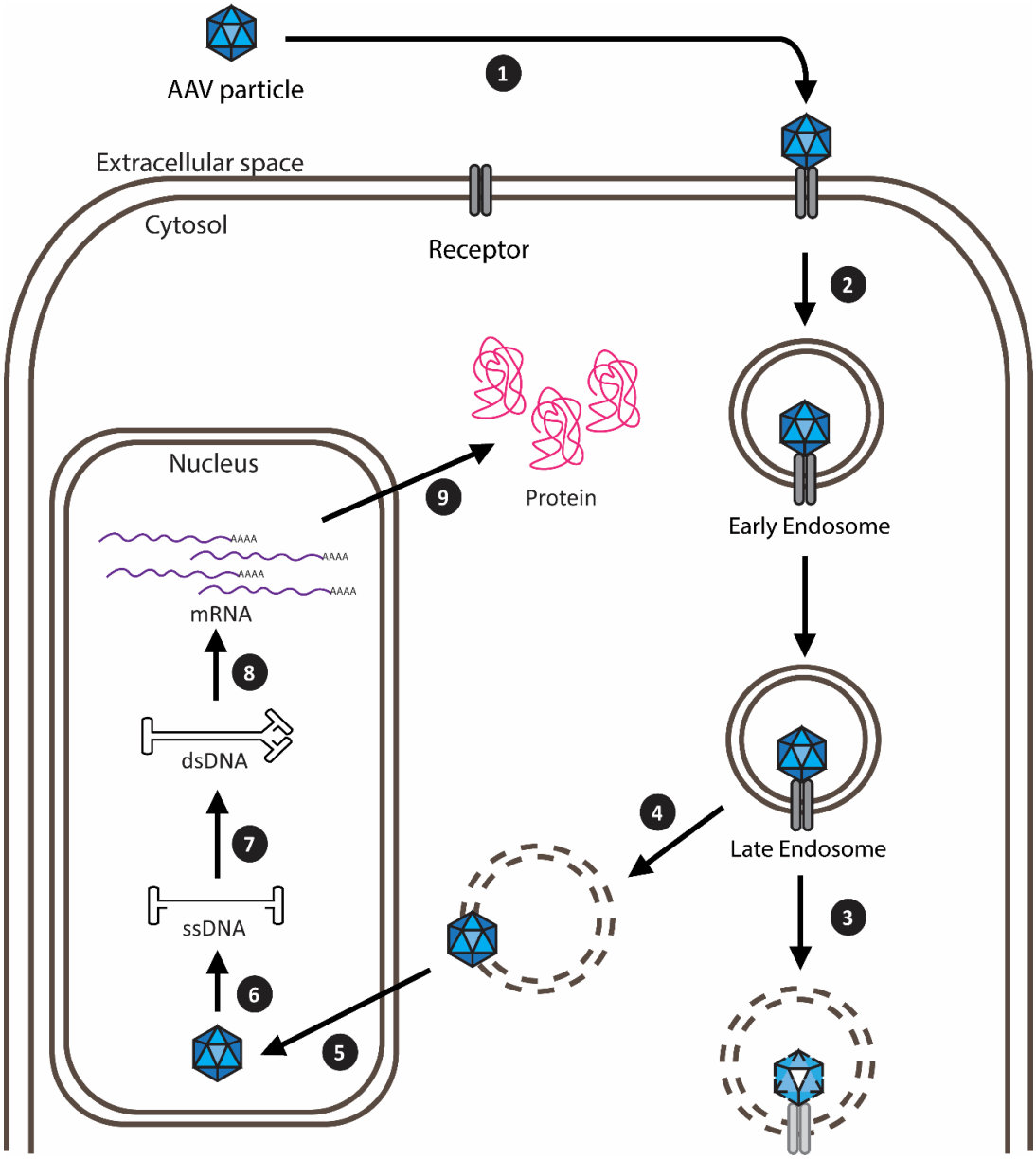

Figure 1-6. AAV transduction process.

Schematic representation of the AAV transduction process. AAV infection of the target cell starts with the interaction between the AAV particle and the membrane receptor (1), which then leads to the viral particle internalization and the formation of an early endosome (2). The early endosome matures in the late endosome which can be degraded together with its content (3). In alternative, the AVV particle can escape from the late endosome (4) and translocate to the nucleus (5). The AAV particle is then uncoated (6) and the released ssDNA is then converted into dsDNA (7). dsDNA can also be formed by the annealing of two complementary ssDNA genomes deriving from two different AAV particles co-infecting the cell. dsDNA is then transcribed in mRNA (8) which is translated to produce proteins (9).

Twelve naturally occurring AAV serotypes have been isolated to date, and many more have been created by manipulation of capsids through rational design, computationally designed ancestral capsid, and directed evolution (Li *et al.*, 2020). Different serotypes display tropism for distinct cell types. AAV2, which has been largely studied and has been used in a vast number of studies (Howard *et al.*, 2008; Srivastava *et al.*, 1983), for example, is known to have tropism for neurons, although it is not efficiently expressed in all type of neurons, but also for liver and muscle cells (Howard *et al.*, 2008). AAV3 and 10 are known to have tropism for muscular tissue and, in the case of AAV3, also stem cells (Li *et al.*, 2020). Among the serotypes that are able to transduce the CNS, only AAV2, 6 and 9 are known to infect only neuronal cells, while AAV1, 5 and 7 can infect also astrocyte and microglia (Haggerty *et al.*, 2020; Zincarelli *et al.*, 2008). AAV9 is an excellent candidate for CNS targeted therapies as it is able to cross the blood brain barrier (BBB), spreads widely in the brain and presents a high tropism for neuronal cells (Foust *et al.*, 2009; Mendell *et al.*, 2017).

1.6.2.1.2 AAV as viral vector

To use AAV as vectors for gene therapies, the wild-type genome is modified to accommodate an expression cassette and prevent viral replication. Both *rep* and *cap* are deleted, and only the flanking ITRs are retained in the final construct. The deletion of both ORFs increases the cloning capacity to ~4700 bp (the size of the entire wild-type genome) (Li *et al.*, 2020).

As the genes necessary for replication and packaging have been deleted, the production of AAV particles requires *rep*, *cap* and helper genes to be provided in *trans* during the manufacturing process. Two production platforms exist at the moment: transfection of human embryonic kidney 293 (HEK293) cells, either using a triple transfection system, or using a stable mammalian cell line that constitutively expresses the genes necessary for replication (Choi *et al.*, 2006; Clark Reed *et al.*, 1995); and the baculovirus/Sf9 system in which insect Sf9 cells are used for AAV production (Wu *et al.*, 2019).

1.6.3 Gene therapy for the treatment of *SYNGAP1* haploinsufficiency-associated disorder

To date, no conventional or disease-modifying treatments are available for *SYNGAP1* haploinsufficiency-associated disorder. The only currently available therapies are for the management of symptoms, often with limited effectiveness. For example, around 50% of epileptic cases in *SYNGAP1* haploinsufficiency-associated disorder are resistant to current pharmacotherapies (Berryer *et al.*, 2013; Mignot *et al.*, 2016; Okazaki *et al.*, 2017; Parker *et al.*, 2015). Although further studies are necessary to deepen our knowledge of the critical rescue period, genetic rescue studies showed that certain phenotypes associated with *SYNGAP1* haploinsufficiency in mice can be prevented by early reactivation of gene expression (Aceti *et al.*, 2015; Creson *et al.*, 2019). These characteristics, together with its monogenic nature, make *SYNGAP1* haploinsufficiency-associated disorder a good candidate for genetic based therapeutic strategies.

As discussed earlier in the chapter, there are various forms of genetic therapy approaches that can be used to treat genetic diseases. To date, the only published attempts to develop a genetic therapy for the treatment of *SYNGAP1* haploinsufficiency-associated disorder use antisense oligonucleotides (ASO). Two studies investigated the use of ASO to increase the production of SYNGAP1 protein from the wild-type allele by blocking alternative splicing events causing the production of non-coding *SYNGAP1* mRNA (Dawicki-mckenna *et al.*, 2022; Lim *et al.*, 2020). They showed that ASOs, targeting either the intronic region between exon 10 and exon 11 or the alternative 3' region of exon 11, can increase the relative amount of coding *SYNGAP1* mRNA *in vitro.* These approaches are useful in cases of dominant mutations such as *SYNGAP1* haploinsufficiency-associated disorder. It is, in fact, possible to exploit the wild-type allele, upregulating its expression without compromising isoform expression ratio and developmental expression levels. Although there are many advantages, including the relatively low cost of production and versatile design, unmodified ASO have low stability, and cell uptake results very low (Gagliardi *et al.*, 2021). Although chemical modifications and coupling with

delivery systems have allowed a better distribution and stability, a systemic administration is still a challenge (Dhuri *et al.*, 2020; Gagliardi *et al.*, 2021) indeed most ASO therapies targeted to the brain and the CNS use intracerebroventricular (ICV) or intrathecal delivery (Jagasia *et al.*, 2022; Lenk *et al.*, 2020; Milazzo *et al.*, 2021). Moreover, they require repeated administrations, which are challenging in the case of brain delivery, and off-target effects are possible(Crooke *et al.*, 2021; Dhuri *et al.*, 2020; Gagliardi *et al.*, 2021). All these limitations pose serious challenges in the application of ASO approaches for the treatment of the *SYNGAP1* haploinsufficiency-associated disorder.

To my knowledge, there are no reports describing toxicity or adverse phenotypes arising from the overexpression of *SYNGAP1*. Moreover, to my knowledge, there are no reports of duplication of the *SYNGAP1* locus. The monogenic nature of the disorder, its demonstrated partial reversibility in mice, and the apparent absence of over-expression related adverse phenotypes suggest that the delivery of a functional copy of the gene using a gene replacement approach could be a feasible option.

SYNGAP1 expression is mostly confined to the brain tissue, with little to no expression in other organs, and it is limited to neuronal cells (Berryer *et al.*, 2016; Chen *et al.*, 1998; Kim *et al.*, 1998; Moon *et al.*, 2008; Ozkan *et al.*, 2014). Given the limited accessibility of brain tissue, the most promising delivery vector would need to be able to spread widely in the brain and infect terminally differentiated cells. For this reason, AAV was believed to be the best candidate and AAV9 the best serotype, as it presents high tropism for the neuronal cells.

However, the limited knowledge of the potential differential contributions of different *SYNGAP1* isoforms to the pathophysiology of the disease poses serious challenges to the development of such therapy. Another challenge is the large size of the *SYNGAP1* coding sequence, which ranges from ~3300 bp to ~3900 bp, depending on the isoform. As AAV cloning capacity is approximately 5000 bp, including ITRs (Bulcha *et al.*, 2021; Dong *et al.*, 2010; Wu *et al.*, 2010), only ~ 600-1000 bp capacity remains available for the other essential genetic elements including the promoter and polyadenylation (polyA) signal.

As previously mentioned, the majority of pathogenetic mutations identified in SYNGAP1 patients are frameshift mutations, while missense mutations accounts for less than 30% (Berryer et al., 2013; Chevarin et al., 2020; Hamdan et al., 2009, 2011; Iossifov et al., 2012; Kimura et al., 2017; Lee et al., 2020; Mignot et al., 2016; Parker et al., 2015; Rauch et al., 2012; De Rubeis et al., 2014; Vissers et al., 2010; Vlaskamp, Shaw, Burgess, Mei, Montomoli, Xie, C. T. Myers, et al., 2019). It is known that missense mutations as well as frameshift mutations can, in addition to a full protein loss-of-function, lead to the acquisition of new unwanted functions or affect protein turnover (Dobson, 2003; Fukami et al., 2017, 2018; Teng et al., 2009; Thusberg et al., 2009; Zhang et al., 2010, 2012). The effects on protein function and stability of all the identified mutations has not been experimentally evaluated. However, *in vitro* studies conducted on a subset of missense mutations suggested that the pathological impact of this sequence modifications is associated with a partial or complete SYNGAP1 loss-of-function (Berryer et al., 2013; Lee et al., 2020; Zeng et al., 2019). Although it is possible that in some cases, the pathological effect is associated to a gain-of-function of the protein for which gene replacement would not be an effective treatment approach, it is reasonable to assume that it would be effective for a large number of patients.

Even though there are many challenges, the AAV-mediated gene replacement approach represents a valid approach that could be used to treat *SYNGAP1* haploinsufficiency-associated disorder. To date there are no reported attempts to develop a gene replacement therapy for *SYNGAP1*, therefore this project will represent the first proof-of-concept work on the feasibility of such approach.

1.7 HYPOTHESIS AND STUDY AIMS

SYNGAP1 haploinsufficiency-associated disorder, or MRD5, is a developmental disorder characterised by a wide set of clinical phenotypes that dramatically impact the quality of life of affected individuals. Currently, no disease-modifying or curative

therapy is available, and the only therapeutic approaches are symptomatic management treatments, which are often of limited effect (Weldon *et al.*, 2018). In contrast, gene therapy has the potential to treat the root cause of the disorder.

Based on the reversibility of the phenotype and the monogenic nature of the disease, I hypothesised that the restoration of SYNGAP1 levels via AAV-mediated gene replacement during early postnatal development will prevent the appearance or ameliorate the severity of behavioural phenotypes observed in the mouse model of *SYNGAP1* haploinsufficiency-associated disorder.

The aim of this project was to design and evaluate candidate gene therapy constructs to test this hypothesis. To this end, the specific aims of my programme of work were:

1. To establish a robust behavioural phenotypic baseline in mice modelling *SYNGAP1* haploinsufficiency and to develop clear endpoints for the evaluation of the therapeutic efficacy of candidate *SYNGAP1* gene therapy vectors.
2. To assess the ability of designed candidate therapeutic constructs to induce stable expression of SYNGAP1 in neuronal cells in brain areas of interest for the disorder.
3. To assess the therapeutic outcome derived from AAV9-derived SYNGAP1 expression in mice modelling *SYNGAP1* haploinsufficiency-associated disorder.
4. To evaluate tolerability associated to the viral vector treatment and to the exogenous expression of SYNGAP1 in wild-type mice.

CHAPTER 2: MATERIAL AND METHODS

2.1 ANIMALS

All procedures were performed in accordance with the regulations set by the University of Edinburgh and the UK Animals Act 1986.

Syngap1$^{+/-}$ and wild-type mice used for this study were derived from the colony of Professor Peter Kind (University of Edinburgh) and were originally created in the laboratory of Professor Seth Grant (Komiyama *et al.*, 2002), University of Edinburgh. Deletion of the *Syngap1* allele was generated by insertion of the targeting cassette HA-STOP-(IRES)-lacZ-polyA-MC1neo-polyA at the XhoI site present in exon 8, which resulted in the deletion of the genomic DNA spanning between exons 8 and 10, corresponding to the sequence encoding for the C2 and GAP domains. The resulting allele fails to express the SYNGAP1 protein (Komiyama *et al.*, 2002).

The colony was maintained on a C57BL/6JOlaHsd background using a breeding scheme consisting of crossing *Syngap1*$^{+/-}$ C57BL/6JOlaHsd male mice with wild-type *Syngap1*$^{+/+}$ C57BL/6JOlaHsd female mice. Animals were maintained on 12:12 hours light/dark cycles (lights on between 7 am and 7 pm) with access to food and water *ad libitum*.

To prevent animal stress and acclimatise the mice to the experimenter, study subjects were handled prior to the start of the behavioural tests using the following protocol. Handling of subjects that had not been handled before started one week prior the first behavioural experiment and continued for 7 consecutive days in sessions progressively longer, from 5 minutes to 20 minutes. For subsequent experiments, mice were handled for 10 minutes for 3 days prior the start of the first behavioural experiment.

2.2 BEHAVIOURAL TESTING

2.2.1 Open field

Hyperactivity and anxiety were evaluated using the open field test. The apparatus was composed of four custom-made square boxes of 50x50x50 cm, made of white opaque plastic and positioned over an infrared (IR) light-box (Noldus Technology, NL). Each arena was digitally subdivided in two zones: central, with a size of 75% of the total arena, and peripheral. A camera (cat. 104845-10, Basler, DE; objective 4-8mm, 1-14, Computar, JP) overhanging the arenas was used to record the behaviour and the videos were analysed using the EthovisionXT 12 software (Noldus Technology, NL). The experiments were conducted in a dark quiet room with only one source of dimmed light derived from the laptop screen maintained at the lowest brightness setting. At the beginning of each trial the animals were gently placed in the centre of the arena, then removed and returned to the home cage. Between each animal, arenas were cleaned with humid wipes.

The horizontal activity was calculated as distance travelled in the given time, and automatically calculated by the program. The percentage of time spent in the periphery was calculated as:

$$\%\ \text{Time in periphery} = \frac{Time\ in\ periphery\ (s)}{Total\ time\ in\ the\ arena\ (s)}\ x\ 100$$

For the behavioural baseline, animals were tested at 4, 7 and 11 weeks of age for 20 minutes. For therapeutic efficacy studies, animals were tested at 7 and 15 weeks of age for 1 hour.

2.2.2 Elevated plus maze

Spontaneous anxiety-like behaviour was assessed using the elevated plus maze test. The apparatus was composed of a maze made of white opaque plastic with IR light source incorporated (Noldus Technology, NL) and was elevated 75 cm above floor level. The maze consisted of four equally spaced arms, each 30 cm in length and 5 cm

wide, that radiated from a square centre of 5x5 cm. Two opposing arms were enclosed with white opaque walls that were 20 cm in height. The remaining arms were open, with a 5 mm high perimetral border. A camera (cat. 104845-10, Basler, DE; objective 4-8 mm, 1-14, Computar, JP) overhanging the arena was used to record the behaviour and the videos were analysed using the EthovisionXT 12 software (Noldus Technology, NL). The experiments were conducted in a dark quiet room with only one source of dimmed light derived from the laptop screen maintained at the lowest brightness setting. At the start of the test, animals were placed in the centre of the maze, facing one of the open arms. Each subject was then left free to explore the maze for 10 minutes, after which it was removed and returned to the home cage. Between each animal, the maze was cleaned with humid wipes.

The horizontal activity was described as the distance travelled in the given time and was automatically calculated by the program. The number of entries in the open arms was given by the sum of the total frequency in the open arm area, which was calculated by the program. The percentage of time spent in the open arms was calculated as:

$$\% \text{ Time in open arms} = \frac{Time\ in\ open\ arm\ 1\ (s) + Time\ in\ open\ arm\ 2\ (s)}{Total\ time\ in\ the\ maze\ (s)}\ x\ 100$$

For the behavioural baseline, animals were tested at 4, 7 and 11 weeks of age. For therapeutic efficacy studies, animals were tested at 7 and 15 weeks of age for 1 hour.

2.2.3 T-Maze

Working memory was evaluated using an alternation test performed as described in Berryer *et al.* (Berryer *et al.*, 2016) on the T-maze apparatus. The maze was composed of three arms placed in a T shape, departing from a central zone measuring 7.5x7.5 cm. The starting arm was 30 cm in length, 7.5 cm in width, and had a starting box of 7.5x10 cm that was divided from the rest of the maze by a guillotine gate. The two choice arms were placed perpendicular to the starting arm and facing each other.

They were 29.5 cm in length, 7.5 cm in width, and were divided from the centre of the maze by a guillotine gate (Figure 2-1).

Briefly, the test consisted of two free-choice trials repeated for three consecutive days. At the start of the test, the mouse was placed in the starting box, which was closed with the guillotine gate for 30 seconds. The guillotine was then removed, and the animal was allowed to freely explore the maze. The choice of arm was considered complete when the mouse passed the gate point with its entire body. Subsequently, the gate was closed, and the mouse was left in the arm for 10 seconds. At the end of the trial, the animal was returned to the home cage for 50 seconds before the trial was repeated. If the mouse chose the opposite arm in the second trial, it was considered an alternation. The experiments were conducted in a dark, quiet room with only one source of red light. Between each animal, the maze was cleaned with humid wipes.

For the behavioural baseline, animals were tested at 4, 7 and 11 weeks of age.

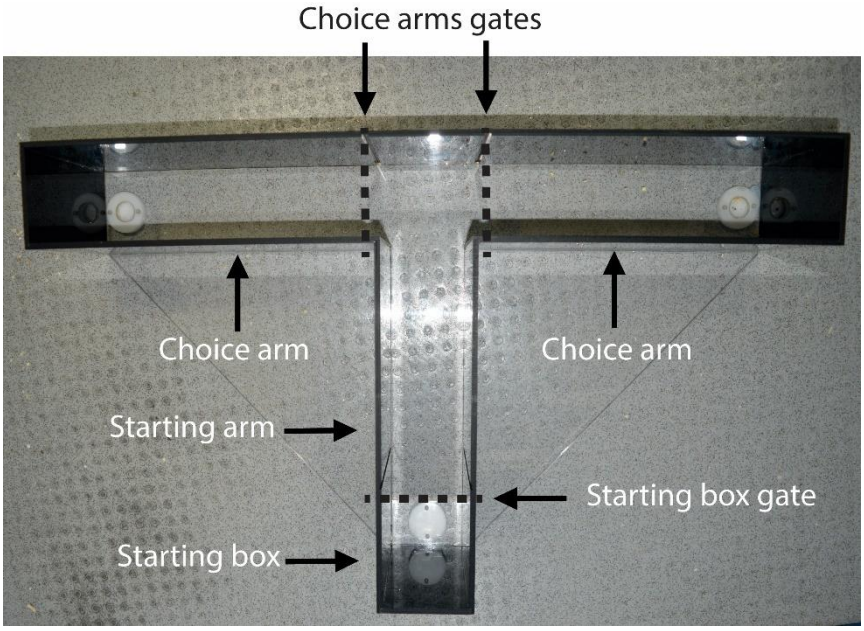

Figure 2-1. T-maze.
Dashed lines represent position of the guillotine gates.

2.2.4 Marble burying

The marble burying test was conducted using a modification of the protocol previously published by Deacon *et al.* (Deacon, 2006b). For this test, rat cages of the dimension of 42x26 cm were filled with 5 cm of wood-chip bedding, pressed, and levelled. Ten glass marbles (assorted colours, with an average diameter of 15 mm) were distributed and equally spaced on the surface (Figure 2-2). The mice were placed in the middle of the cage and were allowed to freely explore and interact with the marbles for 30 minutes. At the end of the period, the mice were removed, and the buried marbles were counted. A marble was counted as buried if covered by bedding for equal or more than two-thirds of its volume. Marbles that fell in the corners as a consequence of the digging activity were also counted as buried even if they were not covered by two-thirds of the volume with bedding material at the end of the 30 minutes. The experiments were conducted in a quiet room with the ceiling lights on. Between each animal, the bedding was changed, and the marbles were cleaned with humid wipes.

For the behavioural baseline, animals were tested at 4, 7 and 11 weeks of age.

Figure 2-2. Marble burying set up.
Ten glass marbles were arranged in two columns of five in a rat cage of 42x26 cm filled with 5 cm of wood-chip bedding material.

2.2.5 Nest building

The nest building test was conducted using a modification of the protocol previously published by Deacon (Deacon, 2006a) while the scoring system was adapted from Kraeuter *et al.* (Kraeuter *et al.*, 2019). For this test mice were individually caged overnight with no environmental enrichment except for 3 g of nesting material (Nestlets, Ancare, USA) and wood-chip bedding. The cages were set one hour before the dark phase and the nest was scored in the first two hours of the light phase.

Briefly, to the nest was assigned a one-to-five score based on the formation of a central portion and surrounding walls. A score of zero was assigned if ≥75% of the starting material remained untouched and not actively used for nest formation. To assess the quality of the nest, the height of each wall was measured, and the average of all quartiles was used for the score. An additional 0.25 was added for each quartile that fell in the subsequent category (Table 2-1).

For the behavioural baseline, animals were tested at 4, 7 and 11 weeks of age.

Table 2-1. Nesting scoring system

Sample image*	Average height**	Score	Increment
	≥75% in weight of Nestlets untouched 0 cm	0	-
	Nestlet shredded but scattered on the cage floor <1 cm	1	+0.25 if part of the material was used to build a wall
	Shredded material flattened against the cage floor ≥1 cm and <2 cm	2	+0.25 for each quartile ≥2 cm and <3 cm
	Walls present in each quartile ≥2 cm and <3 cm	3	+0.25 for each quartile ≥3 cm and <5
	Walls present in each quartile, doughnut-like shape ≥3 cm and <5 cm	4	+0.25 for each quartile ≥5 cm
	Walls present in each quartile, doughnut-like shape ≥5 cm	5	-

*Representative image of different classes of nest, **Average height of the nest's walls. The scoring system was adapted from Kraeuter *et al.* (Kraeuter *et al.*, 2019)

2.2.6 Visual cliff

The visual cliff test was originally developed by Gibson and Walk (Gibson *et al.*, 1960) at Cornell University. For this study, the apparatus was composed of an internal transparent box of 50x50x50 cm made of clear Lexan sheets that composed the inner arena, enclosed in an external L-shaped black opaque plastic box made of black opaque Lexan sheets (Figure 2-3a). The external box floor of dimensions 25x50 cm was in direct contact with the internal box, while the other 25x50 cm was placed at a height of 30 cm under the internal box, creating the virtual drop and dividing the arena into a shallow and deep side (Figure 2-3b). The L-shaped floor was covered by a photographic opaque chess print of 4x4 cm blue squares. Lights were placed under the floor to create homogeneous illumination of approximately 60 Lux.

For the test, mice were placed on the edge of the visual cliff, on the shallow side of the arena, and allowed to explore for 5 minutes. A camera (Logitech,USA) overhanging the arena was used to record each trial and the videos were analysed offline using the EthovisionXT 12 software (Noldus Technology, NL). Between each animal the inner box was cleaned with humid wipes.

The horizontal activity was described as the distance travelled in the given time and was automatically calculated by the program. The latency to first entry in the deep side of the arena was automatically calculated by the program and its quality was checked by the experimenter. The first entry into the deep side was considered to occur when the entire body of the mouse passed the edge of the cliff. The number of transitions was calculated as the sum of times the mouse crossed the cliff edge while moving across both sides of the arena.

The percentage of time spent in the deep side of the arena was calculated as:

$$\%\ \text{Time in deep} = \frac{Time\ in\ deep\ area\ (s)}{Total\ time\ in\ the\ arena\ (s)} \times 100$$

For the behavioural baseline, animals were tested at 7 and 15 weeks of age.

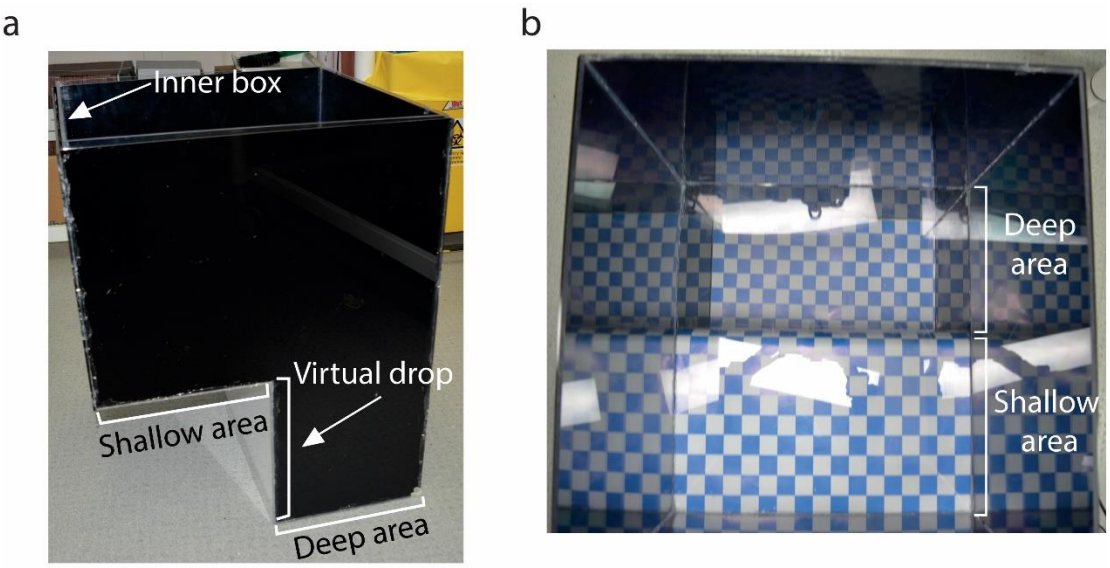

Figure 2-3. Visual cliff set up.
The L shape external box (a), composed of black opaque plastic, formed the visual cliff dividing the internal arena into a shallow and deep area (b).

2.2.7 Platform departure test

Platform departure test was used to evaluate the presence of risk-taking behaviour. The test, developed by Matsuoka *et al.* (Matsuoka *et al.*, 2005), was used to describe behaviour abnormalities in *Syngap1*$^{+/-}$ mice by Kilinc *et al.* (Kilinc *et al.*, 2018).

The apparatus was composed of a 2-liter glass beaker measuring 18 cm in height and 13 cm in width, as well as a camera (Canon Eos, JP) to record behaviour. The animals were placed on top of the upside-down beaker (Figure 2-4a) and allowed to explore for 10 minutes. If the animals jumped from the platform onto the table during this period, they were placed back on the beaker. It was considered a partial departure when both mouse forepaws were on the vertical wall of the beaker (Figure 2-4b) while a full departure was considered to occur when the mouse left the platform with its entire body (Figure 2-4c). Between animals the beaker was cleaned with humid wipes.

Recorded videos were manually scored offline to count the number of partial and full departures and as well as the latency to first departure.

For the behavioural baseline and therapeutic efficacy studies animals were tested at 7 and 15 weeks of age.

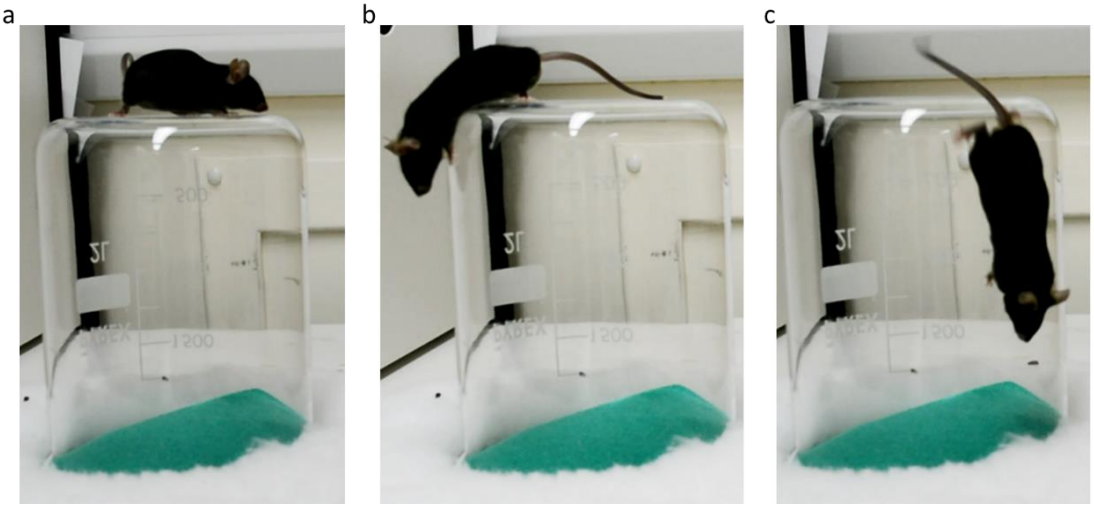

Figure 2-4. Platform departure test.
At the beginning of the test mice were placed on top of the beaker (a) and the number of partial (b) and full (c) departures were evaluated.

2.2.8 Motion Sequencing

Motion sequencing (MoSeq) is a technique developed in the laboratory of Professor Sandeep R. Datta (Harvard University) (Wiltschko *et al.*, 2015).

For this test, mice were placed in an arena measuring 40x40x25 cm made of 10 mm thick sheets of black matt acrylic plastic to prevent the formation of reflections. Each session was recorded for 10 minutes in complete darkness and using a 3D IR Microsoft Kinect depth camera (Microsoft Kinect 2, Microsoft, USA) positioned above the arena at a height of 74 cm. Between each animal, the arena was cleaned with a 10% sodium hypochlorite solution, 1% Alconox (Alconox, USA), and 70% ethanol in that order.

The Kinect camera was connected to a PC via USB 3.0, and video acquisition was carried out using a custom C++ graphical user interface, Kinect2-Nidaq, developed in the Datta laboratory, at 30 frames per second. Data were streamed in real-time to an external hard drive (5 T, Seagate, USA) for storage. The acquired videos were cropped from 512x424 pixels to a final resolution of 260x260 pixels to prevent depth

distortion outside the arena. A flip classifier was adapted for a cropping area relative to the area occupied by the mouse of 60 x 60 pixels. The videos were then analysed using the MoSeq code (v2) provided by the Datta laboratory, and the pipeline described in Wiltschko *et al.* (Wiltschko *et al.*, 2015, 2021). MoSeq, which is programmed in Python, was used to extract the position and morphometry of the mouse from the raw data orientation. Using principal component analysis, the extracted data were then dimensionally reduced. Subsequently, an Autoregressive Hierarchical Dirichlet Process Hidden Markov Model was fit on the processed data. This model, unattended, identifies syllables, unique and highly stereotyped movements of about 300 ms which, combined, are responsible for the animal's whole movement repertoire. Additionally, the algorithm generates a summary of various parameters such as speed, acceleration, position in the arena, height, syllable frequency of usage, etc. The frequency of usage of the top 51 syllables identified was used to investigate genotype differences between wild-type and *Syngap1*$^{+/-}$ mice.
The transitional relationship between syllables was investigated by calculating the transition probability. To do this, the probability of a transition of each module, or syllable, to any other module was calculated. Subsequently, the probability that two modules were occurring one after the other in the sequence was computed.

For therapeutic efficacy study mice were tested at 15 weeks of age.

2.2.9 Neonatal intracranial injections

For the experiments described in this thesis, only male mice were used. Male PND1/2 mice were treated by direct ICV injection, as described below.

The cage containing the litter to be injected and the mother was carefully transported to the appropriate room where a surgical area was previously set up. To ensure the sterility of the injection area, all the surfaces were cleaned with appropriate products, and sterile gloves were worn during the procedure.

Mouse pups were removed from the cage and sexed; female mice were returned to the home cage while male mice were placed on a heating pad covered with clean paper tissue and enclosed to prevent falls.

One at a time mice were moved from the enclosed portion of the heat pad to the injection area, scalp was rubbed with iodine solution and carefully dried using a sterile cotton stick. The viral vector or vehicle was delivered intracerebroventricularly using an ultra-fine gauge dental needle (30G, 21mm length, cat. 1108343, Sopira, Kulzer, DE) connected to a 50 or 100 μl Hamilton syringe (Hamilton, USA) via a fine tube. Injection sites were anterior to lambda, 1 mm from the middle line, and 3 mm in dept. Constant depth was maintained using a needle guard cut to leave 3 mm from the top of the needle. To minimize backflow, injections were carried out slowly (over a time of 30 seconds), and the needle was left in place for approximately 50 seconds after the end of the injection.

At the end of the procedure, mice were returned to the home cage. To prevent mother distress and minimize rejection, mice were rubbed in home cage bedding.

2.3 GENOTYPING

Genomic DNA was extracted from ear biopsies of adult mice or tail tips from neonates.

For standard genotyping DNA was extracted using DirectPCR (cat. 102-T, Viagen, USA). For each sample, 40 μl of DirectPCR + 0.4 μl protease K (0.4 μg/μl, cat. AM2546, ThermoFisher Scientific, USA) were added to a 0.2 ml thin-walled tube containing the tissue sample, and extraction was carried out using the condition listed in Table 2-2 in the C1000 Touch Thermal Cycler (BioRad, USA).

For one day genotyping, DNAreleasy (cat. LS02, Anachem, UK) was used. For each sample, 20 μl of DNAreleasy were added to a 0.2 ml thin-walled tube containing the tissue sample and extraction was carried out using the condition listed in Table 2-3 in the C1000 Touch Thermal Cycler (BioRad, USA).

Table 2-2. DirectPCR reaction conditions.

Temperature	Duration
55°C	4 hours
85°C	45 minutes
12°C	Infinite

Table 2-3. DNAreleasy reaction conditions.

Temperature	Duration
75°C	5 minutes
96°C	2 minutes
12°C	Infinite

Primers were designed to amplify the wild-type *Syngap1* allele and the knockout allele (Table 2-4). Two separate Polymerase Chain Reaction (PCR) reaction mix (Table 2-5) were set up in a 0.2 ml thin-walled tube and carried out following the cycling condition listed in Table 2-6 that were equal for both reactions. PCR reactions were performed using the C1000 Touch Thermal Cycler (BioRad, USA).

Table 2-4. Genotyping primers.

Primer*	Sequence 5'-3'	Fragment size
WT_F	CCCATATCCACCTTCCTCAGAGT	96 bp
WT_R	CCAAGGGCAGGGCAGG	
KO_F	CGATCGTAATCACCCGAGTGT	57 bp
KO_R	CCGTGGCCTGACTCATTCC	

*F indicates forward primer, R reverse primer. WT=wild-type; KO=knockout.

Table 2-5. Genotyping PCR reaction mix.

Component	Volume*
Dreamtaq Mastermix 2X (ThermoFisher Scientific)	13 μl
Forward Primer	1 μl (0.4 μM)
Reverse Primer	1 μl (0.4 μM)
H_2O	To 2 5μl

*Volumes refer per sample.

Table 2-6. Genotyping PCR reaction condition.

Step	Temperature	Time
Initial denaturation	95°C	4 minutes
	X 30 cycles	
Denaturation	95°C	30 seconds
Annealing	58°C	30 seconds
Extension	72°C	1 minute
Final extension	72°C	10 minutes
Hold	12°C	Infinite

Presence/absence of PCR product was then evaluated via agarose gel electrophoresis. Wild-type and knockout reactions were run along with a molecular weight marker (Low molecular weight ladder, cat. N3233S, New England Biolab, USA) on a 3% agarose gel (3 g of agarose cat. 50004, SeaKem LE agarose, Lonza, CH) in 1x Tris/Borate/EDTA buffer (0.089 M EDTA, 0.089 M Tris base, 0.089 M $B(OH)_3$).

2.4 PLASMID AMPLIFICATION

2.4.1 Bacterial transformation

E. coli Subcloning Efficiency DH5α competent cells (cat. 18265017, ThermoFisher Scientific, USA) were used for the amplification of mammalian expression plasmid.
50 μl of DH5α cells were thawed on ice, and after complete defrosting, they were mixed with an appropriate volume of plasmid containing 10 ng of DNA by gentle pipetting. The mixture was then incubated on ice for 30 minutes and subsequently exposed to heat shock using a water bath, pre-warmed at 42°C, for 20 seconds. After a 2-minutes incubation on ice, 950 μl of pre-warmed Super Optimal broth with Catabolite repression (SOC) medium (cat. 15544034, ThermoFisher Scientific, USA) was added to the vial, and the tubes were incubated for an hour at 37°C at 225 rpm.

C3040H stable competent cells (cat. C3040H, New England Biolab, USA) were used for the amplification of AAV expression plasmids containing ITRs.

50 μl of cells were thawed on ice for 10 minutes, 10 ng of plasmid were added to the defrosted cell suspension, and the mixture gently mixed by flicking. The mixture was then incubated for 30 minutes on ice. After incubation, heat shock was carried out in a water bath for 30 seconds at 42°C, and then the mixture was incubated on ice for 5 minutes. 950 μl of room temperature NEB 10-beta/Stable Outgrowth Medium (cat. B9035S, New England Biolab, USA) was added, and tubes were incubated for an hour at 30°C at 250 rpm.

Regardless of the type of cells used, 200 μl of transformation mixture was spread on pre-warmed at 37°C Luria-Bertani (LB) agar plates containing appropriate antibiotics (kanamycin 0.05 mg/ml or ampicillin 0.1 mg/ml) and incubated overnight at 37°C.

2.4.2 Mini amplification of plasmid

Single colonies were picked from each plate and cultured in 3 ml of LB medium containing the appropriate antibiotics (kanamycin 0.05 mg/ml or ampicillin 0.1 mg/ml) in a loosely capped 15 ml Falcon tube. Incubation was carried out overnight at 250 rpm at 37°C, for mammalian expression plasmids, or 30°C, for AAV expression plasmids containing ITRs. The following day, cultures were removed from the incubator and 1.5 ml of culture was transferred to a clean 1.5 ml tube and centrifuged at >10000xg for 30 seconds. After discarding the supernatant, the remaining 1.5 ml of culture was added to the same 1.5 ml tube and centrifuged at >10000xg for 30 seconds. Plasmid DNA was purified using the PureYield Plasmid Miniprep System (cat. A1223, Promega, UK) as per manufacturer instructions.

2.4.3 Maxi amplification of plasmid

Single colonies were picked from each plate, inoculated in 3 ml of LB medium, with appropriate antibiotics (kanamycin 0.05 mg/ml or ampicillin 0.1 mg/ml), and cultured in a loosely capped 15 ml Falcon tube at 37°C for 1 hour at 250 rpm to prepare a starter culture. This was then added to 100 ml LB medium, supplemented with

appropriate antibiotics (kanamycin 0.05 mg/ml or ampicillin 0.1 mg/ml), in a 250 ml glass flask and cultured overnight at 250 rpm at 37°C, for mammalian expression plasmids, or 30°C, for AAV expression plasmids containing ITRs. The following day, cultures were removed from the incubator, divided in two 50 ml Falcon tubes, and centrifuged at 3000xg for 30 minutes at 4°C. Plasmid DNA was purified using the Maxi Prep kit (cat. 12963, QIAGEN, DE) following manufacturer instructions.

2.5 DNA AND RNA CONCENTRATION DETERMINATION

Plasmid concentration and quality were assessed using the Nanodrop 1000 (ThermoFisher Scientific, USA) which measures the UV absorbance of the DNA and RNA solution between 200 and 300 nm. The optical density ratio at a wavelength of 260 nm and 280 nm was used to measure the quality of the samples, and values in the range of 1.8-2.0 were considered indicators of acceptable purity. For DNA and RNA quantification, 1 μl of the solution was used.

2.6 PLASMID ENZYMATIC DIGESTION

Plasmids were digested using restriction enzymes to generate the DNA fragments required for subsequent cloning or to validate/verify the plasmid sequence. Single or double digestions were carried out when required. Reaction mixtures were prepared as described in Table 2-7 in 0.2 ml thin-walled tubes and incubated for one hour at 37°C in the C1000 Touch Thermal Cycler (BioRad, USA). Depending on the combination of restriction enzymes, the reaction buffer changed based on manufacturer instructions.

Table 2-7. Enzymatic digestion reaction mixture.

Component	Volume*
DNA	X μl (1μg)**
Buffer	1 μl
Enzyme 1 (New England Biolab)	1 μl
Enzyme 2 (New England Biolab)	1 μl
H_2O	To 50 μl

*Volumes refer per sample.
**X=Sample volumes. Volumes vary depending on samples concentration.

2.7 CLONING

Cloning was performed using the In-Fusion HD cloning kit (cat. 638909, Takara Bio, USA) following the manufacturer's instructions for spin-column purified PCR fragments. Plasmid backbone was obtained via restriction enzyme digestion as described in Section 2.6 followed by fragment purification using the DNA clean and concentrator kit (cat. D4005, Zymo Research, USA). Insert fragment, in the form of gBlock, was synthesised by Integrated DNA Technologies, USA. Ligation reaction mix, reported in Table 2-8, was prepared in 0.2 ml thin-walled tubes and subsequently incubated for 15 minutes at 50°C in the C1000 Touch Thermal Cycler (BioRad, USA). 2.5 μl of ligation reaction was used to transform C3040H stable competent cells (cat. C3040H, New England Biolab, USA) as described in Section 2.4.1.

Table 2-8. In-Fusion ligation reaction mixture.

Component	Volume*
DNA insert	X μl (50 ng)**
Linearised vector	X μl (50 ng)**
5x In-Fusion HD Enzyme Premix	2 μl
H_2O	To 10 μl

*Volumes refer per sample.
** X=Sample volumes. Volumes vary depending on samples concentration.

2.8 AAV9 VECTOR PRODUCTION

AAV9/JeT-*hSYNGAP1_Myc*-SpA (Chapter 5) was produced using the triple transfection of HEK-293 cells method, quality controlled, and titrated by the Barcelona vector core (Spain). Purification was performed via iodixanol-based ultracentrifugation, and titre was determined via picogreen assay. The titre of the stock solution received from the producer was of 5E13 vg/ml.

AAV9/hSYN1-*hSYNGAP1_Myc*-SV40 (Chapter 6) was produced by the ViroVek vector core (USA) using the Baculovirus system in insect Sf9 cells by infection with rBV-inCap9-inRep-kozak-hr2 and rBV- hSYN1-*hSYNGAP1_Myc*-SV40 plasmids. Viral vector preparation quality control and titration were also performed by the producer. Purification was performed via two rounds of Caesium Chloride ultracentrifugation, the Caesium Chloride was then removed via buffer exchange with two PD-10 desalting columns. The final AAVs were buffer exchanged to PBS + 0.001 % Pluronic F68. The vial vector titre was determined via quantitative real time PCR (qPCR). The titre of the stock solution received from the producer was 2.17E13 vg/ml.

2.9 PLASMID AND VIRAL VECTORS PREPARATION QUALITY CONTROL

2.9.1 Viral DNA extraction

Viral vectors preparation were subjected to in-house quality controls such as sequencing via MiSeq and evaluation of vector genome intactness via alkaline gel electrophoresis. For these experiments, viral DNA genome was first extracted and then processed depending on the protocol to follow.

Viral vector DNA extraction was conducted by Ms Amanda Morris. For sequencing, 2E12 viral genome (vg) were used, while for the alkaline gel experiment, 5E10 vg were used. A 100 µl reaction was set up in 0.2 ml thin-walled tubes as described in Table 2-9 and subsequently incubated at 37°C for 30 minutes. 50 µl of the DNAase treated

sample were then incubated firstly at 55°C for 1 hour and then at 95°C for 10 minutes to carry out proteinase K treatment (reaction mixture reported in Table 2-10).

Table 2-9. DNase treatment reaction mixture.

Component	Volume*
10X DNase Buffer (Roche)	10 μl
1% Pluronic-F 68 (ThermoFisher Scientific)	5 μl
DNase I (Roche)	4 μl
Viral Vector	X μl**
H_2O	To 100 μl

*Volumes refer per sample.
**Minimum volume 10 μl, volumes vary depending on samples concentration.

Table 2-10. Proteinase K treatment reaction mixture.

Component	Volume*
10x Proteinase K Buffer (10mM Tris, 10mM EDTA, 1% SDS)	10 μl
Proteinase K (Invitrogen)	2.5 μl
DNase treated Sample	50 μl
H_2O	To 100 μl

*Volumes refer per sample.

The resulting DNA was then purified using the DNA clean and concentrator kit (Zymo Research, USA) following manufacturer instructions, and eluted in 15 μl of nuclease free water.

For MiSeq sequencing, ssDNA was first incubated at 95°C for 5 minutes and converted in dsDNA using the Klenow polymerase (New England Biolab, USA). The reaction was prepared as described in Table 2-11 and incubated at 37°C for 1 hour. DNA was then purified using the DNA clean and concentrator kit (cat. D4005, Zymo Research, USA) following manufacturer instructions, and eluted in 15 μl of nuclease free water.

Table 2-11. Klenow Polymerase reaction mix.

Component	Volume*
ssDNA	14 μl
dNTPs	2 μl
Random hexamers (Integrated DNA Technologies)	1.2 μl
NEB Buffer2 (New England Biolab)	2 μl
Klenow polymerase (New England Biolab)	1 μl

*Volumes refer per sample.

2.9.2 Viral vector and whole plasmid DNA sequencing

Sequencing was performed by Ms Amanda Morris using MiSeq technology (Illumina, USA). Prior to sequencing, viral vectors DNA was first extracted, purified, and then converted in dsDNA as described in Section 2.9.1. The dsDNA was then used to prepare barcoded libraries using Illumina DNA PCR-Free Library Prep (cat. 20041794), Illumina DNA/RNA UD Indexes Set (cat. 20027213) and Illumina DNA PCR-Free Primer Kit R1 Sequencing (cat. 20041796) (Illumina, USA) following manufacturer instructions.

Prior to sequencing, libraries were first diluted to 4 nM, then NaOH (final concentration 0.001 mM) was added, and samples were incubated at room temperature for 5 minutes. 990 μl of pre-chilled buffer HT1 (cat. 20015892, Illumina, USA) was added, and then a PhiX was added. Sequencing was carried out on MiSeq machine (Illumina, USA) using the MiSeq Reagent kit Box1 and 2 (cat. MS-102-2002, Illumina, USA) following manufacturer instructions.
For whole plasmid sequencing, an input of 300 ng was used, and samples were directly used for library preparation without prior treatment.

Sequence analysis was carried out by Dr Paul Ross using the scripts reported in Appendix A.

2.9.3 Alkaline gel

Alkaline gel electrophoresis was performed by Ms Amanda Morris. For Alkaline gel electrophoresis, 250 ng of viral ssDNA, extracted as described in Section 2.9.1, was used.

To 10 µl of DNA solution, 10 µl of DNase solution (0.01 M Tris pH 7.5, 0.01 M CaCl2, 0.01 M MgCl2, 100 µg DNase in H2O) was added, which was then vortexed to mix and incubated at 37°C for 1 hour. Subsequently, 5 µl of 0.5 M EDTA, 2 µl of 10% SDS and 7 µl of 5x loading dye (0.4 M NaOH, 0.025 M EDTA, 0.09 g Ficol PM 400, few crystals of Xylene Cyanol in H_2O) were added and the solution was incubated at room temperature for 10 minutes. Prior to the electrophoretic run, the 1% alkaline gel (1% agarose (cat. 50004, SeaKem LE agarose, Lonza, CH), 0.25 M NaOH, 0.5m M EDTA in H_2O) was equilibrated in 1x running buffer (0.05 M NaOH, 0.001 M EDTA in H_2O) at 4°C for 10 minutes. The gel was then loaded with 20 µl of samples together with 10 µl of the molecular weight marker 1 kb DNA Ladder (cat. B7025, New England Biolab, USA) and run at 12 V for 24 hours at 4°C.

After the completion of the electrophoretic run, the gel was rinsed in double distilled water and neutralised with two washes of the neutralization buffer (0.5 M Tris-Cl pH 7.5, 1 M NaCl in H_2O) at room temperature for 20 minutes under gentle rocking. Subsequently, the gel was washed two times for 10 minutes in 1x Tris-Acetate-EDTA (TAE) buffer (40 Mm Tris (pH 7.6) 20 mM acetic acid, 1mM EDTA) and then stained with 1x SYBR gold (cat. S11494, ThermoFisher Scientific, USA) in 1x TAE buffer at room temperature for 1 hour with gentle rocking. After two washes with double distilled water, the gel was imaged using the Gel Imager (BioRad, USA).

2.10 CELL CULTURE

2.10.1 Revival of HEK293A cells stored in liquid nitrogen

HEK293A cells were stored in liquid nitrogen in dimethyl sulfoxide (DMSO) at a cell count of 2E6 and revived when necessary.

Cells were thawed quickly in a pre-warmed water bath at 37°C until completely defrosted. Thawed cells were then diluted in 9 ml of pre-warmed Dulbecco's modified eagle medium (DMEM, cat. 41965-039, ThermoFisher Scientific, USA) supplemented with 10% foetal bovine serum heat inactivated (cat. 26140, ThermoFisher Scientific, USA), 2mM L-Glutamine (cat. 25030081, ThermoFisher Scientific, USA), 100 U/ml of penicillin and 100 μg/ml of streptomycin (cat. 15140148, ThermoFisher Scientific, USA) and 1x minimum essential media non-essential amino acids (cat. 11140050, ThermoFisher Scientific, USA) and centrifuged at 150xg for 5 minutes. The cell pellet was subsequently resuspended in 1 ml of pre-warmed cell media, and the resuspension was added to 25 ml of pre-warmed cell media. Cells were cultured at 37°C in a humidified atmosphere conditioned with 5% CO_2 in 175 cm^2 TC treated flasks (cat. 660175, Greiner Bio-One, UK).

2.10.2 HEK293A cell sub-culturing

HEK293A cells passage was performed to prevent overgrowth and therefore cell death. Each cell culture was visually inspected, and subculturing was performed when a confluence of about 80% was reached.

Firstly, culture media was removed using a vacuum pump and the culture was washed with 10 ml of 1x Phosphate Buffered Saline (PBS) (cat. 14190144, Gibco, ThermoFisher Scientific, USA), pre-warmed at 37°C. After removal of the PBS, 3 ml of TrypLE Express enzyme (cat. 12604013, ThermoFisher Scientific, USA) was added, and the flask was incubated at 37°C for 3 minutes. Subsequently, the flask was gently shaken to facilitate cells detachment, 7 ml of fresh supplemented DMEM media was added and the resulting suspension transferred to a 15 ml falcon tube. 20 μl of resuspended cell culture was added to 20 μl of Trypan Blue (cat. 15250061, Thermofisher Scientific, USA) and cells were counted using the Countess II (Invitrogen, USA) apparatus. The appropriate volume containing 2E6 cells was then added to a flask containing 25 ml of pre-warmed DMEM media and returned to the incubator at 37°C in a humidified atmosphere conditioned with 5% CO_2.

For the work described in this thesis, cells at passages 15-25 of *in vitro* culture were used.

For the fluorescence immunocytochemistry experiment, after cell counting, HEK293A cells were seeded in 24 well-plates containing Poly-L-Ornithine/Fibronectin (PLO-FN) coated coverslip (13 mm). For the coating, sterile coverslips were added to the 24 well-plate, 1 ml of PLO-FN was added to each well and left in incubation overnight at 37°C. The coating mixture was removed by aspiration and the plate was left to dry. Subsequently, 5E4 cells were seeded per well.

For the immunoblotting experiment, 5E5 cells per well were seeded in 6 well-plate without coverslip.

2.10.3 HEK293A cells transfection

After 24h from seeding, at 70-90% of confluence, HEK293A cells were transfected using Lipofectamine 2000 (cat. 11668019, ThermoFisher Scientific, USA). In Table 2-12 are reported reagents volumes. The reaction was optimised for the transfection of 2.5 μg of DNA for a 6 well-plate and 1 μg for a 24 well-plate of a plasmid of 3500 bp. To transfect equimolar amount of each plasmid in study, volumes of plasmid DNA to use were calculated as follows:

$$\mu l \text{ of plasmid} = \frac{plasmid\ size\ (kb) \times N(\mu g)/\ 3.5\ kb}{plasmid\ concentration\ (\mu g/(\mu l))}$$

Where N indicates the μg of 3500 bp plasmid to use for transfection of cells seeded in a 6 well or 24 well-plate.

Briefly, reaction mix, reported in Table 2-12 was prepared as per manufacturer instructions. The appropriate amount of mixture was added to each well, the plate was gently tapped to mix the solution with the medium and then incubated for 48 hours at 37°C.

Table 2-12. Component for cell transfection.

Component	6 well-plate*	24 well-plate*
Lipofectamine 2000 (ThermoFisher Scientific)	9 μl	2 μl
DNA	X μl**	X μl**
Opti-MEM	To 250 μl	To 50 μl

*Volumes refer per well.

** X=Sample volumes. Volumes vary depending on samples concentration.

2.10.4 Fluorescence immunocytochemistry

48 hours after transfection, cells were removed from the incubator and processed for fluorescence immunocytochemistry.

Culture media was removed, and cells were washed two times with 1x PBS (Gibco, ThermoFisher Scientific, USA) and fixed for 10 minutes with 4% paraformaldehyde (PFA, cat. 158127, Sigma, USA) at room temperature. Subsequently, 1 ml of permeabilization solution (0.1% Triton-X (cat. X100, Sigma, USA) in 1x PBS) was applied for 5 minutes at room temperature. Then cells were washed two times with 1x PBS (Gibco, ThermoFisher Scientific, USA) and blocking solution ((1 ml of 0.05% Triton-X (Sigma, USA) + 10% goat serum (cat. G9023, Sigma, USA) in 1x PBS (Gibco, ThermoFisher Scientific, USA)) was applied for 1 hour under gentle rocking at room temperature. Cells were then incubated overnight at 4°C on a shaker with the appropriated primary antibodies (Table 2-13) diluted in 0.05% Triton-X (Sigma, USA) + 1% BSA (Bovine serum albumin, cat. BP9700-100, ThermoFisher Scientific, USA) in 1x PBS (Gibco, ThermoFisher Scientific, USA)**.** The following day, primary antibody solution was removed, samples were washed three times with 1x PBS for 10 minutes and then incubated with the appropriate secondary antibodies diluted in 0.05% Triton-X (Sigma, USA) + 1% BSA (Fisher Scientific) in 1x PBS (Gibco, ThermoFisher Scientific, USA) (Table 2-14) for 1 hour under gentle rocking. Subsequently, coverslips were washed three times with 1x PBS (Gibco, ThermoFisher Scientific, USA) for 10 minutes and mounted on glass slides using the VECTASHIELD® HardSet™ Antifade Mounting Medium with DAPI (cat. H-1500-10, Vector Lab, USA).

Images were captured at the Leica DM5500B fluorescent microscope (Leica Bioscience, DE) using the 20x (∞/0.17/D, HCX PL FLUOROTAR, 20x/0.50) and 40x objective (∞/0.17/D, HCX PL FLUOROTAR, 40x/0.75). Microscope acquisition settings were calibrated on the mock-transfected cells and length of exposure, light source power and gain were selected to eliminate the background noise. Settings were then maintained constant across treatments.

Table 2-13. Immunofluorescence primary antibodies.

Antibody	Dilution	Origin	Reference
Anti-Myc	1:500	Rat	Abcam, 9E10
Anti-SYNGAP1	1:1000	Rabbit	ThermoFisher Scientific, PA1-046
Anti-FLAG	1:500	Mouse	Millipore, F1804

Table 2-14. Immunofluorescence secondary antibodies.

Antibody	Dilution	Fluorochrome	Reference
Anti-Rabbit	1:1000	647	Cell Signalling Technology, 4414
Anti-Rat	1:1000	488	Cell Signalling Technology, 4416
Anti-Mouse	1:1000	488	Abcam, 150113

2.10.4.1 Image analysis

The percentage of positive cells was calculated as a ratio between the number of Myc-positive cells and DAPI-stained nuclei. Cells were counted using the Cell Counter plugin (Identifier legacy:Cell_Counter) of ImageJ, Fiji (https://imagej.nih.gov/ij/).

2.11 WESTERN BLOTTING

2.11.1 Sample preparation

2.11.1.1 Cultured cells

HEK293A were transfected as previously described in Section 2.10.3. 48 hours post-transfection cells were processed for immunoblotting. Culture media was removed, cells were washed two times with 1x PBS (Gibco, ThermoFisher Scientific, USA) and

then lysed by scraping in 200 ml of RIPA buffer (10 mM Tris-Cl (pH 8.0) (cat. AM9855G ThermoFisher Scientific, USA), 140 mM NaCl (Sigma, USA), 1 mM EDTA (15575-038, ThermoFisher Scientific, USA), 1% Triton X-100 (Sigma, USA), 0.1% sodium deoxycholate (Sigma, USA), 0.1% Sodium Dodecyl Sulphate (SDS) (cat. 1610416, BioRad, USA), 1x protease inhibitors (cat. A32953, ThermoFisher Scientific, USA)). The lysate was then sonicated for 30 seconds using the Branson Ultrasonic 2800 cleaner and boiled in 1x Laemmli buffer (2% SDS (Sigma, USA), 2.5% β-mercaptoethanol (Sigma, USA), 10% glycerol (Sigma, USA), 0.002% bromophenol blue (Sigma, USA), 0.06M Tris-HCl (Sigma, USA)) for 10 minutes at 95°C. For long-term storage, samples were kept at -80°C.

2.11.1.2 Tissue

Animals were sacrificed by cervical dislocation, the brain was removed and regions of interest were dissected, collected in 1.5 ml tubes or prefilled 2 ml bead mill tubes (ThermoFisher Scientific, USA) and flash frozen in dry ice. If not processed immediately, samples were kept at -80°C. Tissue samples were homogenised for 20 seconds using the Bead Mill 24 (cat. 15-340-153, Fisherbrand, ThermoFisher Scientific, USA) in 500 ml of RIPA buffer. The homogenate was then sonicated for 30 seconds using the Branson Ultrasonic 2800 cleaner and protein concentration was quantified using the DC Protein Assay kit (cat. 5000112, BioRad, USA) as will be described in Section 2.11.2. Subsequently, the samples were boiled in 1x Laemmli buffer for 10 minutes at 95°C.

2.11.1.3 Synaptosomal preparation

Synaptosomal preparation was obtained from the hippocampus of left hemispheres, the protocol used was adapted from the method described by Bermejo *et al.* (Bermejo *et al.*, 2014) (Figure S-3).

Briefly, mice were sacrificed by cervical dislocation, the brain was removed, dissected and the hippocampus was homogenised using 2 ml KIMBLE dounce glass tissue grinder (Sigma, USA) with 20 strokes over 30 seconds in 1.6 ml of homogenisation

buffer (4 mM HEPES (cat. 15630080, Gibco, ThermoFisher Scientific, USA), 0.32 M sucrose (Sigma, USA), 1x protease inhibitor (ThermoFisher Scientific, USA)). 100 μl of homogenate was reserved to constitute the input fraction. The remaining homogenate was collected in a 2 ml tube and centrifuged at 900xg for 10 minutes at 4°C. The supernatant (S1) was transferred to a new 2 ml tube, the pellet resuspended in 1 ml of homogenisation buffer and then centrifuged at 900xg for 10 minutes at 4°C. The supernatant (S1') was transferred to a new 1 ml tube while the pellet, resuspended in 300 μl of homogenisation buffer, constituted the nuclear fraction P1. S1 and S1' were centrifuged at 10000xg for 15 minutes at 4°C, 500 μl of the S1 supernatant were transferred to a new 1 ml tube and constituted the cytoplasmic fraction (S2) while S1' supernatant was discarded. S1 and S1' pellets were merged, resuspended in 1 ml of homogenisation buffer, and centrifuged at 10000xg for 15 minutes at 4°C. The supernatant was discarded, and the pellet, resuspended in 200 μl of homogenisation buffer, constituted the synaptosomal fraction (P2). To each fraction was added 1/9 volume of 10% Triton-X (Sigma, USA), sonicated for 30 seconds, and quantified using DC Protein Assay kit (BioRad, USA) following the protocol described in Section 2.11.2. Samples were then boiled in 1x Laemmli buffer for 10 minutes at 95°C and stored long-term at -80°C.

2.11.2 Protein quantification

After sonication, 10 μl of sample were transferred to a new tube. The colorimetric assay used for the protein quantification has a saturation concentration of 2 mg/ml of protein. It is therefore important to dilute the samples to reach a final concentration which lay in between the lowest detectable concentration (0.125 mg/ml) and the saturation concentration (2 mg/ml). Tissue homogenates were diluted 1:5 while for subcellular fractions, input and synaptosomal fractions were diluted 1:2, nuclear fraction was diluted 1:5 and cytosolic fraction was quantified undiluted. Samples were diluted using the same buffer used for the homogenisation. Protein quantification was carried out using DC Protein Assay kit (BioRad, USA). Briefly, 5 μl of sample, 10-fold serial dilution at a known concentration of BSA

standards (2 mg/ml, 1 mg/ml, 0.5 mg/ml, 0.25 mg/ml, 0.125 mg/ml, cat. 5000007, BioRad, USA) and a blank were distributed in triplicates in an untreated 96 well-plate (cat. 260836, ThermoFisher Scientific, USA). 25 µl of Buffer A' (25 µl of Buffer S per 1000 µl of Buffer A) was added to each well, followed by 200 µl of Buffer B. Plates were incubated at room temperature for 15 minutes with gentle rocking, then read at the CLARIOstart (BMG Labtech, DE).

Quantification was carried out using Excel (Microsoft, USA). Firstly, the percent coefficient of variance was calculated over the absorbance values of the triplicate of each sample using the formula =STDEV(absorbance)/AVERAGE(absorbance). If it resulted above 1% and a clear outlier was identifiable this was removed, and the average was calculated over the remaining two replicates. If it was not possible to identify the outlier the average was calculated over the three replicates. If <1%, the average was calculated over the three replicates. The average absorbance of the standards was then used to construct a standard curve. *m* and *q* of the tendency line (y = *m*x+*q*) to the standard curve were extrapolated using Excel (Microsoft, USA) and protein concentration was calculated with the formula:

$$\text{Protein concentration (µg/µl)} = \frac{Mean\ Absorbance - m}{q}$$

If samples quantified were diluted, the calculated protein concentration was multiplied by the dilution factor.

2.11.3 Protein electrophoresis and immunoblotting

1.5 mm thick SDS-PAGE hand cast mini gels were prepared and run using the Mini-Protean Tetra system (BioRad, USA). Depending on the size of the protein of interest, resolving gels at 8%, 10% or 12% of acrylamide (40% acrylamide/bis solution, 37 5:1, BioRad, USA) concentration were prepared while a 4% acrylamide stacking gel was always used.

Equal quantities of protein were loaded onto the gel alongside a protein molecular weight marker (Precision Plus Protein Dual Color Standard, cat. 1610374, BioRad, USA). Protein electrophoresis was carried out in 1x running buffer (25 mM Tris, 192 mM glycine, 0.1% SDS, pH 8.3, cat. 1610732, BioRad, USA) at 100V for 2 hours.
Proteins were transferred to 0.45 μm nitrocellulose membranes (BioRad, USA) by wet electroblotting in 1x transfer buffer (25 mM Tris, 192 mM glycine, 20% methanol, pH 8.3, cat. 1610734, BioRad, USA) at 85 V for 2 hours or at 35 V overnight.

At the end of the transfer, membranes were firstly washed four times in double distilled water and subsequently stained for total protein using the Revert 700 Total Protein Staining kit (cat. 926-11016, Li-Cor, USA) as per manufacturer instruction. Membranes were then imaged at the Odyssey (Li-Cor, USA) scanner at 1.5 of intensity. Subsequently, membranes were de-stained using the de-staining solution and washed twice with 1x Tris Buffered Saline (TBS) (cat. 1706435, BioRad, USA) + 0.1% Tween-20 (cat. 1706531, BioRad, USA) before applying the blocking solution for 1 hour with gentle rocking. Blocking solutions used for each antibody are reported in Table 2-15**.** Primary antibodies, diluted as described in Table 2-15**,** were incubated overnight at 4°C with gentle rocking. The following day, membranes were washed three times for 10 minutes with 1x TBS (BioRad, USA)+ 0.1% Tween-20 (BioRad, USA) and then incubated with the secondary antibody (Table 2-16) diluted 1:10000 in the appropriate blocking solution for 1 hour at room temperature with rocking. The blocking solution used for the dilution of the secondary antibody matched the one used for the primary antibody.
It was observed that the use of the Intercept Li-Cor TBS blocking solution (cat. 927-60001, Li-Cor, USA) or 5% milk blocking (BioRad, USA) produced the same quality of staining.
Membranes were then washed three times for 10 minutes with rocking followed by several washes in 1x TBS (BioRad, USA) and scanned at the Odyssey (Li-Cor, USA) scanner at appropriate scanning intensity.
If necessary, membranes were stripped and re-probed. For this procedure, membranes were washed in double distilled water, incubated for 10 minutes with 1x

stripping solution (Millipore, DE) and then washed several times in double distilled water and one time in 1x TBS (BioRad, USA) + 0.1% Tween-20 (BioRad, USA) before applying the blocking solution.

Table 2-15. Immunoblotting primary antibodies.

Antibody	Origin	Dilution	Blocking	Reference
Anti-SYNGAP1	Rabbit	1:2000	5% Milk or Li-Cor TBS Blocking	ThermoFisher Scientific, PA1046
Anti-PSD95	Mouse	1:2000	Li-Cor TBS Blocking	ThermoFisher Scientific, MA1045
Anti-FLAG	Mouse	1:1500	Li-Cor TBS Blocking	Millipore, F1804
Anti-Myc	Rabbit	1:750	5% Milk or Li-Cor TBS Blocking	Abcam, 9106
Anti-Histone3	Rabbit	1:10000	Li-Cor TBS Blocking	Abcam, 97968
Anti-GAPDH	Mouse	1:5000	Li-Cor TBS Blocking	Abcam, 9484

Table 2-16. Immunoblotting secondary antibodies.

Species reactivity	Conjugated fluorophore	Reference
Anti-Mouse	680	Li-Cor, 926-32212
Anti-Mouse	800	Li-Cor, 926-68062
Anti-Rabbit	680	Li-Cor, 926-32213
Anti-Rabbit	800	Li-Cor, 926-68073

2.11.4 Analysis

Immunoblots images were analysed using the Image Studio software (v5.2, Li-Cor). Total protein staining was used as loading control and for normalisation of the band signal. The background signal was averaged using the top/bottom option.

For the total protein staining, a rectangular shape was drawn vertically across the entire length of each lane, sufficiently long to include part of the background on both the upper and lower end of each lane.

For the bands relative to the proteins of interest, a box was drawn around the band, sufficiently large to include part of the background.

Quantification was carried out using Excel (Microsoft, USA). The signal from the protein of interest was first divided by the total protein signal of the respective lane. Each sample normalised signal was subsequently normalised over the average normalised signal of each gel. The gel normalised signal of each sample was then normalised to the average of control sample values to obtain fold-change values of the relative intensity. In Chapters 5 and 6 SYNGAP1 signal was normalised to the average signal of the vehicle control while the signal derived from the fusion peptides (Myc or FLAG) was normalised to the average signal of the higher viral vector-treated (1E11 vg/mouse). In Appendix C.1 signal was normalised to the average of the input fraction.

2.12 AAV9 PROTEIN CAPSID ANALYSIS

For this experiment, 1 mm thick 8% acrylamide gel was used. The gel preparation and electrophoresis method is described in Section 2.11.3.

Viral samples were prepared by mixing 5 μl of viral vector stock, 7 μl of 1x PBS (Gibco, ThermoFisher Scientific, USA) and 4 μl of 4x Laemmli buffer and incubated at 90°C for 2 minutes. 16 μl of the sample were then loaded alongside the molecular weight marker Precision Plus Protein Dual Color Standard (cat. 1610374, BioRad, USA).

At the end of the electrophoresis run, the gel was removed from the glass plate, washed two times in double distilled water and then incubated at room temperature for 15 minutes with InstantBlue Coomassie stain (cat. ab119211, Abcam, UK). The gel was then rinsed in double distilled water and the gel image was acquired with a camera.

2.13 VIRAL VECTOR BIODISTRIBUTION ANALYSIS

2.13.1 DNA isolation

DNA was isolated from 4% PFA transcardially perfused mice. The cortex, hippocampus, thalamus, striatum, and cerebellum were collected from the right hemisphere of each brain by microdissection in 1.5 ml tubes. 180 µl of buffer ATL and 20 µl of proteinase K were added to each sample, mixed using a vortex and incubated at 56°C on a heat block overnight. The following day, samples were first incubated for 1 hour at 90°C and then DNA was isolated using the Blood and Tissue extraction kit (QIAGEN, DE) following the manufacturer's instructions. DNA was eluted in 100 µl of nuclease free water (QIAGEN, DE) and stored at -20°C.

2.13.2 qPCR

To evaluate viral vector biodistribution, the absolute quantification with standard curve method was used. Viral vector copies per sample were calculated as absolute number of viral vector DNA relative to the absolute number of diploid genomes, calculated as the number of *Actb* (Actin) gene copies divided by 2, in the same sample.

Standard curves were created using a 10-fold serial dilution of a standard containing a known number of target DNA copies. Two standards were used: the plasmid containing the therapeutic cassette, for the quantification of the viral vector genome and a gene fragment (gBlock, Integrated DNA Technologies, USA) containing a portion of the murine *Actb* gene.

DNA copy number in each standard sample was determined based on the standard sample concentration and the size of the fragment using the formula:

$$\text{Number of copies} = \frac{DNA\ cocentration\ (ng/\mu l) \times Avogadros's\ number}{DNA\ sequence\ length\ (bp) \times ng\ conversion\ factor \times bp\ weight\ (Da)}$$

Where:

Avogadro's number = 6.022×10^{23}

ng conversion factor = $1x10^{9}$

average base pair (bp) weight = 650 Da

Reactions were carried out in MicroAmp Fast Optical 96-Well Reaction Plate (cat. 4346906, Applied Biosystem, ThermoFisher Scientific, USA) using the StepOnePlus Real-Time PCR System (Applied Biosystem, ThermoFisher Scientific, USA). Reactions were prepared as described in Table 2-17 while primers and their reaction concentrations are reported in Table 2-18. Cycling conditions are reported in Table 2-19.

Table 2-17. qPCR reaction.

Component	Volume
Perfecta SYBR Green ROX (Quanta Bio)	10 μl
Primer mix	1.2 μl
DNA	2 μl
H_2O	To 18 μl

Table 2-18. Primers for qPCR.

Primer*	Sequence 5'-3'	Fragment size	Final concentration
mAct_F	AGCCATGTACGTAGCCATCC	228 bp	600 nM
mAct_R	CTCTCAGCTGTGGTGGTGAA		
qJeT_F1	GTTAGGGCGGAGCCAATC	150 bp	300 nM
qJeT_R1	AGAACCGCGACCCAAATC		
qSYN_F2	GGAGGAGTCGTGTCGTG	111 bp	300 nM
qSYN_R2	TGTCATCGTCATCCTTGTAATC		

*F indicates forward primer, R reverse primer.

Table 2-19. qPCR cycling condition

Step	Temperature	Time
Initial Denaturation	95°C	10 minutes
X40		
Denaturation	95°C	15 seconds
Annealing	60°C	30 seconds
Extension	60°C	30 seconds
Melt Curve		
Dissociation	95°C	15 seconds
	60°C (+0.3°C to 95°C)	1 minute
	95°C	15 seconds

2.13.3 Quantification

Data were extracted from the StepOnePlus Real-Time PCR System and analysed using Excel (Microsoft). Firstly, the percent coefficient of variance was calculated over cycle threshold (Ct) values triplicate for each sample using the formula =STDEV(Ct)/AVERAGE(Ct), and outlier removed as described in Section 2.11.2. The average of the replicates for the standard curve was used to calculate the R^2 goodness-to-fit value (acceptable values are between 0.98 and 1).

The slope of the standard curve was calculated using the SLOPE function as SLOPE($\log_{10}$ of the DNA copies, Ct values observed). Similarly, the standard curve intercept was calculated as INTERCEPT($\log_{10}$ of the DNA copies, Ct values observed). The slope was then used to calculate the efficiency of amplification (E_{AMP}) and the percent efficiency of amplification (E_{AMP}%) as:

1- $$E_{AMP} = 10^{\left(-\frac{1}{\text{slope}}\right)} \quad \text{or} \quad E_{AMP}\% = (E_{AMP}-1)\text{x}100$$

For an accurate quantification, E_{AMP} needs to be between 1.9 and 2.10, values above and below could lead to a decreased sensitivity and an increased chance of a false positive.

DNA copies/µl of the "unknown samples" were then calculated as:

2- $$\text{DNA copies/reaction} = E_{AMP}^{(\text{Intercept-Ct})}$$

3- DNA copies/μl of sample = $\frac{DNA\ copies/reaction}{2}$

Copies of vector genome per diploid genome were calculated as:

4- Vector genome per diploid genome = $\frac{Absolute\ copies\ of\ viral\ vector}{Absolute\ copies\ of\ Actb/2}$

2.14 mRNA LEVEL ANALYSIS

2.14.1 RNA isolation

Animals were sacrificed by cervical dislocation, and the brain was removed. RNA was isolated from dissected hippocampi collected in prefilled 2 ml bead mill tubes (ThermoFisher Scientific, USA), flash-frozen on dry ice and stored at -80°C. RNA isolation was performed using RNeasy Mini kit (cat. 74104, QIAGEN, DE).

30 mg of tissue were homogenised for 20 seconds using the Bead Mill 24 (Fisherbrand, ThermoFisher Scientific, USA) in buffer RTL + β-mercaptoethanol (Sigma, USA). Subsequently, the homogenised tissue was transferred to RNeasy spin column, and samples were treated as per manufacturer's instructions. On-column DNase digestion was performed. Purified RNA was eluted in 40 μl nuclease free water and stored at -80°C.

2.14.2 Reverse transcription-PCR (RT-PCR)

600 ng of RNA were used for the retro transcription. RNA samples were treated with DNase to eliminate DNA contamination using RQ1 DNase digestion kit (cat. M6101, Promega, UK). DNase reaction was set up as in Table 2-20 and incubated for 30 minutes at 37°C.

Table 2-20. DNase reaction mix.

Component	Volume*
RNA	X μl (600 ng)**
10x reaction buffer	2 μl
DNase	2 μl
H_2O	To 20 μl

*Volumes refer per sample.
** Sample volumes. Volumes vary depending on samples concentration.

Subsequently, 2 μl of RQ1 DNase stop were added and the reaction was incubated at 65°C for 10 minutes followed by 1 minute on ice. Two separate reactions were set up using the treated RNA, +Reverse Transcriptase (RT) and -RT (in presence or absence of RT) as described in Table 2-21. After mixing, the solutions were incubated for 5 minutes at 65°C and then 1 minute on ice.

Table 2-21. Random hexamers reaction mix.

Component	Volume*	
	+RT	**-RT**
RNA	10 μl	10 μl
dNTP	1 μl	1 μl
Random hexamers (10 μM) (Integrated DNA Technologies)	2.8 μl	2.8 μl
H_2O	To 13 μl	To 13 μl

*Volumes refer per sample.

Reverse transcription reactions mixtures were prepared as described in Table 2-22 and cDNA synthesis was carried out using the cycling condition reported in Table 2-23. cDNA samples were stored at -20°C.

Table 2-22. RT reaction mix.

Component	Volume*	
	+RT	**-RT**
RNA solution	13 μl	13 μl
0.1M DTT (ThermoFisher Scientific)	1 μl	1 μl
First-strand buffer (ThermoFisher Scientific)	4 μl	4 μl
RNase OUT (ThermoFisher Scientific)	1 μl	-
Superscript III (ThermoFisher Scientific)	1 μl	-
H_2O	-	2 μl

*Volumes refer per sample.

Table 2-23. RT cycling conditions.

Temperature	Duration
25°C	5 minutes
50°C	60 minutes
70°C	15 minutes
4°C	Infinite

2.14.3 qPCR

SYNGAP1/Syngap1 mRNA molecules were evaluated using absolute quantification with the standard curve method. Standard curves were constructed following the same procedure presented for the qPCR reported in Section 2.13.2.

Three separate reactions were set up to amplify a fragment specific for the mouse *Syngap1* transcript, for the vector-derived *SYNGAP1* mRNA and for the endogenous *Actb* mRNA. The primers used are reported in Table 2-24. Mouse_F2 refers to the forward primer used for the amplification of the mouse endogenous transcript, while Vector_F2 is used for the amplification of the vector-derived mRNA. Primer Pan_R1 indicates the reverse primer able to anneal to both the endogenous and exogenous mRNA and was used in combination with the specific forward primer (Figure S-20). Reactions were carried out in MicroAmp Fast Optical 96-Well Reaction Plate (Applied Biosystem, ThermoFisher Scientific, USA) using the StepOnePlus Real-Time PCR

System (Applied Biosystem, ThermoFisher Scientific, USA). The reaction mix is reported in Table 2-17 while cycling conditions are reported in Table 2-19.

Table 2-24. qRT-PCR primers.

Primer*	Sequence 5'-3'	Fragment size	Final concentration
Vector_F2	CCACCTCTAAGCCTAGAAGC	76 bp	300 nM
Mouse_F2	CCACCTCCAAGCCCCGCTCG		600 nM
Pan_R1	GCAGGCAGGTTGTTAAACTC		300/600 nM
mAct_F	AGCCATGTACGTAGCCATCC	228 bp	300 nM
mAct_R	CTCTCAGCTGTGGTGGTGAA		

*F indicates forward primer, R reverse primer.

2.14.4 Quantification

Extrapolation of transcript copies was carried out as described in Section 2.13.3 up to point 3. The absolute number of *SYNGAP1* and *Syngap1* mRNA molecules were normalised to the internal control *Actb*, indicated in the text and figures as *SYNGAP1/Actb* and *Syngap1/Actb.* Subsequent normalisations are specified in the text.

2.15 STATISTICS

Statistical analysis was carried out using GraphPad software PRISM 9. Parametric testes (two-tailed Student's t-test, One-way ANOVA and Two-way ANOVA and repeated measures counterpart) or non-parametric tests (two-tailed Mann-Whitney, Kruskal-Wallis and Log-rank test) were used based on the nature of the data. The test used for each comparison and multiple comparison tests are specified in the text.

For parametric tests, normality was assumed but not tested while equal variance was not assumed, and Welch's correction was used.

To define statistical significance $p < 0.05$ was used.

No power calculation was performed to determine samples sizes. The *n* used was based on previous published works.

Treatments were assigned pseudo-randomly to the first litter of each breeding pair, if any other litter from a previously used breeding pair was needed, a treatment different from the first one was delivered.

Experimenter was blind to genotype and treatment.

CHAPTER 3: DEFINITION OF A ROBUST BEHAVIOURAL BASELINE

3.1 INTRODUCTION

From its discovery in 1998 by Kim *et al.* (Kim *et al.*, 1998) to the identification of the first patient carrying a pathogenic mutation (Hamdan *et al.*, 2009) to now, SYNGAP1 has been widely studied. Several constitutive knockouts (Kim *et al.*, 2003; Komiyama *et al.*, 2002; Vazquez *et al.*, 2004) and conditional knockout/rescue (Clement *et al.*, 2012; Knuesel *et al.*, 2005; Muhia *et al.*, 2012) mouse models have been independently created to study gene and protein function and its role in the pathophysiology of the disease. Although they were all generated on the same C57Bl6/J background they differ in the targeting cassette used. Moreover, as in the case of Guo *et al.* (Guo *et al.*, 2009), they have been separately backcrossed on different strains, such as 129sv/ev, to circumvent breeding issues (Table 1-1).

Although all the developed lines have been extensively characterised, in most cases, each study focused on a specific age of testing and across studies a wide range was considered. The youngest was at PND16 (Verma *et al.*, 2022) while the oldest was >50 weeks old (Nakajima *et al.*, 2019). Only two studies conducted an extensive phenotypic characterisation, Muhia *et al.* (Muhia *et al.*, 2010) used *Syngap1*$^{+/-}$ mice generated by Vazquez *et al.* (Vazquez *et al.*, 2004) and Nakajima *et al.* (Nakajima *et al.*, 2019) used the *Syngap1*$^{+/-}$ mice generated by Komiyama *et al.* (Komiyama *et al.*, 2002).

It is widely known that genetic background, as well as different ages of testing, can affect behavioural output (Crawley *et al.*, 1997; Montagutelli, 2000; Wolfer *et al.*, 2002). Moreover, there is an intrinsic variability associated with behavioural assessment due to the experimenter, breeding strategy, facility environment, and testing room conditions which also makes replicating behavioural data more challenging.

For all of these reasons, I evaluated the robustness of previously published results to set the baseline for the work presented in this thesis. Among the many available tests, I chose multiple paradigms of short length that offered the chance to automate the analysis. I also decided to extend the behavioural testing to include paradigms not previously used to phenotype *Syngap1*$^{+/-}$ mice.

3.2 AIM

The work presented in this chapter aimed to design and optimise a robust battery of behavioural tests in a mouse model of *SYNGAP1* haploinsufficiency-associated disorder to be used as endpoints to evaluate the efficacy of the gene therapy products. To this end, wild-type and *Syngap1*$^{+/-}$ mice were tested in a series of behavioural phenotyping tests to establish the baseline consequences of *Syngap1* haploinsufficiency in my *Syngap1*$^{+/-}$ mice colony.

3.3 STUDY PLAN

Detailed methodology for each test used has been presented in Chapter 2. Briefly, cohorts of wild-type and *Syngap1*$^{+/-}$ male mice were tested with the open field, elevated plus maze, T-maze, marble burying and nest building tests, in this order, at three different developmental stages: 4, 7 and 11 weeks of age in a longitudinal study. Due to the breeding difficulties encountered with the *Syngap1* colony, not all the *Syngap1*$^{+/-}$ and wild-type mice included in the analysis were generated and tested in a single large experiment. To reach the desired *n* for each group, animals were divided in cohorts and recruitment spanned over three months.

A portion of the animals entered the study at the beginning (4 weeks of age) while a second group of mice begun the study at 7 weeks of age. The genotype effect at each time point was evaluated by pooling the animals that were tested at the same age,

while to evaluate the effect of re-exposure, only animals that were tested at both 7 and 11 weeks of age were included in the analysis.

Two additional cohorts of animals were tested using, in this order, the visual cliff and platform departure tests at 7 and at 15 weeks of age in a cross-sectional study. As above, due to the breeding difficulties not all the *Syngap1*$^{+/-}$ and wild-type mice included in the analysis were generated and tested in a single large experiment. To reach the desired *n* for each group, animals were divided in cohorts and recruitment spanned over three months.

The rationale for repeating the tests at different ages was to evaluate the robustness of each behaviour across time in a longitudinal study. For gene therapy studies, it is of pivotal to evaluate treatment effects across time. For example, tolerability issues associated with the treatment can develop later. For this reason, it was crucial to test for behavioural abnormalities that are consistently present throughout the lifespan of the animal.

3.4 RESULTS

3.4.1 General conditions

Although reduced brain size, associated with smaller volumes of single brain areas, has been recorded in *Syngap1*$^{+/-}$ mice, the difference in body weight between genotypes had not been investigated before (Kilinc *et al.*, 2018). Therefore, the developmental body weight trajectory was investigated in our colony. The growth chart in Figure 3-1 shows body weights in relation to age for both wild-type and *Syngap1*$^{+/-}$ mice. Across the 9 weeks considered (from 3 weeks to 12 weeks of age) *Syngap1*$^{+/-}$ mice did not display a significantly lower body weight compared to wild-type littermates, except at 10 weeks of age (Figure 3-1; Mixed Effects Model; genotype x age $F_{(9, 280)}$=1.782 p=0.0714, Age $F_{(1.829, 5689)}$=597 p<0.0001, genotype $F_{(1, 35)}$=6.530 p=0.0151; Šídák multiple comparison results are reported in Table S-1).

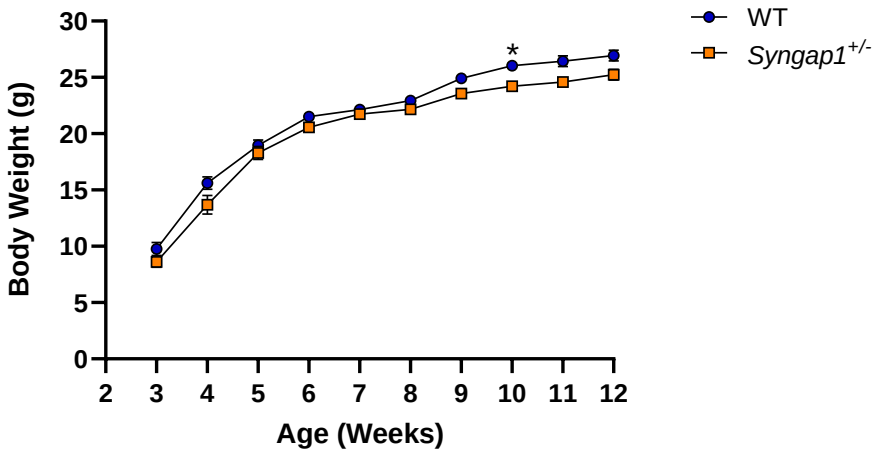

Figure 3-1. Syngap1$^{+/-}$ and wild-type mice showed a comparable body weight across development.
Growth curve of *Syngap1*$^{+/-}$ and wild-type (WT) mice. Animals have been weighed weekly starting from the third week of age until 12 weeks old. Mixed Effects Model, data presented as mean ± standard error of the mean (SEM). * p<0.05.

3.4.2 Open Field

Hyperactivity is a well-established phenotype in *Syngap1*$^{+/-}$ mice, replicated by several groups independently (Berryer *et al.*, 2016; Guo *et al.*, 2009; Muhia *et al.*, 2009, 2010; Nakajima *et al.*, 2019).

To investigate the locomotor activity, wild-type and *Syngap1*$^{+/-}$ mice were tested using the open field test. Three parameters were investigated: distance travelled in 20 minutes, to evaluate hyperactivity, distance travelled in each 5 minutes time bin, to evaluate habituation to the arena, and percentage of time spent in the periphery of the arena, to evaluate anxiety.

The increased horizontal activity was observed in *Syngap1*$^{+/-}$ mice as early as 4 weeks of age (Figure 3-2a; two-tailed Student t-test with Welch's correction, mean ± SEM; wild-type n=9, 7138 ± 614.6; *Syngap1*$^{+/-}$ n=8, 10361 ± 613.4; $t_{(14.94)}$=3.711, p=0.0210). Distance travelled by *Syngap1*$^{+/-}$ mice was higher than distance travelled by wild-type littermates at each time bin but both genotypes showed partial habituation to the arena (Figure 3-2b; Repeated Measure (RM) Two-way ANOVA, wild-type n=9,

Syngap1$^{+/-}$ n=8, genotype x time $F_{(3, 45)}$=0.6356 p=0.5960, time $F_{(2.079, 31.19)}$=45.06 p<0.0001, genotype $F_{(1, 15)}$=17.28 p=0.0013; multiple comparisons results are reported in Table S-2). Although 20 minutes is a short time to observe complete habituation to the environment, this measure is indicative of the fact that the increased distance travelled observed in the *Syngap1*$^{+/-}$ mice was not associated with a lack of habituation but with an overall increased locomotion. *Syngap1*$^{+/-}$ mice also presented a reduced preference for the periphery of the arena (Figure 3-2c; two-tailed Mann-Whitney test, median(95% Confidence Interval (CI)); wild-type n=9, 65.54 (54.22 to 70.76) %; *Syngap1*$^{+/-}$ n=8, 46.76(39.90 to 56.58) %; U=13, p=0.0274) that could be interpreted as reduced anxiety, as described for the elevated plus maze test (Guo *et al.*, 2009; Muhia *et al.*, 2010; Nakajima *et al.*, 2019).

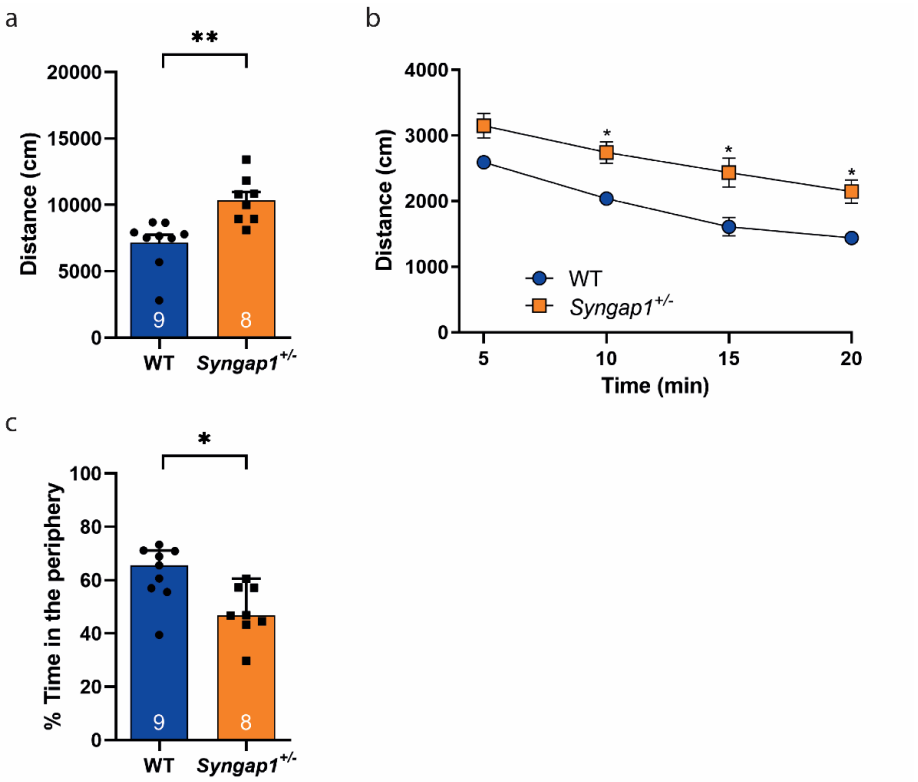

Figure 3-2. At 4 weeks of age Syngap1$^{+/-}$ mice presented increased locomotor activity and increased preference for the peripheral area of the arena.
Total distance travelled in 20 minutes (a) and distance travelled in four intervals of 5 minutes each (b) for *Syngap1*$^{+/-}$ and wild-type (WT) mice in the open field at 4 weeks of age. Stars (*) above each bin represent the results of multiple comparison tests between genotypes. Each data point represents the mean distance travelled over the preceding 5 minutes. The percentage of time in the periphery (c) was also measured for both genotypes at 4 weeks of age. Circles and squares represent single animals. Numbers within the bars represent the n of each group.
a) Two-tailed Student t-test with Welch's correction, data presented as mean ± SEM. b) RM Two-way ANOVA with Šídák multiple comparison test for genotype effect, data presented as mean ± SEM. c) Two-tailed Mann-Whitney test, data presented as median and 95% CI. * $p<0.05$, ** $p<0.01$.

The significant difference in horizontal activity between genotypes was observed also at 7 weeks of age with *Syngap1*$^{+/-}$ mice showing increased horizontal activity compared to wild-type controls (Figure 3-3a; two-tailed Student t-test with Welch's correction, mean ± SEM; wild-type n=14, 6989 ± 386.6 cm; *Syngap1*$^{+/-}$ n=15, 12956 ± 600.6 cm; $t_{(23.63)}=7.084$, $p<0.0001$). Habituation to the arena was again similar in the two genotypes (Figure 3-3b; RM Two-way ANOVA; wild-type n=14, 6989 ± 386.6; *Syngap1*$^{+/-}$ n=15; genotype x time $F_{(3, 81)}=0.2918$ $p=0.8312$, time $F_{(1.356, 36.60)}=10.57$

p=0.0010, genotype $F_{(1,\ 27)}$=42.27 p<0.0001; multiple comparisons results are reported in Table S-3). For what concern time spent in the periphery, wild-type and *Syngap1*$^{+/-}$ mice showed comparable behaviour (Figure 3-3c; two-tailed Mann–Whitney test, median(95% CI); wild-type n=14, 57.87(50.17 to 62.70) %; *Syngap1*$^{+/-}$ n=15, 48.78(45.18 to 53.90) %; U=62, p=0.0630).

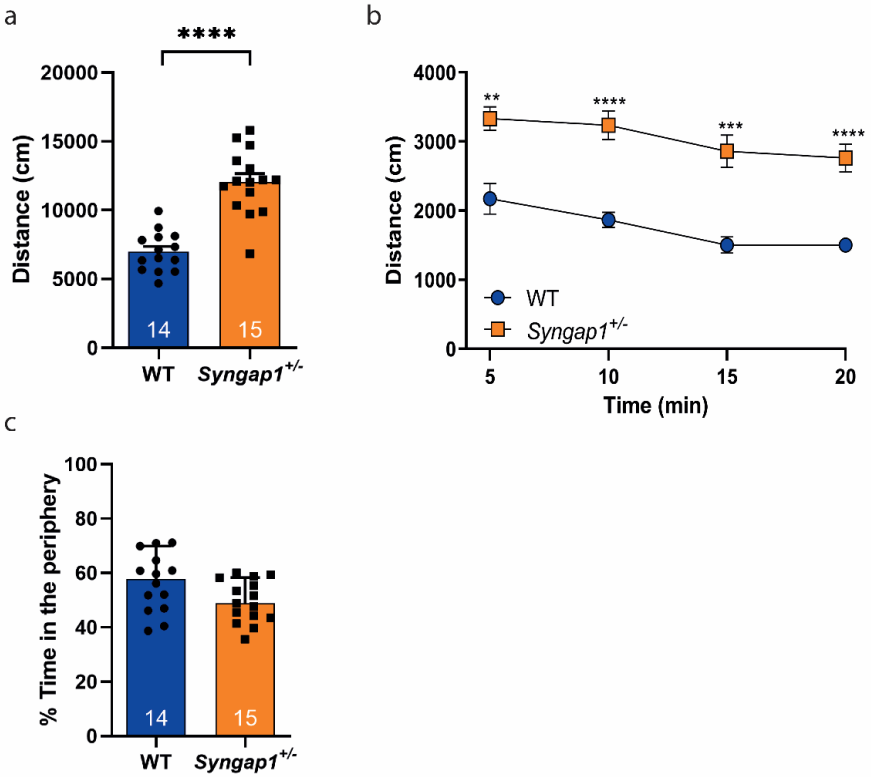

Figure 3-3. At 7 weeks of age, Syngap1*$^{+/-}$ *mice displayed increased locomotion.
Total distance travelled in 20 minutes (a) and distance travelled in four intervals of 5 minutes each (b) for *Syngap1*$^{+/-}$ and wild-type (WT) mice in the open field at 7 weeks of age. Stars (*) above each bin represent the results of multiple comparison tests between genotypes. Each data point represents the mean distance travelled over the preceding 5 minutes. The percentage of time in the periphery (c) was also measured for both genotypes at 7 weeks of age. Circles and squares represent single animals. Numbers within the bars represent the n of each group.
a) Two-tailed Student t-test with Welch's correction, data presented as mean ± SEM. b) RM Two-way ANOVA with Šídák multiple comparison test for genotype effect, data presented as mean ± SEM. c) Two-tailed Mann-Whitney test, data presented as median and 95% CI. **** p<0.0001.

Analysis of horizontal activity showed that hyperactivity was also observed at 11 weeks of age (Figure 3-4a; two-tailed Student t-test with Welch's correction, mean ± SEM; wild-type n=14, 6000 ± 284.8 cm; *Syngap1*$^{+/-}$ n=15, 13671 ± 744.5 cm; $t_{(17.98)}$=9,624, p<0.0001). *Syngap1*$^{+/-}$ mice did not show a preference for the centre of the arena compared to wild-type littermates (Figure 3-4c; two-tailed Mann–Whitney test, median(95% CI); wild-type n=14, 53.24(41.30 to 62.36) %; *Syngap1*$^{+/-}$ n=15, 47.73(40.96 to 49.06) %; U= 69, p=0.01225).

At 11 weeks of age, distance travelled over time remained constant across bins for both genotypes (Figure 3-4b; RM Two-way ANOVA; wild-type n=14, *Syngap1*$^{+/-}$ n=15, genotype x time $F_{(3, 81)}$=1.046 p=0.3770, time $F_{(2.631, 71.02)}$=1.472 p=0.2326, genotype $F_{(1, 27)}$=87.73 p<0.0001; Šídák multiple comparisons results are reported in Table S-4).

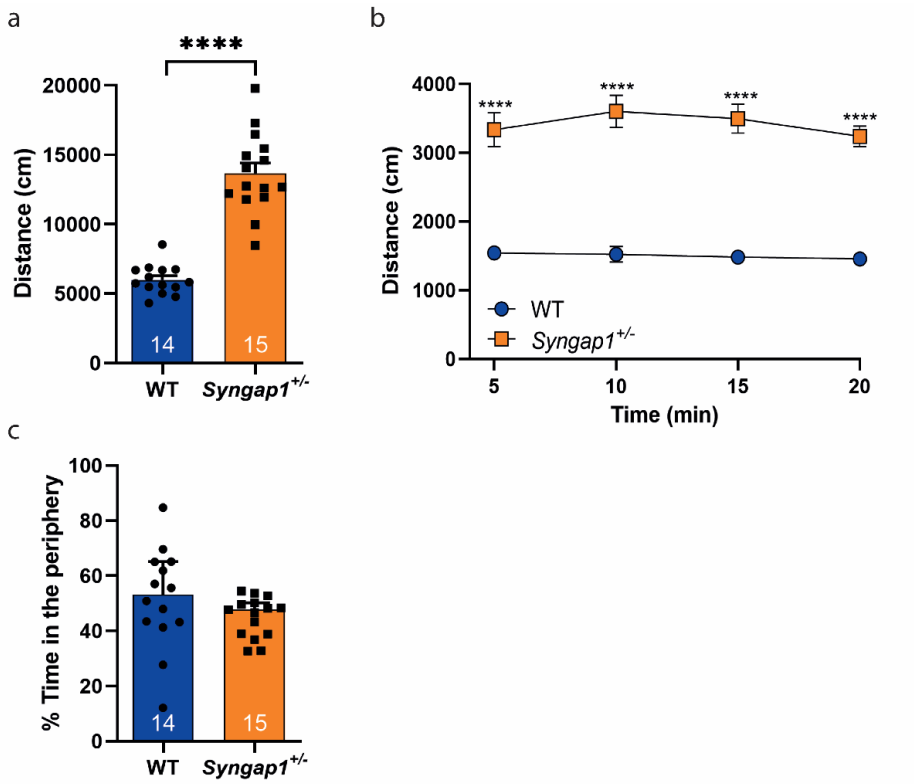

Figure 3-4. At 11 weeks of age, Syngap1$^{+/-}$ mice displayed increased locomotion.
Total distance travelled in 20 minutes (a) and distance travelled in four intervals of 5 minutes each (b) for *Syngap1*$^{+/-}$ and wild-type (WT) mice in the open field at 11 weeks of age. Stars (*) above each bin represent the results of multiple comparison tests between genotypes. Each data point represents the mean distance travelled over the preceding 5 minutes. The percentage of time in the periphery (c) was also measured for both genotypes at 11 weeks of age. Circles and squares represent single animals. Numbers within the bars represent the n of each group.
a) Two-tailed Student t-test with Welch's correction, data presented as mean ± SEM. b) RM Two-way ANOVA with Šídák multiple comparison test for genotype effect, data presented as mean ± SEM. c) Two-tailed Mann-Whitney test, data presented as median and 95% CI. **** p<0.0001

It is possible that the difference in habituation observed across ages was associated with overall habituation to the arena due to re-exposure.

To test this, I compared the distance travelled at 7 and 11 weeks of age. No difference was observed for both wild-type and *Syngap1*$^{+/-}$ mice (Figure 3-5; RM Two-way ANOVA, wild-type n=14, 7 weeks 6989 ± 386.6 cm, 11 weeks 6000 ± 284.8 cm. *Syngap1*$^{+/-}$ n=15, 7 weeks 12056 ± 600.6 cm, 11 weeks 13671 ± 744.5 cm; genotype x time $F_{(2, 27)}$=3.823 p=0.0610, time $F_{(1, 27)}$=0.2213 p=0.6418, genotype $F_{(1, 27)}$=261.7 p<0.0001; Šídák multiple comparisons test results are reported in Table S-5). For this

comparison, only 7 and 11 weeks have been used as these groups contain matching individuals. It is important to note that some mice were exposed to the test also at 4 weeks of age.

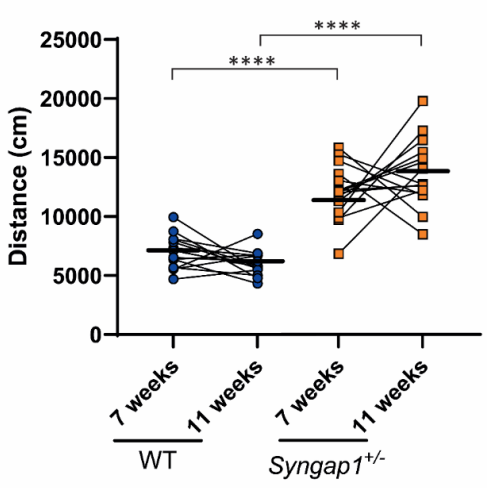

Figure 3-5. No habituation to the open field test was observed for both genotypes
Distance travelled in the open field by wild-type (WT) and *Syngap1*$^{+/-}$ mice at 7 and 11 weeks of age. Circles and squares represent single animals, black horizontal bars represent the mean. Wild-type n=14, *Syngap1*$^{+/-}$ n=15.
RM Two-way ANOVA. **** p<0.0001.

3.4.3 Elevated Plus Maze

Mice, and rodents in general, tend to spend more time in dark enclosed areas compared to open spaces and prefer contact with boundary walls. An increase in time spent away from the boundary walls or enclosed spaces in favour of open spaces can be interpreted as a reduction of anxiety and a test widely used to evaluate anxiety-related behaviours is the elevated plus maze test (Lister, 1987). For this test, mice are placed in a maze composed of two open arms, with no boundary walls, and two closed arms, with boundary walls, placed perpendicularly forming a plus sign. It is considered reduced anxiety when mice spend more time in open arms.

Anxiety disorders have been described in *SYNGAP1* patients (Klitten *et al.*, 2011), while reduction of anxiety has been extensively described in *Syngap1*$^{+/-}$ mice (Berryer

et al., 2016; Clement *et al.*, 2012; Guo *et al.*, 2009; Nakajima *et al.*, 2019) suggesting the possibility of a species-conserved phenotype.

For this study, time spent in the open arms and distance travelled in the given time were assessed. These parameters were then correlated to evaluate the effect of hyperactivity on this phenotype. As defined in Chapter 2, mice that jumped from the maze were excluded from the analysis. Two *Syngap1*$^{+/-}$ mice jumped at 7 weeks and two at 11 weeks.

At 4 weeks of age *Syngap1*$^{+/-}$ mice displayed increased locomotor activity in the maze, in accordance with the open field test result (Figure 3-6a; two-tailed Student t-test with Welch correction, mean ± SEM; wild-type n=9, 1727 ± 55.98 cm; *Syngap1*$^{+/-}$ n=8, 2377 ± 210.4 cm; $t_{(7.991)}$=2.986, p=0.0175). *Syngap1*$^{+/-}$ mice spent less time compared to wild-type controls in the open arms of the maze suggesting a reduction of anxiety (Figure 3-6b; two-tailed Mann–Whitney test; median(95% CI); wild-type n=9, 18.45(14.13 to 35.49) %; *Syngap1*$^{+/-}$ n=8, 39.06(30.46 to 52.37) %; U=12, 95% p=0.0206).

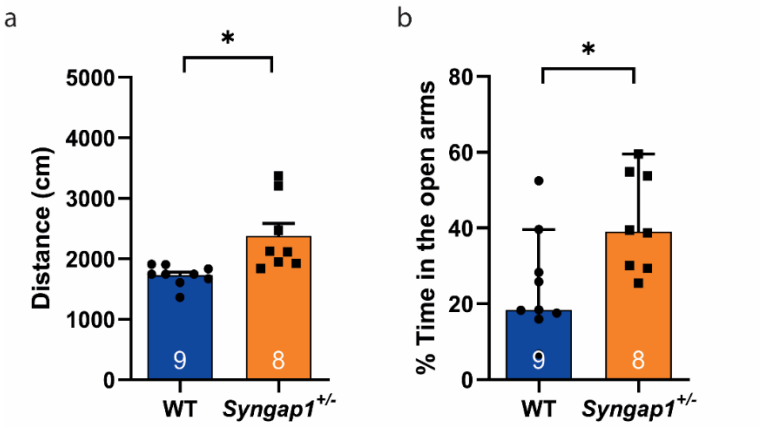

Figure 3-6. At 4 weeks of age, Syngap1*$^{+/-}$ *mice showed increased locomotion activity and increased time spent in open arms.
Total distance travelled (a) and percentage of time spent in the open arms of the maze (b) by wild-type (WT) and *Syngap1*$^{+/-}$ mice at 4 weeks of age. Circles and squares represent single animals. Numbers within the bars represent the n of each group.
a) Two-tailed Student t-test with Welch correction, data presented as mean ± SEM.
b) Two-tailed Mann-Whitney test, data presented as median and 95% CI. * p<0.05.

It is still not clear whether the phenotype observed during the elevated plus maze is a direct consequence of the hyperactivity or if it is truly a reduction of anxiety. To investigate the relationship between distance travelled and time spent in open arms, I analysed their correlation using the Pearson test.

In *Syngap1*$^{+/-}$ mice, the distance travelled in the maze and the number of entries in the open arm, both overall increased, were strongly correlated, suggesting that *Syngap1*$^{+/-}$ mice were prone to move more over the entire maze instead of moving only in the open arms (Figure 3-7b; two-tailed Pearson correlation*; Syngap1*$^{+/-}$ n=8, $r_{(6)}$=0.8561, p=0.0067). However, the two parameters did not display a strong correlation in wild-type mice, where it suggested that the overall distance travelled was more "in arm" rather than "across arms" (Figure 3-7a; two-tailed Pearson correlation; wild-type n=9, $r_{(7)}$=0.4525, p=0.2213).

For both genotypes, the distance travelled showed a weak correlation with the total time spent in the open arms suggesting that, although *Syngap1*$^{+/-}$ mice cover more distance across the entire maze, more distance travelled was not always associated with an increased time in the open arms (Figure 3-7c and d; two-tailed Pearson correlation; wild-type n=9, $r_{(7)}$=0.3745, p=0.3208, *Syngap1*$^{+/-}$ n=8 $r_{(6)}$=0.4307, p=0.2868). Correlation analysis between the number of entries in the open arms and the total time spent in the open arms suggested, for *Syngap1*$^{+/-}$ mice, that the number of entries was not predictive of the amount of time spent in the open arms. The two parameters were correlated in wild-type controls (Figure 3-7e and f; two-tailed Pearson correlation; wild-type n=9, $r_{(7)}$=0.6765, p=0.0454; *Syngap1*$^{+/-}$ n=8 $r_{(6)}$=0.3843, p=0.3473). The low number of subjects present in both groups could cause an underestimation or overestimation of the correlation.

All considered, these results suggested that at 4 weeks of age there was no strong evidence of hyperactivity influence over the time spent in the open arms.

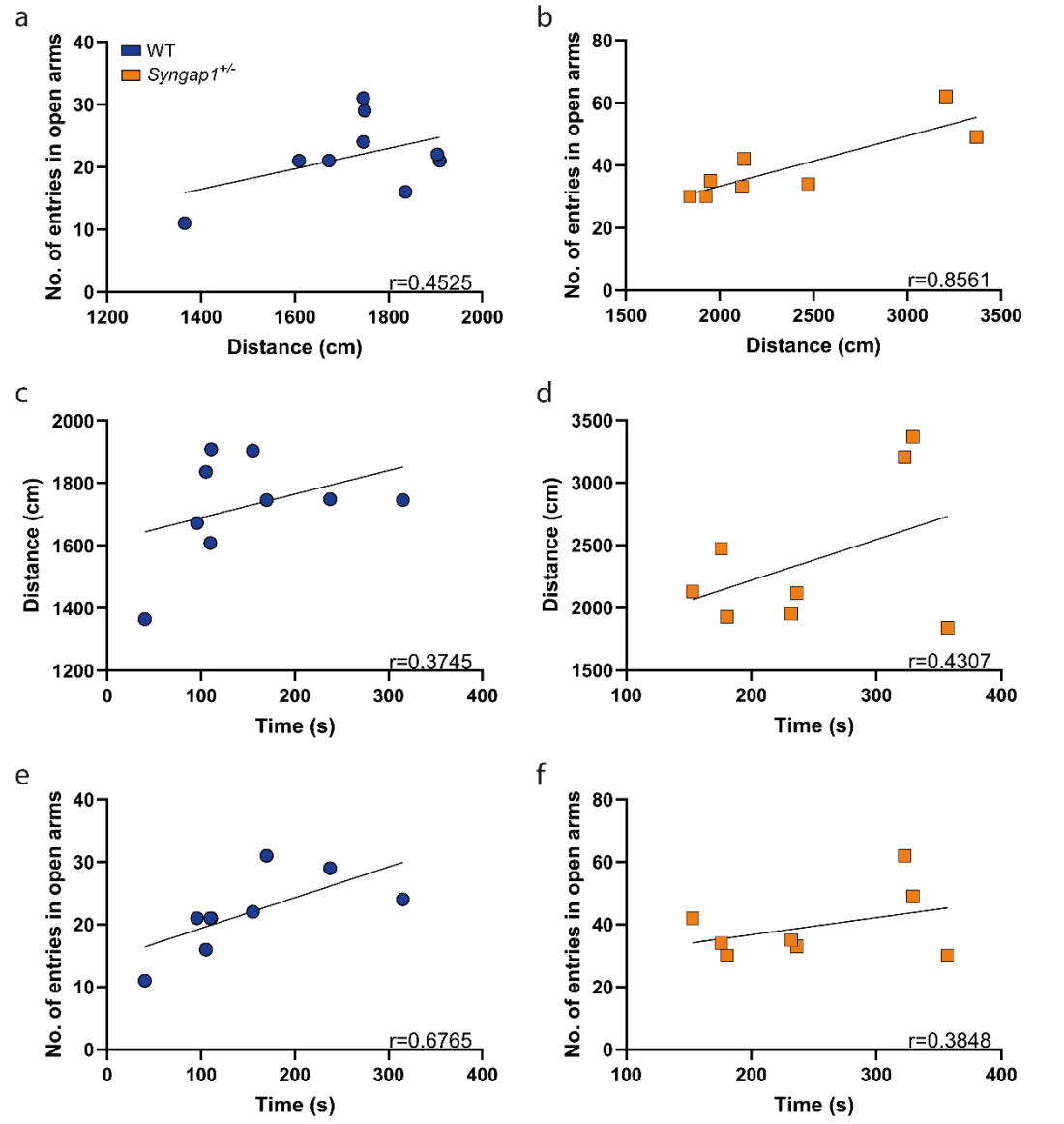

Figure 3-7. At 4 weeks of age, the length of time spent in the open arms was not influenced by hyperactivity in Syngap1$^{+/-}$ mice.

Correlation between distance travelled and the number of entries in the open arms for wild-type (WT) (a) and *Syngap1*$^{+/-}$ (b) mice. Correlation between distance travelled and time spent in the open arms for wild-type (c) and *Syngap1*$^{+/-}$ (d) mice. Correlation between time spent and the number of entries in the open arms for wild-type (e) and *Syngap1*$^{+/-}$ (f) mice. Circles and squares represent single animals. Mice tested at 4 weeks of age.

Two-tailed Pearson correlation. Wild-type n=8, *Syngap1*$^{+/-}$ n=9.

Similar to what was observed during the open field test, at 7 weeks of age *Syngap1*$^{+/-}$ mice travelled a longer distance in the maze (Figure 3-8a; two-tailed Student t-test with Welch correction, mean ± SEM; wild-type n=14, 2132 ± 107.6 cm; *Syngap1*$^{+/-}$

n=13, 2122 ± 101.1 cm; t(24.99)=4.844, p<0.0001) and spent more time in the open arms (Figure 3-8b; two-tailed Mann–Whitney test, median(95% CI); wild-type n=14, 13.84(9.303 to 21.94) %; *Syngap1*$^{+/-}$ n=13, 34.53(28.66 to 44.10) %; U=17, p<0.0001) compared to wild-type controls.

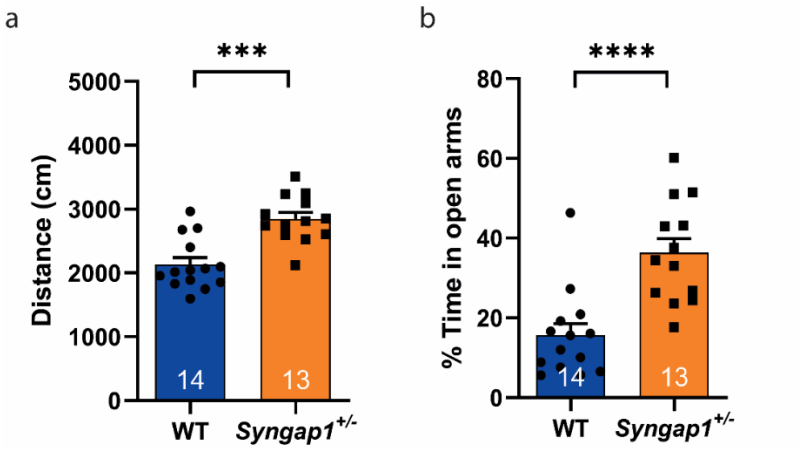

Figure 3-8. At 7 weeks of age, Syngap1$^{+/-}$ mice showed increased horizontal activity and increased time in the open arms.
Total distance travelled (a) and percentage of time spent in the open arms of the maze (b) by wild-type (WT) and *Syngap1*$^{+/-}$ mice at 7 weeks of age. Circles and squares represent single animals. Numbers within the bars represent the n of each group.
a) Two-tailed Student t-test with Welch correction, data presented as mean ± SEM. b) Two-tailed Mann-Whitney test, data presented as median and 95% CI. *** p<0.001, **** p<0.0001.

At 7 weeks of age, the analysis of correlations among different parameters detected suggested that the putative anxiety-like behaviour observed in *Syngap1*$^{+/-}$ mice was dependent on the level of horizontal activity. The number of entries in the open arms did correlate with the distance travelled for both the wild-type and *Syngap1*$^{+/-}$ mice (Figure 3-9a and b, two-tailed Pearson correlation; wild-type n=14, $r_{(12)}$=0.5799, p=0.0297; *Syngap1*$^{+/-}$ n=13, $r_{(11)}$=0.6722, p=0.0118). Similar results were observed for the distance over the total time spent in the open arms for the *Syngap1*$^{+/-}$ mice while weak evidence of correlation was observed for the wild-type controls (Figure 3-9c and d; two-tailed Pearson correlation; wild-type n=14, $r_{(12)}$=0.4083, p=0.1472; *Syngap1*$^{+/-}$ n=13, $r_{(11)}$=0.6341, p=0.0005). On the other hand, in both genotypes, a correlation was observed between the number of entries in the open arms and total

time spent in the open arms (Figure 3-9e and f; two-tailed Pearson correlation; wild-type n=14, $r_{(12)}$=0.8271, p=0.0454*; Syngap1*$^{+/-}$ n=15, $r_{(11)}$=0.8650, p=0.0002), which suggested that in both groups more entries could be associated to more time spent in the open arm.

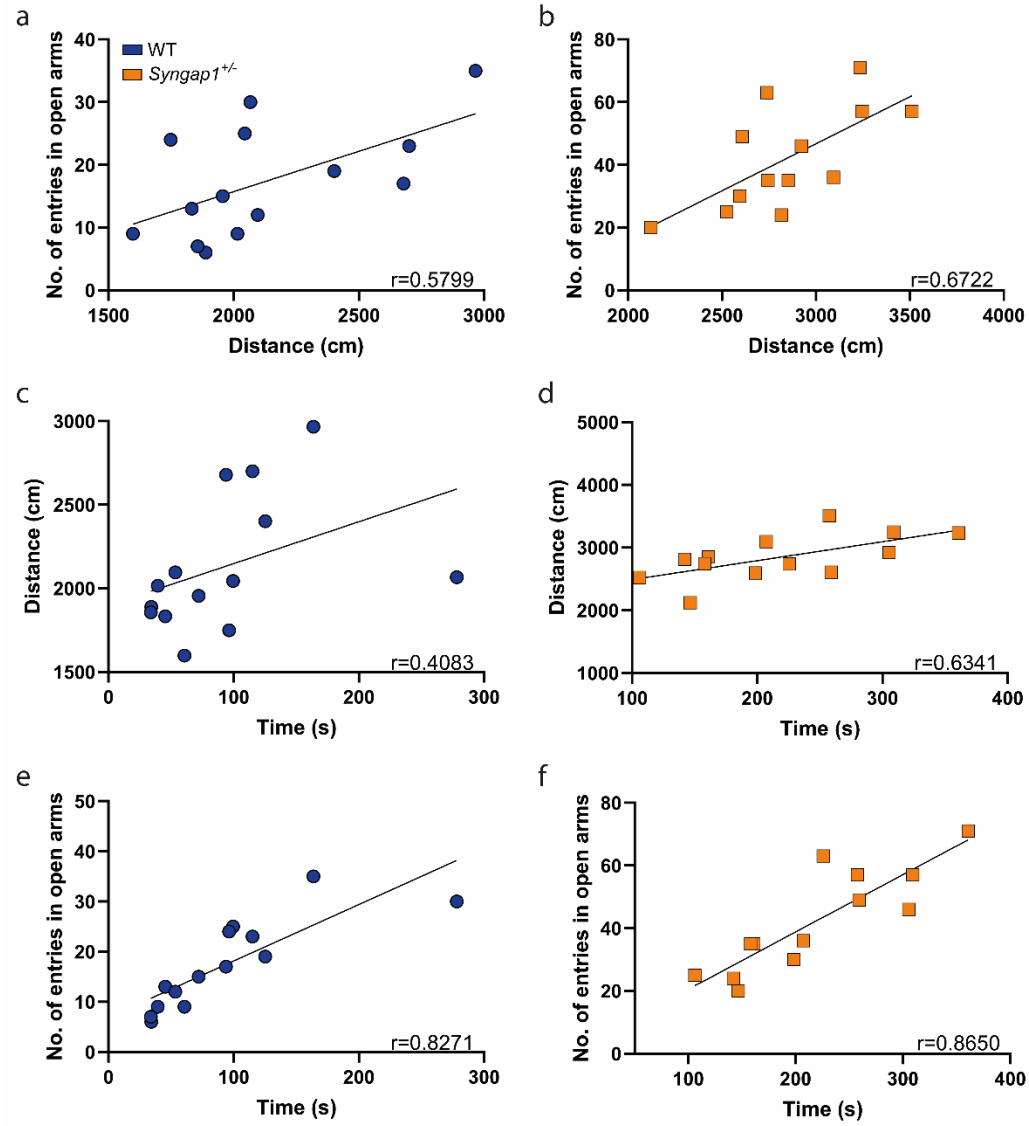

Figure 3-9. At 7 weeks of age, the length of time spent in the open arms was influenced by hyperactivity in Syngap1$^{+/-}$ mice.

Correlation between distance travelled and the number of entries in the open arms for wild-type (WT) (a) and *Syngap1*$^{+/-}$ (b) mice. Correlation between distance travelled and time spent in the open arms for wild-type (c) and *Syngap1*$^{+/-}$ (d) mice. Correlation between time spent and the number of entries in the open arms for wild-type (e) and *Syngap1*$^{+/-}$ (f) mice. Circles and squares represent single animals. Mice tested at 7 weeks of age.

Two-tailed Pearson correlation. Wild-type n=14, *Syngap1*$^{+/-}$ n=13.

Syngap1$^{+/-}$ mice presented increased locomotion at 11 weeks of age (Figure 3-10a; two-tailed Student t-test with Welch's correction, mean ± SEM; wild-type n=18, 1692 ± 134.0 cm; *Syngap1*$^{+/-}$ n=17, 3170 ± 135.3 cm; $t_{(32.95)}$=7.765, p<0.0001) and increased time in open arms (Figure 3-10b; two-tailed Mann–Whitney test, median(95% CI); wild-type n=18, 8.365(6.864 to 13.38) %; *Syngap1*$^{+/-}$ n=17, 33.93(28.94 to 41.34) %; U=4, p<0.0001).

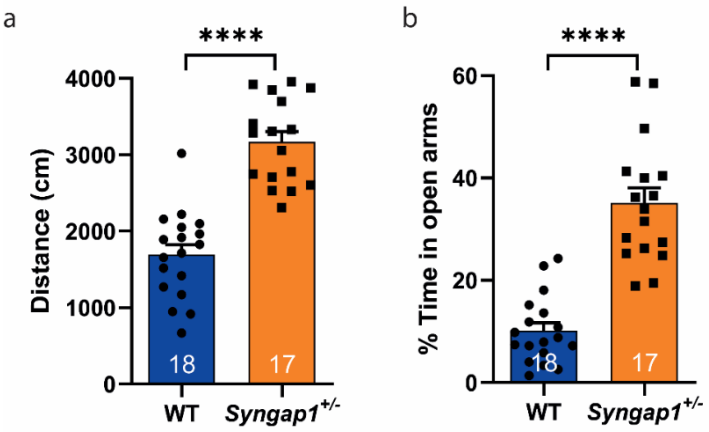

Figure 3-10. At 11 weeks of age, Syngap1$^{+/-}$ mice showed increased horizontal activity and increased time in the open arms.
Total distance travelled (a) and percentage of time spent in the open arms of the maze (b) by wild-type (WT) and *Syngap1*$^{+/-}$ mice at 11 weeks of age. Circles and squares represent single animals. Numbers within the bars represent the n of each group.
a) Two-tailed Student t-test with Welch correction, data presented as mean ± SEM.
b) Two-tailed Mann-Whitney test, data presented as median and 95% CI. **** p<0.0001

Correlation analysis showed that the entries in the open arm were strongly correlated with distance travelled in wild-type mice (Figure 3-11a; two-tailed Pearson correlation; wild-type n=18, $r_{(16)}$=0.8635, p<0.0001) as well as in *Syngap1*$^{+/-}$ mice (Figure 3-11b; two-tailed Pearson correlation; *Syngap1*$^{+/-}$ n=17, $r_{(15)}$=0.7592, p=0.0004). Wild-type mice showed a correlation for both distance over total time spent in the open arms (Figure 3-11c; two-tailed Pearson correlation; wild-type n=18, $r_{(16)}$=0.8277, p<0.0001) and the number of entries in the open arms over total time spent in the open arms (Figure 3-11e; two-tailed Pearson correlation; wild-type n=18, $r_{(16)}$=0.8976, p<0.0001). On the other hand, *Syngap1*$^{+/-}$ mice showed a milder

correlation for the same parameters (Figure 3-11d and f; two-tailed Pearson correlation; *Syngap1*$^{+/-}$ n=17, (d) $r_{(15)}$=0.6463, p=0.0051; (f) $r_{(15)}$=0.6634, p=0.0037).

Except at 7 weeks of age, the correlation between time spent in the open arms and distance travelled in the given time was similar between wild-type and *Syngap1*$^{+/-}$ mice suggesting that the result of the test was overall influenced by the mice's locomotor activity. Locomotor activity in *Syngap1*$^{+/-}$ mice at all ages reflects on a higher number of entries in the open arms. Except at 4 weeks of age, mice that perform more entries were also the ones that spent more time in the open arms, suggesting a higher activity in between equivalent arms (close to close or open to open), and this seemed to be present in the wild-type as much as in the *Syngap1*$^{+/-}$ mice.

Overall, it is not possible to exclude that the amount of time spent in the open arms is influenced by the level of activity in the maze, but results suggest that this is true for wild-type as well.

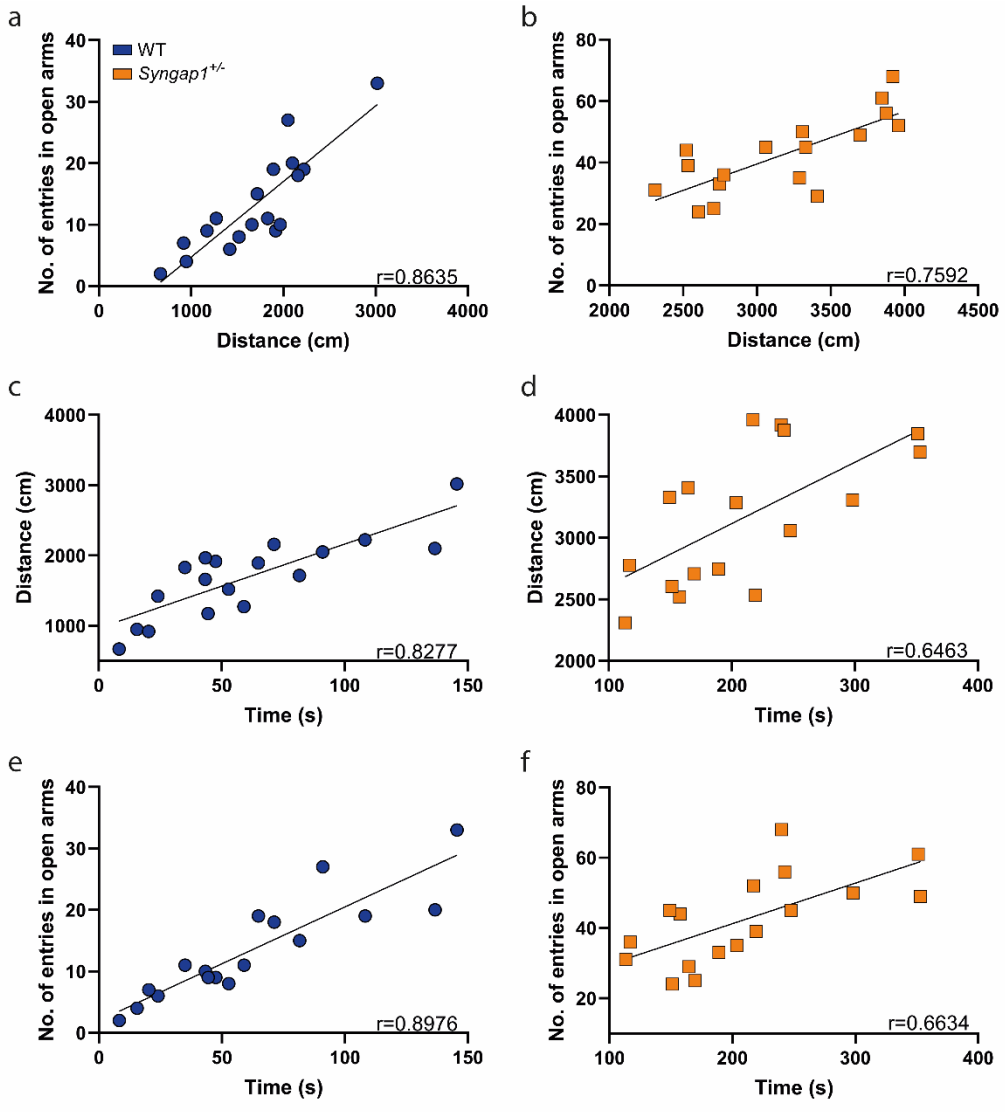

Figure 3-11. At 11 weeks of age, the length of time spent in the open arms was mildly influenced by hyperactivity in Syngap1$^{+/-}$ mice.

Correlation between distance travelled and the number of entries in the open arms for wild-type (WT) (a) and *Syngap1*$^{+/-}$ (b) mice. Correlation between distance travelled and time spent in the open arms for wild-type (c) and *Syngap1*$^{+/-}$ (d) mice. Correlation between time spent and the number of entries in the open arms for wild-type (e) and *Syngap1*$^{+/-}$ (f) mice. Circles and squares represent single animals. Mice tested at 11 weeks of age.

Two-tailed Pearson correlation. Wild-type n=18, *Syngap1*$^{+/-}$ n=17.

Opposite of what was observed in the open field, wild-type mice showed habituation to the elevated plus maze while *Syngap1*$^{+/-}$ mice maintained a constant behaviour across exposures (Figure 3-12; RM Two-way ANOVA, wild-type n=14, 7 weeks 15.62 ± 2.92 %, 11 weeks 7.28 ± 0.96 %; *Syngap1*$^{+/-}$ n=11, 7 weeks 33.61 ± 3.39 %. 11 weeks

31.45 ± 2.94 %; genotype x time $F_{(1, 23)}$=2.601 p=0.1204, time $F_{(1, 23)}$=7.448 p=0.0118, genotype $F_{(1, 23)}$=43.47 p<0.0001; Šídák multiple comparisons results are reported in Table S-6). For this analysis, mice that were not included in the 7 weeks time point were excluded from the 11 weeks time point and vice versa, a RM Two-way ANOVA was performed on the modified data set. Habituation was tested only for the percentage of time spent in the open arms as this is the core phenotype investigated by this test.

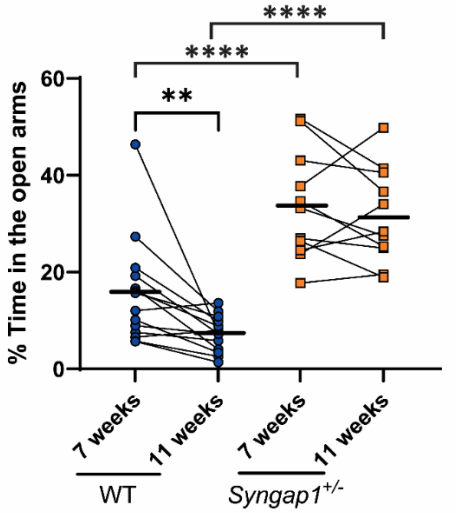

Figure 3-12. Wild-type mice showed habituation to the elevated plus maze.
Percentage of time spent in the open arms of the elevated plus maze by wild-type (WT) and *Syngap1*$^{+/-}$ mice at 7 and 11 weeks of age. Circles and squares represent single animals, black horizontal bars represent the median. Wild-type n=14, *Syngap1*$^{+/-}$ n=11.
RM Two-way ANOVA. ** p<0.01, **** p<0.0001.

3.4.4 T-maze

Exploration of the novel over already known elements in the environment is a common trait in rodents. This intrinsic animal behaviour can be used to evaluate deficits in different types of memory. In particular, the exploration of a novel part of the maze, defined as spontaneous alternation, has been used to evaluate working memory (Dember *et al.*, 1958; Montgomery, 1952). It is considered spontaneous alternation when untrained mice choose to explore a new part of the maze instead of a previously explored one.

Previous work showed that *Syngap1*$^{+/-}$ mice present a working memory deficit (Berryer *et al.*, 2016; Guo *et al.*, 2009; Muhia *et al.*, 2010) as they tend to not alternate the goal arm of a T-maze in consecutive trials.

In this work, I aimed to replicate previously published data by Berryer *et al.* (Berryer *et al.*, 2016). Briefly, mice were tested on three consecutive days, each day was composed of two trials. During the first trial, mice choose to enter one of the two goal arms, after the inter-trial period mice were exposed to the maze again and it was considered a spontaneous alternation if the unexplored arm was chosen. For this test no reinforcement was used.

Juvenile *Syngap1*$^{+/-}$ mice did not present impairments in the ability to alternate between the known and novel arm of the maze (Figure 3-13a; two-tailed Mann-Whitney test, median(95% CI); wild-type n=9, 67.00(50.34 to 90.55) %; *Syngap1*$^{+/-}$ n=8, 67.00(62.48 to 88.02) %; U=33, p=0.9506). At 7 weeks of age, although a percentage of *Syngap1*$^{+/-}$ mice higher than wild-type fail to alternate across the three days of testing, the two groups presented an overall similar behaviour in the maze (Figure 3-13b; two-tailed Mann-Whitney test, median(95% CI); wild-type n=18, 67.00(52.97 to 84.14) %; *Syngap1*$^{+/-}$ n=19, 67.00(32.03 to 69.76) %; U=127, p=0.1727). When mice were tested at 11 weeks of age, the median of *Syngap1*$^{+/-}$ mice able to perform a correct spontaneous alternation was reduced compared to wild-type mice but the difference was not significant (Figure 3-13c; two-tailed Mann-Whitney test, median(95% CI); wild-type n=18, 67.00(43.67 to 71.22) %; *Syngap1*$^{+/-}$ n=19, 33(30.97 to 63.77) %; U=141.5, p=0.3633).

The findings described here are in contrast with previously published data. The mice tested with this paradigm did not show an overall impairment in working memory.

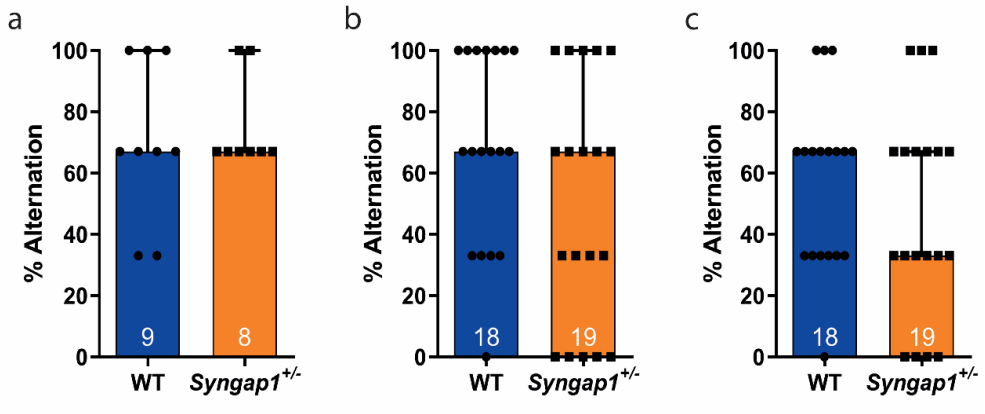

Figure 3-13. Syngap1$^{+/-}$ mice did not show differences in working memory compared to wild-type controls.
Percentage of alteration events of wild-type (WT) and *Syngap1*$^{+/-}$ mice at 4 weeks of age (a), 7 weeks of age (b) and 11 weeks of age (c). Circles and squares represent single animals. Numbers within the bars represent the n of each group.
Two-tailed Mann-Whitney test, data presented as median and 95% CI.

3.4.5 Marble burying

An aspect of *Syngap1*$^{+/-}$ mice behaviour not previously explored is repetitive behaviour. A common sign of repetitive behaviour is increased self-grooming, which usually manifests with bald patches on the animal. Although in our colony mice occasionally presented a patch of absent fur, this was not particular to the *Syngap1*$^{+/-}$ genotype.

Marble burying is a widely used test in which the interaction with the marbles is quantified based on how many objects have been buried in the bedding after a defined amount of time. An increased level of burying can be associated with the presence of repetitive behaviour (Thomas *et al.*, 2009), and this test has been previously adopted in published works to evaluate the presence of such behaviour in mouse models of autism (Silverman *et al.*, 2010).

At 4 weeks of age, *Syngap1*$^{+/-}$ mice showed a reduced burying phenotype, with only 2 mice burying one or more marbles out of 10. Wild-type mice tended to interact more with the marbles, although the number of buried objects resulted low as well

(Figure 3-14a; two-tailed Mann-Whitney test, median(95% CI); wild-type n=9, 2(0.64 to 2.92); *Syngap1*$^{+/-}$ n=8, 0.00(-0.25 to 1); U=16.50, p=0.0468).

At 7 and 11 weeks of age, both genotypes interacted more with the marbles (measured solely by the number of buried marbles) with high intra-group variability. At 7 weeks, genotypes performed significantly different during the task, with *Syngap1*$^{+/-}$ mice burying fewer marbles compared to wild-type mice (Figure 3-14b; two-tailed Mann-Whitney test, median(95% CI); wild-type n=17, 7.00(4.36 to 7.52); *Syngap1*$^{+/-}$ n=18, 4.00(1.97 to 5.14); U=79.50, p=0.0136). However, the genotype difference was not present at 11 weeks with mice of both genotypes burring a similar number of marbles (Figure 3-14c; two-tailed Mann-Whitney test, median(95% CI); wild-type n=18, 7.00(4.14 to 7.52); *Syngap1*$^{+/-}$ n=19, 6.00(3.07 to 6.72); U=144.3, p=0.4257).

The increased interaction with the marbles in subsequent exposures to the task could be associated with increased habituation to the setup that would lead to a decreased cage exploration and to increased attention/interaction with the marbles. Mice at 4 weeks of age were not habituated to the testing cage prior to the exposure to the marbles and this could explain the observed result.

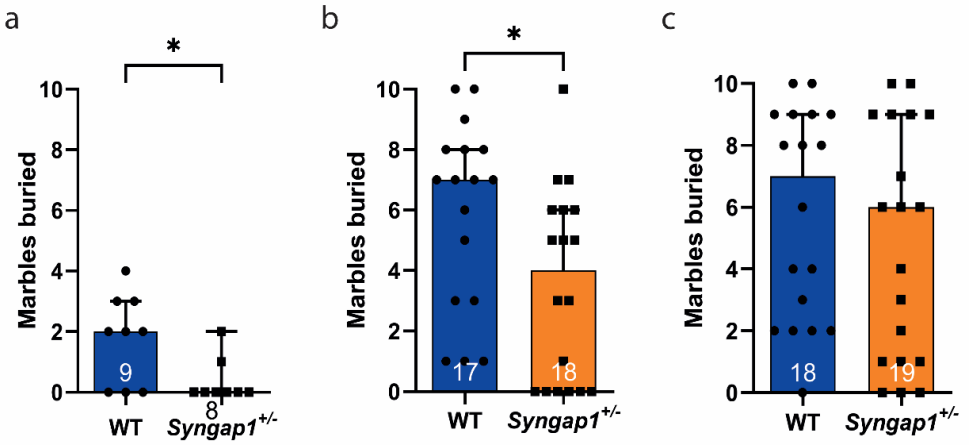

Figure 3-14. The marble burying test did not show repetitive behaviour in Syngap1$^{+/-}$ mice.

The number of marbles buried by wild-type (WT) and *Syngap1*$^{+/-}$ mice at 4 weeks of age (a), 7 weeks of age (b) and 11 weeks of age (c). Circles and squares represent single animals. Numbers within the bars represent the n of each group.
Two-tailed Mann-Whitney test, data presented as median and 95% CI. * p<0.05.

3.4.6 Nest building

As previously discussed in Chapter 1, *Syngap1*$^{+/-}$ mice present a lack of LTP (Kim *et al.*, 2003; Komiyama *et al.*, 2002; Ozkan *et al.*, 2014) and circuital abnormalities (Clement *et al.*, 2012; Ozkan *et al.*, 2014) in the hippocampus. Previous work suggested that dysfunctions in this brain region are linked to the development of hyperactivity (Bast *et al.*, 2003; Gray *et al.*, 1983) and impairments in the nesting and burrowing ability (Cunningham *et al.*, 2003). Decreased ability to build complex nests has been widely described in mouse models of autism (Delorey *et al.*, 2008; El-kordi *et al.*, 2013; Han *et al.*, 2012; Moretti *et al.*, 2005).

Rodents, like many animals in general, present the innate behaviour to build a nest using materials found in the environment. For laboratory animals, the complexity and structure of the nest built using the environmental enrichments present in the cage, has been used to evaluate mice's well-being and social behaviour (Moretti *et al.*, 2005). However, as it involves shredding and building, it can also be used to measure motor functions (Deacon, 2006a).

Muhia *et al.* (Muhia *et al.*, 2010) showed that *Syngap1*$^{+/-}$ female mice, but not male, perform poorly during the rotarod test, with shorter latency to fall. In this published work, it is unclear if this deficit is the consequence of motor impairments and/or lack of coordination, or a tendency of the heterozygous mice to jump from the rotating treadmill. Although this deficit was observed only in female *Syngap1*$^{+/-}$ mice, it was interesting to evaluate the presence of a motor deficit in our colony. The observed phenotype may be influenced by hyperactivity, as the rotarod test involves locomotion and measure motor learning, coordination and balance (Pritchett *et al.*, 2003). Even though it is difficult to predict how hyperactivity can affect a test in which locomotion is not part of the measured output, I hypothesised that the nest building test could be only minimally affected by the increased locomotion present in *Syngap1*$^{+/-}$ mice.

In this test, a score is assigned to each nest, from 0 (untouched material) to 5 (dome-like shape) (Chapter 2). An average score lower than that observed in wild-type controls would suggest motor deficits in the *Syngap1*$^{+/-}$ mice.

At 4 weeks of age, due to the low number of subjects included, the test was likely to be underpowered therefore no statistical analysis will be presented for this time point (Figure 3-15a). At 7 weeks of age *Syngap1*$^{+/-}$ and wild-type mice behaved similarly, with an average nest score of ~2 (Figure 3-15b; two-tailed Mann-Whitney test, median(95% CI); wild-type n=14, 2.12(1.78 to 2.80); *Syngap1*$^{+/-}$ n=15, 2.00(1.71 to 2.55); U=95, p=0.6681). At 11 weeks of age, the *Syngap1*$^{+/-}$ mice nest score was significantly lower compared to wild-type controls (Figure 3-15c; two-tailed Mann-Whitney test, median(95% CI); wild-type n=18, 2.25(2.01 to 2.74); *Syngap1*$^{+/-}$ n=19, 2.00(1.14 to 2.01); U=88.50, p=0.0082).

Overall, although a difference was observed at 11 weeks of age, the absence of a difference at an earlier time point might suggest that motor functions are not influenced by genotype.

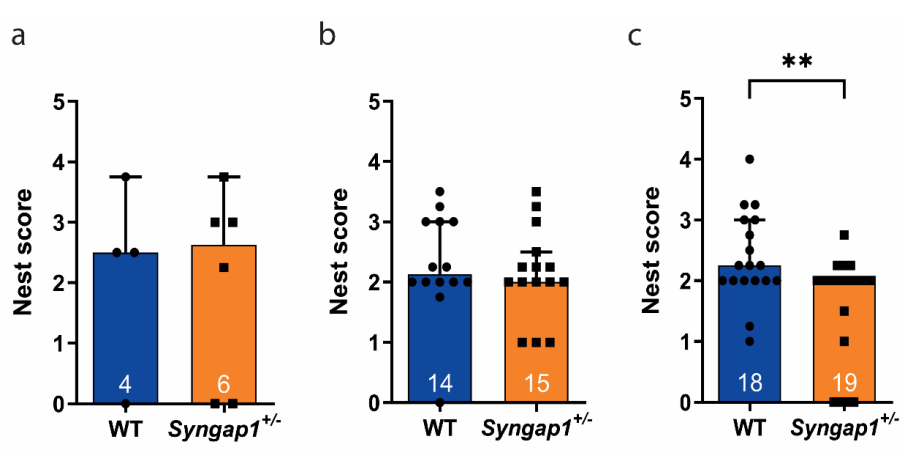

Figure 3-15. The nest building test did not identify a strong genotype difference.
Nest of wild-type (WT) and *Syngap1*$^{+/-}$ mice at 4 weeks of age (a), 7 weeks of age (b) and 11 weeks of age (c). Circles and squares represent single animals. Numbers within the bars represent the n of each group.
Two-tailed Mann-Whitney test result presented as median and 95% CI. ** p<0.01.

3.4.7 Risk-taking behaviour

A decreased sense of risk, such as climbing and jumping from heights, is a characteristic reported by patients families (Weldon *et al.*, 2018). Interestingly, ADHD, which is often described in MRD5 patients, has been associated with a decreased sense of risk and impulsivity (Dekkers *et al.*, 2016).

Risk-taking like behaviour has been recently described in *Syngap1*$^{+/-}$ mice by Kilinc *et al.* (Kilinc *et al.*, 2018) by modelling the reduction of fear of heights or reduced suppression of impulsivity using a platform departure paradigm defined as the cliff avoidance test. For this test, mice are placed on a high object and allowed to explore and leave the platform for 10 minutes. It is considered risk-taking behaviour if they show increased departure compared to wild-type controls.

A possible explanation for this behaviour could be a visual misperception of the drop, and in this case, an increased number of departures would not be connected to increased risk-taking behaviour. However, previous work showed that *Syngap1*$^{+/-}$ mice are able to identify a submerged platform (Morris water maze, Komiyama *et al.*, 2002) and can perform object recognition tasks (Muhia *et al.*, 2010), suggesting the absence of vision impairments.

It is important to note that volume reduction in some cortical areas, in particular the visual cortex, has been described in *Syngap1*$^{+/-}$ mice by Kilinc *et al.* (Kilinc *et al.*, 2018). Although *Syngap1*$^{+/-}$ mice are not blind as mentioned before, they might present an imperfect depth perception.
As depth perception has never been investigated in *Syngap1*$^{+/-}$ mice, I sought to investigate this using the visual cliff paradigm (Gibson *et al.*, 1960). In parallel, I investigated if the risk-taking behaviour described by Kilinc *et al.* (Kilinc *et al.*, 2018) was reproducible in our colony.

Based on results presented earlier in the chapter, time points for all further tests were changed to 7 and 15 weeks.

3.4.7.1 Visual Cliff

The visual cliff, first described by Gibson *et al.* (Gibson *et al.*, 1960), has been used to evaluate depth perception in humans and animals. Subjects are placed in an area composed of a transparent floor under which is placed a patterned floor, usually checkerboard-like. The arena is then divided into two areas, one where the transparent floor is placed in direct contact with the patterned floor, here defined as "shallow", and one where the patterned floor is placed at 30 cm below the arena transparent floor, here defined as "deep", forming the visual cliff. Upon presentation of the visual cliff, the subject's behaviour is recorded.

In this paradigm four parameters were recorded:

- total distance travelled in the given time and number of transitions between the areas, as a measure of hyperactivity.
- time to first in the deep, as a measure of risk-taking behaviour and to assess depth perception.
- percentage of time spent in the deep, as a measure of anxiety.

The animals tested at 7 and 15 weeks were naïve mice with no prior exposure to this paradigm or any other tests.

As observed in both the open field test and in the elevated plus maze, *Syngap1*$^{+/-}$ mice present a significant increase in distance travelled (Figure 3-16a; two-tailed Student t-test with Welch's correction, mean ± SEM; wild-type n=17, 1617 ± 161.1; *Syngap1*$^{+/-}$ n=10, 2682 ± 216.0; $t_{(17.95)}$=3.953, p=0.0009) as well as in the number of transitions between the two areas (Figure 3-16b; two-tailed Student t-test with Welch's correction, mean ± SEM; wild-type n=17, 18.13 ± 2.17; *Syngap1*$^{+/-}$ n=10, 32.00 ± 3.08; $t_{(17.37)}$=3.678, p=0.0018), indicating that the presence of a cliff did not limit the activity in both sides of the arena. Although *Syngap1*$^{+/-}$ mice, on average, spent more time in the deep part of the arena (Figure 3-16c; two-tailed Mann-Whitney test, median(95% CI); wild-type n=17, 42.64(36.23 to 47.16); *Syngap1*$^{+/-}$ n=10, 32.54(26.21 to 39.24); U=33, p=0.0306), the two genotypes appeared to have a similar response to the presentation of the cliff with a similar time to first in the

deep (Figure 3-16d; two-tailed Student t-test with Welch's correction, mean ± SEM; wild-type n=17, 34.37 ± 12.61; *Syngap1*$^{+/-}$ n=10, 24.30 ± 4.71; $t_{(16.41)}$=0.7481, p=0.4650). One wild-type subject presented a very high latency to first in the deep (~180 seconds), compared to the average of the group (~30 seconds), which could be considered as an outlier. Given the intrinsic variability of behavioural tests, this was not removed from the analysis.

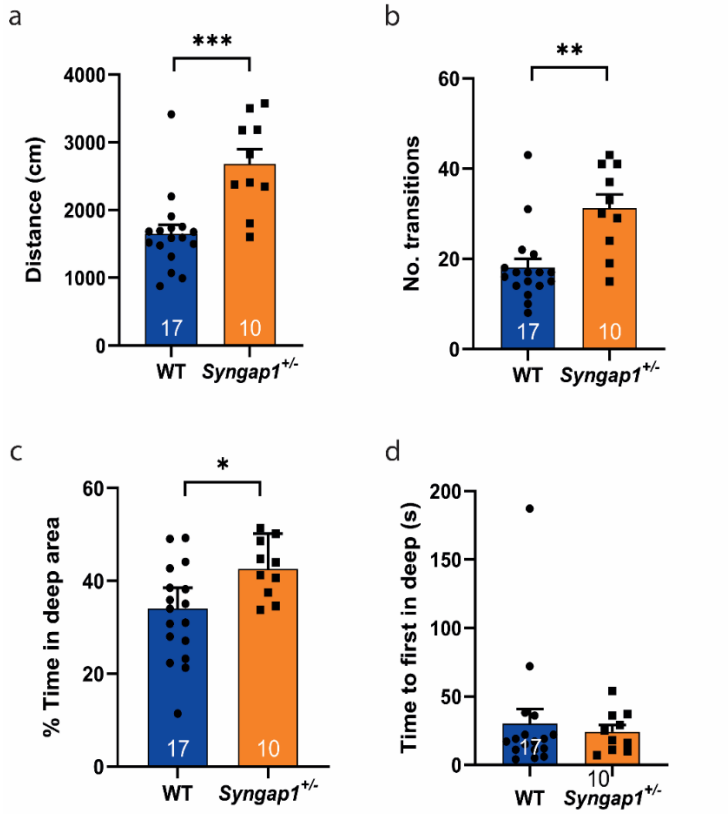

Figure 3-16. At 7 weeks of age, Syngap1*$^{+/-}$ *mice presented a mild preference for the deep area but time to first in the deep was not affected by the genotype.
Distance travelled after 5 minutes (a), number of transitions between shallow and deep area (b), percentage of time spent in the deep area (c) and latency to first cross the border between the shallow and the deep area of the arena (d) by wild-type (WT) and *Syngap1*$^{+/-}$ mice at 7 weeks of age. Circles and squares represent single animals. Numbers within or under the bars represent the n of each group.
a,b,d) Two-tailed Student t-test with Welch correction, data presented as mean ± SEM. c) Two-tailed Mann-Whitney test, data presented as median and 95% CI.
* p<0.05, ** p<0.01, *** p<0.001.

As discussed before, hyperactivity appears to be the most prominent phenotype in *Syngap1*$^{+/-}$ mice. To further investigate how this could potentially influence the

results of the visual cliff test, the correlation between distance travelled, number of transitions and time spent in the deep was investigated.

As expected, transitions strongly correlated with the total distance travelled in both genotypes (Figure 3-17a and b; two-tailed Pearson correlation; wild-type n=17, $r_{(15)}$=0.9513, p<0.0001; *Syngap1*$^{+/-}$ n=10, $r_{(8)}$=0.9808, p<0.0001). In contrast, distance travelled did not appear to be predictive of the amount of time spent in the deep area by the wild-type mice (Figure 3-17c; two-tailed Pearson correlation; wild-type n=17, $r_{(15)}$=0.2402, p=0.3530). In *Syngap1*$^{+/-}$ mice only weak evidence of a correlation was observed (Figure 3-17d; two-tailed Pearson correlation; *Syngap1*$^{+/-}$ n=10, $r_{(8)}$=0.4758, p=0.1646). These results did not compose strong enough evidence to conclude that the phenotype observed during this test was a direct consequence of the hyperactive phenotype in *Syngap1*$^{+/-}$ mice at this age.

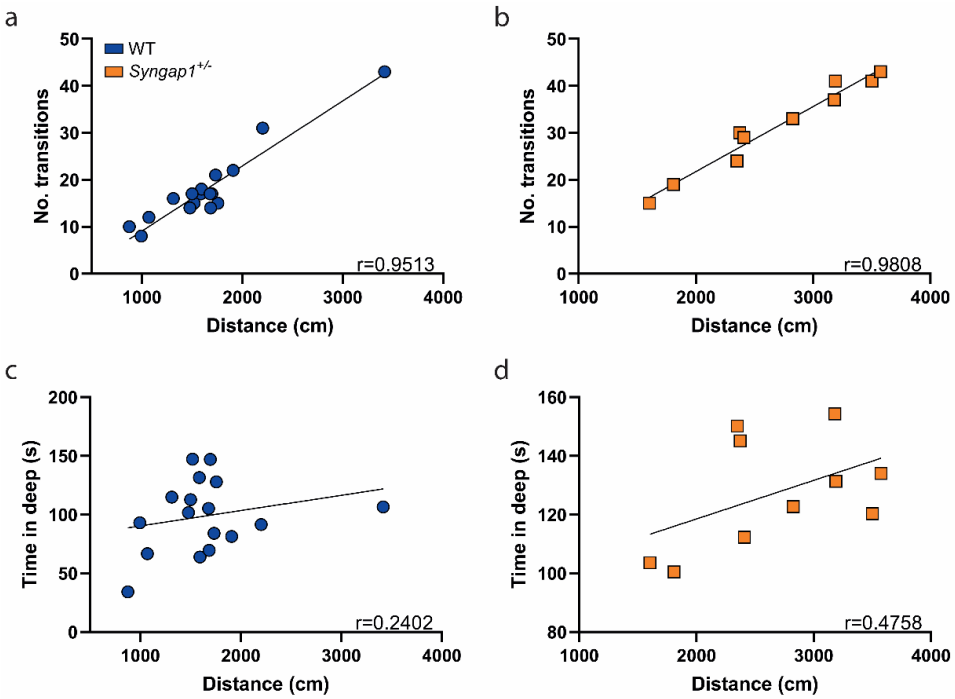

Figure 3-17. At 7 weeks of age, the length of time spent in the deep area was mildly affected by hyperactivity in Syngap1$^{+/-}$ mice.

Correlation between distance travelled and number of transitions between areas for wild-type (WT) (a) and *Syngap1*$^{+/-}$ (b) mice. Correlation between distance travelled and time spent in the deep area for wild-type (c) and *Syngap1*$^{+/-}$ (d) mice. Circles and squares represent single animals. Mice tested at 7 weeks of age.

Two-tailed Pearson correlation. Wild-type n=17, *Syngap1*$^{+/-}$ n=10.

Syngap1$^{+/-}$ mice tested at 15 weeks of age presented an increased horizontal activity (Figure 3-18a; two-tailed Student t-test with Welch's correction, mean ± SEM; wild-type n=17, 1692 ± 106.7; *Syngap1*$^{+/-}$ n=13, 3084 ± 208.1; $t_{(18.19)}$=5.951, p<0.0001) and an increased number of transitions between the areas (Figure 3-18b; two-tailed Student t-test with Welch correction, mean ± SEM; wild-type n=17, 17.35 ± 2.89; *Syngap1*$^{+/-}$ n=13, 35.08 ± 1.53; $t_{(18.57)}$=5.413, p<0.0001). *Syngap1*$^{+/-}$ mice showed also a preference for the deep area, compared to wild-type controls (Figure 3-18c; two-tailed Mann–Whitney test, median(95% CI), wild-type n=17, 25.06(22.55 to 33.72); *Syngap1*$^{+/-}$ n=13, 35.19(30.01 to 46.26); U=57, p=0.0249), but there was no detectable genotype effect in the time to first in the deep area (Figure 3-18d; two-tailed Student t-test with Welch correction, mean ± SEM; wild-type n=17, 25.82 ± 4.00; *Syngap1*$^{+/-}$ n=13, 29.51 ± 5.76; $t_{(26.86)}$=0.5261, p=0.6031).

In both genotypes it was observable a strong correlation between the number of transitions and distance travelled (Figure 3-19a and b; two-tailed Pearson correlation; wild-type n=17, $r_{(15)}$=0.9311, p<0.0001; *Syngap1*$^{+/-}$ n=10, $r_{(11)}$=0.9030, p<0.0001) but distance did not show correlation with the total time spent in the deep area of the arena (Figure 3-19c and d; two-tailed Pearson correlation; wild-type n=17, $r_{(15)}$=0.4418, p=0.0758; *Syngap1*$^{+/-}$ n=10, $r_{(11)}$=0.3931, p=0.2061).

Overall, these results suggested that *Syngap1*$^{+/-}$ mice had a preference for the deep area, which matched with the observation during the elevated plus maze test, although the effect size was relatively small for both time points considered (difference of the mean ± SEM; 7 weeks, 9.62 ± 3.60; 15 weeks, 10.00 ± 4.44). The correlation study did not present strong enough evidence of a direct effect of the hyperactive phenotype over the time they spent in the deep area. As for depth perception, the test did not suggest any difference between genotypes.

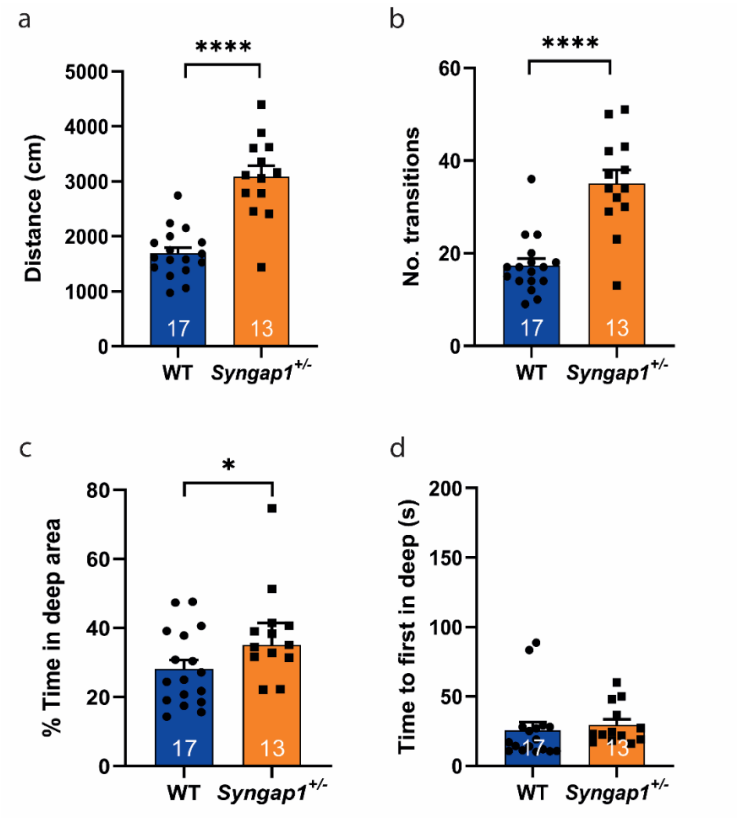

Figure 3-18. Behaviour at 15 weeks recapitulated what was observed at 7 weeks of age.

Distance travelled after 5 minutes (a), number of transitions between shallow and deep area (b), percentage of time spent in the deep area (c) and latency to first cross the border between the shallow and the deep area of the arena (d) by wild-type (WT) and *Syngap1*$^{+/-}$ mice at 15 weeks of age. Circles and squares represent single animals. Numbers within the bars represent the n of each group.

a,b,d) Two-tailed Student t-test with Welch correction, data presented as mean ± SEM. c) Two-tailed Mann-Whitney test, data presented as median and 95% CI.

* $p<0.05$, **** $p<0.0001$.

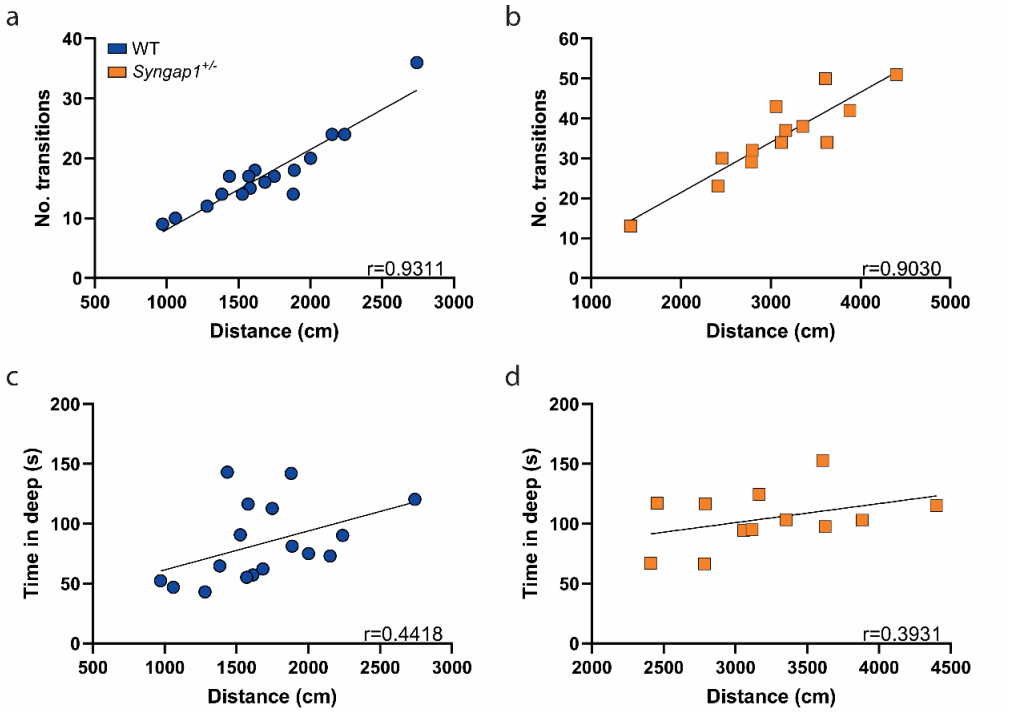

Figure 3-19. At 15 weeks of age, the length of time spent in the deep area was not affected by hyperactivity in Syngap1$^{+/-}$ mice.
Correlation between distance travelled and the number of transitions between areas for wild-type (WT) (a) and *Syngap1*$^{+/-}$ (b) mice. Correlation between distance travelled and time spent in the deep area for wild-type (c) and *Syngap1*$^{+/-}$ (d) mice. Circles and squares represent single animals. Mice tested at 15 weeks of age.
Two-tailed Pearson correlation. Wild-type n=17, *Syngap1*$^{+/-}$ n=13.

3.4.7.2 Platform departure test

Platform departure, or cliff avoidance, test has been previously used to measure impulsive behaviour in mice (Matsuoka *et al.*, 2005) and more recently to evaluate risk-taking like behaviour in *Syngap1*$^{+/-}$ mice (Kilinc *et al.*, 2018).

As a measure of risk-taking behaviour, two events are recorded: the number of partial departures, when the mice are looking over the edge of the platform with both forepaws on the vertical wall; and the number of full departures when the mice leave the platform with the entire body. The time to the first departure was also recorded.

At 7 weeks of age *Syngap1*$^{+/-}$ mice showed a significative increase in the number of partial departures compared to wild-type controls (Figure 3-20a; two-tailed Student t-test with Welch's correction, mean ± SEM; wild-type n=17, 25.94 ± 3.74; *Syngap1*$^{+/-}$

n=10, 65.50 ± 8.48; $t_{(12.57)}$=4.266, p=0.0010). While no wild-type mice never performed a full departure, *Syngap1*$^{+/-}$ mice left the platform multiple times and 50% did it before 5 minutes (Figure 3-20b; median(95% CI); wild-type n=17, 0 ± 3.17; *Syngap1*$^{+/-}$ n=10, 9 ± 3.17; Figure 3-20c; Log-rank (Mantel-Cox) test, wild-type n=17, median time to first=undefined; *Syngap1*$^{+/-}$ n=10, median time to first=5.65. $\chi^2_{(1)}$=13.98, p=0.0002). Due to the absence of variability in the wild-type group in Figure 3-20, no statistical test was performed on this comparison.

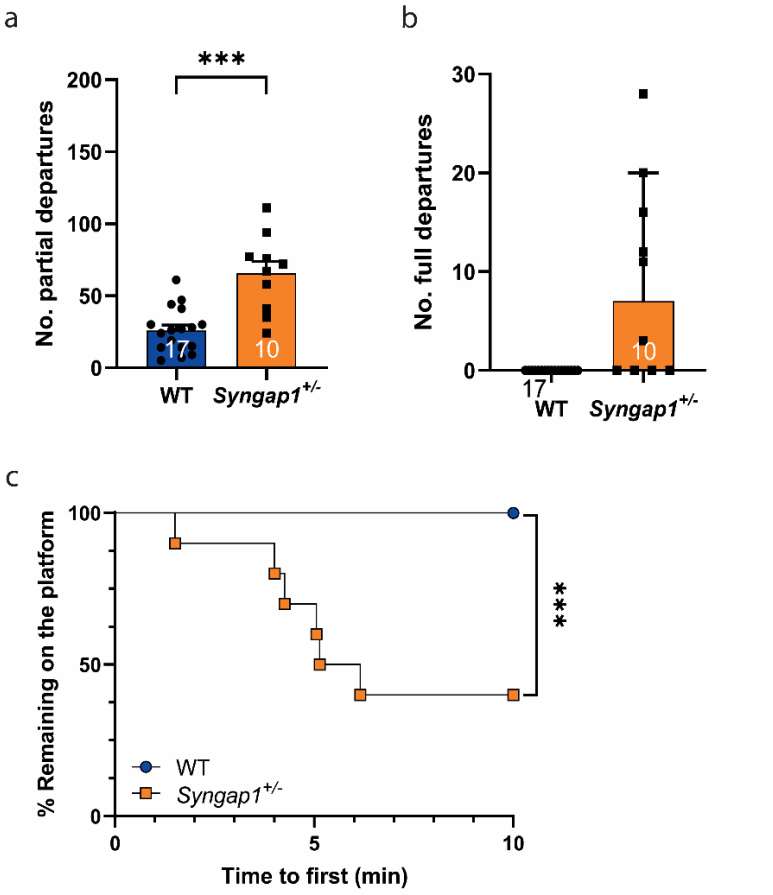

Figure 3-20. At 7 weeks of age, Syngap1*$^{+/-}$ *mice performed more partial and full departures compared to wild-type mice.

Number of partial departures (a), full departures from the platform (b) and percentage of mice remaining on the platform and time to first departure (c) performed by wild-type (WT) and *Syngap1*$^{+/-}$ mice at 7 weeks of age. Circles and squares represent single animals. Numbers within or under the bars represent the n of each group.

a) Two-tailed Student t-test with Welch correction, data presented as mean ± SEM. b) Data presented as median and 95% CI. c) Log-rank (Mantel-Cox) test *** p<0.001.

I evaluated the effect of hyperactivity on the departures performed during the platform departure test. In absence of a more appropriate parameter of activity during this test, the number of partial departures and full departures were correlated to the total distance travelled during the visual cliff. As the same mice have gone through the same tests, distance travelled and departures were matched, and correlation evaluated.

While there was only a mild correlation between the activity in the arena and the number of partial departures among wild-type mice (Figure 3-21a; two-tailed Pearson correlation; wild-type n=17, $r_{(15)}$=0.4265 p=0.0878), a strong correlation was observed in *Syngap1*$^{+/-}$ mice (Figure 3-21b; two-tailed Pearson correlation; *Syngap1*$^{+/-}$ n=10, $r_{(8)}$=0.8267, p=0.0032) suggesting the correlation between the increased number of partial departures and the hyperactive phenotype. On the other hand, the number of full departures did not correlate with the distance travelled for both genotypes (Figure 3-21c and d; two-tailed Pearson correlation; wild-type n=17, $r_{(15)}$=undetermined, p=undetermined; *Syngap1*$^{+/-}$ n=10, $r_{(8)}$=-0.0169, p=0.9630) suggesting that the observed phenotype could be a genuine increased risk-taking like behaviour.

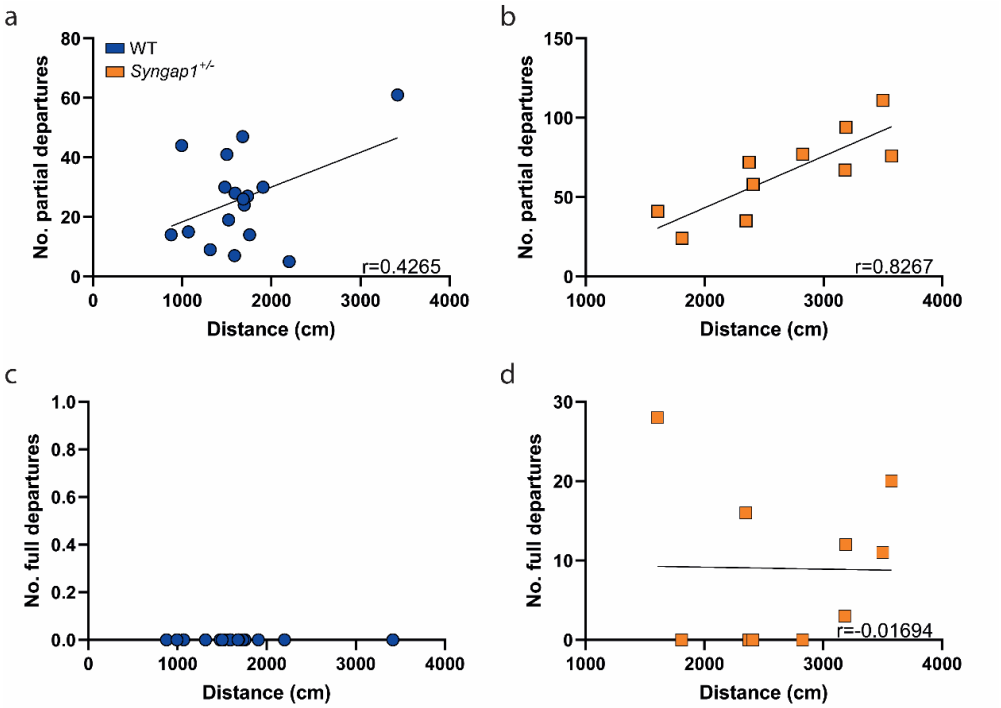

Figure 3-21. At 7 weeks the number of full departures did not correlate with hyperactivity.

Correlation between distance travelled in 5 minutes in the visual cliff arena and number of partial departures from the platform for wild-type (WT) (a) and *Syngap1*$^{+/-}$ (b) mice. Correlation between distance travelled in 5 minutes in the visual cliff arena and number of full departures for the platform from wild-type (c) and *Syngap1*$^{+/-}$ (d) mice. Circles and squares represent single animals. Mice tested at 7 weeks of age. Two-tailed Pearson correlation. Wild-type n=17, *Syngap1*$^{+/-}$ n=10.

At 15 weeks of age *Syngap1*$^{+/-}$ mice showed a significantly higher number of partial departures compared to wild-type controls (Figure 3-22a; two-tailed Student t-test with Welch's correction, mean ± SEM; wild-type n=17, 14.65 ± 1.81; *Syngap1*$^{+/-}$ n=13, 64.38 ± 10.51; $t_{(12.73)}$=4.663, p=0.0005). Similar was observed for the number of full departures (Figure 3-22b; two-tailed Mann-Whitney test, median(95%CI); wild-type n=17, 0.00(-0.24 to 1.54); *Syngap1*$^{+/-}$ n=13, 2.00(1.25 to 7.21), U=59.50, p=0.0145). Furthermore, *Syngap1*$^{+/-}$ mice were more prone to leave the platform sooner compared to wild-type mice (Figure 3-22c; Log-rank (Mantel-Cox) test; wild-type n=17, median time to first=undefined; *Syngap1*$^{+/-}$ n=13, median time to first=6.46. $\chi^2_{(1)}$= =4.897, p=0.0269).

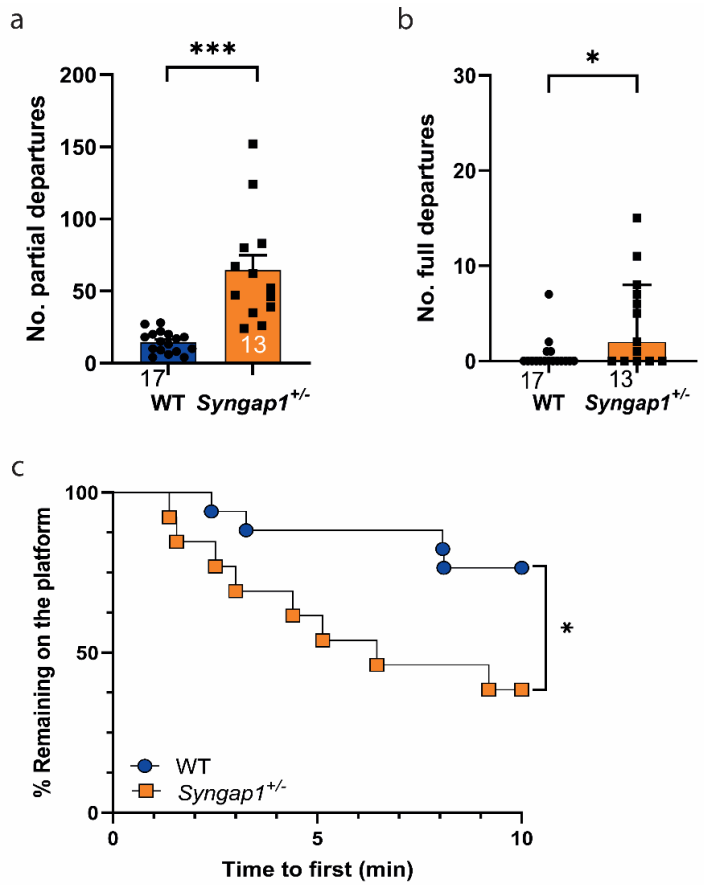

Figure 3-22. At 15 weeks of age, Syngap1$^{+/-}$ mice were more prone to perform partial and full departures compared to wild-type mice.

Number of partial departures (a), full departures (b) and percentage of mice remaining on the platform and time to first departure (c) performed by wild-type (WT) and *Syngap1*$^{+/-}$ mice 15 weeks of age. Circles and squares represent single animals. Numbers within or under the bars represent the n of each group.
a) Two-tailed Student t-test with Welch correction, data presented as mean ± SEM. b) Data presented as median and 95% CI. c) Log-rank (Mantel-Cox) test * $p<0.05$, *** $p<0.01$.

At 15 weeks of age I observed a weak evidence of correlation between horizontal activity and partial departures in both genotypes (Figure 3-23a and b; two-tailed Pearson correlation; wild-type n=17, $r_{(15)}=0.4279$, p=0.0866; *Syngap1*$^{+/-}$ n=13, $r_{(11)}=0.4306$, p=0.1419). The high number of wild-type mice remaining on the platform at 15 weeks of age poses a challenge for the interpretation of the statistical test that needs to be interpreted with caution. Nonetheless, the analysis showed weak statistical evidence of also for full departures in both genotypes (Figure 3-23c

and d; two-tailed Pearson correlation; wild-type n=17, $r_{(15)}$=0.1241, p=0.6351; *Syngap1*$^{+/-}$ n=13, $r_{(11)}$=0.4283, p=0.1400).

While it is not possible to exclude that hyperactivity influences the number of partial departures it appeared that number of full departures was less influenced by the increased locomotion.

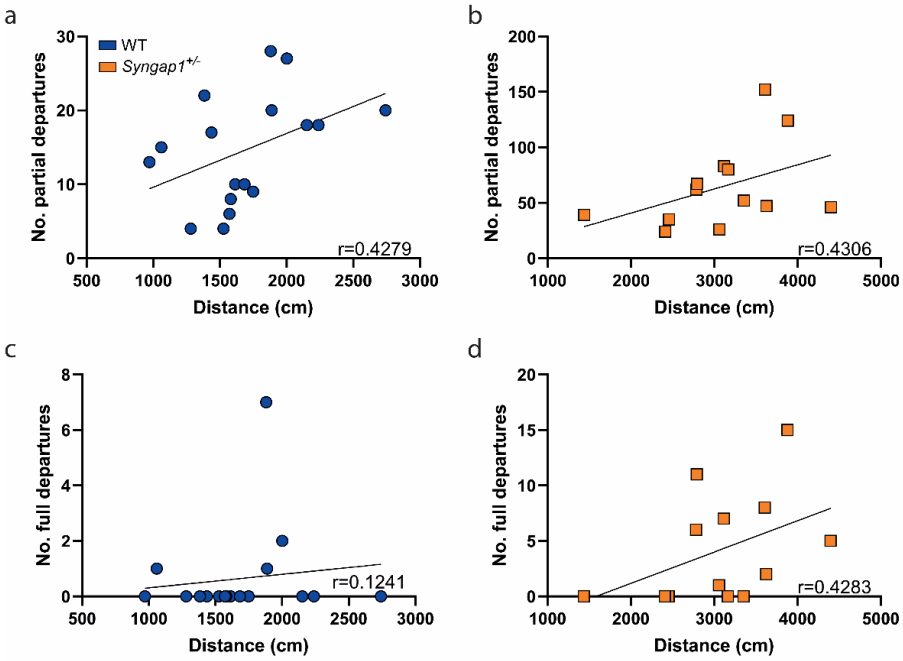

Figure 3-23. At 15 weeks of age, the number of partial and full departures did not show a strong correlation with hyperactivity.
Correlation between distance travelled in 5 minutes in the visual cliff arena and number of partial departures from the platform for wild-type (WT) (a) and *Syngap1*$^{+/-}$ (b) mice. Correlation between distance travelled in 5 minutes in the visual cliff arena and number of full departures from the platform for wild-type (c) and *Syngap1*$^{+/-}$ (d) mice. Circles and squares represent single animals. Mice tested at 7 weeks of age. Two-tailed Pearson correlation. Wild-type n=17, *Syngap1*$^{+/-}$ n=13.

The subjects used for the two developmental time points presented in this section were not the same. Mice exposed to the tests at 7 weeks of age were not retested at 15 weeks therefore the 15 weeks group had no previous exposure to the visual cliff and the platform departure test. For this reason, it was not possible to evaluate habituation at this stage, but it was evaluated during the therapeutic efficacy study presented in Chapter 5.

3.5 DISCUSSION

Since the discovery of the SYNGAP1 protein by Kim *et al.* (Kim *et al.*, 1998) and later with the identification of *SYNGAP1* as a risk factor for ID/ASD, many animal models have been created, independently, by several research groups (Kim *et al.*, 2003; Komiyama *et al.*, 2002; Vazquez *et al.*, 2004) and their behaviour has been extensively studied.

The work presented in this chapter aimed to identify a robust, highly reproducible behavioural phenotyping battery to be used in future therapeutic efficacy studies of candidate viral vectors. To this end, I investigated previously published phenotypes to evaluate their presence in my colony while also studying novel paradigms.
I demonstrated the presence of hyperactivity, anxiety-like phenotypes and risk-taking like behaviour but I was not able to reproduce the working memory impairment observed by Berryer *et al.* (Berryer *et al.*, 2016). As previously shown (Andrews *et al.*, 2018; Bailey *et al.*, 2006), many factors influencing animal behaviour that can potentially impact the reproducibility of phenotypes, such as mouse genetic background, housing conditions, and testing conditions.

In accordance with published data (Berryer *et al.*, 2016; Guo *et al.*, 2009; Komiyama *et al.*, 2002; Nakajima *et al.*, 2019; Verma *et al.*, 2019), I showed that during the open field test, *Syngap1*$^{+/-}$ mice presented a constitutive increased locomotion activity at all three ages considered, while showing a comparable level of intra-trial habituation to the arena to wild-type controls (Figure 3-2, Figure 3-3, Figure 3-4). In contrast to what was previously published (Berryer *et al.*, 2016; Guo *et al.*, 2009; Muhia *et al.*, 2010; Nakajima *et al.*, 2019), *Syngap1*$^{+/-}$ mice did not show a preference for the centre of the arena, except at 4 weeks of age. Decreased time in the periphery has been associated with anxiety reduction, and although *Syngap1*$^{+/-}$ mice spent more time in the centre, there was not enough evidence of a genotype difference.

As previously reported (Berryer *et al.*, 2016; Guo *et al.*, 2009; Muhia *et al.*, 2010; Nakajima *et al.*, 2019), *Syngap1*$^{+/-}$ mice, together with increased locomotor activity,

showed an increased amount of time spent in the open arms of the elevated plus maze at all considered ages (Figure 3-6, Figure 3-8 and Figure 3-10). As suggested before by Dawson *et al.* (Dawson *et al.*, 1995), locomotor activity can affect the readouts of the elevated plus maze test. To this end, I investigated the correlation between horizontal activity and various parameters extrapolated from the elevated plus maze behavioural analyses (Figure 3-7, Figure 3-9 and Figure 3-11). Results suggested that locomotor activity affects the time spent in the open arms in a similar fashion in both genotypes. The effect of hyperactivity was stronger at 7 weeks, where the time spent in the open arms was strongly correlated with distance travelled among *Syngap1*$^{+/-}$ mice. With all considered caveats, horizontal activity does likely affect measures of anxiety to some extent, but this is true for both genotypes. Even though the elevated plus maze is widely considered a valid system for the investigation of anxiety, the discussion on its reliability in presence of hyperactivity is still open to question (Guo *et al.*, 2009; Hogg, 1996; Holmes *et al.*, 2000; Kilinc *et al.*, 2018; Korte *et al.*, 2003; Lister, 1987; Nakajima *et al.*, 2019; Rodgers *et al.*, 1997).

Working memory impairments have been described in *Syngap1*$^{+/-}$ mice by several groups using different experimental designs (Berryer *et al.*, 2016; Clement *et al.*, 2012; Guo *et al.*, 2009; Muhia *et al.*, 2010; Nakajima *et al.*, 2019). In this work, I aimed to evaluate the presence of working memory deficit in my colony using the protocol described by Berryer *et al.* (Berryer *et al.*, 2016), in which working memory was assessed by spontaneous alternations in the T-maze. Despite using the same protocol and mouse line, I failed to observe the same genotype difference.
An explanation could be found in possible environmental differences in which the experiment took place. While for the experiment presented in this thesis was conducted in a dark room, the previous study stated that low light levels were kept.

Another problem that I encountered with the experimental design is the characteristics of the data collected. As alternation was evaluated over three consecutive trials, the alternation percentage that each mouse could achieve was 33, 66 and 100%, producing a not normally distributed dataset. Therefore, I used a non-

parametric test to circumvent the normality issue. It is possible that with such distribution, a weak genotype difference might have not been detected by the analysis. Increasing the number of trials that each mouse performed would create a dataset where each animal can assume a wider spectrum of values, increasing the chances to identify small differences between groups.

Repetitive behaviours, or stereotypies, have been described in many animal models of autism. They can assume different forms, in some cases, they manifest as increased self-grooming, as for *Shank3b*$^{-/-}$ mice (Peça *et al.*, 2011). In others they can be a continuous circling movement that can be driven by increased activity, as in the case of *Scn1a*$^{+/-}$ mice (Han *et al.*, 2012). Although stereotypies have been described in *Syngap1*$^{+/-}$ mice and have been defined as single beam breaks during open field test (Guo *et al.*, 2009; Nakajima *et al.*, 2019), the presence of repetitive behaviour was not been investigated before.

The marble burying test has been considered over the years as a mean to measure anxiety in mice, as it was observed that the administration of anxiolytic drugs led to a reduction of marble buried in a given time (Borsini *et al.*, 2002; Njung'e *et al.*, 1991). More recent studies suggested that the marble burying test measures repetitive behaviour rather than anxiety induced by novelty (Takeuchi *et al.*, 2002; Thomas *et al.*, 2009). To this end, *Syngap1*$^{+/-}$ and wild-type mice were tested using marble burying test, where an increased number of buried marbles compared to wild-type controls is defined as repetitive or compulsive behaviour. Interestingly, *Syngap1*$^{+/-}$ mice buried fewer marbles than wild-type littermates when tested at 4 and 7 weeks, while they presented comparable behaviour at 11 weeks (Figure 3-14). For this test, simple interaction with the marbles, such as sniffing and whisking, was not recorded. As a personal observation, *Syngap1*$^{+/-}$ mice were less interested in the object in the cage and spent most of their time exploring, which is in accordance with the hyperactive phenotype observed in previous experiments.

An increased repetitive behaviour would lead to the burying of more marbles compared to its absence. However, *Syngap1*$^{+/-}$ mice appeared to interact less with the marbles, which allow to exclude the presence of repetitive behaviour in our

cohorts. It is possible also that the result was a direct consequence of little or no habituation to the cage for the first two time points, in conjunction with the high horizontal activity that these mice showed during other tests (open field and elevated plus maze). Hyperactivity could influence the number of marbles that appear buried, running around the cage and stepping on the marbles, could cause them to be pushed under the bedding and, therefore, be counted as buried. However, this was not observed during this test since the number of marbles buried by *Syngap1*$^{+/-}$ mice was lower. It is interesting to note that other knockout mouse models for proteins involved in synaptic maturation/function and neuronal development, that present hyperactivity and reduction of anxiety, exhibit the same tendency to bury fewer marbles compared to wild-type controls (Fox *et al.*, 2013; Katayama *et al.*, 2022; Longatti *et al.*, 2021; Lugo *et al.*, 2014; Moy *et al.*, 2014; Stohn *et al.*, 2016). In particular, the *Grin1* knockout mouse model, while showing over-grooming, marble burying failed to highlight the presence of repetitive behaviour with mutant mice burying fewer marbles compared to wild-type controls (Moy *et al.*, 2014). This might again suggest that hyperactivity could influence the readout of the test. On the other hand, it is possible that the high level of activity reduced the general interest in the novel object and therefore led to a smaller number of buried marbles.

SYNGAP1 patients, in association with ID, ASD and seizures, may present physical features such as ataxia and gait instability (Hamdan *et al.*, 2011; Mignot *et al.*, 2016; Parker *et al.*, 2015; Vlaskamp *et al.*, 2019). While *Syngap1*$^{+/-}$ mice do not present gross physical abnormalities, although a volume reduction of some brain areas has been described (Kilinc *et al.*, 2018), previous publications suggested the presence of motor deficits when tested on the rotarod (Muhia *et al.*, 2010; Nakajima *et al.*, 2019). Muhia *et al.* (Muhia *et al.*, 2010) observed that *Syngap1*$^{+/-}$ female mice perform poorly on the rotarod test, with a shorter latency to fall. After the completion of this study, Nakajima *et al.* (Nakajima *et al.*, 2019) observed a similar phenotype in male *Syngap1*$^{+/-}$ mice. In both publications, it was suggested that the phenotype was caused by motor impairment, although the cause of the fall (jumping from the moving rod, rolling with the rod, or passively rotating with the rod) was not specified.

In the same publications, Nakajima *et al.* (Nakajima *et al.*, 2019) did not observe gait abnormalities and Muhia *et al.* (Muhia *et al.*, 2010) reported no impairments during the hanging wire test. Excluding gait dysfunctions, lack of gross coordination and muscle weakness it is possible that the phenotype observed on the rotarod, if not a direct consequence of hyperactivity, is associated with the loss of more fine motor control.

The nest building test, based on the innate rodent behaviour to build a nest for thermoregulation, reproduction and shelter (Deacon, 2006a; Latham *et al.*, 2004), is generally used to evaluate overall well-being, social behaviour and motor function in mice (Arras *et al.*, 2007; Deacon, 2006a; Huang *et al.*, 2013; Jirkof, 2014), and deficits in this test have been extensively described in animal models of autism (Delorey *et al.*, 2008; El-kordi *et al.*, 2013; Han *et al.*, 2012; Moretti *et al.*, 2005). Interestingly, and contrary to what was observed for the marble burying test, in the nest building test *Syngap1*$^{+/-}$ mice performed as well as the wild-type controls during the first two time points, while at 11 weeks they underperformed (Figure 3-15). As the phenotype was not present across ages it is difficult to determine the cause of the difference. If the underperforming of *Syngap1*$^{+/-}$ mice was due to a genotype effect, we would expect to see a similar difference at all considered ages. It is worth considering that, although nest building was chosen because is a system that might not be affected by hyperactivity, it is not completely possible to exclude its influence. Cage monitoring showed that *Syngap1*$^{+/-}$ mice present increased activity during the dark phase compared to wild-type controls (Nakajima *et al.*, 2019). As young mice are overall more active than older mice, and nest building takes place during the dark phase, it is possible that hyperactivity influence the ability to build the nest more at earlier time points.

A reduced sense of risk is a phenotype reported by parents of MRD5 individuals (Weldon *et al.*, 2018). A previously published paper investigated the presence of this behaviour with a cliff avoidance paradigm in mice at two different ages, PND21 and PND60 (Kilinc *et al.*, 2018), and found that *Syngap1*$^{+/-}$ mice perform a higher number of partial and full departures compared to wild-type controls. Moreover, they

observed that overall, a higher percentage of *Syngap1*$^{+/-}$ mice depart from the platform in the given time. *Syngap1*$^{+/-}$ mice can locate a platform (Komiyama *et al.*, 2002; Muhia *et al.*, 2010), which suggests that they are not blind. On the other hand, Kilinc *et al.* (Kilinc *et al.*, 2018) showed that a reduction of volume in certain brain areas, including many areas related to visual function, is present in *Syngap1*$^{+/-}$ mice. It is possible that this structural modification could lead to visual processing misfunctions, but the presence or the extent of which is currently unknown.

To test both risk-taking like behaviour and depth perception, *Syngap1*$^{+/-}$ mice were subjected to the visual cliff paradigm. Although *Syngap1*$^{+/-}$ mice showed an overall preference for the deep area, they behaved similarly to wild-type controls in terms of the time taken to first enter the deep zone (Figure 3-16 and Figure 3-18). It is likely that once the mice entered the deep area and realized that no physical drop was present, they did not perceive the deep area as different from the shallow area. Therefore, the time to first in deep was used as an indication of risk-taking behaviour and to evaluate depth perception. Mice, and rodents in general, are not prone to jump from heights, and if they are able to correctly understand the presence of the virtual drop, they should not be prone to cross the shallow-to-deep border. While impaired depth perception could induce the subject to not avoid the cliff edge (Desai *et al.*, 2020; Fox, 1965; Niknam *et al.*, 2019), I did not observe differences in this behaviour which would suggest normal depth perception.

The arena design used for this experiment lacked the tactile stimuli of a physical drop. In fact, the arena floor was flat, and the sense of drop was induced only by the difference in the floor pattern. This might have impacted the ability of both wild-type and *Syngap1*$^{+/-}$ mice to fully perceive the drop. To improve the design, a raised platform could be placed over the edge of the cliff, covered with the same pattern used for the floor.

In the platform departure test, I was able to replicate the result reported by Kilinc *et al.* (Kilinc *et al.*, 2018), at both 7 and 15 weeks of age (Figure 3-20 and Figure 3-22). The number of partial departures was higher in *Syngap1*$^{+/-}$ mice, however, it is not possible to exclude that these are a direct consequence of the hyperactive

phenotype, as they showed a strong correlation with the distance travelled during the visual cliff test at 7 weeks of age (Figure 3-21a and b) but not at 15 weeks (Figure 3-23a and b). On the other hand, results suggested that full departures are mostly independent of hyperactivity at both ages tested (Figure 3-21c and d, Figure 3-23c and d). Although it is not possible to exclude the presence of visual processing impairments, it appeared that platform departure is an appropriate test to model risk-taking behaviour in this line.

Intra and inter-trial habituation can affect behavioural outcomes by decreasing or increasing genotype difference if the investigated genotypes respond differently to re-exposure to the same test. It has been shown that different strains show a different level of habituation to the open field after three consecutive days of exposure (Bolivar, 2009). Bolivar and colleagues (Bolivar, 2009) showed that among the considered strains, C57BL/6J presents high intra and inter-session habituation. As shown in Figure 3-5, both wild-type mice and *Syngap1*$^{+/-}$ mice did not show habituation to the open field arena, but the wild-type mice's percentage of time spent in the open arms of the elevated plus maze decreased after re-exposure (Figure 3-12). The inter-session period given to the animals in this experiment might have not been sufficient to avoid habituation, which is a recurrent issue in longitudinal studies such as this.

SYNGAP1 is one of the most abundant protein in the post-synaptic compartment (Chen et al., 1998; Kim et al., 1998), along with PSD95 (Husi et al., 2001; Migaud et al., 1998). Via PSD95, and other scaffolding proteins, SYNGAP1 interacts with NMDAR and works as the principal effector of its signalling pathways (Chen et al., 1998; Kim et al., 1998). Several studies have shown how SYNGAP1 regulates AMPAR trafficking and spine morphology in a NMDAR-dependent manner (Carlisle et al., 2008; Komiyama et al., 2002; Rumbaugh et al., 2006; Vazquez et al., 2004; Walkup et al., 2015). Due to the close relationship between SYNGAP1 and NMADR, it is possible to observe a behavioural phenotypic overlap between NMDAR blockade in rodents and mice carrying mutation of the *Syngap1* gene, such as, reduced life-span (Forrest et

al., 1994; Komiyama et al., 2002), increased horizontal activity and stereotypic movements (Berryer et al., 2016; Facchinetti et al., 1993; Guo et al., 2009; Komiyama et al., 2002; Nakajima et al., 2019; Ozkan et al., 2014; Tricklebank et al., 1989; Wangen et al., 1997), and reduced prepulse inhibition (Guo et al., 2009; Nakajima et al., 2019; Wiseman Harris et al., 2003). Guo and colleagues (Guo et al., 2009) showed that treatment with the NMADR antagonist MK-801 modified the horizontal activity of wild-type mice, while *Syngap1*$^{+/-}$ mice appeared unaffected, suggesting that hyperactivity could be a downstream effect of the impairment of the NMADR-regulated pathways. Further studies will be necessary to understand which phenotypes are associated to the deregulation of such pathways and which are caused by separate regulatory activities of SYNGAP1.

3.6 CONCLUSIONS

This work aimed to identify robust behavioural phenotype outcomes that present throughout development, to allow the testing of therapeutic efficacy at different ages.

It was identified that 7 and 11 weeks of age were the most appropriate time points to consider. At 7 weeks, mice are still considered to be juvenile, but they have lost part of the intrinsic increased activity observable at younger ages. Moreover, testing mice again at 11 weeks allowed more comprehensive monitoring of phenotype and possible adverse effects of the treatments.

The hyperactivity phenotype, measured in the open field, and decreased anxiety-like behaviour, measured in the elevated plus maze, were present in our cohort of *Syngap1*$^{+/-}$ mice at all tested ages. These tests were demonstrated to be effective and unbiased, as an automated tracking system was used. On the other hand, working memory deficits, motor impairments or repetitive behaviours using the T-maze, nest

building and marble burying respectively were not detected. Moreover, the visual cliff did not show depth perception issues in *Syngap1*$^{+/-}$ mice.

Risk-taking-like behaviour was investigated, and it was present at both considered ages. Platform departure test proved to be easily replicable, inexpensive and simple to execute. Although video scoring is not automated, the two recorded events are easily detectable, limiting experimenter error.

In conclusion, based on the results obtained in this work, I decided that the behavioural phenotyping battery for the therapeutic efficacy study would be composed of open field, elevated plus maze and platform departure. Moreover, the data collected in this preliminary work allowed the refinement of testing conditions leading to the identification of the age of testing: 7 and 15 weeks.

CHAPTER 4: *IN VITRO* TESTING OF CANDIDATE THERAPEUTIC CASSETTES

4.1 INTRODUCTION

The aim of the work presented in this thesis was the assessment of the feasibility of a gene therapy approach for the treatment of *SYNGAP1* haploinsufficiency-associated disorder.

Gene therapy is based on the concept that the delivery of a DNA sequence to patients' cells, using viral or non-viral vectors, can prevent or ameliorate symptoms associated with the malfunctioning of a gene (Bulcha *et al.*, 2021). Among the different types of gene therapies available, the work of this thesis aimed to evaluate if a gene replacement approach, which involves the replacement of an existing non-working gene with a functional one, can prevent or ameliorate the symptoms associated with loss-of-function mutations in the *SYNGAP1* gene (Blömer *et al.*, 1996; Bulcha *et al.*, 2021; Ingusci *et al.*, 2019; Shahryari *et al.*, 2019).

To achieve a therapeutic effect, the replacement gene, defined as the transgene, must be expressed in the appropriate tissue and cell type, and delivered at an appropriate time point to maximise phenotypic rescue. Moreover, the level of transgene expression achieved by the therapeutic construct should be as close as possible to the physiological level. The fulfilment of these requirements pose a challenge for the development of effective gene therapies; therefore, it is important to develop rational designs of candidate therapeutic expression cassettes able to behave as similarly as possible to the wild-type gene.

Human *SYNGAP1* encodes for multiple isoforms, all of which contain a common central region composed of the C2 and GAP domains but differ at the N- and C-terminals (Figure 1-1). Five different N-termini, termed A1, A2, B, C and D, are produced by alternative transcription start sites, and four C-termini, α1, α2, β, and γ,

are produced by alternative splicing events (Figure 1-2) (Chen *et al.*, 1998; Gou *et al.*, 2020; Kim *et al.*, 1998; McMahon *et al.*, 2012; Moon *et al.*, 2008).

An early study on isoform functions *in vitro* (McMahon *et al.*, 2012) suggested that each variable N- and C-terminal of SYNGAP1 contribute, independently, to the regulation of synaptic function and strength. In particular, they showed that Aα1 leads to an overall decrease of synaptic strength, Bα2 to an increase while Aα2 showed a neutral effect.

Studies on the relative abundance of isoforms across development suggest a fine temporal regulation of their expression (Gou *et al.*, 2020; McMahon *et al.*, 2012). McMahon and colleagues (McMahon *et al.*, 2012) showed, at the mRNA levels, that A and B N-terminal isoforms expression is stable during the early stages of development, to then peak at PND14 and decrease in adulthood. They also showed that the C isoforms are mostly expressed later in life, with low levels of expression before PND14 and stable expression in adulthood. Gou *et al.* (Gou *et al.*, 2020) instead investigated the temporal expression of C-terminal isoforms. They showed that α1 is the most abundant isoform in adulthood while α2 and β have a higher expression during early stages of development.

SYNGAP1 is a large gene spanning ~34 kb on chromosome 6, with a coding sequence of ~4000 bp, depending on the isoform considered. Large genes impact the choice of functional elements that can be used to drive and regulate transgene expression (primarily a promoter and polyA signal), due to packaging constraints of the delivery vector. AAV has a packaging capacity of ~4700-5000 bp (ITR to ITR), in which a promoter, transgene and polyA signal must be incorporated (Bulcha *et al.*, 2021). Therefore, in a *SYNGAP1* therapeutic cassette, most of the AAV genomic space is taken up by the transgene coding sequence alone. The *SYNGAP1* endogenous promoter, which would be predicted to provide more physiological regulation of transgene expression, has not yet been fully characterised. Well-characterised, constitutive promoters commonly used in gene therapy cassettes, such as CAG or CBh (containing a Cytomegalovirus (CMV) enhancer, chicken beta-actin (CBA) promoter,

and hybrid intron), would be expected to produce a high level of transgene expression. However, the use of these promoters (which are 800-1600 kb in size) with a SYNGAP1 transgene would exceed AAV packaging capacity. Therefore, our choice was restricted to small promoters, in the range of 200-500 nucleotides.

As *SYNGAP1* is primarily expressed in the brain, where it performs its role as a regulator of synaptic function, it was necessary to use a promoter that is known to drive expression in neurons. For this reason, the minimal *Mecp2* promoter, MeP229 (Gray *et al.*, 2011), was initially considered a candidate promoter to drive *SYNGAP1* expression.

MeCP2 is a widely expressed protein that is especially abundant in the CNS, in postnatal neurons (LaSalle *et al.*, 2001). MeP229 is a minimal promoter based on the sequence of the core regulatory element of the murine *Mecp2* promoter, which was developed by Gray *et al.* (Gray *et al.*, 2011) and has been previously utilised to drive transgene expression in gene therapy constructs (Gadalla *et al.*, 2013, 2017).

JeT is a short synthetic promoter created from the combination of functional elements of different promoters. It includes the SV40 early promoter, human ubiquitin C and β-actin promoters transcription binding sites, together with their respective Sp1 transcription factor consensus sequences (Tornoe *et al.*, 2002). It has previously been employed for gene therapy approaches due to its activity in the CNS and relatively high expression compared to promoters of similar size (Bailey *et al.*, 2018; Chen *et al.*, 2022; Gadalla *et al.*, 2017; Tornoe *et al.*, 2002).

4.2 AIM

The rationale of the work presented in this chapter was to design candidate therapeutic cassettes and to evaluate their expression *in vitro* to assess their appropriateness for further *in vivo* studies. To this end specific aims were:

- To generate a candidate therapeutic construct expressing the *SYNGAP1* transgene.
- To evaluate the ability of the chosen promoters to express the SYNGAP1 protein *in vitro*.

4.3 STUDY PLAN

Plasmid MeP229-*hSYNGAP1_Aα1*, MeP229-*hSYNGAP1_Aα2* and MeP229-*hSYNGAP1_Bα1* were designed by Dr Ralph D. Hector and were synthetised by GeneArt (ThermoFisher Scientific, USA). The plasmid JeT-*hSYNGAP1_Aα1* was cloned in-house as described in Section 2.7.

The ability of MeP229 and JeT promoter to drive the expression of SYNGAP1 was evaluated via fluorescence immunocytochemistry and immunoblotting as described in Section 2.10 and Section 2.11. Briefly, HEK293A cells were cultured and transfected with the appropriate plasmid using Lipofectamine 2000 (ThemoFisher Scientific, USA). Subsequently, cells were processed for immunocytochemistry (PFA fixation followed by immunolabelling) or immunoblotting (preparation of cell lysate followed by protein electrophoresis and immunoblotting).

4.4 RESULTS

4.4.1 SYNGAP1 expression was detected *in vitro* after transient transfection with mammalian expression plasmids

As previously mentioned, McMahon and colleagues (McMahon *et al.*, 2012) characterised *in vitro* the activity of three SYNGAP1 isoforms, Aα2, Aα1 or Bα2, suggesting that they modulate synaptic activity differently. Moreover, the expression of these three isoforms appeared to be differentially regulated during development suggesting a development-related function. Given the available data, it was interesting to evaluate the therapeutic effect in *Syngap1*$^{+/-}$ mice of the Aα2, Aα1 or Bα2 isoforms, therefore they were used for the initial design of three candidate therapeutic constructs.

For all constructs, transgene expression was driven by an upstream MeP229 promoter fragment and transcription terminated by the addition of a downstream Synthetic polyA signal (SpA) (Figure 4-1). The SpA was described for the first time by Levitt *et al.* (Levitt *et al.*, 1989), and is a short (50 bp), synthetic polyA signal derived from the rabbit β globin gene.

The Kozak sequence, a conserved nucleotide sequence that serves as protein translation initiation site (Kozak, 1986), is boosted in these constructs by the addition of two cytosine nucleotides between the end of the MeP229 promoter and the ATG start codon of the *SYNGAP1* transgene. The addition of these two cytosine nucleotides to promote transgene expression in a gene therapy cassette was previously described by Grey *et al.* (Gray *et al.*, 2011).

To be able to distinguish transgenic SYNGAP1 protein from endogenously expressed SYNGAP1, a Myc peptide was fused to the C-terminus of the SYNGAP1 transgene (Figure 4-1 and Figure 4-2).

Gene therapy constructs were synthesised and cloned by GeneArt (ThermoFisher Scientific, USA) in two different types of backbone:

- Mammalian expression plasmid pMK.

- AAV expression plasmid pX551.

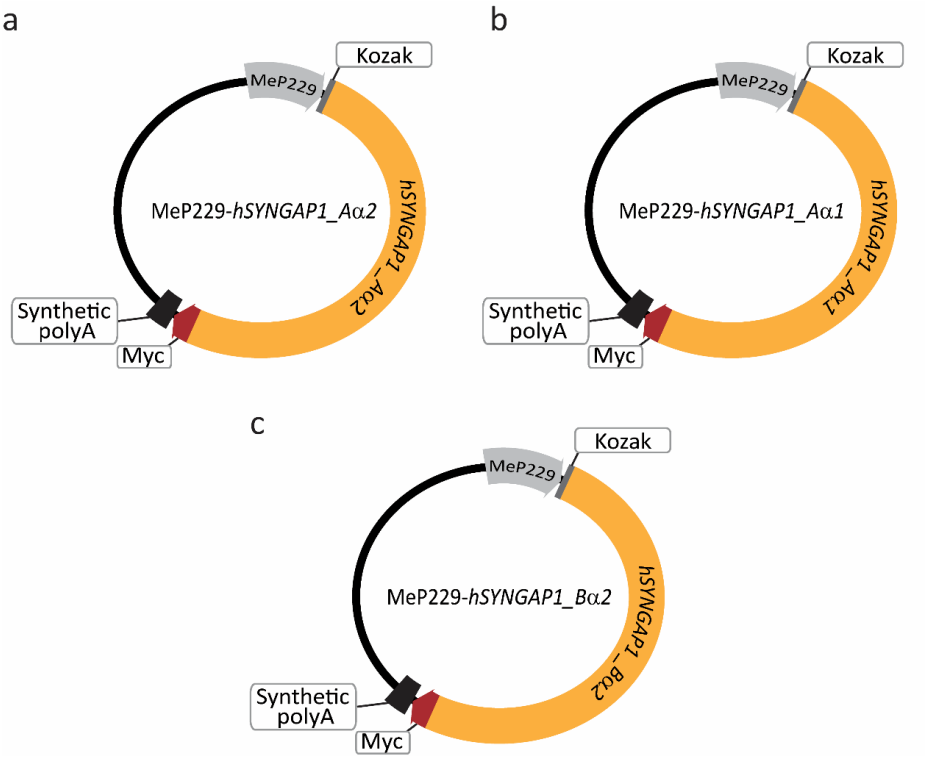

Figure 4-1. Schematic representation of the MePP229-hSYNGAP1 plasmids
MePP229-*hSYNGAP1_Aα2* (a), *Aα1* (b) and *Bα2* (c) plasmids were designed by Dr Ralph Hector and synthesised by GeneArt (ThermoFisher Scientific, USA). pMK and pX551 presented the same expression cassette and differ in the backbone sequence and gene for antibiotic resistance, kanamycin for pMK and ampicillin for pX551.

Figure 4-2. MeP229-hSYNGAP1 plasmids sequence alignment.

Sequences of MeP229-*hSYNGAP1_Aα1, Aα2, Bα2* plasmids aligned using Clustal Omega (EMBL, www.ebi.ac.uk/Tools/msa/clustalo). The promoter sequence is highlighted in grey. Myc sequence is highlighted in dark red and SpA in black, the Kozak sequence is indicated by red underlined characters. The coding sequence, in yellow, is shown only for the 5' and 3' regions which are isoform-specific, "/ /" indicates sequence break. * Indicates nucleotides match.

To evaluate the ability of MeP229 to drive the expression of *SYNGAP1,* an initial *in vitro* experiment was performed using the pMK mammalian expression plasmids. To this end, HEK293A cells were used as they are easily transfected and can express a wide range of transgenes (Chow *et al.*, 2011; Thomas *et al.*, 2005). HEK293A cells were transfected with the MeP229-*hSYNGAP1* pMK plasmids and immunolabelled with anti-SYNGAP1 and anti-Myc antibodies to evaluate transgene expression. Mock-transfected controls were used to verify the specificity of immunolabelling.

As shown by the immunolabelling of the mock-transfected HEK293A cells (Figure 4-3) it appeared that SYNGAP1 was not endogenously expressed or expressed at a subthreshold level. A plasmid expressing MeCP2-Myc (Sinnett *et al.*, 2017) under the control of the same MeP229 promoter used in the candidate therapeutic constructs, was used as a positive control for transfection and promoter activity. The signal associated with the immunolabelling of Myc, in the cells transfected with MeP229-*hSYNGAP1* plasmids*,* was localised in spheroid bodies. These resulted accumulated in the cytoplasm as HEK293A cells do not possess the subcellular compartment where SYNGAP1 is normally shuttled, the synapse. The signal associated with anti-SYNGAP1 antibodies had a similar distribution, although it appeared to be more diffused rather than restricted to the puncta positive for Myc. This difference in the appearance of the labelling could be associated with the intrinsic differences in the detection of the two antibodies more than non-specific labelling.

While MeP229-*hMECP2-Myc* transfection showed a relatively high number of cells positive for Myc, only few cells transfected with MeP229-*hSYNGAP1* plasmids were double positive for SYNGAP1 and Myc immunolabelling (Figure 4-4; mean ± SEM; MeP229-*hSYNGAP1_Aα2*, n=1, 2.40; MeP229-*hSYNGAP1_Aα1*, n=1, 0.64; MeP229-*hSYNGAP1_Bα2*, n=1, 1.26; MeP229-*hMECP2-Myc*, n=1, 14.21). It is important to note that this experiment was initially designed to be only qualitative, therefore no replicates were performed. The quantification reported here refers to only a single experiment with the data points reported in Figure 4-4 referring to the quantification

of multiple fields of view derived from a single immunolabelled coverslip and not acquired randomly.

It is known that the size of the transfected plasmid can affect transfection efficiency (Yin *et al.*, 2005) but, as equimolar amounts of plasmid were used for each transfection mix, likely the difference in the percentage of positive cells was not associated with this. A low level of transgene expression could explain the observed difference. As the image acquisition settings, light source power and exposure, were set up based on the background signal present in the mock-transfected cells, if the intensity of the signal was at the same level as the background noise this would result below detection. Under these circumstances, cells that have been transfected would appear negative even if some protein was being produced from the plasmid.

Overall, these preliminary results suggested that MeP229 was active in HEK293A cells, and it was able to drive expression of the three SYNGAP1 isoforms albeit only to low levels.

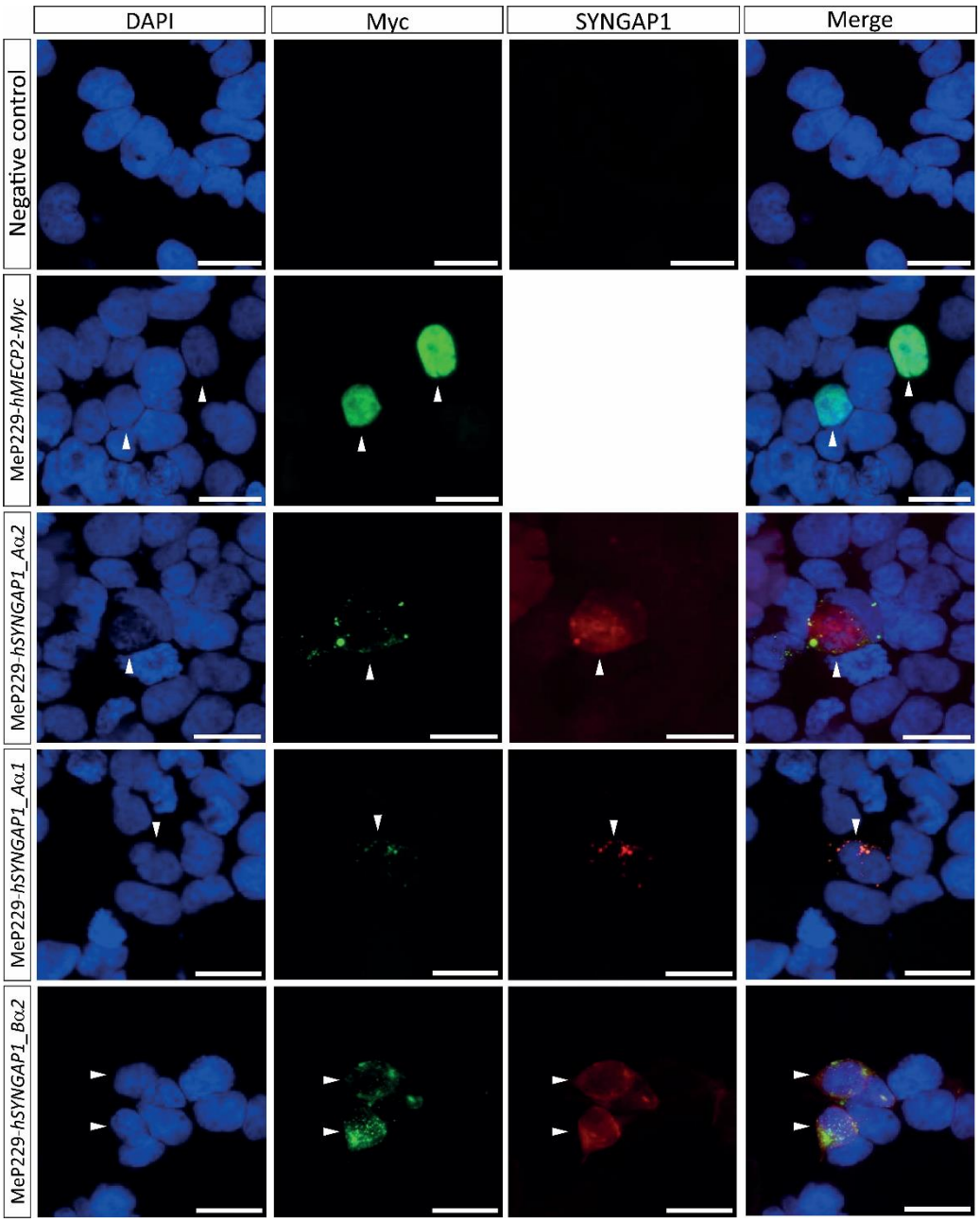

Figure 4-3. Myc and SYNGAP1 expression was detected in vitro after transfection with all three mammalian expression plasmids.

Representative fluorescence immunocytochemistry of transfected HEK293A cells. Negative control indicates mock-transfected cells, MeP229-*hMECP2-Myc* was used as a positive control. White arrowheads indicate cells positive for SYNGAP1 and Myc immunolabelling or only Myc in the case of MeP229-*hMECP2-Myc* transfected cells. Blue: DAPI staining; Green: immunolabelling of Myc; Red: immunolabelling of SYNGAP1. Bars indicate 25μm.

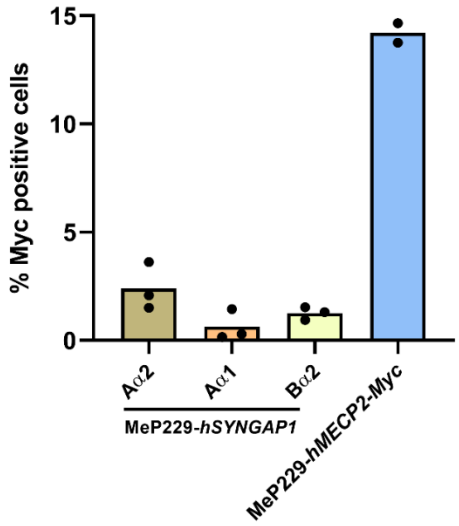

Figure 4-4. The positive control MeP229-hMECP2-Myc presents a number of Myc-positive cells between 6 and 21x higher than MeP229-hSYNGAP1 plasmids.
Quantification of fluorescence immunocytochemistry of HEK293A cells transfected with either the MeP229-*hSYNGAP1* plasmids or the positive control MeP229-*hMECP2-Myc.* The percentage of Myc-positive cells was calculated as the ratio between Myc-positive cells and the number of DAPI-stained nuclei per field of view and expressed as mean. Points represent the quantification of single field of views derived from the same coverslip for each plasmid, data points are not independent. Fields of views used for the quantification were acquired with the 20x or the 40x objective.

4.4.2 Development of an alternative candidate therapeutic construct

Preliminary results from the *in vitro* testing showed that, although the positive control MeP229-*hMECP2-Myc* produced a robust expression of the transgene, only weak expression was obtained from the MeP229-*hSYNGAP1* plasmids. Although MeP229 was able to drive the expression of MeCP2, results suggested that it was less efficient in the expression of SYNGAP1. For this reason, I decided to assess an alternative promoter to drive the expression of the therapeutic construct.

JeT (Tornoe *et al.*, 2002) was chosen as a new promoter due to its proven ability to effectively drive therapeutic transgene expression (Bailey *et al.*, 2018; Chen *et al.*, 2022; Gadalla *et al.*, 2017). It has been described that the presence of certain intronic sequences between the promoter and the transgene can also increase expression (Powell *et al.*, 2015) therefore, in addition to the JeT core, a short synthetic intron of

156 bp was added downstream to the promoter (Kikuchi *et al.*, 2014; de la Garza-Rodea *et al.*, 2011) (Figure 4-5).

Several published works have reported an overall increased neuronal excitability in *Syngap1*$^{+/-}$ mice, which is believed to be one of the underlying causes of the epileptic phenotype in patients (Clement *et al.*, 2012, 2013; Ozkan *et al.*, 2014). McMahon *et al.* (McMahon *et al.*, 2012) showed that expression of the Aα1 isoform in *Syngap1*$^{-/-}$ primary neurons led to a reduction of mEPSC amplitude and frequency. Moreover, compared to the other two isoforms, the expression of Aα1 caused the silencing of a higher portion of transfected neurons.

It is known that the α1 isoforms contain the C-terminal QTRV amino acid sequence which composes the PDZ binding motif necessary for the interaction with the PSD complex (Zeng *et al.*, 2016) but it was not clear yet which could have been the most promising isoform to use for gene therapy application. The presence of the PBM only in the α1-containing isoforms might suggest its prime role in synaptic activity regulation. For these reasons, I decided to move forward with only the Aα1 isoform for the new construct.

a

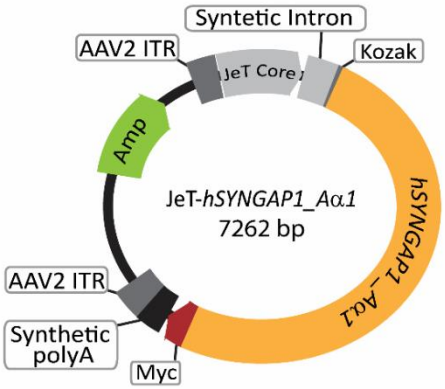

b

cctgcaggcagctgcgcgctcgctcgctcactgaggccgcccgggcgtcgggcgacctttggtcgcccggcctca
gtgagcgagcgagcgcgcagagagggagtggccaactccatcactaggggttcctGGATCCGGGCGGAGTTAGGG
CGGAGCCAATCAGCGTGCGCCGTTCCGAAAGTTGCCTTTTATGGCTGGGCGGAGAATGGGCGGTGAACGCCGATG
ATTATATAAGGACGCGCCGGGTGTGGCACAGCTAGTTCCGTCGCAGCCGGGATTTGGGTCGCGGTTCTTGTTTGT
GGATCCCTGTGATCGTCACTTGGTAAGTCACTGACTGTCTATGCCTGGGAAAGGGTGGGCAGGAGATGGGGCAGT
GCAGGAAAAGTGGCACTATGAACCCTGCAGCCCTAGGAATGCATCTAGACAATTGTACTAACCTTCTTCTCTTTC
CTCTCCTGACAGTCCGGATCCGGAAACCATGAGCAGGTCTCGAGCCTCCATCCATCGGGGGAGCATCCCCGCGAT
GTCCTATGCCCCCTTCAGAGATGTACGGGGACCCTCTATGCACCGAACCCAATACGTTCATTCCCCGTATGATCG
TCCTGGTTGGAACCCTCGGTTCTGCATCATCTCGGGGAACCAGCTGCTCATGCTGGATGAGGATGAGATACACCC
CCTACTGATCCGGGACCGGAGGAGCGAGTCCAGTCGCAACAAACTGCTGAGACGCACAGTCTCCGTGCCGGTGGA
GGGGCGGCCCCACGGCGAGCATGAATACCAC / / AAGAGGCTGCTCGACGCTCAGAGAGGCAGCTTCCCCCC
TTGGGTCCAACAAACCCGCGTGGGATCCGGGCCCTTCGAACAAAAACTCATCTCAGAAGAGGATCTGGTCGACTA
GCGTACGAATAAAGAGCTCAGATGCATCGATCAGAGTGTGTTGGTTTTTTGTGTGGCGGCCGCaggaaccctag
tgatggagttggccactccctctctgcgcgctcgctcgctcactgaggccgggcgaccaaaggtcgcccgacgcc
cgggctttgcccgggcggcctcagtgagcgagcgagcgcgcag

Figure 4-5. JeT-hSYNGAP1_Aα1 plasmid scheme and sequence.
Plasmid scheme (a) and gene therapy construct sequence (b) of the alternative therapeutic construct JeT-*hSYNGAP1_Aα1*. 5' and 3' ITRs are highlighted in dark grey and are shown in lower case characters, JeT core promoter sequence is highlighted in light grey while the synthetic intron sequence is highlighted in light grey and underlined. Myc sequence is highlighted in dark red and SpA in black. Kozak sequence is indicated by red underlined characters. The coding sequence, in yellow, is only shown for the 5' and 3' regions, "/ /" indicates sequence break.

To generate the new JeT-*hSYNGAP1_Aα1* plasmid I used the pX551 AAV expression plasmid MeP229-*hSYNGAP1_Aα1*.

The backbone, of about 2890 bp, presented a unique XbaI restriction site upstream of the MeP229 promoter, while the construct presented a unique BspEI between the end of the promoter sequence and the start of the *hSYNGAP1_Aα1* coding sequence.

These two sites were used for the removal of MeP229 and the cloning of the new regulatory sequences.

The MeP229-*hSYNGAP1_Aα1* plasmid was firstly digested using XbaI and BspEI (Figure 4-6). This allowed the removal of the MeP229 fragment and the linearisation of the plasmid, verified by gel electrophoresis (Figure 4-7). Subsequently, the purified linearized plasmid was ligated with JeT promoter fragment, produced as a gBlock (Integrated DNA Technologies, USA), using the InFusion kit as described in Chapter 2 (Figure 4-6).

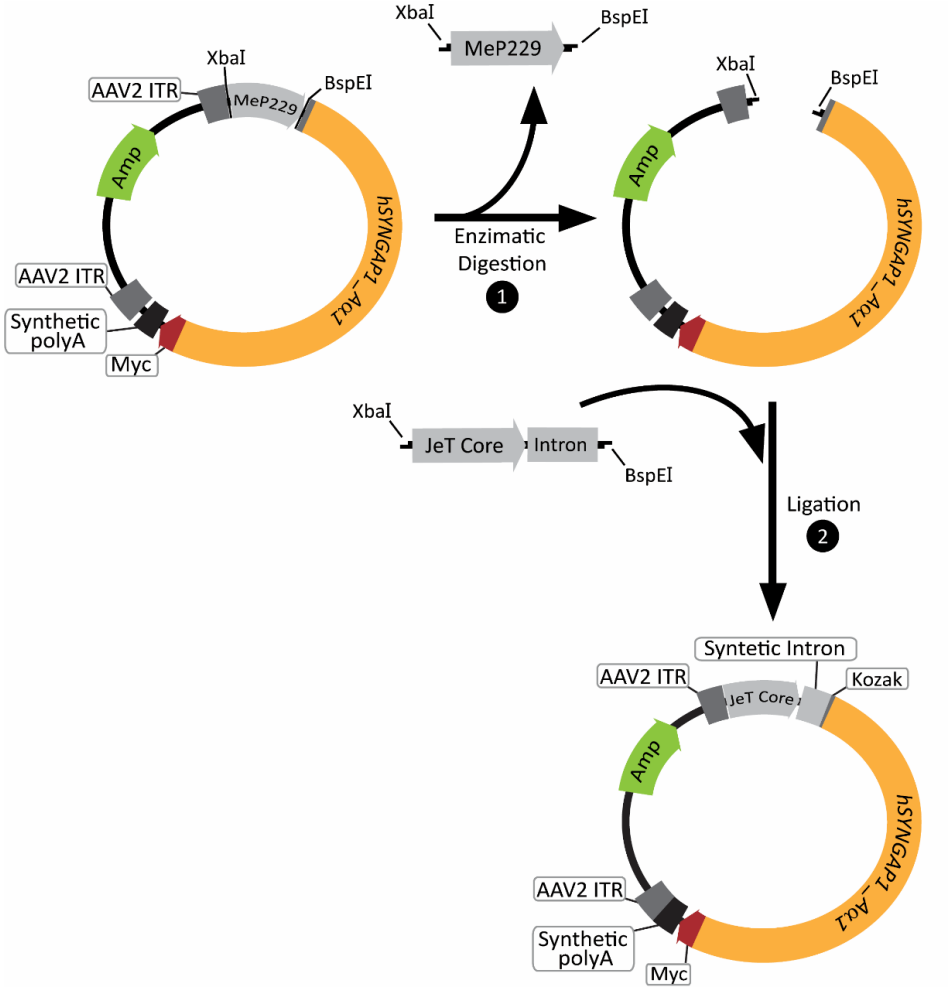

Figure 4-6. Cloning strategy for JeT-hSYNGAP1_Aα1 construct.
Schematic representation of cloning strategy used to produce JeT-*hSYNGAP1_Aα1*. Plasmid coding for *SYNGAP1* Aα1 was digested with XbaI and BspEI for the removal of MeP229 (1). The ligation reaction was then performed to insert the JeT promoter in the linearised plasmid (2). Amp= Ampicillin resistance gene.

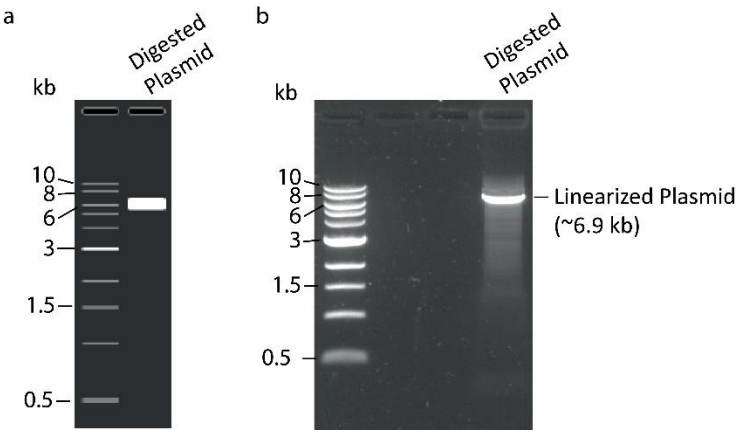

Figure 4-7. Enzymatic digestion of MeP229-hSYNGAP1_Aα1 plasmid.
Predicted (b) and experimentally obtained (c) representative agarose gel showing bands derived from enzymatic digestion of MeP229-*hSYNGAP1_Aα1* plasmid with XbaI and BspEI. 1 kb DNA Ladder (New England Biolab, USA) was loaded in Lane 1 as molecular weight marker.

The ligation reaction was subsequently transformed in competent cells and multiple colonies were picked for plasmid DNA mini amplification.

To ensure the correct structure of the cloned plasmid, purified DNA from each colony was enzymatically digested. ITRs are highly recombinogenic sites therefore an important quality control check is to evaluate that no recombination occurred during bacterial plasmid replication. To this end, purified plasmids were digested with the restriction enzyme SmaI (Figure 4-8). JeT-*hSYNGAP1_Aα1* presents four cutting sites for SmaI, three inside the two ITRs and one in the coding sequence (Figure 4-8a). As a further confirmation of the correct plasmid structure, purified DNA was double digested also with BamHI and EcoRI (Figure 4-8a).

As shown in Figure 4-8b, the pattern and size of fragments obtained matched the predicted pattern after both SmaI and BamHI+EcoRI digestion.

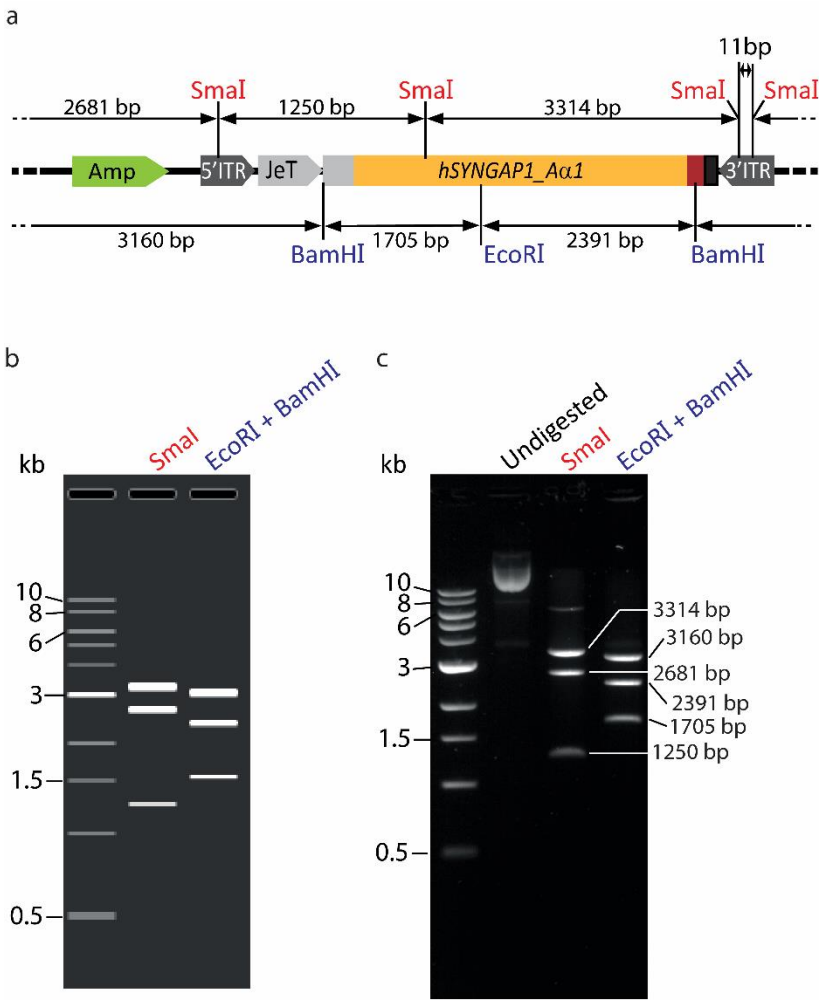

Figure 4-8. Enzymatic digestion for JeT-hSYNGAP1_Aα1 plasmid validation showed the correct insertion of the promoter.

Schematic representation of the JeT-*hSYNGAP1_Aα1* plasmid showing restriction enzyme sites and expected band-size for SmaI, BamHI and EcoRI (a). Predicted (b) and experimentally obtained (c) representative agarose gel showing bands derived from the enzymatic restriction of JeT-*hSYNGAP1_Aα1* plasmid. 1 kb DNA Ladder (New England Biolab, USA) was loaded in Lane 1 as molecular weight marker.

Correct DNA sequence was also confirmed via MiSeq whole plasmid sequencing (sequencing reaction was performed by Ms Amanda Morris and sequence analysis by Dr Paul Ross).

4.4.3 Myc-tagged protein was detectable in HEK293A cells transfected with the JeT-*hSYNGAP1_Aα1* plasmid

The earlier pilot study (Section 4.4.1) was conducted using the gene therapy constructs expressed in the standard mammalian expression plasmid pMK, which do not contains ITRs (Figure 4-1 and Figure 4-2). For viral vector production the presence of the ITRs flanking the therapeutic cassette are necessary as they are required for the viral vector genome packaging. Prior to the viral production, I, therefore, established whether the AAV expression plasmids, which contain the ITRs (Figure 4-9a, b and c), were able to express SYNGAP1 *in vitro.*

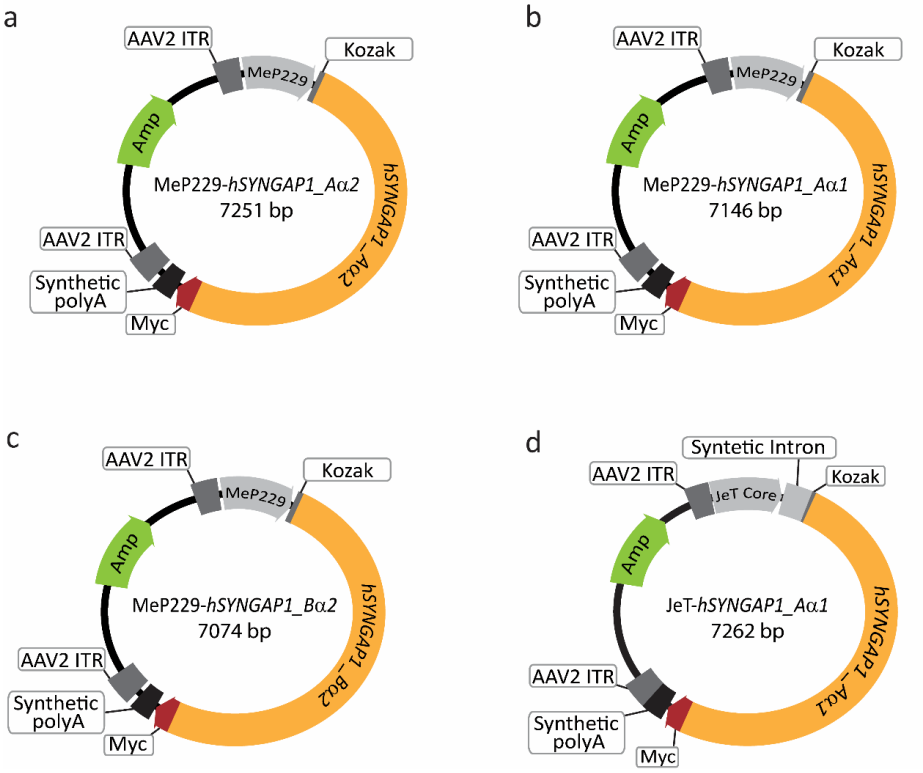

Figure 4-9. AAV expression plasmid schematic representation.
pX551 AAV expression plasmids expressing Aα2 (a), Aα1 (b) and Bα2 (c) retain the same insert present in the mammalian expression plasmid, but in this case, it is flanked by AAV2 ITRs. JeT-*hSYNGAP1_Aα1* plasmid structure (d). Amp=Ampicillin.

The MeP229-*hSYNGAP1* AAV expression plasmids were produced, together with the mammalian expression plasmids, by GeneArt (ThermoFisher Scientific, USA), however, plasmid DNA was further propagated, by mini amplification, in the

laboratory. As mentioned before, ITRs are highly recombinogenic therefore the AAV plasmids were digested with restriction enzymes to verify the integrity of the plasmid and evaluate possible recombination events. To this end, plasmids were digested with either SmaI or EcoRI+HindIII, as shown in Figure 4-10. The gel electrophoresis showed that the pattern of bands obtained after the enzymatic digestion (Figure 4-10e) matched with the expected band pattern (Figure 4-10d), confirming the correct structure of the plasmids.

HEK293A cells were transfected with equimolar amounts of MeP229-*hSYNGAP1_Aα2*, *Aα1, Bα2* and the JeT-*hSYNGAP1_Aα1* AAV expression plasmid together with the positive control plasmid MeP229-*hMECP2-Myc* (Figure 4-11).

Of the five plasmids tested, several Myc-positive cells per field-of-view were detected in cells transfected with MeP229-*hMECP2-Myc* while few sparse faint double positive cells for Myc and SYNGAP1 were detected in cells transfected with JeT-*hSYNGAP1_Aα1*. As shown in Figure 4-11, no signal associated with either anti-Myc or anti-SYNGAP1 immunolabelling was detectable in the cells transfected with the three MeP229 regulated plasmids encoding SYNGAP1 isoforms.

Given that the Myc signal was detected in the positive control MeP229-*hMECP2-Myc* and JeT-*hSYNGAP1_Aα1* transfected cells, it is likely that the absence of positive cells in the MeP229-*hSYNGAP1* transfected cells was not related to the transfection protocol. Nonetheless, although some punctate immunolabeling was detectable for JeT-*hSYNGAP1_Aα1*, this was relatively faint, especially for the anti-SYNGAP1 antibody-associated signal (Figure 4-11).

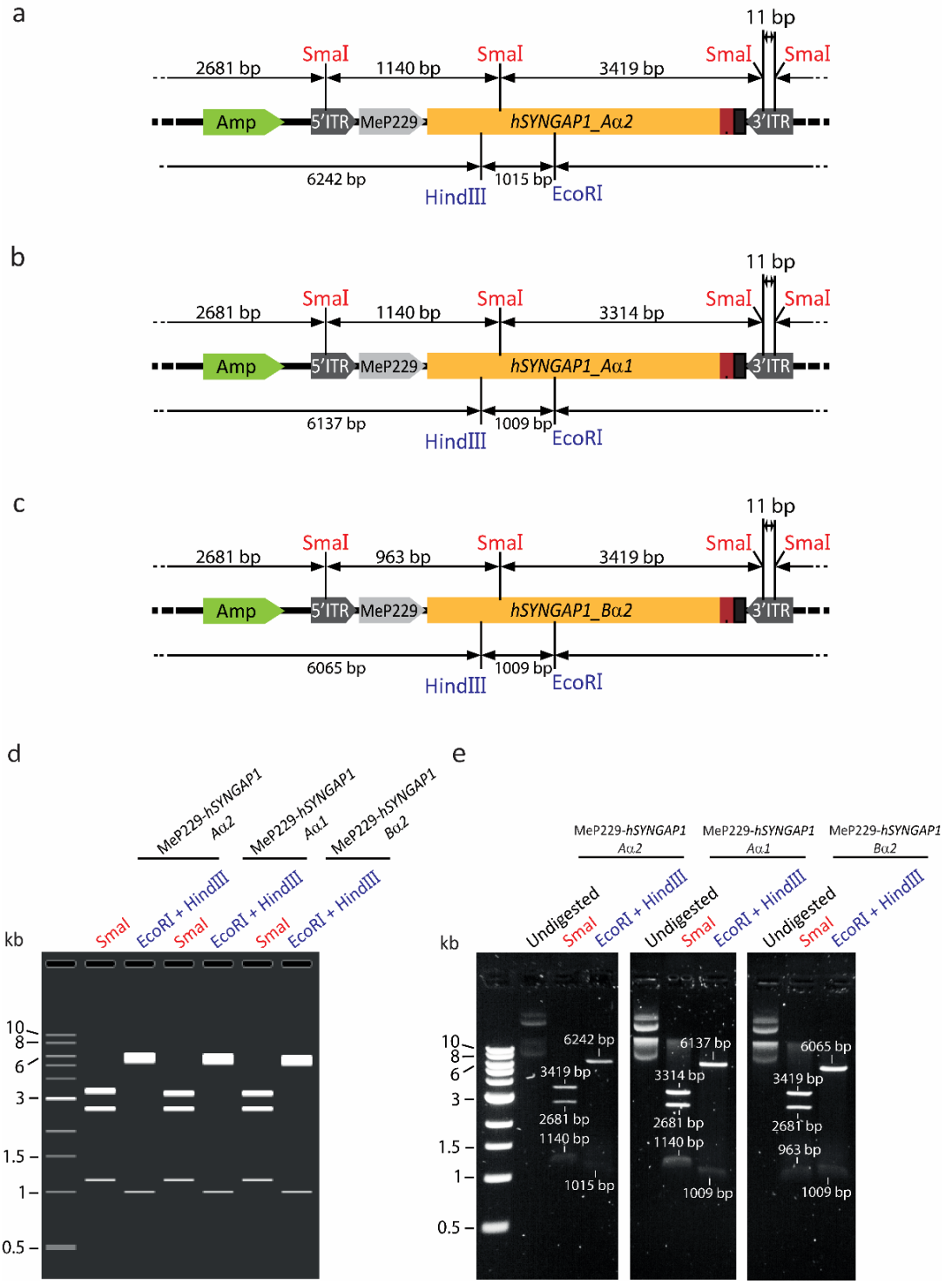

Figure 4-10. Digestion confirms the expected sequence and integrity of the ITRs. Schematic representation of MeP229-*hSYNGAP1_Aα2* (a), MeP229-*hSYNGAP1_Aα1* (b), MeP229-*hSYNGAP1_Bα2* (c) showing restriction enzyme sites and expected band-size after SmaI, BamHI and EcoRI digestion. Predicted (d) and experimentally obtained (e) representative agarose gels showing bands derived from enzymatic digestion. 1 kb DNA Ladder (New England Biolab, USA) was loaded in Lane 1 as molecular weight marker.

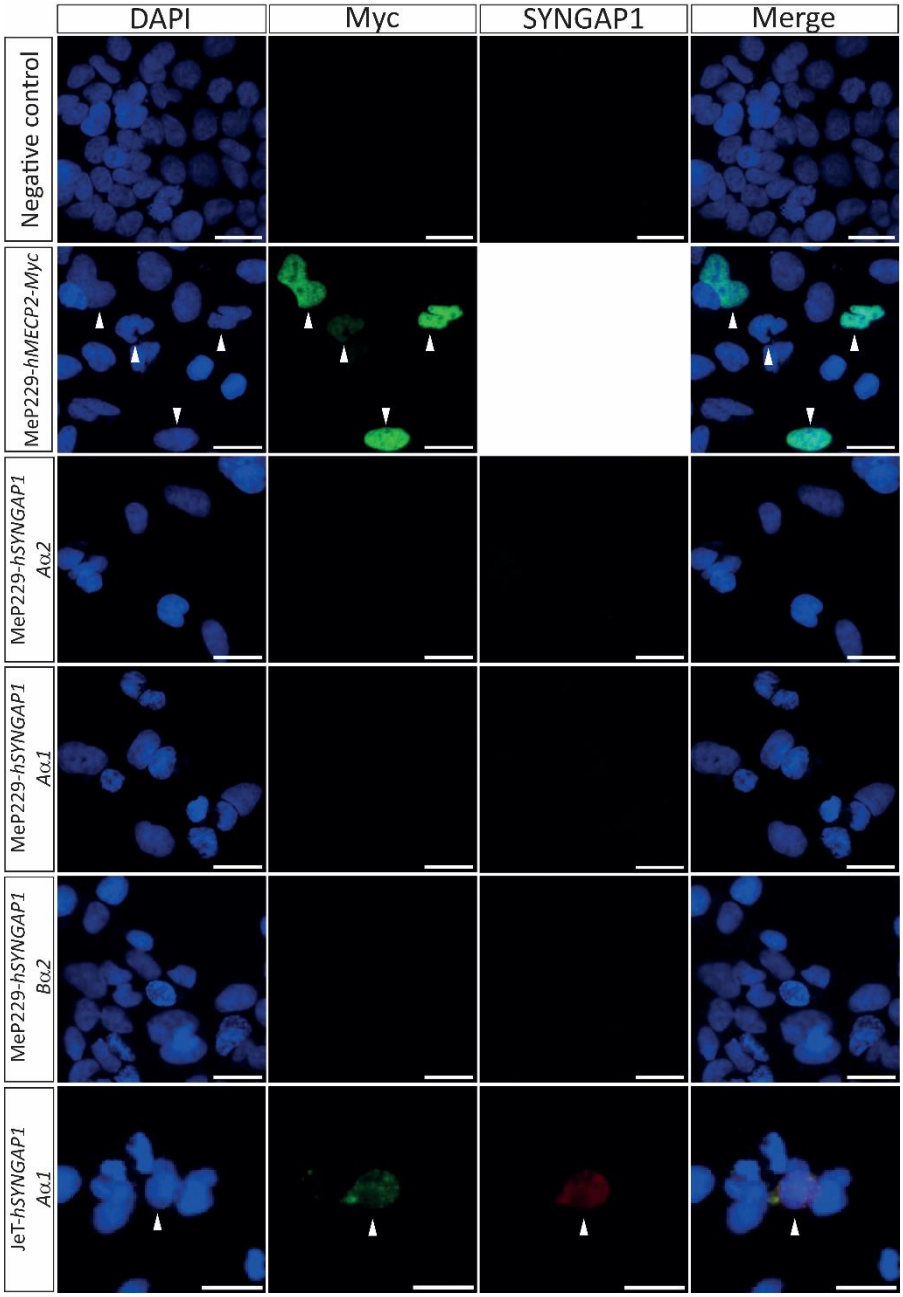

Figure 4-11. Few sparse cells were detected after HEK293A cells transfection with JeT-hSYNGAP1_Aα1 AAV expression plasmid.

Representative images of HEK293A cells transfected with the MeP229-*hSYNGAP1_Aα2*, *Aα1*, *Bα2* and JeT-*hSYNGAP1_Aα1* expressing plasmid. Negative control indicates mock-transfected cells, MeP229-*hMECP2-Myc* was used as a positive control. White arrowheads indicate cells positive for SYNGAP1 and Myc immunolabelling or only Myc in the case of MeP229-*hMECP2-Myc* transfected cells. Blue: DAPI staining; Green: immunolabelling of Myc; Red: immunolabelling of SYNGAP1. Bars indicate 25μm.

Similarly, to what was discussed for the fluorescence immunocytochemistry experiment presented in Section 4.4.1, the absence of SYNGAP1-Myc-positive cells could be associated with the intrinsic detection threshold of the assay. For this reason, using the same transfection protocol, I decided to test the presence of plasmid-derived SYNGAP1 by immunoblot of protein lysate derived from transfected HEK293A cells.

As shown in Figure 4-12, the positive control MeP229-*hMECP2-Myc* presented an intense Myc-positive band at around 70 kDa while a band at around 150 kDa, positive to both Myc and SYNGAP1, was detected in the protein lysate of JeT-*hSYNGAP1_Aα1* transfected cells. The MeP229-*hSYNGAP1* plasmids produced band with a lower intensity around 150 kDa positive to both Myc and SYNGAP1 (Figure 4-12). Total protein staining, used as a loading control, showed that the amount of total protein loaded in each lane was similar.

Quantification of the signal associated with SYNGAP1 showed that the expression of the transgene driven by JeT promoter was between 70x and 260x higher compared to what was observed in the MeP229 regulated plasmids (Figure 4-13a; mean ± SEM; negative control, n=2, 1.00 ± 0.73; MeP229-*hSYNGAP1_Aα2*, n=2, 3.08 ± 1.04; MeP229-*hSYNGAP1_Aα1,* n=2, 3.34 ± 1.60; MeP229-*hSYNGAP1_Bα2*, n=2, 11.37 ± 0.32; JeT-*hSYNGAP1_Aα1*, n=2, 803.4 ± 159.9).

A similar trend was observable for Myc. Myc signal quantification showed that the JeT-*hSYNGAP1_Aα1* plasmid-derived SYNGAP1 was lower, ~2x, compared to the amount of MeCP2-Myc produced by the MeP229-*hMECP2-Myc* plasmid, but between 38x and 150x times higher than the amount of Myc-tagged protein produced from the MeP229-*hSYNGAP1* plasmids (Figure 4-13b; mean ± SEM; negative control, n=2, 1.00 ± 0.11; MeP229-*hSYNGAP1_Aα2*, 3.80 ± 0.54; MeP229-*hSYNGAP1_Aα1,* n=2, 6.15 ± 4.82; MeP229-*hSYNGAP1_Bα2*, n=2, 24.09 ± 2.69; JeT-*hSYNGAP1_Aα1*, n=2, 928.8 ± 181.2; MeP229-*hMECP2-Myc*, n=2, 1940 ± 290.9). It is important to note that the data points in this experiment refer to technical replicates and are not independent, therefore should be interpreted with caution.

As an intense band was detected for the positive control MeP229-*hMECP2-Myc,* it is likely that the low amount of protein detected in the protein lysate from MeP229-*hSYNGAP1-Myc* transfected cells was not due to the low transcriptional activity of the promoter. Instead, it is possible that the combination of MeP229 and *SYNGAP1* was the driver of such a scarce level of expression.

Together with the strong band around 150 kDa (molecular weight of Aα1 isoform is ~148kDa), fainter bands, positive to both Myc and SYNGAP1, of lower molecular weights were present in the JeT-*hSYNGAP1_Aα1* transfected samples. Apart from the negative control, bands at the same molecular weight, although with a considerably lower intensity, were present also in the other samples. These lower molecular weight bands could have been produced by aberrant transcription or translation of the plasmid, which would give rise to truncated proteins, or caused by sample degradation. As no sequence abnormalities were detected after MiSeq whole plasmid sequencing, samples were likely compromised during preparation and therefore those low molecular weight bands were associated with protein degradation.

These results showed that the MeP229 promoter was active in HEK293A cells and was able to drive the expression of the MeCP2 protein that was detectable above the noise by both fluorescence immunocytochemistry and immunoblotting. Although the signal detected during immunocytochemistry from the JeT-*hSYNGAP1_Aα1* plasmid was relatively low compared to MeCP2 expressing plasmid, few sparse Myc-positive cells were detectable. Moreover, a clear strong band in the JeT-*hSYNGAP1_Aα1* plasmid-treated sample, positive for both Myc and SYNGAP1, was detectable in protein lysates of transfected cells by immunoblotting.

Given these preliminary results, it was decided to not pursue a therapeutic study with MeP229 regulated constructs and instead focus future efforts using JeT-*hSYNGAP1_Aα1*.

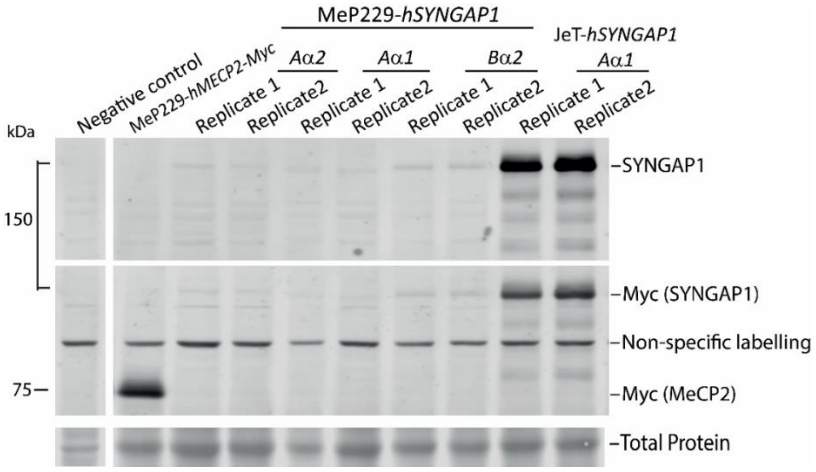

Figure 4-12. Immunoblot of HEK293A transfected cells showed positive bands for all tested plasmids.

Representative immunoblot of protein lysates from HEK293A cells transfected with the MeP229-*hMECP2-Myc,* MeP229-*SYNGAP1_Aα2*, *Aα1*, *Bα2* and JeT-*hSYNGAP1_Aα1* plasmids. The MeCP2 encoding plasmid was used as a positive control for transfection and for blotting. The total protein is shown as a loading control. Image used for quantification is reported in Figure S-26. Replicates refer to samples derived from different wells seeded with the same transfection mix. The gel was used at a concentration of bis-acrylamide of 8%.

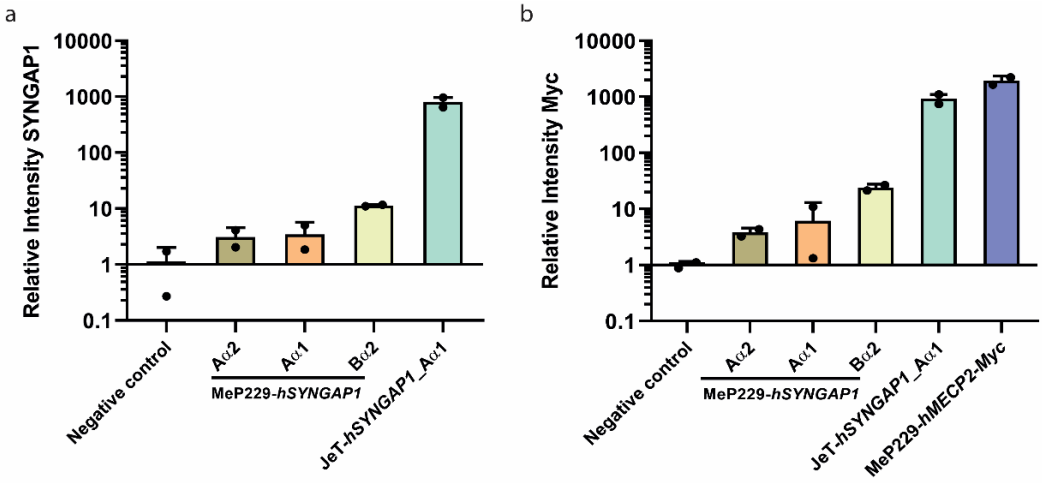

Figure 4-13. The JeT promoter was able to drive a higher expression of SYNGAP1 compared to the MeP229 promoter.

Quantification of SYNGAP1 (a) and Myc (b) signal in transfected HEK293A cells protein lysate. SYNGAP1 and Myc-positive bands relative intensity was first normalised to the total protein staining and subsequently normalised on the relative signal detected in the negative control. Negative control indicates mock-transfected cells. Log_{10} scale is used for the y axes, data are represented as mean ± SEM. Points represent technical replicates.

4.5 DISCUSSION

The rationale of the work presented in this chapter was to assess the expression of different *SYNGAP1* isoforms, reported to cause physiologically distinct effects, (McMahon *et al.*, 2012) in a gene therapy context. To this end, constructs expressing three different SYNGAP1 isoforms, Aα1, Bα2 and Aα2 were designed. Before moving to the *in vivo* testing of therapeutic efficacy, the ability of the designed constructs to express the SYNGAP1 isoform encoded by the transgene was tested *in vitro* in HEK293A cells.

The experiments showed that, despite being able to detect plasmid-derived SYNGAP1 from the MeP229 promoter (Gray *et al.*, 2011) regulated mammalian expression plasmids (Figure 4-3), this result was not reproduced with the AAV expression plasmids (Figure 4-11). On the other hand, SYNGAP1 protein was detectable from the plasmid encoding the Aα1 isoform under the control of the JeT promoter (Figure 4-11 and Figure 4-12) (Tornoe *et al.*, 2002).

The *in vitro* system chosen to test the ability of the candidate therapeutic cassette to express SYNGAP1 was HEK293A cells. HEK293 cell lines have been commonly used for the production of recombinant proteins, among which many neuronal markers such as neurotransmitter receptors and ion channels, due to their ease of transfection and ability to perform the post-translational modification and folding necessary to produce functional proteins (Thomas *et al.*, 2005). HEK293 cells have also been extensively used for functional studies of opsins (Chow *et al.*, 2011). Moreover, HEK293T cells were used in several publications for the expression of SYNGAP1 (Araki *et al.*, 2015, 2020; Zeng *et al.*, 2016). Although the absence of the synaptic compartment does not allow to study the plasmid-derived protein subcellular localisation and functionality, as the aim of this work was to only evaluate therapeutic cassette expression, this system was deemed appropriate for the aim.

An initial pilot study was conducted using the mammalian expression plasmids that differ from the AAV expression plasmid with respect to the backbone sequence and the absence of ITRs. This preliminary study showed that, albeit very weakly, the

MeP229-*hSYNGAP1* plasmids were able to express the three different SYNGAP1 isoforms. As expected, due to the absence of the synaptic compartment, SYNGAP1 associated signal localised in the cytoplasm, forming spheroid bodies (Figure 4-3). The signal associated with the staining of the MeCP2-Myc protein, derived from the positive control MeP229-*hMECP2-Myc*, appeared to be stronger compared to the signal derived from the expression of the MeP229-*hSYNGAP1* plasmids. Quantification of the Myc-positive cells showed that the transfection efficiency of MeP229-*hSYNGAP1* plasmids was lower compared to what was observed for the MeP229-*hMECP2-Myc* plasmid. As previously mentioned, transfection efficiency can be influenced by the size of the plasmid transfected (~3500 bp for the MeP229-*hMECP2-Myc* plasmid versus the ~6000 bp of the MeP229-*hSYNGAP1* plasmids) (Yin *et al.*, 2005), however, as equimolar amounts of plasmid were used, it is unlikely that the result was influenced by this phenomenon.

The low number of Myc-positive detected cells can be associated with the intrinsic characteristic of the assay used. I previously mentioned that light source intensity and exposure were optimised on the background noise of the mock-transfected cells to prevent the capturing of background noise in plasmid-transfected cells. If the signal associated with the immunolabelling is too faint and below the detection threshold, equal or lower to the background noise, even if transfected cells were expressing SYNGAP1 they would have appeared negative. More sensitive alternative methods could have been used for the investigation, such as flow cytometry, but they were not adopted for the work presented here.

The *in vitro* fluorescence immunocytochemistry experiment was repeated using the MeP229-*hSYNGAP1* AAV expression plasmids. On this occasion no positive cells were detected for SYNGAP1 and Myc immunolabelling, while MeCP2, derived from the expression of MeP229-*hMECP2-Myc,* was detectable (Figure 4-11). As for the experiment with the mammalian expression plasmid, the absence of Myc-positive cells was likely to be associated to a sub-threshold level of therapeutic cassette expression.

When transgene expression was tested via immunoblotting of HEK239A cell protein lysates, it appeared that a very low level of plasmid-derived SYNGAP1 was achieved from all three evaluated plasmids (Figure 4-12). Quantification of the Myc-positive band showed that the positive control plasmid MeP229-*hMECP2-Myc* was achieving a protein expression between ~80 and ~600x time more than what produced by the MeP229-*hSYNGAP1* plasmids (Figure 4-13). This result confirms that the failure to observe cells positive for anti-SYNGAP1 and anti-Myc immunolabelling in the fluorescence immunocytochemistry experiment was likely to be a result of the sensitivity of the assay and not to a complete lack of SYNGAP1 expression from the MeP229-*hSYNGAP1* plasmids.

Together with the MeP229-*hSYNGAP1* plasmids, the JeT-*hSYNGAP1_Aα1* was tested in parallel. As seen in Figure 4-13, the level of Myc-tagged SYNGAP1 derived from the expression of the JeT regulated plasmid was about 2x lower than what was seen with the MeP229-*hMECP2-Myc* plasmid, but it resulted considerably higher than what seen for the MeP229-*hSYNGAP1* plasmids (between 38x and 150x times higher).

The difference observed between the levels of Myc-tagged SYNGAP1 and Myc-tagged MeCP2 could also be associated with a different half-life of the proteins. To my knowledge, the turn-over of SYNGAP1 has not yet been investigated, but data suggest that MeCP2 half-life is around 24 hours (Sheikha *et al.*, 2017).

Mutations in the DNA sequence of the expression cassette could impact the expression levels of the transgene, both at the transcription and translation levels. All plasmids underwent quality checks which involved enzymatic digestion (Figure 4-8 and Figure 4-10) and whole plasmid sequencing using MiSeq. These systems confirmed the appropriate structure of the plasmids and excluded deletion or insertions, even at single nucleotide level. MiSeq is a sensitive technique that allows to reach higher read depth compared to Sanger sequences due to the high number of reads generated per single DNA fragment. It is therefore a more reliable technique for the sequencing of GC-rich regions such as the promoters and the ITRs (which present about ~70% of GC content).

It is important to note that the sequence of the JeT-*hSYNGAP1_Aα1* plasmid and the MeP229-*hSYNGAP1_Aα1* plasmid were identical except only for the promoter sequence, excluding the possibility that the backbone structure and sequence might have had an impact on the transgene expression.

MeP229 and JeT regulated plasmid contained a subtly different boosted Kozak sequences at the ATG start codon. Analysis of the sequences present in these plasmids/expression cassettes showed similar reliability in the usage of the boosted Kozak sequence across all constructs (a score of ~0.70 for the MeP229-*hSYNGAP1* plasmids and ~0.80 for the JeT-*hSYNGAP1* plasmids; https://atgpr.dbcls.jp/).

It is known that the minimal promoters based on the murine endogenous *Mecp2* promoter are able to efficiently drive the expression of MeCP2 (Gadalla *et al.*, 2013, 2017; Sinnett *et al.*, 2017) and other genes such as CRISPR-Cas9 (Swiech *et al.*, 2015). However, recent unpublished data shows that MePP29 appears to be unable to drive high expression of other genes *in vitro* (unpublished data, personal communication, Dr Ralph D. Hector). It is therefore possible that the low protein level of plasmid-derived SYNGAP1 achieved from the expression of the MeP229 regulated plasmids was a result of an altered, and unexpected, transgene-promoter interaction.

SYNGAP1 is one of the most abundant proteins of the PSD (Hamdan *et al.*, 2011; Zeng *et al.*, 2016, 2019) and it has been demonstrated to be dosage sensitive as a protein reduction of about the 50% leads to the development of the *SYNGAP1* haploinsufficiency associated-disorder (Hamdan *et al.*, 2009; Komiyama *et al.*, 2002). It was therefore important to develop a therapeutic construct able to drive high expression of the SYNGAP1 protein. Given the apparently weak expression observed with the MeP229-*hSYNGAP1* plasmids, the MeP229 promoter was excluded as a candidate element in a therapeutic cassette and instead JeT promoter was chosen (Tornoe *et al.*, 2002).

At the time of the work presented in this chapter, isoform-specific functions were not well delineated. An early study presented by McMahon and colleagues (McMahon *et al.*, 2012) suggested that the different N- and C-termini have different roles in the

regulation of synaptic function and their association gives rise to a characteristic modulation of synaptic strength. Zeng *et al.* (Zeng *et al.*, 2016) showed that the CC domain is important for SYNGAP1-PSD interaction suggesting that the α1 isoform has a role in the regulation of synaptic activity. These were the reasons that led to the choice of Aα1 as an initial construct for the therapeutic efficacy study.

4.6 CONCLUSION

To summarise, protein from the newly cloned JeT-*hSYNGAP1_Aα1* was detectable both via fluorescence immunocytochemistry and immunoblotting of HEK293A transfected cells. On the other hand, MeP229-*hSYNGAP1* expressing plasmids showed little to no expression *in vitro*. These preliminary results suggested that JeT-*hSYNGAP1_Aα1* plasmid was the best candidate to move on to the next stage of therapeutic testing.

CHAPTER 5: *A*SSESSMENT OF THE SECOND GENERATION CANDIDATE GENE THERAPY CONSTRUCT JET-*hSYNGAP1_Aα1* THERAPEUTIC EFFICACY *IN VIVO*

5.1 INTRODUCTION

The purpose of the work presented in this chapter was to move into a phase of my research where I began to assess the therapeutic potential of gene therapy vectors in mice modelling the *SYNGAP1* haploinsufficiency-associated disorder. In particular, I tested the therapeutic efficacy of the candidate gene therapy cassette JeT-*hSYNGAP1_Aα1*.

I introduced in Chapter 4 the rationale behind the use of the JeT promoter and the choice of the Aα1 isoform. Briefly, the JeT promoter is a short synthetic promoter created by the combination of functional elements of different promoters, which is able to drive the expression of a transgene in the CNS (Bahey *et al.*, 2017; Bailey *et al.*, 2018; Chen *et al.*, 2022; Tornoe *et al.*, 2002). To increase the transgene expression, a short synthetic intron was added between the core promoter region and the transgene (Kikuchi *et al.*, 2014; de la Garza-Rodea *et al.*, 2011; Powell *et al.*, 2015).

Based on previously published data, it was decided to clone the JeT promoter and synthetic intron in the Aα1-expressing plasmid among the three originally designed constructs. This isoform contains the PDZ binding motif that mediates the interaction with the PSD and presents the highest negative effect on synaptic strength (McMahon *et al.*, 2012).

Previously published works failed to precisely define the phenotypes rescue window in *Syngap1*$^{+/-}$ mice, although data suggest that an early intervention could be the most promising approach (Aceti *et al.*, 2015; Creson *et al.*, 2019; Ozkan *et al.*, 2014; Verma *et al.*, 2022). Aceti *et al.* (Aceti *et al.*, 2015) showed that normalisation of expression levels at PND1 can prevent the insurgence of haploinsufficiency-

associated symptoms while normalisation at PND21 rescued only the fear conditioning phenotype. For this reason, it was decided to deliver the gene therapy vector at PND1-2.

Gene therapy treatments *in vivo* can be delivered using different routes of administration, and the choice of which route to use is based on various factors such as the target tissue and age of delivery. *SYNGAP1* expression is primarily limited to the brain, where it is expressed at high levels in the cortex, hippocampus, and striatum (Kim *et al.*, 2003; Knuesel *et al.*, 2005; Moon *et al.*, 2008; Porter *et al.*, 2005; Tomoda *et al.*, 2004). It was important to use an administration route that ensured maximal transduction in this tissue and areas of interest. Intravenous administration has been used before to target the brain (Foust *et al.*, 2009), but this method of administration causes a large amount of vector to be sequestered in the hepatic tissue, causing toxicity. Direct brain injections have the advantage to maximise transduction in the brain and limiting it to other tissues. Among the possible routes for direct brain delivery, ICV injections allow a brain-wide spread of the vector (Belur *et al.*, 2021; Galvan *et al.*, 2021; Hughes *et al.*, 2018; McLean *et al.*, 2014) when administered at a neonatal stage (Hughes *et al.*, 2018; McLean *et al.*, 2014). Although it is not considered a translational administration route, ICV is known to allow efficient transduction of cortical areas, hippocampus and striatum (Chakrabarty *et al.*, 2013).

AAV has been extensively used for gene therapy applications due to its ability to infect both dividing and non-diving cells, wide tropism, and ability to induce stable long-lasting transgene expression (Bouard *et al.*, 2009; Penaud-Budloo *et al.*, 2018). Compared to other vectors, AAV has a relatively small cloning capacity, ~5000 bp, but it presents relatively low immunogenicity, low toxicity for the host cell, and does not commonly undergo recombination with the host genome (Bulcha *et al.*, 2021; Gardlík *et al.*, 2005; Ritter *et al.*, 2002; Sakuma *et al.*, 2012). AAV9 is the most promising for CNS-targeted gene therapy approaches as it is able to cross the BBB and has high tropism for neuronal cells (Foust *et al.*, 2009; Mendell *et al.*, 2017).

5.2 AIM

The aim of the work presented in this chapter was to evaluate the therapeutic efficacy of ssAAV9 vector expressing the human *SYNGAP1* Aα1 isoform. To this end specific aims were:

- To evaluate viral vector-derived transgene expression *in vivo* in disease-relevant brain areas such as cortex and hippocampus.
- To evaluate whether the gene therapy vector can ameliorate the behavioural phenotypes observed in *Syngap1*$^{+/-}$ mice.
- To assess the tolerability of transgene expression in wild-type mice.

5.3 STUDY PLAN

Detailed methodology is provided in Chapter 2. Briefly, the viral vector (Figure 4-5 and Figure 5-1a) was delivered via ICV injections in PND1-2 neonatal wild-type and *Syngap1*$^{+/-}$ male mice at three doses: 1E10, 5E10 and 1E11 vg/mouse, or vehicle (PBS) as control. To reach the desired *n* for each treatment group, mice were recruited in groups and the period of injections spanned over four months. Treatments were assigned to litters as described in Section 2.15. Initially, mice were treated with 5E10 vg/mouse and vehicle, subsequently 1E10 and 1E11vg/mouse doses were added. Testing of all treatment groups resulted partially overlapped due to the longitudinal nature of the study.

Mice were monitored and behaviourally phenotyped at 7 and then at 15 weeks of age using, in this order and in consecutive days, the open field, elevated plus maze and platform departure test, as described in Figure 5-1b. Mice treated with 5E10 vg/mouse and vehicle were sacrificed between 20 and 22 weeks of age, while mice treated with 1E10 and 1E11vg/mouse were sacrificed between 28 and 31 weeks of age.

The candidate therapeutic viral vector (Figure 5-1a) used for the work presented in this chapter expresses the human Aα1 *SYNGAP1* isoform under the regulation of the synthetic JeT promoter. Downstream to JeT was inserted a short synthetic intron (Kikuchi *et al.*, 2014; de la Garza-Rodea *et al.*, 2011; Powell *et al.*, 2015). To distinguish between endogenous and viral vector-derived SYNGAP1 protein, a Myc fusion peptide was added to the C-terminal of SYNGAP1. A variation of the SpA reported by Levitt and colleagues (Levitt *et al.*, 1989) was used. The construct was vectorised as ssDNA using AAV9 capsid pseudotyped (when expression cassettes are designed using ITRs belonging to one serotype then, during viral vector production, the most suited capsid is chosen, depending on the type of cell to transduce) with AAV2 ITRs at Barcelona Vector Core (Barcelona, Spain) as described in Section 2.8. The ssAAV2/9/JeT-*hSYNGAP1_Aα1-Myc-SpA* vector (Figure 5-1a) will be referred as AAV9/JeT-*hSYNGAP1* forward in the text while the plasmid will be referred to as JeT-*hSYNGAP1_Aα1.*

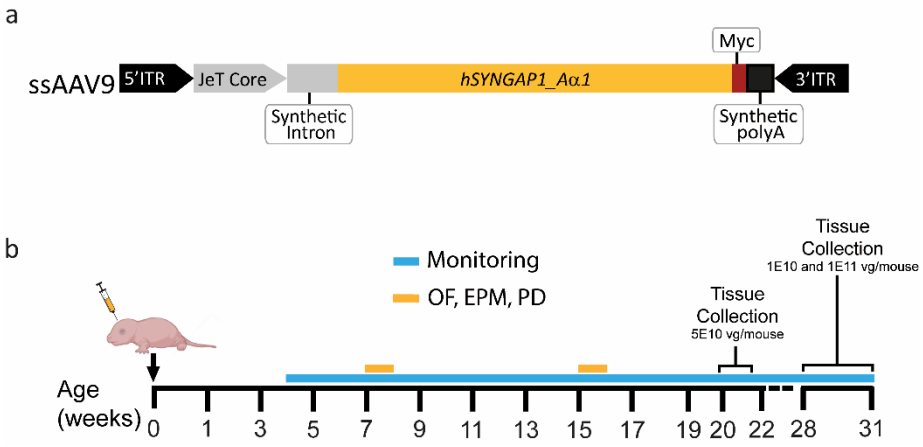

Figure 5-1. Schematic representation of the AAV9/JeT-hSYNGAP1 and experimental plan.

Schematic representation of the AAV9/JeT-*hSYNGAP1* construct (a) where the sequence of the Myc-tagged human Aα1 *SYNGAP1* was cloned under the control of the JeT promoter and the regulation of AAV2 ITRs. The experimental plan (b) involved the dosing of wild-type and *Syngap1*$^{+/-}$ mice via ICV injection with 1E10, 5E10 or 1E11 vg/mouse or vehicle as control. As detailed in the methods section, mice were then monitored and tested on consecutive days using open field (OF), elevated plus maze (EPM) and platform departure (PD) at 7 and then at 15 weeks of age.

5.4 RESULTS

5.4.1 Viral vector-derived SYNGAP1-Myc was detectable in cortex and hippocampus of treated wild-type mice

After confirmation of correct expression *in vitro*, shown in Chapter 4, the plasmid JeT-*hSYNGAP1_Aα1* was vectorised as ssDNA and packaged in an AAV9 capsid.

The correct packaged DNA sequence was confirmed by viral vector DNA sequencing using MiSeq. As shown in Table 5-1, a large percentage of reads, ~96%, aligned on the construct sequence, while less than 1% of reads covered the plasmid backbone sequence and the rep-cap sequence of the helper. Moreover, the analysis did not detect DNA sequences of other origins, such as bacterial genomic sequence, that could have been associated to contaminants. This experiment confirmed the correctness of the packaged sequence. MiSeq sequencing was performed by Ms Amanda Morris and sequence analysis by Dr Paul Ross.

Table 5-1. AAV9/JeT-hSYNGAP1 sequence quality evaluation via MiSeq.

Mapped sequence	Percentage of reads
AAV9/JeT-*hSYNGAP1*	96.08%
AAV9/JeT-*hSYNGAP1* plasmid backbone	0.36%
Helper Rep-Cap	0.36%

AAV9/JeT-*hSYNGAP1* expression was first tested *in vivo* in a qualitative pilot study. The presence of SYNGAP1-Myc was evaluated after five weeks from injection at three different doses: 5E10, 1E11, and 2E11 vg/mouse. As shown in Figure 5-2, immunoblot of protein lysate from viral vector-treated wild-type mice cortex and hippocampus showed the presence of the Myc-tagged SYNGAP1 which migrated at the same molecular weight as the native SYNGAP1 protein. Protein levels were not quantified for this experiment as the aim was only to demonstrate viral vector transgene expression in brain areas of interest: cortex and hippocampus. Viral vector-derived protein quantification is described in Figure 5-15 and Figure 5-16.

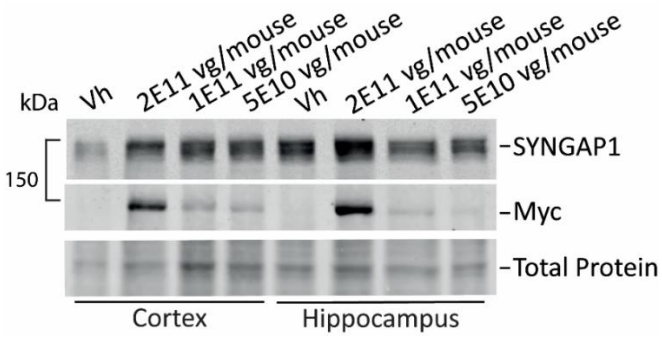

Figure 5-2. SYNGAP1-Myc derived from AAV9/JeT-hSYNGAP1 expression was detectable in cortex and hippocampus protein lysates after five weeks from the injection.

Representative qualitative immunoblot of cortex and hippocampus protein lysates from wild-type treated tissue after 5 weeks post-treatment with vehicle (Vh) or viral vector at doses of 5E10, 1E11 and 2E11 vg/mouse. SYNGAP1 endogenous protein migrates at a molecular weight of ~148 KDa. Similarly, viral vector-derived SYNGAP1-Myc migrated at a molecular weight of ~148 KDa. Total protein was used as loading control. The gel was used at a concentration of bis acrylamide of 8%.

5.4.2 AAV9/JeT-*hSYNGAP1* treatment in *Syngap1*$^{+/-}$ mice showed a trend toward the amelioration of the risk-taking behaviour

After establishing detectable brain expression *in vivo,* I moved on to the therapeutic phase of the study. As shown in Figure 5-1b, wild-type and *Syngap1*$^{+/-}$ mice were ICV dosed at PND1-2 with the AAV9/JeT-*hSYNGAP1* therapeutic vector at doses of 1E10, 5E10 and 1E11 vg/mouse. These doses were chosen based on the preliminary results shown by the pilot study presented in Section 5.4.1. As clear expression was detectable at 5E10 and 1E11 vg/mouse, and 2E11 vg/mouse was not further tested. Moreover, only *Syngap1*$^{+/-}$ mice were dosed with the highest viral genome per mouse, 1E11 vg/mouse, to prevent tolerability issues due to *SYNGAP1* overexpression.

Mice were subjected to a behavioural pipeline of assessments defined during the study presented in Chapter 3. The first of these was the open field test, followed by elevated plus maze and platform departure tests.

One wild-type mouse injected with 5E10 vg/mouse was removed from the study prior to testing at 15 weeks for health issues not related to the treatment.

5.4.2.1 Open Field

A robust hyperactive phenotype is reported for *Syngap1*$^{+/-}$ mice in several published works (Aceti *et al.*, 2015; Berryer *et al.*, 2016; Guo *et al.*, 2009; Komiyama *et al.*, 2002; Muhia *et al.*, 2010; Nakajima *et al.*, 2019; Ozkan *et al.*, 2014) and this result was reproduced in my baseline studies (Chapter 3). I therefore next went on to assess the candidate therapeutic vector AAV9/JeT-*hSYNGAP1* ability to prevent or ameliorate such phenotype using the open field test. Subjects were allowed to explore a square arena for 1 hour while their behaviour was monitored using the EthovisionXT 12 software (Noldus). After video analysis, the total distance travelled in the given time and distance travelled per 15 minutes time bins were extrapolated.

Consistent with what was previously observed in published works and with my results shown in Chapter 3, *Syngap1*$^{+/-}$ mice travelled longer distances when compared to wild-type controls (Figure 5-3a; two-tailed Student's t-test with Welch's correction, mean ± SEM; wild-type n=16, 17833 ± 1499 cm; *Syngap1*$^{+/-}$ n=19, 31796 ± 1291 cm; $t_{(31.90)}$=7.059, p<0.0001). Wild-type viral vector-treated mice's behaviour was comparable to what was observed in vehicle-treated animals, suggesting that the treatment did not modify the behaviour (Figure 5-3b; Welch's ANOVA, mean ± SEM; vehicle n=16, 17833 ± 1499 cm; 1E10 vg/mouse n=18, 17937 ± 1757 cm; 5E10 vg/mouse n=14, 20258 ± 1056 cm; $W_{(2.00,\ 29.51)}$=1.149, p=0.3309). However, no modification of the hyperactive phenotype was observed among viral vector-treated *Syngap1*$^{+/-}$ mice (Figure 5-3c; Welch's ANOVA, mean ± SEM; vehicle n=19, 31796 ± 1291 cm; 1E10 vg/mouse n=13, 37985 ± 3434 cm; 5E10 vg/mouse n=17, 36081 ± 1706 cm; 1E11 vg/mouse n=14, 35953 ± 2178 cm, $W_{(3.00,\ 28.95)}$=2.083, p=0.1242).

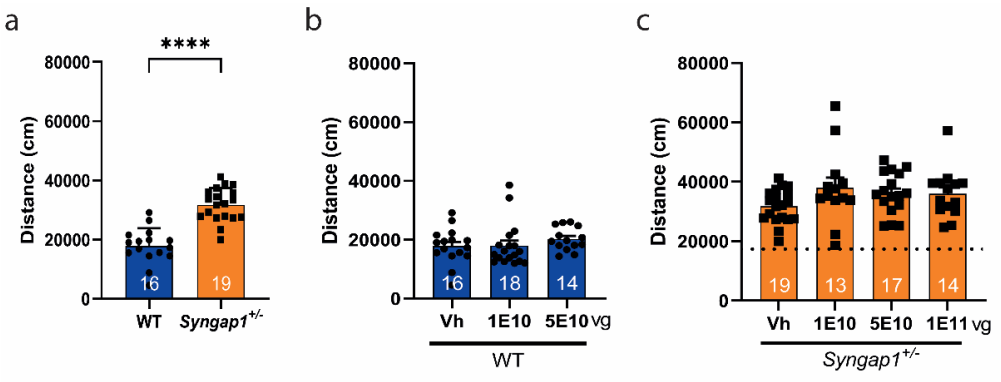

Figure 5-3. At 7 weeks of age, AAV9/JeT-hSYNGAP1 treatment did not affect the hyperactivity phenotype observed during the open field test.

Total distance travelled in 1 hour by vehicle (Vh) treated wild-type (WT) and *Syngap1*$^{+/-}$ mice (a) and by wild-type (b) and *Syngap1*$^{+/-}$ mice (c) of all treatment groups at 7 weeks of age. Dotted line represents wild-type behaviour. Circles and squares represent single animals. Numbers within the bars represent the n of each group.

Data presented as mean ± SEM. a) Two-tailed Student's t-test with Welch's correction. b,c) Welch's ANOVA. **** p<0.0001.

Increased locomotor activity in *Syngap1*$^{+/-}$ mice appeared to not be associated with a lack of habituation when compared to wild-type controls at 7 weeks of age, in agreement with results shown in Chapter 3 (Figure 5-4a; RM Two-way ANOVA; vehicle(WT), n=16, vehicle(*Syngap1*$^{+/-}$), n=19; genotype x time $F_{(3,\ 99)}$=4.840, p=0.0035; time $F_{(3,\ 99)}$=158.4, p<0.0001; genotype $F_{(1,\ 33)}$=50.39, p<0.0001; multiple comparisons tests results are reported in Table S-7). Analysis of viral vector-treated *Syngap1*$^{+/-}$ mice showed no variation in habituation rate after treatment (Figure 5-4b; RM Two-way ANOVA; vehicle(*Syngap1*$^{+/-}$), n=19, 1E10 vg/mouse n=13, 5E10 vg/mouse n=17, 1E11 vg/mouse n=17; treatment x time $F_{(9,\ 177)}$=0.2293, p=0.9742; time $F_{(1.942,\ 114.6)}$=233.6, p<0.0001; treatment $F_{(3,\ 59)}$=1.655, p=0.1866, Tukey's multiple comparisons test are reported in Table S-8).

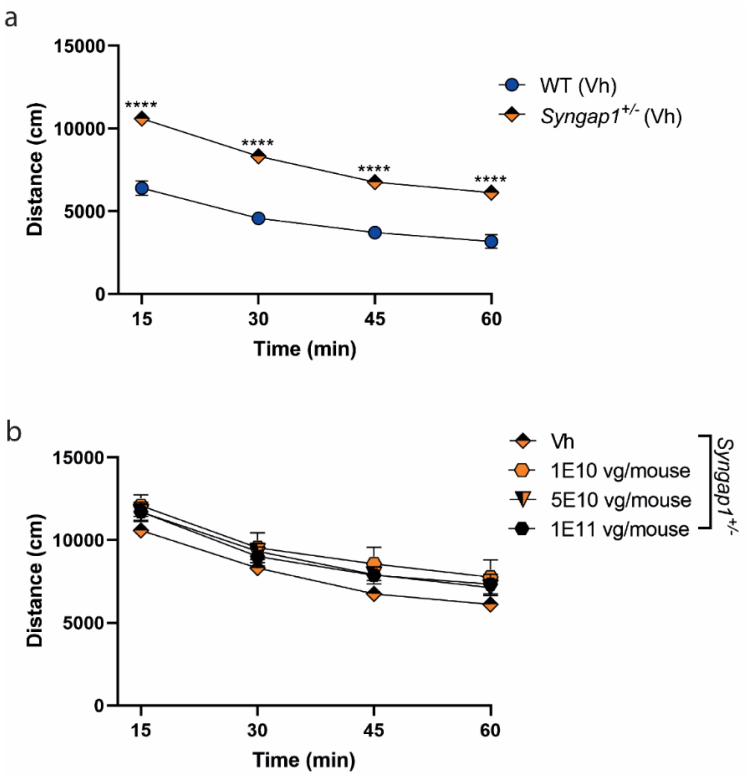

Figure 5-4. At 7 weeks of age, Syngap1$^{+/-}$ mice presented comparable levels of habituation to wild-type mice in the open field. AAV9/JeT-hSYNGAP1 treatment did not affect behaviour over time.

Wild-type (WT) and *Syngap1*$^{+/-}$ vehicle (Vh) treated mice (a) and *Syngap1*$^{+/-}$ vehicle and viral vector-treated mice (b) distance travelled for 15 minutes time bins at 7 weeks of age. Each data point represents the mean distance travelled over the preceding 15 minutes. Stars (*) above each bin represent the results of multiple comparison tests between genotypes. Wild-type (Vh) n=16, *Syngap1*$^{+/-}$ (Vh) n=19, 1E10 vg/mouse n=13, 5E10 vg/mouse n=17, 1E11 vg/mouse n=14.
Data presented as mean ± SEM. RM Two-way ANOVA with multiple comparison tests. **** p<0.0001.

The large difference in distance travelled between wild-type and *Syngap1*$^{+/-}$ vehicle-treated mice was present at 15 weeks of age (Figure 5-5a; two-tailed Student's t-test with Welch's correction, mean ± SEM; wild-type n=16, 13208 ± 701.5 cm; *Syngap1*$^{+/-}$ n=19, 34876 ± 1699 cm; $t_{(23.83)}$=11.79, p<0.0001). Analysis of vector-treated wild-type mice showed no evident issue with treatment tolerability, as mice of all groups presented a comparable behaviour (Figure 5-5b; Welch's ANOVA, mean ± SEM; vehicle n=16, 13208 ± 701.5 cm; 1E10 vg/mouse n=17, 14007 ± 1633 cm; 5E10 vg/mouse n=14, 13110 ± 865.5 cm; $W_{(2.00,\ 27.68)}$=0.1194, p=0.8879). Considering

Syngap1$^{+/-}$ mice treated with the AAV9/JeT-*hSYNGAP1* viral vector, data did not suggest the presence of treatment effect on the hyperactivity phenotype (Figure 5-5c; Welch's ANOVA, mean ± SEM; vehicle n=19, 34876 ± 1699 cm; 1E10 vg/mouse n=13, 39964 ± 5175 cm; 5E10 vg/mouse n=17, 42659 ± 3211 cm; 1E11 vg/mouse n=14, 38814 ± 1727 cm; $W_{(3.00, 29.50)}$=1.835, p=0.1626).

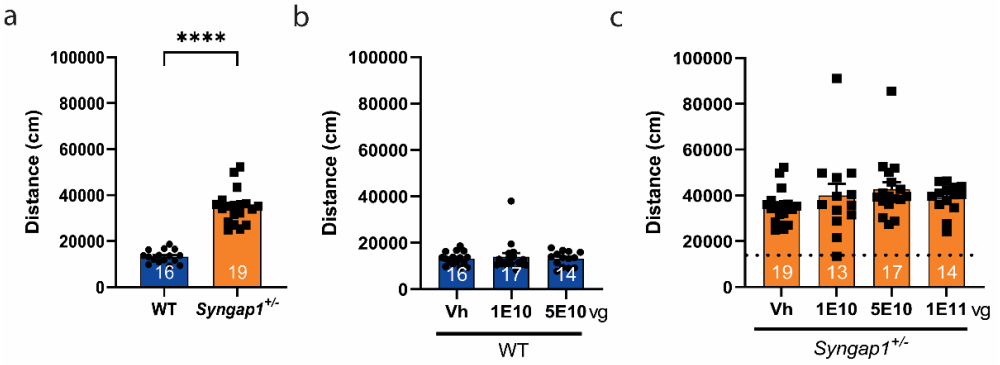

Figure 5-5. At 15 weeks of age, AAV9/JeT-hSYNGAP1 treated Syngap1$^{+/-}$ mice did not show amelioration of the hyperactivity phenotype.

Total distance travelled in 1 hour by vehicle (Vh) treated wild-type (WT) and *Syngap1*$^{+/-}$ mice (a) and by wild-type (b) and *Syngap1*$^{+/-}$ mice (c) of all treatment groups at 15 weeks of age. Circles and squares represent single animals. Dotted line represents wild-type behaviour. Numbers within the bars represent the n of each group.

Data presented as mean ± SEM. a) Two-tailed Student's t-test with Welch's correction. b,c) Welch's ANOVA. **** p<0.0001.

Wild-type mice presented a higher difference in distance travelled per time bins, while *Syngap1*$^{+/-}$ mice horizontal activity resulted more stable across time (Figure 5-6a; RM Two-way ANOVA; vehicle(WT), n=16, vehicle(*Syngap1*$^{+/-}$), n=19; genotype x time $F_{(3, 99)}$=3.432, p=0.0200; time $F_{(2.199, 72.58)}$=21.67, p<0.0001; genotype $F_{(1, 33)}$=121.7, p<0.0001; multiple comparisons tests results are reported in Table S-9).

Viral vector treatment in *Syngap1*$^{+/-}$ mice did not impact the distance travelled in each 15-minutes time bin over time (Figure 5-6b; RM Two-way ANOVA; vehicle(*Syngap1*$^{+/-}$), n=19, 1E10 vg/mouse n=13, 5E10 vg/mouse n=17, 1E11 vg/mouse n=17; treatment x time $F_{(9, 177)}$=1.897, p=0.0550; time $F_{(2.321, 137.0)}$=10.19, p<0.0001; treatment $F_{(3, 59)}$=1.300, p=0.2829; Tukey's multiple comparisons test results are reported in Table S-10).

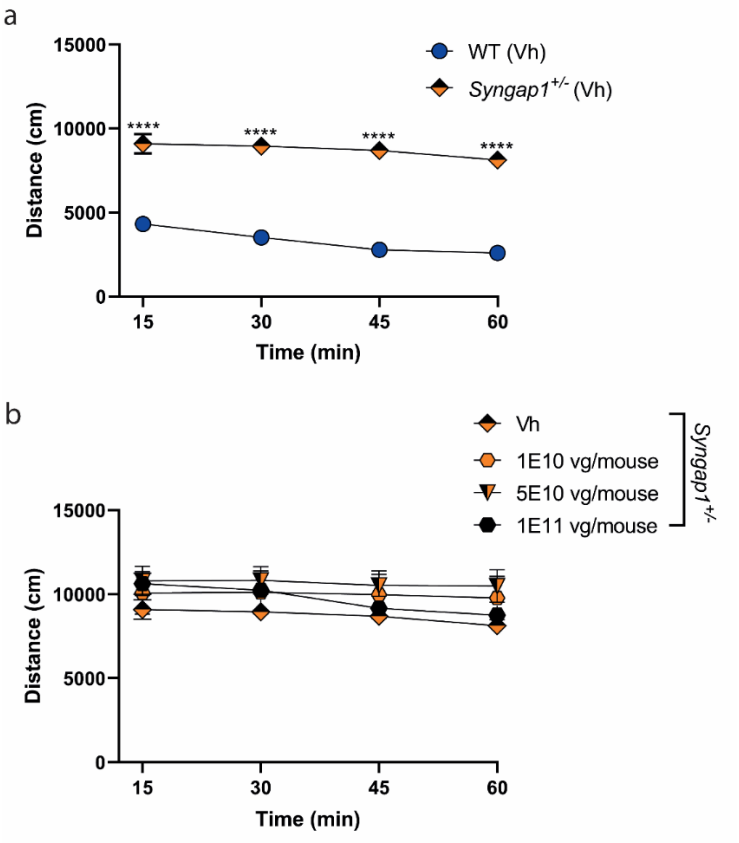

Figure 5-6. AAV9/JeT-hSYNGAP1 treatment did not affect distance travelled over time during open field when mice are tested at 15 weeks of age.
Wild-type (WT) and *Syngap1*$^{+/-}$ vehicle (Vh) treated mice (a) and *Syngap1*$^{+/-}$ vehicle and viral vector-treated mice (b) distance travelled per 15 minutes time bins at 15 weeks of age. Each data point represents the mean distance travelled over the preceding 15 minutes. Stars (*) above each bin represent the results of multiple comparison tests between genotypes. Wild-type (Vh) n=16, *Syngap1*$^{+/-}$ (Vh) n=19, 1E10 vg/mouse n=13, 5E10 vg/mouse n=17, 1E11 vg/mouse n=14.
Data presented as mean ± SEM. RM Two-way ANOVA with multiple comparison tests. **** p<0.0001.

5.4.2.2 Elevated plus maze

Reduced anxiety, measured as time spent in the open arms of the elevated plus maze, is a well-established phenotype in *Syngap1*$^{+/-}$ mice (Berryer *et al.*, 2016; Guo *et al.*, 2009; Muhia *et al.*, 2010; Nakajima *et al.*, 2019). In accordance with published results (Berryer *et al.*, 2016; Guo *et al.*, 2009; Muhia *et al.*, 2010; Nakajima *et al.*, 2019), I showed in Chapter 3 that the increased time spent in open arms was present in the *Syngap1*$^{+/-}$ mouse line used for this study. I, therefore, proceeded to evaluate the therapeutic effect of the candidate gene therapy construct AAV9/JeT-*hSYNGAP1* on

such behaviour. Wild-type and *Syngap1*$^{+/-}$ mice were exposed to the elevated plus maze on the subsequent day after the open field test for 10 minutes (Figure 5-1b). Videos were analysed using the EthovisionXT 12 software (Noldus) and, distance travelled, and time spent in the open arms were extrapolated.

As defined in Chapter 2, subjects that jumped out of the maze were excluded from the analysis. At 7 weeks, two *Syngap1*$^{+/-}$ vehicle-treated mice were excluded. At 15 weeks, three *Syngap1*$^{+/-}$ mice were excluded: one treated with vehicle, one with 5E10 vg/mouse and one with 1E11 vg/mouse.

At both 7 and 15 weeks of age, heterozygous mice showed increased horizontal activity (Figure 5-7a and Figure 5-8a; two-tailed Student's t-test with Welch's correction, mean ± SEM; 7 weeks, wild-type n=16, 2228 ± 87.60 cm; *Syngap1*$^{+/-}$ n=17, 3167 ± 131.9 cm; $t_{(27.52)}$=5.933, p<0.0001; 15 weeks, wild-type n=16, 1738 ± 94.62 cm; *Syngap1*$^{+/-}$ n=16, 2448 ± 117.4 cm; $t_{(28.70)}$=4.714, p<0.0001) and increased time in the open arms compared to wild-type controls (Figure 5-7d and Figure 5-8d; two-tailed Mann-Whitney test, median(95% CI); 7 weeks, wild-type n=16, 17.48(15.69 to 20.97) %; *Syngap1*$^{+/-}$ n=19, 41.65(38.20 to 44.83) %; U=2, p<0.0001. 15 weeks, wild-type n=16, 11.01(9.55 to 17.61) %; *Syngap1*$^{+/-}$ n=19, 27.83(22.76 to 33.73) %; U=33, p=0.0002).

In wild-type mice at 7 weeks of age, viral vector treatment did not affect activity in the maze (Figure 5-7b; Welch's ANOVA, mean ± SEM; vehicle n=16, 2228 ± 87.50 cm; 1E10 vg/mouse n=18, 2303 ± 108.7 cm; 5E10 vg/mouse n=14, 2420 ± 92.69 cm; $W_{(2.00, 29.79)}$=1.119, p=0.9275) or percentage of time spent in the open arms (Figure 5-7e; Kruskal-Wallis test, median(95% CI); vehicle n=16, 17.48(15.69 to 20.97) %; 1E10 vg/mouse n=18, 15.77(12.48 to 19.06) %; 5E10 vg/mouse n=14, 19.59(16.16 to 23.02) %; H=6.9, p=0.0317; Dunn's multiple comparisons test results are reported in Table S-11).

Syngap1$^{+/-}$ mice treated with AAV9/JeT-*hSYNGAP1* did not show a difference in activity levels (Figure 5-7c; Welch's ANOVA, mean ± SEM; vehicle n=17, 3167 ± 131.9

cm; 1E10 vg/mouse n=13, 3490 ± 292.9 cm; 5E10 vg/mouse n=17, 3340 ± 112.9 cm; 1E11 vg/mouse n=14, 3362 ± 118.3 cm; $W_{(3.00,\ 29.52)}$=0.5765, p=0.6350) nor normalisation of the percentage of time spent in the open arms (Figure 5-7f; Kruskal-Wallis test, median(95% CI); vehicle n=17, 41.65(38.20 to 44.83) %; 1E10 vg/mouse n=13, 41.60(34.41 to 51.51) %; 5E10 vg/mouse n=17, 40.86(36.18 to 46.34) %; 1E11 vg/mouse n=14, 38.96(32.42 to 47.21) %; H=0.8910, p=0.8276).

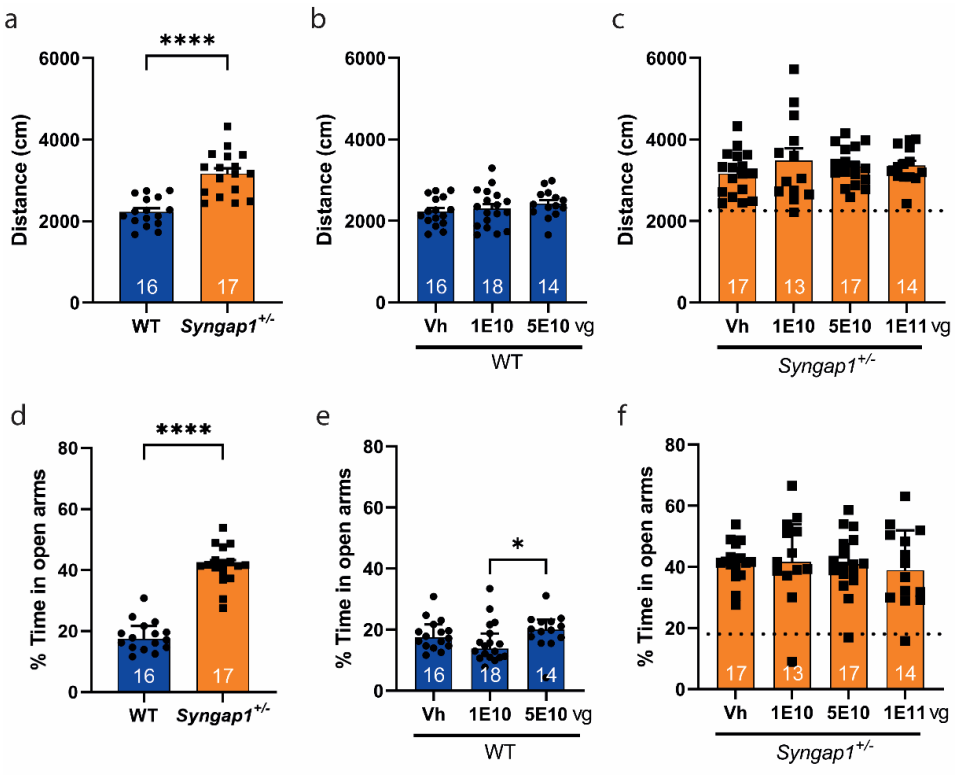

Figure 5-7. At 7 weeks of age, the time spent in the open arm by AAV9/JeT-hSYNGAP1 treated mice was comparable to vehicle-treated controls.

Total distance travelled in 10 minutes by vehicle (Vh) treated wild-type (WT) and *Syngap1*$^{+/-}$ mice (a) and by wild-type (b) and *Syngap1*$^{+/-}$ mice (c) of all treatment groups in the elevated plus maze at 7 weeks of age. Percentage of time spent in the open arms by vehicle-treated wild-type and *Syngap1*$^{+/-}$ mice (d) and by wild-type (e) and *Syngap1*$^{+/-}$ mice (f) of all treatment groups at 7 weeks of age. Dotted line represents wild-type behaviour. Circles and squares represent single animals. Numbers within the bars represent the n of each group.

a) Two-tailed Student's t-test with Welch's correction. b,c) Welch's ANOVA. Mean ± SEM.

d) Two-tailed Mann-Whitney test. e,f) Kruskal-Wallis test. Median and 95% CI.

* $p<0.05$, **** $p<0.0001$.

At 15 weeks of age, a significant decrease in the percentage of time spent in open arms was observed in wild-type mice treated with 5E10 vg/mouse compared to vehicle controls (Figure 5-8e; Kruskal-Wallis test, median(95% CI); vehicle n=16, 11.01(9.55 to 17.61) %; 1E10 vg/mouse n=17, 6.60(4.13 to 7.67) %; 5E10 vg/mouse n=14, 8.67(4.47 to 14.43) %; H=9.76, p=0.0076; Dunn's multiple comparisons test results are reported in Table S-12). However, the level of activity in these mice remained comparable to the one observed in vehicle controls, both during the open

field (Figure 5-5b) and during the elevated plus maze test (Figure 5-8b; Welch's ANOVA, mean ± SEM; vehicle n=16, 1738 ± 94.62 cm; 1E10 vg/mouse n=17, 1431 ± 120.7 cm; 5E10 vg/mouse n=14, 1612 ± 133.5 cm; $W_{(2.00, 28.14)}$=1.957, p=0.1719).
Syngap1$^{+/-}$ mice hyperactivity phenotype in the maze appeared to worsen in a dose-dependent manner (Figure 5-8c; Welch's ANOVA, mean ± SEM; vehicle n=16, 2448 ± 117.4 cm; 1E10 vg/mouse n=13, 2918 ± 257.2 cm; 5E10 vg/mouse n=16, 3017 ± 108.1 cm; 1E11 vg/mouse n=13, 3388 ± 167.5 cm; $W_{(3.00, 27.68)}$=7.735, p=0.0044; Dunnett's T3 multiple comparison test results are reported in Table S-13) but, similarly to what was noted in the wild-type group, this was not observed during the open field (Figure 5-5c). As no general condition abnormalities were reported for both wild-type and *Syngap1*$^{+/-}$ viral vector-treated mice, it is likely that these differences were not associated with the treatment.

Data showed no treatment-related improvement in the percentage of time spent in the open arms by *Syngap1*$^{+/-}$ viral vector-treated mice (Figure 5-8f; Kruskal-Wallis test, median(95% CI); vehicle n=16, 27.83(22.76 to 33.73) %; 1E10 vg/mouse n=13, 25.64(19.36 to 32.65) %; 5E10 vg/mouse n=16, 35.27(26.52 to 38.83) %; 1E11 vg/mouse n=13, 34.74(26.23 to 37.46) %; H=3.791, p=0.2849).

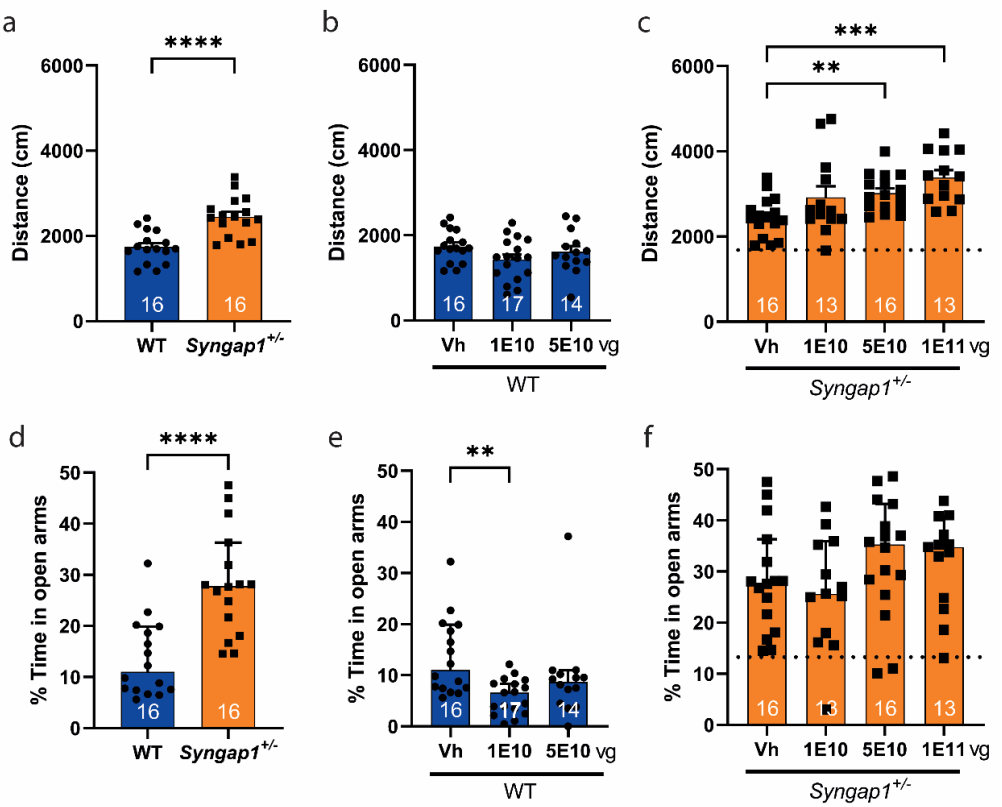

Figure 5-8. Treatment did not affect the percentage of time in the open arms in AAV9/JeT-hSYNGAP1 treated Syngap1$^{+/-}$ mice at 15 weeks of age.

Total distance travelled in 10 minutes by vehicle (Vh) treated wild-type (WT) and *Syngap1*$^{+/-}$ mice (a) and by wild-type (b) and *Syngap1*$^{+/-}$ mice (c) of all treatment groups in the elevated plus maze at 15 weeks of age. Percentage of time spent in the open arms by vehicle-treated wild-type and *Syngap1*$^{+/-}$ mice (d) and by wild-type (e) and *Syngap1*$^{+/-}$ mice (f) of all treatment groups at 15 weeks of age. Dotted line represents wild-type behaviour. Circles and squares represent single animals. Numbers within the bars represent the n of each group.

a) Two-tailed Student's t-test with Welch's correction. b,c) Welch's ANOVA with Dunnett's T3 multiple comparisons test. Mean ± SEM.

d) Two-tailed Mann-Whitney test. e,f) Kruskal-Wallis test with Dunn's multiple comparisons test. Median and 95% CI.

** p<0.01, *** p<0.01 **** p<0.0001.

5.4.2.3 Platform departure test

Families of *SYNGAP1* affected individuals report a reduced sense of risk (Weldon *et al.*, 2018), phenotype that was observed also in *Syngap1*$^{+/-}$ mice in the form of increased departures from an elevated platform compared to wild-type littermates (Kilinc *et al.*, 2018). This represents one of the most promising behaviours as it appears to be conserved across species, providing an important translatable measure

to evaluate the therapeutic efficacy of gene therapy constructs. In Chapter 3, I showed how this behaviour was present in the *Syngap1*$^{+/-}$ mouse line used for this study; therefore, I proceeded to evaluate the effect of AAV9/JeT-*hSYNGAP1* treatment on this behaviour. As described in Chapter 2, mice were placed on a 2-litre beaker and allowed to explore for 10 minutes; the number of partial and full departures were counted offline and formed the measures to evaluate the presence of risk-taking behaviour. As described in Figure 5-1b, this test was performed on the subsequent day of the elevated plus maze test.

At 7 weeks of age *Syngap1*$^{+/-}$ mice performed a significantly higher number of partial departures (Figure 5-9a; two-tailed Student's t-test with Welch's correction, mean ± SEM; wild-type n=16, 18.69 ± 2.85; *Syngap1*$^{+/-}$ n=19, 35.53 ± 3.72; $t_{(32.05)}$=3.592, p=0.0011) and full departures (Figure 5-9d; two-tailed Mann-Whitney test, median(95% CI); wild-type n=16, 0.00(-0.8486 to 2.35); *Syngap1*$^{+/-}$ n=19, 5.00(5.427 to 14.57); U=33.50, p<0.0001).

Wild-type mice behaviour was not affected by the treatment for both partial departures (Figure 5-9b; Welch's ANOVA, mean ± SEM; vehicle n=16, 18.69 ± 2.85; 1E10 vg/mouse n=18, 20.83 ± 3.46; 5E10 vg/mouse n=14, 14.79 ± 2.27; $W_{(2.00, 29.86)}$=1.227, p=0.3075) and full departures (Figure 5-9e; Kruskal-Wallis test, median(95% CI); vehicle n=16, 0.00(-0.85 to 2.35; 1E10 vg/mouse n=18, 0.00(-0.60 to 3.27); 5E10 vg/mouse n=14, 0.00(-0.13 to 1.41); H=1.223, p=0.5424).

Syngap1$^{+/-}$ mice treated with AAV9/JeT-*hSYNGAP1* vector did not show a modification in the number of partial departures (Figure 5-9c; Welch's ANOVA, mean ± SEM; vehicle n=19, 35.53 ± 3.72; 1E10 vg/mouse n=13, 36.92 ± 5.13; 5E10 vg/mouse n=17, 44.29 ± 5.55; 1E11 vg/mouse n=14, 33.86 ± 6.28; $W_{(3.00, 30.47)}$=0.6777, p=0.5725), however, both low and high dose viral vector-treated mice showed a reduced tendency to leave the platform (Figure 5-9f; Kruskal-Wallis test, median(95% CI); vehicle n=19, 5.00(5.43 to 14.57); 1E10 vg/mouse n=13, 6.00(2.50 to 14.89); 5E10 vg/mouse n=17, 17.00(9.28 to 21.89); 1E11 vg/mouse n=14, 0.50(1.64 to 11.64); H=6.426, p=0.0926). This effect was more evident when observing the percentage of

mice leaving the platform in function of time (Figure 5-9g; Log-rank (Mantel-Cox) test; vehicle(WT) n=16, median time to first=undefined; vehicle(*Syngap1*$^{+/-}$) n=19, median time to first=4.16 min, 1E10 vg/mouse n=13, median time to first=6.14 min, 5E10vg/mouse n=17, median time to first=3.49 min, 1E11vg/mouse n=14, median time to first=8.55 min; vehicle(WT) vs vehicle(*Syngap1*$^{+/-}$) $\chi^2_{(1)}$=22.50, p<0.0001; vehicle(*Syngap1*$^{+/-}$) vs 1E10 vg/mouse $\chi^2_{(1)}$=1.649, p=0.1991; vehicle(*Syngap1*$^{+/-}$) vs 5E10 vg/mouse $\chi^2_{(1)}$=0.1066, p=0.7441; vehicle(*Syngap1*$^{+/-}$) vs 1E11 vg/mouse $\chi^2_{(1)}$=3.837, p=0.0501).

In this experiment, a smaller percentage of mice treated with 1E10 and 1E11 vg/mouse left the platform in the given time. It is interesting to note that, when tested, the difference between vehicle and 1E11 vg/mouse treated *Syngap1*$^{+/-}$ mice was close to significance, p=0.0501.

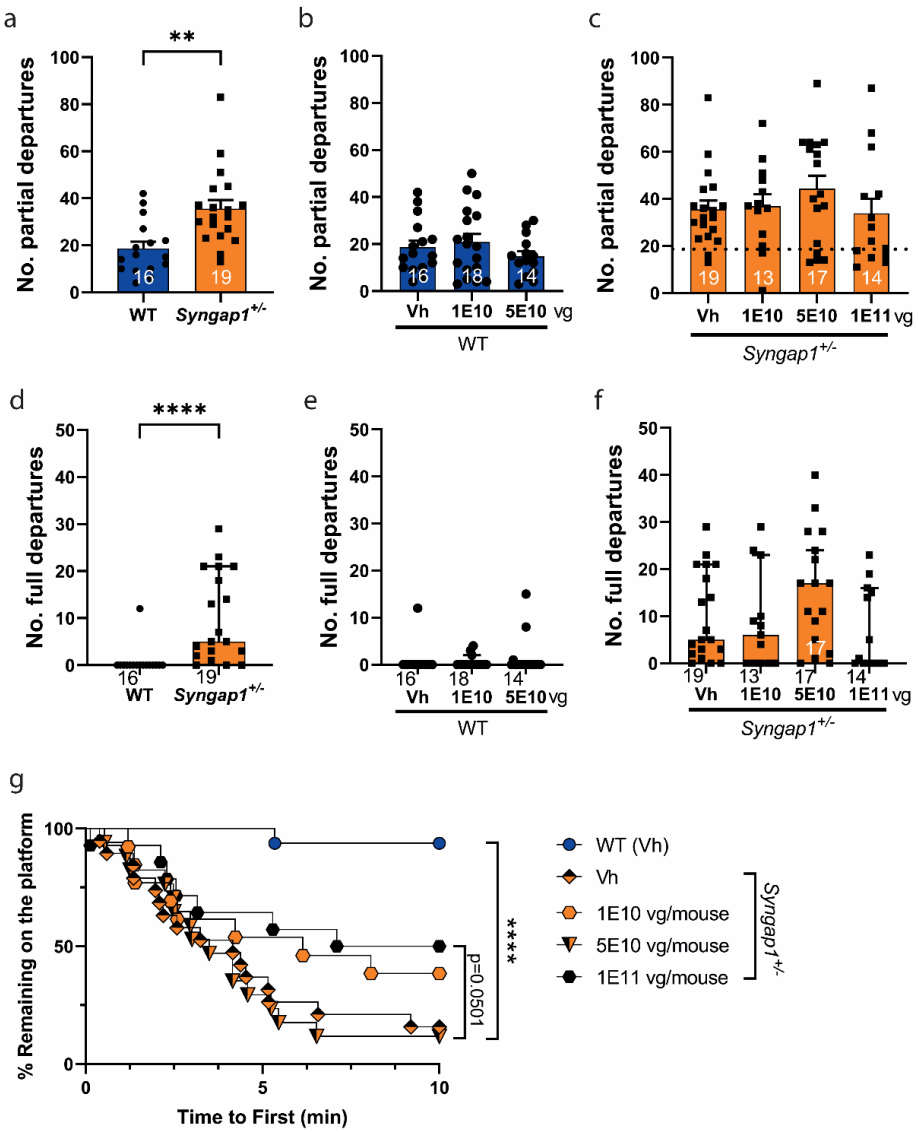

Figure 5-9. At 7 weeks of age, AAV9/JeT-hSYNGAP1 treated Syngap1$^{+/-}$ mice showed delayed departure time from the platform.

Number of partial departures performed by vehicle (Vh) treated wild-type (WT) and *Syngap1*$^{+/-}$ mice (a) and by wild-type (b) and *Syngap1*$^{+/-}$ mice (c) of all treatment groups at 7 weeks of age. Number of full departures performed by vehicle-treated wild-type and *Syngap1*$^{+/-}$ mice (d) and by wild-type (e) and *Syngap1*$^{+/-}$ (f) of all treatment groups at 7 weeks of age. Percentage of vehicle-treated wild-type and *Syngap1*$^{+/-}$ mice of all treatment groups (g) that remained on the platform and time to first departure at 7 weeks of age. Dotted line represents wild-type behaviour. Circles and squares represent single animals. Numbers within or under the bars represent the n of each group.

a) Two-tailed Student's t-test with Welch's correction. b,c) Welch's ANOVA. Mean ± SEM.

d) Two-tailed Mann-Whitney test. e,f) Kruskal-Wallis test. Median and 95% CI.

g) Log-rank (Mantel-Cox) test. ** p<0.01, **** p<0.0001.

At 15 weeks of age, vehicle-treated *Syngap1*$^{+/-}$ mice were more prone to perform partial (Figure 5-10a; two-tailed Student's t-test with Welch's correction, mean ± SEM; wild-type n=16, 8.62 ± 1.37; *Syngap1*$^{+/-}$ n=19, 36.32 ± 3.79; $t_{(22.53)}$=6.866, p<0.0001) and full departures (Figure 5-10d; two-tailed Mann-Whitney test, median(95% CI); wild-type n=16, 0.00(-0.46 to 2.33); *Syngap1*$^{+/-}$ n=19, 14.00(8.08 to 16.24); U=28.50, p<0.0001) when compared to wild-type vehicle-treated mice.

Analysis of wild-type viral vector-treated mice showed no difference with vehicle-treated mice (Figure 5-10b and e; partial departures, Welch's ANOVA, mean ± SEM; vehicle n=16, 8.62 ± 1.34; 1E10 vg/mouse n=17, 5.82 ± 2.32; 5E10 vg/mouse n=14, 8.21 ± 1.71; $W_{(2.00,\ 28.26)}$=0.5387, p=0.5894; full departures, Kruskal-Wallis test, median(95% CI); vehicle n=16, 0.00(-0.46 to 2.33); 1E10 vg/mouse n=17, 0.00(-0.63 to 8.27); 5E10 vg/mouse n=14, 0.00(-0.58 to 1.58); H=1.669, p=0.4340).

Treatment did not affect the number of partial departures performed by vehicle and viral vector-treated *Syngap1*$^{+/-}$ mice overall (Figure 5-10c; Welch's ANOVA, mean ± SEM; vehicle n=19, 36.32 ± 3.79; 1E10 vg/mouse n=13, 25.77 ± 6.14; 5E10 vg/mouse n=17, 37.35 ± 6.14; 1E11 vg/mouse n=14, 29.86 ± 6.65; $W_{(3.00,\ 29.87)}$=0.8996, p=0.4529). On the other hand, AAV9/JeT-*hSYNGAP1* treated *Syngap1*$^{+/-}$ mice performed a reduced number of full departures compared to vehicle-treated mice with the vehicle (Figure 5-10f; Kruskal-Wallis test, median(95% CI); vehicle n=19, 14.00(8.08 to 16.24); 1E10 vg/mouse n=13, 3.00(0.82 to 18.10); 5E10 vg/mouse n=17, 7.00(3.52 to 10.95); 1E11 vg/mouse n=14, 5.00(3.41 to 14.74); H=3.925, p=0.2696).

A shift in the curve of animals departing from the platform was observed, with the 1E10 and 1E11 vg/mouse treatment groups showing the lowest percentage of *Syngap1*$^{+/-}$ mice departing from the platform (Figure 5-10g; Log-rank (Mantel-Cox) test; vehicle(WT) n=16, median time to first=undefined; vehicle(*Syngap1*$^{+/-}$) n=19, median time to first=3.16 min, 1E10 vg/mouse n=13, median time to first=6.41 min, 5E10vg/mouse n=17, median time to first=4.59 min, 1E11vg/mouse n=14, median time to first=6.65 min; vehicle(WT) vs vehicle(*Syngap1*$^{+/-}$) $\chi^2_{(1)}$=21.49, p<0.0001; vehicle(*Syngap1*$^{+/-}$) vs 1E10 vg/mouse $\chi^2_{(1)}$=3.661, p=0.0557; vehicle(*Syngap1*$^{+/-}$) vs

5E10 vg/mouse $\chi^2_{(1)}$=0.4369, p=0.5086; vehicle(*Syngap1*$^{+/-}$) vs 1E11 vg/mouse $\chi^2_{(1)}$=2.649, p=0.1036).

In all treatments, about 50% of mice departed around 5 minutes from the start, while 50% of vehicle-treated *Syngap1*$^{+/-}$ mice left the platform after 3-3.5 minutes.

Due to the nature of the data set presented in Chapter 3, it was not possible to investigate habituation after re-exposure to the platform departure test. It is possible that the decreased number of full departures observed in 1E10 and 1E11 vg/mouse-treated *Syngap1*$^{+/-}$ mice was associated with habituation to the test. For this reason, I investigated whether re-exposure to the task would modify the response in the two genotype groups, and to this end, I analysed the number of partial and full departures performed by the vehicle-treated mice. Both wild-type and *Syngap1*$^{+/-}$ mice did not show habituation in the number of partial departures (Figure 5-11a; RM Two-way ANOVA; wild-type n=16, 7 weeks=18.69 ± 2.85, 15 weeks=8.62 ± 1.37; *Syngap1*$^{+/-}$ n=19, 7 weeks=35.53 ± 3.72, 15 weeks=36.32 ± 3.80; genotype x time $F_{(1, 33)}$=3.403 p=0.0741, time $F_{(1, 33)}$=2.485 p=0.1245, genotype $F_{(1, 33)}$=40.02 p<0.0001; Šídák multiple comparison test results are reported in Table S-14).

Only one wild-type subject left the platform at 7 weeks of age, while three did at 15 weeks of age. Such reduced variance in the dataset posed a challenge to the statistical analysis, nonetheless it appeared that re-exposure to the task did not modify the behaviour of wild-type nor *Syngap1*$^{+/-}$ mice (Figure 5-11b; RM Two-way ANOVA; wild-type n=16, 7 weeks=0.75 ± 0.75, 15 weeks=0.93 ± 0.65; *Syngap1*$^{+/-}$ n=19, 7 weeks=10.00 ± 2.18, 15 weeks=12.16 ± 1.94; genotype x time $F_{(1, 33)}$=0.599 p=0.4446, time $F_{(1, 33)}$=0.8482 p=0.3638, genotype $F_{(1, 33)}$=27.06 p<0.0001; Šídák multiple comparison test results are reported in Table S-15).

These results suggest that the reduction of departures observed in viral vector-treated *Syngap1*$^{+/-}$ mice was not caused by a habituation effect.

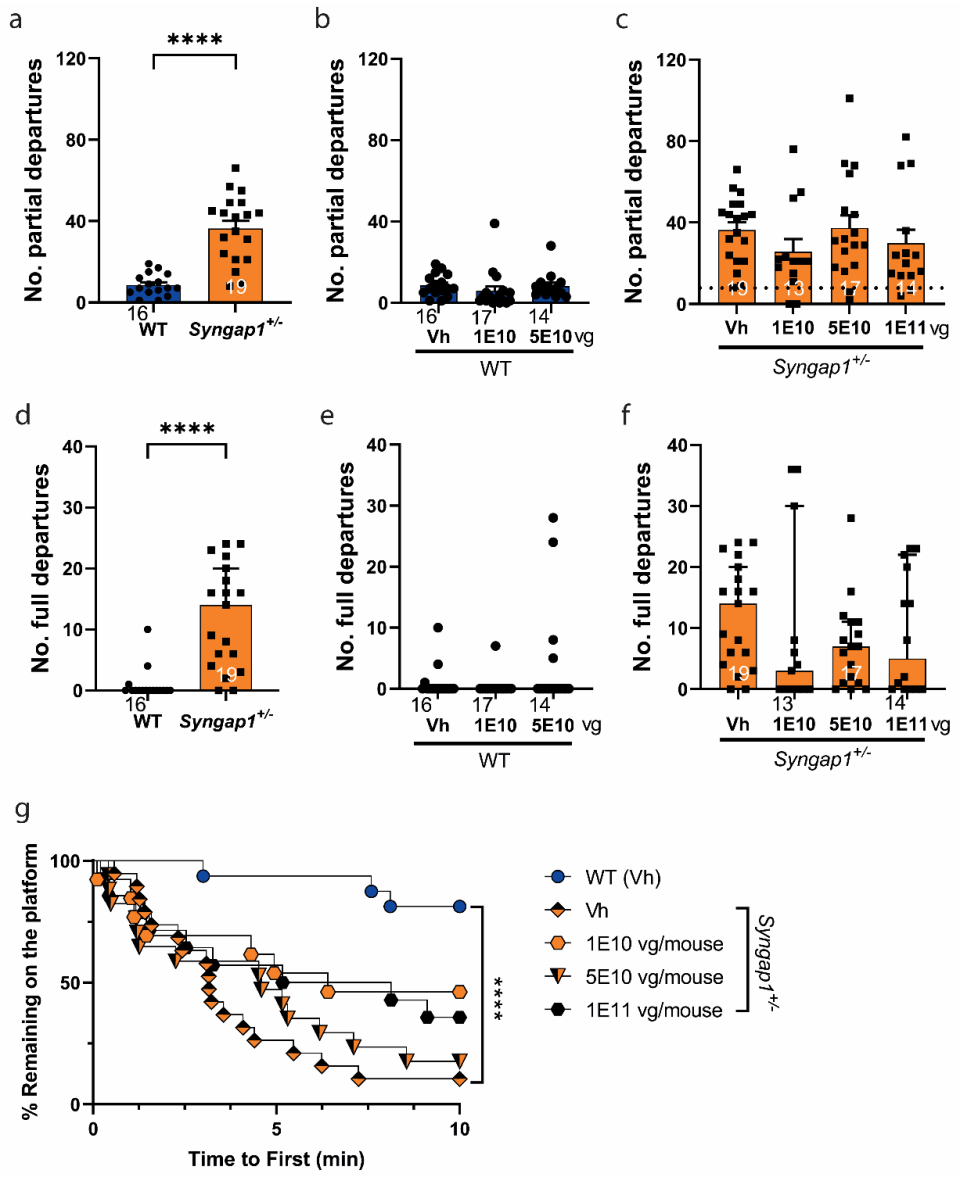

Figure 5-10. 15-weeks-old AAV9/JeT-hSYNGAP1 treated Syngap1$^{+/-}$ mice performed a reduced number of full departures and departed from the platform later in time.

Number of partial departures performed by vehicle (Vh) treated wild-type (WT) and *Syngap1*$^{+/-}$ mice (a) and by wild-type (b) and *Syngap1*$^{+/-}$ mice (c) of all treatment groups at 15 weeks of age. Number of full departures performed by vehicle-treated wild-type and *Syngap1*$^{+/-}$ mice (d) and by wild-type (e) and *Syngap1*$^{+/-}$ (f) of all treatment groups at 15 weeks of age. Percentage of vehicle-treated wild-type and *Syngap1*$^{+/-}$ mice of all treatment groups (g) that remained on the platform and time to first departure at 15 weeks of age.

Dotted line represents wild-type behaviour. Circles and squares represent single animals. Numbers within or under the bars represent the n of each group.

a) Two-tailed Student's t-test with Welch's correction. b,c) Welch's ANOVA. Mean ± SEM.

d) Two-tailed Mann-Whitney test. e,f) Kruskal-Wallis test. Median and 95% CI.

g) Log-rank (Mantel-Cox) test. **** p<0.0001.

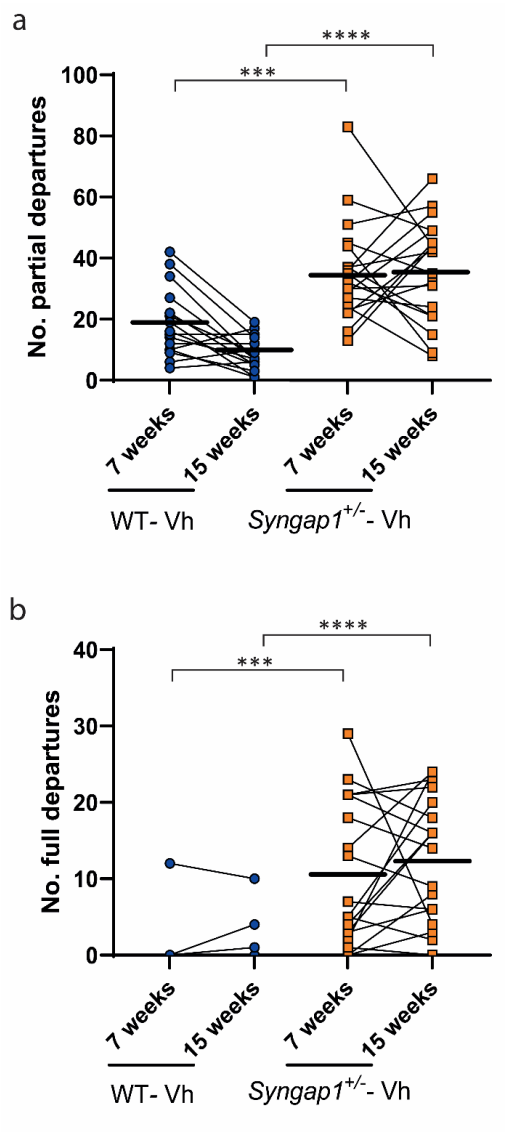

Figure 5-11. Wild-type and Syngap1$^{+/-}$ mice did not show habituation to the platform departure test.

Number of partial departures (a) and number of full departures (b) performed by wild-type and *Syngap1*$^{+/-}$ mice at 7 weeks and 15 weeks of age. Circles and squares represent single animals. Data related to the vehicle-treated wild-type and *Syngap1*$^{+/-}$ mice. Dark black bars represent the means. Wild-type n=16, *Syngap1*$^{+/-}$ n=19.
RM Two-way ANOVA. *** p<0.001, **** p<0.0001.

5.4.3 Biodistribution analysis showed a high number of viral vector genomes in cortex and striatum while a lower distribution was observed in hippocampus and thalamus

Following the *in vivo* phase of the study, I proceeded to assess the viral vector biodistribution. The aim of this experiment was to relate the functional findings with viral vector distribution in different brain areas. I quantified the viral vector genome in the cortex, hippocampus, striatum, thalamus, and cerebellum using qPCR. I used absolute quantification via the standard curve method, which allowed me to calculate the number of viral vector genomes per diploid genome measured as the number of copies of Actb, using standards of known titre. The methodology is detailed in Chapter 2 and primers sequence and optimization process are reported in Appendix C, Section C.3.

Cortex and hippocampus were previously identified as regions where levels of SYNGAP1 are high (Knuesel *et al.*, 2005; Moon *et al.*, 2008; Porter *et al.*, 2005; Tomoda *et al.*, 2004) and where the majority of circuit and cellular dysfunctions associated with *SYNGAP1* haploinsufficiency were observed (Barnett *et al.*, 2006; Michaelson *et al.*, 2018; Muhia *et al.*, 2012; Ozkan *et al.*, 2014). *SYNGAP1* is also expressed in striatum (Knuesel *et al.*, 2005; Moon *et al.*, 2008; Porter *et al.*, 2005; Tomoda *et al.*, 2004). Investigation of biodistribution in thalamus and cerebellum, where SYNGAP1 is expressed at low levels (Gou *et al.*, 2020; Moon *et al.*, 2008; Porter *et al.*, 2005), aimed to understand the viral vector spread.

Cortical samples, collected from the somatomotor and motor cortex, presented the highest levels of vector biodistribution (Figure 5-12a; Welch's ANOVA, mean ± SEM; vehicle n=3, 4.04E-5 ± 2.61E-5 vg/dg; 1E10 vg/mouse n=3, 0.31 ± 0.10 vg/dg; 5E10 vg/mouse n=3, 1.65 ± 0.75 vg/dg; 1E11 vg/mouse n=3, 4.70 ± 0.74 vg/dg; $W_{(3.00, 3.333)}$=12.85, p=0.0252; Dunnett's T3 multiple comparison test results are reported in Table S-16).

Low copy number of viral vector genomes were recorded instead in the cerebellum and thalamus (Figure 5-12e and d; cerebellum, Welch's ANOVA, mean ± SEM; vehicle n=3, 6.05E-5 ± 4.59E-5 vg/dg; 1E10 vg/mouse n=3, 0.0018 ± 0.001 vg/dg; 5E10 vg/mouse n=3, 0.017 ± 0.006 vg/dg; 1E11 vg/mouse n=3, 0.051 ± 0.013 vg/dg; $W_{(3.00, 2.999)}$=6.128, p=0.0734. Thalamus; Welch's ANOVA, mean ± SEM; vehicle n=3, 0.00017 ± 8.43E-5 vg/dg; 1E10 vg/mouse n=3, 0.026 ± 0.011 vg/dg; 5E10 vg/mouse n=3, 2.53 ± 2.00 vg/dg; 1E11 vg/mouse n=3, 1.11 ± 0.49 vg/dg; $W_{(3.00, 3.336)}$=3.027, p=0.1791).

Analysis showed that the hippocampus presented about half the number of viral vector genomes seen in cortex, suggesting a reduced distribution in this area (Figure 5-12b; Welch's ANOVA, mean ± SEM; vehicle n=3, 1.02E-4 ± 5.42E-5 vg/dg; 1E10 vg/mouse n=3, 0.12 ± 0.064 vg/dg; 5E10 vg/mouse n=3, 0.84 ± 0.44 vg/dg; 1E11 vg/mouse n=3, 2.48 ± 1.10 vg/dg; $W_{(3.00, 3.333)}$=2.957, p=0.1840).
Similarly it was observed in the striatum (Figure 5-12c; ; Welch's ANOVA, mean ± SEM; vehicle n=3, 0.0008 ± 0.0006 vg/dg; 1E10 vg/mouse n=3, 0.33 ± 0.076 vg/dg; 5E10 vg/mouse n=3, 1.02 ± 0.18 vg/dg; 1E11 vg/mouse n=3, 3.03 ± 0.96 vg/dg; $W_{(3.00, 3.334)}$=14.56, p=0.0210 vg/dg; Dunnett's T3 multiple comparison test results are reported in Table S-17).

Overall, the viral vector reached both regions of interest: cortex and hippocampus, with minimal distribution in areas where SYNGAP1 is normally found in trace amounts: thalamus and cerebellum.

The high intra-group variability observed could be associated with the quality of the injections, which depends on the correct placement of the needle or the occurrence of backflow. The former could result in a higher distribution in regions where only a limited number of vector copies are detected, such as the thalamus. The latter would cause the delivery of a reduced number of viral particles, as a portion of the particles would not reach the tissue, increasing the variability among subjects for the same brain area.

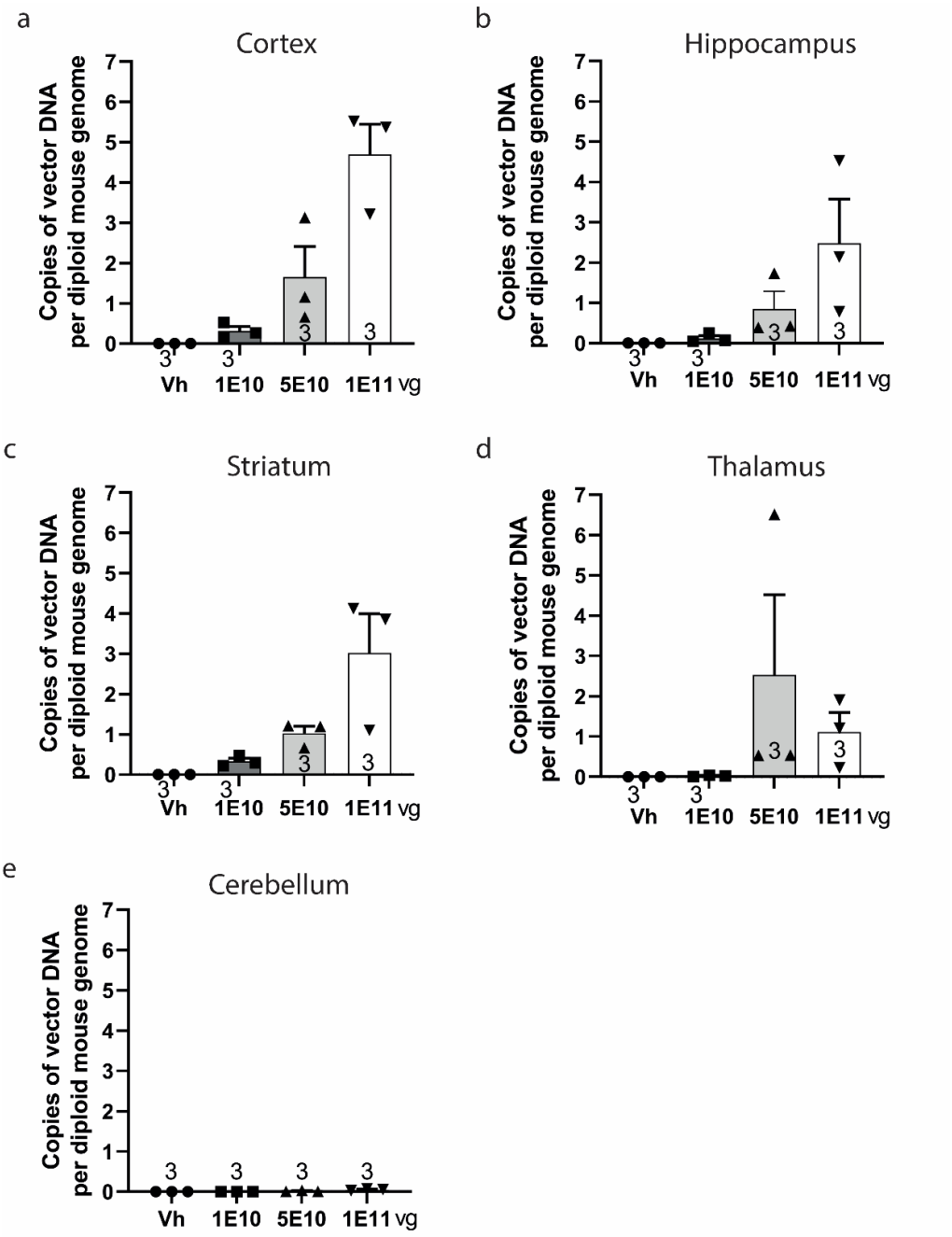

Figure 5-12. AAV9/JeT-hSYNGAP1 viral vector biodistribution analysis showed a dose-dependent trend in cortex, hippocampus and striatum.

Number of viral genomes per diploid genome in cortex (a), hippocampus (b), striatum (c), thalamus (d) and cerebellum (e). Vh=vehicle.

Points represent single animals. Numbers within or under/above the bars represent the n of each group.

Data presented as mean ± SEM. Welch's ANOVA with Dunnett's T3 multiple comparisons test.

5.4.4 Viral vector-derived SYNGAP1 was detectable in the synaptic compartment and showed a dose-dependent expression in cortex

Early rescue studies suggested that the circuit malfunctions observed in forebrain areas are likely to be one of the main causes of the core phenotypes observed in *Syngap1*$^{+/-}$ mice (Muhia *et al.*, 2012; Ozkan *et al.*, 2014) while more recent publications suggest the involvement of SSC and visual cortex in the pathophysiology of the disease (Kilinc *et al.*, 2018; Michaelson *et al.*, 2018). Although no published data is available at the moment, it is reasonable to think that restoring SYNGAP1 expression to near wild-type levels in these areas would be necessary to fully rescue the phenotype observed in *Syngap1*$^{+/-}$ mice.

To investigate the underlying causes of the modest therapeutic effect observed, I evaluated the levels of exogenous protein expressed in the hippocampus and cortex following AAV9/JeT-*hSYNGAP1* treatment. Moreover, to evaluate the ability of the vector-derived protein to localise in the synaptic compartment, where it exerts its primary functions, I investigated its subcellular compartment distribution.

Antibodies used for the quantification of SYNGAP1 and Myc were optimised to obtain linearity of detection as shown in Appendix C, Section C.2.

5.4.4.1 Confirmatory experiments showed that Syngap1$^{+/-}$ *mice express about half the amount of SYNGAP1 protein compared to wild-type controls*

The mouse model used for this work was generated by the in-frame insertion of a targeting vector, causing the deletion of the region spanning exon 8, 9 and 10 (for a detailed description refer to Chapter 2). As a result, *Syngap1*$^{+/-}$ mice are reported to express approximately half the level of SYNGAP1 protein observed in wild-type mice (Komiyama *et al.*, 2002).

To confirm this finding, I evaluated SYNGAP1 levels in protein lysate from cortex and hippocampus derived from wild-type and *Syngap1*$^{+/-}$ mice via immunoblotting. As the 5E10 vg/mouse treatment group was sacrificed at 20-22 weeks of age while mice treated with 1E10 and 1E11 vg/mouse were sacrificed at 28-31 weeks of age, the two

groups were analysed separately. Endogenous SYNGAP1 level was evaluated in age-matched groups.

At 20 weeks of age, in the cortex, *Syngap1*$^{+/-}$ mice showed a ~50% reduction of SYNGAP1 protein (Figure 5-13b; two-tailed Student's t-test with Welch's correction, mean ± SEM; wild-type, n=3 1.00 ± 0.03; *Syngap1*$^{+/-}$, n=3 0.48 ± 0.02; $t_{(3.939)}$=13.85, p=0.0002). A reduction of about half was observed at 28 weeks of age, although the comparison between genotypes did not result significant (Figure 5-13c; two-tailed Student's t-test with Welch's correction, mean ± SEM; wild-type, n=3 1.00 ± 0.14; *Syngap1*$^{+/-}$, n=3 0.60 ± 0.11; $t_{(3.795)}$=2.240, p=0.0923).

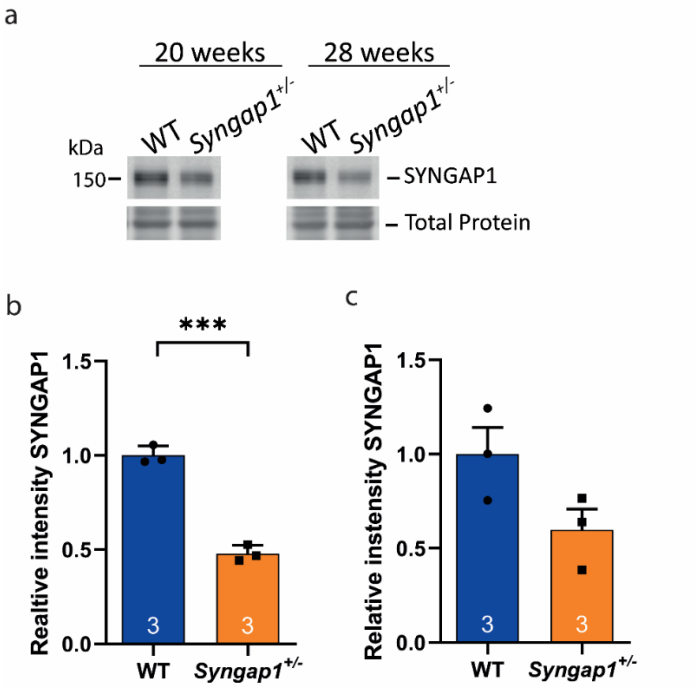

Figure 5-13. About 50% reduction of SYNGAP1 protein was detected in protein lysate derived from cortex of Syngap1$^{+/-}$ mice.
Representative immunoblot of cortex protein lysate from wild-type and *Syngap1*$^{+/-}$ mice cortex at 20 weeks and 28 weeks of age (a) labelled with anti-SYNGAP1 antibody. Immunoblot quantification for samples collected at 20 weeks of age (b) and 28 weeks of age (c). SYNGAP1 signal was normalised to the average signal detected in wild-type tissue. Total protein was used as loading control. Images used for quantification are reported in Figure S-27. The gel was used at a concentration of bis acrylamide of 10%. Circles and squares represent single animals. Numbers within the bars represent the n of each group.
Data presented as mean ± SEM, two-tailed Student's t-test with Welch's correction. *** p<0.001.

In the hippocampus, at both tested ages, a significant reduction of SYNGAP1 levels was detected in tissue from *Syngap1*$^{+/-}$ mice relative to wild-type (Figure 5-14b and c; two-tailed Student's t-test with Welch's correction, mean ± SEM; 20 weeks, wild-type n=3 1.00 ± 0.12; *Syngap1*$^{+/-}$, n=3 0.53 ± 0.08; $t_{(3.456)}$=3.10, p=0.0441. 28 weeks, wild-type n=3 1.00 ± 0.03; *Syngap1*$^{+/-}$, n=3 0.44 ± 0.05; $t_{(3.158)}$=8.74, p=0.0026).

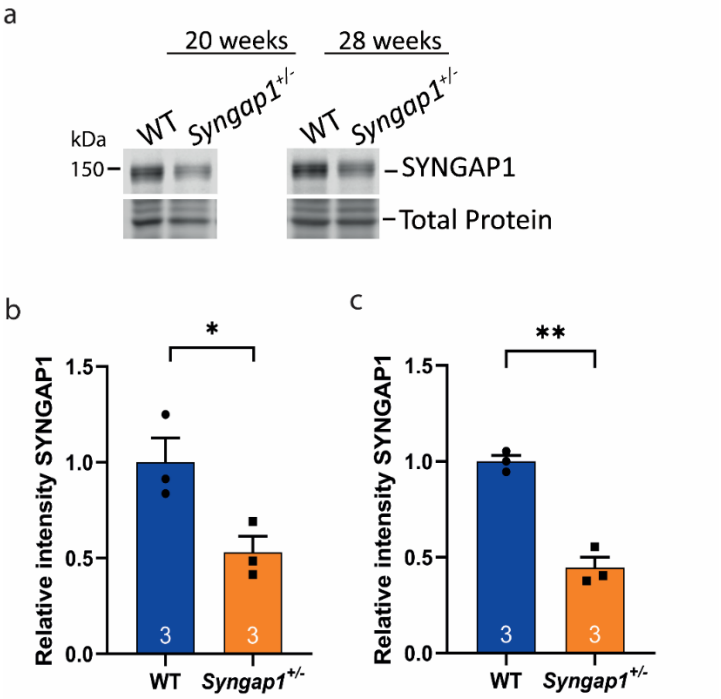

Figure 5-14. A reduction of SYNGAP1 protein of about 50% was detected in protein lysate derived from hippocampus of Syngap1$^{+/-}$ mice.

Representative immunoblot of hippocampus protein lysate from wild-type and *Syngap1*$^{+/-}$ mice cortex at 20 weeks and 28 weeks of age (a) labelled with anti-SYNGAP1 antibody. Immunoblot quantification for samples collected at 20 weeks of age (b) and 28 weeks of age (c). SYNGAP1 signal was normalised to the average signal detected in wild-type tissue. Total protein was used as loading control. Images used for quantification are reported in Figure S-28. The gel was used at a concentration of bis acrylamide of 10%. Circles and squares represent single animals. Numbers within the bars represent the n of each group.

Data presented as mean ± SEM, two-tailed Student's t-test with Welch's correction. * p<0.05, ** p<0.01.

5.4.4.2 Increase of absolute levels of SYNGAP1 was observable in cortex but not in hippocampus of viral vector-treated Syngap1$^{+/-}$ mice

I then proceeded to evaluate level of exogenous protein achieved in cortex and hippocampus of *Syngap1*$^{+/-}$ treated mice.

In the cortex of *Syngap1*$^{+/-}$ mice, at all considered viral vector doses, Myc-tagged protein was detectable and when the signal associated to Myc immunolabelling was quantified a dose-dependent increase in expression was detected (Figure 5-15e; Welch's ANOVA, mean ± SEM; vehicle, n=6 0.01 ± 0.003; 1E10 vg/mouse, n=6 0.30 ± 0.11; 1E11 vg/mouse, n=6 1.00 ± 0.08; $W_{(2.00,\ 6.684)}$=68.14, p<0.0001, Dunnett's T3 multiple comparison test results are reported in Table S-18). Similarly, in 5E10 vg/mouse treated mice, SYNGAP1-Myc was detected above noise level (Figure 5-15c; two-tailed Student's t-test with Welch's correction, mean ± SEM; vehicle, n=6 0.03 ± 0.009; 5E10 vg/mouse, n=6 1.00 ± 0.15; $t_{(5.033)}$=6.445, p=0.0013).

As the anti-SYNGAP1 antibody recognises both human and mouse-derived protein, it is possible to compare the absolute level of SYNGAP1 present in viral vector and vehicle-treated tissue to evaluate if an increase was achieved after viral vector treatment. The signal observed in viral vector-treated tissue is given by the sum of the endogenous and exogenous SYNGAP1 protein.

In the tissue treated with 5E10 vg/mouse a significant increase in absolute levels of SYNGAP1, with a range of 1x to 1.8x of vehicle control, was observed (Figure 5-15b; two-tailed Student's t-test with Welch's correction, mean ± SEM; vehicle, n=6 1.00 ± 0.07; 5E10 vg/mouse, n=6 1.42 ± 0.11; $t_{(8.447)}$=3.206, p=0.0116). Cortex derived from mice treated with 1E11 vg/mouse showed an average, non-significant, increase in SYNGAP1 protein ranging from 1x to 2.2x of vehicle control, while scarce, if no, increase was observed for tissue injected with 1E10 vg/mouse (0.3 to 0.9x of wild-type levels) (Figure 5-15d; Welch's ANOVA, mean ± SEM; vehicle, n=6 1.00 ± 0.15; 1E10 vg/mouse, n=6 1.18 ± 0.20; 1E11 vg/mouse, n=6 1.51 ± 0.22; $W_{(2.00,\ 9.702)}$=1.724, p=0.2288).

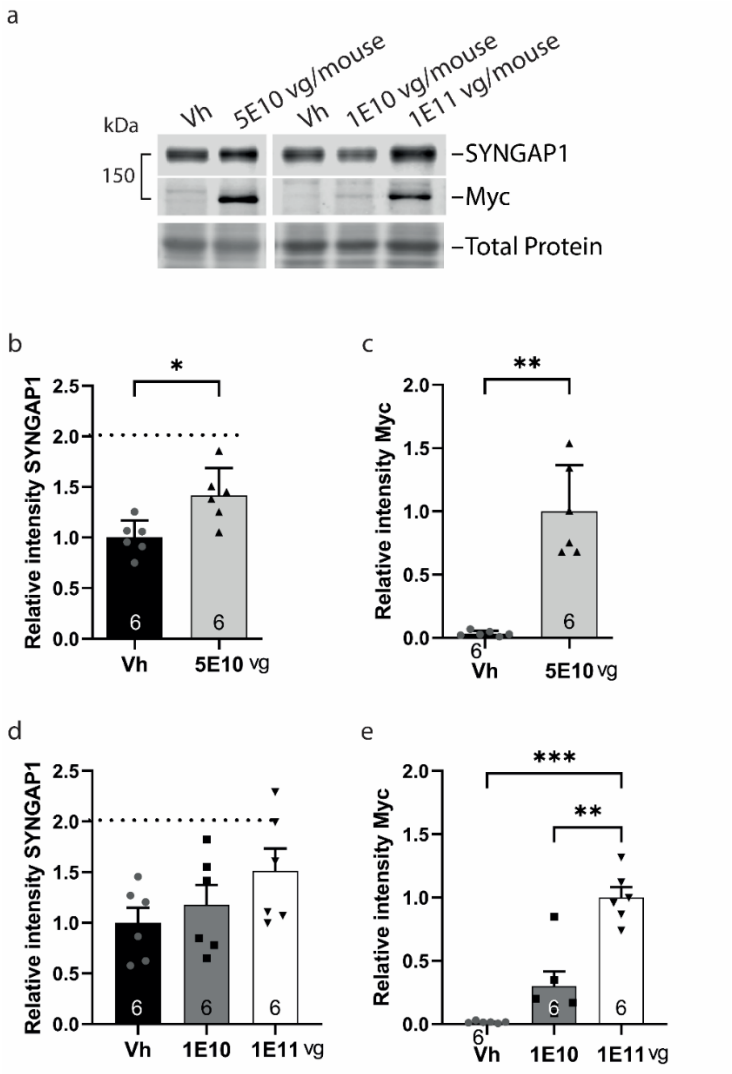

Figure 5-15. AAV9/JeT-hSYNGAP1 viral vector-derived protein dose-dependent expression was observed in cortex.

Representative immunoblot of cortex protein lysate labelled with anti-Myc and anti-SYNGAP1 antibodies (a). Quantification of SYNGAP1 (normalised to vehicle treated) and Myc (normalised to 1E11 vg/mouse treated) in cortex derived from *Syngap1*$^{+/-}$ mice treated with vehicle (Vh) or 5E10 vg/mouse (b and c) and vehicle or 1E10 and 1E11 vg/mouse (d and e).

Cortex of mice treated with 5E10 vg/mouse and correspondent controls was collected at 20-22 weeks of age. Cortex of mice treated with 1E10 and 1E11 vg/mouse and correspondent control was collected at 28-31 weeks of age. Dotted line represents wild-type levels. Total protein was used as loading control. Images used for quantification are reported in Figure S-29. The gel was used at a concentration of bis acrylamide of 10%. Points represent single animals. Numbers within or under the bars represent the n of each group.

Data presented as mean ± SEM. a,b) Two-tailed Student's t-test with Welch's correction. c,d) Welch's ANOVA with Dunnett's T3 multiple comparisons test.

* p<0.05, **p<0.01, ***p<0.001.

When protein expression was evaluated in hippocampus, tissue treated with viral vector at a dose of 1E10 vg/mouse showed a very low amount of Myc-tagged protein, while higher levels were detected in tissue treated with 1E11 vg/mouse (Figure 5-16a and e). Quantification showed a non-significant difference in relative amounts of the Myc-tagged protein between low and high doses (Figure 5-16e; Welch's ANOVA, mean ± SEM; vehicle, n=6 -0.01 ± 0.05; 1E10 vg/mouse, n=6 0.12 ± 0.05; 1E11 vg/mouse, n=6 1.00 ± 0.30; $W_{(2.00,\ 8.932)}$=6.157, p=0.0169; Dunnett's multiple comparison test results are reported in Table S-19). SYNGAP1-Myc protein was detected in the lysate of 5E10 vg/mouse treated tissue (Figure 5-16c; two-tailed Student's t-test with Welch's correction, mean ± SEM; vehicle, n=6 -0.04 ± 0.08; 5E10 vg/mouse, n=6 1.00 ± 0.33; $t_{(5.644)}$=3.034, p=0.0248).

Quantification of absolute levels of SYNGAP1 protein showed that no increase in the absolute levels of SYNGAP1 was observed in viral vector-treated tissue compared to vehicle control for all considered doses (Figure 5-16b; two-tailed Student's t-test with Welch's correction, mean ± SEM; vehicle, n=6 1.00 ± 0.15; 5E10 vg/mouse, n=6 0.81 ± 0.08; $t_{(7.959)}$=1.111, p=0.2989. Figure 5-16d; Welch's ANOVA, mean ± SEM; vehicle, n=6 1.00 ± 0.04; 1E10 vg/mouse, n=6 0.60 ± 0.14; 1E11 vg/mouse, n=6 0.72 ± 0.14; $W_{(2.00,\ 7.691)}$=4.473, p=0.0995).

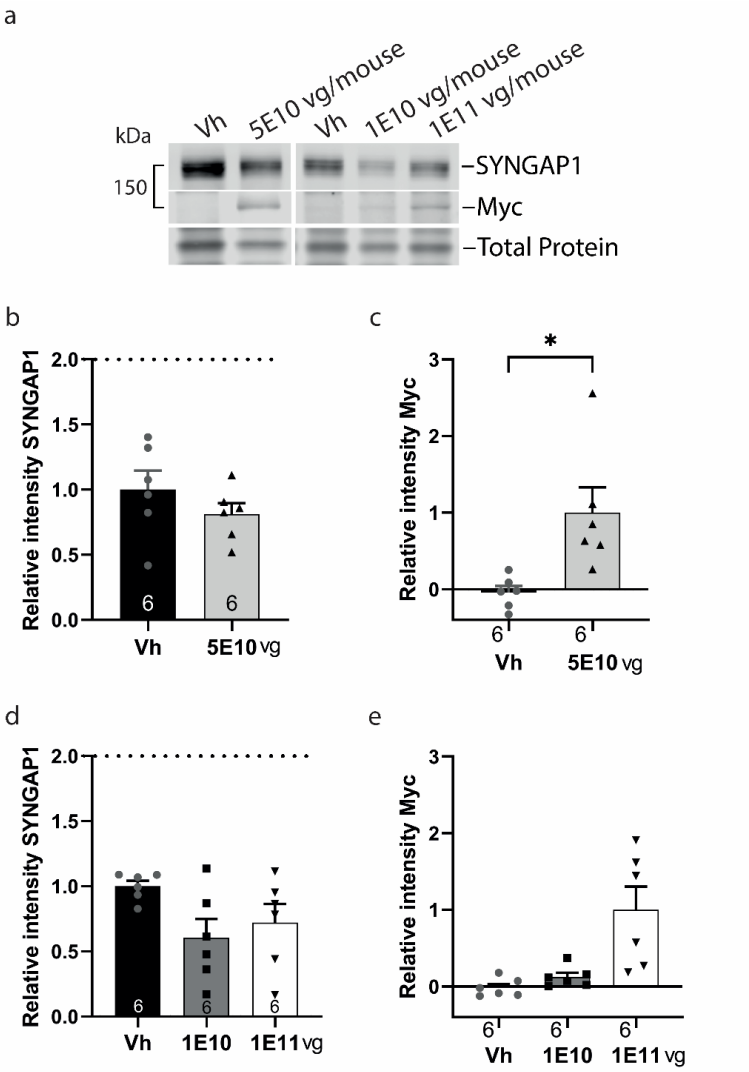

Figure 5-16. AAV9/JeT-hSYNGAP1 viral vector-derived SYNGAP1 was detectable in the hippocampus via immunoblot analysis of protein lysate.

Representative immunoblot of hippocampus protein lysate labelled with anti-Myc and anti-SYNGAP1 antibodies (a). Quantification of SYNGAP1 (normalised to vehicle treated) and Myc (normalised to 1E11 vg/mouse treated) in hippocampus derived from *Syngap1*$^{+/-}$ mice treated with vehicle (Vh) or 5E10 vg/mouse (b and c) and vehicle or 1E10 and 1E11 vg/mouse (d and e).

Hippocampus of mice treated with 5E10 vg/mouse and correspondent controls was collected at 20-22 weeks of age. Hippocampus of mice treated with 1E10 and 1E11 vg/mouse and correspondent control was collected at 28-31 weeks of age. Points represent single animals. Dotted line represents wild-type levels. Numbers within or under the bars represent the n of each group. Total protein was used as loading control. Images used for quantification are reported in Figure S-30. The gel was used at a concentration of bis acrylamide of 10%.

Data presented as mean ± SEM. a,b) Two-tailed Student's t-test with Welch's correction. c,d) Welch's ANOVA with Dunnett's T3 multiple comparisons test.

* $p<0.05$.

5.4.4.3 Vector-derived protein correctly localised in the synaptic compartment

α1 isoform of SYNGAP1 protein exerts its primary function in the synaptic compartment (Guo *et al.*, 2009; Komiyama *et al.*, 2002; Krepischi *et al.*, 2010; Walkup *et al.*, 2016), and although the protein can be identified in other subcellular compartments depending on the isoform considered (Gou *et al.*, 2020), it is the most enriched isoform in the synaptic compartment (Araki *et al.*, 2020).

The subcellular expression of the viral vector-derived Myc-tagged SYNGAP1 protein was assessed by evaluating the presence or absence within the synaptosomal fraction of hippocampal samples. For this, I used a modification of a previously published protocol from Bermejo *et al.* (Bermejo *et al.*, 2014). The original protocol allows the isolation of a highly enriched PSD fraction via a series of centrifugation steps and a final step of ultracentrifugation step in the presence of a sucrose gradient. For this study, obtaining a highly enriched PSD fraction was not necessary. The optimisation steps are described in Appendix C, Section C.1.

As this protocol was implemented later during the study, only tissue deriving from animals injected with AAV9/JeT-*hSYNGAP1* at the doses of 1E10 and 1E11 vg/mouse were processed for synaptosomal preparation.

The optimised protocol allowed for better enrichment of synaptic markers in the synaptosomal fraction compared to the input, but a large amount of protein was lost during the first step of centrifugation, which caused high contamination of the nuclear fraction (Figure 5-17). As shown in Figure 5-16, Myc-tagged SYNGAP1 was detected in hippocampal tissue treated with the 1E10 vg/mouse dose at very low levels. In the subcellular fractions prepared from 1E10 vg/mouse injected tissue, the Myc signal was not detectable. Exogenous SYNGAP1 was instead detected in tissue treated with the 1E11 vg/mouse dose (Figure 5-17). The presence of signal associated to the Myc fusion peptide in the synaptosome fraction, and its depletion from the cytosolic fraction, suggested the correct translocation of the viral vector-derived protein to the synaptic compartment.

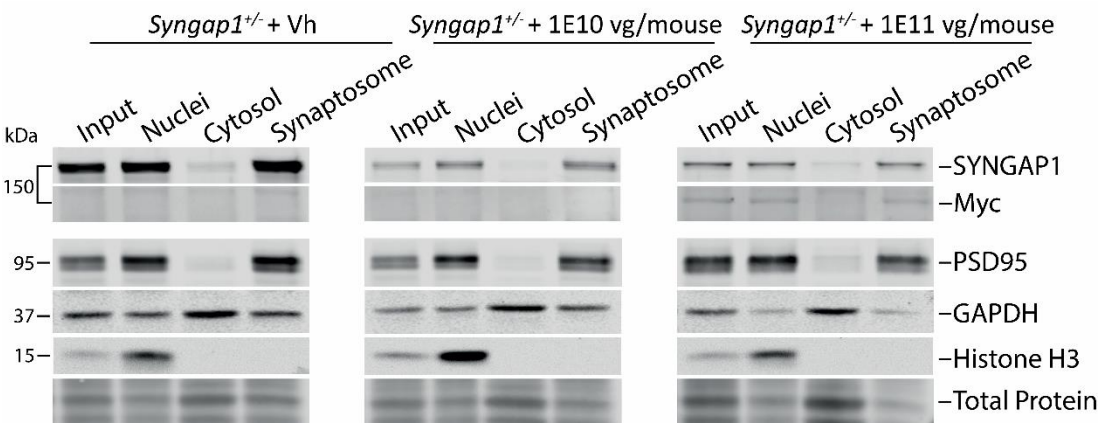

Figure 5-17. AAV9/JeT-hSYNGAP1 derived SYNGAP1-Myc was present in the synaptosomal fraction and resulted undetectable in the cytosolic compartment.
Representative immunoblot of synaptosomal preparation of whole hippocampi and labelled with subcellular fraction-specific markers. Tissue from vehicle (Vh) and viral vector-treated *Syngap1*$^{+/-}$mice collected at 28-31 weeks of age. The gel was used at a concentration of bis acrylamide of 12%.

5.5 DISCUSSION

The aim of the work presented in this chapter was to evaluate the ability of the second generation candidate gene therapy construct expressing the human *SYNGAP1* Aα1 isoform to rescue the behavioural phenotype observed in the *SYNGAP1* haploinsufficiency mouse model. Behavioural phenotyping of *Syngap1*$^{+/-}$ mice treated with 1E10, 5E10 and 1E11 vg/mouse showed a trend toward the amelioration of the risk-taking behaviour, while hyperactivity and increased time spent in the open arms of the elevated plus maze were unaffected. Analysis of absolute levels of SYNGAP1 showed limited variation, and SYNGAP1 remained at sub-physiological levels.

As discussed in Chapter 3, hyperactivity emerges to be one of the most prominent behavioural phenotypes present in *Syngap1*$^{+/-}$ mice. It has been reported in previous publications that hippocampal dysfunction may lead to increased locomotor activity and anxiety disorders (Bannerman *et al.*, 2003; Bast *et al.*, 2003; Deacon *et al.*, 2002; Gray *et al.*, 1983; Pouzet, 1999; Wiley *et al.*, 1995).

Muhia *et al.* (Muhia *et al.*, 2012) showed how the total absence of SYNGAP1 expression in the hippocampus of 8-weeks-old mice caused a significant increase of horizontal activity but not a reduction of anxiety. Ozkan *et al.* (Ozkan *et al.*, 2014) showed that induction of haploinsufficiency in forebrain areas induced the development of the phenotypes typically observed in the germline *Syngap1*$^{+/-}$ mouse model. The same paper reported that induction of *Syngap1* expression limited to forebrain areas was not sufficient to prevent the development of hyperactivity, suggesting the involvement of extra-cortical areas that have not yet been identified in the development of such behaviours. Although data are still limited, published results suggest that the cortex and hippocampus are not the sole players in the development of hyperactivity, but they are likely to be key elements. It is, therefore, reasonable to think that to observe an improvement of the hyperactivity phenotype, it is important to reach a high level of transduction and exogenous protein expression in these areas.

In treated hippocampi, absolute levels of SYNGAP1 protein were not significantly increased above the sensitivity of the anti-SYNGAP1 assay (Figure 5-16).
Immunoblot staining with anti-Myc antibody showed that tissue treated with the 1E10 vg/mouse dose presented very low levels of Myc-tagged SYNGAP1, which was in accordance with the result shown by the anti-SYNGAP1 assay (Figure 5-16e). These findings were consistent with data from the biodistribution analysis, which showed relatively low copy numbers per diploid genome in the 1E10 vg/mouse-treated tissue. The low levels of vector-derived protein detected in the hippocampus could explain the lack of treatment effects on hyperactivity.

Cellular and circuital dysfunction, together with structural abnormalities, have been described during development in cortex of *Syngap1*$^{+/-}$ mice, particularly in the SSC and prefrontal cortex (Aceti *et al.*, 2015; Michaelson *et al.*, 2018). Michaelson *et al.* (Michaelson *et al.*, 2018) observed reduced excitability and connectivity of glutamatergic neurons in the SSC of *Syngap1*$^{+/-}$ mice, resulting in a reduction of touch-related activity. Altered sensory processing is a reported phenotype in *SYNGAP1*

patients (Michaelson *et al.*, 2018). Kilinc *et al.* (Kilinc *et al.*, 2018) showed that cortical regions, including many related to the visual system and secondary SSC, presented a reduction in volume. It is possible that these structural and functional changes in areas of sensory stimuli processing are one of the underlying causes of the increased impulsivity and risk-taking behaviour observed in *Syngap1*$^{+/-}$ mice.

The variation of absolute levels of SYNGAP1 protein observed in the cortex was in the range of 0.6 (for 1E10 vg/mouse) to 2.2x (for 1E11 vg/mouse treated mice) the levels observed in the *Syngap1*$^{+/-}$ vehicle controls Although this increment did not significantly differ from the vehicle, it is possible that the trend toward the reduction of the number of full departures performed by viral vector-treated *Syngap1*$^{+/-}$ mice during the platform departures test (Section 5.4.2.3) was associated to the variation in SYNGAP1 levels.

It is known that the JeT promoter is a relatively weak promoter compared to more commonly used regulatory elements such as the CMV promoter (Tornoe *et al.*, 2002). Despite this, the level of viral vector-derived SYNGAP1 expression achieved in this experiment was lower than expected, as only in the cortex treated with a viral vector at a dose of 5E10 vg/mouse was a significant difference observable in absolute levels of SYNGAP1. The reason for such results could be associated with the intrinsic technical limitations of the assay used. I demonstrated that SYNGAP1 antibody detection is linear, but this does not consider the intrinsic sensitivity of the assay. The non-significant difference seen in the cortex and hippocampus (Figure 5-15 and Figure 5-16), could be caused by a relatively low sensitivity of the antibody to small changes in protein quantity.

Another element to consider is that the comparison performed was between the increment given by the expression of a single isoform over the total of the endogenous isoforms expressed in the tissue. In fact, the antibody used for this assay recognises a region of SYNGAP1 that is common to all isoforms, while the viral vector produces only one isoform, Aα1. When the analysis was performed the entire SYNGAP1 positive band was quantified as it was not possible to distinguish bands

associated with the single isoforms. It is possible that the small increase caused by the expression of one isoform was not detectable over the noise presented by the unrelated isoforms. Consequently, I may have underestimated how much protein was actually produced from the therapeutic cassette. The use of isoform-specific antibodies would allow a better understanding of the variation in Aα1 level in viral vector-treated mice. C-terminal specific antibodies have been developed in-house by laboratories studying SYNGAP1 (Araki *et al.*, 2020; Gou *et al.*, 2020) and one α1 specific antibody is commercially distributed, but at the time of the work presented in this thesis, it was not available. Future experiments investigating α1 level with this antibody would be important for a better understanding of viral vector SYNGAP1 expression.

In addition to what was previously discussed, another assumption made for the immunoblot quantification is that the antibody can detect vector-derived (human) and endogenous (mouse) SYNGAP1 with the same efficiency. The protein sequence is highly conserved between species and, as reported by the antibody manufacturer, the region where the epitope is localised presents only one amino acid change between mouse/rat and human. For this reason, and because it is not known if the amino acid change is localised in the antigenic sequence, we assumed equal affinity. However, this was not experimentally tested.

The trend toward the reduction of the number of full departures appeared to not be dose-dependent. The most significant difference was seen with the 1E10 and 1E11 vg/mouse doses, while mice treated with 5E10 vg/mouse were indistinguishable from controls treated with vehicle. The amount of Myc-tagged protein detected in tissue treated with 1E10 vg/mouse was about one-third that of the high-dose treated tissue. Assuming that the amount of protein produced by the 5E10 vg/mouse dose was intermediate between the other two doses, it remains unclear why the putative trend toward ameliorating risk-taking behaviour was observed with the lowest dose and not with 5E10 vg/mouse. It is possible that this trend was due to chance rather than a genuine effect of the treatment.

A possible explanation for the absence of a dose-dependent response during the platform departure test may reside in the distribution of treatments across groups and time. Initially, only vehicle and 5E10 vg/mouse viral vector dose were injected, and only later were mice treated with the 1E10 and 1E11 vg/mouse. Due to the longitudinal nature of this study, even though mice treated with vehicle and 5E10 vg/mouse were injected before starting the injections for the 1E10 and 1E11 vg/mouse doses, the timing of tests for all groups overlapped (15-week-old 5E10 vg/mouse treated mice were tested in the same period as 7-week-old 1E10 or 1E11 vg/mouse treated mice). Although nothing in the housing or testing environment was different between groups, it is possible that this difference might have impacted to some extent the behavioural outcome.

SYNGAP1 presents a CC domain at the C-terminus, which allows the protein to interact with other SYNGAP1 molecules and form trimers. Protein trimerization play an important role in its ability to interact with PSD95 and the PSD more broadly (Zeng *et al.*, 2016). As the SYNGAP1 protein expressed by the viral vector presented an intact CC domain and PDZ binding motif, I hypothesised that the presence of a C-terminal fused Myc peptide would not impact the normal protein function and localisation.

More recent publications have provided deeper insight into the importance of an intact, unmodified C-terminus. Araki *et al.* (Araki *et al.*, 2020) showed that the α1 isoform carrying a mutation in the CC domain, which disrupt liquid-liquid phase transition and prevent protein trimerization, is less enriched at the synapses and it is not able to regulate plasticity events. They demonstrated that mutant α1 behaves similarly to wild-type β isoform, as its expression can rescue the arborisation phenotype observed in haploinsufficiency condition and only partially affect LTP. More recently, Kilinc *et al.* (Kilinc *et al.*, 2022) showed that mice expressing normal levels of the wild-type β and α2 isoform but harbouring a α1 carrying missense mutations in the PBM, present cellular and behavioural phenotypes comparable to *Syngap1*$^{+/-}$ mice.

I showed that SYNGAP1-Myc was detectable in the synaptic compartment while it was depleted from the cytosol, suggesting correct subcellular localisation (Figure 5-17). As LTP and cellular structure were not investigated in this work, it is not clear if the Myc-tagged SYNGAP1 is able to exert all the functions in which it is involved. Although the effect of the presence of an extra element at the C-terminus it is still not elucidated, it is possible that the presence of the Myc peptide may have impacted the protein's ability to form trimers and therefore affect its ability to rescue the plasticity and behavioural phenotype (Araki *et al.*, 2020; Kilinc *et al.*, 2022). Investigating the ability of the C-terminal Myc-tagged SYNGAP1 protein to form trimers and the same interactome seen in wild-type tissue would allow us to understand the impact of such modifications.

5.6 CONCLUSION

To summarise, I have shown that viral vector-derived Myc-tagged SYNGAP1 was detectable *in vivo* five weeks after the injection of the AAV9/JeT-*hSYNGAP1* viral vector.

I showed that the treatment did not affect behaviour in the open field or in the elevated plus maze, but a modest therapeutic effect was observed during the platform departure test. 1E10 and 1E11 vg/mouse treated *Syngap1*$^{+/-}$ mice showed a reduction in the number of full departures and perform the first full departure later in time.

Dose-dependent expression of vector-derived SYNGAP1 was detected in cortex and hippocampus using a sensitive anti-Myc antibody. However, quantification of absolute levels of SYNGAP1 protein showed a not significant increase in cortex, while no increment was observed in hippocampus. This suggests that only a relatively low level of viral vector-derived protein was achieved, and the consequent inability to reach wild-type physiological levels.

In terms of protein localisation, I demonstrated that viral vector-derived protein was detectable in the synaptosomal fraction and depleted from cytosolic compartment, adopting the pattern of subcellular localisation seen with the endogenous protein.

To conclude, the risk-taking behaviour of viral vector-treated *Syngap1*$^{+/-}$ mice showed a trend toward amelioration. It was not elucidated whether the modest effect was associated with too little expression of the viral vector-encoded protein or if the delivered protein was not able to exert the full spectrum of the wild-type protein functions due to the presence of the C-terminal Myc fusion peptide. For this reason, a third-generation therapeutic cassette was designed with the aim to improve the expression of SYNGAP1. This is presented in Chapter 6.

CHAPTER 6: *A*SSESSMENT OF THE THIRD GENERATION CANDIDATE GENE THERAPY CONSTRUCT hSYN1-*hSYNGAP1(OPT)_Aα1* THERAPEUTIC EFFICACY *IN VIVO*

6.1 INTRODUCTION

The therapeutic efficacy study conducted using the second generation AAV9/JeT-*hSYNGAP1,* as detailed in Chapter 5, showed the potential of gene therapy for the amelioration of risk-taking behaviour. It is possible that the limited effect observed on behaviour was a consequence of the relatively low expression of vector-derived protein in disease-relevant brain regions such as the cortex and hippocampus that could have been associated with the relatively weak strength of the promoter used, JeT.

With the aim of improving transgene expression, and possibly therapeutic efficacy, the gene therapy cassette was redesigned by modifying the promoter, regulatory elements and codon-optimising the transgene sequence.

Synapsins are a family of phosphoproteins expressed in both excitatory and inhibitory neurons, involved in the regulation of synaptic vesicle trafficking and neurotransmitter release (Greengard *et al.*, 1993; Song *et al.*, 2016). The human *SYNAPSIN1* promoter (hSYN1) is a short promoter fragment (~470 bp) with neuronal-specific activity (Kügler *et al.*, 2003). This promoter has been shown to drive transgene expression in cortical areas of interest for this project, like cortex, hippocampus and striatum (McLean *et al.*, 2014). Given the reduced size and the predicted expression pattern, it was decided to substitute the JeT promoter with the hSYN1 promoter.

It is well-established that SYNGAP1 forms trimers through the association of its C-terminal CC domain (Zeng *et al.*, 2016). Mutations in the CC domain prevent trimerization, limiting the ability of the protein to exert isoform-specific functions and

to associate with the PSD without completely abolishing the synaptic compartment localisation (Araki *et al.*, 2020; Kilinc *et al.*, 2022; Zeng *et al.*, 2016).

I demonstrated in Chapter 5, that even in the presence of the C-terminal fusion peptide Myc, vector-derived protein localised in the synaptic compartment, but I did not investigate the ability of the tagged protein to form trimers. To circumvent the theoretical issue that a C-terminal tag could disrupt this important protein-protein interaction, and therefore function, I decided to design a new vector where the tag, in this case FLAG, was placed at the N-terminus. A fusion peptide in this position is not predicted to interfere with other protein-protein interactions. The FLAG peptide, which is an artificial octapeptide tag (Hopp *et al.*, 1988), is highly hydrophilic, reducing the likelihood of abnormal folding of the protein to which it is fused (Terpe, 2003).

In the genetic code, each amino acid, except methionine and tryptophan, is encoded by two or more codons (Crick *et al.*, 1961; Nirenberg *et al.*, 1963). Although theoretically, each amino acid could be represented in the coding sequence of genes by any of its respective codons with the same probability, it has been observed that this was not the case. Codon usage refers to the frequency at which different codons appear in the DNA, and the non-random usage of each codon is defined as codon usage bias, which correlates with the relative abundance of tRNA (Air *et al.*, 1976; Fiers *et al.*, 1975; Ikemura, 1981). Optimising a gene sequence by removing rare codons and substituting them with more commonly used ones, without changing the amino acid sequence, is defined codon optimisation and it has the ability to improve protein expression (Burgess-Brown *et al.*, 2008; Disbrow *et al.*, 2003). The process is widely used in gene therapy constructs where the sequence is optimised for expression in humans (Brown *et al.*, 2018; Ward *et al.*, 2011). The rationale for such an approach is to improve the translational application of the construct, but also to improve the expression of the transgene. Indeed, Brown *et al.* (Brown *et al.*, 2018) and Ward *et al.* (Ward *et al.*, 2011) showed that a codon-optimised sequence for expression in humans, when tested in mice, produced higher levels of protein compared to the same non-codon-optimised sequence. For these reasons, in the new

expression cassette, the codon-optimised sequence for expression in humans of the Aα1 isoform was used.

MoSeq is an ethologically relevant technique that allows the analysis of 3D mouse movements for the identification of single stereotypic behaviours, defined as “syllables” (short 3D motifs of behaviour spanning about 300 ms), and how they relate to each other to identify what has been defined as "behavioural grammar" (Wiltschko *et al.*, 2015). This is possible as the system detects regular elements in the overall behaviour and uses them to identify syllables and the probability and pattern of transition between them (Wiltschko *et al.*, 2015, 2021). To this end, MoSeq uses 3D videos captured using a depth camera and a machine learning algorithm that uncovers underlying modular components of behaviour. An important feature of the system is that the machine learning is unsupervised, meaning that the system is able to identify the stereotyped behaviour without the need for the experimenter to define the behavioural parameters to quantify (Dennis *et al.*, 2021). Thanks to these characteristics, MoSeq has been used to investigate the genotype effect on core behavioural elements (Hadjas *et al.*, 2020; Rudolph *et al.*, 2020; Silachev *et al.*, 2022), understanding how specific circuits shape behaviour (Markowitz *et al.*, 2018; Pisanello *et al.*, 2017) and evaluate the effects of pharmacological treatments (Wiltschko *et al.*, 2021).

6.2 AIM

The aim of the study presented in this chapter was to evaluate the ability of a newly designed third generation ssAAV9 *hSYNGAP1* vector to ameliorate the phenotypes observed in *Syngap1*$^{+/-}$ mice. To this end specific aims were:

- To evaluate the ability of the chosen promoter to express the SYNGAP1 protein *in vitro*.
- To evaluate the expression of the transgene *in vivo* in brain regions relevant to the disease, such as cortex and hippocampus.

- To extend the phenotypic characterisation of *Syngap1*$^{+/-}$ mice by establishing a new behavioural paradigm using MoSeq.
- To evaluate the potential of the designed candidate gene therapy cassette to ameliorate the behavioural abnormalities observed in *Syngap1*$^{+/-}$ mice.
- To evaluate transgene expression tolerability in wild-type mice.

6.3 STUDY PLAN

Detailed methodology is reported in Chapter 2. Briefly, the viral vector (Figure 6-1a) was delivered via ICV injection in PND1-2 neonatal wild-type and *Syngap1*$^{+/-}$ mice at two doses, 5E10 vg/mouse and 1E11 vg/mouse, or vehicle (PBS) as control. To reach the desired *n* for each treatment group, mice were recruited in groups and the period of injections spanned over five months. Treatments were assigned to litters as described in Section 2.15.

Mice were monitored and behaviourally phenotyped at 7 and then at 15 weeks of age using, in this order and in consecutive days, the open field, elevated plus maze and platform departure test, as described in Figure 6-1c. MoSeq was performed only at 15 weeks of age, at the end of the behavioural test battery, with at least one day of rest after the platform departure test. Mice were sacrificed at 25 weeks of age.

The plasmid expressing the human codon-optimised *SYNGAP1* Aα1 isoform was synthesised by GeneArt (ThermoFisher Scientific, USA) (Figure 6-1a and b). Gene expression was driven by the hSYN1 promoter, and transcription was terminated by the addition of a downstream SV40 polyA signal. A FLAG fusion peptide was added to the N-terminus to enable the detection of the viral vector-derived protein and discriminate it from native SYNGAP1. Similarly to AAV9/JeT-*hSYNGAP1,* the Kozak sequence (Kozak, 1986), indicated in Figure 6-1b with red underlined characters, was boosted by the addition of two cytosine nucleotides before the first ATG codon. The hSYN1-*FLAG-hSYNGAP1_Aα1(opt)-SV40* therapeutic cassette was vectorised as

ssDNA using AAV9 capsid pseudotyped with AAV2 ITRs using Baculovirus packaging system by ViroVek (USA) as described in Section 2.8.

The ssAAV2/9/hSYN1-*FLAG-hSYNGAP1_Aa1(opt)-SV40* will be referred to as AAV9/hSYN1-*hSYNGAP1* in the rest of the chapter, and the plasmid as hSYN1-*hSYNGAP1.*

The gene therapy cassette was designed by Dr Ralph D. Hector who also performed codon optimisation for expression in humans using the GeneOptimiser software (ThermoFisher Scientific, USA).

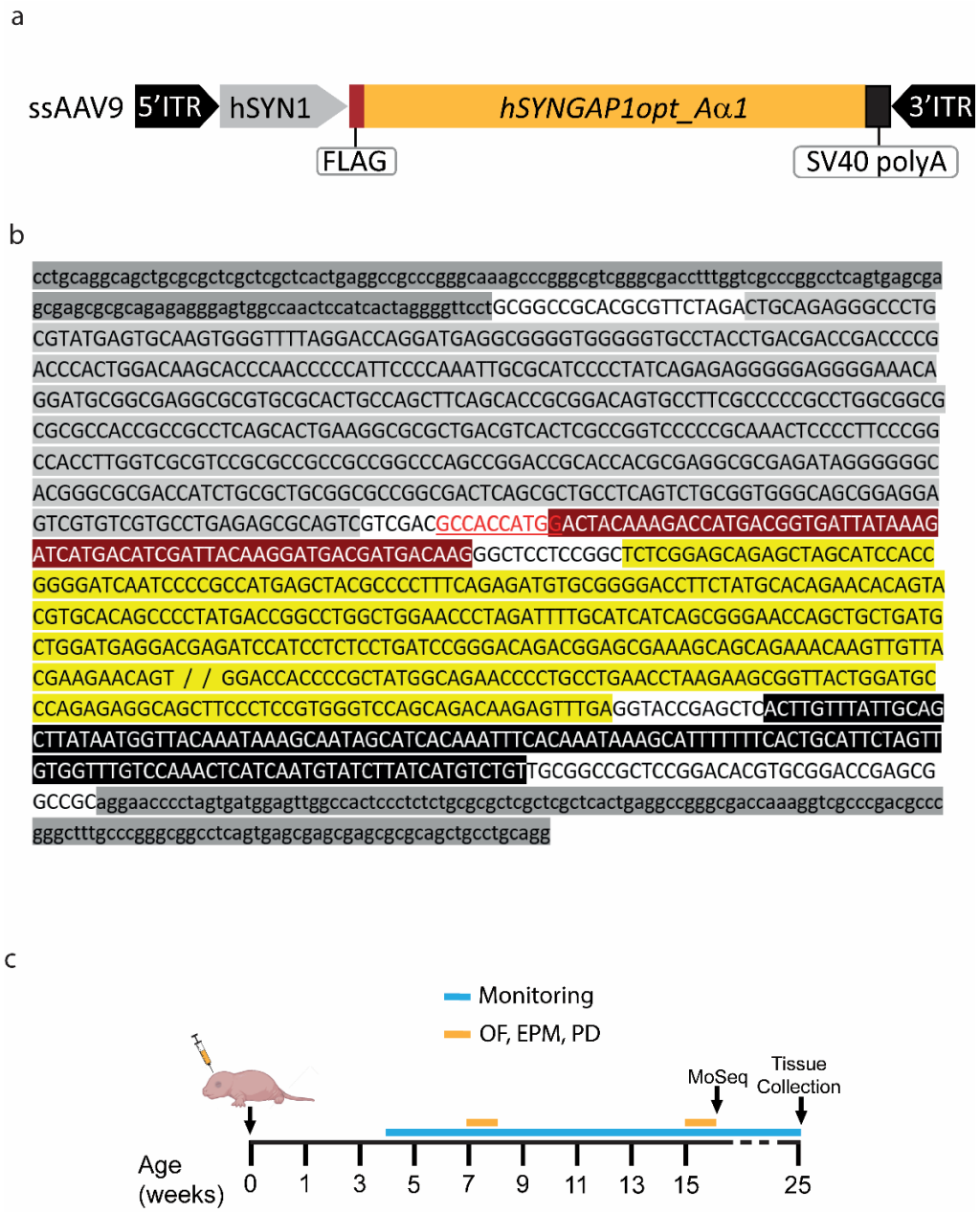

Figure 6-1. Schematic of the new generation gene therapy construct and experimental plan.

Schematic representation of the AAV9/hSYN1-*hSYNGAP1* construct (a) and its sequence (b). 5' and 3' ITRs are highlighted in dark grey and are shown in lowercase characters, hSYN1 promoter sequence is highlighted in light grey. FLAG peptide sequence is highlighted in dark red and SV40 polyA in black. Kozak sequence is indicated by red underlined characters. The coding sequence, in yellow, is only shown for the 5' and 3' regions, "/ / /" indicates sequence break. The experimental plan (c) involved the dosing of wild-type and *Syngap1*$^{+/-}$ mice via ICV injection with 5E10 or 1E11 vg/mouse or vehicle as control. As detailed in the methods section, mice were then monitored and tested on consecutive days in open field (OF), elevated plus maze (EPM) and platform departure (PD) at 7 and 15 weeks of age. Motion sequencing (MoSeq) was performed at the end of the behavioural pipeline at 15 weeks of age.

6.4 RESULTS

6.4.1 Viral vector-derived FLAG-SYNGAP1 protein was detectable *in vitro* and *in vivo*

As part of the quality control pipeline, upon reception from GeneArt (ThermoFisher Scientific, USA), the hSYN1-*hSYNGAP1* (Figure 6-2a) whole plasmid sequence was confirmed using MiSeq as described in Chapter 2. Moreover, as for the expression cassettes presented in Chapter 4, before moving to viral vector production, the ability of the hSYN1 promoter to drive the expression of the transgene was tested *in vitro.*

hSYN1-*hSYNGAP1* was transfected in HEK293A cells and the presence of plasmid-derived FLAG-SYNGAP1 protein was investigated by fluorescence immunocytochemistry. MeP229-*hMECP2-Myc* was used as positive control for the transfection experiment (Figure 6-2b). Mock-transfected cells (negative control) were used to verify the specificity of immunostaining (Figure 6-2c).

Similarly to what was observed in Chapter 4, Myc immunolabelling of the positive control transfected cells showed multiple Myc-positive cells per field of view (Figure 6-2b), while only a few cells resulted positive for SYNGAP1 and FLAG immunolabeling in wells transfected with the hSYN1-*hSYNGAP1* plasmid (Figure 6-2c). Nonetheless, this experiment confirmed that hSYN1 can drive the expression of the codon-optimised *hSYNGAP1 in vitro.*

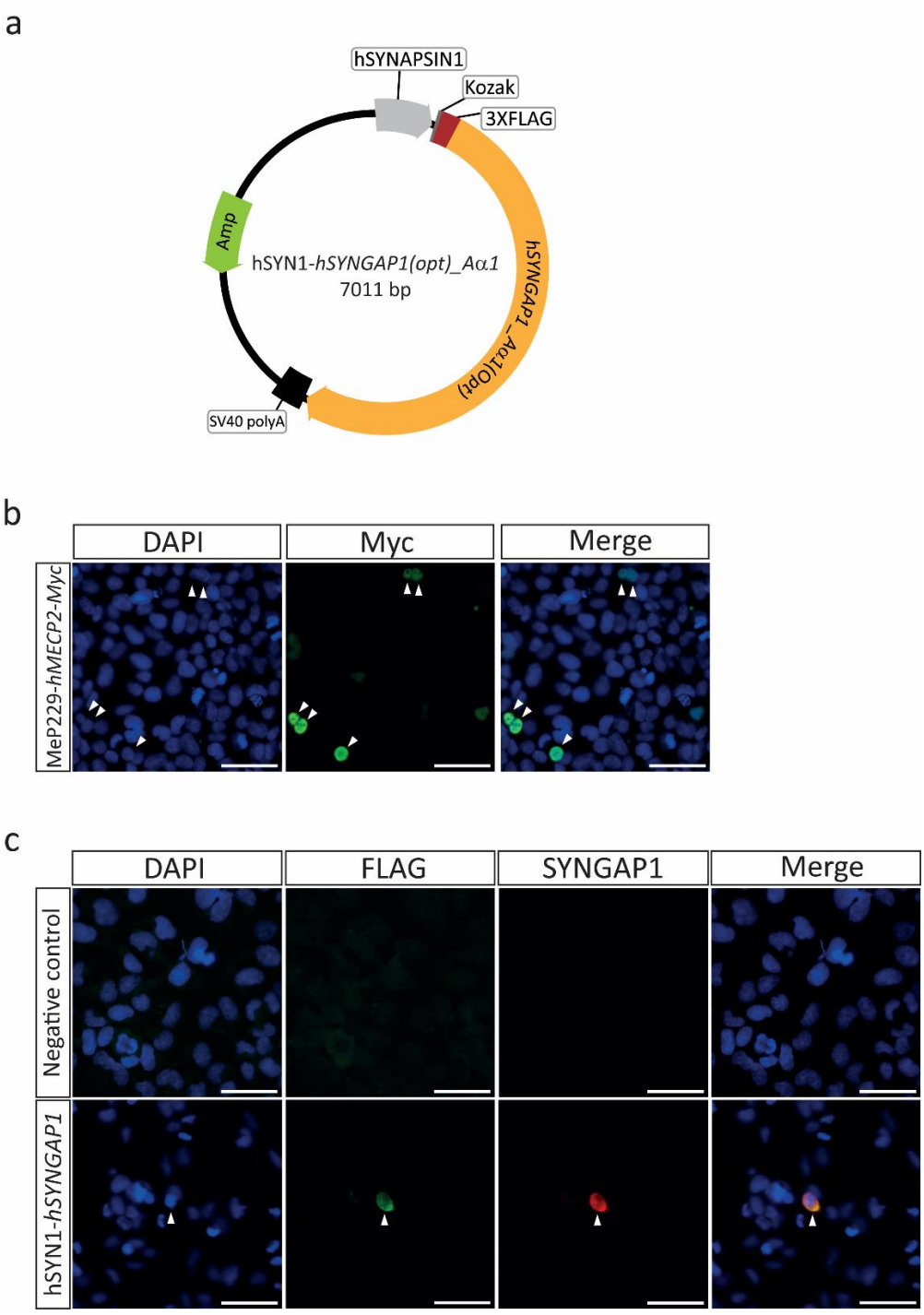

Figure 6-2. FLAG-tagged SYNGAP1 was detectable in HEK293A cells transfected with the hSYN1-hSYNGAP1 plasmid.

Schematic representation of the plasmid used for transfection (a). Representative fluorescence immunocytochemistry of HEK293A cells transfected with the positive control MeP229-*hMECP2-Myc* plasmid (b) or the hSYN1-*hSYNGAP1* plasmid (c). White arrowheads indicate cells positive for SYNGAP1 and FLAG immunolabelling or Myc in the case of MeP229-*hMECP2-Myc* transfected cells. Blue: DAPI staining; Green: immunolabelling of Myc (b) or FLAG (c); Red: immunolabelling of SYNGAP1. Bars indicate 50 μm.

Following verification of expression *in vitro* and confirmation of sequence via MiSeq, the plasmid was vectorised by ViroVek (USA) using the baculovirus/Sf9 cells production system.

As part of the quality control process, the integrity of the viral vector AAV9/hSYN1-*hSYNGAP1* DNA sequence was evaluated via MiSeq. As shown in Table 6-1, ~94% of reads aligned to the construct sequence, indicating that the packaged sequence was correct. In addition, the analysis did not detect DNA sequence deriving from other organisms, such as bacteria, which would indicate contamination of the viral vector preparation.

Whole plasmid and viral vector genome sequencing were performed by Ms Amanda Morris, and sequence analysis by Dr Paul Ross.

Table 6-1. AAV9/hSYN1-hSYNGAP1 sequence quality evaluation via MiSeq.

Mapped sequence	Percentage of reads
AAV9/hSYN1-*hSYNGAP1*	94.26%
AAV9/hSYN1-*hSYNGAP1* plasmid backbone	0.05%
Helper Rep-Cap	0.03%

Before commencing an extended in vivo therapeutic efficacy study for the novel gene therapy cassette, a qualitative pilot study was conducted in wild-type mice to assess AAV9/hSYN1-*hSYNGAP1* expression *in vivo.* The aim of this study was to evaluate viral vector transgene expression in disease-relevant brain regions such as the cortex and hippocampus. The presence of the viral vector-derived protein was evaluated after five weeks post-injection at two different doses, 5E10 and 1E11 vg/mouse. Immunoblot of protein lysate from the cortex and hippocampus confirmed the presence of FLAG-tagged SYNGAP1, which appeared to migrate at the same molecular height as the endogenous SYNGAP1 (~148 kDa) (Figure 6-3). Quantification of viral vector-derived protein is described in Figure 6-19 and Figure 6-20.

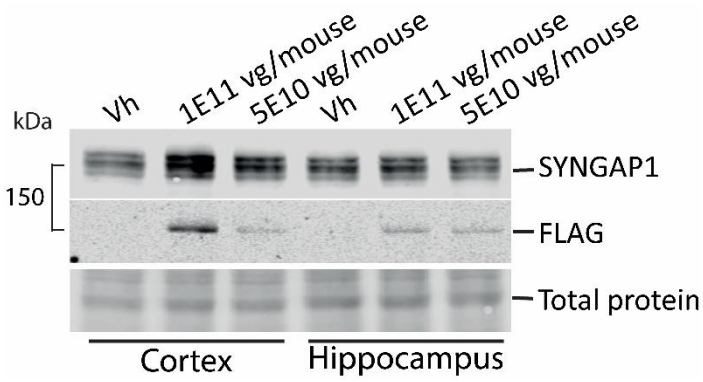

Figure 6-3. FLAG-tagged viral vector-derived SYNGAP1 was detectable in cortex and hippocampus after five weeks from injection.
Representative qualitative immunoblot of cortex and hippocampus protein lysate from wild-type treated tissue after 5 weeks post-treatment with vehicle (Vh) or viral vector at doses of 5E10 and 1E11 vg/mouse. SYNGAP1 endogenous protein migrates at a molecular weight of ~148 KDa. Similarly, viral vector-derived SYNGAP1 migrated at a molecular weight of ~148 KDa. Total protein was used as loading control. The gel was used at a concentration of bis acrylamide of 10%.

6.4.2 AAV9/hSYN1-*hSYNGAP1* treated *Syngap1*$^{+/-}$ mice showed a trend toward amelioration of the risk-taking behaviour

As shown in Chapter 3, *Syngap1*$^{+/-}$ mice present increased horizontal activity, higher percentage of time in the open arms of the elevated plus maze and have a higher tendency to leave an elevated platform.

In Chapter 5, it was shown that treatment with AAV9/JeT-*hSYNGAP1* resulted in a trend toward the amelioration of risk-taking behaviour in *Syngap1*$^{+/-}$ mice, with viral vector dosed *Syngap1*$^{+/-}$ mice showing a reduced tendency to leave the platform. It was hypothesised that the limited treatment effect could have been associated with the low level of viral vector-derived protein expressed in disease-relevant brain regions such as the cortex and hippocampus.

After confirming the ability of the hSYN1 promoter to express the transgene *in vitro* and establishing detectable brain expression of AAV9/hSYN1-*hSYNGAP1 in vivo*, an efficacy study was set up to evaluate the ability of *SYNGAP1* Aα1 expression to ameliorate phenotypes associated with *SYNGAP1* haploinsufficiency. The behavioural

phenotyping battery included open field, elevated plus maze, platform departure test and MoSeq, as detailed in Chapter 2 and described in Figure 6-1c.

6.4.2.1 Open field

Syngap1$^{+/-}$ mice present an increased locomotor activity, resulting in a higher distance travelled over time in the open field when compared to wild-type littermates. Hyperactivity is a highly reproducible phenotype (Aceti *et al.*, 2015; Berryer *et al.*, 2016; Guo *et al.*, 2009; Komiyama *et al.*, 2002; Muhia *et al.*, 2010; Nakajima *et al.*, 2019; Ozkan *et al.*, 2014) and as demonstrated in Chapter 3 and 5, this phenotype is also observed in the *Syngap1*$^{+/-}$ mouse line used for the work presented in this thesis.

The effect of the viral vector treatment on the hyperactive phenotype was assessed using the open field test, as described in Chapter 2. Briefly, mice treated with 5E10 and 1E11 vg/mouse AAV9/hSYN1-*hSYNGAP1* were exposed to the open field test for 1 hour, and the distance travelled over the total time and per 15-minutes was measured.

At 7 weeks of age a clear genotype difference was observed between *Syngap1*$^{+/-}$ and wild-type mice (Figure 6-4a; two-tailed Student's t-test with Welch's correction, mean ± SEM; wild-type n=16, 23763 ± 1906 cm; *Syngap1*$^{+/-}$ n=16, 36870 ± 2105 cm; $t_{(29.71)}$=4.616, p<0.0001). Wild-type viral vector-treated mice did not show difference in horizontal activity when compared to vehicle-treated mice, suggesting that the viral vector treatment did not modify this behaviour (Figure 6-4b; Welch's ANOVA, mean ± SEM; vehicle n=16, 23763 ± 1906 cm; 5E10 vg/mouse n=18, 21417 ± 1289 cm; 1E11 vg/mouse n=21, 22694 ± 1491 cm; $W_{(2,32.81)}$=0.5518, p=0.5812).
When comparing viral vector and vehicle-treated *Syngap1*$^{+/-}$ mice, no amelioration of hyperactivity was observed at either dose (Figure 6-4c; Welch's ANOVA, mean ± SEM; vehicle n=16, 36870 ± 2105 cm; 5E10 vg/mouse n=14, 36169 ± 1888 cm; 1E11 vg/mouse n=13, 37930 ± 2698 cm; $W_{(2,25.61)}$=0.1404, p=0.8697).

The hyperactivity observed in *Syngap1*$^{+/-}$ mice was not associated with a lack of habituation as both vehicle-treated genotype groups showed the same level of intra-trial habituation (Figure 6-5a; RM Two way ANOVA; vehicle(WT), n=16, vehicle(*Syngap1*$^{+/-}$), n=16; genotype x time $F_{(3, 90)}$=0.509, p=0.6771; time $F_{(2.716, 81.47)}$=162.0, p<0.0001; genotype $F_{(1, 30)}$=27.91, p<0.0001; multiple comparisons tests results are reported in Table S-25).

The habituation was not affected by viral vector treatment in *Syngap1*$^{+/-}$ mice (Figure 6-5b; RM Two away ANOVA; vehicle(*Syngap1*$^{+/-}$), n=16, 5E10 vg/mouse n=14, 1E11 vg/mouse n=13; treatment x time $F_{(6, 120)}$=0.911, p=0.4892; time $F_{(2.188, 87.51)}$=161.7, p<0.0001; treatment $F_{(2, 40)}$=0.155, p=0.8571, Tukey's multiple comparisons test results are reported in Table S-26).

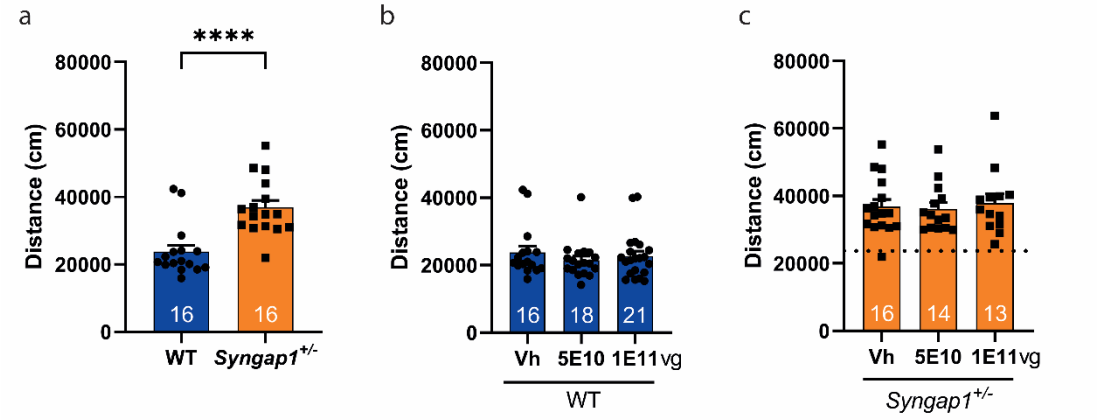

Figure 6-4. At 7 weeks of age, Syngap1*$^{+/-}$ *mice hyperactivity was not affected by AAV9/hSYN1-hSYNGAP1 viral vector treatment.

Total distance travelled in 1 hour by vehicle (Vh) treated wild-type (WT) and *Syngap1*$^{+/-}$ mice (a) and by wild-type (b) and *Syngap1*$^{+/-}$ mice (c) of all treatment groups at 7 weeks of age. Dotted line represents wild-type behaviour. Circles and squares represent single animals. Numbers within the bars represent the n of each group. Data presented as mean ± SEM. a) Two-tailed Student's t-test with Welch's correction. b,c) Welch's ANOVA. **** p<0.0001.

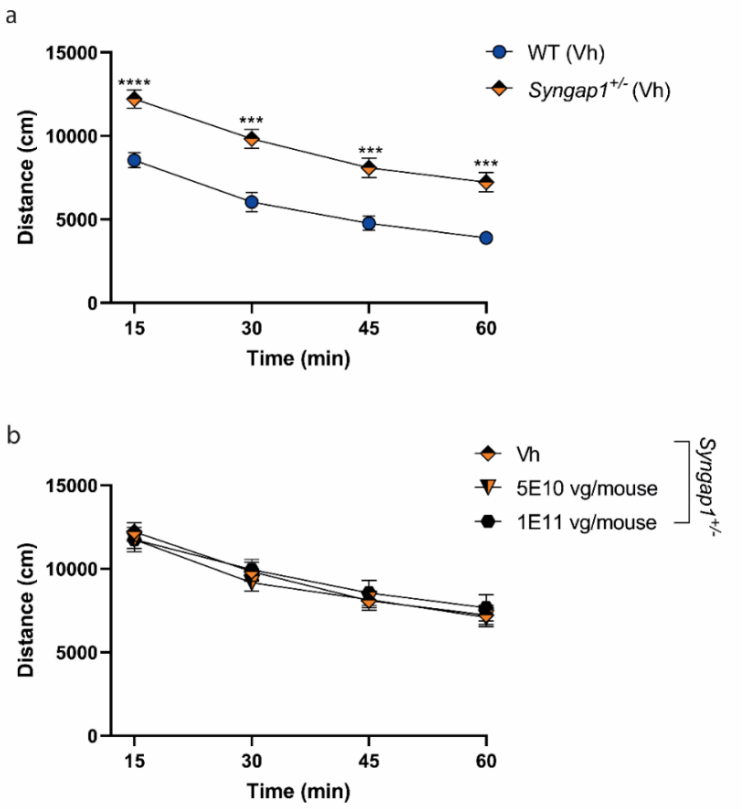

Figure 6-5. At 7 weeks of age, Syngap1$^{+/-}$ mice habituation was not affected by AAV9/hSYN1-hSYNGAP1 viral vector treatment.

Wild-type (WT) and *Syngap1*$^{+/-}$ vehicle (Vh) treated mice (a) and *Syngap1*$^{+/-}$ vehicle and viral vector-treated mice (b) distance travelled for 15 minutes time bins at 7 weeks of age. Each data point represents the mean distance travelled over the preceding 15 minutes. Stars (*) above each bin represent the results of multiple comparison tests between genotypes. Wild-type (Vh) n=16, *Syngap1*$^{+/-}$ (Vh) n=16, 5E10 vg/mouse n=14, 1E11 vg/mouse n=13.
Data presented as mean ± SEM. RM Two-way ANOVA with Šídák multiple comparisons test. *** p<0.001, **** p<0.0001.

At 15 weeks of age the increased horizontal activity observed in *Syngap1*$^{+/-}$ vehicle-treated mice (Figure 6-6a; two-tailed Student's t-test with Welch's correction, mean ± SEM; wild-type n=16, 17308 ± 1242 cm; *Syngap1*$^{+/-}$ n=16, 40588 ± 2351 cm; $t_{(22.77)}$=8.757, p<0.0001) was not modified by the viral vector treatment at all considered doses (Figure 6-6c; Welch's ANOVA test, mean ± SEM; vehicle, n=16, 40588 ± 2351 cm; 5E10 vg/mouse n=14, 43997 ± 5946 cm; 1E11 vg/mouse n=13, 43518 ± 8321 cm; $W_{(2,19.89)}$=0.1774, p=0.8388).

Similarly, AAV9/hSYN1-*hSYNGAP1* did not induce modification of the behaviour in wild-type mice (Figure 6-6b; Welch's ANOVA test, mean ± SEM; vehicle n=16, 17308 ± 1242 cm; 5E10 vg/mouse n=18, 16877 ± 1335 cm; 1E11 vg/mouse n=21, 20321 ± 2437 cm; $W_{(2,34.24)}$=0.7762, p=0.4681).

At 15 weeks of age, in accordance with the results shown in Chapter 3, wild-type and *Syngap1*$^{+/-}$ mice showed reduced habituation to the arena (Figure 6-7a; RM Two away ANOVA; vehicle(WT), n=16, vehicle(*Syngap1*$^{+/-}$), n=16; genotype x time $F_{(3, 90)}$=3.550, p=0.0176; time $F_{(2.039, 61.17)}$=28.55, p<0.0001; genotype $F_{(1, 30)}$=76.68, p<0.0001; multiple comparisons tests results are reported in Table S-27).

The viral vector treatment did not modify habituation in *Syngap1*$^{+/-}$ mice, which resulted comparable to vehicle controls (Figure 6-7b; RM Two away ANOVA; vehicle(*Syngap1*$^{+/-}$), n=16, 5E10 vg/mouse n=14, 1E11 vg/mouse n=13; treatment x time $F_{(6, 120)}$=1.504, p=0.1824; time $F_{(1.590, 63.61)}$=4.296, p=0.0252; treatment $F_{(2, 40)}$=0.111, p=0.8952, Tukey's multiple comparisons for test results are reported in Table S-28).

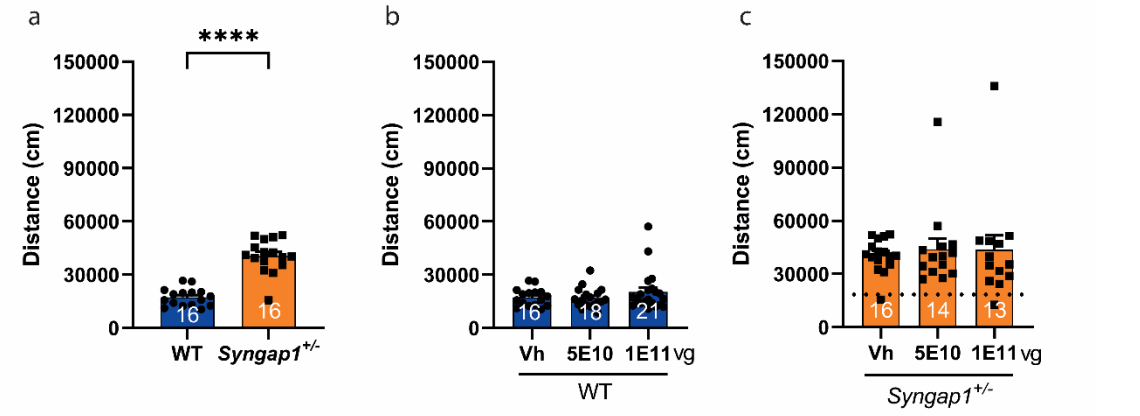

Figure 6-6. At 15 weeks of age, Syngap1*$^{+/-}$ *mice hyperactivity in the open field was not ameliorated by AAV9/hSYN1-hSYNGAP1 viral vector treatment.

Total distance travelled in 1 hour by vehicle (Vh) treated wild-type (WT) and *Syngap1*$^{+/-}$ mice (a) and by wild-type (b) and *Syngap1*$^{+/-}$ mice (c) of all treatment groups at 15 weeks of age. Circles and squares represent single animals. Dotted line represents wild-type behaviour. Numbers within the bars represent the n of each group.

Data presented as mean ± SEM. a) Two-tailed Student's t-test with Welch's correction. b,c) Welch's ANOVA. **** p<0.0001.

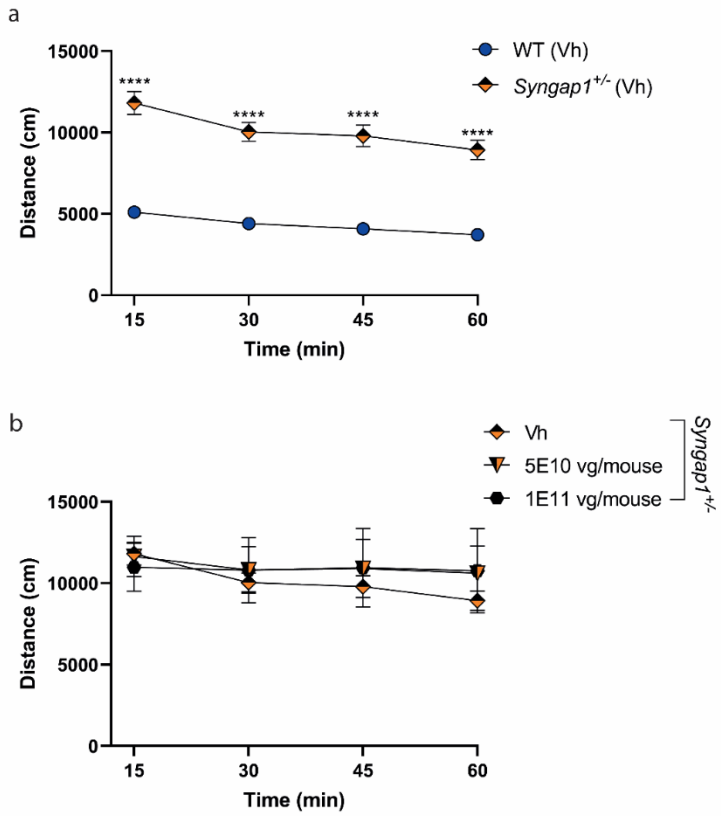

Figure 6-7. At 15 weeks of age, AAV9/hSYN1-hSYNGAP1 and vehicle-treated Syngap1$^{+/-}$ mice showed comparable distance travelled over time.

Wild-type (WT) and *Syngap1*$^{+/-}$ vehicle (Vh) treated mice (a) and *Syngap1*$^{+/-}$ vehicle and viral vector-treated mice (b) distance travelled per 15 minutes time bins at 15 weeks of age. Each data point represents the mean distance travelled over the preceding 15 minutes. Stars (*) above each bin represent the results of multiple comparison tests between genotypes. Wild-type (Vh) n=16, *Syngap1*$^{+/-}$ (Vh) n=16, 5E10 vg/mouse n=14, 1E11 vg/mouse n=13.

Data presented as mean ± SEM. RM Two-way ANOVA with Šídák multiple comparisons test. **** p<0.0001.

6.4.2.2 Elevated Plus Maze

Several publications have shown that *Syngap1*$^{+/-}$ mice present reduced anxiety levels, which is evidenced by the increased time spent in the open arms of the elevated plus maze (Berryer *et al.*, 2016; Guo *et al.*, 2009; Muhia *et al.*, 2010; Nakajima *et al.*, 2019). In agreement with these works (Berryer *et al.*, 2016; Guo *et al.*, 2009; Muhia *et al.*, 2010; Nakajima *et al.*, 2019), I also observed a similar increase in time spent in the open arms (Chapters 3 and 5), and therefore, I used the elevated plus maze to evaluate the therapeutic effect of the newly designed AAV9/hSYN1-*hSYNGAP1* on

this behaviour. As presented in Chapter 5, the elevated plus maze test was conducted on the day following the open field test, and treated *Syngap1*$^{+/-}$ and wild-type mice were tested on the elevated plus maze for 10 minutes and, and the distance travelled and time spent in the open arms were extrapolated (Figure 6-1c).

As defined in Chapter 2, subjects that jumped out of the maze were excluded from the analysis. At 7 weeks, one *Syngap1*$^{+/-}$ mouse treated with 1E11 vg/mouse was excluded while at 15 weeks one *Syngap1*$^{+/-}$ mouse treated with vehicle was excluded.

At 7 weeks of age increased horizontal activity was present in *Syngap1*$^{+/-}$ mice when compared to wild-type mice, in agreement with the results of the open field test and previously shown results (Chapters 3 and 5) (Figure 6-8a; two-tailed Student's t-test with Welch's correction, mean ± SEM; wild-type n=16, 2462 ± 201.5 cm; *Syngap1*$^{+/-}$ n=16, 3349 ± 265.0 cm; $t_{(28)}$=2.666, p=0.0126).
Viral vector treatment did not alter the distance travelled in the maze by wild-type mice (Figure 6-8b; Welch's ANOVA test, mean ± SEM; vehicle n=16, 2462 ± 201.5 cm; 5E10 vg/mouse n=18, 2349 ± 63.08 cm; 1E11 vg/mouse n=21, 2650 ± 126.7 cm; $W_{(2,28.23)}$=2.242, p=0.1248).
Similarly, *Syngap1*$^{+/-}$ mice behaviour was not affected by the treatment, with the viral vector injected mice indistinguishable from the vehicle-treated (Figure 6-8c; Welch's ANOVA test, mean ± SEM; vehicle n=16, 3349 ± 265.0 cm; 5E10 vg/mouse n=14, 3228 ± 141.2 cm; 1E11 vg/mouse n=12, 3665 ± 205.9 cm; $W_{(2, 24.30)}$=1.494, p=0.2443).

The percentage of time spent in the open arms was significantly different between wild-type and *Syngap1*$^{+/-}$ vehicle-treated mice (Figure 6-8d; two-tailed Mann-Whitney test, median(95% CI); wild-type n=16, 21.09(16.38 to 26.94) %; *Syngap1*$^{+/-}$ n=16, 40.70(33.80 to 47.62) %; U=32, p=0.0001).
Similar to what was observed for total distance travelled, the percentage of time spent in the open arms of the maze was not affected by the viral vector treatment in wild-type (Figure 6-8e; Kruskal-Wallis test, median(95% CI); vehicle n=16, 21.09(16.38 to26.94) %; 5E10 vg/mouse n=18, 21.51(18.71 to 26.03) %; 1E11 vg/mouse n=21, 29.80(22.71 to 36.58) %; $H_{(2)}$=4.728, p=0.0940) and in *Syngap1*$^{+/-}$ mice (Figure 6-8f,

Kruskal-Wallis test, median(95% CI); vehicle n=16, 40.70(33.80 to 47.62) %; 5E10 vg/mouse n=14, 42.62(38.02 to 51.28) %; 1E11 vg/mouse n=12, 46.68(38.09 to 53.16) %; $H_{(2)}$=1.664, p=0.4352).

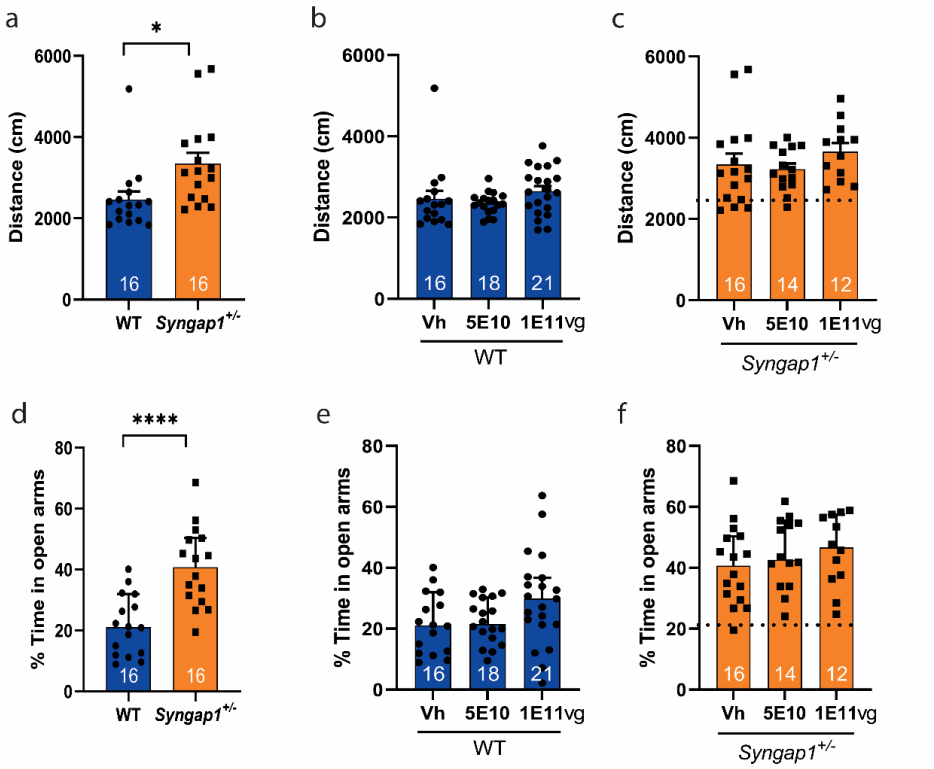

Figure 6-8. At 7 weeks of age, the percentage of time spent in the open arms of the elevated plus maze was not altered in AAV9/hSYN1-hSYNGAP1 treated Syngap1$^{+/-}$ mice.

Total distance travelled in 10 minutes by vehicle (Vh) treated wild-type (WT) and *Syngap1*$^{+/-}$ mice (a) and by wild-type (b) and *Syngap1*$^{+/-}$ mice (c) of all treatment groups in the elevated plus maze at 7 weeks of age. Percentage of time spent in the open arms by vehicle-treated wild-type and *Syngap1*$^{+/-}$ mice (d) and by wild-type (e) and *Syngap1*$^{+/-}$ mice (f) of all treatment groups at 7 weeks of age. Dotted line represents wild-type behaviour. Circles and squares represent single animals. Numbers within the bars represent the n of each group.
a) Two-tailed Student's t-test with Welch's correction. b,c) Welch's ANOVA. Mean ± SEM.
d) Two-tailed Mann-Whitney test. e,f) Kruskal-Wallis test. Median and 95% C.
* p<0.05, **** p<0.0001.

Syngap1$^{+/-}$ mice showed an increased horizontal activity also at 15 weeks of age (Figure 6-9a; two-tailed Student's t-test with Welch's correction, mean ± SEM; wild-

type n=16, 1844 ± 149.7 cm; *Syngap1*$^{+/-}$ n=15, 3553 ± 307.6 cm; $t_{(20.35)}$=4.995, p<0.0001).

Total distance travelled was not affected by the treatment in both wild-type (Figure 6-9b; Welch's ANOVA test, mean ± SEM; vehicle n=16, 1844 ± 149.7 cm; 5E10 vg/mouse n=18, 1955 ± 100.2 cm; 1E11 vg/mouse n=21, 2070 ± 140.3 cm; $W_{(2,32.89)}$=0.5969, p=0.5564) and *Syngap1*$^{+/-}$ mice (Figure 6-9c; Welch's ANOVA test, mean ± SEM; vehicle n=15, 3553 ± 307.6 cm; 5E10 vg/mouse n=14, 3571 ± 284.7 cm; 1E11 vg/mouse n=13, 3390 ± 254.4 cm; $W_{(2,25.99)}$=0.1341, p=0.8751).

Syngap1$^{+/-}$ mice spent more time in the open arms of the maze compared to wild-type controls (Figure 6-9d; two-tailed Mann-Whitney test, median(95% CI); wild-type n=16, 12.85(8.22 to 16.52) %; *Syngap1*$^{+/-}$ n=15, 41.74(26.68 to 45.78) %; U=32, p=0.0003).

The viral vector treatment did not affect the percentage of time spent in the open arms by *Syngap1*$^{+/-}$ (Figure 6-9f; Kruskal-Wallis test, median(95% CI); vehicle n=15, 41.74(26.68 to 45.78) %; 5E10 vg/mouse n=14, 37.48(30.27 to 48.17) %; 1E11 vg/mouse n=13, 35.63(25.13 to 46.65) %; $H_{(2)}$=0.2727, p=0.8725) and wild-type mice (Figure 6-9e; Kruskal-Wallis test, median(95% CI); vehicle n=16, 12.85(8.22 to 16.52 %); 5E10 vg/mouse n=18, 16.33(12.00 to 22.17) %; 1E11 vg/mouse n=21, 20.15(12.96 to 23.80) %; $H_{(2)}$=2.711, p=0.2578).

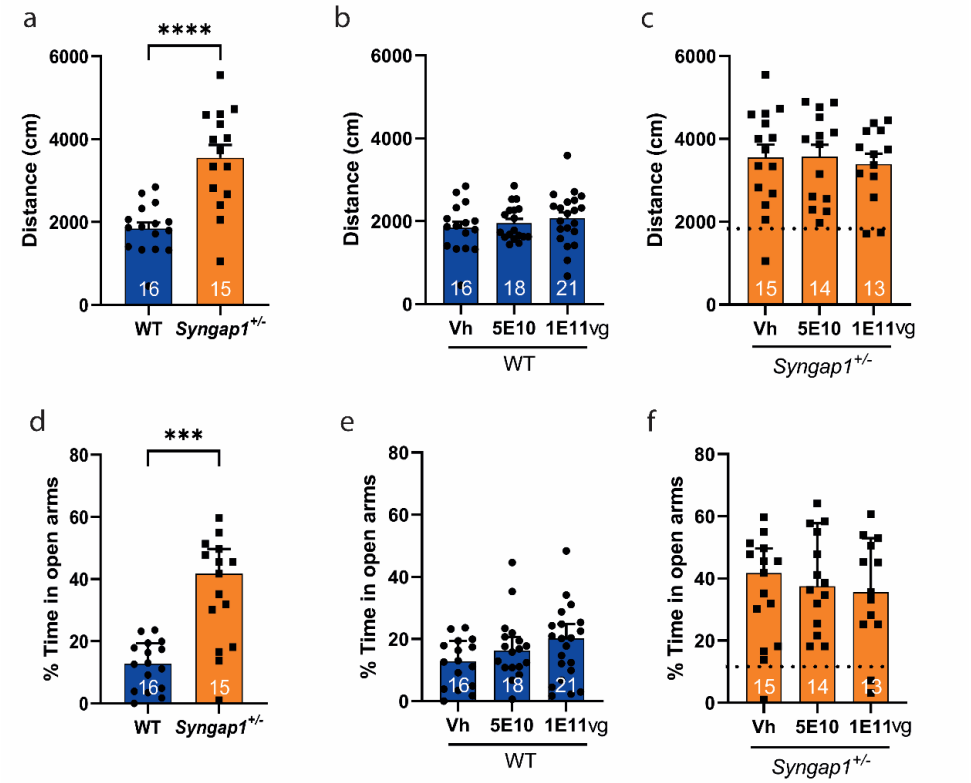

Figure 6-9. At 15 weeks of age, the percentage of time spent in the open arms of the elevated plus maze was not altered in AAV9/hSYN1-hSYNGAP1 treated Syngap1$^{+/-}$ mice.

Total distance travelled in 10 minutes by vehicle (Vh) treated wild-type (WT) and *Syngap1*$^{+/-}$ mice (a) and by wild-type (b) and *Syngap1*$^{+/-}$ (c) of all treatment groups in the elevated plus maze at 15 weeks of age. Percentage of time spent in the open arms by vehicle-treated wild-type and *Syngap1*$^{+/-}$ mice (d) and by wild-type (e) and *Syngap1*$^{+/-}$ mice (f) of all treatment groups at 15 weeks of age. Dotted line represents wild-type behaviour. Circles and squares represent single animals. Numbers within the bars represent the n of each group.

a) Two-tailed Student's t-test with Welch's correction. b,c) Welch's ANOVA. Mean ± SEM.

d) Two-tailed Mann-Whitney test. e,f) Kruskal-Wallis test. Median and 95% C.

*** p<0.001, **** p<0.0001.

6.4.2.3 Platform departure test

As previously shown in Chapter 3, an increased number of departures from an elevated platform, which has been interpreted as an increase in risk-taking behaviour, was detectable in *Syngap1*$^{+/-}$ mice when compared to wild-type littermates. In Chapter 5, I showed that AAV9/JeT-*hSYNGAP1* treated *Syngap1*$^{+/-}$ mice

showed promising results in this test, with a trend towards the reduction of the number of full departures.

I assessed the therapeutic effect of the AAV9/hSYN1-*hSYNGAP1* viral vector using the same paradigm described in Chapters 3 and 5. Mice were placed on top of a 2-litre beaker and allowed to explore for 10 minutes, and the number of partial and full departures were counted. This test was performed at 7 and then at 15 weeks of age the day after the elevated plus maze test (Figure 6-1c).

Consistent with what has been shown in previous chapters, wild-type and *Syngap1*$^{+/-}$ mice presented a significant difference in the number of partial departures and total departure at 7 weeks of age, with the *Syngap1*$^{+/-}$ mice being overall more active on the platform (Figure 6-10a and d; partial departures, two-tailed Student's t-test with Welch's correction, mean ± SEM; wild-type n=16, 6.00 ± 1.26; *Syngap1*$^{+/-}$ n=16, 21.63 ± 2.94; $t_{(20.31)}$=4.885, p<0.0001. Full departureks, two-tailed Mann-Whitney test, median(95% CI); wild-type n=16, 0.00(-0.29 to 1.79); *Syngap1*$^{+/-}$ n=16, 8.00(4.54 to 14.71); U=17.50, p<0.0001).

Although 5E10 vg/mouse treated wild-type mice performed significantly more partial departures compared to vehicle controls, in light of what was observed in previous tests and based on the fact that the difference between vehicle and 1E11 vg/mouse did not appear significant, this variation was not considered to be associated with poor treatment tolerability (Figure 6-10b; Welch's ANOVA, mean ± SEM; vehicle n=16, 6.00 ± 1.26; 5E10 vg/mouse n=18, 12.56 ± 1.95; 1E11 vg/mouse n=21, 14.90 ± 3.99; $W_{(2,32.39)}$=5.304, p=0.0102; Dunnett's T3 multiple comparisons test results are reported in Table S-29).

No difference in the number of full departures was observed among AAV9/hSYN1-*hSYNGAP1* viral vector-treated wild-type mice (Figure 6-10e; Kruskal-Wallis test, median(95% CI); vehicle n=16, 0.00(-0.29 to 1.79); 5E10 vg/mouse n=18, 0.00(0.33 to 4.11); 1E11 vg/mouse n=21, 0.00(-0.001 to 7.24); $H_{(2)}$=1.268, p=0.5305).

Similarly, the number of partial departures performed by viral vector-treated *Syngap1*$^{+/-}$ mice appeared to not be affected (Figure 6-10c; Welch's ANOVA test,

mean ± SEM; vehicle n=16, 21.63 ± 2.94; 5E10 vg/mouse n=14, 32.86 ± 5.64; 1E11 vg/mouse n=13, 23.23 ± 2.65; $W_{(2,25)}$=1.542, p=0.2336).

Interestingly, although the general full departures behaviour did not appear modified by the treatment in *Syngap1*$^{+/-}$ mice, it was possible to observe an increase in the number of animals that did not perform any departure at all (Figure 6-10f; Kruskal-Wallis test, median(95% CI); vehicle n=16, 8.00(4.54 to 14.71); 5E10 vg/mouse n=14, 11.50(6.92 to 15.23); 1E11 vg/mouse n=13, 8.00(3.52 to 14.33); $H_{(2)}$=1.496, p=0.4734), which was confirmed by the reduced fraction of 1E11 vg/mouse viral vector-treated *Syngap1*$^{+/-}$ mice departing form the platform shown in Figure 6-10g (Log-rank (Mantel-Cox) test, vehicle(WT) n=16, median time to first=undefined; vehicle(*Syngap1*$^{+/-}$) n=16, median time to first=3.30, 5E10vg/mouse n=14, median time to first=2.38, 1E11vg/mouse n=13, median time to first=3.78; vehicle(WT) vs vehicle(*Syngap1*$^{+/-}$) $\chi^2_{(1)}$=23.64, p<0.0001; vehicle(*Syngap1*$^{+/-}$) vs 5E10vg/mouse $\chi^2_{(1)}$=0.057, p=0.8108; vehicle vs 1E11vg/mouse $\chi^2_{(1)}$=1.28, p=0.2581).

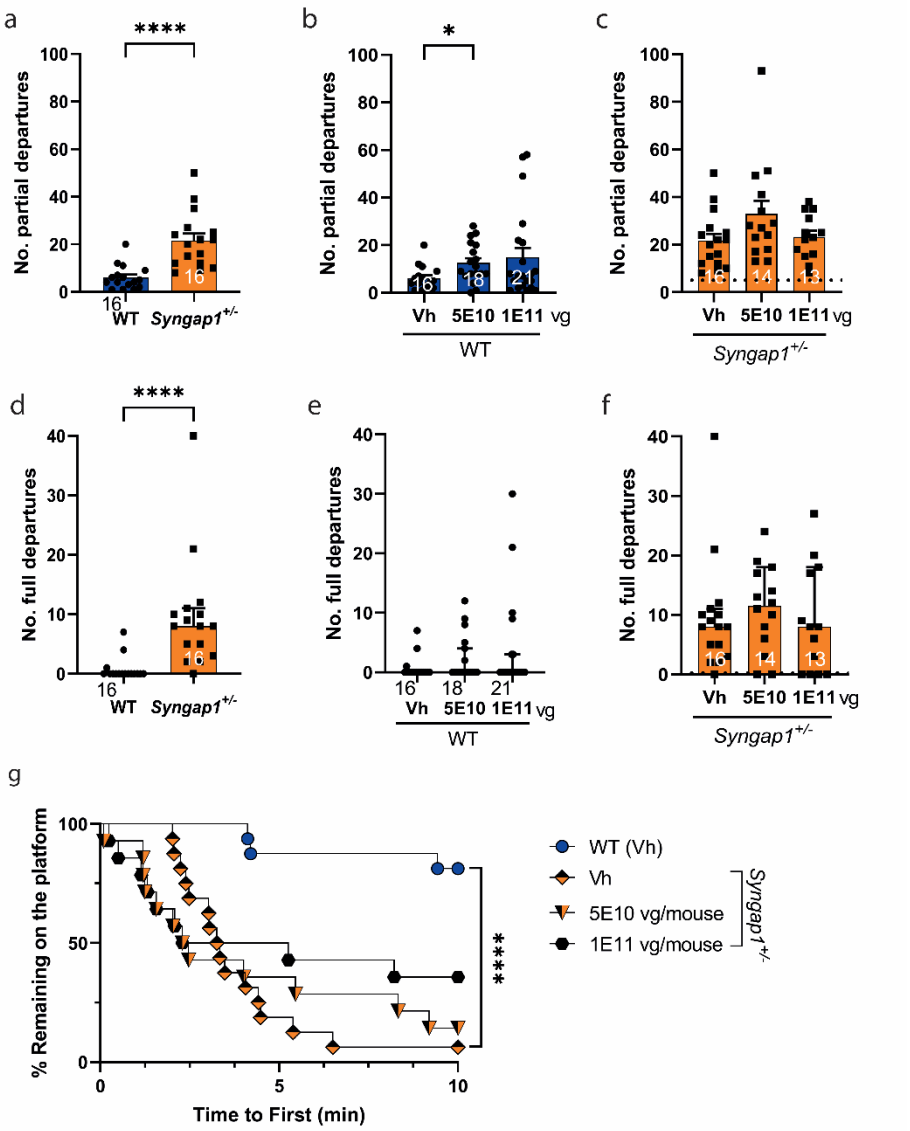

Figure 6-10. At 7 weeks of age, a reduced number of AAV9/hSYN1-hSYNGAP1 treated Syngap1$^{+/-}$ mice left the platform in the given time.

Number of partial departures performed by vehicle (Vh) treated wild-type (WT) and *Syngap1*$^{+/-}$ mice (a) and by wild-type (b) and *Syngap1*$^{+/-}$ mice (c) of all treatment groups at 7 weeks of age. Number of full departures performed by vehicle-treated wild-type and *Syngap1*$^{+/-}$ mice (d) and by wild-type (e) and *Syngap1*$^{+/-}$ (f) of all treatment groups at 7 weeks of age. Percentage of vehicle wild-type and *Syngap1*$^{+/-}$ mice of all treatment groups (g) that remained on the platform and time to first departure at 7 weeks of age. Dotted line represents wild-type behaviour. Circles and squares represent single animals. Numbers within or under the bars represent the n of each group.

a) Two-tailed Student's t-test with Welch's correction. b,c) Welch's ANOVA. Mean ± SEM.

d) Two-tailed Mann-Whitney test. e,f) Kruskal-Wallis test. Median and 95% CI.

g) Log-rank (Mantel-Cox) test. * $p<0.05$, **** $p<0.0001$.

At 15 weeks of age vehicle-treated wild-type and *Syngap1*$^{+/-}$ mice performed a significantly different number of partial and full departures compared to wild-type mice (Figure 6-11a and d; partial departures, two-tailed Student's t-test with Welch's correction, mean ± SEM; wild-type n=16, 8.50 ± 3.43; *Syngap1*$^{+/-}$ n=16, 32.50 ± 4.03; $t_{(29.26)}$=4.535, p<0.0001. Full departures, two-tailed Mann-Whitney test, median(95% CI); wild-type n=16, 0.00(-0.008 to 0.63); *Syngap1*$^{+/-}$ n=16, 8.50(4.87 to 20.01); U=15.50, p<0.0001).

Partial and full departures were similar between viral vector and vehicle-treated wild-type mice (Figure 6-11b and e; partial departures, Welch's ANOVA, mean ± SEM; vehicle n=16, 8.50 ± 3.43; 5E10 vg/mouse n=18, 8.11 ± 2.35; 1E11 vg/mouse n=21, 8.40 ± 33.46; $W_{(2,\ 32.37)}$=0.005, p=0.9949. Full departures, Kruskal-Wallis test, median(95% CI); vehicle n=16, 0.00(-0.008 to 0.63); 5E10 vg/mouse n=18, 0.00(0.30 to 4.48); 1E11 vg/mouse n=21, 0.00(-0.50 to 4.50); $H_{(2)}$=1.083, p=0.5818).

Although viral vector treatment in *Syngap1*$^{+/-}$ mice did not affect the partial departures behaviour (Figure 6-11c; Welch's ANOVA test, mean ± SEM; vehicle n=16, 32.50 ± 4.03; 5E10 vg/mouse n=14, 36.21 ± 5.07; 1E11 vg/mouse n=13, 31.31 ± 7.03; $W_{(2,24.44)}$=0.2167, p=0.8067), analysis of the number of full departures and percentage of individuals remaining on the platform suggested a treatment effect for the 1E11 vg/mouse viral vector dose group (Figure 6-11f and g), which performed a reduced number of jumps from the platform, although not significant (Figure 6-11f; Kruskal-Wallis test, median(95% CI); vehicle n=16, 8.50(4.87 to 20.01); 5E10 vg/mouse n=14, 9.00(5.65 to 14.21); 1E11 vg/mouse n=13, 3.00(0.38 to 12.08); $H_{(2)}$=3.71, p=0.1564), and about 30% of subjects did not leave the platform in the given time (Figure 6-11g; Log-rank (Mantel-Cox) test, vehicle(WT) n=16, median time to first=undefined; vehicle(*Syngap1*$^{+/-}$) n=16, median time to first=3.59, 5E10vg/mouse n=14, median time to first=3.73, 1E11vg/mouse n=13, median time to first=3.39; vehicle(WT) vs vehicle(*Syngap1*$^{+/-}$) $\chi^2_{(1)}$=13.73, p=0.0002; vehicle(*Syngap1*$^{+/-}$) vs 5E10vg/mouse $\chi^2_{(1)}$=0.6870, p=0.6870; vehicle(*Syngap1*$^{+/-}$) vs 1E11vg/mouse $\chi^2_{(1)}$=1.004, p=0.3163).

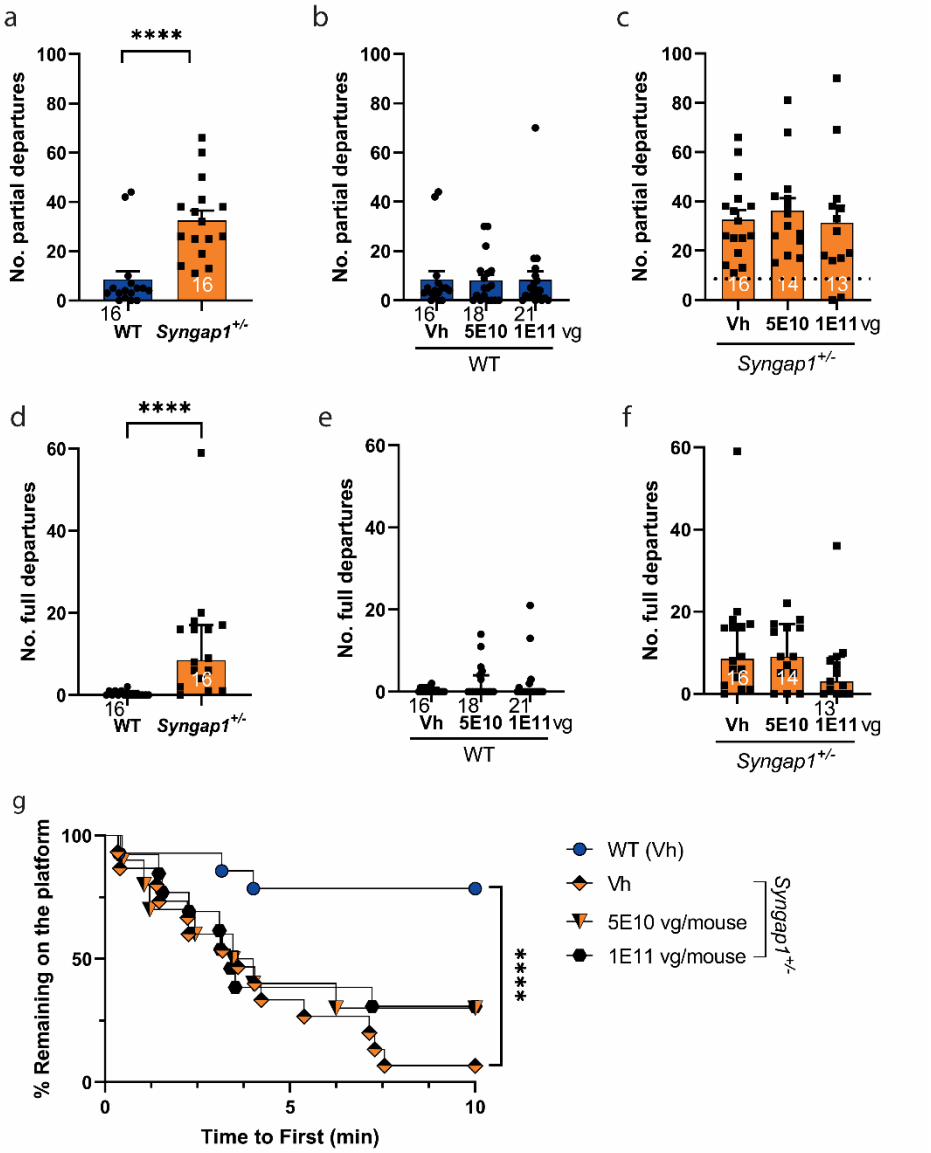

Figure 6-11. At 15 weeks of age, AAV9/hSYN1-hSYNGAP1 high dose treated Syngap1$^{+/-}$ mice showed higher propensity to remain on the platform compared to vehicle-treated controls.

Number of partial departures performed by vehicle (Vh) treated wild-type (WT) and *Syngap1*$^{+/-}$ mice (a) and by wild-type (b) and *Syngap1*$^{+/-}$ mice (c) of all treatment groups at 15 weeks of age. Number of full departures performed by vehicle-treated wild-type and *Syngap1*$^{+/-}$ mice (d) and by wild-type (e) and *Syngap1*$^{+/-}$ (f) of all treatment groups at 15 weeks of age. Percentage of vehicle wild-type and *Syngap1*$^{+/-}$ mice of all treatment groups (g) that remained on the platform and time to first departure at 15 weeks of age. Dotted line represents wild-type behaviour. Circles and squares represent single animals. Numbers within or under the bars represent the n of each group.

a) Two-tailed Student's t-test with Welch's correction. b,c) Welch's ANOVA. Mean ± SEM.

d) Two-tailed Mann-Whitney test. e,f) Kruskal-Wallis test. Median and 95% CI.

g) Log-rank (Mantel-Cox) test. **** p<0.0001.

6.4.3 MoSeq analysis revealed a strong genotype effect but did not identify behaviour modification after viral vector treatment

As seen in previous chapters, hyperactivity in *Syngap1*$^{+/-}$ mice is likely to be the most prominent phenotype, and it is possible that this strong phenotype influences other behaviours to some extent. If this is true, discriminating between what is and what is not a consequence of increased locomotor activity is not possible. To identify novel systems for performing behavioural phenotyping of *Syngap1*$^{+/-}$ mice and to test the therapeutic effects of viral vector treatment, experimental cohorts injected with vehicle or AAV9/hSYN1-*hSYNGAP1* were tested using MoSeq (Wiltschko *et al.*, 2015).

As shown in Figure 6-1c, MoSeq was performed at the end of the behavioural battery at 15 weeks of age. Mice were placed in an open field arena and allowed to explore for 10 minutes while the behaviour was recorded using a depth camera. Videos were then analysed using the MoSeq algorithm as detailed in Chapter 2.

After comparing wild-type and *Syngap1*$^{+/-}$ vehicle-treated mice, it was possible to identify a clear genotype effect in syllable usage (Figure 6-12). The algorithm identified 51 common syllables of which less than 50% (17 out of 51, statistical results reported in Table S-30) had a comparable usage between the two genotypes.

The system also analysed the overall horizontal activity, which was consistently higher in *Syngap1*$^{+/-}$ mice, as observed during other behavioural paradigms.

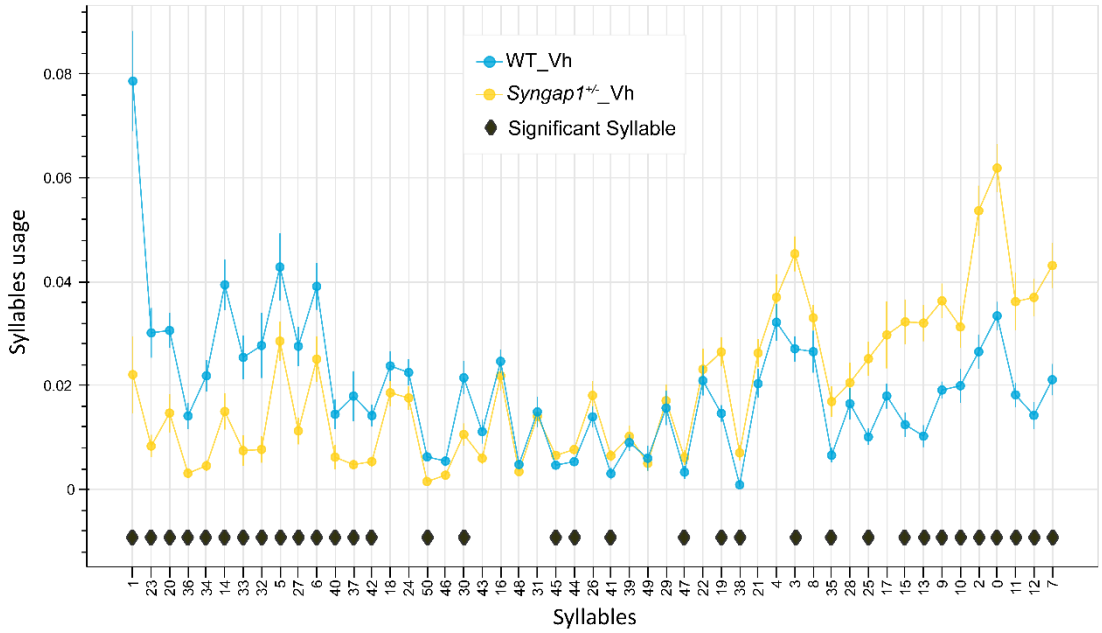

Figure 6-12. Syllables usage analysis revealed a clear genotype difference.
Syllable usage in wild-type (WT) and *Syngap1*$^{+/-}$ vehicle (Vh) treated mice. Data are organised on the base of the level of difference in usage. At the centre are the syllables with a common level of usage between genotypes. On the left-hand side are reported the syllables with higher usage in the wild-type, on the right are reported the syllables mostly used by *Syngap1*$^{+/-}$ mice.
Data presented as mean ± SEM, two-tailed Mann-Whitney test. Wild-type (Vh) n=19, *Syngap1*$^{+/-}$ (Vh) n=17. Black diamonds indicate a significant difference, $p<0.05$.

Together with the level of usage of each syllable, the system also allows the calculation of the syllable-to-syllable probability of transition and pattern. These data are represented using state maps, as seen in Figure 6-13, where each node represents a syllable, and the size of the node is proportional to the level of usage. The lines connecting the syllables represent the likelihood of transition between the connected syllables: the thicker the line, the more likely the transition will happen.

The comparison of wild-type and *Syngap1*$^{+/-}$ vehicle-treated mice state maps reveals a large difference in syllable-to-syllable likelihood of transition (Figure 6-13). As seen in Figure 6-12, syllable 1 is the most used by wild-type mice, with a high probability of transition to syllable 33 (Figure 6-13a). The opposite is observed in *Syngap1*$^{+/-}$ mice, where syllable 1 shows low level of usage with a scarce probability of transitioning to syllable 33.

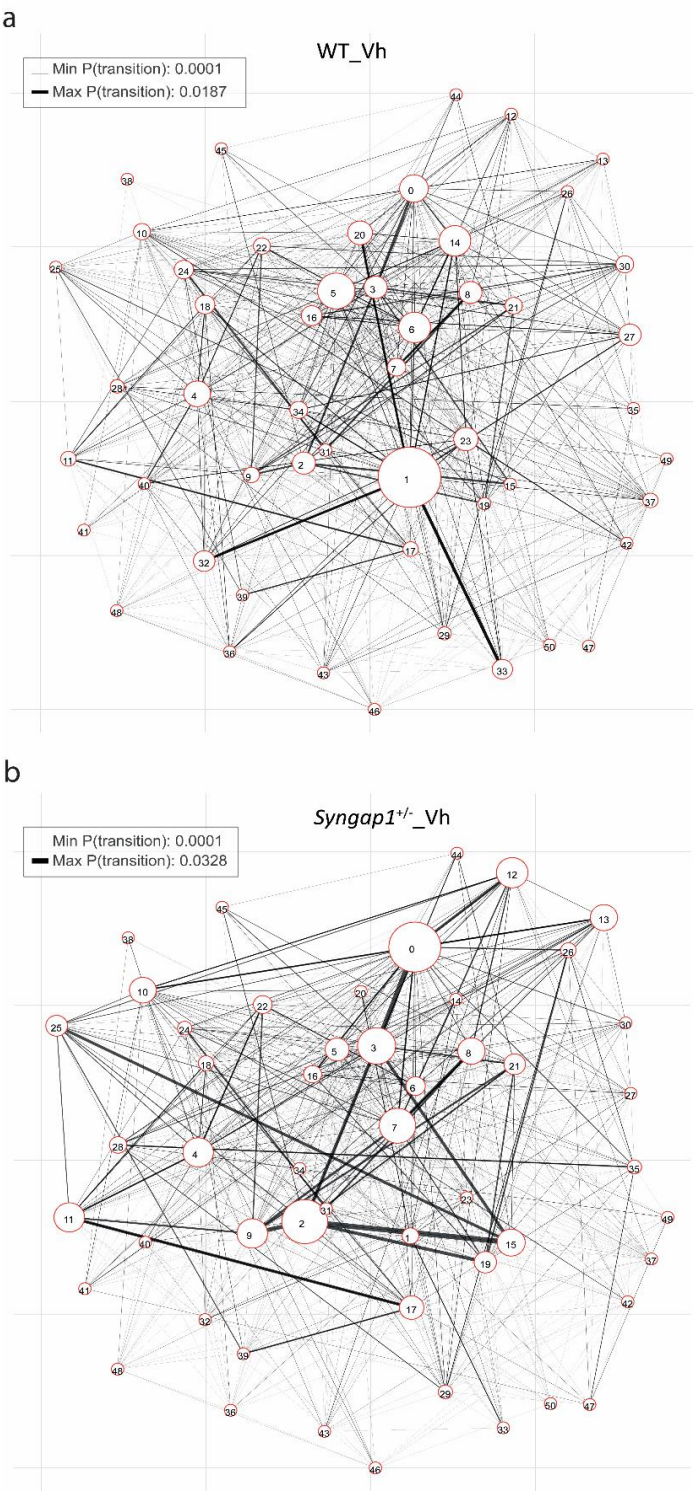

Figure 6-13. Genotype affects, together with the syllable usage, also the likelihood of syllable-to-syllable transition.

State maps representing syllables (nodes) and the likelihood of transition (edges) between syllables of wild-type (WT) (a) and *Syngap1*$^{+/-}$ vehicle (Vh) treated mice (b). The size of the node is proportional to the syllables level of usage while the thickness of the connecting lines is proportional to the probability that the indicated transition will occur. Wild-type (Vh) n=19, *Syngap1*$^{+/-}$ (Vh) n=17.

Similar to what showed in previous sections, the effect of viral vector treatment on behaviour was also evaluated in wild-type mice. The overall syllables usage between vehicle and viral vector-treated wild-type mice resulted similarly, with only a small subset of syllables that resulted differentially used between treatments (Figure 6-14, statistical tests results are reported in Table S-31 and Dunn's multiple comparison tests results are reported in Table S-32).

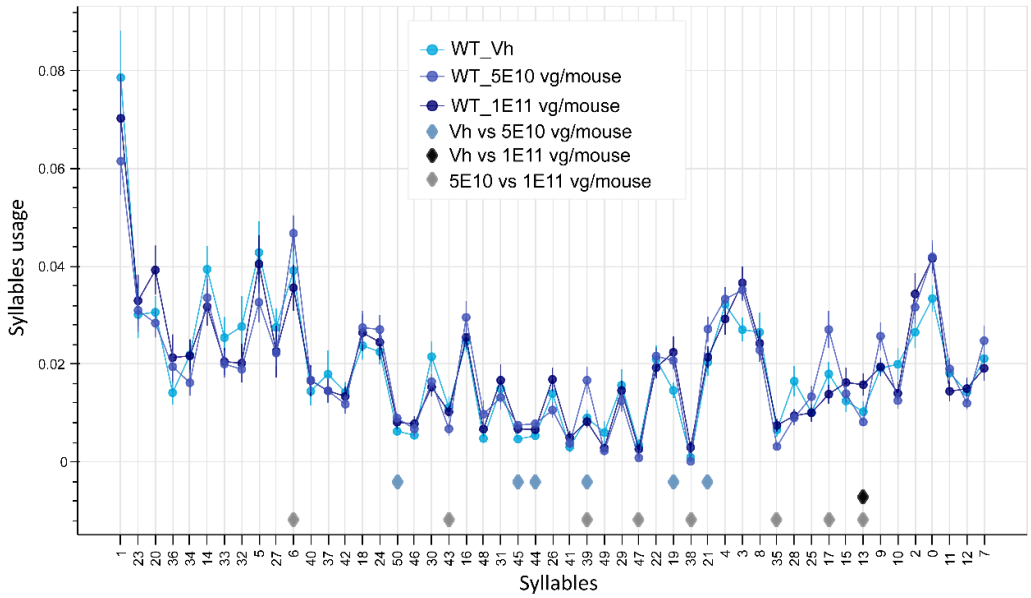

Figure 6-14. Comparison between vehicle and AAV9/hSYN1-hSYNGAP1 injected wild-type mice did not highlight overt tolerability issues associated with the treatment.

Syllables usage in vehicle (Vh) and viral vector-treated wild-type (WT) mice.
Data presented as mean ± SEM, Kruskal-Wallis test with Dunn's multiple comparison test. Vehicle n=19, 5E10 vg/mouse n=18, 1E10 vg/mouse n=21. Diamonds indicate a significant difference, $p<0.05$.

Analysis of the state maps generated for vehicle and viral vector wild-type treatment groups showed a comparable overall pattern of syllable-to-syllable transition (Figure 6-15). Single syllable representation (size of the node), as also seen in Figure 6-13, is broadly similar.

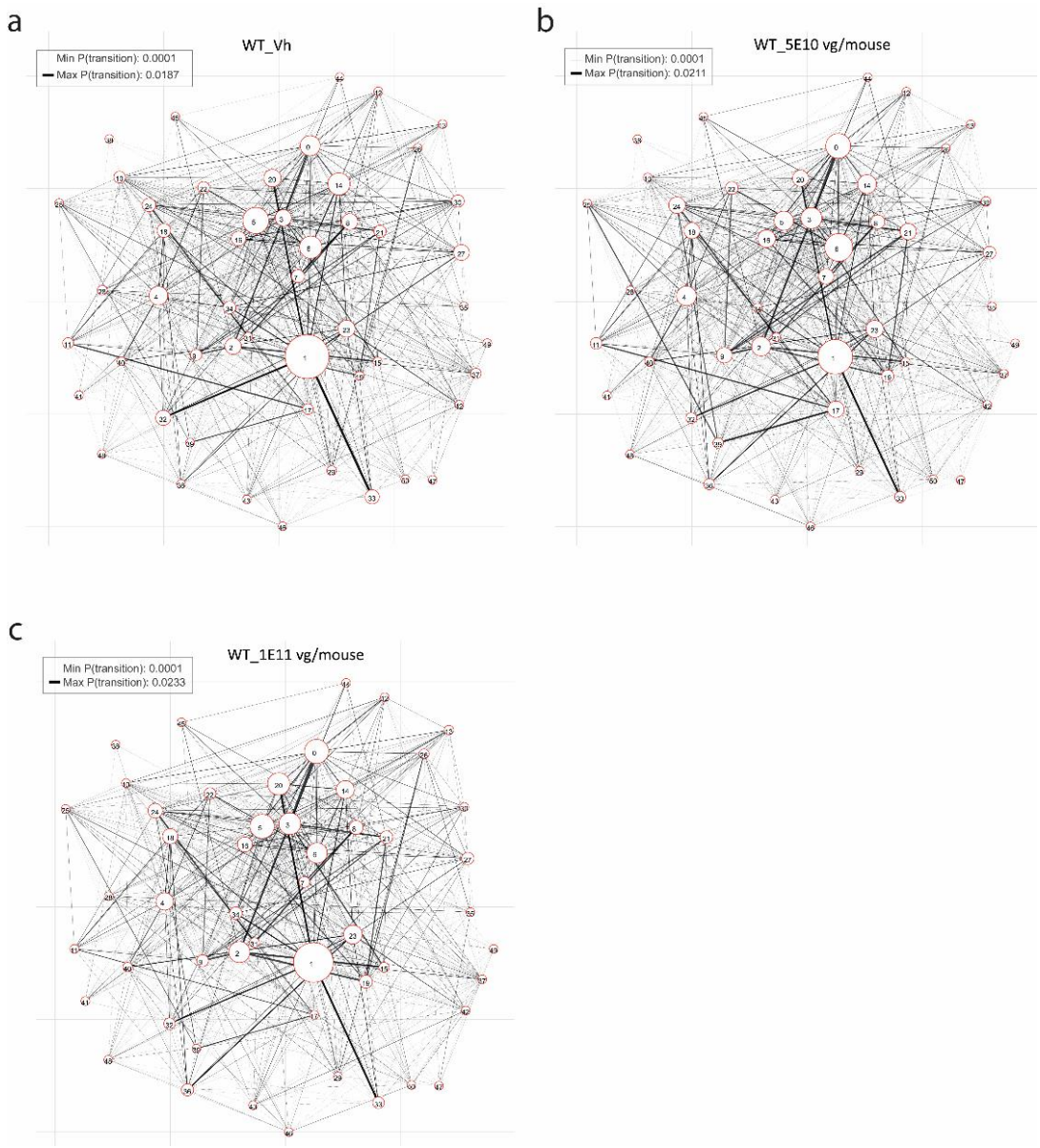

Figure 6-15. Syllable transition pattern was comparable among treatment groups in wild-type mice.

State maps representing syllables (nodes) and the likelihood of transition (edges) between syllables of wild-type (WT) mice treated with vehicle (Vh) (a), 5E10vg/mouse (b) or 1E11vg/mouse (c). The size of the node is proportional to the syllables level of usage while the thickness of the connecting lines is proportional to the probability that the indicated transition will occur. Vehicle n=19, 5E10 vg/mouse n=18, 1E10 vg/mouse n=21.

As described in the previous section, no behavioural modification was observed among wild-type viral vector-treated mice, with the only exception for the number of partial departures at 7 weeks of age. MoSeq is regarded as an extremely sensitive

technique, able to discern between doses of the same treatment (Wiltschko *et al.*, 2021). It is possible that although no overt tolerability issues were observed, the treatment was causing subtle behavioural changes, which caused a modification in a subset of syllables.

Overall, viral vector treatment did not affect syllables usage among *Syngap1*$^{+/-}$ mice (Figure 6-16). Only three out of 51 syllables were differentially used among treatment groups, of which only syllable 45 was originally significantly different between wild-type and *Syngap1*$^{+/-}$ vehicle-treated mice (statistical results are reported in Table S-33 and Dunn's multiple comparison tests results are reported in Table S-34). Interestingly, among the syllables that had a significant different usage between wild-type and *Syngap1*$^{+/-}$ vehicle-treated mice, *Syngap1*$^{+/-}$ viral vector-treated mice showed improvement in five syllables (5, 25, 9, 11 and 7). The difference between vehicle and viral vector-treated mice was not significant, but these five syllables from either 5E10 or 1E11 vg/mouse, or both treatment groups, presented a more similar usage to wild-type rather than to *Syngap1*$^{+/-}$ vehicle-treated mice.

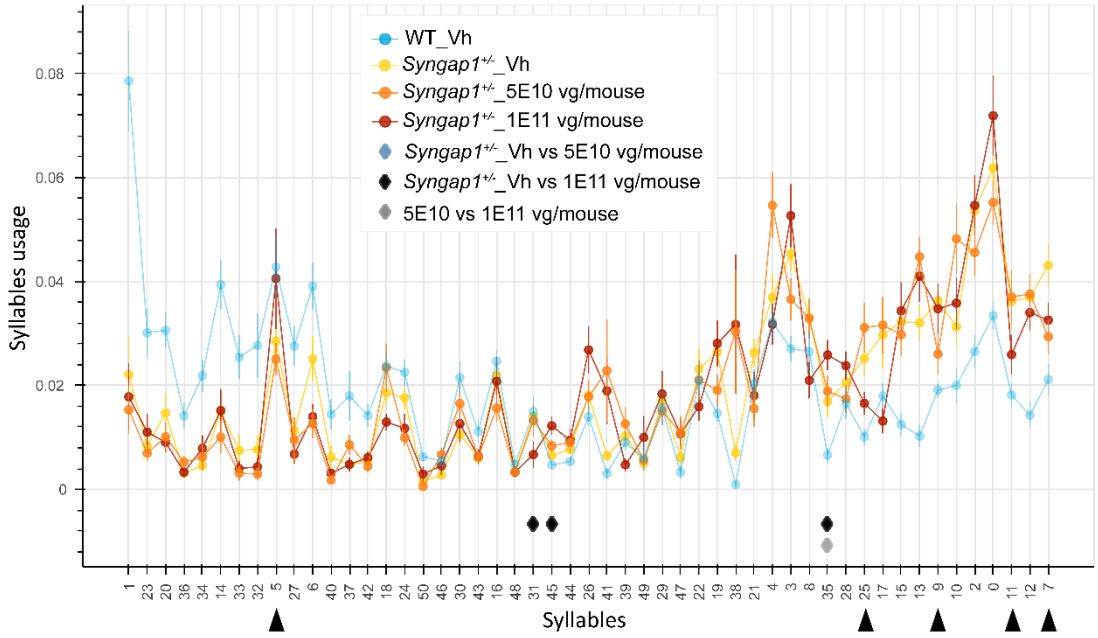

Figure 6-16. AAV9/hSYN1-hSYNGAP1 and vehicle-treated Syngap1$^{+/-}$ mice presented a similar syllables usage pattern.

Syllable usage in vehicle (Vh) and viral vector-treated *Syngap1*$^{+/-}$ mice. Diamonds indicate a significant difference. Black arrows indicate syllables where the usage by viral vector-treated *Syngap1*$^{+/-}$ mice was similar to the wild-type (WT) usage.
Data presented as mean ± SEM, Kruskal-Wallis test with Dunn's multiple comparison test. Vehicle n=17, 5E10 vg/mouse n=13, 1E10 vg/mouse n=13. $p<0.05$.

No clear difference was observed when comparing the state maps of syllable-to-syllable likelihood of transition of vehicle (Figure 6-17a) and AAV9/hSYN1-*hSYNGAP1* treated *Syngap1*$^{+/-}$ mice (Figure 6-17b and c), apart from subtle changes in transition likelihood of the syllables mentioned before (5, 25, 9, 11 and 7) which appeared more similar to wild-type vehicle-treated mice (Figure 6-13).

These subtle changes are difficult to quantify, and as they were not present over most of the syllables and syllable-to-syllable transition, overall, MoSeq analysis did not suggest the presence of a treatment effect.

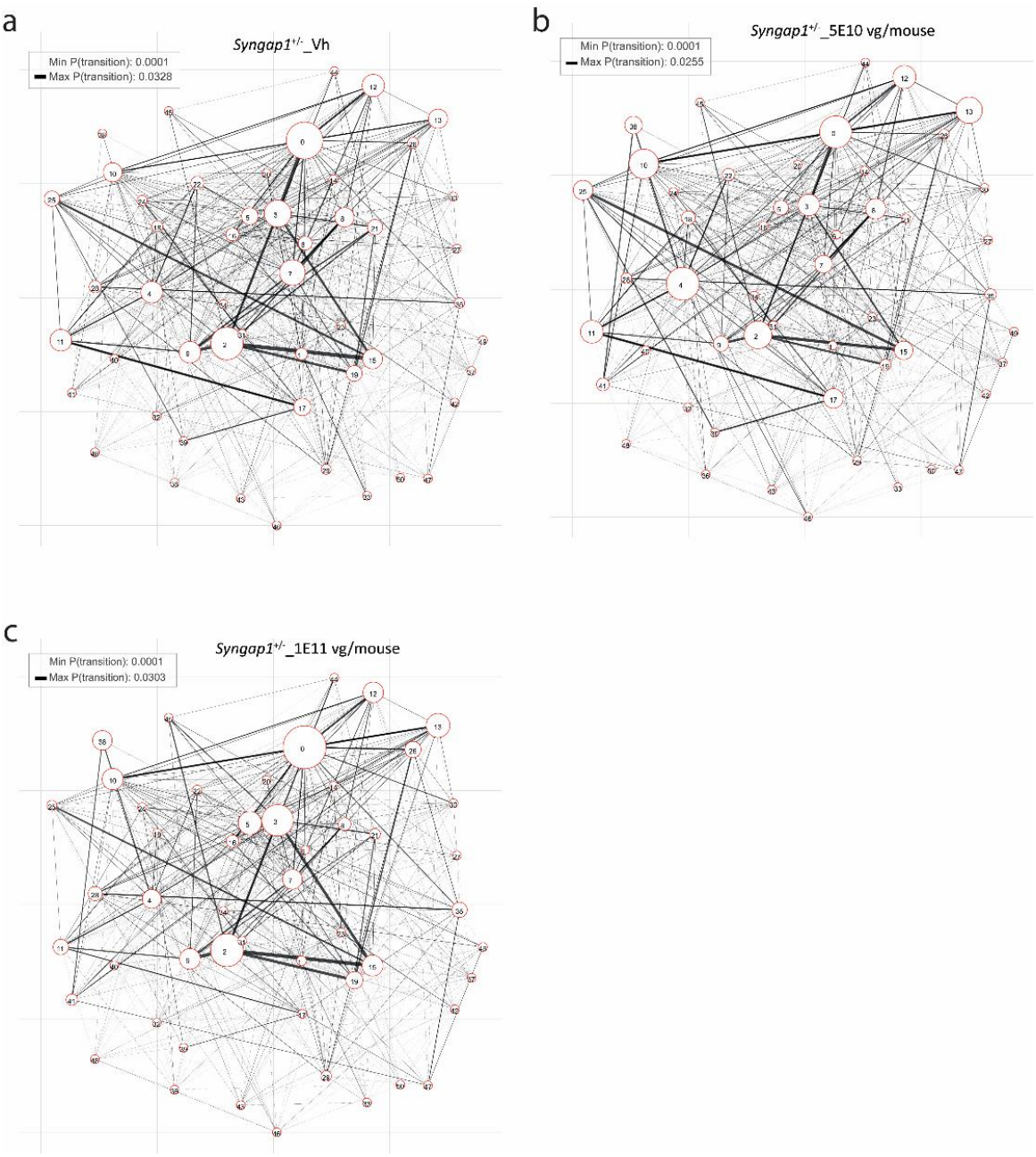

Figure 6-17. The syllable transition pattern was comparable across treatment groups in Syngap1$^{+/-}$ mice.

State maps representing syllables (nodes) and the likelihood of transition (edges) between syllables of *Syngap1*$^{+/-}$ mice treated with vehicle (Vh) (a), 5E10vg/mouse (b) or 1E11vg/mouse (c). The size of the node is proportional to the syllables level of usage while the thickness of the connecting lines is proportional to the probability that the indicated transition will occur. Vehicle n=17, 5E10 vg/mouse n=13, 1E10 vg/mouse n=13.

6.4.4 AAV9/JeT-*hSYNGAP1* viral vector genome was detected in the cortex, hippocampus, thalamus and striatum

Post hoc viral vector biodistribution analysis was performed with the aim to correlate the effects observed during the behavioural phenotyping and the viral vector distribution in the brain.

Specifically, viral vector biodistribution was assessed in the cortex, hippocampus and striatum, which are considered to be important regions in the pathophysiology of the disease (Knuesel *et al.*, 2005; Moon *et al.*, 2008; Porter *et al.*, 2005; Tomoda *et al.*, 2004). Biodistribution was also analysed in thalamus and cerebellum, which were chosen to evaluate viral vector spread. To this end, qPCR and absolute quantification, via standard curve method were used. The methodology is detailed in Chapter 2 and primer sequences and optimization process is reported in Appendix C, Section C.4.

In all considered regions, no dose-response was observed with an average number of copies similar between doses. It is to be noted that the dataset was quite variable, with samples with very few vector copies per diploid genome for both tested viral vector doses. As expected, cerebellum presented the lowest number of AAV9/hSYN1-*hSYNGAP1* genomes per diploid genomes (Figure 6-18e; Welch's ANOVA, mean ± SEM; vehicle n=3, 9.64E-6 ± 7.40E-6 vg/dp; 5E10 vg/mouse n=5, 0.0046 ± 0.00013 vg/dp; 1E11 vg/mouse n=5, 0.0073 ± 0.0014 vg/dp; $W_{(2.00,\ 5.334)}$=16.78, p=0.0050; Dunnett's T3 multiple comparison test results are reported in Table S-39).
Cortical samples, collected from the somatomotor and motor cortex, and hippocampus appeared to have a similar vector distribution (Figure 6-18a and b; cortex, Welch's ANOVA, mean ± SEM; vehicle n=3, 1.2E-5 ± 4.47E-6 vg/dp; 5E10 vg/mouse n=5, 0.82 ± 0.33 vg/dp; 1E11 vg/mouse n=5, 0.61 ± 0.22 vg/dp; $W_{(2.00,\ 5.333)}$=5.896, p=0.0446. Hippocampus, Welch's ANOVA, mean ± SEM; vehicle n=3, 2.07E-5 ± 1.19E-5 vg/dp; 5E10 vg/mouse n=5, 0.57 ± 0.29 vg/dp; 1E11 vg/mouse n=5, 0.58 ± 0.15 vg/dp; $W_{(2.00,\ 5.333)}$=8.443, p=0.0223; Dunnett's T3 multiple comparison test results are reported in Table S-35 and Table S-36).

Similar viral vector copy number was detected in striatum and thalamus (Figure 6-18c and d; striatum, Welch's ANOVA, mean ± SEM; vehicle n=3, 5.34E-5 ± 3.98E-5 vg/dp; 5E10 vg/mouse n=5, 1.01 ± 0.71 vg/dp; 1E11 vg/mouse n=5, 0.47 ± 0.14 vg/dp; $W_{(2.00, 5.333)}$=6.070, p=0.0422. Thalamus, Welch's ANOVA, mean ± SEM; vehicle n=3, 8.30E-6 ± 5.65E-6 vg/dp; 5E10 vg/mouse n=5, 0.60 ± 0.25 vg/dp; 1E11 vg/mouse n=5, 0.24 ± 0.06 vg/dp; $W_{(2.00, 5.333)}$=9.568, p=0.0172; Dunnett's T3 multiple comparison test results are reported in Table S-37 and Table S-38).

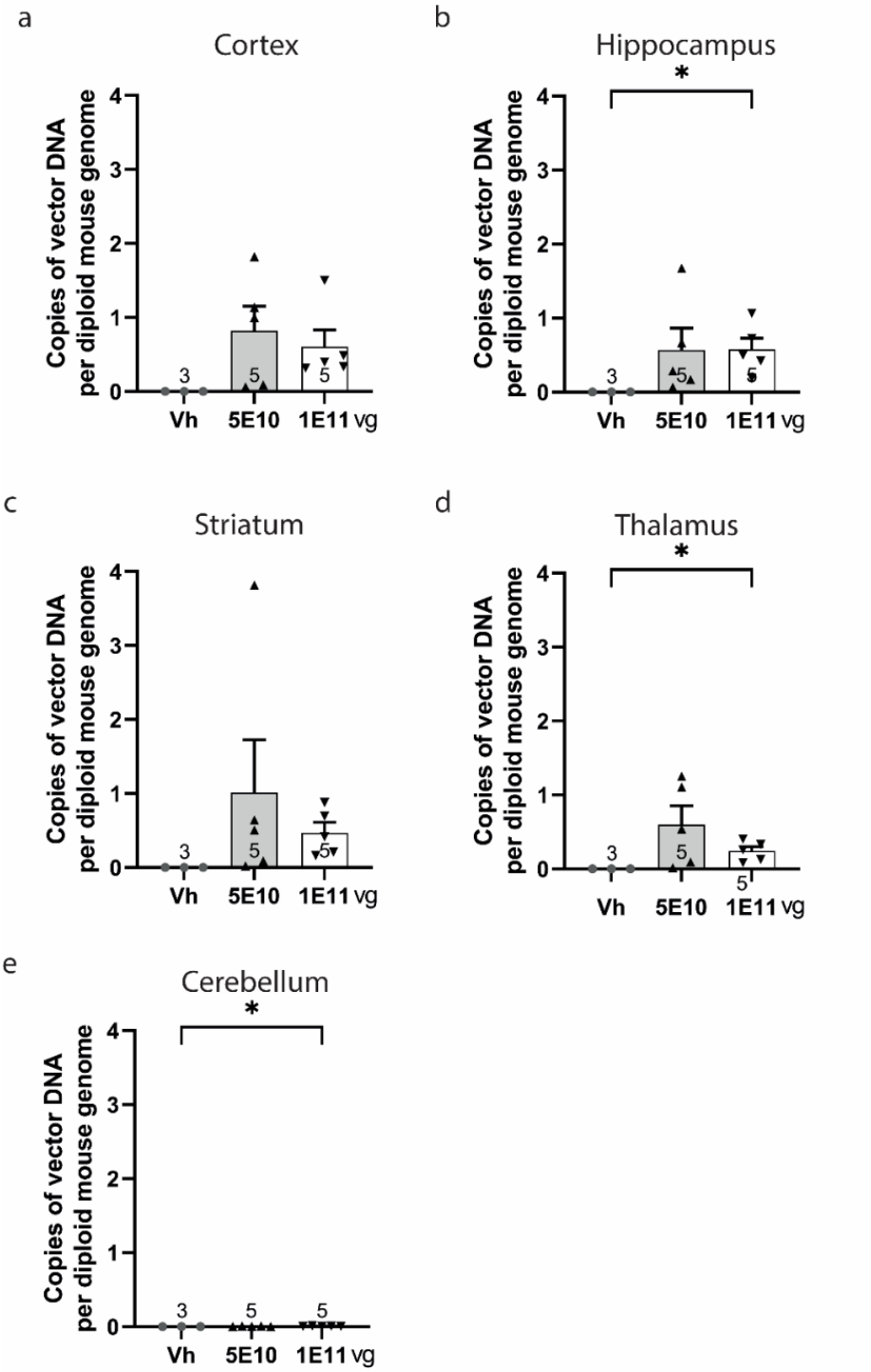

Figure 6-18. Biodistribution analysis showed the presence of the AAV9/hSYN1-hSYNGAP1 viral vector in the cortex, hippocampus, striatum and thalamus.
Number of viral genomes per diploid genome in cortex (a), hippocampus (b), striatum (c), thalamus (d) and cerebellum (e). Points on the graphs represent single animals. Numbers within or under/above the bars represent group n. Vh=Vehicle. Data presented as mean ± SEM. Welch's ANOVA with Dunnett's T3 multiple comparisons test. * $p<0.05$.

6.4.5 Viral vector-derived FLAG-SYNGAP1 was detectable in the cortex and hippocampus and showed a subcellular compartment localisation comparable to the endogenous SYNGAP1

After completing the behavioural phenotyping, I proceeded to assess the level of exogenous protein expression achieved with the third generation gene therapy vector AAV9/hSYN1-*hSYNGAP1*. The goal was to establish a correlation between protein levels and behavioural outcomes. Specifically, I measured the levels of FLAG-SYNGAP1 derived from the viral vector in the cortex and hippocampus of *Syngap1*$^{+/-}$ mice treated with either the vector or vehicle. Additionally, I investigated the subcellular localization of the exogenous protein.

In the whole cortex lysates, AAV9/hSYN1-*hSYNGAP1* derived protein signal was detectable (Figure 6-19a) and signal derived from the immunolabelling of the FLAG peptide was suggestive of dose-dependent protein expression (Figure 6-19c; Welch's ANOVA test, mean ± SEM; vehicle n=6, 0.02 ± 0.01; 5E10 vg/mouse n=6, 0.51 ± 0.24; 1E11 vg/mouse n=5, 1.00 ± 0.22; $W_{(2,\ 6.719)}$=10.53, p=0.0085; Dunnett's T3 multiple comparisons test are reported in Table S-40).

When the absolute level of SYNGAP1 protein was quantified in the same samples, no increase relative to the vehicle control was observed (Figure 6-19b; Welch's ANOVA test, mean ± SEM; vehicle n=6, 1.00 ± 0.16; 5E10 vg/mouse n=6, 1.01 ± 0.15; 1E11 vg/mouse n=5, 1.05 ± 0.02; $W_{(2,\ 6.911)}$=0.095, p=0.9102).

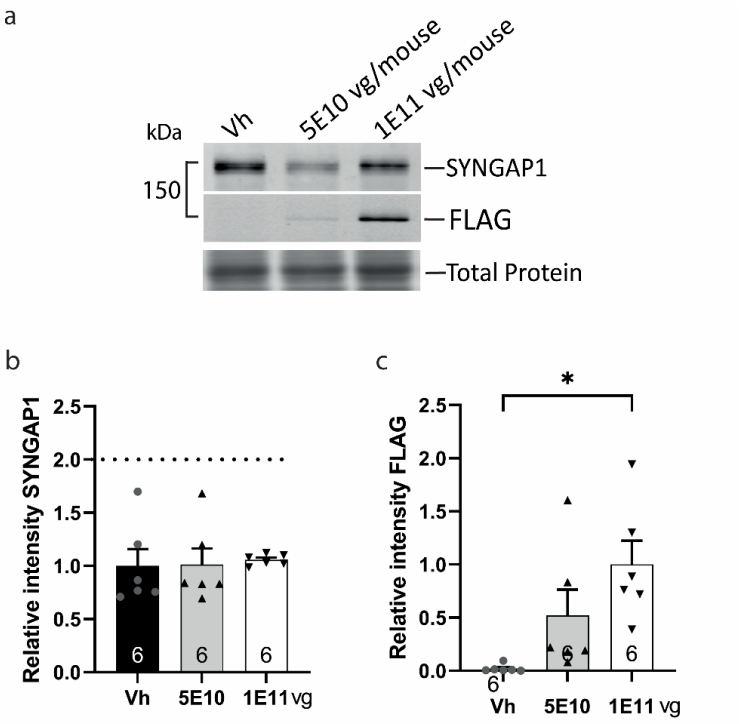

Figure 6-19. AAV9/hSYN1-hSYNGAP1 viral vector-derived SYNGAP1 was detectable via immunoblot analysis in cortical protein lysate.
Representative immunoblot of cortex protein lysate labelled with anti-FLAG and anti-SYNGAP1 antibodies (a). Quantification of SYNGAP1 (b, normalised to vehicle treated) and FLAG (c, normalised to 1E11 vg/mouse treated) signal in tissues treated with 1E10 and 1E11 vg/mouse or vehicle (Vh).
Tissue from *Syngap1*$^{+/-}$ treated mice was collected at 25-26 weeks of age. Dotted line represent wild-type levels. Total protein was used as loading control. Images used for quantification are reported in Figure S-33. Points represent single animals. Numbers within or under the bars represent the n of each group. The gel was used at a concentration of bis-acrylamide of 10%. Data presented as mean ± SEM. Welch's ANOVA with Dunnett's T3 multiple comparisons test. * $p<0.05$.

Similar to what was observed for AAV9/JeT-*hSYNGAP1* (Chapter 5), in whole hippocampal preparation, FLAG-SYNGAP1 was detected (Figure 6-20a), however, vector-derived protein did not cause an increase in absolute levels of SYNGAP1 protein when compared to vehicle-treated *Syngap1*$^{+/-}$ tissue (Figure 6-20b; Welch's ANOVA test, mean ± SEM; vehicle n=6, 1.00 ± 0.15; 5E10 vg/mouse n=6, 0.85 ± 0.11; 1E11 vg/mouse n=6, 0.74 ± 0.15; $W_{(2, 9.764)}=0.7462$, $p=0.4994$).

Analysis of the signal associated to the FLAG peptide suggested a dose-dependent trend in the expression of the exogenous protein (Figure 6-20c; Welch's ANOVA test,

mean ± SEM; vehicle n=6, 0.04 ± 0.01; 5E10 vg/mouse n=6, 0.52 ± 0.15; 1E11 vg/mouse n=6, 1.00 ± 0.27; $W_{(2,\ 6.755)}$=10.01, p=0.0095; Dunnett's T3 multiple comparisons test results are reported in Table S-41).

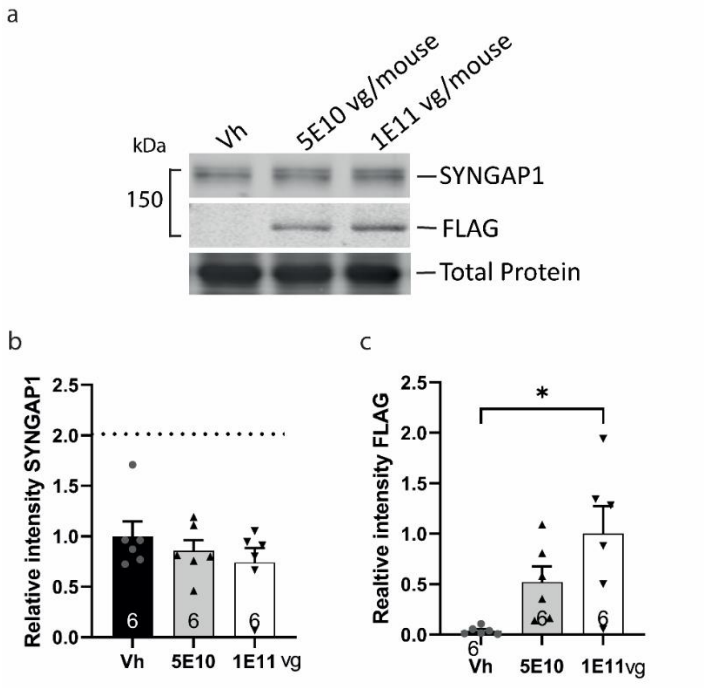

Figure 6-20. AAV9/hSYN1-hSYNGAP1 viral vector-derived SYNGAP1 was detectable via immunoblot analysis of hippocampal protein lysate.
Representative immunoblot of hippocampus protein lysate labelled with anti-FLAG and SYNGAP1 antibodies (a). Quantification of SYNGAP1 (b, normalised to vehicle treated) and FLAG (c, normalised to 1E11 vg/mouse treated) signal in tissues treated with 1E10 and 1E11 vg/mouse or vehicle (Vh).
Tissue from *Syngap1*$^{+/-}$ treated mice was collected at 25-26 weeks of age. Dotted line represent wild-type levels. Images used for quantification are reported in Figure S-34. Points represent single animals. Numbers within or under the bars represent the n of each group. The gel was used at a concentration of bis-acrylamide of 10%. Data presented as mean ± SEM. Welch's ANOVA with Dunnett's T3 multiple comparisons test. * p<0.05.

The subcellular localisation of vector-derived protein was examined using the synaptosomal preparation protocol as described in Chapter 2.

Immunoblot analysis of subcellular fractions showed the correct localisation of the vector-derived protein in the synaptic compartment, with little or no signal associated with the FLAG peptide detected in the cytosolic compartment. This

subcellular compartment distribution closely resembled the localization of the endogenous protein (Figure 6-21). As previously noted in Chapter 5, nuclear fraction contamination by synaptic marker was observed in these preparations, but the absence of Histone H3 from the cytosolic and synaptosome fractions confirmed the successful depletion of nuclei.

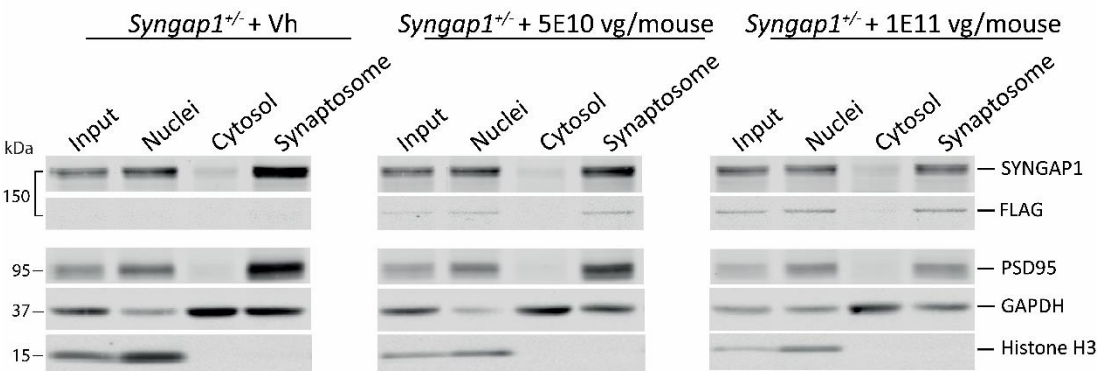

Figure 6-21. AAV9/hSYN1-hSYNGAP1 viral vector FLAG-SYNGAP1 resulted present in the synaptosome fraction and absent from the cytosolic fraction, mimicking endogenous SYNGAP1 localisation.
Representative immunoblot of synaptosomal preparation of whole hippocampi and labelled with subcellular fraction-specific markers. Tissue from vehicle (Vh) and viral vector-treated *Syngap1*$^{+/-}$mice collected at 25-26 weeks of age. The gel was used at a concentration of bis acrylamide of 12%.

6.4.6 *SYNGAP1* viral vector-derived mRNA molecules were detected in treated tissue

It has been shown before that codon optimisation can increase transgene expression when compared to a non-codon-optimised sequence (Brown *et al.*, 2018; Burgess-Brown *et al.*, 2008; Disbrow *et al.*, 2003; Ward *et al.*, 2011). Therefore, higher levels of viral vector-derived SYNGAP1 were expected despite the relatively low number of viral vector genome copies detected in these regions.

To evaluate if the low levels of the vector-derived SYNGAP1 were due to issues during the therapeutic cassette transcription, the number of viral vector-derived *SYNGAP1* transcripts were quantified from total RNA extracted from whole hippocampi using the absolute quantification via standard curve method.

To compare the amount of endogenous *Syngap1* and exogenous *SYNGAP1* mRNA molecules it was necessary to design primers specific for the amplification of the mouse and the viral vector sequence with no cross-reaction. The presence of mismatches between endogenous and exogenous sequences, due to intrinsic differences between human and mouse sequences and the effect of the codon optimisation, was used to design viral vector and mouse-specific forward primers. The detailed methodology was presented in Chapter 2 while primer sequence and reactions optimisation are reported in Appendix C, Section C.5.

To evaluate viral vector-derived *SYNGAP1* transcripts in relation to endogenous *Syngap1* mRNA, the absolute number of molecules of *SYNGAP1* and endogenous *Syngap1* mRNA calculated were normalised to the number of *Actb* mRNA molecules for each sample (this normalisation is indicated in figures and figure legends as *Syngap1/Actb* or *SYNGAP1/Actb*). This corrects for any variation in the RNA input. Further normalisations are specified for each comparison.

Confirmatory quantification of endogenous *Syngap1* mRNA showed that, as expected, *Syngap1*$^{+/-}$ mice presented a reduction of about 50% of *Syngap1* mRNA molecules compared to wild-type controls (Figure 6-22; Student's t-test with Welch's correction, mean ± SEM; wild-type n=3, 1.00 ± 0.15; *Syngap1*$^{+/-}$ n=3, 0.44 ± 0.04; $t_{(2.226)}$=3.521, p=0.0616). These data were in accordance with what was observed at the protein level shown in Chapter 5, with *Syngap1*$^{+/-}$ mice expressing about half the amount of SYNGAP1 protein present in wild-type controls.

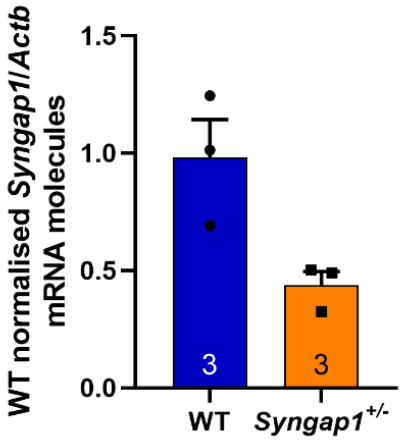

Figure 6-22. Syngap1$^{+/-}$ mice, compared to wild-type controls, showed a reduction of Syngap1 mRNA molecules of about half compared to wild-type controls.
Syngap1/Actb molecules in wild-type (WT) and *Syngap1*$^{+/-}$ vehicle-treated mice normalised to the average number of *Syngap1* mRNA molecules present in the wild-type control. Tissue from whole hippocampi of 25 weeks old vehicle-treated mice, dots represent single animals. Numbers within the bars represent the n of each group. Data presented as mean ± SEM, Student's t-test with Welch's correction.

When the *Actb* normalised absolute copies of viral vector-derived *SYNGAP1* mRNA were compared between treatment groups, results were suggestive of a dose-dependent response (Figure 6-23a; Welch's ANOVA test among treated *Syngap1*$^{+/-}$ mice, mean ± SEM; *Syngap1*$^{+/-}$ Vh n=3, 0.00003 ± 0.00003; 5E10 vg/mouse n=3, 0.01 ± 0.0.003; 1E11 vg/mouse n=3, 0.02 ± 0.012; $W_{(2, 2.667)}$=5.173, p=0.1203).

To evaluate the fold-change of viral vector-derived *SYNGAP1* transcripts in comparison to the wild-type *Syngap1* mRNA molecules, *Actb* normalised *SYNGAP1* mRNA molecules of each group were normalised over the *Syngap1/Actb* mRNA molecules present in the wild-type controls. A 2.5-fold and a 6-fold increase over wild-type level was observed for 5E10 vg/mouse and 1E11 vg/mouse viral vector-treated *Syngap1*$^{+/-}$ mice respectively (Figure 6-23b; mean ± SEM; wild-type Vh n=3 0.0001 ± 7.87%-5; *Syngap1*$^{+/-}$ Vh n=3 0.007 ± 0.007, 1E11 vg/mouse n=3 2.56 ± 0.86, 5E10 vg/mouse 6.28 ± 3.12). It was possible to perform this comparison as the absolute quantification considers the different efficiency of amplification of the different reactions by calculating the number of mRNA molecules based on known standards.

Data showed that mRNA derived from the transcription of the viral vector was detectable and that, at the highest viral vector dose tested, a 6-fold increase was observed.

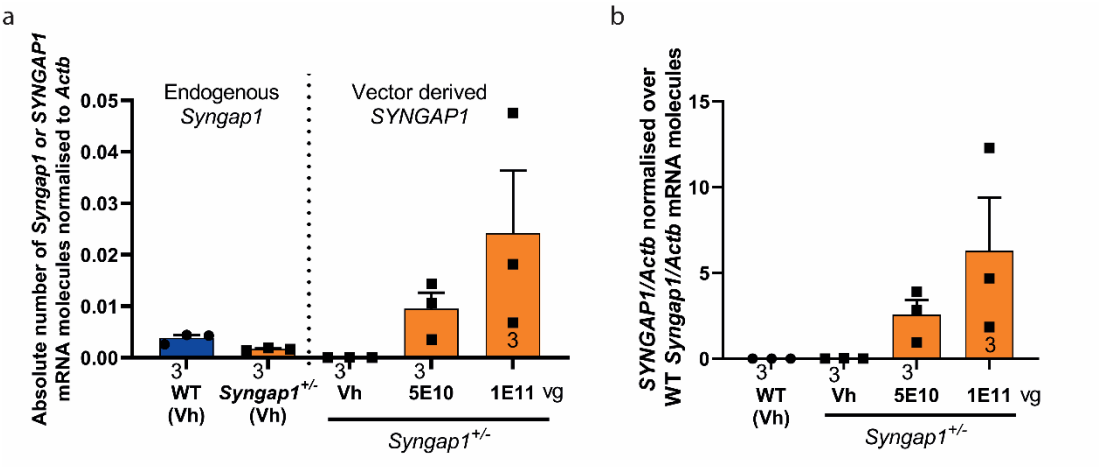

Figure 6-23. At both AAV9/hSYN1-hSYNGAP1 viral vector doses tested, a higher number of exogenous derived SYNGAP1 mRNA was detected compared to the wild-type control.

Syngap1/Actb mRNA molecules in wild-type (WT) and *Syngap1*$^{+/-}$ vehicle (Vh) treated mice (left panel); *SYNGAP1/Actb* mRNA molecules in *Syngap1*$^{+/-}$ vehicle and viral vector-treated mice (right panel) (a). Fold increase of *SYNGAP1/Actb* mRNA molecules normalised over the average of the wild-type (WT) vehicle (Vh) endogenous *Syngap1/Actb* mRNA molecules (b). Tissue from whole hippocampi of 25 weeks old vehicle and viral vector-treated mice. Circles and squares represent single animals. Numbers within or under the bars represent the n of each group. Data presented as mean ± SEM, a) Student's t-test with Welch's correction.

6.4.7 Quality control of therapeutic viral vector preparation showed correct ratio among viral vector capsid protein, but alkaline gel suggested viral genome packaging issues

The quality of the viral vector preparation is defined by several parameters such as the presence of empty capsids, incomplete encapsidation, encapsidation of fragmented genomes or DNA fragments derived from the production system or contaminants. All these factors can strongly influence transduction efficiency (Schnödt *et al.*, 2017).

Using next generation sequencing to analyse the sequence composition of the AAV prep, encapsidation of DNA derived from the production system and contaminants was shown to be minimal. As previously shown in Table 6-1, 94% of sequence reads aligned to the construct sequence (ITR to ITR). Less than 1% of all reads aligned to the rep-cap, helper and plasmid backbone sequences.

The formation of an empty capsid is caused by a failure during DNA packaging and it is considered a contaminant of viral vector preparations, as their presence decrease transduction efficiency and increase the chances of an immune response (Gao *et al.*, 2014; Hösel *et al.*, 2012). A strategy to decrease empty capsid contamination is to purify the viral vector preparation using Caesium chloride density gradient ultracentrifugation. As the AAV9/hSYN1-*hSYNGAP1* vector was purified using this strategy it is likely that the observed low vector distribution was not associated with the presence of a high percentage of the empty capsids.

The outer shell of AAV is composed of three viral capsid proteins, VP1, VP2 and VP3, arranged in an icosahedral structure with a ratio among proteins of 1:1:10 (Naso *et al.*, 2017). Recent studies have shown that vector capsid follows a stochastic assembly which leads to the formation of capsid with a variable ratio between VP1, VP2 and VP3 (Wörner *et al.*, 2021). Moreover, it was shown that different viral vector production systems can differently affect the VP ratio (Kohlbrenner *et al.*, 2005; Mietzsch *et al.*, 2015). A large difference between the expected ratio and the observed one can be an indication of a problem during viral vector preparation and low quality.

SDS-PAGE gel electrophoresis followed by Coomassie staining, as detailed in Chapter 2, was performed to evaluate the VP ratio of the AAV9/JeT-*hSYNGAP1* and AAV9/hSYN1-*hSYNGAP1* viral vector (Figure 6-24), and the resulting image was subsequently visually inspected by a collaborator. AAV9/JeT-*hSYNGAP1* presented a fourth band, around 60 kDa, which could be associated with partial degradation of the viral vector preparation. This degradation could be due to the relatively long time passed between the viral vector production and this test (~2 years). AAV9/hSYN1-

hSYNGAP1 vector presented a smaller amount of VP1 and 2 compared to VP3 but the difference was not large enough to suggest issues in capsid formation.

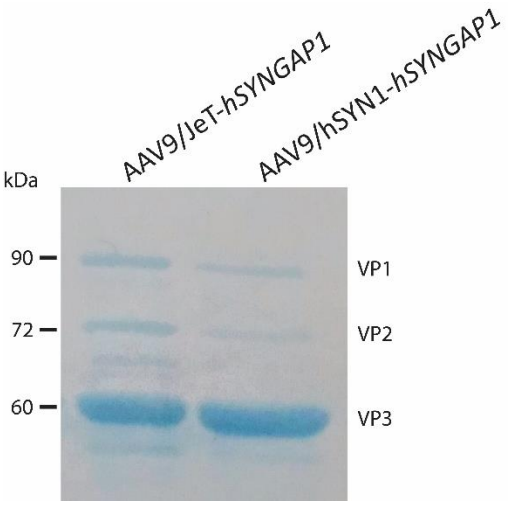

Figure 6-24. SDS-PAGE of the candidate therapeutic viral vector showed correct proportion among viral vector capsid proteins.
Coomassie staining of SDS-PAGE of AAV9/JeT-*hSYNGAP1* and AAV9/hSYN1-*hSYNGAP1* viral vectors showing the three viral vector capsid proteins, VP1, VP2 and VP3.

Exceeding the packaging capacity of wild-type AAV can also lead to packaging problems. Wild-type AAV genomic DNA has a total size of ~4700 bp (including ITRs), however, several studies have been conducted to evaluate if larger cassettes can be packaged into AAV capsid (Dong *et al.*, 1996; Grieger *et al.*, 2005; Wu *et al.*, 2006). Although one study claimed that cassettes up to 8000 bp could be packaged intact (Allocca *et al.*, 2008), more recent works showed that only genomes smaller than 5000 bp can be efficiently packaged in AAV capsid without genomic fragmentation (Dong *et al.*, 2010; Wu *et al.*, 2010).

AAV9/JeT-*hSYNGAP1* has a genome size of 4654 bp, including ITRs, which is comparable to wild-type AAV. AAV9/hSYN1-*hSYNGAP1* has a genome size of 4970 bp, which exceeds wild-type AAV capacity, but is still under the 5000 bp limit frequently identified in the literature (Dong *et al.*, 1996; Grieger *et al.*, 2005; Wu *et al.*, 2006). At this upper limit, it is possible that packaging problems occurred during AAV9/hSYN1-*hSYNGAP1* production. The presence of fragmented genomes in the viral vector

preparation could, in part, explain the low viral vector copy number seen with the biodistribution assay because fragmented genomes would be unable to complete cell transduction. Alkaline gel electrophoresis can be used to evaluate viral genome fragmentation (Schnödt *et al.*, 2017). An intact, well-packaged genome would be visualised as a single strong band at the expected genome size (ITR to ITR). As shown in Figure 6-25, AAV9/JeT-*hSYNGAP1* was visualised as a strong band of ~4700 bp, with a smear underneath, indicating that most capsids contain the full-length genome, but partial/fragmented species are present. For AAV9/hSYN1-*hSYNGAP1* the expected band of ~5000 bp was weaker, with a stronger smear underneath, indicating a higher proportion of partial/fragmented species present in this preparation.

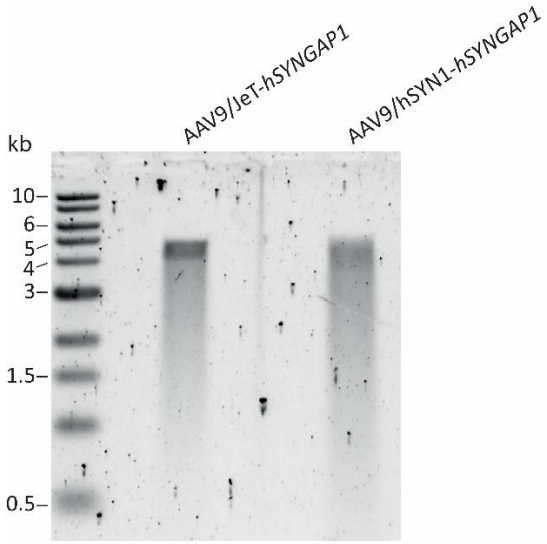

Figure 6-25. Alkaline gel electrophoresis of AAV9/hSYN1-hSYNGAP1 genomic DNA did not show a single clear band.
Alkaline gel electrophoresis of AAV9/JeT-*hSYNGAP1* (lane 2) and AAV9/hSYN1-*hSYNGAP1* (lane 5) viral vectors. 250 ng of viral DNA were loaded. DNA processing and alkaline gel electrophoresis were performed by Ms Amanda Morris.

Overall, the quality controls showed that, while both vectors presented a normal capsid protein ratio, AAV9/hSYN1-*hSYNGAP1* showed packaging issues which could explain the results presented in the previous sections.

6.5 DISCUSSION

The aim of the work presented in this chapter was to evaluate a new gene therapy construct designed to improve the therapeutic outcome observed with the AAV9/JeT-*hSYNGAP1* viral vector presented in Chapter 5. However, behavioural analysis of the new AAV9/hSYN1-*hSYNGAP1* viral vector-treated *Syngap1*$^{+/-}$ mice showed only a limited treatment effect. Mice treated with 1E11 vg/mouse exhibited a trend toward amelioration of the behaviour during the platform departure test, but hyperactivity and time spent in the open arms of the elevated plus maze appeared unaffected. Additionally, post hoc analysis of protein expression showed no increase in absolute levels of SYNGAP1 in cortical areas and hippocampus.

As shown in Chapter 5, Myc-tagged SYNGAP1 was detectable in both cortex and hippocampus, although viral vector expression only led to a subtle increase of absolute levels of SYNGAP1 protein. For this new construct, regulatory elements were modified with the aim of increasing protein expression. Firstly, the hSYN1 promoter, which has neuronal-specific activity and high levels of expression in brain regions of interest such as the cortex, hippocampus and striatum, was used (McLean *et al.*, 2014). Secondly, the polyA signal was modified by substituting the SpA with the SV40 polyA. Studies have shown that the SV40 polyA signal increases transgene expression by 2.5-fold compared to SpA (Choi *et al.*, 2014). In association to the modification of the regulatory elements, another important change consisted in the usage of a codon-optimised *SYNGAP1* sequence instead of the wild-type human sequence used for the JeT-*hSYNGAP1* construct. In particular, the sequence was codon-optimised using the codon usage found in the human genome. Mouse and human codon usage are similar and this approach has been applied before for other gene therapy cassette designs (Brown *et al.*, 2018; Ward *et al.*, 2011). Lastly, the tag element necessary to distinguish the vector-derived protein from the endogenous SYNGAP1 was changed to FLAG and positioned at the N-terminal of the protein. This was done to avoid possible impacts on protein trimerization that could lead to

impairment of protein functions (Araki *et al.*, 2020; Kilinc *et al.*, 2022; Zeng *et al.*, 2016).

Although the vector was designed to improve the level of expression observed with the previous construct, post hoc analysis of treated tissue showed no increase in the absolute levels of SYNGAP1 protein when compared to vehicle-treated mice, in both the cortex and hippocampus. Quantification using the anti-FLAG antibody showed that the difference in levels of expression, although not statistically significant, had a dose-dependent trend, with 5E10 vg/mouse dose producing about half the amount seen with 1E11 vg/mouse (Figure 6-19 and Figure 6-20). However, the large spread of the dataset made drawing conclusions challenging.

There are several possible reasons why such a limited amount of viral vector-derived protein was observed, such as the level of transcription, translation and protein stability. Moreover, as discussed in Chapter 5, a low assay sensitivity or the lack of an isoform-specific antibody could lead to an underestimation of protein levels.

To evaluate the level of transcription, I quantified the mRNA copies produced by the viral vector and compared them to the level of endogenous mRNA. As shown in Figure 6-23, the hippocampi of *Syngap1*$^{+/-}$ mice treated with the AAV9/hSYN1-*hSYNGAP1* at the higher dose (1E11 vg/mouse) showed a 6-fold increase over wild-type endogenous *Syngap1* mRNA levels, while 5E10 vg/mouse treatment led to a 2.5-fold increase. It appeared from this analysis that a dose-response, although not significant, was present between treatments, and that the amount of mRNA produced from the expression of the viral vector was higher than wild-type endogenous *Syngap1* transcript. Correlation between mRNA levels and protein levels is widely discussed; studies demonstrated that correlation between mRNA and protein is not high, at least not for every transcript (Liu *et al.*, 2002; Tian *et al.*, 2004). There are many steps between the synthesis of an mRNA molecule and the quantification of a protein, such as the availability of ribosomes, mRNA degradation and protein half-life (Liu *et al.*, 2002; Tian *et al.*, 2004). Moreover, it is important to consider, as mentioned before, the sensitivity of the assays used, which can

considerably impact the result. It is therefore not surprising to observe a discrepancy between mRNA and protein level.

The FLAG signal was detected in protein lysate of tissue treated with both doses, confirming that mRNA molecules were translated to some extent. Although a compromised 3D protein structure could lead to the targeting of the produced protein for degradation (Kriegenburg *et al.*, 2012), the intrinsic chemical property of the FLAG peptide (Terpe, 2003) make this event unlikely. However, codon optimization of the DNA sequence could have affected the translation process.

The codon optimisation process assumes that the usage of synonymous codons does not affect the protein structure. The velocity at which mRNA is read and translated by ribosomes is important for protein folding, and substitution of specific pausing signals could potentially compromise protein structure (Spencer *et al.*, 2012; Tsai *et al.*, 2008) leading to misfolding and degradation. The detection of FLAG-SYNGAP1 in treated tissue suggested that this did not occur for the translation of all transcripts.

The codon adaptation index (CAI) is a measure of the synonymous codon usage bias and is used to predict gene expression levels (Sharp *et al.*, 1986). A CAI of 1 is considered optimal, therefore the closer the calculated CAI is to 1, higher is the predicted level of expression. The wild-type and codon-optimized SYNGAP1 sequences had similar CAI values: 0.79 for the wild-type sequence and 0.91 for the codon-optimized gene (GenScript Rare Codon Analysis tool, GeneScript, USA).

Viral vector biodistribution analysis showed no significant difference in the number of viral vector copies per diploid genome between the two doses (Figure 6-18) across all brain regions. The relatively small increase of 2x between the low and the high dose may explain the absence of a clear dose-response effect between 5E10 and 1E11 vg/mouse.

The viral vector distribution appeared relatively homogeneous in the different brain areas, except for the cerebellum, where a lower transduction efficiency was observed. High intra-group variability was observed, which could be associated with

variable injection quality, determined by the correct placement of the needle or the occurrence of backflow. However, this would only partially explain the absence of a difference between doses. For example, in the case of the 5E10 vg/mouse treatment, the samples corresponding with the highest and second-highest genome copies per diploid genomes for each area always corresponded to the same two animals. If the variability was solely associated with sub-optimal injections, such as misplacement of the needle leading to direct injection into the neuropil, we would expect to see a high number of viral genomes in an unexpected area, such as the thalamus, and a low number in an area that is usually well transduced, such as the cortex. In the case of backflow, the viral particles injected into the tissue would be less than the estimated amount, leading to a reduced number of transduced cells. The injection protocol was developed to prevent backflow, but this can still occur.

The alkaline gel electrophoresis analysis indicated a possible packaging issue. As shown in Figure 6-25, a large portion of viral particles appeared to contain fragmented versions of the gene therapy cassette, as only a faint band was visible at the expected molecular weight. This result may explain the viral vector biodistribution results and the low level of protein detected in both doses. Particles with fragmented genomes are not transcriptionally active and cannot transduce cells unless a rare recombination event occurs (Wu *et al.*, 2010), in which multiple viral particles with complementary genomic fragments enter the same cell at the same time.

Although the MiSeq sequencing results indicated that viral vector preparation did not contain contaminants, this assay is not suitable for evaluating the presence of truncated genomes. To confirm the presence of fragmented genomes, a more appropriate system would have been needed, such as digital droplet PCR (ddPCR) or charge detection mass spectrometry (CDMS).

The analysis of the behavioural outcome of treated *Syngap1*$^{+/-}$ mice showed that viral vector treatment did not impact the hyperactive phenotype or the anxiety-like behaviours. If the hippocampus is to be considered a key area for the development of hyperactivity and anxiety disorders (Bannerman *et al.*, 2003; Bast *et al.*, 2003;

Deacon *et al.*, 2002; Gray *et al.*, 1983; Muhia *et al.*, 2012; Ozkan *et al.*, 2014; Pouzet, 1999; Wiley *et al.*, 1995), the low level of expression of the viral vector-derived SYNGAP1 in the area would explain the lack of treatment effect (Figure 6-20).

A trend toward amelioration was instead observed in the risk-taking like behaviour. For partial departures, no difference was observed as AAV9/hSYN1-*hSYNGAP1*-treated *Syngap1*$^{+/-}$ mice performed a comparable number of partial departures to vehicle control mice (Figure 6-10c and Figure 6-11c), while the number of full departures appeared affected by the viral vector treatment. At 7 weeks of age, a smaller percentage of 1E11 vg/mouse treated *Syngap1*$^{+/-}$ mice departed from the platform compared to vehicle-treated controls (Figure 6-10f). Comparing the shape of the Kaplan-Meier curves (Figure 6-10g), vehicle and viral vector-treated mice departed from the platform at a similar rate, while after 5 minutes, almost all vehicle-treated *Syngap1*$^{+/-}$ mice departed, about 50% of 1E11 vg/mouse treated mice were still on the platform. At 15 weeks of age, a higher percentage of 5E10 vg/mouse treated mice did not perform any full departures compared to vehicle controls and mice treated with 1E11 vg/mouse appeared to perform a lower number of full departures compared to vehicle-treated controls (Figure 6-11f). Although the differences observed were not significant, it was suggestive of a modification of the phenotype. As seen in Chapter 5, it is possible that due to the lack of statistical evidence, the trend observed is associated with a spurious effect rather than to a treatment effect.

MoSeq is a highly sensitive, ethologically-relevant, system that allows for the evaluation of the 3D mouse behaviour in a fully automated and unbiased way (Wiltschko *et al.*, 2015). Here, I showed, for the first time, the use of this system to phenotype *Syngap1*$^{+/-}$ mice. MoSeq highlighted the presence of a genotype difference (Figure 6-12), characterised by the differential usage of a large portion of the identified syllables (34 out of 51 identified syllables were differentially used between genotypes). State maps showed that the likelihood of syllable-to-syllable transition was also affected by the genotype (Figure 6-13).

When comparing vehicle and viral vector-treated *Syngap1*$^{+/-}$ mice, no treatment effect was observed. Three syllables were statistically different between vehicle and 1E11 vg/mouse treated *Syngap1*$^{+/-}$ mice, and one between vehicle and 5E10 vg/mouse treated mice (Figure 6-16 and Figure 6-17), but for all of them, the overall usage did not result in a pattern more similar to the wild-type.

Among the syllables in which usage was statistically different between wild-type and *Syngap1*$^{+/-}$ vehicle-treated mice, for five (Figure 6-16, indicated by the black arrows), the usage by viral vector-treated *Syngap1*$^{+/-}$ mice resulted more similar to wild-type vehicle mice usage. Syllable-to-syllable likelihood of transition was not considerably impacted by the treatment, suggesting that viral vector expression did not modify the general grammar used by the *Syngap1*$^{+/-}$ mice (Figure 6-17).

Comparison between vehicle and viral vector-treated wild-type mice (Figure 6-14) showed that the usage of a few syllables was different after treatment but none of them was differentially used by both treatments at the same time. As there was no overlap between treatments and there was also no dose-dependent response, it is difficult to interpret the results, but it is possible that the treatment causes subtle behavioural changes not detectable with other tests.

6.6 CONCLUSION

To summarise, I showed that the newly designed hSYN1-*hSYNGAP1* therapeutic cassette was expressed *in vitro* and that SYNGAP1 derived from the expression of the AAV9-hSYN1-*hSYNGAP1* viral vector was detected *in vivo* after five weeks post-injection.

I showed that no increase in absolute levels of SYNGAP1 was observed in cortex and hippocampus of AAV9/hSYN1-*hSYNGAP1* treated mice when compared to vehicle controls but viral vector-derived protein was detected in this tissue using the highly sensitive anti-FLAG immunoblot assay. Despite the low level of protein detected, the

mRNA produced from the viral vector transcription was 6-fold higher than the level of endogenous *Syngap1* mRNA produced in wild-type tissue.

Quality control of viral vector preparation showed a capsid composition in the normal range, but alkaline gel electrophoresis highlighted a concerning potential issue with the viral vector genome packaging.

Behaviourally, I showed that hyperactivity and anxiety-like phenotypes were not rescued by the treatment, but a dose-dependent trend toward amelioration was observed for the risk-taking behaviour. I also demonstrated that MoSeq can be a powerful tool for the investigation of the phenotypes caused by *SYNGAP1* haploinsufficiency. The test highlighted a strong genotype difference but failed to show a clear treatment effect. Interestingly, the usage of five syllables appeared ameliorated by the treatment but the difference with the vehicle-treated controls was not significant.

To conclude, given the limited effects observed and the challenges encountered with the vector presented in this chapter, this therapeutic cassette will not be used for future studies. Improvements of the design are needed to generate a therapeutic construct able to drive robust expression of SYNGAP1 in brain areas of interest.

CHAPTER 7: GENERAL DISCUSSION

The aim of the work presented in this thesis was to evaluate the potential of a gene therapy approach to prevent or ameliorate the behavioural phenotypes observed in the mouse model of *SYNGAP1* haploinsufficiency-associated disorder.

SYNGAP1 haploinsufficiency-associated disorder, characterised by ID, seizures, ASD and sleep disorders, and for which no canonical therapies are currently available, is caused by loss-of-function mutations in the *SYNGAP1* gene (Agarwal *et al.*, 2019; Berryer *et al.*, 2013; Hamdan *et al.*, 2009, 2011; Mignot *et al.*, 2016; Vlaskamp *et al.*, 2019; Weldon *et al.*, 2018).

In this chapter, I will summarise and discuss more broadly the major findings presented in this thesis and their significance in respect to the current and future studies on gene therapy approaches for *SYNGAP1* haploinsufficiency-associated disorder. I will also discuss the limitations of the methodology used, the technical difficulties encountered and future experiments that would integrate and extend the work presented here.

7.1 IDENTIFICATION OF A ROBUST BATTERY OF BEHAVIOURAL PHENOTYPES

In Chapter 3, I assessed several behavioural phenotypes in *Syngap1*$^{+/-}$ mice with the aim to develop a robust battery of behavioural tests to use for the evaluation of the putative therapeutic effects elicited by the gene therapy treatments.

I evaluated the following: hyperactivity, anxiety, working memory, motor skills, repetitive behaviour, risk-taking behaviour and depth perception. In Chapter 6, I also presented the results of the MoSeq experiment, a newly developed machine-learning analysis system that allows the evaluation of mouse behaviours in an ethologically appropriate way (Wiltschko *et al.*, 2015).

In accordance with published studies (Aceti *et al.*, 2015; Berryer *et al.*, 2016; Clement *et al.*, 2012; Guo *et al.*, 2009; Muhia *et al.*, 2010; Nakajima *et al.*, 2019), I showed a strong genotype effect in the distance travelled over time using the open field test and I investigated the intra and inter-trial habituation to the test (Figure 3-2, Figure 3-3, Figure 3-4 and Figure 3-5). I also demonstrated the presence of an anxiety reduction phenotype, which has been previously described in the literature (Aceti *et al.*, 2015; Berryer *et al.*, 2016; Clement *et al.*, 2012; Guo *et al.*, 2009; Muhia *et al.*, 2010; Nakajima *et al.*, 2019) and is defined as the increased time spent in the open arms of the elevated plus maze (Figure 3-6, Figure 3-8 and Figure 3-10). In order to evaluate if hyperactivity influences this phenotype, I evaluated the correlation between the distance travelled and time spent in the open arms (Figure 3-7, Figure 3-9 and Figure 3-11).

Several publications link hyperactive behaviour, as well as anxiety disorders, to hippocampal dysfunctions (Bast *et al.*, 2003; Deacon *et al.*, 2005; Gray *et al.*, 1983; Hannigan *et al.*, 1984; Pouzet, 1999). The investigation of the connection between dysfunction of brain areas and behavioural phenotype observed in *Syngap1*$^{+/-}$ mice showed that hippocampus, together with other forebrain areas, appear to be involved in the development of hyperactivity (Muhia *et al.*, 2012; Ozkan *et al.*, 2014). Basal ganglia, together with striatum and the nucleus accumbens are considered fundamental structures for motor control (Jones *et al.*, 1980; Markowitz *et al.*, 2018; Nicola, 2007; Roseberry *et al.*, 2016) and it is possible that functional impairments of these brain regions could, in part, be the driver of locomotor abnormalities. While SYNGAP1 expression has been observed in the basal ganglia during embryonic development (Porter *et al.*, 2005), in adulthood, it is mostly expressed in the cortex, hippocampus, striatum, and, at relatively low levels, in the olfactory bulb and cerebellum (Gou *et al.*, 2020; Porter *et al.*, 2005). The striatum and the nucleus accumbens are other regions that could potentially drive the development of hyperactivity.

Other previously reported phenotypes in *Syngap1*$^{+/-}$ mice include working memory deficits and risk-taking behaviours (Berryer *et al.*, 2016; Guo *et al.*, 2009; Kilinc *et al.*, 2018; Muhia *et al.*, 2010; Nakajima *et al.*, 2019).

I investigated the presence of memory impairments using the protocol presented by Berryer and co-workers (Berryer *et al.*, 2016) based on a spontaneous alternation paradigm. In contrast to the results previously published, I showed that at all ages tested, *Syngap1*$^{+/-}$ mice presented a behaviour comparable to wild-type control mice (Figure 3-13). It is known that behavioural tests outcomes can be influenced by many factors such as the age of testing, housing condition and experimental room condition (Andrews *et al.*, 2018; Bailey *et al.*, 2006; Crawley *et al.*, 1997; Montagutelli, 2000; Wolfer *et al.*, 2002). Although the age of testing was not specified, it appeared that Berryer *et al.* (Berryer *et al.*, 2016) used juvenile mice around 5 weeks of age, which match the age of mice used in this work. The major difference between the two experimental setups, and possibly one of the causes of the different results, could be the level of light in the room. Berryer *et al.* (Berryer *et al.*, 2016) performed the experiment with a low level of light while this experiment was performed in a dark room with only one source of red light.

The identification of behavioural phenotypes conserved across species is very important for the evaluation of the viral vector therapeutic efficacy. The increased propension to risky behaviours has been described in both *SYNGAP1* patients (Weldon *et al.*, 2018) and in the mouse model of *SYNGAP1* haploinsufficiency-associated disorders (Kilinc *et al.*, 2018). I was able to observe the same phenotype at both ages tested, 7 and 15 weeks (Figure 3-20 and Figure 3-22), in which *Syngap1*$^{+/-}$ mice performed a significant higher number of partial and full departures from the platform. Moreover, I showed that the number of full departures performed by *Syngap1*$^{+/-}$ mice did not appear to be a direct consequence of hyperactivity (Figure 3-21 and Figure 3-23).

It is possible that the increased risk-taking behaviour observed in *SYNGAP1* patients and *Syngap1*$^{+/-}$ mice results from the combination of multiple factors, such as

structural, circuital, and cellular changes in areas responsible for processing sensory and visual stimuli (Carreño-Muñoz *et al.*, 2021; Michaelson *et al.*, 2018), as well as a consequence of other behavioural impairments such as ADHD.

ADHD, which has been found comorbid in a high proportion of *SYNGAP1* haploinsufficiency-associated disorder patients (Agarwal *et al.*, 2019; Holder *et al.*, 2018; Klitten *et al.*, 2011; Weldon *et al.*, 2018), has been associated in many cases with risk-taking behaviour and increased impulsivity (Dekkers *et al.*, 2016). The etiology of this disorder has not been elucidated yet, although mutations in several genes have been identified in affected individual (Faraone *et al.*, 2005; Lasky-Su *et al.*, 2007; Mortimer *et al.*, 2019; Won *et al.*, 2011). Given the complexity of the disorder, the identification of a specific brain region involved in its pathophysiology is difficult, but it is likely multiple areas are affected. Several studies have suggested the involvement of the prefrontal cortex, striatum, basal ganglia, and cerebellum (Castellanos *et al.*, 2012; Cortese *et al.*, 2012; Durston *et al.*, 2011; Giedd *et al.*, 2001; Leo *et al.*, 2013; Mortimer *et al.*, 2019).

Impairments in tactile stimuli processing have been described both in patients and in *Syngap1*$^{+/-}$ mice by Michaelson and colleagues (Michaelson *et al.*, 2018), who demonstrated the inability of *Syngap1*$^{+/-}$ mice to use tactile stimuli to discriminate objects in an object recognition task. Additionally, hypoexcitability of excitatory neurons of layers 2 and 3 of SSC, which is associated with impaired experience-induced plasticity, has been described (Michaelson *et al.*, 2018).

Vision impairments have not been commonly observed as a phenotype in *SYNGAP1* affected individuals (Kilinc *et al.*, 2018; Weldon *et al.*, 2018). However, a recent study suggested the presence of an alteration of visual and auditory stimuli processing in humans (Carreño-Muñoz *et al.*, 2021). *Syngap1*$^{+/-}$ mice blindness has been excluded as they are able to navigate in the Morris water maze test (Komiyama *et al.*, 2002; Muhia *et al.*, 2010); however, to the best of my knowledge, there are no published studies investigating visual acuity. Furthermore, *Syngap1*$^{+/-}$ mice are able to perform the object recognition test (Muhia *et al.*, 2010), but when tested in a visual discrimination task, they showed a deficit in the ability to discriminate between

different visual stimuli (Horner *et al.*, 2021). However, analysis of depth perception using the visual cliff test (Gibson *et al.*, 1960) did not reveal a difference between wild-type and *Syngap1*$^{+/-}$ mice (Figure 3-16 and Figure 3-18). These data suggested that the increased number of partial and full departures are not associated to visual impairment but, rather, could be a consequence of an impairment in the processing of these stimuli.

I demonstrated that *Syngap1*$^{+/-}$ mice do not present stereotypic behaviour (Figure 3-14) and motor skills impairments (Figure 3-15). However, they exhibit a statistically significant different syllables usage compared to wild-type mice.

The MoSeq test allows researchers to identify short, stereotyped elements in the mouse behaviour, defined as syllables, using 3D videos of mice that move freely in an open field arena (Wiltschko *et al.*, 2015). As shown in Chapter 6, the comparison of syllables usage in wild-type and *Syngap1*$^{+/-}$ mice showed a profound genotype difference (Figure 6-12). Similarly, differences were observed between the genotype groups in the syllable-to-syllable likelihood of transition (Figure 6-13).
As a large number of brain circuits affected by *Syngap1* haploinsufficiency have been described, it was not surprising to observe such a large genotype effect on syllable usage and in the syllable-to-syllable transition pattern. As mentioned earlier, striatum plays a crucial role in motor functions (Nicola, 2007), and it is known that lesions in the dorsolateral striatum affect the pattern of actions sequencing (Berridge *et al.*, 1987). A recent publication showed how lesions in the striatum can significantly modify the representation of individual syllables and the syllable-to-syllable likelihood of transition (Markowitz *et al.*, 2018). As mentioned previously, SYNGAP1 expression in the striatum begins early in development and its expression is maintained into adulthood (Gou *et al.*, 2020; Porter *et al.*, 2005). It is plausible that haploinsufficiency in this brain region is the primary driver of the phenotype observed with the MoSeq.

7.2 *IN VIVO* THERAPEUTIC EFFICACY TEST HIGHLIGHTED THE CHALLENGES FOR THE DEVELOPMENT OF A GENE REPLACEMENT THERAPY FOR *SYNGAP1* HAPLOINSUFFICIENCY-ASSOCIATED DISORDER

This first proof-of-concept study highlighted the many difficulties posed by the *SYNGAP1*/SYNGAP1 biology for the development of an effective gene therapy treatment, some of which are summarised in Table 7-1.

Table 7-1. Challenges posed by SYNGAP1 biology.

***SYNGAP1/*SYNGAP1 characteristic**	**Challenge**
SYNGAP1 coding sequence is about 3900 bp.	The length of the coding sequence strongly limits the choice of regulatory elements to use for the therapeutic cassette.
Different *SYNGAP1* haploinsufficiency phenotypes show a different rescue window but this is likely to close early in life for core behavioural abnormalities.	The therapeutic cassette needs to be delivered very early in life and needs to reach high level of protein expression quickly.
SYNGAP1 expression levels vary during development and result different in different areas of the brain.	Delivering the therapeutic cassette in the brain areas more likely to drive the behavioural abnormalities.
SYNGAP1 presents multiple isoforms which exert different functions and are differently regulated during development in different areas of the brain.	Only the coding sequence of one isoform can be delivered. The need to deliver the appropriate isoform in the appropriate brain region at the right age.
SYNGAP1 is dosage sensitive.	*SYNGAP1* haploinsufficiency phenotype is caused by a too low amount of SYNGAP1, it is therefore likely that to restore normal functions the therapeutic cassette will need to reach close to physiological levels of expression. No information are available regarding overt toxicity caused by the overexpression of *SYNGAP1.*

SYNGAP1 coding sequence (~3900 bp) considerably limits the choice of regulatory elements to be used in a gene therapy cassette (Bulcha *et al.*, 2021).

To achieve an expression pattern and temporal regulation as close as possible to that of the endogenous protein, the ideal regulatory element would be the endogenous promoter. However, early work on SYNGAP1 by McMahon and colleagues (McMahon et al., 2012) suggested that the SYNGAP1 promoter presents a complex sequence and composition, and proposed the existence of at least two different promoters that drive and regulate the expression of different isoforms. More recently, investigation of the promoter structure and sequence (personal communication, Dr Ralph D. Hector) revealed that the SYNGAP1 promoter, 3'UTR and regulatory elements (intronic and distal) span over a length of several kilobases. Furthermore, the presence of a neighbouring gene poses a serious challenge to identifying the regulatory elements necessary for SYNGAP1 expression. The absence of a well-characterised promoter sequence and the large size make the SYNGAP1 endogenous promoter not suitable for a gene replacement approach.

As *SYNGAP1* expression in adulthood is limited to the brain (Porter *et al.*, 2005), promoters were chosen to maximise expression in neuronal cells. For the first generation constructs, expressing the Aα1, Aα2 or Bα2 *SYNGAP1,* the minimal MeCP2 promoter, MeP229 promoter, was chosen (Gray *et al.*, 2011). Due to the promoter's relatively small size (229 bp) and activity in post-mitotic neurons, it was considered a good candidate to regulate SYNGAP1 expression.

For the second generation construct, the JeT promoter was used instead, which is active in neuronal cells and has been proven successful in the gene therapy context (Bailey *et al.*, 2018; Chen *et al.*, 2022; Gadalla *et al.*, 2017; Tornoe *et al.*, 2002). For the third-generation construct, a neuronal-specific promoter, human SYNAPSIN1, was used. hSYN1 is active in both excitatory and inhibitory neurons and brain regions of interest for *SYNGAP1* (Kügler *et al.*, 2003).

Post hoc analysis of treated cortex and hippocampus showed that both JeT and hSYN1 led to a low level of viral vector-derived protein. Many factors, which I will

discuss further on, might have contributed to this, but investigating alternative regulatory elements might be necessary to obtain higher levels of expression.

I previously described the spatial and temporal SYNGAP1 expression pattern during development (Gou *et al.*, 2020; Kim *et al.*, 2003; Knuesel *et al.*, 2005; Moon *et al.*, 2008; Porter *et al.*, 2005; Tomoda *et al.*, 2004). I also discussed that various behavioural phenotypes appear to present different rescue windows, but core behaviours such as hyperactivity and reduced anxiety are likely rescuable only early in life (Aceti *et al.*, 2015; Clement *et al.*, 2012; Creson *et al.*, 2019; Verma *et al.*, 2019). Therefore, delivering the gene therapy cassette expressing SYNGAP1 as early as possible would be ideal to prevent the insurgence of the highest number of behavioural abnormalities. Although prenatal gene therapy delivery is possible, it was not considered at this stage due to the scarce possibility to translate it into the clinic (Massaro *et al.*, 2018; Peranteau *et al.*, 2020; Rashnonejad *et al.*, 2019). It was demonstrated that restoring SYNGAP1 expression at PND1 can prevent the development of core phenotypes such as hyperactivity and reduced anxiety (Aceti *et al.*, 2015), which demonstrates the feasibility of postnatal treatment.

In Chapter 1, I presented the various types of viral vectors commonly used for gene therapy and their characteristics (Bulcha *et al.*, 2021; Gardlík *et al.*, 2005; Lee *et al.*, 2017; Palella *et al.*, 1988; Ritter *et al.*, 2002). To maximise neuronal transduction, obtain a broad spread in the brain and achieve a stable long-term expression of the transgene, I used AAV vectors, and in particular the serotype 9. These vectors are the gold standard for CNS-targeted gene therapy approaches (Bouard *et al.*, 2009; Penaud-Budloo *et al.*, 2018) and have successfully been used in several gene therapy treatments (Bailey *et al.*, 2018; Chen *et al.*, 2022; Gadalla *et al.*, 2013; Hughes *et al.*, 2018; Massaro *et al.*, 2020; Presa *et al.*, 2021; Rashnonejad *et al.*, 2019; Wang *et al.*, 2017).

Following ICV injection, AAV9 genomes are primarily detected in the brain and spinal cord, with traces found in heart, liver, and muscular tissue (Presa *et al.*, 2021; Tanenhaus *et al.*, 2022). When evaluating viral vector biodistribution in the brain, the

highest amount of viral vector occurs in the cortex, olfactory bulb, striatum, and hippocampus, but it can be detected also in other brain regions such as the thalamus and brainstem (Belur *et al.*, 2021; Chakrabarty *et al.*, 2013; Hughes *et al.*, 2018; McLean *et al.*, 2014). It was observed that the extent of the distribution in the brain was also dependent on the age of administration with a wider spread at a younger age (PND0) (Chakrabarty *et al.*, 2013). Due to the SYNGAP1 profile of expression in adulthood (Gou *et al.*, 2020; Kim *et al.*, 2003; Knuesel *et al.*, 2005; Moon *et al.*, 2008; Porter *et al.*, 2005; Tomoda *et al.*, 2004), ICV was adopted for this work.

The results of viral vector biodistribution for AAV9/JeT-*hSYNGAP1* (Figure 5-12) were overall in accordance with the literature (Belur *et al.*, 2021; Chakrabarty *et al.*, 2013; Hughes *et al.*, 2018; McLean *et al.*, 2014), with the highest viral vector copy number in the cortex, hippocampus and striatum and little to no distribution to the thalamus and cerebellum. However, the number of viral vector genomes of AAV9/hSYN1-*hSYNGAP1* in the cortex, hippocampus, striatum, and thalamus were very similar (Figure 6-18). It is possible that not enough vector reached important regions, such as the hippocampus, even though both viral vectors distributed in brain regions of interest for SYNGAP1. To address this issue, alternative AAV capsids could be investigated. In recent years, there have been many efforts to develop highly penetrating AAV capsids with high tropism for neuronal cells, broader spread in the brain, and de-targeting of other tissues such as the liver (Challis *et al.*, 2022; Chatterjee *et al.*, 2022; Meng *et al.*, 2021; Yao *et al.*, 2022).

Studies aimed to understand isoforms-specific subcellular localisation, timing of expression, and functions (Araki *et al.*, 2020; Gou *et al.*, 2020; Kilinc *et al.*, 2022; Li *et al.*, 2001; McMahon *et al.*, 2012; Moon *et al.*, 2008; Zeng *et al.*, 2016) have suggested that isoforms containing $\alpha 1/\alpha 2$ C-terminus are primarily involved in regulating synaptic function and are the most enriched in the synaptic compartment/PSD. The β isoform, which is less enriched at PSD, is the dominant isoform in the cytoplasm and is involved in the regulation of cellular structure (Araki *et al.*, 2020; Gou *et al.*, 2020; Kilinc *et al.*, 2022; Zeng *et al.*, 2016).

Less information is available regarding the functionality and temporal expression pattern of the N-terminal isoforms and how they are associated to the different C-terminal (Gou *et al.*, 2020; McMahon *et al.*, 2012). McMahon and colleagues (McMahon *et al.*, 2012) investigated the developmental-dependent expression of three different N-terminal variants at the mRNA level. Their data suggested that A and B are more involved in early stage of development, while C is more critical later in life. As the aim of this project was to express SYNGAP1 early in life to prevent or ameliorate the insurgence of haploinsufficiency-associated phenotype, it was reasonable to express an isoform that has a high level of expression in early stages of development. Based on the information provided by the work from McMahon and colleagues (McMahon *et al.*, 2012), three constructs were initially designed to express respectively the Aα1, Aα2 or Bα2 isoform. In parallel, the second generation of expression cassette was generated, but initially, only the Aα1 expression cassette was produced. Based on more recently published works (Araki *et al.*, 2020; Gou *et al.*, 2020) it was decided to maintain the Aα1 isoform for the third generation construct.

It is possible that the N-terminal variants play crucial roles during the period between its peak of expression at PND14 and adulthood and that it is required for the correct synaptic function later in life. Therefore, the limited treatment effect observed could be a consequence of the isoform chosen. More information on N-terminal isoforms-specific function and how they associate with different C-terminal variants is needed for a more rational development of future therapeutic cassettes.

A trend toward the amelioration of the risk-taking behaviour was observed in *Syngap1*$^{+/-}$ mice treated with AAV9/JeT-*hSYNGAP1* and AAV9/hSYN1-*hSYNGAP1* candidate therapeutic vectors. Interestingly, the effect observed was similar for both viral vectors, with an apparent reduction of the percentage of mice departing from the platform and in the total number of full departures, but no effect was seen on the number of partial departures.

I previously discussed the possible involvement of the cortex in the pathophysiology of the risk-taking behaviour. It is possible that the observed trend toward the amelioration in viral vector-treated mice is correlated to the higher biodistribution of the therapeutic vector and the level of expression of viral vector-derived SYNGAP1 protein in this area. It is worth noting that the cortical samples used for biodistribution analysis and protein quantification corresponded to the somatomotor and motor cortex and they did not include SSC and visual cortex areas. Therefore, it is not possible to infer distribution or expression in these regions.

The evaluation of viral vector-derived SYNGAP1 expression in cortical areas showed that tissues treated with 1E11 vg/mouse of AAV9/JeT-*hSYNGAP1* showed an absolute level of SYNGAP1 protein in the range of 1x to 2.2x (average 1.5x) protein levels observed in the *Syngap1*$^{+/-}$ vehicle-treated control. Interestingly, tissue treated with 5E10 vg/mouse showed a similar increase in SYNGAP1 levels (between 1x and 1.8x, average of 1.4x over vehicle control), but no modification of the risk-taking behaviour (Figure 5-15).

For AAV9/hSYN1-*hSYNGAP1*, a very low amount of exogenous protein was detected in the cortex of viral vector-treated *Syngap1*$^{+/-}$ mice. The highest dose tested, 1E11 vg/mouse, produced an average of only about 1.05x of vehicle control, while 5E10 vg/mouse produced 1x the amount of absolute SYNGAP1 level observed in *Syngap1*$^{+/-}$ vehicle-treated mice (Figure 6-19). However, risk-taking behaviour has not been previously investigated in genetic rescue experiments, therefore it is not known to which extent the phenotype can be ameliorated.

The evaluation of locomotor activity in the open field showed no amelioration of the hyperactive phenotype, with AAV9/JeT-*hSYNGAP1*-treated *Syngap1*$^{+/-}$ mice exhibiting behaviour comparable to vehicle controls at both ages tested (Figure 5-3 and Figure 5-5). Similar results were observed for the anxiety-like behaviour, where vector-treated *Syngap1*$^{+/-}$ mice were indistinguishable from the vehicle-treated mice (Figure 5-7 and Figure 5-8). Treatment with AAV9/hSYN1-*hSYNGAP1* yielded comparable results with no amelioration of the hyperactivity or anxiety-like phenotypes (Figure 6-4, Figure 6-6, Figure 6-8 and Figure 6-9).

Evaluation of AAV9/JeT-*hSYNGAP1* and AAV9/hSYN1-*hSYNGAP1* vector-derived SYNGAP1 protein in hippocampi of treated *Syngap1*$^{+/-}$ mice showed no increase of absolute levels of SYNGAP1 protein (Figure 5-16 and Figure 6-20). Although it is not possible to exclude other factors, it is possible that the lack of amelioration of these phenotypes was due to the low level of expression in the hippocampus. As mentioned earlier, the involvement of the hippocampus and other forebrain regions in the development of hyperactivity has been suggested by Muhia *et al.* (Muhia *et al.*, 2012) and by Ozkan *et al.* (Ozkan *et al.*, 2014), which is consistent with previous studies (Bannerman *et al.*, 2003; Bast *et al.*, 2003; Deacon *et al.*, 2002; Gray *et al.*, 1983; Pouzet, 1999; Wiley *et al.*, 1995). It is known that the highest expression level detected in the brain for SYNGAP1 is the hippocampus (Gou *et al.*, 2020). Therefore, restoring normal levels of SYNGAP1 in the area may ameliorate the hyperactive phenotype but not necessarily abolish it.

I mentioned before the possible involvement of the striatum in the modulation of motor activity (Jones *et al.*, 1980; Nicola, 2007; Roseberry *et al.*, 2016). Protein levels were not investigated in this brain region, but viral vector distribution data suggested that a similar amount of AAV9/JeT-*hSYNGAP1* and AAV9/hSYN1-*hSYNGAP1* reached hippocampus and striatum. It is reasonable to conclude that a similarly low level of expression was achieved here.

AAV9/hSYN1-*hSYNGAP1* treated mice were additionally tested using MoSeq. However, considering the treatment effect among *Syngap1*$^{+/-}$ mice, the test did not highlight a clear effect of the therapeutic vector. Interestingly, for five syllables, the usage in viral vector-treated *Syngap1*$^{+/-}$ mice appeared to be ameliorated compared to vehicle-treated mice, although the difference between treatments was not significant (Figure 6-16). An in-depth analysis of the types of movements described by each syllable and how they relate to each other might allow a better understanding of how the treatment affects *Syngap1*$^{+/-}$ mice behaviour.

The ability to rescue the syllable usage phenotype by genetic rescue has not been investigated. It will be crucial to determine if the phenotype is reversible, to what

extent, and if a rescue window is present. This information could be used in the future to evaluate the therapeutic efficacy of treatments.

Treatment tolerability issues may be associated to a toxic effect caused by the overexpression of the transgene, as seen for gene therapies developed for the treatment of Rett syndrome (Gadalla *et al.*, 2017; Sinnett *et al.*, 2017), or to the intrinsic toxicity associated with the viral vector used (Fader *et al.*, 2022; Kishimoto *et al.*, 2022; Shirley *et al.*, 2020). AAVs and viral vectors, in general, can elicit a strong immune response which can cause severe damage to the treated organism (Shirley *et al.*, 2020). In the case of intravenous delivery, hepatotoxicity can be observed due to a large amount of viral vector sequestered in the liver, which can cause localised inflammation (Kishimoto *et al.*, 2022). Moreover, degeneration of the dorsal root ganglion has been observed after cerebrospinal fluid delivery or intravenous delivery of AAV (Fader *et al.*, 2022; Hordeaux *et al.*, 2020; Sirivelu *et al.*, 2021). These toxic effects are more prominent at high viral vector dosages (Fader *et al.*, 2022; Kishimoto *et al.*, 2022). For example, with an intravenously delivered dose higher than 5E13 vg/kg in rats or 3.3E13 vg/dose in monkeys, with intrathecal delivery, severe dorsal root ganglion toxicity was observed (Fader *et al.*, 2022).

AAV9/JeT-*hSYNGAP1* and AAV9/hSYN1-*hSYNGAP1* vector treatments did not show overt tolerability issues. Wild-type viral vector-treated mice did not present any deterioration of general conditions, had normal motility, good grooming behaviour, and normal in-cage behaviour. Similarly, no abnormalities were observed during behavioural tests for all viral vectors treated wild-type mice.

The absence of overexpression-associated toxicity is not surprising given the low amount of exogenous protein detected in viral vector-treated tissue. Moreover, to my knowledge, there are no reported affected individuals with microduplication of the *SYNGAP1* locus.

After ICV delivery, only limited liver transduction has been observed (Presa *et al.*, 2021; Tanenhaus *et al.*, 2022); therefore, as no alteration of the general condition of viral vector-treated mice was observed, the presence of viral vector genomes in this

tissue and hepatotoxicity were not investigated. Degeneration of the dorsal root ganglion is often associated with ataxia (Fader *et al.*, 2022; Hordeaux *et al.*, 2020; Sirivelu *et al.*, 2021); however, the absence of motility problems and gait abnormalities in viral vector-treated mice ruled out this phenomenon.

MoSeq analysis of vehicle and AAV9/hSYN1-*hSYNGAP1*-treated wild-type mice showed differences in the usage of a subset of syllables between dose groups (Figure 6-14). Interestingly, no overlap was observed between the two doses administered, differences between vehicle and viral vector-treated mice were mostly observed for the 5E10 vg/mouse dose, and only in one case vehicle differed from 1E11 vg/mouse group. As viral vector-treated mice did not exhibit signs of general health detriment, these differences were not considered signs of poor treatment tolerability. However, the high sensitivity of the assay could have potentially highlighted treatment-associated behavioural modifications that will require further investigation.

As previously mentioned, one of the factors that led to a modest therapeutic effect for both tested gene therapy constructs was likely associated with the low levels of exogenous protein expression achieved. The two constructs presented substantial differences in the regulatory elements and coding sequences used for the *SYNGAP1* gene, making a direct comparison difficult. The JeT promoter is considered a relatively weak promoter but is able to yield levels of expression, on average, higher than other promoters of comparable size (Tornoe *et al.*, 2002). It is therefore not surprising to see only a relatively small variation in absolute levels of SYNGAP1 protein. On the other hand, the AAV9/hSYN1-*hSYNGAP1* was designed with the aim to outperform the previous construct; however, SYNGAP1 protein level analysis showed no changes in absolute levels of SYNGAP1. This construct uses the hSYN1 promoter which, despite the size, has been shown to be able to drive high level of transgene expression in a neuronal-specific fashion (Massaro *et al.*, 2020). The AAV9/hSYN1-*hSYNGAP1* uses the SV40 polyA construct uses the SV40 polyA, which has been shown to drive higher levels of expression compared to SpA (Choi *et al.*, 2014). Moreover, the wild-type human sequence was replaced into a codon-optimised one. Possible issues with translation were not investigated; however, the

levels of in the treated hippocampal tissue were evaluated. Analysis showed that viral vector-derived *SYNGAP1* mRNA was, on average, 6 times higher than the endogenous *Syngap1* mRNA observed in wild-type vehicle-treated hippocampal tissue (Figure 6-23). Discrepancies between the relative amount of transcript and the amount of protein produced have been described before (Liu *et al.*, 2002; Tian *et al.*, 2004), but this result shows that the viral vector transcription can potentially surpass the wild-type levels.

The *SYNGAP1* coding sequence used for the third generation viral vector was codon-optimised for expression in humans, as previously discussed in Chapter 6. Codon optimization has been used in gene therapy for the purpose of improving expression, with varying success (Brown *et al.*, 2018; Cantore *et al.*, 2012; Huston *et al.*, 2011; Raab *et al.*, 2010). While it can improves expression in some cases, it has been shown to interfere with transcription initiation, mRNA stability, translation and even introduce alternative transcription start sites and cryptic splicing sites, and micro RNA binding sites (Fåhraeus *et al.*, 2016; Firth, 2014; Gamble *et al.*, 2016; Harigaya *et al.*, 2017; Kelsic *et al.*, 2016; Lorenz *et al.*, 2015; Mauro *et al.*, 2014). As only the full-length protein was detected after immunoblot analysis of protein lysate, it is reasonable to assume that the transgene is correctly transcribed, and the mRNA correctly translated. However, it is still possible that the sequence modification might have created a new regulatory sequence in the mRNA which could target it for degradation or lead to translational stall. Further investigation is required to evaluate these possibilities.

The inability to detect an increase in the absolute levels of SYNGAP1 using the anti-SYNGAP1 antibody could also be associated with a limitation of the approach used. I discussed in Chapter 5 how the presence of multiple SYNGAP1 isoform might have led to the underestimation of the viral vector-derived protein levels. I will discuss this in more detail in the technical limitation of the immunoblot approach in Section 7.4.

Another element to consider is the quality of the viral preparation. As discussed in Chapter 6, when the size of the gene therapy cassette reaches the upper limit of the

cloning capacity, ~5000 bp (Bulcha *et al.*, 2021), it is possible to observe truncation of the encapsidated viral genomes (Dong *et al.*, 2010; Wu *et al.*, 2010). The resulting viral particles would not be able to fully transduce the target cell, reducing therefore the transduction efficiency observed (Wu *et al.*, 2010). While alkaline gel electrophoresis did not show issues with the AAV9/JeT-*hSYNGAP1* viral vector, it suggested packaging problems for the AAV9/hSYN1-*hSYNGAP1* vector (Figure 6-25). To better evaluate the presence and the extent of viral genome fragmentation, further analysis using more appropriate and sensitive methodology such as ddPCR or CDMS is necessary. ddPCR is a new generation PCR technique that presents high sensitivity and which would allow the evaluation of viral vector genome integrity (Furuta-hanawa *et al.*, 2019). CDMS is a mass spectrometry approach that allows to detect the presence of viral vector capsids containing partial viral genome and empty capsid (Pierson *et al.*, 2019).

It was shown that interference with the C-terminal protein-protein interaction impairs SYNGAP1 functionality, cellular localization, and potentially, the ability to rescue behavioural abnormalities (Araki *et al.*, 2020; Kilinc *et al.*, 2022). Analysis of protein localisation via synaptosomal preparation showed that Myc-tagged SYNGAP1 is detectable in the synaptic compartment but not in the cytosol, with a pattern similar to endogenous SYNGAP1 (Figure 5-17). The subcellular localisation experiments, presented in Chapter 5 suggested that the Myc fusion peptide did not impair subcellular localisation. On the other hand, this experiment ruled out the possibility that the C-terminal Myc could impair protein functionality to some extent. Similar results were observed for AAV9/hSYN1-*hSYNGAP1* vector-treated tissue, in which FLAG-tagged SYNGAP1 recapitulated endogenous wild-type SYNGAP1 localisation (Figure 6-21).

To further evaluate the ability of both Myc and FLAG-tagged SYNGAP1 to interact with elements of the PSD, it would be necessary to perform a co-immunoprecipitation. This technique would allow for a better understanding of whether the viral vector-derived protein can form the same interactome observed

for the wild-type protein, which is essential for the synaptic activity regulation function of SYNGAP1.

To overcome some of the many challenges encountered during the development of a candidate gene therapy for *SYNGAP1* haploinsufficiency-associated disorder, such as the need to choose the isoform to deliver and the level of expression to achieve, alternative approaches such as ASO or CRISPR (clustered regularly interspaced short palindromic repeats)-Cas could be considered. I have discussed in Chapter 1 the pros and cons of the ASO system (Dhuri *et al.*, 2020; Gagliardi *et al.*, 2021). Nonetheless, it is a valid method, currently under study in the context of *SYNGAP1* haploinsufficiency (Dawicki-mckenna *et al.*, 2022; Lim *et al.*, 2020), which would allow to upregulate SYNGAP1 expression without the limitation of re-introducing only one isoform. Moreover, as the endogenous wild-type allele expression is exploited, the temporal and spatial developmental expression regulation would be maintained. This approach has been successfully adopted for the treatment of Dravet syndrome (Lenk *et al.*, 2020; Wengert *et al.*, 2022) and spinal muscular atrophy (Passini *et al.*, 2011).
Loss-of-function of the *SYNGAP1* gene is in many cases caused by single nucleotide mutations (Figure 1-4) (Vlaskamp *et al.*, 2019). Patients carrying single nucleotide mutation would be ideal candidates for a CRISPR-Cas approach, as this system would allow for reversion of the mutation and restoration of the wild-type sequence, thus normalizing protein levels (Karimian *et al.*, 2019).
Side by side therapeutic studies utilizing different modes of therapeutic correction are necessary to assess the most suitable for the *SYNGAP1* haploinsufficiency-associated disorder.

7.3 TECHNICAL CONSIDERATIONS

The major technical issue encountered during this project was associated with the *Syngap1*$^{+/-}$ mouse model. I have extensively discussed the behavioural phenotypes present in the model, and although the genotype difference is profound, only a very limited subset of behaviours was affected or at least that I was able to efficiently measure. Hyperactivity is considered the main phenotype present that could potentially lead to a misinterpretation of other results. To circumvent this problem, I investigated behaviours which do not involve locomotion, or in which locomotion is not the primary readout, such as the platform departure test and the MoSeq. Despite this, the behavioural panel of tests is still limited and efforts to individuate new, robust behavioural abnormalities would be fundamental to further investigate the therapeutic effect of the candidate gene therapy vectors.

It is also important to consider the construct validity of the model. SYNGAP1 haploinsufficiency-associated disorder is classified as an haploinsufficiency disorder as the identified mutation are classified as loss-of-function. It is known that a subset of missense mutation do not completely abolish protein function (Berryer et al., 2013; Zeng et al., 2019). It is not known if one of the many missense or frameshift mutations causes gain-of-function of SYNGAP1. The mouse model used for the work presented in this thesis models only the complete loss of expression of one allele, but it does not consider the possible presence of normal levels of protein with reduced functionality (Berryer et al., 2013; Zeng et al., 2019) or the acquisition of new functions. Although it can still be considered a valid model of the disease, it would be informative for future studies to develop new animal models that recapitulate these conditions.

Immunohistochemistry is a widely used technique for the evaluation of the viral vector transduction efficiency and of protein localisation within the cell. For transduction efficiency, the percentage of transduced cells is evaluated based on the number of cells positive for the immunolabelling of the exogenous protein over the number of DAPI positive nuclei present in the field of view considered. This procedure

can be used when the exogenous protein localises in the nucleus or in the soma/cytoplasm of target cells. In the case of SYNGAP1, the predicted localisation of the viral vector-derived protein is the synapse, which poses a challenge for investigating transduction efficiency using an immunohistochemistry approach. It would not be possible to evaluate the fraction of cells per field of view that are positive for the exogenous protein. Moreover, the difficulties to obtain a full knockout sample to optimise SYNGAP1 detection made the usage of this approach to evaluate subcellular localisation challenging. Therefore, alternative approaches, such as immunoblotting and subcellular fractionation, were used.

The technical limitation of the immunoblot is mainly associated with the sensitivity of the assay and the linearity of detection of the antibody used. Before performing full-scale protein quantification, immunoblot staining has been optimised, and the linearity of detection has been evaluated for all the antibodies used, as shown in Appendix C, Section C.2. However, the sensitivity of the assay was not evaluated.

Fractionation of whole hippocampi homogenates allowed me to evaluate the presence of the vector-derived protein in the synaptic compartment. However, it lacks the ability to evaluate colocalization and protein-protein interactions. Moreover, the large amount of synaptic-specific proteins pelleted in the nuclear fraction makes an accurate quantification challenging.

I have discussed that, even if SYNGAP1 is unbale to form trimers via its C-terminal CC domain, it can still localise at the synapse. However, data suggests that the direct interaction with the PSD is reduced (Araki *et al.*, 2020; Zeng *et al.*, 2016). Further evaluation of the interaction of the viral vector-derived SYNGAP1 with the PSD complex is necessary to have a better understanding of the protein functionality. To this end, an immunoprecipitation could be used to evaluate if the expressed protein can form the interactome seen in wild-type condition. Another technique that could be used to evaluate co-localisation would be immunofluorescence tomography, which would allow for the visualisation at high resolution of the viral vector-derived SYNGAP1 localisation.

Amygdala has been described as exerting a pivotal function in emotional processing, anxiety regulation and fear response (Davis, 1992; Davis et al., 1994; Kalin et al., 2004; Rauch et al., 2004; Roozendaal et al., 2009; Tye et al., 2011). In particular, it has been observed that the lesion of the central nucleus of the amygdala (Kalin et al., 2004) or pharmacological or optogenetic-induced hypoexicitability of this region (Davis et al., 1994; Tye et al., 2011) causes reduction of anxiety and fear-related behaviours, similar to what is observed in *Syngap1*$^{+/-}$ mice (Clement et al., 2012; Komiyama et al., 2002; Nakajima et al., 2019). Porter and colleagues (Porter et al., 2005) showed that SYNGAP1 is expressed in the amygdaloid complex throughout development and its expression is maintained in adulthood, suggesting the involvement of this brain region in the pathophysiology of the disease. It would have been therefore appropriate to also evaluate a delivery system that would have allowed viral vector distribution to this brain region. Biodistribution to the amygdaloid complex was not investigated in this study, but it would be interesting to evaluate this in future works.

Statistical analysis is crucially important for the correct interpretation of the results. In this work, groups have been analysed for each genotype separately, as the aim was to evaluate the effect of the treatment for each genotype, tolerability in wild-type mice and therapeutic effect in *Syngap1*$^{+/-}$ mice. This analysis does not take in consideration genotype x treatment interaction or the effect of repeated exposures. Therefore, for a more comprehensive and accurate analysis, it would be advisable to reanalyse the data using a three-way ANOVA.

7.4 SIGNIFICANCE

SYNGAP1 haploinsufficiency-associated disorder is a genetic disorder that is considered one of the most common causes of ID (Berryer *et al.*, 2013; Hamdan *et al.*, 2009, 2011; Rauch *et al.*, 2012), for which no treatment is currently available. Reversal studies showed that early, but not late, restoration of normal protein levels prevents the insurgence of most of the haploinsufficiency-associated phenotypes (Aceti *et al.*, 2015; Creson *et al.*, 2019).

My thesis provided the first proof-of-concept study on the feasibility of a gene therapy approach for the treatment of *SYNGAP1* haploinsufficiency-associated disorder. My results highlighted the many challenges posed by SYNGAP1 biology for the development of an effective gene replacement treatment. Nonetheless, my results suggest that a gene therapy approach could be a feasible option to treat *SYNGAP1* haploinsufficiency-associated disorder.

7.5 FUTURE EXPERIMENTS

This project was designed to determine the potential for gene therapy in a mouse model of *SYNGAP1* haploinsufficiency-associated disorder by testing the therapeutic efficacy of a series of rationally designed constructs. The limited non-significant amelioration observed in *Syngap1*$^{+/-}$ viral vector-treated mice could be associated to a series of factors which were discussed in previous sections. The results from this thesis highlight the necessity of a better understanding of SYNGAP1 functions and of the limitations associated with the animal model used. Therefore, I would like to suggest the following future experiments:

1. It is possible that the limited effect observed after viral vector treatment is associated with the low expression level of the viral vector protein achieved. Unfortunately, the large size of the *SYNGAP1* coding sequence (~3900 bp) occupies most of the available cloning space of AAV9, restricting the choice of

regulatory elements. The development of a *SYNGAP1* mini gene, where non-functionally relevant portions of the protein are removed to decrease the coding sequence length, would widen the choice of regulatory elements. This approach has been successfully used for the development of gene therapy for the treatment of Duchenne muscular dystrophy (Foster *et al.*, 2008; le Guiner *et al.*, 2017). As shown in Figure 1-4, the absence of mutation hotspots along the SYNGAP1 gene makes difficult to identify a region that could be deleted without impacting its function. Nonetheless, it is possible that the reintroduction of a protein that retains, at least, the C2-GAP fragment, which corresponds to the catalytic domain of the protein, might be able to ameliorate the phenotype observed in SYNGAP1 patients. To test this hypothesis, I would recommend constructing a library of mini gene designs presenting different combinations of N- and C-terminal regions and to evaluate their therapeutic efficacy.

2. The high level of horizontal activity showed by *Syngap1*$^{+/-}$ mice is a potential confounding factor for other behavioural abnormalities readouts. Given the promising results observed with the candidate therapeutic vectors, I would suggest to evaluate their therapeutic efficacy in *SYNGAP1* haploinsufficiency models that do not show the hyperactive phenotype but present cognitive and memory deficits, such as the rat model presented in Katsanevaki *et al.* (Katsanevaki *et al.*, 2020).

3. Another explanation for the small effect of the treatment could be related to the isoform expressed. Kilinc *et al.* (Kilinc *et al.*, 2022) showed that the absence of functional α1/α2 C-terminal containing isoforms is likely to be the factor causing the haploinsufficiency phenotype. However, it is important to consider the complex genetic context present in these models. Moreover, here are no data available currently regarding the importance and function of each N-terminus *in vivo*. An important experiment to determine which isoform/isoforms are necessary to be re-expressed to observe the maximum therapeutic efficacy would be the generation of mouse/rat lines which express only one full-length SYNGAP1 isoform. I would suggest evaluating cellular and behavioural

abnormalities in the *Syngap1*$^{+/isoform}$ model but also investigating the survival of *Syngap1*$^{isoform/isoform}$ animals.

4. SYNGAP1 expression pattern throughout development and distribution in the brain has been investigated by multiple laboratories, setting an important base for the understanding of the behavioural abnormalities observed (Gou *et al.*, 2020; Kim *et al.*, 2003; Knuesel *et al.*, 2005; McMahon *et al.*, 2012; Moon *et al.*, 2008; Porter *et al.*, 2005; Tomoda *et al.*, 2004). Muhia *et al.* (Muhia *et al.*, 2012) and Ozkan *et al.* (Ozkan *et al.*, 2014) suggested the involvement of forebrain regions in the development of hyperactivity but the importance of other regions is still to be elucidated.

   Before moving on with further *SYNGAP1* gene therapy studies, it will be important not only to understand which regions are fundamental to traduce to obtain the maximum therapeutic efficacy but also if there are region-specific derived behavioural abnormalities. An approach to investigate this would be parenchymal injections of viral vector expressing *SYNGAP1* in different brain areas such as the hippocampus, striatum, SSC, visual cortex and amygdala.

7.6 SUMMARY

To conclude, in this thesis, I showed the identification of a robust battery of behavioural tests for the assessment of the therapeutic efficacy of candidate gene therapy constructs. Subsequently, I demonstrated the potential and the challenges that need to be overcome for the development of an effective gene therapy approach for the treatment of *SYNGAP1* haploinsufficiency-associated disorder. Several factors could have impacted the poor therapeutic outcome, such as the inappropriate choice of the SYNGAP1 isoform, low levels of viral vector-derived protein expression, and inadequate therapeutic vector distribution across the brain. Further studies are necessary to define important elements of SYNGAP1 biology for the rational development of future gene therapy vectors.

Unix code script for the analysis of plasmid DNA sequencing data.

```
#!/bin/sh
### PlasmidSeq script by A.Saveliev, 2017
### Assumes that bbmap is in PATH, NOVOPlasty in home directory, denovo seed fasta in
/media/sf_vm_shared/seeds
### Script must find project folders in /media/sf_vm_shared/PlasmidSeq directory. Each folder must
have 3 files: one plasmid .fa, a pair of MiSeq 2x250 bp fastq.gz's
set -eux pipefail
### Clears out previous results
rm -rf /home/ubuntu/projects/sequencing/plasmid-seq/results/first-pass/*
rm -rf /home/ubuntu/projects/sequencing/plasmid-seq/final_report_1/*
### set up loop
for i in $(ls /home/ubuntu/projects/sequencing/plasmid-seq/data/)
do
 results=/home/ubuntu/projects/sequencing/plasmid-seq/results/first-pass/$i/
  mkdir ${results}
  cd /home/ubuntu/projects/sequencing/plasmid-seq/data/$i/
  # generate seed file by pulling out first read from fastq file
  echo ">first_read_seed_seq" >> ${results}seed.fasta
  seqkit seq -s *R1*fastq.gz | head -n 1 >> ${results}seed.fasta
  # unset variables
  FBLEN=""
  FBSEQ=""
  LOTNUMBER=""
  SAMPLENUMBER=""
  READ1=""
  READ2=""
   # remove BBMap fasta index if exists
  rm -rf ref
   # assign 2 variables  based on fastq.gz names
  LOTNUMBER=$(echo *.gz | awk -F'[_]' '{print $1}')
  SAMPLENAME=$(echo *.gz | awk -F'[_]' '{print $1 "_" $2}')
   # create a new fasta reference file with a simple name
  cp *.fa ${results}$LOTNUMBER.fasta
   # extract fasta sequence, remove control characters, write fasta body to file
  sed  '1d' ${results}$LOTNUMBER.fasta | tr -d '\n \r' > ${results}$LOTNUMBER.body.fasta
   # assign variable to fasta body DNA length
  FBLEN=$(cat ${results}$LOTNUMBER.body.fasta | wc -m)
   # assign variable to fasta body DNA sequence
  FBSEQ=$(cat ${results}$LOTNUMBER.body.fasta)
   # shift fasta by 500 bp (move tail to head)
  rm -f ${results}$LOTNUMBER.movetail.fasta
  grep '>' ${results}$LOTNUMBER.fasta > ${results}$LOTNUMBER.movetail.fasta
  echo ${FBSEQ:$FBLEN-500:$FBLEN} | tr -d '\n \r' >> ${results}$LOTNUMBER.movetail.fasta
  echo ${FBSEQ:0:$FBLEN-500} >> ${results}$LOTNUMBER.movetail.fasta
   # perform read pre-processing in BBDuk
  bbduk.sh overwrite=t ref=/home/ubuntu/miniconda3/envs/bioinfo/opt/bbmap-38.87-
0/resources/adapters.fa ktrim=r k=23 mink=11 hdist=1 tpe tbo qtrim=r trimq=10
in1="$SAMPLENAME"_L001_R1_001.fastq.gz in2="$SAMPLENAME"_L001_R2_001.fastq.gz
```

```
out1=${results}"$SAMPLENAME"_L001_R1_001.clean.fastq.gz
out2=${results}"$SAMPLENAME"_L001_R2_001.clean.fastq.gz minlen=250
   # gunzip pre-processed fastq files, use them for alignment and denovo assembly
  gunzip -kf ${results}*.clean.fastq.gz
   # perform alignment in BBMap, write ref, sam, bam, bai. Change maxindel value as needed.
  bbmap.sh overwrite=t in1=${results}"$SAMPLENAME"_L001_R1_001.clean.fastq.gz
in2=${results}"$SAMPLENAME"_L001_R2_001.clean.fastq.gz
ref=${results}$LOTNUMBER.movetail.fasta outm=${results}$LOTNUMBER.movetail.mapped.sam
maxindel=2000 outu=${results}$LOTNUMBER.movetail.unmapped.sam

  echo ""
  echo -e "\e[1;34mStarting bamscript from BBTools as embedded...\e[0m"
  echo ""

  #BBTools bs.sh inserted below
    echo "Note: This script is designed to run with the amount of memory detected by BBMap."
  echo "      If Samtools crashes, please ensure you are running on the same platform as BBMap,"
  echo "      or reduce Samtools' memory setting (the -m flag)."
  echo "Note: Please ignore any warnings about 'EOF marker is absent'; this is a bug in samtools that
occurs when using piped input."
  samtools view -bhu ${results}$LOTNUMBER.movetail.mapped.sam | samtools sort -m 2G -@ 3 -o
${results}$LOTNUMBER.movetail.mapped_sorted.bam
  samtools index ${results}$LOTNUMBER.movetail.mapped_sorted.bam
  echo "Note: Please ignore any warnings about 'EOF marker is absent'; this is a bug in samtools that
occurs when using piped input."
  samtools view -bhu ${results}$LOTNUMBER.movetail.unmapped.sam | samtools sort -m 2G -@ 3 -o
${results}$LOTNUMBER.movetail.unmapped_sorted.bam
  samtools index ${results}$LOTNUMBER.movetail.unmapped_sorted.bam

 #BBTools bs.sh ends
    echo ""
  echo -e "\e[1;34mFinished bamscript from BBTools\e[0m"
  echo ""
  # perform variant calling in CallVariants, write as VCF
  callvariants.sh overwrite=t in=${results}$LOTNUMBER.movetail.mapped.sam
ref=${results}$LOTNUMBER.movetail.fasta out=${results}$LOTNUMBER.movetail.vcf rarity=0.01
maf=0.01
  ### process VCF, build simplified variant table
    # extract VCF header, write to file
  head -n +52 ${results}$LOTNUMBER.movetail.vcf > ${results}$LOTNUMBER.movetail.header.txt
    # extract VCF body, write to file
  tail -n +53 ${results}$LOTNUMBER.movetail.vcf > ${results}$LOTNUMBER.movetail.body.txt
    # restore original fasta coordinates, write to new txt file as VCF body
  awk '$2>0 {$2=$2-500} 1'  OFS='\t' ${results}$LOTNUMBER.movetail.body.txt | awk '$2<1
{$2='$FBLEN'+$2} 1' OFS='\t' > ${results}$LOTNUMBER.unshift.vcf.txt
    # append VCF header and new rearranged VCF body, write to rearranged file. This is to archive a
full VCF with the restored coordinates.
  cat ${results}$LOTNUMBER.movetail.header.txt ${results}$LOTNUMBER.unshift.vcf.txt >
${results}$LOTNUMBER.unshift.vcf
    ### process new rearranged VCF body
    # replace semicolons with tabs, write to tab-delimited txt file
  tr ';' '\t' <  ${results}$LOTNUMBER.unshift.vcf.txt >  ${results}$LOTNUMBER.unshift.vcf.tab.txt
  # make summary vcf containing only name, position, ref, alt, sequence_depth, and alternative allele
fraction
```

```
  cat ${results}$LOTNUMBER.unshift.vcf.tab.txt | cut -f 1,2,4,5,17,20 >
${results}$LOTNUMBER.summary.txt
    # extract specific columns, write to a new txt file
  cut -f1-2,4-6,11,30-34  ${results}$LOTNUMBER.unshift.vcf.tab.txt >
${results}$LOTNUMBER.unshift.vcf.tab.simple.txt
    # sort by revised allele frequency, write to a new txt file
  sort -rk 9 ${results}$LOTNUMBER.unshift.vcf.tab.simple.txt >
${results}$LOTNUMBER.unshift.vcf.tab.simple.sortedbyRAF.txt
    ### build final report
    # append new column names to report
  echo -e "PLASMID\tPOS\tREF\tALT\tQUAL\tTYPE\tDEPTH\tAF\tRAF\tSB\tDP4" >>
${results}$LOTNUMBER.FINAL.report.txt
    # append new variant body, sorted by revised allele frequency
  cat ${results}$LOTNUMBER.unshift.vcf.tab.simple.sortedbyRAF.txt >>
${results}$LOTNUMBER.FINAL.report.txt
    # remove keys, keep numbers only
  sed -i 's/TYP=//g; s/DP=//g; s/RAF=//g; s/AF=//g; s/SB=//g'  ${results}$LOTNUMBER.FINAL.report.txt

  # comment out the next line to debug
  #rm -f $LOTNUMBER.unshift.vcf.txt $LOTNUMBER.unshift.vcf.tab.txt
$LOTNUMBER.unshift.vcf.tab.simple.txt $LOTNUMBER.unshift.vcf.tab.simple.sortedbyRAF.txt
$LOTNUMBER.movetail.header.txt $LOTNUMBER.movetail.body.txt $LOTNUMBER.body.fasta
   # remove BBMap index
  rm -rf ref
    ### start denovo assembly in NOVOPlasty
    # create variables from pre-processed fasta file names
  READ1=${results}$(basename *_R1_001.clean.fastq)
  READ2=${results}$(basename *_R2_001.clean.fastq)
  # remove temporary fastq files
  rm -rf ${results}*.clean.fastq*
  # move files needed for final anlysis to final_report folder
  cp ${results}*movetail.fasta ${results}*.summary.txt ${results}*.mapped_sorted.bam*
/home/ubuntu/projects/sequencing/plasmid-seq/final_report_1/
done

### Clears out previous results
rm -rf /home/ubuntu/projects/sequencing/plasmid-seq/results/second-pass/*
rm -rf /home/ubuntu/projects/sequencing/plasmid-seq/final_report_2/*

### set up loop
for i in $(ls /home/ubuntu/projects/sequencing/plasmid-seq/data/)
do
  results=/home/ubuntu/projects/sequencing/plasmid-seq/results/second-pass/$i/
  mkdir ${results}
  cd /home/ubuntu/projects/sequencing/plasmid-seq/data/$i/
  # generate seed file by pulling out first read from fastq file
  echo ">first_read_seed_seq" >> ${results}seed.fasta
  seqkit seq -s *R1*fastq.gz | head -n 1 >> ${results}seed.fasta
  # unset variables
  FBLEN=""
  FBSEQ=""
  LOTNUMBER=""
  SAMPLENUMBER=""
  READ1=""
  READ2=""
```

```
 # remove BBMap fasta index if exists
 rm -rf ref
 # assign 2 variables  based on fastq.gz names
 LOTNUMBER=$(echo *.gz | awk -F'[_]' '{print $1}')
 SAMPLENAME=$(echo *.gz | awk -F'[_]' '{print $1 "_" $2}')

 # create a new fasta reference file with a simple name
 cp *.fa ${results}$LOTNUMBER.fasta
 # extract fasta sequence, remove control characters, write fasta body to file
 sed  '1d' ${results}$LOTNUMBER.fasta | tr -d '\n \r' > ${results}$LOTNUMBER.body.fasta
 # assign variable to fasta body DNA length
 FBLEN=$(cat ${results}$LOTNUMBER.body.fasta | wc -m)
 # assign variable to fasta body DNA sequence
 FBSEQ=$(cat ${results}$LOTNUMBER.body.fasta)
 # shift fasta by 500 bp (move tail to head)
 rm -f ${results}$LOTNUMBER.movetail.fasta
 grep '>' ${results}$LOTNUMBER.fasta > ${results}$LOTNUMBER.movetail.fasta
 echo ${FBSEQ:$FBLEN-500:$FBLEN} | tr -d '\n \r' >> ${results}$LOTNUMBER.movetail.fasta
 echo ${FBSEQ:0:$FBLEN-500} >> ${results}$LOTNUMBER.movetail.fasta
 # perform read pre-processing in BBDuk
 bbduk.sh overwrite=t ref=/home/ubuntu/miniconda3/envs/bioinfo/opt/bbmap-38.87-
0/resources/adapters.fa ktrim=r k=23 mink=11 hdist=1 tpe tbo qtrim=rl trimq=30
in1="$SAMPLENAME"_L001_R1_001.fastq.gz in2="$SAMPLENAME"_L001_R2_001.fastq.gz
out1=${results}"$SAMPLENAME"_L001_R1_001.clean.fastq.gz
out2=${results}"$SAMPLENAME"_L001_R2_001.clean.fastq.gz minlen=50
 # gunzip pre-processed fastq files, use them for alignment and denovo assembly
 gunzip -kf ${results}*.clean.fastq.gz
 # perform alignment in BBMap, write ref, sam, bam, bai. Change maxindel value as needed.
 bbmap.sh overwrite=t in1=${results}"$SAMPLENAME"_L001_R1_001.clean.fastq.gz
in2=${results}"$SAMPLENAME"_L001_R2_001.clean.fastq.gz
ref=${results}$LOTNUMBER.movetail.fasta outm=${results}$LOTNUMBER.movetail.mapped.sam
maxindel=10 outu=${results}$LOTNUMBER.movetail.unmapped.sam

 echo ""
 echo -e "\e[1;34mStarting bamscript from BBTools as embedded...\e[0m"
 echo ""

 #BBTools bs.sh inserted below
 echo "Note: This script is designed to run with the amount of memory detected by BBMap."
 echo "      If Samtools crashes, please ensure you are running on the same platform as BBMap,"
 echo "      or reduce Samtools' memory setting (the -m flag)."
 echo "Note: Please ignore any warnings about 'EOF marker is absent'; this is a bug in samtools that
occurs when using piped input."
 samtools view -bhu ${results}$LOTNUMBER.movetail.mapped.sam | samtools sort -m 2G -@ 3 -o
${results}$LOTNUMBER.movetail.mapped_sorted.bam
 samtools index ${results}$LOTNUMBER.movetail.mapped_sorted.bam
 echo "Note: Please ignore any warnings about 'EOF marker is absent'; this is a bug in samtools that
occurs when using piped input."
 samtools view -bhu ${results}$LOTNUMBER.movetail.unmapped.sam | samtools sort -m 2G -@ 3 -o
${results}$LOTNUMBER.movetail.unmapped_sorted.bam
 samtools index ${results}$LOTNUMBER.movetail.unmapped_sorted.bam

#BBTools bs.sh ends
 echo ""
 echo -e "\e[1;34mFinished bamscript from BBTools\e[0m"
```

```
 echo ""
 # perform variant calling in CallVariants, write as VCF
 callvariants.sh overwrite=t in=${results}$LOTNUMBER.movetail.mapped.sam
ref=${results}$LOTNUMBER.movetail.fasta out=${results}$LOTNUMBER.movetail.vcf rarity=0.01
maf=0.01

 ### process VCF, build simplified variant table
 # extract VCF header, write to file
 head -n +52 ${results}$LOTNUMBER.movetail.vcf > ${results}$LOTNUMBER.movetail.header.txt
 # extract VCF body, write to file
 tail -n +53 ${results}$LOTNUMBER.movetail.vcf > ${results}$LOTNUMBER.movetail.body.txt
 # restore original fasta coordinates, write to new txt file as VCF body
 awk '$2>0 {$2=$2-500} 1'  OFS='\t' ${results}$LOTNUMBER.movetail.body.txt | awk '$2<1
{$2='$FBLEN'+$2} 1' OFS='\t' > ${results}$LOTNUMBER.unshift.vcf.txt
 # append VCF header and new rearranged VCF body, write to rearranged file. This is to archive a full
VCF with the restored coordinates.
 cat ${results}$LOTNUMBER.movetail.header.txt ${results}$LOTNUMBER.unshift.vcf.txt >
${results}$LOTNUMBER.unshift.vcf

 ### process new rearranged VCF body
 # replace semicolons with tabs, write to tab-delimited txt file
 tr ';' '\t' <  ${results}$LOTNUMBER.unshift.vcf.txt >  ${results}$LOTNUMBER.unshift.vcf.tab.txt
 # make summary vcf containing only name, position, ref, alt, sequence_depth, and alternative allele
fraction
 cat ${results}$LOTNUMBER.unshift.vcf.tab.txt | cut -f 1,2,4,5,17,20 >
${results}$LOTNUMBER.summary.txt
 # extract specific columns, write to a new txt file
 cut -f1-2,4-6,11,30-34  ${results}$LOTNUMBER.unshift.vcf.tab.txt >
${results}$LOTNUMBER.unshift.vcf.tab.simple.txt
 # sort by revised allele frequency, write to a new txt file
 sort -rk 9 ${results}$LOTNUMBER.unshift.vcf.tab.simple.txt >
${results}$LOTNUMBER.unshift.vcf.tab.simple.sortedbyRAF.txt

 ### build final report
 # append new column names to report
 echo -e "PLASMID\tPOS\tREF\tALT\tQUAL\tTYPE\tDEPTH\tAF\tRAF\tSB\tDP4" >>
${results}$LOTNUMBER.FINAL.report.txt
 # append new variant body, sorted by revised allele frequency
 cat ${results}$LOTNUMBER.unshift.vcf.tab.simple.sortedbyRAF.txt >>
${results}$LOTNUMBER.FINAL.report.txt
 # remove keys, keep numbers only
 sed -i 's/TYP=//g; s/DP=//g; s/RAF=//g; s/AF=//g; s/SB=//g'  ${results}$LOTNUMBER.FINAL.report.txt
 # comment out the next line to debug
 #rm -f $LOTNUMBER.unshift.vcf.txt $LOTNUMBER.unshift.vcf.tab.txt
$LOTNUMBER.unshift.vcf.tab.simple.txt $LOTNUMBER.unshift.vcf.tab.simple.sortedbyRAF.txt
$LOTNUMBER.movetail.header.txt $LOTNUMBER.movetail.body.txt $LOTNUMBER.body.fasta
 # remove BBMap index
 rm -rf ref

 ### start denovo assembly in NOVOPlasty
 # create variables from pre-processed fasta file names
 READ1=${results}$(basename *_R1_001.clean.fastq)
 READ2=${results}$(basename *_R2_001.clean.fastq)
 # clean up and create a new config file for NOVOPlasty
 rm -f ${results}config_plasmid.txt
```

```
  touch ${results}config_plasmid.txt
  # assign NOVOPLasty config values, seed location, preprocessed fasta files, append all to
config_plasmid.txt file
  echo "Project" >> ${results}config_plasmid.txt
  echo "-----------------------" >> ${results}config_plasmid.txt
  echo "Project name        = $LOTNUMBER" >> ${results}config_plasmid.txt
  echo "Type                = mito" >> ${results}config_plasmid.txt
  echo "Genome Range        = "$((FBLEN-1000))" "-" "$((FBLEN+1000))"" >>
${results}config_plasmid.txt
  echo "K-mer               = 39"  >> ${results}config_plasmid.txt
  echo "Max memory          = " >> ${results}config_plasmid.txt
  echo "Extended log        = 0" >> ${results}config_plasmid.txt
  echo "Save assembled reads = no" >> ${results}config_plasmid.txt
  echo "Seed Input          = ${results}seed.fasta" >> ${results}config_plasmid.txt
  echo "Reference sequence   = " >> ${results}config_plasmid.txt
  echo "Variance detection   = no " >> ${results}config_plasmid.txt
  echo "Heteroplasmy        = " >> ${results}config_plasmid.txt
  echo "HP exclude list     = " >> ${results}config_plasmid.txt
  echo "Chloroplast sequence = " >> ${results}config_plasmid.txt

  echo "Dataset 1: " >> ${results}config_plasmid.txt
  echo "-----------------------" >> ${results}config_plasmid.txt
  echo "Read Length         = 250" >> ${results}config_plasmid.txt
  echo "Insert size = 450" >> ${results}config_plasmid.txt
  echo "Platform            = illumina" >> ${results}config_plasmid.txt
  echo "Single/Paired       = PE" >> ${results}config_plasmid.txt
  echo "Combined reads      = " >> ${results}config_plasmid.txt
  echo "Forward reads       = " $READ1 >> ${results}config_plasmid.txt
  echo "Reverse reads       = " $READ2 >> ${results}config_plasmid.txt

  echo "Optional" >> ${results}config_plasmid.txt
  echo "-----------------------" >> ${results}config_plasmid
  echo "Insert size auto    = yes" >> ${results}config_plasmid.txt
  echo "Insert Range        = 1.6" >> ${results}config_plasmid.txt
  echo "Insert Range strict  = 1.2" >> ${results}config_plasmid.txt
  echo "Use Quality Scores   = no" >> ${results}config_plasmid.txt

  # run NOVOPlasty
  perl  ~/tools/NOVOPlasty/NOVOPlasty3.7.2.pl -c ${results}config_plasmid.txt
  # remove temporary fastq files
  rm -rf ${results}*.clean.fastq*
  # move NOVOplasty output files to results folder
  mv *ontigs* *contigs* log*  *fasta ${results} || true
  # move files needed for final anlysis to final_report folder
  cp ${results}C*.fasta ${results}*movetail.fasta ${results}*.summary.txt
${results}*.mapped_sorted.bam* /home/ubuntu/projects/sequencing/plasmid-seq/final_report_2/
done
```

Unix code script for the analysis of viral vector DNA sequencing data.

```
#!/bin/sh
### Script for analysis of MiSeq data from AAV virus DNA. Expects individual folders for each construct with two fastq.gz files and
### ref seq file containing transgene cassette (including ITRs), vector backbone, rep/cap plasmid, helper plasmid, HEK293 Ad5 sequence

set -eux pipefail

### Round 1 analysis with very loose quality filtering and allowing for presence of large indels
### Clears out previous results
rm -rf /home/ubuntu/projects/sequencing/plasmid-seq/results/first-pass/*
rm -rf /home/ubuntu/projects/sequencing/plasmid-seq/final_report_1/*
### set up loop
for i in $(ls /home/ubuntu/projects/sequencing/plasmid-seq/data/)
do
 results=/home/ubuntu/projects/sequencing/plasmid-seq/results/first-pass/$i/
 mkdir ${results}
 cd /home/ubuntu/projects/sequencing/plasmid-seq/data/$i/
 # unset variables
 LOTNUMBER=""
 SAMPLENUMBER=""
  # remove BBMap fasta index if exists
 rm -rf ref
  # assign 2 variables  based on fastq.gz names
 LOTNUMBER=$(echo *.gz | awk -F'[_]' '{print $1}')
 SAMPLENAME=$(echo *.gz | awk -F'[_]' '{print $1 "_" $2}')
  # create a new fasta reference file with a simple name
 cp *.fa ${results}$LOTNUMBER.fasta
 # perform read pre-processing in BBDuk
 bbduk.sh overwrite=t ref=/home/ubuntu/miniconda3/envs/bioinfo/opt/bbmap-38.87-0/resources/adapters.fa ktrim=r k=23 mink=11 hdist=1 tpe tbo qtrim=r trimq=10 in1="$SAMPLENAME"_L001_R1_001.fastq.gz in2="$SAMPLENAME"_L001_R2_001.fastq.gz out1=${results}"$SAMPLENAME"_L001_R1_001.clean.fastq.gz out2=${results}"$SAMPLENAME"_L001_R2_001.clean.fastq.gz minlen=250
 # gunzip pre-processed fastq files, use them for alignment and denovo assembly
 gunzip -kf ${results}*.clean.fastq.gz
  # perform alignment in BBMap, write ref, sam, bam, bai. Change maxindel value as needed.
 bbmap.sh overwrite=t in1=${results}"$SAMPLENAME"_L001_R1_001.clean.fastq.gz in2=${results}"$SAMPLENAME"_L001_R2_001.clean.fastq.gz scafstats=${results}$LOTNUMBER.stats ref=${results}$LOTNUMBER.fasta outm=${results}$LOTNUMBER.mapped.sam outu=${results}$LOTNUMBER.unmapped.fq
 samtools view -bhu ${results}$LOTNUMBER.mapped.sam | samtools sort -m 2G -@ 3 -o ${results}$LOTNUMBER.mapped_sorted.bam
 samtools index ${results}$LOTNUMBER.mapped_sorted.bam
#  samtools view -bhu ${results}$LOTNUMBER.unmapped.sam | samtools sort -m 2G -@ 3 -o ${results}$LOTNUMBER.unmapped_sorted.bam
#  samtools index ${results}$LOTNUMBER.unmapped_sorted.bam
 cp ${results}*fasta* ${results}*.mapped_sorted.bam* /home/ubuntu/projects/sequencing/plasmid-seq/final_report_1/

done
```

```
### Round 2 of analysis with more stringent quality and indel length requirements
### Clears out previous results
rm -rf /home/ubuntu/projects/sequencing/plasmid-seq/results/second-pass/*
rm -rf /home/ubuntu/projects/sequencing/plasmid-seq/final_report_2/*
### set up loop
for i in $(ls /home/ubuntu/projects/sequencing/plasmid-seq/data/)
do
 results=/home/ubuntu/projects/sequencing/plasmid-seq/results/second-pass/$i/
 mkdir ${results}
 cd /home/ubuntu/projects/sequencing/plasmid-seq/data/$i/
 # unset variables
 LOTNUMBER=""
 SAMPLENUMBER=""
  # remove BBMap fasta index if exists
 rm -rf ref
  # assign 2 variables  based on fastq.gz names
 LOTNUMBER=$(echo *.gz | awk -F'[_]' '{print $1}')
 SAMPLENAME=$(echo *.gz | awk -F'[_]' '{print $1 "_" $2}')
  # create a new fasta reference file with a simple name
 cp *.fa ${results}$LOTNUMBER.fasta
 # perform read pre-processing in BBDuk
 bbduk.sh overwrite=t ref=/home/ubuntu/miniconda3/envs/bioinfo/opt/bbmap-38.87-
0/resources/adapters.fa ktrim=r k=23 mink=11 hdist=1 tpe tbo qtrim=rl trimq=20
in1="$SAMPLENAME"_L001_R1_001.fastq.gz in2="$SAMPLENAME"_L001_R2_001.fastq.gz
out1=${results}"$SAMPLENAME"_L001_R1_001.clean.fastq.gz
out2=${results}"$SAMPLENAME"_L001_R2_001.clean.fastq.gz minlen=50
 # gunzip pre-processed fastq files, use them for alignment and denovo assembly
 gunzip -kf ${results}*.clean.fastq.gz
 # perform alignment in BBMap, write ref, sam, bam, bai. Change maxindel value as needed.
 bbmap.sh overwrite=t in1=${results}"$SAMPLENAME"_L001_R1_001.clean.fastq.gz
in2=${results}"$SAMPLENAME"_L001_R2_001.clean.fastq.gz scafstats=${results}$LOTNUMBER.stats
ref=${results}$LOTNUMBER.fasta outm=${results}$LOTNUMBER.mapped.sam
outu=${results}$LOTNUMBER.unmapped.fq
 samtools view -bhu ${results}$LOTNUMBER.mapped.sam | samtools sort -m 2G -@ 3 -o
${results}$LOTNUMBER.mapped_sorted.bam
 samtools index ${results}$LOTNUMBER.mapped_sorted.bam

 # samtools view -bhu ${results}$LOTNUMBER.unmapped.sam | samtools sort -m 2G -@ 3 -o
${results}$LOTNUMBER.unmapped_sorted.bam
 #samtools index ${results}$LOTNUMBER.unmapped_sorted.bam
 cp ${results}*fasta* ${results}*.mapped_sorted.bam*
/home/ubuntu/projects/sequencing/plasmid-seq/final_report_2/

echo ""
echo "==============ANALYSIS COMPLETED==============="
echo ""

done
```

Table S-1. Body weight comparisons, Šídák multiple comparison.

Age in weeks	Wild-type n	*Syngap1*$^{+/-}$ n	Mean Diff. (g)	95% CI	t	df*	p value
3	14	15	1.158	-0.3794 to 2.696	1.550	25.56	0.7615
4	14	15	1.914	-0.1625 to 3.990	1.901	24.35	0.5119
5	14	15	0.6638	-0.8798 to 2.207	0.8829	26.66	0.9923
6	14	15	0.9571	-0.1557 to 2.070	1.766	26.63	0.6057
7	18	18	0.4056	-0.5497 to 1.361	0.8628	33.94	0.9934
8	19	18	0.7810	-0.1174 to 1.739	1.657	33.64	0.6770
9	19	18	1.348	0.3196 to 2.376	2.672	31.41	0.1124
10	19	18	1.829	0.6791 to 2.979	3.233	33.88	0.0270
11	19	18	1.849	0.5129 to 3.185	2.811	34.54	0.0780
12	17	18	1.704	0.3356 to 3.072	2.534	32.90	0.1510

*df = degrees of freedom.

Table S-2. RM Two-way ANOVA, 4 weeks of age.

	Mean Diff. (cm)	95% CI	t	df*	p value
Genotype effect, Šídák multiple comparison test					
5 min	554.4	-71.58 to 1180	2.654	10.51	0.0897
10 min	702.1	154.9 to 1249	3.843	10.53	0.0118
15 min	827.8	59.63 to 1596	3.151	11.99	0.0330
20 min	705.9	114.4 to 1297	3.667	9.343	0.0193
Time effect, Tukey's multiple comparison test					
Syngap1$^{+/-}$					
5 min vs 10 min	406.4	-165.2 to 978.0	3.329	7.00	0.1746
5 min vs 15 min	711.6	-67.53 to 1491	4.276	7.00	0.0726
5 min vs 20 min	1003	433.2 to 1573	8.239	7.00	0.0028
10 min vs 15 min	305.2	-200.2 to 810.6	2.827	7.00	0.2736
10 min vs 20 min	596.8	260.1 to 933.6	8.298	7.00	0.0027
15 min vs 20 min	291.6	-138.4 to 721.6	3.175	7.00	0.2008
WT					
5 min vs 10 min	554.1	218.3 to 889.9	7.473	8.00	0.0033
5 min vs 15 min	985.0	488.1 to 1482	8.977	8.00	0.0010
5 min vs 20 min	1155	904.1 to 1405	20.860	8.00	<0.0001
10 min vs 15 min	430.9	76.69 to 785.1	5.509	8.00	0.0192

10 min vs 20 min	600.7	299.7 to 901.7	9.038	8.00	0.0010
15 min vs 20 min	169.8	-254.6 to 594.2	1.812	8.00	0.5982

*df = degrees of freedom.

Table S-3. RM Two-way ANOVA, 7 weeks of age.

Wild-type vs *Syngap1*$^{+/-}$	**Mean Diff. (cm)**	**95% CI**	**t**	**df***	**p value**
5 min	1158	404.0 to 1912	4.123	24.85	0.0015
10 min	1372	733.2 to 2011	5.836	21.43	<0.0001
15 min	1357	642.8 to 2070	5.189	20.42	0.0002
20 min	1260	655.1 to 1865	5.709	19.61	<0.0001
Time effect, Tukey's multiple comparison test					
Syngap1$^{+/-}$					
5 min vs 10 min	94.8	-687.9 to 877.6	0.4981	14.00	0.9844
5 min vs 15 min	472.6	-292.5 to 1238	2.539	14.00	0.3158
5 min vs 20 min	569.8	-119.5 to 1259	3.398	14.00	0.1222
10 min vs 15 min	377.8	114.34 to 641.2	5.896	14.00	0.0046
10 min vs 20 min	474.9	197.2 to 752.7	7.028	14.00	0.0010
15 min vs 20 min	97.1	-80.6 to 274.9	2.246	14.00	0.4159
WT					
5 min vs 10 min	309.2	-331.9 to 950.2	2.002	13.00	0.5121
5 min vs 15 min	671.3	0.2 to 1342	4.152	13.00	0.0499
5 min vs 20 min	672.0	-30.3 to 1374	3.972	13.00	0.0626
10 min vs 15 min	362.2	72.6 to 651.8	5.191	13.00	0.0132
10 min vs 20 min	362.9	100.0 to 651.8	5.731	13.00	0.0066
15 min vs 20 min	0.7	-236.8 to 238.2	0.012	13.00	>0.9999

*df = degrees of freedom.

Table S-4. RM Two-way ANOVA, 11 weeks of age.

Wild-type vs *Syngap1*$^{+/-}$	**Mean Diff. (cm)**	**95% CI**	**t**	**df***	**p value**
5 min	1793	1056 to 2529	6.727	18.14	<0.0001
10 min	2080	1373 to 2786	8.050	20.16	<0.0001
15 min	2016	1375 to 2656	8.615	19.77	<0.0001
20 min	1783	1309 to 2258	10.160	22.95	<0.0001

*df = degrees of freedom.

Table S-5. RM Two-way ANOVA, repeated exposures to the open field.

Wild-type vs *Syngap1*$^{+/-}$	Mean Diff. (cm)	95% CI	t	df*	p value
Genotype effect, Šídák multiple comparisons tests between genotypes					
7 weeks	-5067	-847 to -3287	6.548	54.00	<0.0001
11 weeks	-7671	-951 to -5892	9.915	54.00	<0.0001

*df = degrees of freedom.

Table S-6. RM Two-way ANOVA, repeated exposures to the elevated plus maze.

	Mean Diff. (% of time)	95% CI	t	df*	p value
Genotype effect, Šídák multiple comparisons tests between genotypes					
7 weeks	-17.99	-26.60 to -9.37	4.824	46.00	<0.0001
11 weeks	-24.17	-32.79 to -15.55	6.483	46.00	<0.0001
Time effect, Šídák multiple comparisons tests between age					
Wild-type	8.34	2.25 to 14.43	3.278	23.00	0.0066
Syngap1$^{+/-}$	2.15	-4.71 to 9.02	0.751	23.00	0.7089

*df = degrees of freedom.

Table S-7. RM Two way ANOVA, WT(Vh) vs Syngap1$^{+/-}$(Vh), 7 weeks of age.

	Mean Diff. (cm)	95% CI	t	df*	p value
Genotype effect, Šídák multiple comparisons tests between genotypes					
5 min	-4208	-5765 to -2650	7.141	31.16	<0.0001
10 min	-3749	-5217 to -2281	6.726	32.99	<0.0001
15 min	-3051	-4355 to -1747	6.190	30.65	<0.0001
20 min	-2955	-4378 to -1532	5.495	30.48	<0.0001
Time effect, Tukey's multiple comparisons tests within genotypes					
WT (Vh)					
15 min vs 30 min	1817	1081 to 2553	9.12	99.00	<0.0001
15 min vs 45 min	2683	1947 to 3419	13.470	99.00	<0.0001
15 min vs 60 min	3225	2489 to 3961	16.190	99.00	<0.0001
30 min vs 45 min	866	129.9 to 16.02	4.348	99.00	0.0143
30 min vs 60 min	1408	672.1 to 2144	7.070	99.00	<0.0001
45 min vs 60 min	545.2	-193.9 to 1278	2.722	99.00	0.2244
Syngap1$^{+/-}$ (Vh)					
15 min vs 30 min	2275	16000 to 2951	12.450	99.00	<0.0001
15 min vs 45 min	3840	3164 to 4515	21.010	99.00	<0.0001
15 min vs 60 min	4478	3802 to 5153	24.500	99.00	<0.0001
30 min vs 45 min	1564	888.9 to 2240	8.559	99.00	<0.0001
30 min vs 60 min	2202	1527 to 2878	12.050	99.00	<0.0001

*df=degree of freedom. Vh=vehicle, WT=wild-type.

Table S-8. RM Two way ANOVA, time effect, Tukey's multiple comparisons tests within treatment groups at 7 weeks of age.

	Mean Diff. (cm)	95% CI	t	df*	p value
Vh					
15 min vs 30 min	2275	1624 to 2926	13.970	18.00	<0.0001
15 min vs 45 min	3840	3021 to 5448	18.750	18.00	<0.0001
15 min vs 60 min	4478	3507 to 5448	18.440	18.00	<0.0001
30 min vs 45 min	1564	807.8 to 2321	8.264	18.00	<0.0001
30 min vs 60 min	2202	1337 to 3067	10.180	18.00	<0.0001
45 min vs 60 min	637.7	-1.645 to 1277	3.987	18.00	0.0507
1E10 vg/mouse					
15 min vs 30 min	2550	1071 to 4030	7.237	12.00	0.0013
15 min vs 45 min	3522	1621 to 5422	7.781	12.00	0.0007
15 min vs 60 min	4331	2169 to 6492	8.413	12.00	0.0003
30 min vs 45 min	971.3	-85.35 to 2028	3.860	12.00	0.0754
30 min vs 60 min	1780	532.3 to 3028	5.989	12.00	0.0055
45 min vs 60 min	808.8	-77.13 to 1695	3.833	12.00	0.0778
5E10 vg/mouse					
15 min vs 30 min	2368	1744 to 2993	15.330	16.00	<0.0001
15 min vs 45 min	3788	2627 to 4949	13.200	16.00	<0.0001
15 min vs 60 min	4570	3259 to 5881	14.100	16.00	<0.0001
30 min vs 45 min	1419	481.2 to 2358	6.121	16.00	0.0026
30 min vs 60 min	2202	1039 to 3364	7.663	16.00	0.0003
45 min vs 60 min	782.1	181.1 to 1383	5.265	16.00	0.0090
1E11 vg/mouse					
15 min vs 30 min	2705	1740 to 3670	11.640	13.00	<0.0001
15 min vs 45 min	3843	2811 to 4875	15.460	13.00	<0.0001
15 min vs 60 min	4379	3205 to 5553	15.480	13.00	<0.0001
30 min vs 45 min	1138	551.6 to 1724	8.056	13.00	0.0004
30 min vs 60 min	1674	820.6 to 2527	8.143	13.00	0.0003
45 min vs 60 min	536	-165.7 to 1238	3.171	13.00	0.1632
45 min vs 60 min	637.7	-37.77 to 1313	3.489	99.00	0.0715

*df=degree of freedom. Vh=vehicle.

Table S-9. RM Two way ANOVA, WT(Vh) vs Syngap1$^{+/-}$(Vh), 15 weeks of age.

	Mean Diff. (cm)	95% CI	t	df*	p value
Genotype effect, Šídák multiple comparisons tests between genotypes					
5 min	-4785	-6535 to -3036	7.308	26.46	<0.0001
10 min	-5435	-6683 to -4188	11.62	27.05	<0.0001
15 min	-5909	-6980 to -4839	14.75	26.44	<0.0001
20 min	-5538	-6804 to -4272	11.86	21.92	<0.0001
Time effect, Tukey's multiple comparisons tests within genotypes					
WT (Vh)					
15 min vs 30 min	790.3	228.1 to 1353	5.730	15.00	0.0051
15 min vs 45 min	1534	732.0 to 2336	7.796	15.00	0.0003
15 min vs 60 min	1722	933.2 to 2511	8.898	15.00	<0.0001
30 min vs 45 min	743.8	206.9 to 1281	5647	15.00	0.0058
30 min vs 60 min	931.6	374.6 to 1489	6.817	15.00	0.0011
45 min vs 60 min	187.8	-154.8 to 530.5	2.234	15.00	0.4185
Syngap1$^{+/-}$ (Vh)					
15 min vs 30 min	140.4	-553.2 to 834.0	0.809	18.00	0.9391
15 min vs 45 min	410.2	-523.3 to 1344	1.756	18.00	0.6094
15 min vs 60 min	969.3	20.34 to 1918	4.083	18.00	0.0443
30 min vs 45 min	269.8	-324.5 to 864.1	1.815	18.00	0.5847
30 min vs 60 min	828.9	144.9 to 1513	4.844	18.00	0.0146
45 min vs 60 min	559.0	-145.8 to 1264	3.170	18.00	0.1498

*df = degrees of freedom. Vh=vehicle, WT=wild-type.

Table S-10. RM Two way ANOVA, time effect, Tukey's multiple comparisons tests within treatment groups at 15 weeks of age.

	Mean Diff. (cm)	95% CI	t	df*	p value
Vh					
15 min vs 30 min	140.4	-553.2 to 834.0	0.809	18.00	0.9391
15 min vs 45 min	410.2	-523.3 to 1344	1.756	18.00	0.6094
15 min vs 60 min	969.3	20.34 to 1918	4.083	18.00	0.0443
30 min vs 45 min	269.8	-324.5 to 864.1	1.815	18.00	0.5847
30 min vs 60 min	828.9	144.9 to 1513	4.844	18.00	0.0146
45 min vs 60 min	559.0	-145.8 to 1264	3.170	18.00	0.1498
1E10 vg/mouse					
15 min vs 30 min	-42.2	-1200 to 1115	0.153	12.00	0.9995
15 min vs 45 min	102.0	-1369 to 1573	0.291	12.00	0.9967
15 min vs 60 min	297.0	-1010 to 1604	0.954	12.00	0.9046
30 min vs 45 min	144.2	-758.4 to 1047	0.671	12.00	0.9633
30 min vs 60 min	339.2	-369.9 to 1048	2.009	12.00	0.552
45 min vs 60 min	195.1	-675.2 to 1065	0.941	12.00	0.9080
5E10 vg/mouse					
15 min vs 30 min	-24.7	-890.3 to 820.9	0.164	16.00	0.9994
15 min vs 45 min	258.2	-679.4 to 1196	1.114	16.00	0.8589
15 min vs 60 min	294.5	-917.7 to 1507	0.983	16.00	0.8975
30 min vs 45 min	292.9	-627.5 to 1213	1.288	16.00	0.7996
30 min vs 60 min	329.2	-412.4 to 1071	1.796	16.00	0.5938
45 min vs 60 min	36.3	-1385 to 1458	0.103	16.00	0.9999
1E11 vg/mouse					
15 min vs 30 min	388.5	-726.1 to 1503	1.447	13.00	0.7393
15 min vs 45 min	1469	8.2 to 2931	4.174	13.00	0.0486
15 min vs 60 min	1875	89.04 to 3661	4.358	13.00	0.0385
30 min vs 45 min	1081	347.1 to 1815	6.114	13.00	0.0040
30 min vs 60 min	1486	461.0 to 2512	6.017	13.00	0.0045
45 min vs 60 min	405.6	-305.1 to 1116	3.369	13.00	0.3744

*df = degrees of freedom, Vh=vehicle

Table S-11. Dunn's multiple comparison test, wild-type treated, elevated plus maze, 7 weeks.

Treatment comparison	Mean Rank Diff. (% of time)	z	p value
Vh vs 1E10 vg/mouse	7.95	1.653	0.2950
Vh vs 5E10 vg/mouse	-4.87	0.950	>0.9999
1E10 vg/mouse vs 5E10 vg/mouse	-12.82	2.569	0.0306

*df = degrees of freedom. Vh=vehicle.

Table S-12. Dunn's multiple comparison test, wild-type treated, elevated plus maze, 15 weeks.

Treatment comparison	Mean Rank Diff. (% of time)	z	p value
Vh vs 1E10 vg/mouse	14.92	3.125	0.0053
Vh vs 5E10 vg/mouse	-7.69	1.532	0.3765
1E10 vg/mouse vs 5E10 vg/mouse	-7.23	1.462	0.4311

*df = degrees of freedom. Vh=vehicle

Table S-13. Dunnett's T3 multiple comparison test, Syngap1$^{+/-}$ treated, elevated plus maze, 15 weeks.

Treatment comparison	Mean Diff. (cm)	95% CI	t	df*	p value
Vh vs 1E10 vg/mouse	-469.50	-1303.00 to 363.90	1.661	16.94	0.4860
Vh vs 5E10 vg/mouse	-568.60	-1016.00 to -121.00	3.563	29.80	0.0074
Vh vs 1E11 vg/mouse	-939.20	-1527.00 to -351.80	4.593	22.37	0.0008
1E10 vg/mouse vs 5E10 vg/mouse	-99.10	-927.40 to 729.20	0.355	16.21	0.9994
1E10 vg/mouse vs 1E11 vg/mouse	-469.70	-1355.00 to 415.40	1.531	20.63	0.5684
5E10 vg/mouse vs 1E11 vg/mouse	-370.60	-945.60 to 204.30	1.859	21.14	0.3600

*df = degrees of freedom. Vh=vehicle

Table S-14. RM Two-way ANOVA, partial departures, repeated exposures to the platform departure.

Wild-type vs *Syngap1*$^{+/-}$	Mean Diff.	95% CI	t	df*	p value
Genotype effect, Šídák multiple comparisons tests between genotypes					
7 weeks	-16.84	-27.34 to -6.34	3.671	66.00	0.0010
11 weeks	-27.69	-38.19 to -17.19	6.037	66.00	<0.0001

*df = degrees of freedom.

Table S-15. RM Two-way ANOVA, full departures, repeated exposures to the platform departure.

Wild-type vs *Syngap1*$^{+/-}$	Mean Diff.	95% CI	t	df*	p value
Genotype effect, Šídák multiple comparisons tests between genotypes					
7 weeks	-9.25	-14.61 to -3.89	3.947	66.00	0.0004
11 weeks	-11.22	-16.58 to -5.86	4.788	66.00	<0.0001

*df = degrees of freedom.

Table S-16. Dunnett's T3 multiple comparison tests results for viral vector biodistribution in cortex.

Treatment comparison	Mean Diff. (vg/dg)	95% CI	t	df*	p value
Vh vs 1E10 vg/mouse	-0.32	-1.11 to 0.47	3.076	2.000	0.2593
Vh vs 5E10 vg/mouse	-1.65	-7.42 to 4.12	2.185	2.000	0.4297
Vh vs 1E11 vg/mouse	-4.70	-10.40 to 1.00	6.304	2.000	0.0723
1E10 vg/mouse vs 5E10 vg/mouse	-1.33	-7.15 to 4.49	1.746	2.076	0.5641
1E10 vg/mouse vs 1E11 vg/mouse	-4.38	-10.13 to 1.37	5.820	2.078	0.0841
5E10 vg/mouse vs 1E11 vg/mouse	-3.05	-7.68 to 1.58	2.875	3.999	0.1754

*df = degrees of freedom. Vh=vehicle

Table S-17. Dunnett's T3 multiple comparison tests results for viral vector biodistribution in striatum.

Treatment comparison	Mean Diff. (vg/dg)	95% CI	t	df*	p value
Vh vs 1E10 vg/mouse	-0.33	-0.91 to 0.25	4.318	2.000	0.1454
Vh vs 5E10 vg/mouse	-1.02	-2.39 to 0.35	5.695	2.000	0.0875
Vh vs 1E11 vg/mouse	-3.02	-10.41 to 4.36	3.132	2.000	0.2518
1E10 vg/mouse vs 5E10 vg/mouse	-0.69	-1.71 to 0.33	3.546	2.704	0.1353
1E10 vg/mouse vs 1E11 vg/mouse	-2.69	-10.10 to 4.71	2.781	2.025	0.3038
5E10 vg/mouse vs 1E11 vg/mouse	-2.00	-9.51 to 5.51	2.040	2.138	0.4698

*df = degrees of freedom. Vh=vehicle

Table S-18. Dunnett's T3 multiple comparison tests results for Myc quantification in cortex.

Treatment comparison	Mean Diff.	95% CI	t	df*	p value
Vh vs 1E10 vg/mouse	-0.28	-0.68 to 0.11	2.470	5.009	0.1410
Vh vs 1E11 vg/mouse	-0.98	-1.26 to -0.71	11.99	5.017	0.0002
1E10 vg/mouse vs 1E11 vg/mouse	-0.70	-1.11 to -0.29	4.943	9.027	0.0023

*df = degrees of freedom. Vh=vehicle

Table S-19. Dunnett's T3 multiple comparison tests results for Myc quantification in hippocampus.

Treatment comparison	Mean Diff.	95% CI	t	df*	p value
Vh vs 1E10 vg/mouse	-0.14	-0.35 to 0.07	1.894	9.868	0.2262
Vh vs 1E11 vg/mouse	-1.01	-2.06 to 0.03	3.287	5.255	0.0563
1E10 vg/mouse vs 1E11 vg/mouse	-0.88	-1.93 to 0.18	2.829	5.322	0.0934

*df = degrees of freedom. Vh=vehicle

Table S-20. Dunnett's T3 multiple comparison tests results for PSD95 quantification in subcellular fractionation experiment, protocol 1.

Treatment comparison	Mean Diff.	95% CI	t	df*	p value
Input vs nuclei	-0.56	-1.53 to 0.40	2.134	5.5725	0.3105
Input vs cytosol	0.98	-0.09 to 2.06	0.4773	3.011	0.0639
Input vs synaptosome	-0.11	-.1.10 to 0.87	0.426	5.833	0.9975
Nuclei vs cytosol	1.54	0.68 to 2.40	9.370	3.017	0.0097
Nuclei vs synaptosome	0.45	-0.43 to 1.32	1.873	5.984	0.4185
Cytosol vs synaptosome	-1.10	-2.00 to -0.188	6.319	3.016	0.0298

*df = degrees of freedom.

Table S-21. Dunnett's T3 multiple comparison tests results for Histone H3 quantification in subcellular fractionation experiment, protocol 1.

Treatment comparison	Mean Diff.	95% CI	t	df*	p value
Input vs nuclei	-1.78	-4.12 to 0.56	3.326	4.323	0.1169
Input vs cytosol	1.00	-0.22 to 2.21	4.285	3.001	0.0546
Input vs synaptosome	1.00	-0.22 to 2.22	4.292	3.001	0.0843
Nuclei vs cytosol	2.78	0.25 to 5.30	5.758	3.000	0.0386
Nuclei vs synaptosome	2.78	0.25 to 5.30	5.761	3.000	0.0385
Cytosol vs synaptosome	0.001	-0.01 to 0.02	0.335	5.929	0.9993

*df = degrees of freedom.

Table S-22. Dunnett's T3 multiple comparison tests results for SYNGAP1 quantification in subcellular fractionation experiment, protocol 2.

Treatment comparison	Mean Diff.	95% CI	t	df*	p value
Input vs Nuclei	-0.71	-2.70 to 1.29	2.696	2.251	0.3185
Input vs Cytosol	0.87	-1.07 to 2.80	3.434	2.001	0.2163
Input vs Synaptosome	-0.99	-2.41 to 0.44	3.617	2.632	0.1290
Nuclei vs Cytosol	1.57	1.09 to 2.06	24.72	2.017	0.0049
Nuclei vs Synaptosome	-0.28	-0.91 to 0.34	2.360	3.350	0.3246
Cytosol vs Synaptosome	-1.86	-2.64 to -1.08	18.20	2.007	0.0091

*df = degrees of freedom.

Table S-23. Dunnett's T3 multiple comparison tests results for PSD95 quantification in subcellular fractionation experiment, protocol 2.

Treatment comparison	Mean Diff.	95% CI	t	df*	p value
Input vs nuclei	-0.99	-2.41 to 0.45	2.988	3.780	0.1582
Input vs cytosol	0.84	-0.71 to 2.39	4.133	2.020	0.1571
Input vs synaptosome	-0.79	-1.94 to 0.35	3.628	2.679	0.1280
Nuclei vs cytosol	1.81	-0.16 to 3.80	7.020	2.012	0.0589
Nuclei vs synaptosome	0.18	-1.89 to 2.67	0.6823	2.423	0.9613
Cytosol vs synaptosome	-1.63	-2.29 to 0.98	19.04	2.111	0.0083

*df = degrees of freedom.

Table S-24. Dunnett's T3 multiple comparison tests results for GAPDH quantification in subcellular fractionation experiment, protocol 2.

Treatment comparison	Mean Diff.	95% CI	t	df*	p value
Input vs nuclei	0.28	-1.46 to 2.02	0.8492	3.147	0.9234
Input vs cytosol	-1.93	-3.64 to -0.23	4.949	3.959	0.0328
Input vs synaptosome	-0.12	-2.03 to 1.78	0.2870	3.944	0.9996
Nuclei vs cytosol	-2.22	-3.83 to -0.60	7.188	3.346	0.0208
Nuclei vs synaptosome	-0.41	-2.32 to 1.50	1.117	2.935	0.8175
Cytosol vs synaptosome	1.81	-0.02 to 3.64	4.318	3.818	0.0518

*df = degrees of freedom.

Table S-25. RM Two-way ANOVA, WT(Vh) vs Syngap1$^{+/-}$ (Vh), 7 weeks of age.

	Mean Diff. (cm)	95% CI	t	df*	p
Genotype effect, Šídák multiple comparisons tests between genotypes					
5 min	-3671	-5565 to -1777	5.145	29.18	<0.0001
10 min	-3790	-5932 to -1647	4.687	29.99	0.0002
15 min	-3319	-5273 to -1365	4.529	27.30	0.0004
20 min	-3339	-5085 to -1593	5.176	22.44	0.0001
Time effect, Tukey's multiple comparisons tests within genotypes					
WT (Vh)					
15 min vs 30 min	2502	1528 to 3476	10.470	15.00	<0.0001
15 min vs 45 min	37776	2888 to 4664	17.330	15.00	<0.0001
15 min vs 60 min	4659	3656 to 5662	18.930	15.00	<0.0001
30 min vs 45 min	1275	502.7 to 2047	6.730	15.00	0.0013
30 min vs 60 min	2157	1059 to 3254	8.011	15.00	0.0002
45 min vs 60 min	882.3	43.52 to 1721	4.287	15.00	0.0377
Syngap1$^{+/-}$ (Vh)					
15 min vs 30 min	2383	1480 to 3287	10.750	15.00	<0.0001
15 min vs 45 min	4128	2850 to 5406	13.170	15.00	<0.0001
15 min vs 60 min	4991	3912 to 6070	18.860	15.00	<0.0001
30 min vs 45 min	1745	897.2 to 2593	8.389	15.00	0.0001
30 min vs 60 min	2608	1846 to 3369	13.960	15.00	<0.0001
45 min vs 60 min	862.6	-49.16 to 1774	3.856	15.00	0.0667

*df = degrees of freedom. Vh=vehicle, WT=wild-type.

Table S-26. RM Two way ANOVA, time effect, Tukey's multiple comparisons tests within treatment groups at 7 weeks of age.

	Mean Diff. (cm)	95% CI	t	df*	p value
Vh					
15 min vs 30 min	2383	1480 to 3287	10.750	15.00	<0.0001
15 min vs 45 min	4128	2850 to 5406	13.170	15.00	<0.0001
15 min vs 60 min	4991	3912 to 6070	18.860	15.00	<0.0001
30 min vs 45 min	1745	897.2 to 2593	8.389	15.00	0.0001
30 min vs 60 min	2608	1846 to 3369	13.960	15.00	<0.0001
45 min vs 60 min	862.6	-49.16 to 1774	3.856	15.00	0.0667
5E10 vg/mouse					
15 min vs 30 min	2589	1791 to 3387	13.470	13.00	<0.0001
15 min vs 45 min	3599	2254 to 4945	11.10	13.00	<0.0001
15 min vs 60 min	4665	3220 to 6109	13.410	13.00	<0.0001

30 min vs 45 min	1010	279.7 to 1741	5.741	13.00	0.0065
30 min vs 60 min	2075	991.4 to 3159	7.948	13.00	0.0004
45 min vs 60 min	1065	391.0 to 1739	6.558	13.00	0.0023
1E11 vg/mouse					
15 min vs 30 min	1809	793.0 to 2825	7.475	12.00	0.0010
15 min vs 45 min	3208	1721 to 4694	9.060	12.00	0.0002
15 min vs 60 min	4098	2572 to 5624	11.270	12.00	<0.0001
30 min vs 45 min	1398	140.3 to 2656	4.667	12.00	0.0281
30 min vs 60 min	2289	658.4 to 3919	5.894	12.00	0.0062
45 min vs 60 min	890.3	-218.5 to 1999	3.371	12.00	0.1334

*df = degrees of freedom. Vh=vehicle.

Table S-27. RM Two way ANOVA, WT(Vh) vs Syngap1$^{+/-}$(Vh), 15 weeks of age.

	Mean Diff. (cm)	**95% CI**	**t**	**df***	**p value**
Genotype effect, Šídák multiple comparisons tests between genotypes					
5 min	-6712	-8842 to -4582	8.554	21.74	<0.0001
10 min	-5642	-7441 to -3844	8.455	23.62	<0.0001
15 min	-5706	-7734 to -3678	7.604	22.90	<0.0001
20 min	-5219	-7079 to -3360	7.525	25.26	<0.0001
Time effect, Tukey's multiple comparisons tests within genotypes					
WT (Vh)					
15 min vs 30 min	698.4	-57.09 to 1454	3.768	15.00	0.0748
15 min vs 45 min	1019	114.3 to 1923	4.591	15.00	0.0249
15 min vs 60 min	1388	490.1 to 2285	6.301	15.00	0.0023
30 min vs 45 min	320.4	-135.3 to 776.1	2.865	15.00	0.2221
30 min vs 60 min	689.2	12.57 to 1366	4.152	15.00	0.0452
45 min vs 60 min	369.8	-328.0 to 1066	2.157	15.00	0.4476
Syngap1$^{+/-}$ (Vh)					
15 min vs 30 min	1768	639.7 to 2897	6.387	15.00	0.0021
15 min vs 45 min	2025	780.6 to 3269	6.633	15.00	0.0015
15 min vs 60 min	2880	1242 to 4519	7.165	15.00	0.0007
30 min vs 45 min	256.9	-385.5 to 899.3	1.630	15.00	0.6642
30 min vs 60 min	1112	90.2 to 2135	4.436	15.00	0.0308
45 min vs 60 min	855.5	-110.8 to 1822	3.609	15.00	0.0917

*df = degrees of freedom. Vh=vehicle, WT=wild-type.

Table S-28. RM Two way ANOVA, time effect, Tukey's multiple comparisons tests within treatment groups at 15 weeks of age.

	Mean Diff. (cm)	95% CI	t	df*	p value
Vh					
15 min vs 30 min	1768	639.7 to 2897	6.387	15.00	0.0021
15 min vs 45 min	2025	780.6 to 3269	6.633	15.00	0.0015
15 min vs 60 min	2880	1242 to 4519	7.165	15.00	0.0007
30 min vs 45 min	256.9	-385.5 to 899.3	1.630	15.00	0.6642
30 min vs 60 min	1112	90.2 to 2135	4.436	15.00	0.0308
45 min vs 60 min	855.5	-110.8 to 1822	3.609	15.00	0.0917
5E10 vg/mouse					
15 min vs 30 min	817.5	-932.3 to 2567	1.939	13.00	0.5375
15 min vs 45 min	729.7	-2029 to 3488	1.098	13.00	0.8637
15 min vs 60 min	1021	-1825 to 3868	1.490	13.00	0.7224
30 min vs 45 min	-87.73	-1386 to 1210	0.281	13.00	0.9971
30 min vs 60 min	204.0	-1277 to 1685	0.571	13.00	0.9767
45 min vs 60 min	291.7	-949.1 to 1533	0.976	13.00	0.8991
1E11 vg/mouse					
15 min vs 30 min	171.5	-2397 to 2740	0.280	12.00	0.9971
15 min vs 45 min	25.9	-3588 to 3640	0.030	12.00	>0.9999
15 min vs 60 min	215.0	-3755 to 4185	0.227	12.00	0.9984
30 min vs 45 min	-145.6	-1599 to 1308	0.421	12.00	0.9904
30 min vs 60 min	43.48	-2580 to 2667	0.070	12.00	>0.9999
45 min vs 60 min	189.1	-1663 to 2041	0.429	12.00	0.9898

*df = degrees of freedom. Vh=vehicle.

Table S-29. Dunnett's T3 multiple comparison tests results, wild-type treated, platform departure at 7 weeks.

Treatment comparison	Mean Diff.	95% CI	t	df*	p value
Vh vs 5E10 vg/mouse	-6.56	-12.44 to -0.67	2.882	28.49	0.0255
Vh vs 1E11 vg/mouse	-8.90	-19.61 to 1.80	2.129	23.86	0.1228
5E10 vg/mouse vs 1E11 vg/mouse	-2.35	-13.57 to 8.88	0.529	28.78	0.9337

*df = degrees of freedom. Vh=vehicle.

Table S-30. Syllable usage comparison, WT(Vh) vs Syngap1$^{+/-}$(Vh). Two-tailed Mann-Whitney test.

	WT_Vh n = 19		***Syngap1*$^{+/-}$_Vh n = 17**			
Syllable	**Median**	**95% CI**	**Median**	**95% CI**	**U**	**p**
0	0.028	0.028 to 0.039	0.059	0.052 to 0.072	18	<0.0001
1	0.062	0.058 to 0.099	0.011	0.0064 to 0.038	25	<0.0001
2	0.023	0.020 to 0.033	0.062	0.043 to 0.064	43	<0.0001
3	0.026	0.022 to 0.032	0.040	0.038 to 0.052	53.5	0.0004
4	0.03	0.025 to 0.040	0.034	0.027 to 0.046	146	0.6386
5	0.028	0.029 to 0.056	0.023	0.020 to 0.037	86	0.0158
6	0.037	0.030 to 0.049	0.017	0.016 to 0.034	88	0.0194
7	0.019	0.015 to 0.027	0.04	0.034 to 0.052	44	<0.0001
8	0.024	0.018 to 0.035	0.034	0.028 to 0.038	114	0.1356
9	0.018	0.016 to 0.023	0.035	0.029 to 0.043	41	<0.0001
10	0.018	0.013 to 0.027	0.030	0.023 to 0.040	97	0.0415
11	0.014	0.013 to 0.023	0.029	0.024 to 0.048	70	0.0031
12	0.012	0.0088 to 0.020	0.041	0.029 to 0.045	39	<0.0001
13	0.0064	0.0058 to 0.015	0.031	0.025 to 0.039	28	<0.0001
14	0.041	0.029 to 0.050	0.011	0.0076 to 0.022	45	0.0001
15	0.0092	0.0076 to 0.017	0.039	0.023 to 0.041	58	0.0007
16	0.026	0.020 to 0.029	0.020	0.016 to 0.028	129	0.3147
17	0.017	0.013 to 0.023	0.022	0.016 to 0.043	118	0.1724
18	0.019	0.018 to 0.030	0.019	0.013 to 0.024	126	0.2711
19	0.013	0.011 to 0.018	0.025	0.021 to 0.032	63	0.0013
20	0.028	0.024 to 0.038	0.0072	0.0068 to 0.023	53	0.0003
21	0.018	0.015 to 0.026	0.027	0.021 to 0.032	105	0.0758
22	0.016	0.015 to 0.027	0.021	0.015 to 0.031	149	0.7072
23	0.026	0.020 to 0.040	0.0054	0.0038 to 0.013	25	<0.0001
24	0.019	0.017 to 0.028	0.017	0.013 to 0.022	119	0.1856
25	0.0099	0.0068 to 0.013	0.023	0.018 to 0.032	47	0.0001
26	0.014	0.0098 to 0.018	0.018	0.012 to 0.024	125	0.2573
27	0.025	0.020 to 0.035	0.0079	0.0058 to 0.017	55	0.0005
28	0.014	0.010 to 0.023	0.021	0.012 to 0.029	137	0.4466
29	0.012	0.0087 to 0.023	0.017	0.010 to 0.024	143.5	0.5786
30	0.017	0.015 to 0.028	0.0083	0.0061 to 0.015	73	0.0043
31	0.012	0.0088 to 0.021	0.013	0.010 to 0.018	150	0.7306
32	0.022	0.015 to 0.041	0.0042	0.0023 to 0.013	52	0.0003
33	0.021	0.017 to 0.034	0.0031	0.0012 to 0.014	38	<0.0001
34	0.025	0.015 to 0.028	0.0028	0.0023 to 0.0068	28	<0.0001
35	0.004	0.0036 to 0.0096	0.017	0.011 to 0.023	76.5	0.0061
36	0.014	0.0089 to 0.019	0.0014	0.0012 to 0.0050	53	0.0003
37	0.01	0.0079 to 0.028	0.0043	0.0030 to 0.0065	98.5	0.0457
38	0	-0.0000089 to 0.0018	0.0050	0.0038 to 0.010	30	<0.0001

39	0.01	0.0057 to 0.012	0.010	0.0059 to 0.014	157.5	0.9063
40	0.0096	0.0084 to 0.021	0.0034	0.0012 to 0.011	69	0.0027
41	0.0011	0.00071 to 0.0054	0.0065	0.0043 to 0.0086	56	0.0005
42	0.011	0.0097 to 0.019	0.0054	0.0034 to 0.0073	48	0.0002
43	0.0068	0.0063 to 0.016	0.0050	0.0036 to 0.0084	116	0.1555
44	0.0047	0.0040 to 0.0067	0.0067	0.0060 to 0.0094	91	0.0252
45	0.0037	0.0032 to 0.0061	0.0066	0.0053 to 0.0078	93	0.0294
46	0.0056	0.0034 to 0.0075	0.0017	0.00092 to 0.0045	104	0.0702
47	0.00092	0.00067 to 0.0060	0.0042	0.0031 to 0.0091	98	0.0433
48	0.003	0.0029 to 0.0067	0.0025	0.0017 to 0.0051	125	0.2542
49	0.0011	0.00096 to 0.011	0.0036	0.0017 to 0.0083	141	0.522
50	0.0061	0.0047 to 0.0078	0.00083	0.00067 to 0.0024	30	<0.0001
51	0.0028	0.0021 to 0.0097	0.00069	0.00031 to 0.0041	87	0.0169

Vh=vehicle, WT=wild-type.

Table S-31. Syllable usage comparison among wild-type treatment groups. Kruskal-Wallis test.

	WT_Vh n=19		**WT_5E10 vg/mouse n=18**		**WT_1E11 vg/mouse n=21**			
Syllable	**Median**	**95% CI**	**Median**	**95% CI**	**Median**	**95% CI**	**H**	**p**
0	0.028	0.028 to 0.039	0.039	0.034 to 0.051	0.042	0.035 to 0.048	4.400	0.1132
1	0.062	0.058 to 0.099	0.056	0.042 to 0.076	0.066	0.051 to 0.089	2.160	0.3395
2	0.023	0.020 to 0.033	0.033	0.027 to 0.041	0.030	0.025 to 0.043	2.813	0.2450
3	0.026	0.022 to 0.032	0.035	0.032 to 0.041	0.039	0.030 to 0.044	6.905	0.0317
4	0.030	0.025 to 0.040	0.033	0.027 to 0.038	0.031	0.022 to 0.036	0.670	0.7153
5	0.028	0.029 to 0.056	0.023	0.023 to 0.044	0.027	0.028 to 0.053	3.688	0.1581
6	0.037	0.030 to 0.049	0.046	0.041 to 0.058	0.032	0.026 to 0.045	8.709	0.0128
7	0.019	0.015 to 0.027	0.026	0.021 to 0.034	0.019	0.014 to 0.025	4.509	0.1049
8	0.024	0.018 to 0.035	0.023	0.019 to 0.030	0.021	0.019 to 0.030	0.117	0.9430
9	0.018	0.016 to 0.023	0.023	0.021 to 0.034	0.020	0.016 to 0.023	4.848	0.0885
10	0.018	0.013 to 0.027	0.0095	0.0082 to 0.013	0.011	0.0090 to 0.019	4.490	0.1059
11	0.014	0.013 to 0.023	0.019	0.015 to 0.026	0.014	0.010 to 0.019	3.705	0.1568
12	0.012	0.0088 to 0.020	0.010	0.0089 to 0.015	0.013	0.010 to 0.020	0.397	0.8201

13	0.0064	0.0058 to 0.015	0.0084	0.006 to 0.0099	0.014	0.011 to 0.021	10.040	0.0066
14	0.041	0.029 to 0.050	0.033	0.023 to 0.040	0.031	0.024 to 0.040	1.830	0.4005
15	0.0092	0.0076 to 0.017	0.016	0.011 to 0.019	0.012	0.0099 to 0.023	1.770	0.4127
16	0.026	0.020 to 0.029	0.029	0.023 to 0.039	0.024	0.021 to 0.030	1.109	0.5745
17	0.017	0.013 to 0.023	0.030	0.021 to 0.038	0.015	0.0098 to 0.018	10.380	0.0056
18	0.019	0.018 to 0.030	0.023	0.019 to 0.035	0.021	0.019 to 0.034	0.272	0.873
19	0.013	0.011 to 0.018	0.022	0.017 to 0.026	0.018	0.016 to 0.029	8.229	0.0163
20	0.028	0.024 to 0.038	0.027	0.021 to 0.035	0.034	0.029 to 0.050	3.062	0.2163
21	0.018	0.015 to 0.026	0.028	0.023 to 0.035	0.023	0.017 to 0.026	6.808	0.332
22	0.016	0.015 to 0.027	0.021	0.018 to 0.025	0.019	0.015 to 0.024	1.121	0.571
23	0.026	0.020 to 0.040	0.024	0.019 to 0.032	0.028	0.022 to 0.044	0.351	0.8388
24	0.019	0.017 to 0.028	0.027	0.024 to 0.036	0.019	0.017 to 0.032	4.355	0.1134
25	0.0099	0.0068 to 0.013	0.015	0.0094 to 0.019	0.0098	0.0063 to 0.014	2.478	0.2897
26	0.014	0.0098 to 0.018	0.011	0.0067 to 0.014	0.016	0.012 to 0.022	3.660	0.1604
27	0.025	0.020 to 0.035	0.021	0.018 to 0.030	0.020	0.012 to 0.034	2.604	0.2719
28	0.014	0.010 to 0.023	0.0073	0.0046 to 0.0096	0.0075	0.0067 to 0.012	5.128	0.0770
29	0.012	0.0087 to 0.023	0.0073	0.0059 to 0.016	0.012	0.010 to 0.019	2.133	0.3442
30	0.017	0.015 to 0.028	0.015	0.012 to 0.021	0.014	0.011 to 0.019	1.955	0.3762
31	0.012	0.0088 to 0.021	0.011	0.0084 to 0.020	0.011	0.010 to 0.023	0.353	0.8383
32	0.022	0.015 to 0.041	0.016	0.013 to 0.025	0.017	0.012 to 0.028	1.037	0.5954
33	0.021	0.017 to 0.034	0.017	0.013 to 0.024	0.021	0.015 to 0.026	1.059	0.589
34	0.025	0.015 to 0.028	0.011	0.0089 to 0.020	0.016	0.015 to 0.029	3.643	0.1618
35	0.0040	0.0036 to 0.0096	0.0028	0.0018 to 0.0038	0.0063	0.0047 to 0.010	10.600	0.0050
36	0.014	0.0089 to 0.019	0.014	0.011 to 0.026	0.016	0.011 to 0.031	0.880	0.6442
37	0.010	0.0079 to 0.028	0.011	0.0087 to 0.020	0.014	0.0097 to 0.019	0.256	0.8797
38	0	-0.0000089 to 0.0018	0	-0.000041 to 0.00023	0.00094	0.00048 to 0.0054	14.790	0.0006

39	0.010	0.0057 to 0.012	0.017	0.012 to 0.025	0.0085	0.0056 to 0.011	10.210	0.0061
40	0.0096	0.0084 to 0.021	0.015	0.011 to 0.020	0.014	0.010 to 0.023	0.514	0.7733
41	0.0011	0.00071 to 0.0054	0.0017	0.0014 to 0.0063	0.0031	0.0021 to 0.0078	2.571	0.2765
42	0.011	0.0097 to 0.019	0.0075	0.0063 to 0.012	0.012	0.0094 to 0.017	3.953	0.1386
43	0.0068	0.0063 to 0.016	0.004	0.0028 to 0.0071	0.0097	0.0077 to 0.013	9.738	0.0077
44	0.0047	0.0040 to 0.0067	0.0088	0.0064 to 0.010	0.0058	0.0049 to 0.0082	6.544	0.379
45	0.0037	0.0032 to 0.0061	0.0076	0.0066 to 0.0099	0.0056	0.0044 to 0.0092	7.840	0.0198
46	0.0056	0.0034 to 0.0075	0.0038	0.0024 to 0.0073	0.0058	0.0044 to 0.011	1.590	0.4515
47	0.00092	0.00067 to 0.0060	0	0.000076 to 0.012	0.0011	0.00037 to 0.0048	6.989	0.0304
48	0.0030	0.0029 to 0.0067	0.0032	0.0021 to 0.0093	0.0039	0.0038 to 0.0096	2.287	0.3187
49	0.0011	0.00096 to 0.011	0.0013	0.00064 to 0.0022	0.0011	0.00095 to 0.0047	1.530	0.4653
50	0.0061	0.0047 to 0.0078	0.0087	0.0078 to 0.011	0.0065	0.0052 to 0.011	7.004	0.0301
51	0.0028	0.0021 to 0.0097	0.0029	0.0020 to 0.0072	0.0022	0.0015 to 0.0038	1.624	0.4440

Vh=vehicle, WT=wild-type.

Table S-32. Dunn's multiple comparison test for syllable usage of among wild-type mice treatment groups.

Comparison	Mean Rank diff.	z	p	Mean Rank diff.	z	p
	Syllable 3			**Syllable 38**		
Vh vs 5E10 vg/mouse	-12.000	2.200	0.0870	7.900	1.600	0.3180
Vh vs 1E11 vg/mouse	-13.000	2.400	0.0540	-10.000	2.200	0.0850
5E10 vg/mouse vs 1E11 vg/mouse	-0.530	0.098	>0.9999	-18.000	3.800	0.0004
	Syllable 6			**Syllable 39**		
Vh vs 5E10 vg/mouse	-12.000	2.100	0.0970	-14.000	2.500	0.0350
Vh vs 1E11 vg/mouse	3.600	0.670	>0.9999	2.200	0.410	>0.9999
5E10 vg/mouse vs 1E11 vg/mouse	15.000	2.900	0.0130	16.000	3.000	0.0083
	Syllable 13			**Syllable 43**		
Vh vs 5E10 vg/mouse	1.100	0.190	>0.9999	13.000	2.300	0.0690
Vh vs 1E11 vg/mouse	-14.000	2.600	0.0260	-3.700	0.690	>0.9999
5E10 vg/mouse vs 1E11 vg/mouse	-15.000	2.800	0.0157	-16.000	3.000	0.0078
	Syllable 17			**Syllable 44**		
Vh vs 5E10 vg/mouse	-12.000	2.100	0.1100	-14.000	2.600	0.0320

Vh vs 1E11 vg/mouse	5.700	1.100	0.8690	-6.200	1.200	0.7320
5E10 vg/mouse vs 1E11 vg/mouse	17.000	3.200	0.0044	8.000	1.500	0.4273
	Syllable 19			**Syllable 45**		
Vh vs 5E10 vg/mouse	-15.000	2.800	0.0160	-16.000	2.800	0.0160
Vh vs 1E11 vg/mouse	-11.000	2.000	0.1400	-6.700	1.300	0.6330
5E10 vg/mouse vs 1E11 vg/mouse	4.900	0.900	>0.9999	8.800	1.600	0.3110
	Syllable 21			**Syllable 47**		
Vh vs 5E10 vg/mouse	-14.000	2.500	0.040	11.000	2.000	0.132
Vh vs 1E11 vg/mouse	-2.800	0.530	>0.9999	-2.400	0.460	>0.9999
5E10 vg/mouse vs 1E11 vg/mouse	11	2	0.1336	-13	2.5	0.0356
	Syllable 35			**Syllable 50**		
Vh vs 5E10 vg/mouse	12.000	2.200	0.084	-14.000	2.500	0.039
Vh vs 1E11 vg/mouse	-5.200	0.960	>0.9999	-2.500	0.470	>0.9999
5E10 vg/mouse vs 1E11 vg/mouse	-17	3.2	0.0041	11	2.1	0.1116

Vh=vehicle.

Table S-33. Syllable usage comparison among Syngap1$^{+/-}$ mice treatment groups. Kruskal-Wallis test.

	***Syngap1*$^{+/-}$_Vh n=17**		***Syngap1*$^{+/-}$_5E10 vg/mouse n=13**		***Syngap1*$^{+/-}$_1E11 vg/mouse n=13**			
Syllable	**Median**	**95% CI**	**Median**	**95% CI**	**Median**	**95% CI**	**H**	**p**
0	0.059	0.052 to 0.072	0.060	0.046 to 0.067	0.069	0.055 to 0.089	3.000	0.1964
1	0.011	0.0064 to 0.038	0.0085	0.0052 to 0.030	0.0096	0.0038 to 0.032	0.5387	0.7639
2	0.062	0.043 to 0.064	0.050	0.038 to 0.060	0.055	0.042 to 0.067	1.072	0.5851
3	0.040	0.038 to 0.052	0.042	0.030 to 0.049	0.053	0.039 to 0.066	4.138	0.1263
4	0.034	0.027 to 0.046	0.063	0.037 to 0.069	0.030	0.023 to 0.040	4.107	0.1342
5	0.023	0.020 to 0.037	0.025	0.018 to 0.035	0.027	0.019 to 0.062	3.181	0.2038
6	0.017	0.016 to 0.034	0.011	0.0084 to 0.022	0.011	0.0089 to 0.019	4.054	0.1317
7	0.040	0.034 to 0.052	0.029	0.022 to 0.039	0.034	0.025 to 0.040	5.041	0.0804
8	0.034	0.028 to 0.038	0.036	0.022 to 0.042	0.021	0.013 to 0.029	6.588	0.0371
9	0.035	0.029 to 0.043	0.027	0.020 to 0.039	0.033	0.024 to 0.045	2.459	0.2924
10	0.030	0.023 to 0.040	0.042	0.027 to 0.052	0.030	0.025 to 0.047	1.455	0.4832
11	0.029	0.024 to 0.048	0.043	0.024 to 0.052	0.029	0.018 to 0.034	2.089	0.3519
12	0.041	0.029 to 0.045	0.033	0.025 to 0.042	0.039	0.027 to 0.041	0.900	0.6377

13	0.031	0.025 to 0.039	0.048	0.036 to 0.054	0.032	0.030 to 0.052	4.829	0.094
14	0.011	0.0076 to 0.022	0.0053	0.0042 to 0.020	0.011	0.0063 to 0.024	1.135	0.567
15	0.039	0.023 to 0.041	0.024	0.019 to 0.041	0.034	0.022 to 0.046	0.221	0.8956
16	0.020	0.016 to 0.028	0.013	0.011 to 0.024	0.016	0.011 to 0.031	1.046	0.5927
17	0.022	0.016 to 0.043	0.038	0.016 to 0.044	0.011	0.0080 to 0.018	5.296	0.0708
18	0.019	0.013 to 0.024	0.016	0.011 to 0.034	0.013	0.0094 to 0.017	3.107	0.2115
19	0.025	0.021 to 0.032	0.016	0.013 to 0.028	0.027	0.018 to 0.038	2.602	0.2722
20	0.0072	0.0068 to 0.023	0.0042	0.0038 to 0.019	0.0082	0.0050 to 0.013	1.578	0.4544
21	0.027	0.021 to 0.032	0.013	0.0096 to 0.027	0.013	0.0080 to 0.028	4.791	0.0911
22	0.021	0.015 to 0.031	0.017	0.013 to 0.033	0.016	0.010 to 0.022	2.184	0.3356
23	0.0054	0.0038 to 0.013	0.005	0.0025 to 0.010	0.0061	0.0032 to 0.019	0.4404	0.8023
24	0.017	0.013 to 0.022	0.010	0.0070 to 0.015	0.010	0.0056 to 0.018	4.894	0.0866
25	0.023	0.018 to 0.032	0.027	0.018 to 0.039	0.017	0.012 to 0.021	4.331	0.1147
26	0.018	0.012 to 0.024	0.018	0.011 to 0.028	0.024	0.017 to 0.037	2.452	0.2934
27	0.0079	0.0058 to 0.017	0.0023	0.00018 to 0.023	0.0059	0.0028 to 0.011	2.456	0.2933
28	0.021	0.012 to 0.029	0.014	0.0095 to 0.020	0.022	0.018 to 0.030	4.919	0.0855
29	0.017	0.010 to 0.024	0.014	0.0075 to 0.021	0.015	0.0089 to 0.028	0.3437	0.8421
30	0.0083	0.0061 to 0.015	0.015	0.0079 to 0.028	0.0089	0.0049 to 0.020	1.556	0.4592
31	0.013	0.010 to 0.018	0.011	0.0056 to 0.017	0.0041	0.0011 to 0.012	8.4	0.0150
32	0.0042	0.0023 to 0.013	0.0019	0.00032 to 0.0064	0.0023	0.00085 to 0.0078	2.65	0.2657
33	0.0031	0.0012 to 0.014	0.00077	-0.00013 to 0.0074	0.003	0.00075 to 0.0072	3.357	0.1866
34	0.0028	0.0023 to 0.0068	0.0021	0.0010 to 0.014	0.0046	0.0023 to 0.013	0.503	0.7777
35	0.017	0.011 to 0.023	0.015	0.0099 to 0.021	0.026	0.020 to 0.032	7.907	0.0192
36	0.0014	0.0012 to 0.0050	0.0023	0.0021 to 0.0087	0.00084	0.0011 to 0.0055	3.209	0.2010
37	0.0043	0.0030 to 0.0065	0.0049	0.0029 to 0.011	0.0044	0.0019 to 0.0076	0.560	0.7570

38	0.0050	0.0038 to 0.010	0.020	-0.0013 to 0.063	0.011	0.0026 to 0.061	4.472	0.1059
39	0.010	0.0059 to 0.014	0.0065	0.0032 to 0.016	0.0020	0.0020 to 0.0074	3.851	0.1458
40	0.0034	0.0012 to 0.011	0.0015	0.00074 to 0.0031	0.0023	0.0013 to 0.0049	2.293	0.3178
41	0.0065	0.0043 to 0.0086	0.0094	-0.0049 to 0.047	0.0083	0.0048 to 0.033	4.305	0.1162
42	0.0054	0.0034 to 0.0073	0.0021	0.0011 to 0.0069	0.0059	0.0035 to 0.0087	3.406	0.1821
43	0.005	0.0036 to 0.0084	0.0051	0.0026 to 0.0077	0.0044	0.0030 to 0.0097	0.141	0.9319
44	0.0067	0.0060 to 0.0094	0.0085	0.0051 to 0.014	0.0099	0.0046 to 0.014	0.323	0.8509
45	0.0066	0.0053 to 0.0078	0.0098	0.0066 to 0.012	0.012	0.0085 to 0.016	9.900	0.0072
46	0.0017	0.00092 to 0.0045	0.0047	0.0028 to 0.0065	0.0026	0.00078 to 0.0082	4.650	0.0978
47	0.0042	0.0031 to 0.0091	0.0046	0.0019 to 0.014	0.0070	0.0050 to 0.016	3.044	0.2182
48	0.0025	0.0017 to 0.0051	0.0019	0.0012 to 0.0059	0.0024	0.0010 to 0.0056	0.099	0.9516
49	0.0036	0.0017 to 0.0083	0.0026	0.0014 to 0.0044	0.0046	0.0010 to 0.019	5.342	0.0692
50	0.00083	0.00067 to 0.0024	0	0.00011 to 0.0011	0.00078	-0.00025 to 0.0061	2.529	0.2824
51	0.00069	0.00031 to 0.0041	0.00085	0.00061 to 0.0027	0.002	-0.0078 to 0.035	3.267	0.1953

Vh=vehicle.

Table S-34. Dunn's multiple comparison test for syllable usage of among wild-type treatment groups.

Comparison	Mean Rank diff.	z	p	Mean Rank diff.	z	p
	Syllable 8			Syllable 35		
Vh vs 5E10 vg/mouse	0.410	0.089	>0.9999	1.000	0.220	>0.9999
Vh vs 1E11 vg/mouse	11.000	2.400	0.0560	-11.000	2.400	0.0450
5E10 vg/mouse vs 1E11 vg/mouse	10.00	2.100	0.1010	-12.000	2.500	0.0382
	Syllable 31			Syllable 45		
Vh vs 5E10 vg/mouse	4.700	1.000	0.9160	-9.000	1.900	0.1580
Vh vs 1E11 vg/mouse	13.000	2.900	0.0120	-14.000	3.100	0.0070
5E10 vg/mouse vs 1E11 vg/mouse	8.600	1.700	0.2404	-5.200	1.100	0.8646

Vh=vehicle.

Table S-35. Dunnett's T3 multiple comparison tests results for viral vector biodistribution in cortex.

Treatment comparison	Mean Diff. (vg/dg)	95% CI	t	df*	p value
Vh vs 5E10 vg/mouse	-0.82	-2.075 to 0.43	2.452	4.000	0.1676
Vh vs 1E11 vg/mouse	-0.61	-1.45 to 0.24	2.693	4.000	0.1316
5E10 vg/mouse vs 1E11 vg/mouse	0.21	-1.020 to 1.45	0.529	7.011	0.9315

*df = degrees of freedom. Vh=vehicle.

Table S-36. Dunnett's T3 multiple comparison tests results for viral vector biodistribution in hippocampus.

Treatment comparison	Mean Diff. (vg/dg)	95% CI	t	df*	p value
Vh vs 5E10 vg/mouse	-0.57	-1.67 to 0.53	1.944	4.000	0.2831
Vh vs 1E11 vg/mouse	-0.58	-1.14 to -0.023	3.901	4.000	0.0439
5E10 vg/mouse vs 1E11 vg/mouse	-0.0093	-1.059 to 1.04	0.0285	5.926	>0.9999

*df = degrees of freedom. Vh=vehicle.

Table S-37. Dunnett's T3 multiple comparison tests results for viral vector biodistribution in striatum.

Treatment comparison	Mean Diff. (vg/dg)	95% CI	t	df*	p value
Vh vs 5E10 vg/mouse	-1.015	-3.67 to 1.64	1.429	4.000	0.4792
Vh vs 1E11 vg/mouse	-0.47	-0.99 to 0.047	3.408	4.000	0.0670
5E10 vg/mouse vs 1E11 vg/mouse	0.54	-2.17 to 3.25	0.751	4.303	0.8358

*df = degrees of freedom. Vh=vehicle.

Table S-38. Dunnett's T3 multiple comparison tests results for viral vector biodistribution in thalamus.

Treatment comparison	Mean Diff. (vg/dg)	95% CI	t	df*	p value
Vh vs 5E10 vg/mouse	-0.60	-1.55 to 0.35	2.371	4.000	0.1820
Vh vs 1E11 vg/mouse	-0.24	-0.47 to -0.015	3.989	4.000	0.0408
5E10 vg/mouse vs 1E11 vg/mouse	0.36	0.62 to 1.33	1.380	4.454	0.5026

*df = degrees of freedom. Vh=vehicle.

Table S-39. Dunnett's T3 multiple comparison tests results for viral vector biodistribution in cerebellum.

Treatment comparison	Mean Diff. (vg/dg)	95% CI	t	df*	p value
Vh vs 5E10 vg/mouse	-0.0046	-0.0095 to 000028	3.534	4.00	0.0600
Vh vs 1E11 vg/mouse	-0.0073	-0.013 to -0.0019	5.026	4.00	0.0187
5E10 vg/mouse vs 1E11 vg/mouse	-0.0027	-0.0084 to 0.0031	1.360	7.919	0.4788

*df = degrees of freedom. Vh=vehicle.

Table S-40. Dunnett's T3 multiple comparison tests results for FLAG quantification in cortex.

Treatment comparison	Mean Diff.	95% CI	t	df*	p value
Vh vs 5E10 vg/mouse	-0.50	-1.33 to 0.33	2.039	5.036	0.2333
Vh vs 1E11 vg/mouse	-0.98	-1.74 to -0.22	4.366	50.43	0.0192
5E10 vg/mouse vs 1E11 vg/mouse	-0.48	-1.42 to 0.45	1.454	9.928	0.4192

*df = degrees of freedom. Vh=vehicle.

Table S-41. Dunnett's T3 multiple comparison tests results for FLAG quantification in hippocampus.

Treatment comparison	Mean Diff.	95% CI	t	df*	p value
Vh vs 5E10 vg/mouse	-0.48	-1.01 to -0.04	3.130	5.102	0.0668
Vh vs 1E11 vg/mouse	-0.96	-1.89 to -0.03	3.512	5.032	0.0444
5E10 vg/mouse vs 1E11 vg/mouse	-0.48	-1.40 to 0.45	1.522	7.880	0.3936

*df = degrees of freedom. Vh=vehicle.

APPENDIX C: SUBCELLULAR FRACTIONATION, IMMUNOBLOTTING AND qPCR REACTION PROTOCOL OPTIMISATION

C.1 PROTOCOL OPTIMISATION FOR SYNAPTOSOMAL PREPARATION

In Chapter 2 the optimised protocol for synaptosome preparation is described in detail. Here I am going to discuss the steps of optimisation of the protocol originally described by Bermejo *et al.* (Bermejo *et al.*, 2014)

Volume of homogenisation buffer was not sufficient to obtain an optimal homogenisation of the input tissue

In the original protocol (Bermejo *et al.*, 2014), a starting input of 100-200 mg of tissue was used, which corresponded to about 3/6 hippocampi from different animals (around 30 mg per hippocampus). Here the protocol was adapted for the homogenisation of one hippocampus, therefore the volume of homogenisation needed to be adjusted to avoid excessive dilution.

The modified procedure is described in Figure S-1. Briefly, a whole hippocampus was homogenised in 1 ml of buffer. After the first low speed centrifugation (900xg for 10 minutes) the formed pellet represented the nuclear fraction, while the supernatant was the soluble fraction. The soluble fraction was subsequently centrifuged and the pellet obtained was the synaptosomal fraction 1 while the supernatant corresponded to the cytosolic fraction 1. Synaptosomal fraction 1 was resuspended in buffer and centrifuged again. The obtained pellet corresponded to the final synaptosomal fraction. The two cytosolic fractions were then combined.

Immunoblot analysis showed (Figure S-2a) how, although the protocol led to a poor enrichment of the synaptic marker PSD95 in the synaptosomal fraction (Figure S-2b; Welch's ANOVA, mean ± SEM; n=4, input 1.00 ± 0.20, Nuclei 1.56 ± 0.16, cytosol 0.02 ± 0.01, synaptosome 1.11 ± 0.17, $W_{(3.00,\ 5.024)}$=39.47, p=0.0006, Dunnett's multiple comparisons test results are reported in Table S-20), cytosolic and synaptosomal fractions showed no contamination of nuclear markers (Figure S-2d; Welch's ANOVA,

mean ± SEM; n=4, input 1.00 ± 0.23, nuclei 2.78 ± 0.48, cytosol 0.003 ± 0.003, synaptosome 0.001 ± 0.003, $W_{(3.00,\ 5.986)}$=14.09, p=0.0040, Dunnett's multiple comparisons test results are reported in Table S-21). Moreover, no enrichment of GAPDH protein was observed (Figure S-2c; Welch's ANOVA, mean ± SEM; n=4, input 1.00 ± 0.35, nuclei 0.53 ± 0.12, cytosol 1.39 ± 0.42, synaptosome 0.73 ± 0.13, $W_{(3.00,\ 6.207)}$=1.500, p=0.3045). A considerable amount of PSD95 was lost during the first low spin leading to nuclear fraction contamination.

An improper starting homogenisation could explain this contamination. In fact, it is likely that, if the volume of homogenisation buffer was not sufficient, portions of the cellular membrane together with large protein complexes like the PSD fail to form synaptosomal vesicles. This would lead to the formation of large fragments of insoluble heavy material which would then be pulled down together with the nuclei during the first low speed spin.

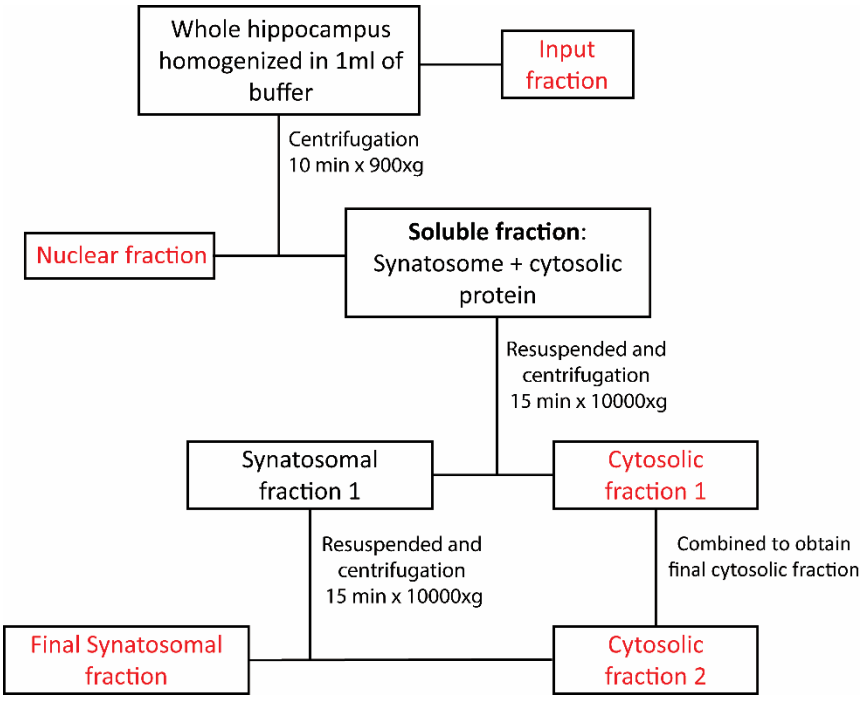

Figure S-1. Schematic representation of the first version of the adapted synaptosomal protocol.
The protocol described here follows the steps described by Bermejo *et al.* (Bermejo *et al.*, 2014) and differs from the original procedure only for the volume of homogenised buffer used, 1 ml. In red are reported the final fractions that were used for immunoblotting.

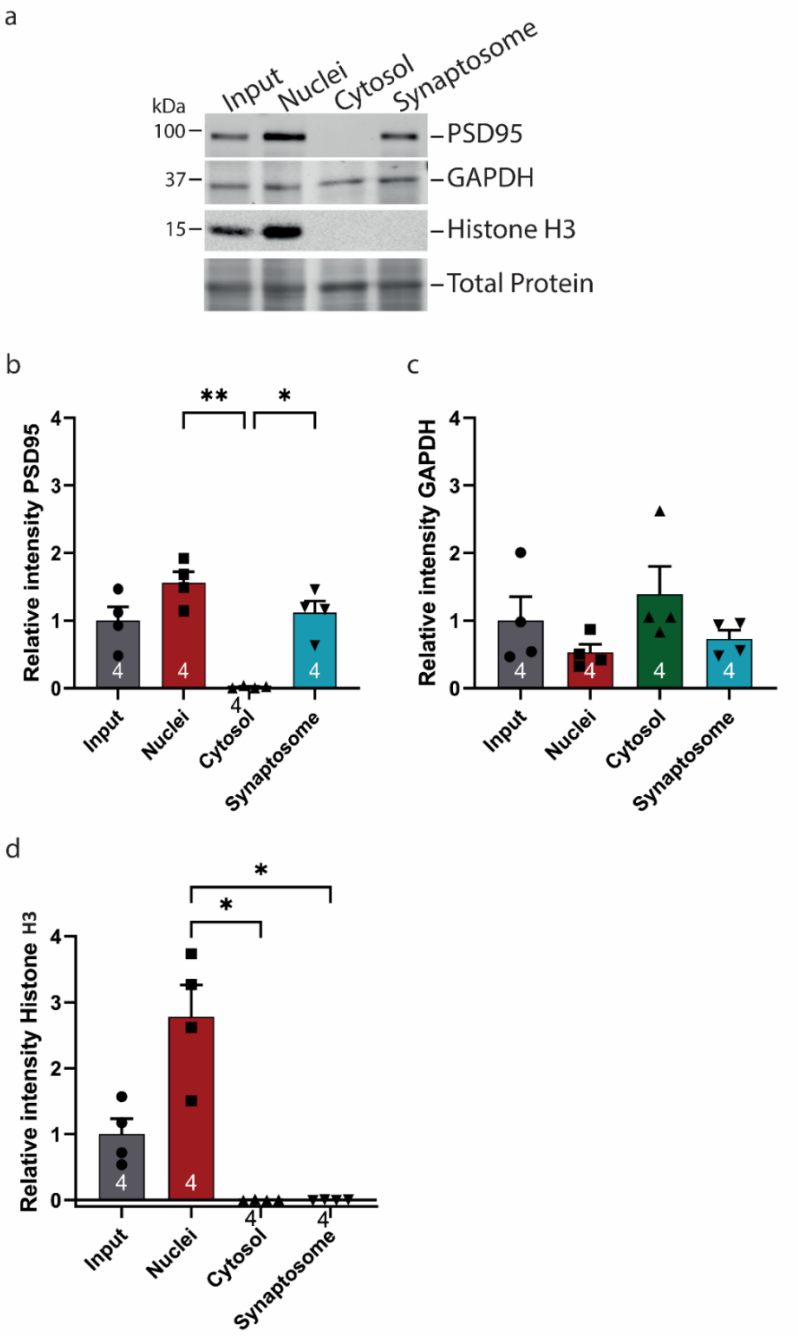

Figure S-2. A relative high amount of synaptic marker PSD95 was present in the nuclear fraction resulting in a scarce synaptosomal fraction enrichment.

Representative immunoblot showing synaptic, cytosolic and nuclear markers (a). Quantification of PSD95 (b), GAPDH (c) and Histone H3 (d) relative amount in the four fractions, normalised over the input. The gel was used at a concentration of bis-acrylamide of 12%. Points represent single animals. Numbers within or under the bars represent the n of each group. Tissue from wild-type naïve mice. Images used for quantification are reported in Figure S-31.

Data presented as mean ± SEM. Welch's ANOVA with Dunnett's T3 multiple comparisons test. * $p<0.05$, ** $p<0.01$.

Modification to the protocol allowed a better enrichment of cytosolic markers

To improve the homogenisation, buffer volume was increased initially up to 2 ml, but this led to an excessive dilution of the cytosolic fraction making it impossible to load a constant amount of protein for all the samples. Therefore, the volume used was lowered to 1.6 ml. Moreover, a washing step of the primary nuclear pull-down was added with the aim to remove as much contaminant as possible. To avoid an excessive dilution of the cytosolic fraction, only the supernatant derived from the first fast spin of the soluble fraction 1 was collected and used for the analysis. The schematic representation of the protocol is described in Figure S-3.

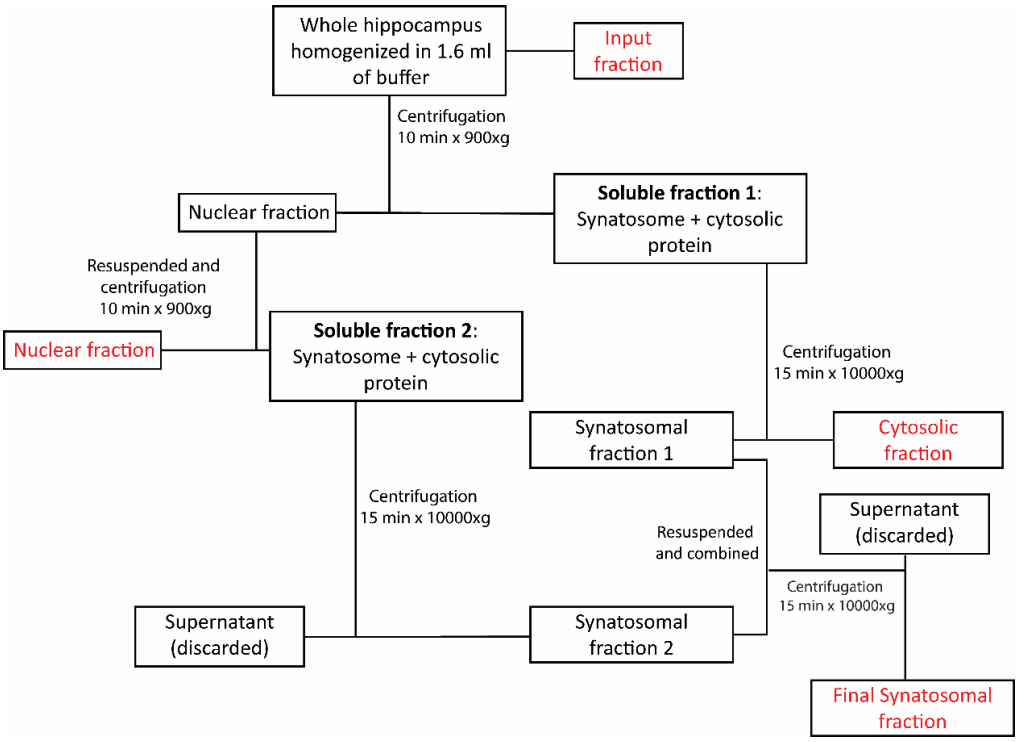

Figure S-3. Schematic representation of the optimised synaptosomal preparation protocol.
In respect to the protocol described in the previous section intermediate steps were added. Homogenisation volume was increased to 1.6 ml, in an attempt to obtain a better homogenisation of the starting hippocampal tissue, and an additional washing step of the nuclear fraction was added. In red are reported the final fractions that were used for immunoblotting.

The analysis of the subcellular fractions immunoblot (Figure S-4a) showed an improvement in the level of enrichment of synaptic marker in the synaptosomal

fraction, however, a high contamination of the nuclear fraction by SYNGAP1 and PSD95 was still present (Figure S-b and c; SYNGAP1, Welch's ANOVA, mean ± SEM; SYNGAP1, n=3, input 1.00 ± 0.25, nuclei 1.70 ± 0.06, cytosol 0.13 ± 0.004, synaptosome 1.99 ± 0.10, $W_{(3.00,\ 3.347)}$=226.8, p=0.0002; Dunnett's multiple comparisons test results are reported in Table S-22. PSD95, n=3, input 1.00 ± 0.20, nuclei 1.98 ± 0.26, cytosol 0.16 ± 0.01, synaptosome 1.79 ± 0.08, $W_{(3.00,\ 3.410)}$=101.8, p=0.0008; Dunnett's multiple comparisons test results are reported in Table S-23). GAPDH enrichment resulted improved (Figure S-4e; Welch's ANOVA, mean ± SEM; n=3, input 1.00 ± 0.29, nuclei 0.71 ± 0.16, cytosol 2.93 ± 0.26, synaptosome 1.13 ± 0.33, $W_{(3.00,\ 4.265)}$=13.44, p=0.0025; Dunnett's multiple comparisons test results are reported in Table S-24), while Histone H3 enrichment and depletion appeared to be comparable to before, although the difference between fractions was not significant (Figure S-4d; Welch's ANOVA, mean ± SEM; n=3, input 1.00 ± 0.34, nuclei 3.69 ± 1.97, cytosol -0.05 ± 0.07, synaptosome -0.02 ± 0.05, $W_{(3.00,\ 3.964)}$=3.106, p=0.2429).

This protocol allowed me to obtain cytosolic fraction free from synaptic markers and to deplete the synaptic fraction from cytosolic markers. This was deemed appropriate to evaluate vector-derived protein distribution between the cytosol and the synaptic compartment.

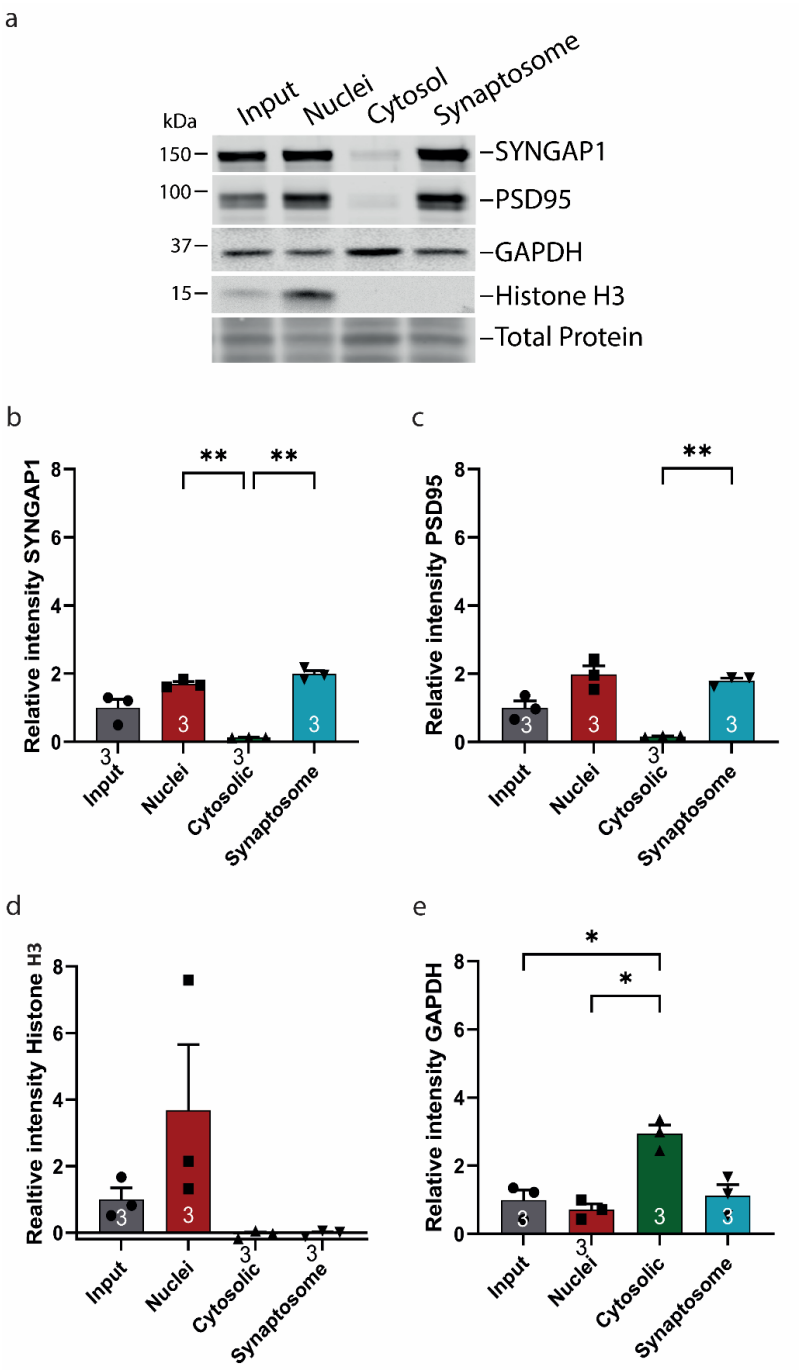

Figure S-4. Protocol optimisation allowed to improve cytosolic markers enrichment. Representative immunoblot showing synaptic, cytosolic and nuclear markers (a). Quantification of SYNGAP1 (b), PSD95 (c), Histone H3 (d) and GAPDH (e) relative amount in the four fractions, normalised over the input. The gel was used at a concentration of bis-acrylamide of 12%. Points represent data from single animals. Numbers within or under the bars represent the n of each group. Tissue from *Syngap1*$^{+/-}$ PBS treated mice. Images used for quantification are reported in Figure S-32.

Data presented as mean ± SEM. Welch's ANOVA with Dunnett's T3 multiple comparisons test. * $p<0.05$, ** $p<0.01$.

C.2 EVALUATION OF THE LINEARITY OF DETECTION OF ANTIBODIES USED FOR IMMUNOBLOT QUANTIFICATION

Antibodies used for the immunoblot quantification shown in Chapters 5 and 6 were tested for linearity of detection. Serial dilution of protein lysate from treated and untreated tissues were loaded an 8% bis-acrylamide gels. Separation, transfer and staining were performed as described in Chapter 2.

Anti-SYNGAP1, at the working dilution of 1:2000, and anti-Myc, at the dilution of 1:750, presented a linear detection for a range of scanning intensities (Figure S-5 and Figure S-6). FLAG antibody, at a dilution of 1:1500, showed linear detection at all tested intensities of scanning (Figure S-7).

As mentioned in Chapter 2, total protein staining was used as loading control and as an internal normalisation control. The linearity of detection of total protein staining was tested with the same protocol described previously for the antibodies. As shown in Figure S-8 the signal resulted linear at the tested scanning intensity of 1.5.

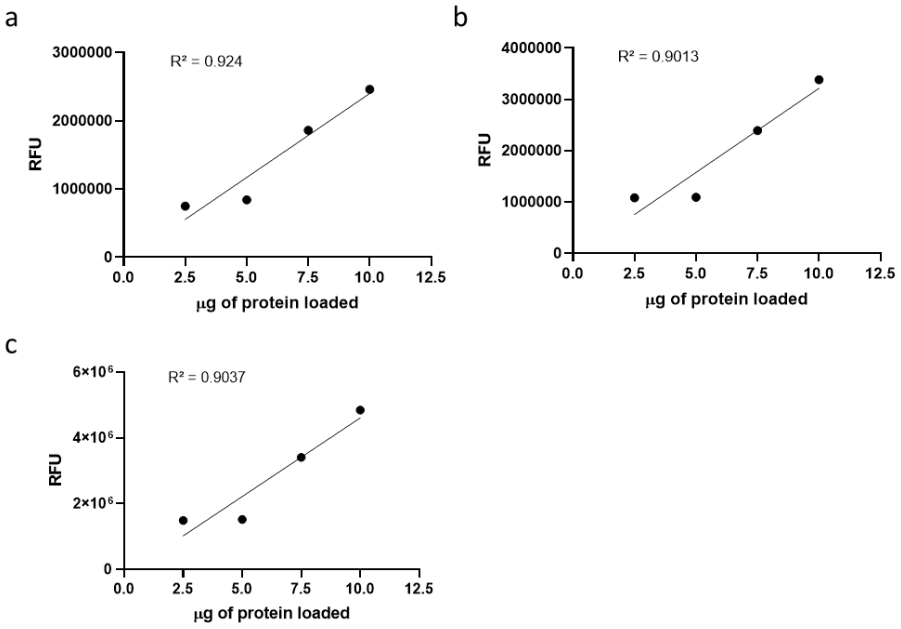

Figure S-5. Anti-SYNGAP1 antibody showed linearity of detection.
Antibody linearity test at 1:2000 dilution scanned at 1.5 (a), 2 (b) and 2.5 (c) scanning intensity at the Li-Cor scanner. RFU=Relative Fluorescence Intensity. R^2 indicates goodness to fit.

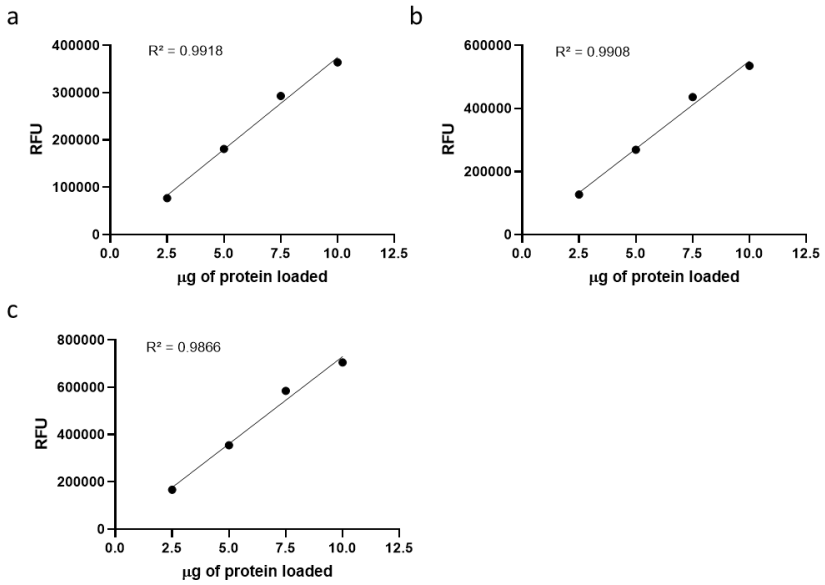

Figure S-6. Anti-Myc antibody showed linearity of detection at each scanning intensity tested.

Antibody linearity test at 1:750 dilution scanned at 1.5 (a), 2 (b) and 2.5 (c) scanning intensity at the Li-Cor scanner. RFU=relative fluorescent unit. R^2 indicates goodness to fit.

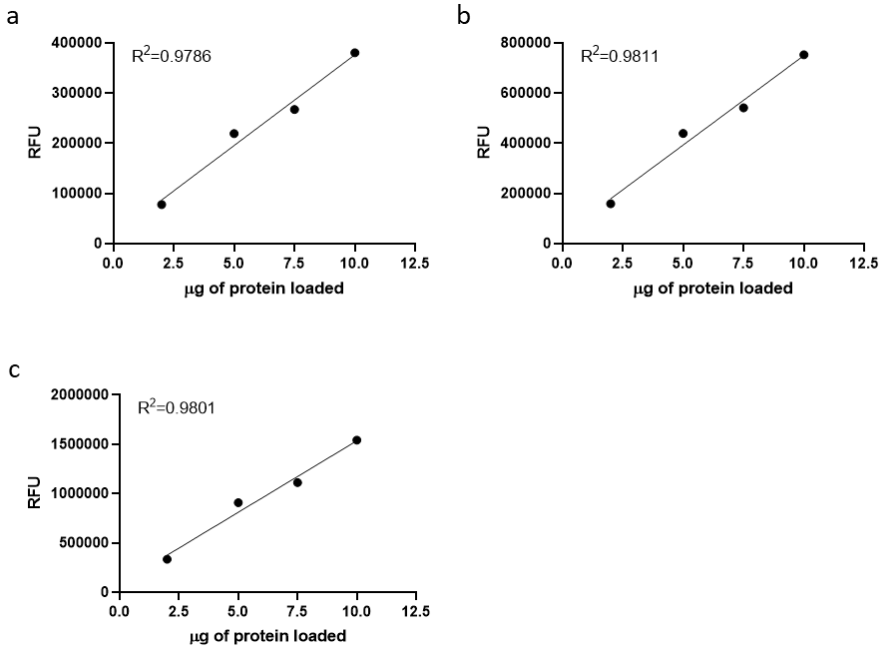

Figure S-7. Anti-FLAG antibody showed linearity of detection at each scanning intensity tested.

Antibody linearity test at 1:1500 dilution scanned at 6 (a), 7 (b) and 8 (c) scanning intensity the Li-Cor scanner. RFU=Relative Fluorescence Intensity. R^2 indicates goodness to fit.

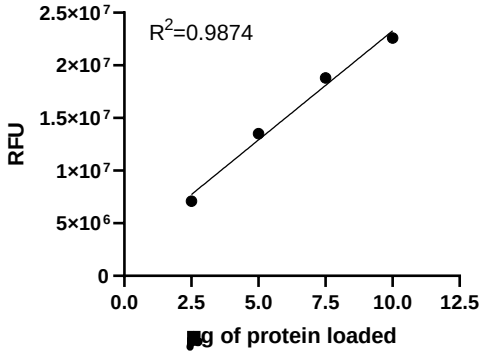

Figure S-8. Total protein staining signal resulted linear under the standard condition used.
Total protein signal of serial dilutions of tissue protein lysates scanned at intensity of 1.5. RFU=relative fluorescent unit. R^2 indicates goodness to fit.

C.3 qPCR REACTION OPTIMISATION FOR AAV9/JET-*hSYNGAP1*

The primer pair for the evaluation of AAV9/JeT-*hSYNGAP1* biodistribution was designed to amplify 150 bp spanning the 5' end of the JeT core region (Figure S-9). *Actb* specific primers were designed by Dr Sophie Thompson to amplify an exonic region of 228 bp of the murine *Actb* gene.

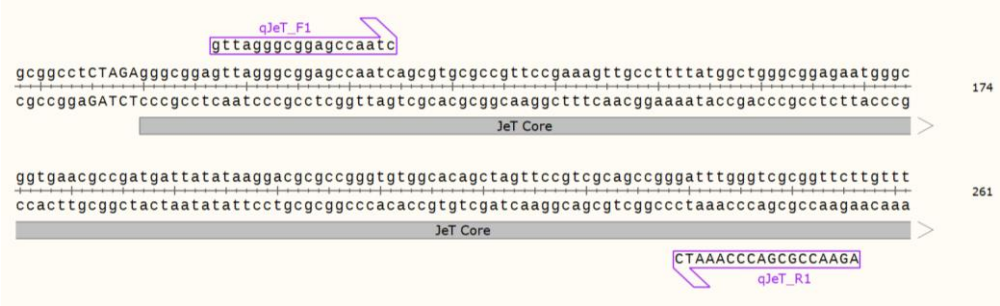

Figure S-9. Primers for viral vector biodistribution analysis were designed to amplify a region of the JeT promoter.
Sequence and position on the therapeutic cassette of the primers used for the evaluation of AAV9/JeT-*hSYNGAP1* biodistribution.

qPCR reaction was optimised in order to achieve an E_{AMP}% between 90 and 110 % and avoid non-specific amplification of the templates. To this end, dilution series of the designed primers were tested.

Primers concentration of 600 nM led to non-specific amplification of the negative control with the generation of a peak overlapping with the one generated from the specific amplification of the positive control and the plasmid (Figure S-10). At 200 nM non-specific amplification was not observed (Figure S-12), but E_{AMP}% was lower than 80 % (Figure S-13c). Although at 300 nM non-specific amplification was observed, the generated peak showed only a minor overlap with the one derived from the amplification of the desired sequence (Figure S-11). Even if E_{AMP}% at 300 nM of primer concentration (Figure S-13b) was 86.11 %, further testing showed that an efficiency above 90 % was achievable with this reaction parameter.

When performing absolute quantification using the standard curve method, the assumption is that the efficiency of amplification of the standard is comparable to the amplification efficiency of the unknown sample. Therefore, it is important to evaluate the amplification efficiency of a representative sample. As shown in Figure S-14, with the same reaction conditions used for plasmid amplification and a primers concentration of 300 nM, it was possible to obtain an amplification efficiency of 89.72 %, similar to the efficiency observed for the amplification of the standard sample. For this reason, I decided to use a primers concentration of 300 nM for the evaluation of AAV9/JeT-*hSYNGAP1* biodistribution.

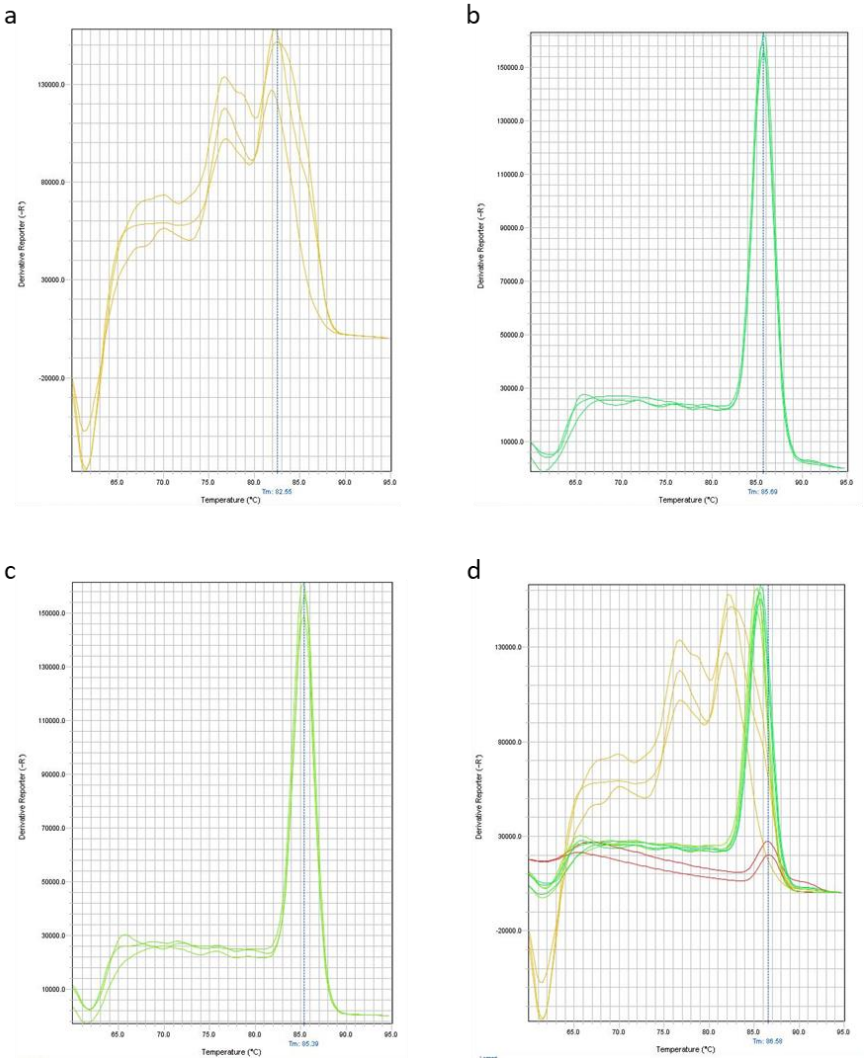

Figure S-10. Reaction performed with 600 nM of reverse and forward primers produced a non-specific fragment with a melting curve overlapping with the expected fragment melting curve.

Melting curves generated from the negative control (a), positive control (b) and plasmid (c) amplification. Merge of all curves is also reported (d). Negative control refers to genomic DNA which does not contain the target sequence. Positive control refers to genomic DNA which contains the target sequence. Red line refers to no template control.

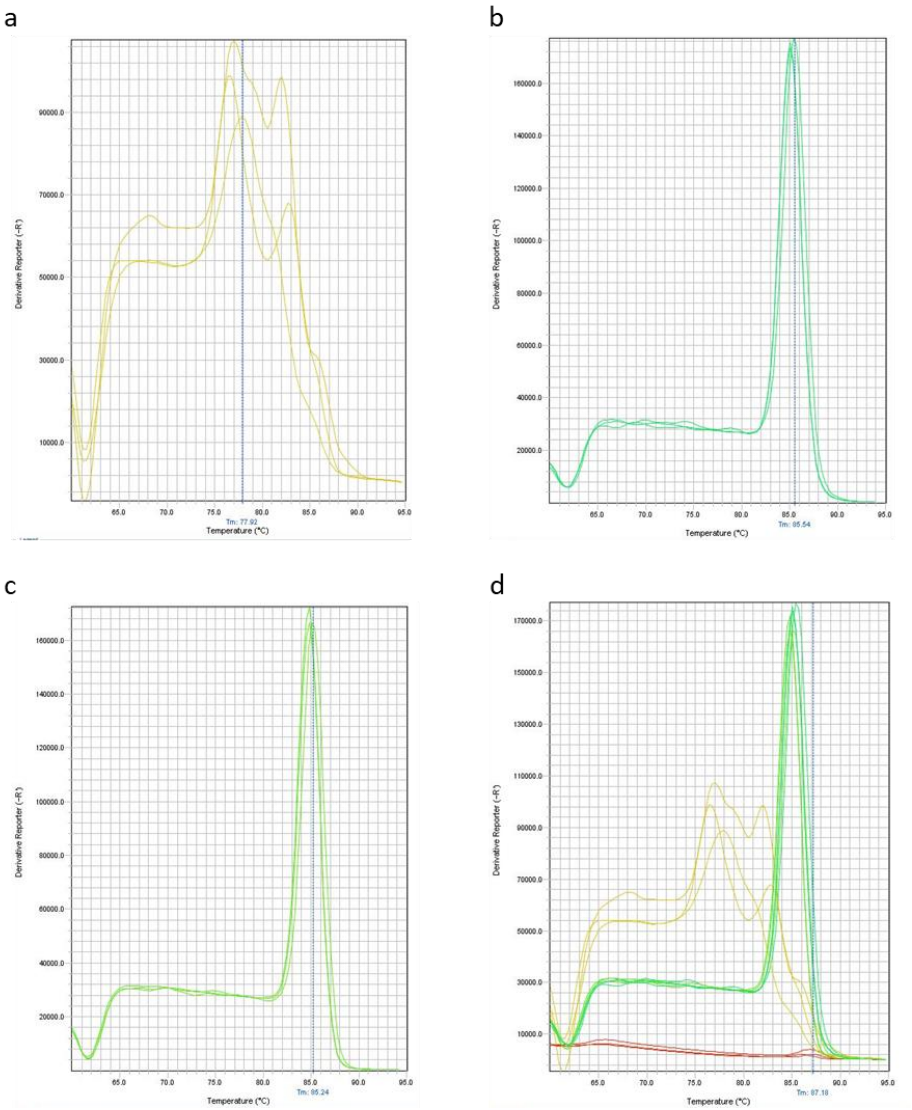

Figure S-11. At a primers concentration of 300 nM the melting curve produced by the non-specific amplification presented a reduced overlapped area with the melting curve produced by the desired fragment.

Melting curves generated from the negative control (a), positive control (b) and plasmid (c) amplification. Merge of all curves is also reported (d). Negative control refers to genomic DNA which does not contain the target sequence. Positive control refers to genomic DNA which contains the target sequence. Red line refers to no template control.

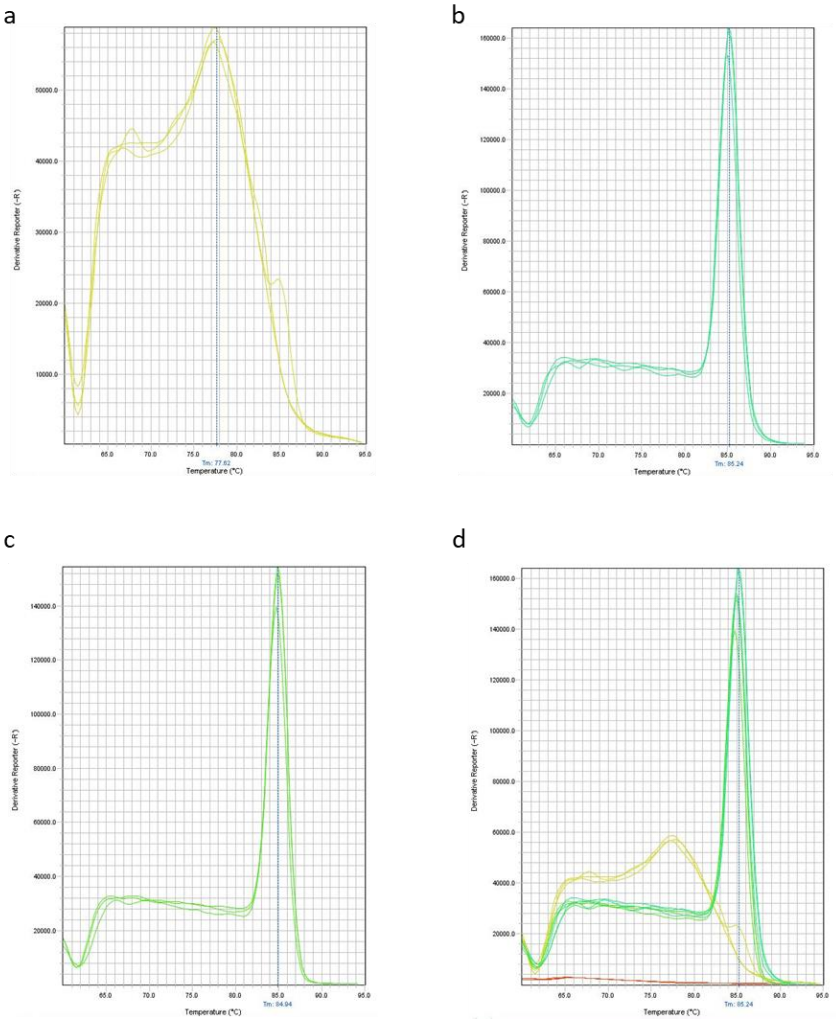

Figure S-12. At a concentration of forward and reverse primers of 200 nM the melting curve associated with the non-specific amplification was distinguishable from the melting curve of the expected fragment.

Melting curves generated from the negative control (a), positive control (b) and plasmid (c) amplification. Merge of all curves is also reported (d). Negative control refers to genomic DNA which does not contain the target sequence. Positive control refers to genomic DNA which contains the target sequence. Red line refers to no template control.

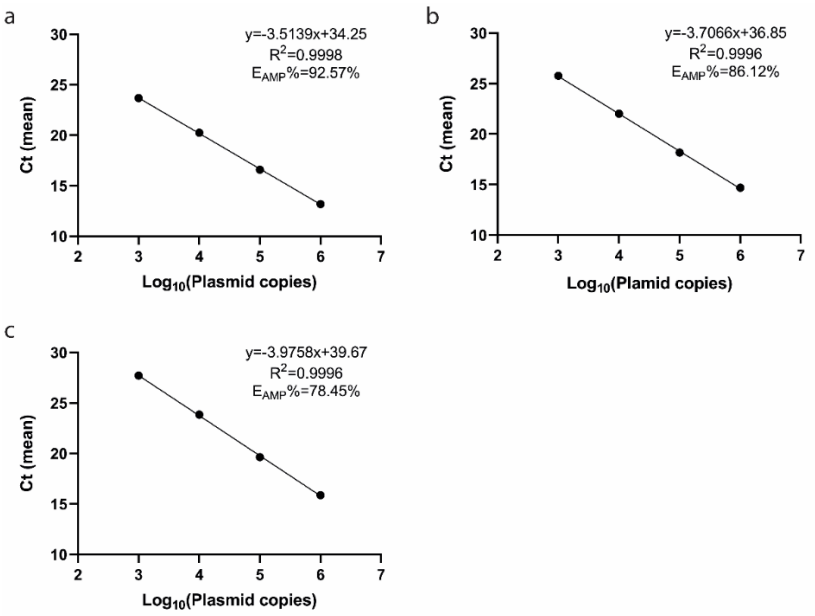

Figure S-13. Amplification efficiency decreased with the decrease in primers concentration.

Standard curves and E_{AMP}% for the amplification reactions with primers at the final concentration of 600 nM (a) 300 nM (b) and 200 nM (c). R^2 indicates goodness to fit. Ct=Cycle threshold, E_{AMP}%= Percent amplification efficiency.

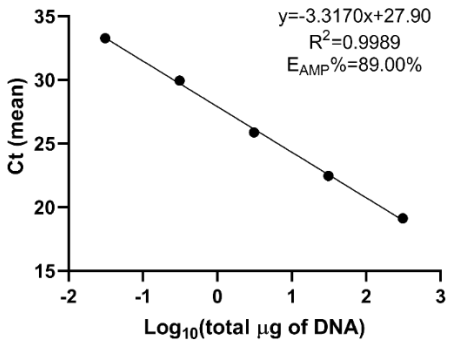

Figure S-14. At the optimised conditions, genomic DNA amplification efficiency was 89%.

Representative standard curves and E_{AMP}% for the amplification of vector-derived SYNGAP1 in serial dilutions of genomic DNA.

Actb amplification reaction has been previously optimised in the lab to work under a spectrum of conditions. Here I will show the reaction efficiency and amplification specificity at the conditions used for this work.

Forward and reverse primers were used at a final concentration of 600 nM. As shown in Figure S-15, with this concentration only one defined peak was produced.

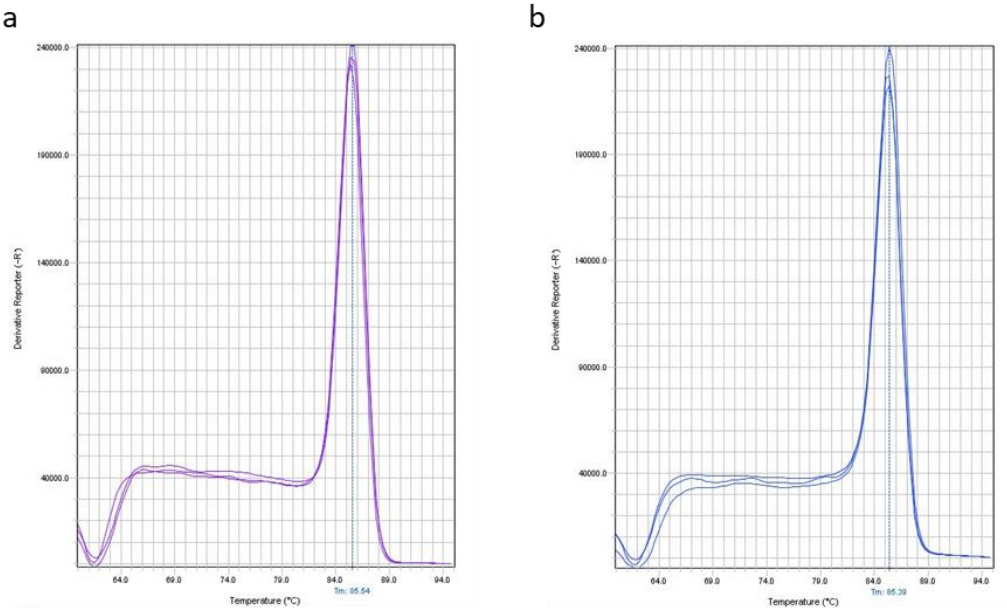

Figure S-15. Analysis of melting curves showed one single defined curve in both Actb standard and positive control amplification.
Melting curves generated from the positive control (a) and the *Actb* standard (b) amplification. Positive control refers to genomic DNA which contains the target sequence.

E_{AMP}% was between 90 and 110 % for both the amplification of the *Actb* standard and for the amplification of the genomic DNA (Figure S-16).

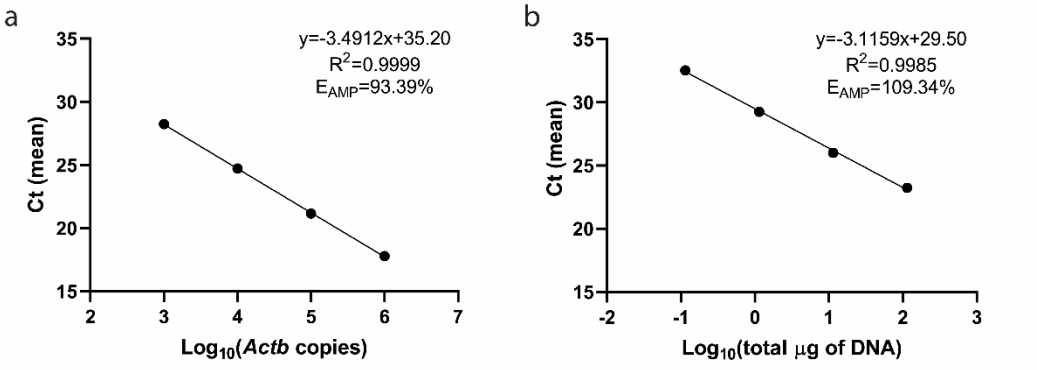

Figure S-16. Genomic DNA and Actb standard were amplified with high efficiency.
Representative standard curves and percent efficiency of amplification (E_{AMP}%) for the amplification reactions of the *Actb* sequence used as standard (a) and genomic DNA (b).

C.4 qPCR REACTION OPTIMISATION FOR AAV9/hSYN1-*hSYNGAP1*

Similar to what was shown in Section C.3, the qPCR reaction for the biodistribution analysis of AAV9/hSYN1-*hSYNGAP1* was optimised to obtain an E_{AMP}% between 90 and 110% for the molecule used as standard and the genomic DNA.

qPCR primers (Figure S-17) at a final concentration 300 nM were used as produced no non-specific amplification and yielded an E_{AMP}% efficiency above 90% for both plasmid and DNA amplification (Figure S-18 and Figure S-19)

Figure S-17. Primers for viral vector biodistribution evaluation were designed to amplify a region spanning the hSYN1 promoter and the FLAG tag.
Sequence and position on the therapeutic cassette of the primers used for the evaluation of AAV9/hSYN1-*hSYNGAP1* biodistribution.

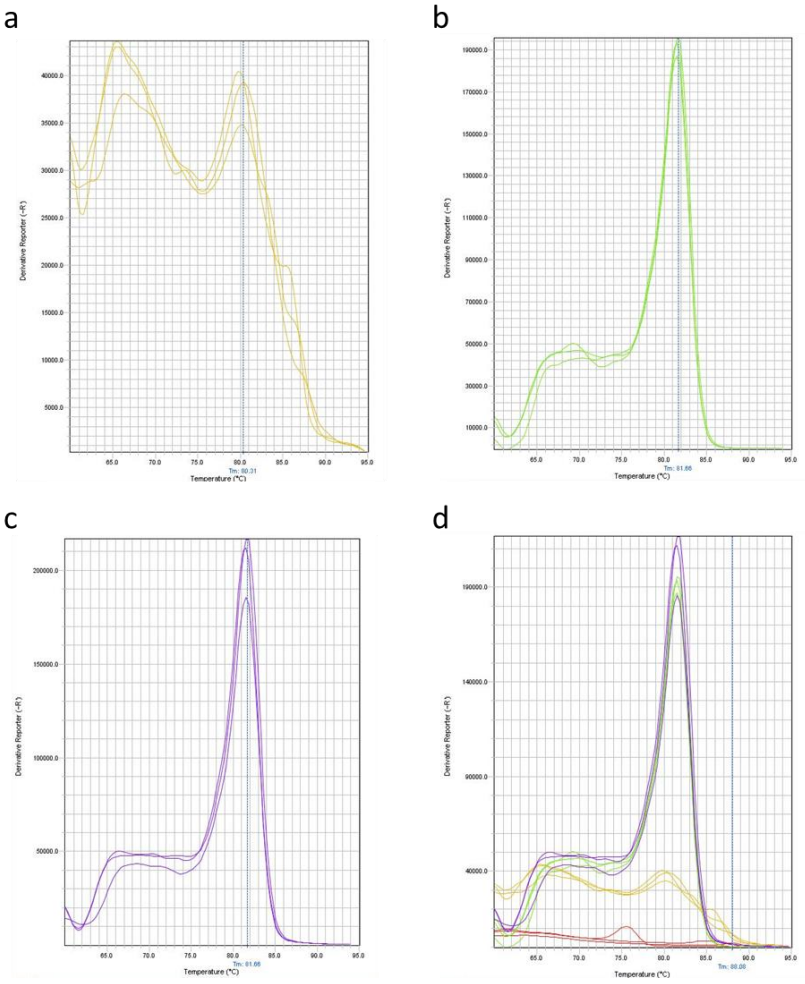

Figure S-18. At forward and reverse primers concentration of 300 nM, non-specific amplification was not observable.

Melting curves generated from the negative control (a), positive control (b) and plasmid (c) amplification. Merge of all curves is also reported (d). Negative control refers to genomic DNA which does not contain the target sequence. Positive control refers to genomic DNA which contains the target sequence. Red line refers to no template control.

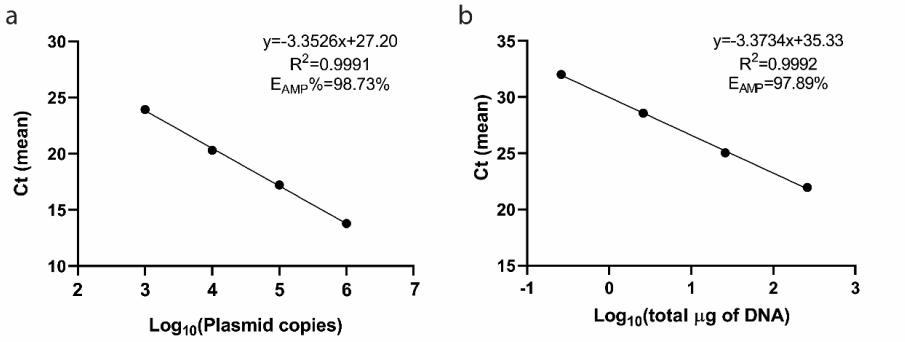

Figure S-19. Reaction efficiency was above 90% for both plasmid and DNA amplification.
Representative standard curves and E_{AMP}% for the amplification reactions with primers at a final concentration of 300 nM for plasmid (a) and DNA (b). R^2 indicates goodness to fit. Ct=Cycle threshold, E_{AMP}%= Percent amplification efficiency.

C.5 qPCR REACTION OPTIMIZATION FOR mRNA QUANTIFICATION

An equivalent approach used for the optimisation of the qPCR viral vector biodistribution reactions was used for the optimisation of the qPCR reaction conditions for the exogenous *SYNGAP1* and endogenous *Syngap1* mRNA quantification.

Two sequence-specific forward primers were designed over a 19 bp stretch containing 7 mismatches (Figure S-20, yellow and green highlighted sequence) present in exon 8 (Figure S-21). The reverse primer (Figure S-20, blue highlighted sequence) was common to both mouse and human sequences.

Analysis of the amplified fragments melting curves showed high amplification specificity (Figure S-22 and Figure S-23).

```
Vector      CAGAGAGCCGTGAAGCCCAACAAGGATAACAGCCGCAGAGTGGACAATGTGCTGAAGCTG
Mouse       CAGAGGGCTGTAAAACCCAACAAGGACAACAGCCGCCGAGTAGATAACGTGCTGAAGCTA
            ***** ** ** ** *********** ********* **** ** ** ***********

Vector      TGGATCATCGAGGCTCGGGAGCTGCCACCTAAAAAAAGATACTACTGCGAGCTGTGTCTG
Mouse       TGGATCATAGAGGCTCGAGAGCTGCCCCCCAAGAAGAGATATTACTGTGAGCTGTGCCTG
            ******** ******** ******** ** ** ** ***** ***** ******** ***

Vector      GACGATATGCTGTACGCCAGAACCACCTCTAAGCCTAGAAGCGCTAGCGGCGACACCGTG
Mouse       GACGACATGCTGTATGCACGAACCACCTCCAAGCCCCGCTCGGCTTCAGGAGACACCGTC
            ***** ******** **  ********** *****  *    ***   ** ********

Vector      TTCTGGGGCGAGCACTTCGAGTTTAACAACCTGCCTGCTGTCCGGGCCCTGAGACTGCAC
Mouse       TTTTGGGGCGAGCACTTTGAGTTTAACAACCTGCCTGCCGTCCGGGCCCTTCGGCTGCAT
            ** ************** ******************** ***********  * *****

Vector      TTGTACCGGGACAGCGATAAGAAACGGAAGAAAGACAAGGCTGGCTACGTGGGCTTGGTG
Mouse       CTGTACCGTGACTCAGACAAAAAGCGGAAGAAGGACAAGGCTGGCTACGTTGGCCTGGTG
             ******* ***   ** ** ** ******** ***************** *** *****

Vector      ACCGTGCCCGTGGCCACACTGGCTGGCAGACACTTCACCGAGCAGTGGTATCCTGTGACA
Mouse       ACTGTTCCAGTGGCCACCCTAGCTGGGCGCCACTTCACAGAGCAGTGGTACCCCGTGACC
            ** ** ** ******** ** *****  * ******** *********** ** *****
```

Figure S-20. hSYN1-hSYNGAP1 and mouse wild-type Syngap1 sequence alignment and primers set for mRNA quantification.
Partial alinement between the hSYN1-*hSYNGAP1* and wild-type mouse sequence was performed with Clustal Omega (www.ebi.ac.uk/Tools/msa/clustalo). In yellow is indicated the hSYN1-*hSYNGAP1* specific forward primer while in green is reported the primer specific for the wild-type mouse sequence. In blue is reported the complementary sequence of the common reverse primer. *Indicates nucleotides match. Mouse sequence NM_001394027.1.

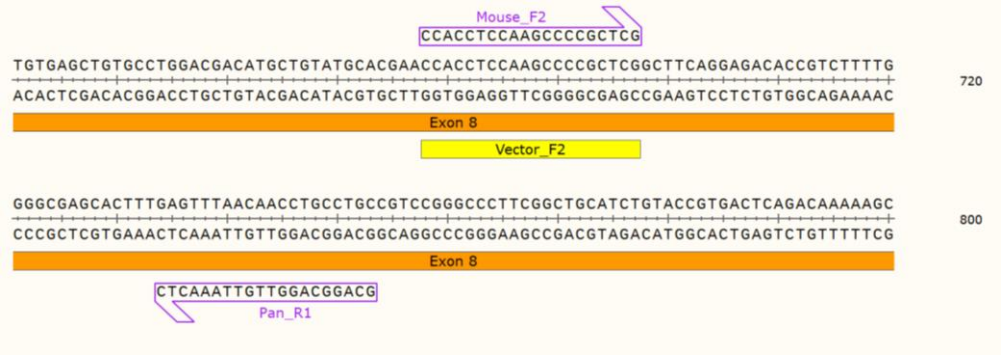

Figure S-21. Primers used for mRNA quantification amplified a region of exon 8.
Graphical representation of the position of the primers on the wild-type mouse sequence. In orange is reported the exonic sequence. Mouse_F2 indicates the mouse-specific forward primer, Vector_F2 is the forward primer specific for the amplification of the viral vector sequence, while Pan_R1 is the common reverse primer. Snapshot from SnapGene software (v5.1.7). Mouse sequence NM_001394027.1.

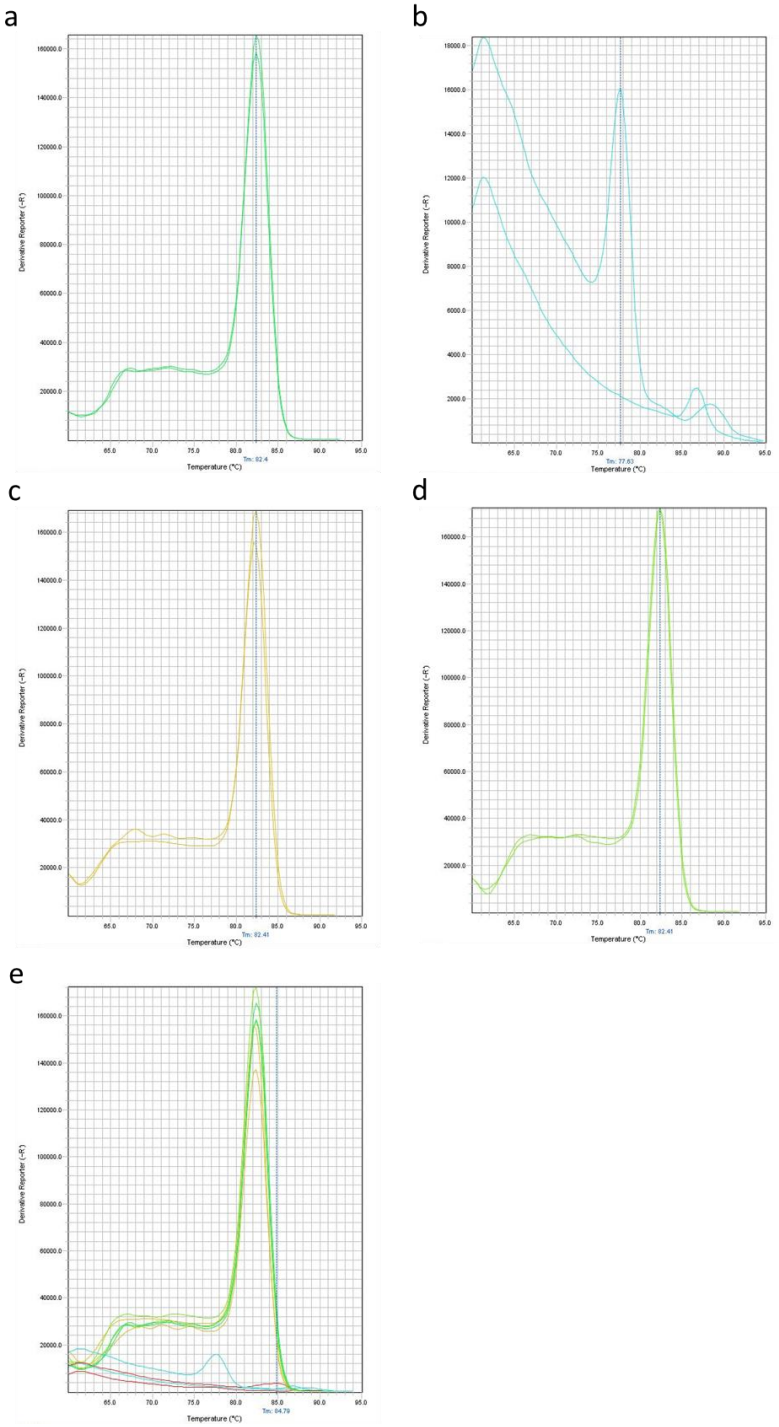

Figure S-22. Primers for the amplification of the endogenous Syngap1 mRNA presented high specificity.

Melting curves generated from the amplification of the fragment used as a standard (a), the hSYN1-*hSYNGAP1* plasmid (b), cDNA derived from PBS treated mouse (c) and cDNA derived from viral vector-treated mouse (d). Merge of all curves is also reported (e). Red line refers to no template control.

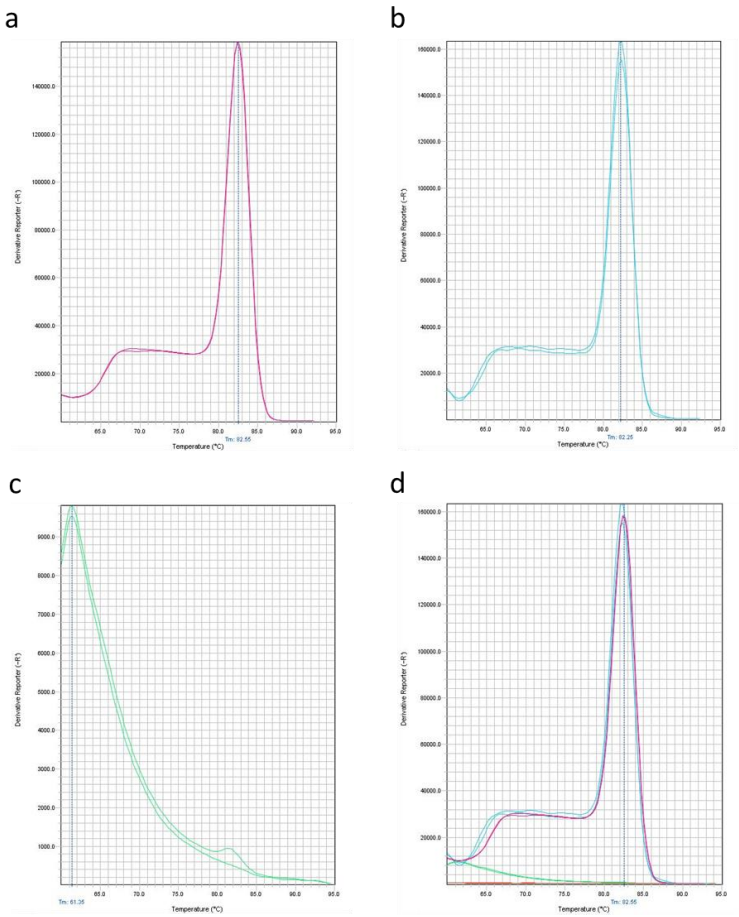

Figure S-23. Primers for the amplification of the exogenous SYNGAP1 mRNA presented high specificity.
Melting curves generated from the amplification of hSYN1-*hSYNGAP1* plasmid used as a standard (a), cDNA derived from viral vector-treated mouse (b) and cDNA derived from PBS treated mouse (c). Merge of all curves is also reported (d). Red line refers to no template control.

As shown in Figure S-24, the amplification efficiency of reactions for the endogenous and viral vector mRNA quantification was between 90 and 110% for both the amplification of the standards and the cDNA samples.

The specificity of amplification of *Actb* primers was described before in Section C.3. Preliminary results showed that the optimal primers concentration for cDNA amplification was 300 nM. In Figure S-25 are reported the amplification efficiencies for the amplification of the standards and the cDNA. In both cases, efficiencies

resulted below the expected 90%, but as they were comparable between samples, mRNA quantification was carried out with these reaction conditions.

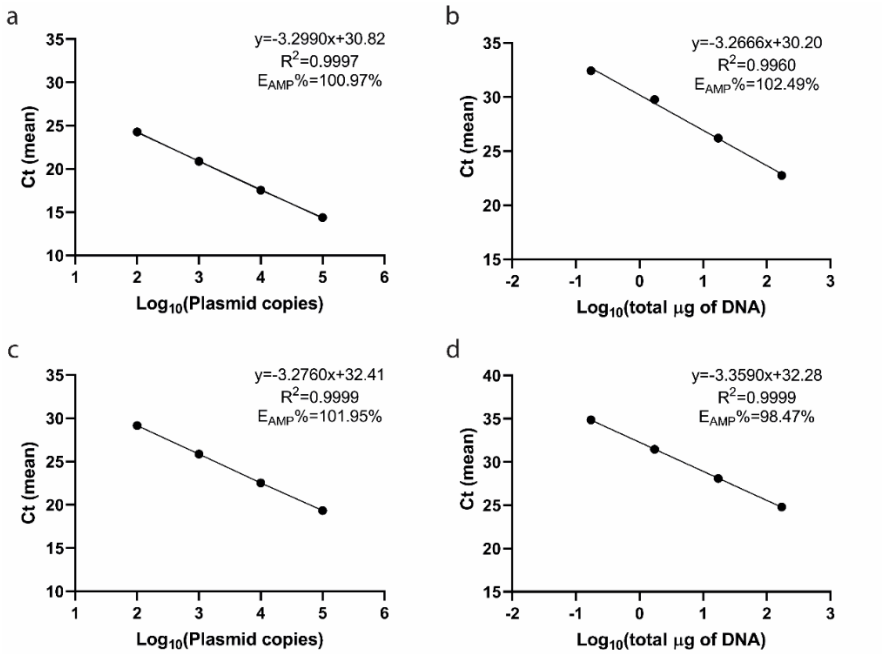

Figure S-24. The amplification efficiency of standards and cDNA sample was comparable for both endogenous Syngap1 and exogenous SYNGAP1 mRNA amplification.

Representative standard curves and E_{AMP}% for the amplification reactions of the endogenous *Syngap1* mRNA sequence used as standard (a) and cDNA (b); viral vector-derived *SYNGAP1* mRNA sequence used as standard (c) and cDNA (d). R^2 indicates goodness to fit. Ct=Cycle threshold, E_{AMP}%= Percent amplification efficiency.

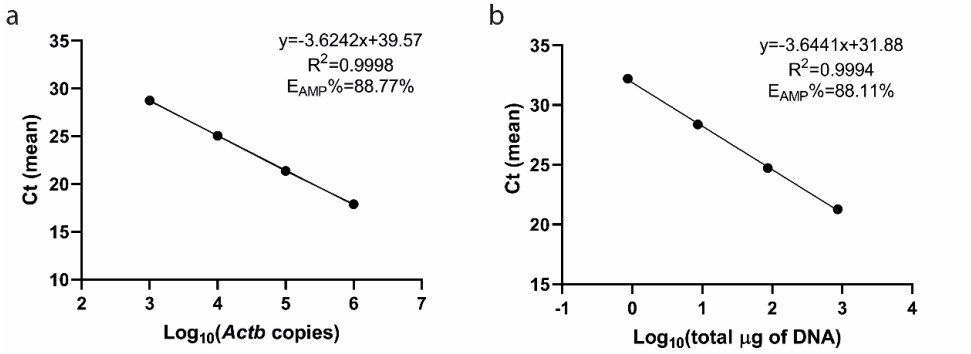

Figure S-25. The amplification efficiency of the Actb sequence was comparable between the standards and cDNA.

Representative standard curves and E_{AMP}% for the amplification reactions of the *Actb* sequence used as standard (a) and genomic DNA (b). R^2 indicates goodness to fit. Ct=Cycle threshold, E_{AMP}%= Percent amplification efficiency.

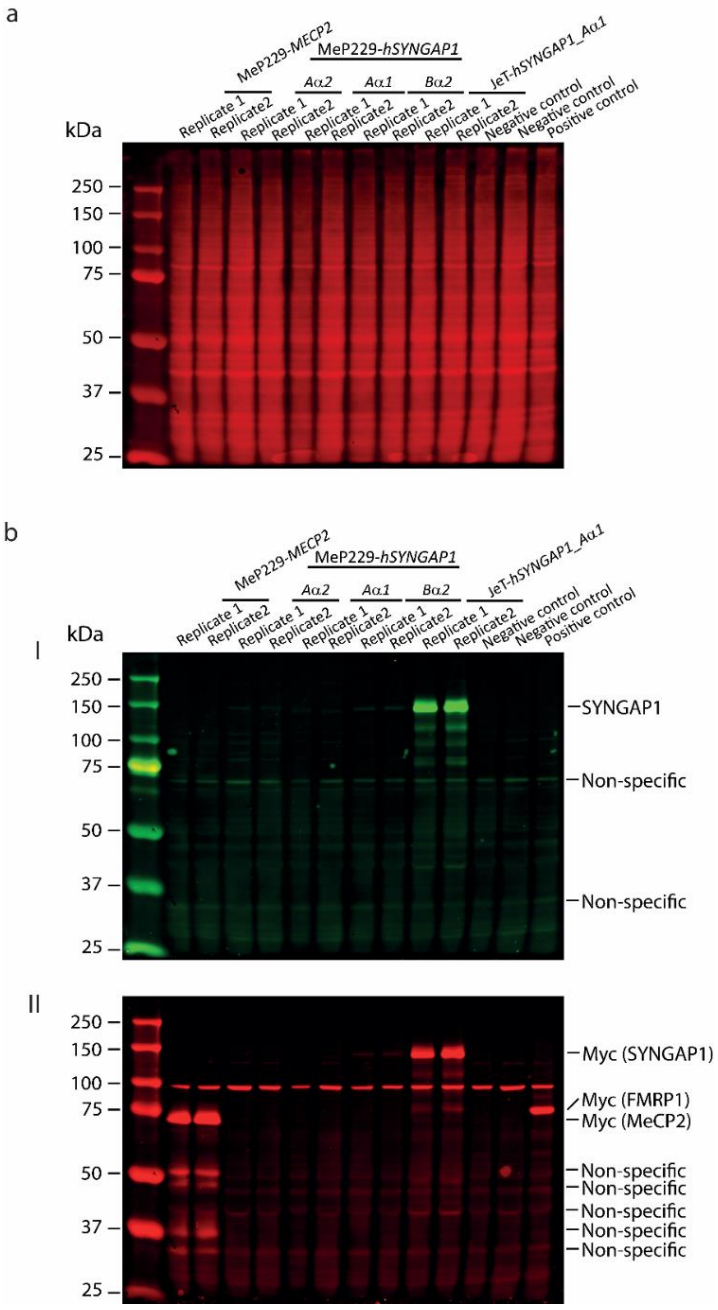

Figure S-26. Immunoblot of HEK293A transfected cells protein lysate.
Total protein staining (a) and anti-SYNGAP1 (b-I, green) and anti-Myc (b-II, red) staining of protein lysate of HEK293A cells transfected with: MeP229-*MECP2-Myc,* MeP229-*hSYNGAP1_Aα2,* MeP229-*hSYNGAP1_Aα1,* MeP229-*hSYNGAP1_Bα2,* JeT-*hSYNGAP1_Aα1.* Negative control indicates mock-transfected HEK293A cells protein lysate. Positive control indicated positive control sample for Myc. Replicates indicate technical replicates. Total protein was used as loading control. The gel was used at a concentration of bis-acrylamide of 8%.

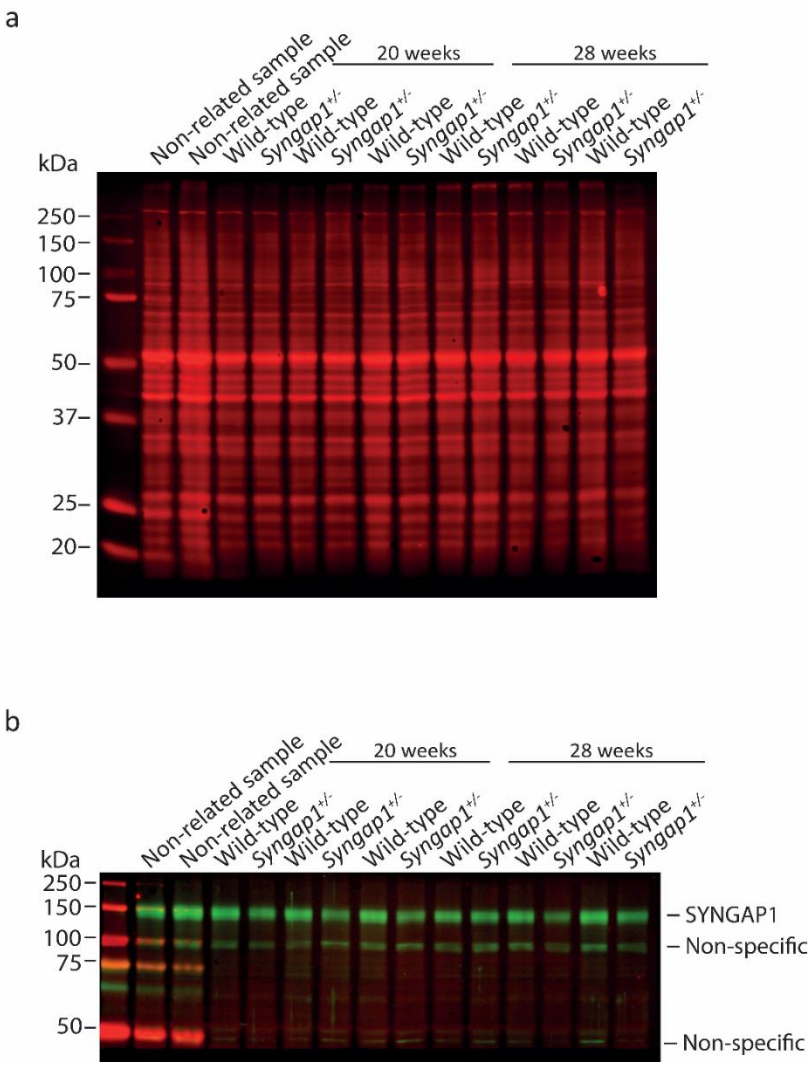

Figure S-27. SYNGAP1 expression in wild-type and Syngap1$^{+/-}$ mice cortex.
Total protein staining (a) and anti-SYNGAP1 (b, green) staining of cortex homogenates from wild-type and *Syngap1*$^{+/-}$ mice collected at 20 weeks of age and 28 weeks of age. Total protein was used as loading control. The gel was used at a concentration of bis acrylamide of 10%.

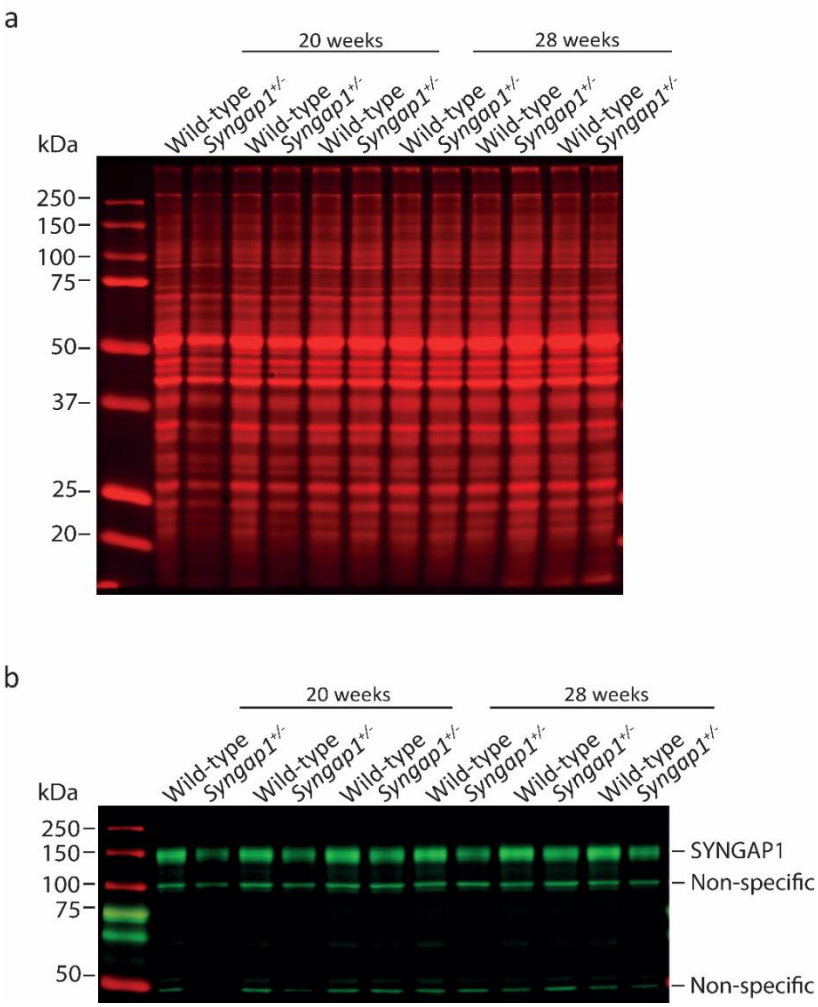

Figure S-28. SYNGAP1 expression in wild-type and Syngap1$^{+/-}$ mice hippocampus.
Total protein staining (a) and anti-SYNGAP1 (b, green) staining of hippocampus homogenates from wild-type and *Syngap1*$^{+/-}$ mice collected at 20 weeks of age and 28 weeks of age. Total protein was used as loading control. The gel was used at a concentration of bis acrylamide of 10%.

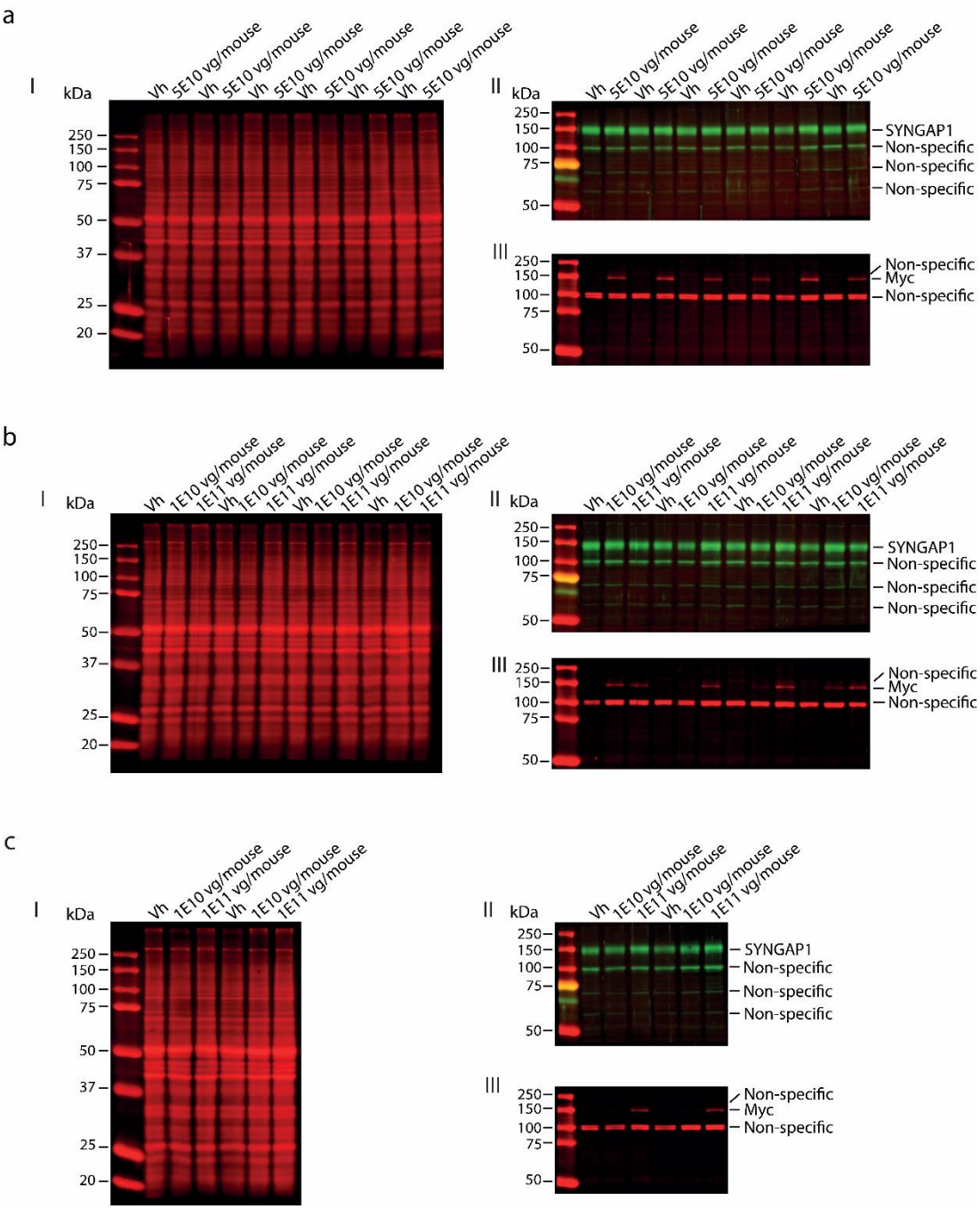

Figure S-29. Endogenous SYNGAP1 and AAV9/JeT-hSYNGAP1 Myc-tagged SYNGAP1 in cortex of Syngap1$^{+/-}$ mice.

Total protein staining (a-I, b-I, c-I) and anti-SYNGAP1 (a-II, b-II, c-II, green) and anti-Myc (a-III, b-III, c-III, red) staining in cortex of *Syngap1*$^{+/-}$ mice treated with vehicle or AAV9/JeT-hSYNGAP1 vector. Total protein was used as loading control. The gel was used at a concentration of bis acrylamide of 10%.

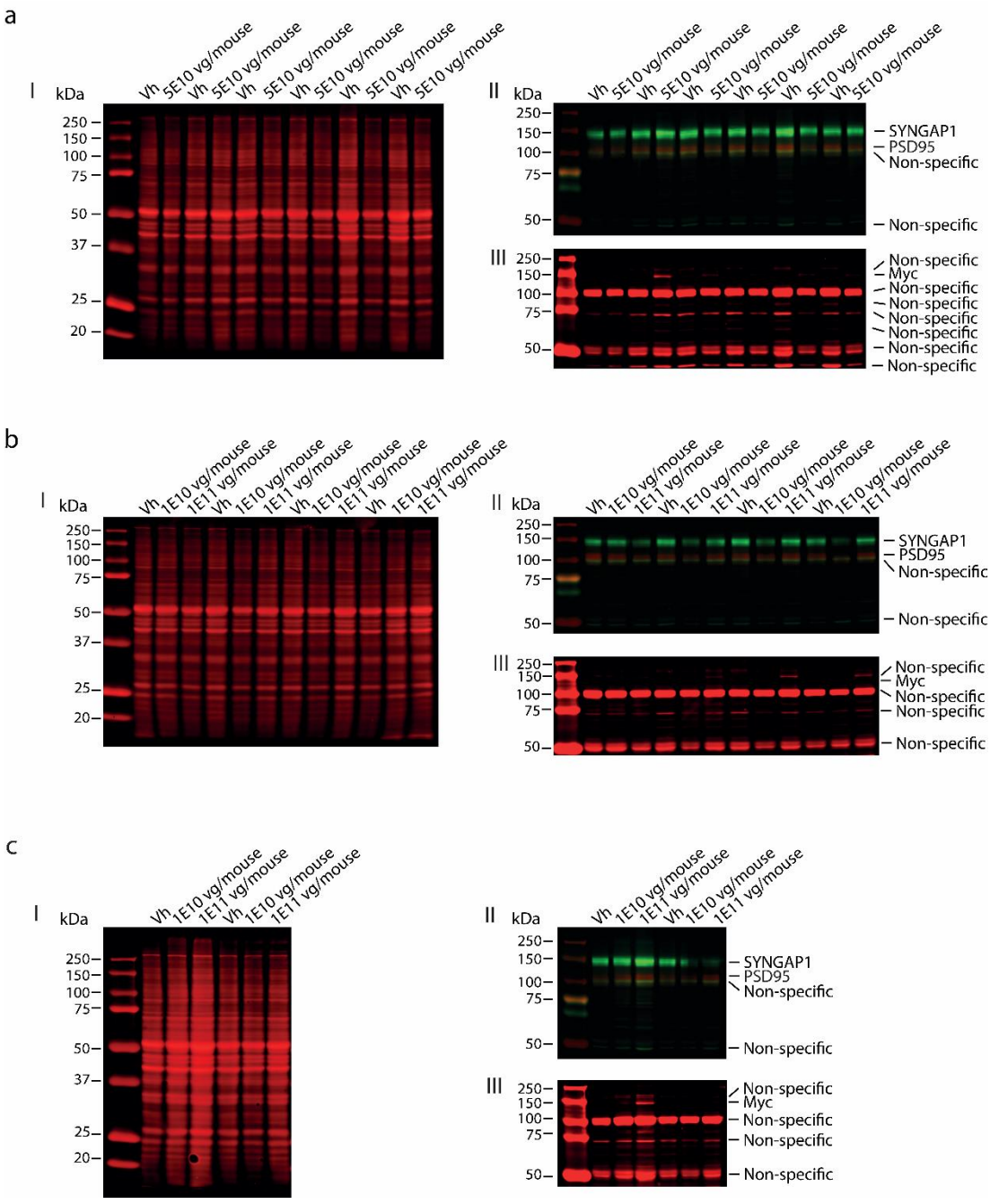

Figure S-30. Endogenous SYNGAP1 and AAV9/JeT-hSYNGAP1 Myc-tagged SYNGAP1 in hippocampus of Syngap1$^{+/-}$ mice.

Total protein staining (a-I, b-I, c-I) and anti-SYNGAP1 (a-II, b-II, c-II, green) and anti-Myc (a-III, b-III, c-III, red) staining in hippocampus of *Syngap1*$^{+/-}$ mice treated with vehicle or AAV9/JeT-hSYNGAP1 vector. Total protein was used as loading control. The gel was used at a concentration of bis acrylamide of 10%.

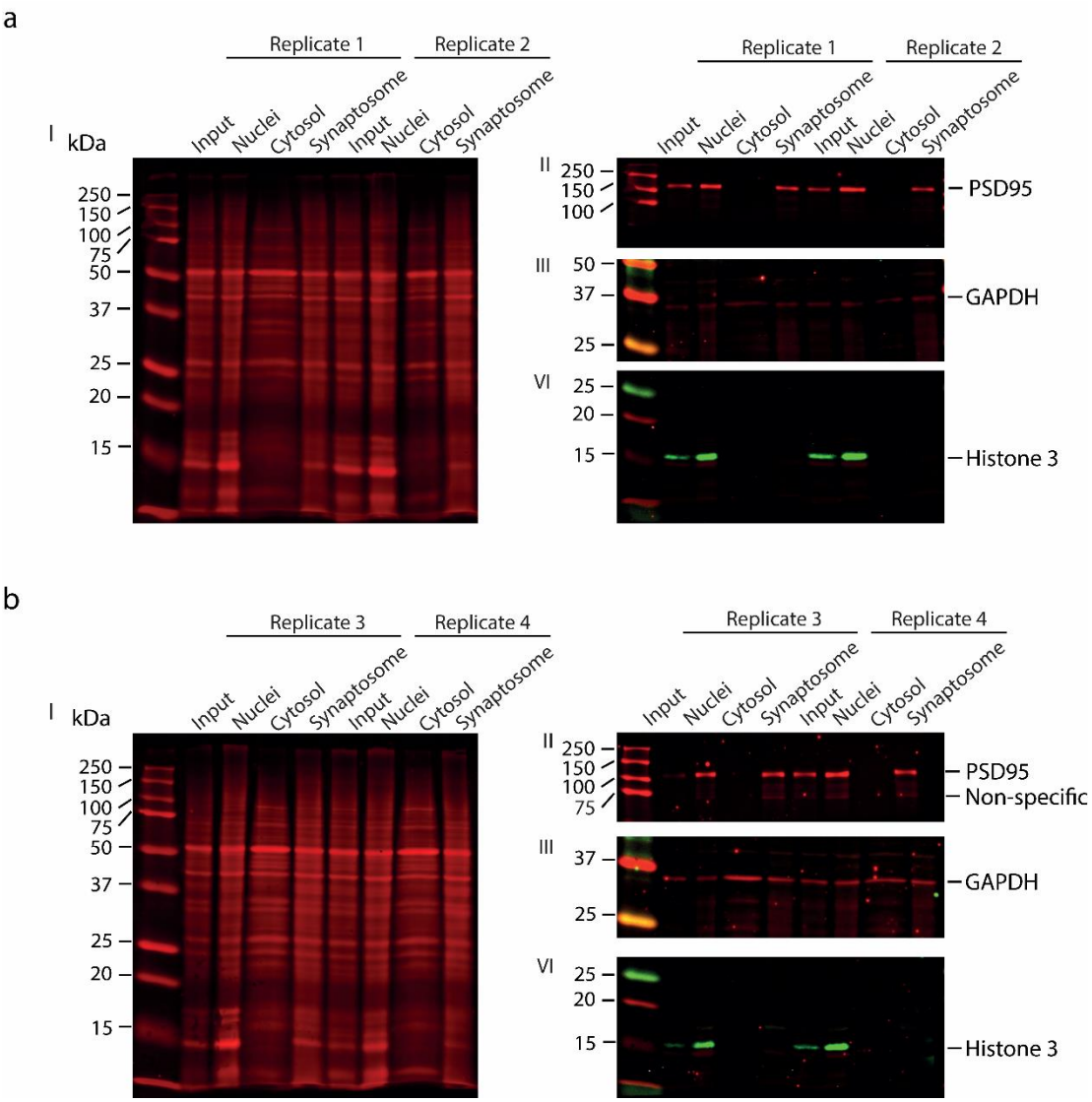

Figure S-31. Subcellular fractionation of hippocampal homogenates using the first version of the protocol.

Total protein staining (a-I, b-I), anti-PSD95 (a-II, b-II, red), anti-GAPDH (a-III, b-III, red) and anti-Histone 3 (a-VI, b-VI, green) staining od subcellular fractions derived from hippocampus of wild-type (replicate 1 and 3) and *Syngap1*$^{+/-}$ (replicate 2 and 4) mice. The comparison was possible as genotypes do not affect levels of the protein investigated. Total protein was used as loading control. The gel was used at a concentration of bis acrylamide of 12%.

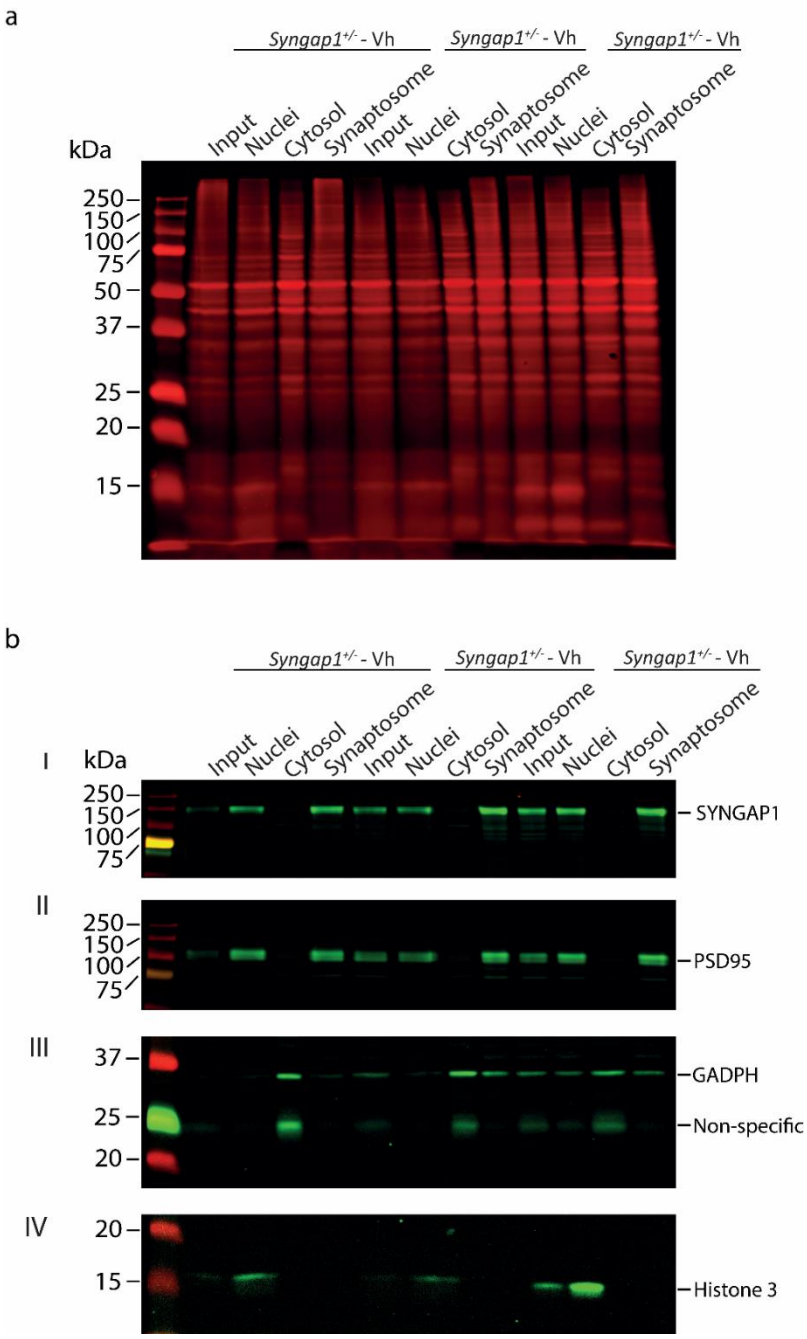

Figure S-32. Subcellular fractionation of hippocampal homogenates using the second version of the protocol.

Total protein staining (a), anti-SYNGAP1 (b-I, green), anti-PSD95 (b-II, green), anti-GAPDH (b-III, green) and anti-Histone 3 (b-IV, green) staining of subcellular fractions derived from hippocampus of *Syngap1*$^{+/-}$ vehicle treated. Total protein was used as loading control. The gel was used at a concentration of bis acrylamide of 12%.

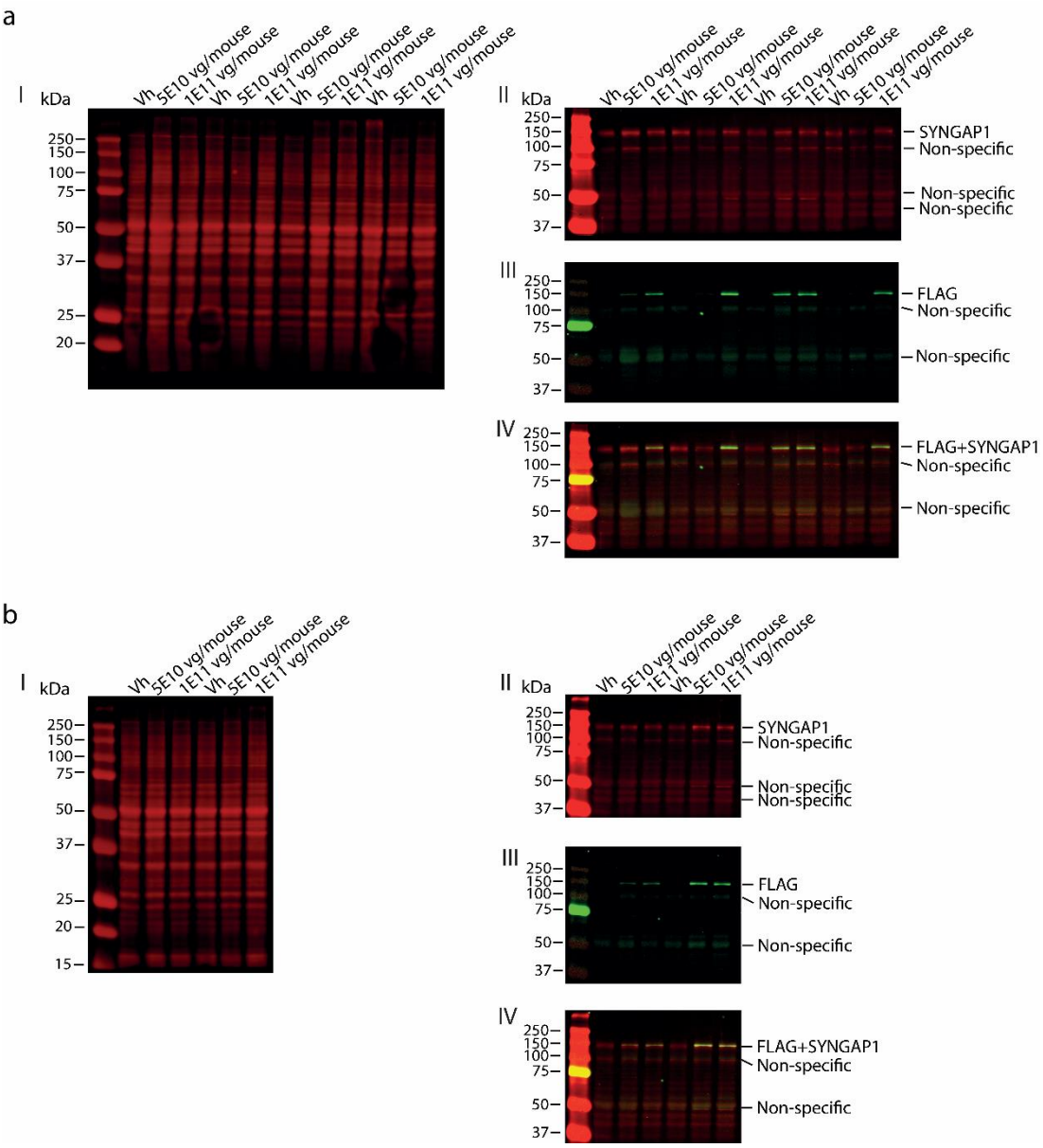

Figure S-33. Endogenous SYNGAP1 and AAV9/hSYN1-hSYNGAP1 FLAG-tagged SYNGAP1 in cortex of Syngap1$^{+/-}$ mice.

Total protein staining (a-I, b-I), anti-SYNGAP1 (a-II, b-II, red) and anti-FLAG (a-III, b-III, green) staining in cortex of *Syngap1*$^{+/-}$ mice treated with vehicle or AAV9/hSYN1-*hSYNGAP1* vector. FLAG and SYNGAP1 channels merge (a-IV and b-IV) reported as reference. Total protein was used as loading control. The gel was used at a concentration of bis acrylamide of 10%.

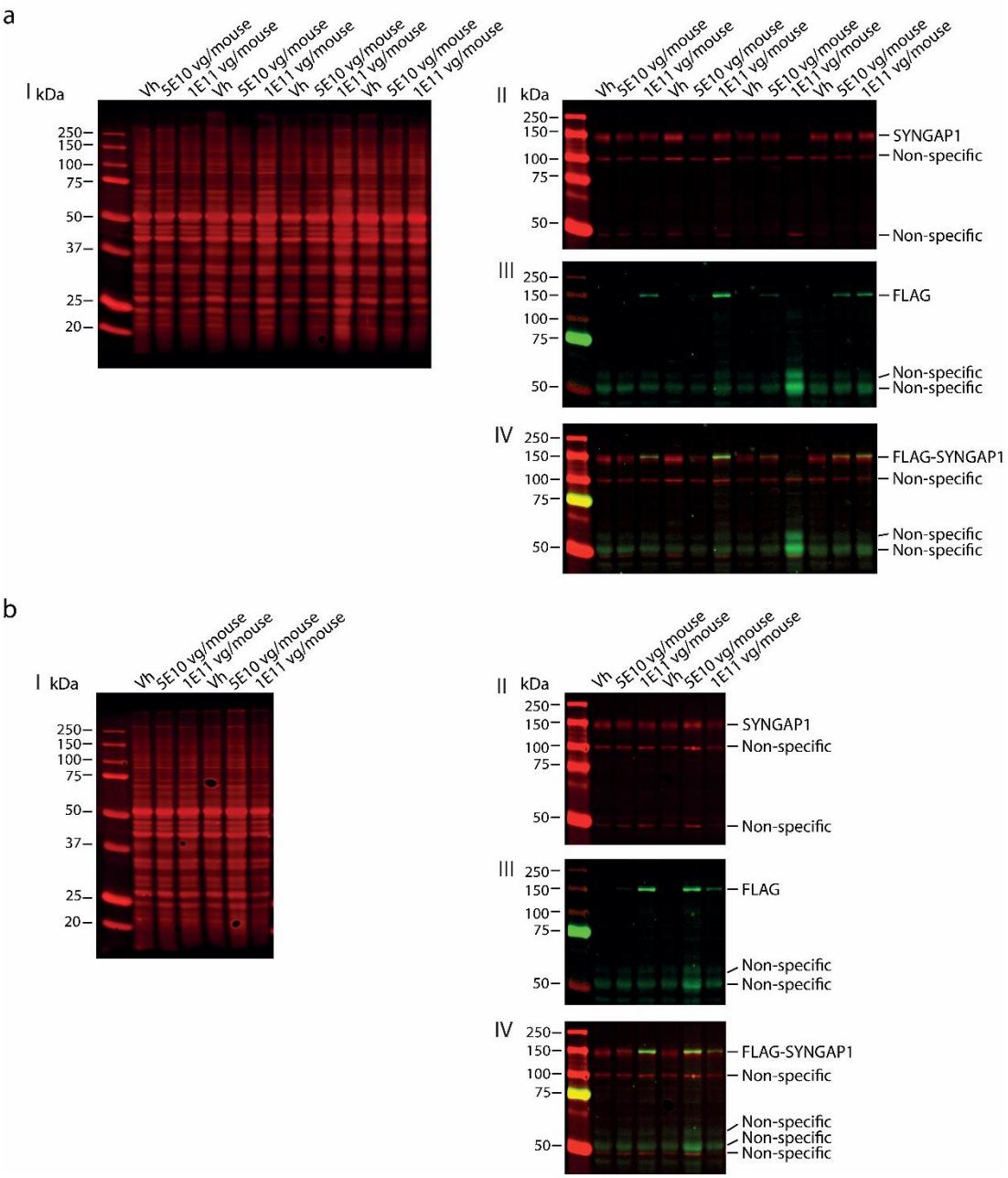

Figure S-34. Endogenous SYNGAP1 and AAV9/hSYN1-hSYNGAP1 FLAG-tagged SYNGAP1 in hippocampus of Syngap1$^{+/-}$ mice.

Total protein staining (a-I, b-I), anti-SYNGAP1 (a-II, b-II, red) and anti-FLAG (a-III, b-III, green) staining in hippocampus of *Syngap1*$^{+/-}$ mice treated with vehicle or AAV9/hSYN1-*hSYNGAP1* vector. FLAG and SYNGAP1 channels merge (a-IV and b-IV) reported as reference. Total protein was used as loading control. The gel was used at a concentration of bis acrylamide of 10%.

Aceti, M., T. K. Creson, T. Vaissiere, C. Rojas, W. C. Huang, Y. X. Wang, R. S. Petralia, ..., and Gavin Rumbaugh. (2015). "Syngap1 Haploinsufficiency Damages a Postnatal Critical Period of Pyramidal Cell Structural Maturation Linked to Cortical Circuit Assembly." *Biol. Psychiatry*, 77(9):805–15.

Agarwal, M., M. V. Johnston, and C. E. Stafstrom. (2019). "SYNGAP1 Mutations: Clinical, Genetic, and Pathophysiological Features." *Int. J. Dev. Neurosci.*, 78:65–76.

Agbandje-McKenna, Mavis, and Jürgen Kleinschmidt. (2011). *AAV Capsid Structure and Cell Interactions*. Vol. 807.

Air, G. M., E. H. Blackburn, A. R. Coulson, F. Galibert, F. Sanger, J. W. Sedat, and E. B. Ziff. (1976). "Gene F of Bacteriophage X174. Correlation of Nucleotide Sequences from the DNA and Amino Acid Sequences from the Gene Product." *J. Mol. Biol.*, 107(4):445–58.

Allocca, M., M. Doria, M. Petrillo, P. Colella, M. Garcia-Hoyos, D. Gibbs, S. R. Kim, A. Maguire, ..., and A. Auricchio. (2008). "Serotype-Dependent Packaging of Large Genes in Adeno-Associated Viral Vectors Results in Effective Gene Delivery in Mice." *J. Clin. Invest.*, 118(5):1955–64.

Andrews, A. M., X. Cheng, S. C. Altieri, and H. Yang. (2018). "Bad Behavior: Improving Reproducibility in Behavior Testing." *ACS Chem Neurosci.*, 9(8):1904–6.

Araki, Y., I. Hong, T. R. Gamache, S. Ju, L. Collado-Torres, J. H. Shin, and R. L. Huganir. (2020). "Syngap Isoforms Differentially Regulate Synaptic Plasticity and Dendritic Development." *Elife*, 9:1–28.

Araki, Y., M. Zeng, M. Zhang, and R. L. Huganir. (2015). "Rapid Dispersion of SynGAP from Synaptic Spines Triggers AMPA Receptor Insertion and Spine Enlargement during LTP." *Neuron*, 85(1):173–89.

Arras, M., A. Rettich, P. Cinelli, H. P. Kasermann, and K. Burki. (2007). "Assessment of Post-Laparotomy Pain in Laboratory Mice by Telemetric Recording of Heart Rate and Heart Rate Variability." *BMC Vet. Res.*, 3:16.

Atchison, C. B., R. W. Casto, and Hammon W. MCD. (1965). "Adenovirus-Associated Virus." *Science (80-.).*, 149:754–55.

Aten, S., A. Kalidindi, H. Yoon, Ga. Rumbaugh, K. R. Hoyt, and K. Obrietan. (2021). "SynGAP Is Expressed in the Murine Suprachiasmatic Nucleus and Regulates Circadian-Gated Locomotor Activity and Light-Entrainment Capacity." *Eur. J. Neurosci.*, 53(3):732–49.

Ayala, GF., M. Dichter, Gumnit RJ., H. Matsumoto, and A. Spencerw. (1973). “Genesis of Epileptic Interictal Spikes. New Knowledge of Cortical Feedback Systems Suggest a Neurophysiological Explanation of Brief Paroxysms.” *Brain Res.*, 4(4):387–88.

Bahey, N., K. Gadalla, M. Rhona, M. Bailey, J. Edgar, and S. Cobb. (2017). “Reduced Axonal Diameter of Peripheral Nerve Fibers in a Mouse Model of Rett Syndrome.” *Neuroscience*, 358:261–68.

Bailey, K. R., N. R. Rustay, and J. N. Crawley. (2006). “Behavioral Phenotyping of Transgenic and Knockout Mice: Practical Concerns and Potential Pitfalls.” *ILAR J.*, 47(2):124–31.

Bailey, R. M., D. Armao, N. K. Sahana, and S. J. Gray. (2018). “Development of Intrathecal AAV9 Gene Therapy for Giant Axonal Neuropathy.” *Mol. Ther. - Methods Clin. Dev.*, 9:160–71.

Bannerman, D. M., M. Grubb, R. M. J. Deacon, B. K. Yee, J. Feldon, and J. N. P. Rawlins. (2003). “Ventral Hippocampal Lesions Affect Anxiety but Not Spatial Learning.” *Behav. Brain Res.*, 139(1–2):197–213.

Lo Barco, T., L. De Gaetano, E. Santangelo, T. Bravi, J. Proietti, G. Cantalupo, I. Brambilla, and F. Darra. (2022). “SYNGAP1-Related Developmental and Epileptic Encephalopathy: The Impact on Daily Life.” *Epilepsy Behav.*, 127:108500.

Lo Barco, T., A. Kaminska, R. Solazzi, C. Cancés, G. Barcia, N. Chemaly, E. Fontana, ..., and Rima Nabbout. (2021). “SYNGAP1 -DEE : A Visual Sensitive Epilepsy.” *Clin. Neurophys.*, 132(4):841–50.

Barnett, M. W., R. F. Watson, T. Vitalis, K. Porter, N. H. Komiyama, P. N. Stoney, T. H. Gillingwater, S. G. Grant, and P. C. Kind. (2006). “Synaptic Ras GTPase Activating Protein Regulates Pattern Formation in the Trigeminal System of Mice.” *J Neurosci.*, 26(5):1355–65.

Bast, T., and J. Feldon. (2003). “Hippocampal Modulation of Sensorimotor Processes.” *Prog. Neurobiol.*, 70:319–45.

Bear, M. F. (2005). “Therapeutic Implications of the MGluR Theory of Fragile X Mental Retardation.” *Genes Brain Behav.*, 4(6):393–98.

Belur, L. R., M. Romero, J. Lee, K. M. Podetz-Pedersen, Z. Nan, M. S. Riedl, L. Vulchanova, ..., and R. Scott McIvor. (2021). “Comparative Effectiveness of Intracerebroventricular, Intrathecal, and Intranasal Routes of AAV9 Vector Administration for Genetic Therapy of Neurologic Disease in Murine Mucopolysaccharidosis Type I.” *Front. Mol. Neurosci.*, 14:618360.

Bermejo, M. K., M. Milenkovic, A. Salahpour, and A. J. Ramsey. (2014). “Preparation

of Synaptic Plasma Membrane and Postsynaptic Density Proteins Using a Discontinuous Sucrose Gradient." *J. Vis. Exp.*, (91):1–8.

Berridge, K. C., and J. C. Fentress. (1987). "Disruption of Natural Grooming Chains." *Psychobiology*, 15(4):336–42.

Berryer, M. H., B. Chattopadhyaya, P. Xing, I. Riebe, C. Bosoi, N. Sanon, ..., J. C. Lacaille, J. L. Michaud, and G. Di Cristo. (2016). "Decrease of SYNGAP1 in GABAergic Cells Impairs Inhibitory Synapse Connectivity, Synaptic Inhibition and Cognitive Function." *Nat. Commun.*, 7:13340.

Berryer, M. H., F. F. Hamdan, L. L. Klitten, R. S. Møller, L. Carmant, J. Schwartzentruber, L. Patry, ..., J. L. Michaud, and G. Di Cristo. (2013). "Mutations in SYNGAP1 Cause Intellectual Disability, Autism, and a Specific Form of Epilepsy by Inducing Haploinsufficiency." *Hum. Mutat.*, 34(2):385–94.

Blömer, U., L. Naldini, I. M. Verma, D. Trono, and F. H. Gage. (1996). "Applications of Gene Therapy to the CNS." *Hum. Mol. Genet.*, 5(REVIEW):1397–1404.

Bolivar, V. J. (2009). "Neurobiology of Learning and Memory Intrasession and Intersession Habituation in Mice : From Inbred Strain Variability to Linkage Analysis." *Neurobiol. Learn. Mem.*, 92:206–14.

Borsini, F., J. Podhorna, and D. Marazziti. (2002). "Do Animal Models of Anxiety Predict Anxiolytic-like Effects of Antidepressants?" *Psychopharmacology (Berl).*, 163:121–41.

Bouard, D., N. Alazard-Dany, and F. L. Cosset. (2009). "Viral Vectors: From Virology to Transgene Expression." *Br. J. Pharmacol.*, 157(2):153–65.

Brown, H. C., P. M. Zakas, S. N. George, E. T. Parker, H. T. Spencer, and C. B. Doering. (2018). "Target-Cell-Directed Bioengineering Approaches for Gene Therapy of Hemophilia A." *Mol. Ther. - Methods Clin. Dev.*, 9(June):57–69.

Bulcha, J. T., Y. Wang, H. Ma, P. W. L. Tai, and G. Gao. (2021). "Viral Vector Platforms within the Gene Therapy Landscape." *Signal Transduct. Target. Ther.*, 6(1).

Buller-peralta, I., J. Maicas-Royo, Z. Lu, S. M. Till, E. R. Wood, P. .. C. Kind, J. Escudero, and A. Gonzalez-sulser. (2022). "Abnormal Brain State Distribution and Network Connectivity in a SYNGAP1 Rat Model." *BioRxiv*,.

Burgess-Brown, N. A., S. Sharma, F. Sobott, C. Loenarz, U. Oppermann, and O. Gileadi. (2008). "Codon Optimization Can Improve Expression of Human Genes in Escherichia Coli: A Multi-Gene Study." *Protein Expr. Purif.*, 59(1):94–102.

Cantore, A., N. Nair, P. Della Valle, M. Di Matteo, J. Màtrai, F. Sanvito, C. Brombin, ..., Marinee Chuah, Luigi Naldini, and Thierry VandenDriessche. (2012). "Hyperfunctional Coagulation Factor IX Improves the Efficacy of Gene Therapy

in Hemophilic Mice." *Blood*, 120(23):4517–20.

Carlisle, H. J., P. Manzerra, E. Marcora, and M. B. Kennedy. (2008). "SynGAP Regulates Steady-State and Activity-Dependent Phosphorylation of Cofilin." *J. Neurosci.*, 28(50):13673–83.

Carreño-Muñoz, M. I., B. Chattopadhyaya, K. Agbogba, V. Côté, S. Wang, M. Lévesque, M. Avoli, ..., and Graziella Di Cristo. (2021). "Sensory Processing Dysregulations as Reliable Translational Biomarkers in SYNGAP1 Haploinsufficiency." *Brain*, 1–16.

Carvill, G. L., S. B. Heavin, S. C. Yendle, J. M. McMahon, B. J. O'Roak, J. Cook, A. Khan, ..., I. E. Scheffer, and H. C. Mefford. (2013). "Targeted Resequencing in Epileptic Encephalopathies Identifies de Novo Mutations in CHD2 and SYNGAP1." *Nat. Genet.*, 45(7):825–30.

Cash, J. N., P. V. Sharma, and J. J. G. Tesmer. (2019). "Structural and Biochemical Characterization of the Pleckstrin Homology Domain of the RhoGEF P-Rex2 and Its Regulation by PIP3." *J. Struct. Biol. X*, 1(July 2018):100001.

Castellanos, F. X., and E. Proal. (2012). "Large-Scale Brain Systems in ADHD: Beyond the Prefrontal- Striatal Model." *Trends Cogn. Sci.*, 16(1):17–26.

Chakrabarty, P., A. Rosario, P. Cruz, Z. Siemienski, C. Ceballos-Diaz, K. Crosby, K. Jansen, ..., and Y. Levites. (2013). "Capsid Serotype and Timing of Injection Determines AAV Transduction in the Neonatal Mice Brain." *PLoS One*, 8(6):0–8.

Challis, R. C., S. R. Kumar, X. Chen, D. Goertsen, G. M. Coughlin, Acacia M. Hori, M. R. Chuapoco, ..., and V. Gradinaru. (2022). "Adeno-Associated Virus Toolkit to Target Diverse Brain Cells." *Annu. Rev. OfNeuroscience*, 45:447–69.

Chatterjee, D., D. J. Marmion, J. L. McBride, F. P. Manfredsson, D. Butler, A. Messer, and J. H. Kordower. (2022). "Enhanced CNS Transduction from AAV.PHP.EB Infusion into the Cisterna Magna of Older Adult Rats Compared to AAV9." *Gene Ther.*, 29:390–97.

Chellappan, D. K., N. S. Sivam, K. X. Teoh, W. P. Leong, T. Z. Fui, K. Chooi, N. Khoo, ..., and K. Dua. (2018). "Gene Therapy and Type 1 Diabetes Mellitus." *Biomed. Pharmacother.*, 108(July):1188–1200.

Chen, H. J., M. Rojas-Soto, A. Oguni, and M. B. Kennedy. (1998). "A Synaptic Ras-GTPase Activating Protein (P135 SynGAP) Inhibited by CaM Kinase II." *Neuron*, 20(5):895–904.

Chen, X., T. Dong, Y. Hu, F. C. Shaffo, N. R. Belur, J. R. Mazzulli, and S. J. Gray. (2022). "AAV9/MFSD8 Gene Therapy Is Effective in Preclinical Models of Neuronal Ceroid Lipofuscinosis Type 7 Disease." *J. Clin. Invest.*, 132(5):146286.

Chérot, E., B. Keren, C. Dubourg, W. Carré, M. Fradin, A. Lavillaureix, A. Afenjar, ..., and C. Mignot. (2018). “Using Medical Exome Sequencing to Identify the Causes of Neurodevelopmental Disorders: Experience of 2 Clinical Units and 216 Patients.” *Clin. Genet.*, 93(3):567–76.

Chevarin, M., Y. Duffourd, R. A. Barnard, S. Moutton, F. Lecoquierre, F. Daoud, P. Kuentz, ..., and L. Faivre. (2020). “Excess of de Novo Variants in Genes Involved in Chromatin Remodelling in Patients with Marfanoid Habitus and Intellectual Disability.” *J. Med. Genet.*, 57(7):466–74.

Cho, K., M. M. Hill, S. Chigurupati, G. Du, R. G. Parton, and J. F. Hancock. (2011). “Therapeutic Levels of the Hydroxmethylglutaryl-Coenzyme A Reductase Inhibitor Lovastatin Activate Ras Signaling via Phospholipase D2.” *Mol. Cell. Biol.*, 31(6):1110–20.

Cho, W., and R. V. Stahelin. (2006). “Membrane Binding and Subcellular Targeting of C2 Domains.” *Biochim. Biophys. Acta*, 1761(8):838–49.

Choi, J., N. Yu, G. Baek, J. Bakes, D. Seo, H. Nam, S. H. Baek, ..., and B. Kaang. (2014). “Optimization of AAV Expression Cassettes to Improve Packaging Capacity and Transgene Expression in Neurons.” *Mol. Brain*, 7(17).

Choi, V. W., A. Asokan, R. A. Haberman, T. J. McCown, and R. J. Samulski. (2006). “Production of Recombinant Adeno-Associated Viral Vectors and Use for in Vitro and in Vivo Administration.” *Curr. Protoc. Neurosci.*, Chapter 4:1–30.

Chow, B. Y., A. S. Chuong, N. C. Klapoetke, and E. S. Boyden. (2011). “Synthetic Physiology: Strategies for Adapting Tools from Nature for Genetically-Targeted Control of Fast Biological Processes.” *Methods Enzym.*, 497:425–43.

Clark, J. D., L. L. Lin, R. W. Kriz, C. S. Ramesha, L. A. Sultzman, A. Y. Lin, N. Milona, and J. L. Knopf. (1991). “A Novel Arachidonic Acid-Selective Cytosolic PLA2 Contains a Ca(2+)-Dependent Translocation Domain with Homology to PKC and GAP.” *Cell*, 65(6):1043–51.

Clark Reed, K., F. Voulgaropoulou, D. M. Fraley, and P. R. Johnson. (1995). “Cell Lines for the Production of Recombinant Adeno-Associated Virus.” *Hum. Gene Ther.*, 6(October):1329–41.

Clement, J. P., M. Aceti, T. K. Creson, E. D. Ozkan, Y. Shi, N. J. Reish, A. G. Almonte, ..., and G. Rumbaugh. (2012). “Pathogenic SYNGAP1 Mutations Impair Cognitive Development by Disrupting Maturation of Dendritic Spine Synapses.” *Cell*, 151(4):709–23.

Clement, J. P., E. D. Ozkan, M. Aceti, C. A. Miller, and G. Rumbaugh. (2013). “SYNGAP1 Links the Maturation Rate of Excitatory Synapses to the Duration of Critical-Period Synaptic Plasticity.” *J. Neurosci.*, 33(25):10447–52.

Cook, E. H., J. T. Masaki, S. J. Guter, and F. Najjar. (2019). “Lovastatin Treatment of a Patient with a De Novo SYNGAP1 Protein Truncating Variant.” *J. Child Adolesc. Psychopharmacol.*, 29(4):321–22.

Cooray, S., S. J. Howe, and A. J. Thrasher. (2012). “Retrovirus and Lentivirus Vector Design and Methods of Cell Conditioning.” Pp. 29–57 in *Methods in Enzymology*. Vol. 507. Elsevier Inc.

Cortese, S., and F. X. Castellanos. (2012). “Neuroimaging of Attention-Deficit/Hyperactivity Disorder: Current Neuroscience-Informed Perspectives for Clinicians.” *Curr. Psychiatry Rep.*, 14(5):1–13.

Crawley, J. N., J. K. Belknap, A. Collins, J. C. Crabbe, W. Frankel, N. Henderson, R. J. Hitzemann, ..., and R. Paylor. (1997). “Behavioral Phenotypes of Inbred Mouse Strains: Implications and Recommendations for Molecular Studies.” *Psychopharmacology (Berl).*, 132:107–24.

Creson, T. K., C. Rojas, E. Hwaun, T. Vaissiere, M. Kilinc, J. Andres, J. L. Holder, ..., and Gavin Rumbaugh. (2019). “Re-Expression of SynGAP Protein in Adulthood Improves Translatable Measures of Brain Function and Behavior.” *Elife*, 8:e46752.

Crick, F., L. Barnett, S. Brenner, and J. Watts-Tobin. (1961). “General Neture of the Genetic Code for Proteins.” *Nature*, 192:1227–32.

Crooke, S. T., X. H. Liang, B. F. Baker, and R. M. Crooke. (2021). “Antisense Technology: A Review.” *J. Biol. Chem.*, 296:100416.

Cunningham, C., R. Deacon, H. Wells, D. Boche, S. Waters, C. Picanco Diniz, H. Scott, J. N. P. Rawlins, and V. H. Perry. (2003). “Synaptic Changes Characterize Early Behavioural Signs in the ME7 Model of Murine Prion Disease.” *Eur. J. Neurosci.*, 17(10):2147–55.

Davis, M. (1992). “The Role of the Amygdala in Fear and Anxiety.” *Annu. Rev. Neurosci.*, 15:353–75.

Davis, M., D. Rainnie, and M. Cassell. (1994). “Neurotransmission in the Rat Amygdala Related to Fear and Anxiety.” *TINS*, 17(5).

Davletov, B. A., and T. C. Südhof. (1993). “A Single C2 Domain from Synaptotagmin I Is Sufficient for High Affinity Ca2+/Phospholipid Binding.” *J Biol Chem*, 268(35):26386–90.

Dawicki-mckenna, J. M., A. J. Felix, E. A. Waxman, C. Congsheng, D. A. Amado, P. T. Ranum, A. Bogush, ..., and B. L. Prosser. (2022). “Mapping PTBP Splicing in Human Brain Identifies Targets for Therapeutic Splice Switching Including SYNGAP1.” *Biorxiv*,.

Dawson, G. R., S. P. Crawford, N. Collinson, S. D. Iversen, and M. D. Tricklebank. (1995). “Evidence That the Anxiolytic-like Effects of Chlordiazepoxide on the Elevated plus Maze Are Confounded by Increases in Locomotor Activity.” *Psychopharmacology (Berl).*, 118(3):316–23.

Daya, Shyam, and Kenneth I. Berns. (2008). “Gene Therapy Using Adeno-Associated Virus Vectors.” *Clin. Microbiol. Rev.*, 21(4):583–93.

Deacon, R. (2006a). “Assessing Nest Building in Mice.” *Nat. Protoc.*, 1(3):1117.

Deacon, R. (2006b). “Digging and Marble Burying in Mice: Simple Methods for in Vivo Identification of Biological Impacts.” *Nat. Protoc.*, 1(1):nprot.2006.20.

Deacon, R. M. J., D. M. Bannerman, and J. N. P. Rawlins. (2002). “Anxiolytic Effects of Cytotoxic Hippocampal Lesions in Rats.” *Behav. Neurosci.*, 116(3):494–97.

Deacon, R. M. J., and J. N. P. Rawlins. (2005). “Hippocampal Lesions, Species-Typical Behaviours and Anxiety in Mice.” *Behav. Brain Res.*, 156(2):241–49.

Dekkers, T. J., A. Popma, J. A. Agelink, V. Rentergem, A. Bexkens, and H. M. Huizenga. (2016). “Risky Decision Making in Attention-Deficit/Hyperactivity Disorder: A Meta-Regression Analysis.” *Clin. Psychol. Rev.*, 45:1–16.

Delorey, T. M., P. Sahbaie, E. Hashemi, G. E. Homanics, and J. D. Clark. (2008). “Gabrb3 Gene Deficient Mice Exhibit Impaired Social and Exploratory Behaviors, Deficits in Non-Selective Attention and Hypoplasia of Cerebellar Vermal Lobules: A Potential Model of Autism Spectrum Disorder.” *Behav. Brain Res.*, 187:207–20.

Dember, W. N., and H. Fowler. (1958). “Spontaneous Alteration Behavior.” *Psycological Bull.*, 6(4):331–36.

Dennis, E. J., A. E. Hady, A. Michaiel, A. Clemens, D. R. Gowan Tervo, J. Voigts, and S. R. Datta. (2021). “Systems Neuroscience of Natural Behaviors in Rodents.” *J. Neurosci.*, 41(5):911–19.

Desai, A., H. Chen, and H. Y. Kim. (2020). “Multiple Mild Traumatic Brain Injuries Lead to Visual Dysfunction in a Mouse Model.” *J. Neurotrauma*, 37(2):286–94.

Dhuri, K., C. Bechtold, E. Quijano, H. Pham, A. Gupta, A. Vikram, and R. Bahal. (2020). “Antisense Oligonucleotides: An Emerging Area in Drug Discovery and Development.” *J. Clin. Med.*, 9(6):1–24.

Ding, W., L. Zhang, Z. Yan, and J. F. Engelhardt. (2005). “Intracellular Trafficking of Adeno-Associated Viral Vectors.” *Gene Ther.*, 12(11):873–80.

Disbrow, G. L., I. Sunitha, C. C. Baker, J. Hanover, and R. Schlegel. (2003). “Codon Optimization of the HPV-16 E5 Gene Enhances Protein Expression.” *Virology*,

311:105–14.

Dobson, C. M. (2003). “Protein Folding and Misfolding Christopher.” *Nature*, 426(December):1–4.

Dong, B., H. Nakai, and W. Xiao. (2010). “Characterization of Genome Integrity for Oversized Recombinant AAV Vector.” *Mol. Ther.*, 18(1):87–92.

Dong, J., P. Fan, and R. A. Frizzell. (1996). “Quantitative Analysis of the Packaging Capacity of Recombinant Adeno-Associated Virus.” *Hum. Gene Ther.*, 7:2101–12.

Durston, S., J. V. Belle, and P. de Zeeuw. (2011). “Circuits in Attention-Deficit/Hyperactivity Disorder Neuroanatomical Substrate for Links Among Prefrontal.” *Biol Psychiatry*, 69:1178–84.

Dutta, S., B. Ray, S. Raut, and C. K. Sahoo. (2021). “Nonviral Gene Therapy: Technology and Application.” *Res. J. Sci. Technol.*, 13(1):13–22.

El-kordi, A., D. Winkler, K. Hammerschmidt, A. Kästner, D. Krueger, A. Ronnenberg, C. Ritter, ..., and Hannelore Ehrenreich. (2013). “Development of an Autism Severity Score for Mice Using Nlgn4 Null Mutants as a Construct-Valid Model of Heritable Monogenic Autism.” *Behav. Brain Res.*, 251:41–49.

Fader, K. A., I. D. Pardo, R. C. Kovi, C. J. Somps, H. H. Wang, V. S. Vaidya, S. K. Ramaiah, and M. P. Sirivelu. (2022). “Circulating Neurofilament Light Chain as a Promising Biomarker of AAV-Induced Dorsal Root Ganglia Toxicity in Nonclinical Toxicology Species.” *Mol. Ther. Methods Clin. Dev.*, 25:264–77.

Fåhraeus, R., M. Marin, and V. Olivares-Illana. (2016). “Whisper Mutations: Cryptic Messages within the Genetic Code.” *Oncogene*, 35(29):3753–59.

Faraone, S. V., R. H. Perlis, A. E. Doyle, J. W. Smoller, J. J. Goralnick, M. A. Holmgren, and P. Sklar. (2005). “Molecular Genetics of Attention-Deficit/Hyperactivity Disorder.” *Biol. Psychiatry*, 57(11):1313–23.

Farid, S. S., and M. J. Jenkins. (2018). “Bioprocesses for Cell Therapies.” Pp. 899–930 in *Biopharmaceutical Processing: Development, Design, and Implementation of Manufacturing Processes*. Elsevier Ltd.

Fiers, W., R. Contreras, F. Duerinck, G. Haegmean, J. Merregaert, W. M. Jou, A. Raeymakers, ..., and M. Van Montagu. (1975). “A-Protein Gene of Bacteriophage MS2.” *Nature*, 256(5515):273–78.

Firth, A. E. (2014). “Mapping Overlapping Functional Elements Embedded within the Protein-Coding Regions of RNA Viruses.” *Nucleic Acids Res.*, 42(20):12425–39.

Foster, H., P. S. Sharp, T. Athanasopoulos, C. Trollet, I. R. Graham, K. Foster, D. J.

Wells, and G. Dickson. (2008). “Codon and MRNA Sequence Optimization of Microdystrophin Transgenes Improves Expression and Physiological Outcome in Dystrophic Mdx Mice Following AAV2 / 8 Gene Transfer.” *Mol. Ther.*, 16(11):1825–32.

Foust, K. D., E. Nurre, C. L. Montgomery, A. Hernandez, C. M. Chan, and B. K. Kaspar. (2009). “Intravascular AAV9 Preferentially Targets Neonatal Neurons and Adult Astrocytes.” *Nat. Biotechnol.*, 27(1):59–65.

Fox, M. A., M. G. Panessiti, F. S. Hall, G. R. Uhl, and D. L. Murphy. (2013). “An Evaluation of the Serotonin System and Perseverative, Compulsive, Stereotypical, and Hyperactive Behaviors in Dopamine Transporter (DAT) Knockout Mice.” *Psychopharmacology (Berl).*, 227:685–95.

Fox, M. W. (1965). “The Visual Cliff Test for the Study of Visual Depth Perception in the Mouse.” *Anim. Behav.*, 13(2–3):232–33.

Fukami, M., E. Suzuki, M. Igarashi, M. Miyado, and T. Ogata. (2018). “Gain-of-Function Mutations in G-Protein–Coupled Receptor Genes Associated with Human Endocrine Disorders.” *Clin. Endocrinol. (Oxf).*, 88(3):351–59.

Fukami, M., Er. Suzuki, Y. Izumi, T. Torii, S. Narumi, M. Igarashi, M. Miyado, ..., and T. Ogata. (2017). “Paradoxical Gain-of-Function Mutant of the G-Protein-Coupled Receptor PROKR2 Promotes Early Puberty.” *J. Cell. Mol. Med.*, 21(10):2623–26.

Funk, A. J., G. Rumbaugh, V. Harotunian, R. E. McCullumsmith, and J. H. Meador-Woodruff. (2009). “Decreased Expression of NMDA Receptor-Associated Proteins in Frontal Cortex of Elderly Patients with Schizophrenia.” *Neuroreport*, 20(11):1019–22.

Furuta-hanawa, B., T. Yamaguchi, and E. Uchida. (2019). “Two-Dimensional Droplet Digital PCR as a Tool for Titration and Integrity Evaluation of Recombinant Adeno-Associated Viral Vectors.” *Hum. Gene Ther. Methods*, 30(4):127–36.

Gadalla, K. K. E., M. E. S. Bailey, R. C. Spike, P. D. Ross, K. T. Woodard, S. N. Kalburgi, L. Bachaboina, ..., S. J. Gray, and S. R. Cobb. (2013). “Improved Survival and Reduced Phenotypic Severity Following AAV9/MECP2 Gene Transfer to Neonatal and Juvenile Male Mecp2 Knockout Mice.” *Mol. Ther.*, 21(1):18–30.

Gadalla, K. K. E., T. Vudhironarit, R. D. Hector, S. Sinnett, N. G. Bahey, M. E. S. Bailey, S. J. Gray, and S. R. Cobb. (2017). “Development of a Novel AAV Gene Therapy Cassette with Improved Safety Features and Efficacy in a Mouse Model of Rett Syndrome.” *Mol. Ther. - Methods. Clin. Dev.*, 5:180–90.

Gagliardi, M., and A. T. Ashizawa. (2021). “The Challenges and Strategies of Antisense Oligonucleotide Drug Delivery.” *Biomedicines*, 9(4).

Galvan, A., T. L. Petkau, A. M. Hill, A. J. Korecki, G. Lu, D. Choi, K. Rahman, ..., and Y. Smith. (2021). “Intracerebroventricular Administration of AAV9-PHP.B SYN1-EmGFP Induces Widespread Transgene Expression in the Mouse and Monkey Central Nervous System.” *Hum. Gene Ther.*, 32(11–12):599–615.

Gamble, C. E., C. E. Brule, K. M. Dean, S. Fields, and E. J. Grayhack. (2016). “Adjacent Codons Act in Concert to Modulate Translation Efficiency in Yeast.” *Cell*, 166(3):679–90.

Gao, K., M. Li, L. Zhong, Q. Su, J. Li, S. Li, R. He, ..., and G. Gao. (2014). “Empty Virions in AAV8 Vector Preparations Reduce Transduction Efficiency and May Cause Total Viral Particle Dose-Limiting Side Effects.” *Mol. Ther. - Methods Clin. Dev.*, 1:9.

Gardlík, R., R. Pálffy, J. Hodosy, J. Lukács, J. Turňa, and P. Celec. (2005). “Vectors and Delivery Systems in Gene Therapy.” *Med Sci Monit*, 11(4):110–21.

Gauthier, J., T. J. Siddiqui, P. Huashan, D. Yokomaku, F. F. Hamdan, N. Champagne, M. Lapointe, ..., and G. A. Rouleau. (2011). “Truncating Mutations in NRXN2 and NRXN1 in Autism Spectrum Disorders and Schizophrenia.” *Hum. Genet.*, 130(4):563–73.

Gibson, E. J., and R. D. Walk. (1960). “The ‘Visual Cliff’.” *Sci. Am.*, 202(4):64–71.

Giedd, J. N., J. Blumenthal, E. Molloy, and F. X. Castellanos. (2001). “Brain Imaging of Attention Deficit / Hyperactivity Disorder.” *Ann. NEW YORK Acad. Sci.*,.

Gou, G., A. Roca-Fernandez, M. Kilinc, E. Serrano, R. Reig-Viader, Y. Araki, R. L. Huganir, C. de Quintana-Schmidt, G. Rumbaugh, and À. Bayés. (2020). “SynGAP Splice Variants Display Heterogeneous Spatio-Temporal Expression and Subcellular Distribution in the Developing Mammalian Brain.” *J. Neurochem.*, 00:1–17.

Goverdhana, S., M. Puntel, W. Xiong, J. M. Zirger, C. Barcia, J. F. Curtin, E. B. Soffer, ..., and M. G. Castro. (2005). “Regulatable Gene Expression Systems for Gene Therapy Applications: Progress and Future Challenges.” *Mol. Ther.*, 12(2):189–211.

Gray, J. A., and N. McNaughton. (1983). “Comparison between the Behavioural Effects of Septal and Hippocampal Lesions: A Review.” *Neurosci. Biobehav. Rev.*, 7(2):119–88.

Gray, S. J., S. B. Foti, J. W. Schwartz, L. Bachaboina, B. Taylor-Blake, J. Coleman, M. D. Ehlers, ..., and R. J. Samulski. (2011). “Optimizing Promoters for Recombinant Adeno-Associated Virus-Mediated Gene Expression in the Peripheral and Central Nervous System Using Self-Complementary Vectors.” *Hum. Gene Ther.*, 22(9):1143–53.

Greengard, P., F. Valtorta, A. J. Czernik, and F. Benfenati. (1993). “Synaptic Vesicle Phosphoproteins and Regulation of Synaptic Function.” *Science (80-.).*, 259:780–85.

Grieger, J. .. C., and R. J. Samulski. (2005). “Packaging Capacity of Adeno-Associated Virus Serotypes: Impact of Larger Genomes on Infectivity and Postentry Steps.” *J. Virol.*, 79(15):9933–44.

le Guiner, C., L. Servais, M. Montus, T. Larcher, M. Allais, V. Franc, ..., and G. Dickson. (2017). “Long-Term Microdystrophin Gene Therapy Is Effective in a Canine Model of Duchenne Muscular Dystrophy.” *Nat. Commun.*, 100.

Guo, X., P. J. Hamilton, N. J. Reish, J. D. Sweatt, C. A. Miller, and G. Rumbaugh. (2009). “Reduced Expression of the NMDA Receptor-Interacting Protein SynGAP Causes Behavioral Abnormalities That Model Symptoms of Schizophrenia.” *Neuropsychopharmacology*, 34(7):1659–72.

Hadjas, L. C., M. M. Schartner, J. Cand, M. C. Creed, V. Pascoli, C. Lüscher, and L. D. Simmler. (2020). “Projection-Specific Deficits in Synaptic Transmission in Adult Sapap3-Knockout Mice.” *Neuropsychopharmacology*, 45:2020–29.

Haggerty, D. L., G. G. Grecco, K. C. Reeves, and B. Atwood. (2020). “Adeno-Associated Viral Vectors in Neuroscience Research.” *Mol. Ther. Methods Clin. Dev.*, 17:69–82.

Hamdan, F. F., H. Daoud, A. Piton, J. Gauthier, S. Dobrzeniecka, M. O. Krebs, R. Joober, ..., and J. L. Michaud. (2011). “De Novo SYNGAP1 Mutations in Nonsyndromic Intellectual Disability and Autism.” *Biol. Psychiatry*, 69(9):898–901.

Hamdan, F. F., J. Gauthier, D. Spiegelman, A. Noreau, Y. Yang, S. Pellerin, S. Dobrzeniecka, ..., and J. L. Michaud. (2009). “Mutations in SYNGAP1 in Autosomal Nonsyndromic Mental Retardation.” *N. Engl. J. Med.*, 360(6):599–605.

Han, S., C. Tai, R. E. Westenbroek, F. H. Yu, C. S. Cheah, G. B. Potter, J. L. Rubenstein, ..., and William A. Catterall. (2012). “Autistic-like Behaviour in Scn1a +- Mice and Rescue by Enhanced GABA-Mediated Neurotransmission.” *Nature*, 489(7416):385–90.

Hannigan, J. H., J. E. Springer, and R. L. Isaacson. (1984). “Differentiation of Basal Ganglia Dopaminergic Involvement in Behavior after Hippocampectomy.” *Brain Res.*, 291:83–91.

Harigaya, Y., and R. Parker. (2017). “The Link between Adjacent Codon Pairs and MRNA Stability.” *BMC Genomics*, 18(1):1–16.

Harris, E., and J. J. Elmer. (2021). “Optimization of Electroporation and Other Non-

Viral Gene Delivery Strategies for T Cells." *Biotechnol. Prog.*, 37(1).

Hogg, S. (1996). "A Review of the Validity and Variability of the Elevated Plus-Maze as an Animal Model of Anxiety." *Pharmacol. Biochem. Behav.*, 54(1):21–30.

Holder, JL Jr, FF Hamdan, and JL. Michaud. (2018). "SYNGAP1-Related Intellectual Disability Syndrome." *Arch. Neurol. Neurosci.*, 1(4):1–4.

Holmes, A., S. Parmigiani, P. F. Ferrari, P. Palanza, and R. J. Rodgers. (2000). "Behavioral Profile of Wild Mice in the Elevated Plus-Maze Test for Anxiety." *Physiol. Behav.*, 71(5):509–16.

Hopp, T. P., K. S. Prickett, V. L. Price, R. T. Libby, C. J. March, D. P. Cerretti, D. L. Urdal, and P. J. Conlon. (1988). "A Short Polypeptide Marker Sequence Useful for Recombinant Protein Identification and Purification." *Bio/Technology*, 6:1204–10.

Hordeaux, J., E. L. Buza, C. Dyer, T. Goode, T. W. Mitchell, L. Richman, N. Denton, ..., and J. M. Wilson. (2020). "Adeno-Associated Virus-Induced Dorsal Root Ganglion Pathology." *Hum. Gene Ther.*, 31(15):808–18.

Horner, A. E., R. H. Norris, R. McLaren-Jones, L. Alexander, N. H. Komiyama, S. G. N. Grant, J. Nithianantharajah, and M. V. Kopanitsa. (2021). "Learning and Reaction Times in Mouse Touchscreen Tests Are Differentially Impacted by Mutations in Genes Encoding Postsynaptic Interacting Proteins SYNGAP1, NLGN3, DLGAP1, DLGAP2 and SHANK2." *Genes, Brain Behav.*, 20(1):1–15.

Hösel, M., M. Broxtermann, H. Janicki, K. Esser, S. Arzberger, P. Hartmann, S. Gillen, ..., and Hildegard Büning. (2012). "Toll-like Receptor 2-Mediated Innate Immune Response in Human Nonparenchymal Liver Cells toward Adeno-Associated Viral Vectors." *Hepatology*, 55(1):287–97.

Howard, D. B., K. Powers, Y. Wang, and B. K. Harvey. (2008). "Tropism and Toxicity of Adeno-Associated Viral Vector Serotypes 1, 2, 5, 6, 7, 8, and 9 in Rat Neurons and Glia in Vitro." *Virology*, 372(1):24–34.

Huang, W., M. Calvo, K. Karu, H. R. Olausen, G. Bathgate, K. Okuse, D. L. H. Bennett, and A. S. C. Rice. (2013). "A Clinically Relevant Rodent Model of the HIV Antiretroviral Drug Stavudine Induced Painful Peripheral Neuropathy." *Pain*, 154(4):560–75.

Hughes, M. P., D. A. Smith, L. Morris, C. Fletcher, A. Colaco, M. Huebecker, J. Tordo, ..., and A. A. Rahim. (2018). "AAV9 Intracerebroventricular Gene Therapy Improves Lifespan, Locomotor Function and Pathology in a Mouse Model of Niemann-Pick Type C1 Disease." *Hum. Mol. Genet.*, 27(17):3079–98.

Le Huray, K. I. P., H. Wang, F. Sobott, and A. C. Kalli. (2022). "Systematic Simulation

of the Interactions of Pleckstrin Homology Domains with Membranes." *Sci. Adv.*, 8(27):1–14.

Husi, H., and S. G. Grant. (2001). "Isolation of 2000-KDa Complexes of N-Methyl-D-Aspartate Receptor and Postsynaptic Density 95 from Mouse Brain." *J. Neurochem.*, 77(1):281–91.

Huston, M. W., N. P. Van Til, T. P. Visser, S. Arshad, M. H. Brugman, C. Cattoglio, A. Nowrouzi, ..., and Gerard Wagemaker. (2011). "Correction of Murine SCID-X1 by Lentiviral Gene Therapy Using a Codon-Optimized IL2RG Gene and Minimal Pretransplant Conditioning." *Mol. Ther.*, 19(10):1867–77.

Ikemura, T. (1981). "Correlation between the Abundance of Escherichia Coli Transfer RNAs and the Occurrence of the Respective Codons in Its Protein Genes: A Proposal for a Synonymous Codon Choice That Is Optimal for the E. Coli Translational System." *J. Mol. Biol.*, 151:389–409.

Ingusci, S., G. Verlengia, M. Soukupova, S. Zucchini, and M. Simonato. (2019). "Gene Therapy Tools for Brain Diseases." *Front. Pharmacol.*, 10(July):1–19.

Iossifov, I., M. Ronemus, D. Levy, Zi. Wang, I. Hakker, J. Rosenbaum, B. Yamrom, ..., and Michael Wigler. (2012). "De Novo Gene Disruptions in Children on the Autistic Spectrum." *Neuron*, 74(2):285–99.

Isaac, J. T. R., R. A. Nicoll, and R. C. Malenka. (1995). "Evidence for Silent Synapses: Implications for the Expression of LTP." *Neuron*, 15(2):427–34.

Jagasia, R., C. Bon, S. V. Rasmussen, S. Badillo, D. Tehler, D. Buchy, M. Berrera, ..., and M. C. Hoener. (2022). "Angelman Syndrome Patient Neuron Screen Identifies a Potent and Selective Clinical ASO Targeting UBE3A-ATS with Long Lasting Effect in Cynomolgus Monkey." *BioRxiv*,.

Jimenez-Gomez, A. S., S. Niu, F. Andujar-Perez, E. A. McQuade, A. Balasa, D. Huss, R. Coorg, ..., and J. L. Holder. (2019). "Phenotypic Characterization of Individuals with SYNGAP1 Pathogenic Variants Reveals a Potential Correlation between Posterior Dominant Rhythm and Developmental Progression." *J. Neurodev. Disord.*, 11(1):1–11.

Jirkof, P. (2014). "Burrowing and Nest Building Behavior as Indicators of Well-Being in Mice." *J. Neurosci. Methods*, 234:139–46.

Jones, D. L., and G. J. Mogenson. (1980). "Nucleus Accumbens to Globus Pallidus GABA Projection Subserving Ambulatory Activity." *Am. J. Physiol.*, 7(1):65–68.

Kalin, N. H., S. E. Shelton, and R. J. Davidson. (2004). "The Role of the Central Nucleus of the Amygdala in Mediating Fear and Anxiety in the Primate." *J. Neurosci.*, 24(24):5506–15.

Karimian, A., K. Azizian, H. Parsian, S. Rafieian, V. Shafiei-Irannejad, M. Kheyrollah, M. Yousefi, M. Majidinia, and B. Yousefi. (2019). “CRISPR/Cas9 Technology as a Potent Molecular Tool for Gene Therapy.” *J. Cell Physiol.*, 234:12267–12277.

Karoly, P. J., D. R. Freestone, R. Boston, D. B. Grayden, D. Himes, K. Leyde, U. Seneviratne, ..., and M. J. Cook. (2016). “Interictal Spikes and Epileptic Seizures: Their Relationship and Underlying Rhythmicity.” *Brain*, 139(4):1066–78.

Katayama, K., N. Morimura, K. Kobayashi, D. Corbett, T. Okamoto, V. G. Ornthanalai, H. Matsunaga, ..., and J. Aruga. (2022). “Slitrk2 Deficiency Causes Hyperactivity with Altered Vestibular Function and Serotonergic Dysregulation.” *IScience*, 25(7):104604.

Katsanevaki, D., S. M. Till, I. Buller-Peralta, T. C. Watson, M. S. Nawaz, D. Arkell, S. Tiwari, V. Kapgal, ..., S. Chattarji, A. Gonzalez-Sulser, O. Hardt, E. R. Wood, and P. C. Kind. (2020). “Heterozygous Deletion of SYNGAP Enzymatic Domains in Rats Causes Selective Learning, Social and Seizure Phenotypes.” *Biorvix*,.

Kelsic, E. D., H. Chung, N. Cohen, J. Park, H. H. Wang, and R. Kishony. (2016). “RNA Structural Determinants of Optimal Codons Revealed by MAGE-Seq.” *Cell Syst.*, 3(6):563-571.e6.

Kikuchi, H., H. Yagi, H. Hasegawa, Y. Ishii, K. Okabayashi, M. Tsuruta, G. Hoshino, A. Takayanagi, and Y. Kitagawa. (2014). “Therapeutic Potential of Transgenic Mesenchymal Stem Cells Engineered to Mediate Anti-High Mobility Group Box 1 Activity: Targeting of Colon Cancer.” *J. Surg. Res.*, 190:134–43.

Kilinc, M., V. Arora, T. K. Creson, C. Rojas, A. A. Le, J. Lauterborn, B. Wilkinson, ..., and Gavin Rumbaugh. (2022). “Endogenous Syngap1 Alpha Splice Forms Promote Cognitive Function and Seizure Protection.” *Elife*, 11:1–34.

Kilinc, M., T. Creson, C. Rojas, M. Aceti, J. Ellegood, T. Vaissiere, J. P. Lerch, and G. Rumbaugh. (2018). “Species-Conserved SYNGAP1 Phenotypes Associated with Neurodevelopmental Disorders.” *Mol. Cell Neurosci.*, 91:140–50.

Kim, J. H., H. K. Lee, K. Takamiya, and R. L. Huganir. (2003). “The Role of Synaptic GTPase-Activating Protein in Neuronal Development and Synaptic Plasticity.” *J Neurosci*, 23(4):1119–24.

Kim, J. H., D. Liao, L. F. Lau, and R. L. Huganir. (1998). “SynGAP: A Synaptic RasGAP That Associates with the PSD-95/SAP90 Protein Family.” *Neuron*, 20(4):683–91.

Kimura, Y., M. Akahira-Azuma, N. Harada, Y. Enomoto, Y. Tsurusaki, and K. Kurosawa. (2017). “Novel SYNGAP1 Variant in a Patient with Intellectual Disability and Distinctive Dysmorphisms.” *Congenit. Anom. (Kyoto).*, 58(6):188–90.

Kishimoto, A., U. Kikkawa, K. Ogita, M. S. Shearman, and Y. Nishizuka. (1989). “The

Protein Kinase C Family in the Brain: Heterogeneity and Its Implications." *Ann. N. Y. Acad. Sci.*, 568(1):181–86.

Kishimoto, T. K., and R. J. Samulski. (2022). "Expert Opinion on Biological Therapy Addressing High Dose AAV Toxicity – ' One and Done ' or ' Slower and Lower '?" *Expert Opin. Biol. Ther.*, 22(9):1067–72.

Klitten, L. L., R. S. Møller, M. Nikanorova, A. Silahtaroglu, H. Hjalgrim, and N. Tommerup. (2011). "A Balanced Translocation Disrupts SYNGAP1 in a Patient with Intellectual Disability, Speech Impairment, and Epilepsy with Myoclonic Absences (EMA)." *Epilepsia*, 52(12):190–93.

Kluger, G., C. Von Stülpnagel-Steinbeis, S. Arnold, K. Eschermann, and T. Hartlieb. (2019). "Positive Short-Term Effect of Low-Dose Rosuvastatin in a Patient with SYNGAP1 -Associated Epilepsy." *Neuropediatrics*, 50(4):266–67.

Knuesel, I., A. Elliott, H. J. Chen, I. M. Mansuy, and M. B. Kennedy. (2005). "A Role for SynGAP in Regulating Neuronal Apoptosis." *Eur J Neurosci*, 21(3):611–21.

Kohlbrenner, E., G. Aslanidi, K. Nash, S. Shklyaev, M. Campbell-Thompson, B. J. Byrne, R. O. Snyder, ..., and Sergei Zolotukhin. (2005). "Successful Production of Pseudotyped RAAV Vectors Using a Modified Baculovirus Expression System." *Mol. Ther.*, 12(6):1217–25.

Komiyama, N. H., A. M. Watabe, H. J. Carlisle, K. Porter, P. Charlesworth, J. Monti, D. J. Strathdee, ..., and S. G. Grant. (2002). "SynGAP Regulates ERK/MAPK Signaling, Synaptic Plasticity, and Learning in the Complex with Postsynaptic Density 95 and NMDA Receptor." *J. Neurosci.*, 22(22):9721–32.

Korte, S. M., and S. F. De Boer. (2003). "A Robust Animal Model of State Anxiety: Fear-Potentiated Behaviour in the Elevated plus-Maze." *Eur. J. Pharmacol.*, 463:163–75.

Kotin, R. M., J. C. Menninger, D. C. Ward, and K. I. Berns. (1991). "Mapping and Direct Visualization of a Region-Specific Viral DNA Integration Site on Chromosome 19q13-Qter." *Genomics*, 10(3):831–34.

Kozak, M. (1986). "Point Mutations Define a Sequence Flanking the AUG Initiator Codon That Modulates Translation by Eukaryotic Ribosomes." *Cell*, 44:283–92.

Kraeuter, A. K., P. C. Guest, and Z. Sarnyai. (2019). "The Nest Building Test in Mice for Assessment of General Well-Being." *Methods Mol Biol*, 1916:87–91.

Krapivinsky, G., I. Medina, L. Krapivinsky, S. Gapon, and D. E. Clapham. (2004). "SynGAP-MUPP1-CaMKII Synaptic Complexes Regulate P38 MAP Kinase Activity and NMDA Receptor-Dependent Synaptic AMPA Receptor Potentiation." *Neuron*, 43(4):563–74.

Krepischi, A. C. V., C. Rosenberg, S. S. Costa, J. A. Crolla, S. Huang, and A. M. Vianna-Morgante. (2010). “A Novel de Novo Microdeletion Spanning the SYNGAP1 Gene on the Short Arm of Chromosome 6 Associated with Mental Retardation.” *Am. J. Med. Genet. Part A*, 152A(9):2376–78.

Kriegenburg, F., L. Ellgaard, and R. Hartmann-Petersen. (2012). “Molecular Chaperones in Targeting Misfolded Proteins for Ubiquitin-Dependent Degradation.” *FEBS J.*, 279(4):532–42.

Kroon, T., M. C. Sierksma, and R. M. Meredith. (2013). “Investigating Mechanisms Underlying Neurodevelopmental Phenotypes of Autistic and Intellectual Disability Disorders: A Perspective.” *Front Syst Neurosci*, 7:1–14.

Kuchenbuch, M., G. D’Onofrio, N. Chemaly, G. Barcia, T. Teng, and R. Nabbout. (2020). “Add-on Cannabidiol Significantly Decreases Seizures in 3 Patients with SYNGAP1 Developmental and Epileptic Encephalopathy.” *Epilepsia Open*, 5(3):496–500.

Kügler, S., E. Kilic, and M. Bähr. (2003). “Human Synapsin 1 Gene Promoter Confers Highly Neuron-Specific Long-Term Transgene Expression from an Adenoviral Vector in the Adult Rat Brain Depending on the Transduced Area.” *Gene Ther.*, 10(4):337–47.

de la Garza-Rodea, A. S., I. van der Velde, H. Boersma, M. A. F. V. Gonçalves, D. W. van Bekkum, A. A. F. de Vries, and S. Knaän-Shanzer. (2011). “Long-Term Contribution of Human Bone Marrow Mesenchymal Stromal Cells to Skeletal Muscle Regeneration in Mice.” *Cell Transplant.*, 20:217–31.

LaSalle, J. M., J. Goldstine, D. Balmer, and C. M. Greco. (2001). “Quantitative Localization of Heterogeneous Methyl-CpG-Binding Protein 2 (MeCP2) Expression Phenotypes in Normal and Rett Syndrome Brain by Laser Scanning Cytometry.” *Hum. Mol. Genet.*, 10(17):1729–40.

Lasky-Su, J., T. Banaschewski, J. Buitelaar, B. Franke, K. Brookes, E. Sonuga-Barke, R. Ebstein, ..., and Stephen V. Faraone. (2007). “Partial Replication of a DRD4 Association in ADHD Individuals Using a Statistically Derived Quantitative Trait for ADHD in a Family-Based Association Test.” *Biol. Psychiatry*, 62(9):985–90.

Latham, N., and G. Mason. (2004). “From House Mouse to Mouse House: The Behavioural Biology of Free-Living Mus Musculus and Its Implications in the Laboratory.” *Appl. Anim. Behav. Sci.*, 86:261–89.

Lee, C. S., E. S. Bishop, R. Zhang, X. Yu, E. M. Farina, S. Yan, C. Zhao, ..., Russell R. Reid, and Tong Chuan He. (2017). “Adenovirus-Mediated Gene Delivery: Potential Applications for Gene and Cell-Based Therapies in the New Era of Personalized Medicine.” *Genes Dis.*, 4(2):43–63.

Lee, J., S. Ha, S. T. Lee, S. G. Park, S. Shin, J. R. Choi, and K. A. Cheon. (2020). “Next-Generation Sequencing in Korean Children With Autism Spectrum Disorder and Comorbid Epilepsy.” *Front. Pharmacol.*, 11:585.

Lemmon, M. A. (2004). “Pleckstrin Homology Domains: Not Just for Phosphoinositides.” *Biochem Soc Trans*, 32(6):707–11.

Lemmon, M. A. (2008). “Membrane Recognition by Phospholipid-Binding Domains.” *Nat. Rev. Mol. Cell Biol.*, 9(2):99–111.

Lenk, G. M., P. Jafar-nejad, S. F. Hill, L. D. Huffman, C. E. Smolen, J. L. Wagnon, H. Petit, ..., and M. H. Meisler. (2020). “Scn8a Antisense Oligonucleotide Is Protective in Mouse Models of SCN8A Encephalopathy and Dravet Syndrome.” *Ann. OfNeurology*, 87:339–46.

Leo, D., and R. R. Gainetdinov. (2013). “Transgenic Mouse Models for ADHD.” 259–71.

Levitt, N., D. Briggs, A. Gil, and N. J. Proudfoot. (1989). “Definition of an Efficient Synthetic Poly(A) Site.” *Genes Dev.*, 3(7):1019–25.

Li, C., and R. J. Samulski. (2020). “Engineering Adeno-Associated Virus Vectors for Gene Therapy.” *Nat. Rev. Genet.*, 21(4):255–72.

Li, W., A. Okano, Q. B. Tian, K. Nakayama, T. Furihata, H. Nawa, and T. Suzuki. (2001). “Characterization of a Novel SynGAP Isoform, SynGAP-Beta.” *J. Biol. Chem.*, 276(24):21417–24.

de Ligt, J., M. H. Willemsen, B. W. M. Van Bon, T. Kleefstra, H. G. Yntema, T. Kroes, A. T. Vulto-van Silfhout, ..., J. A. Veltman, and L. E. L. M. Vissers. (2012). “Diagnostic Exome Sequencing in Persons with Severe Intellectual Disability.” *New Engl J Med.*, 367(20):1921–29.

Lim, Ki. H., Z. Han, H. Y. Jeon, J. Kach, E. Jing, S. Weyn-vanhentenryck, M. Downs, ..., and Isabel Aznarez. (2020). “Antisense Oligonucleotide Modulation of Non-Productive Alternative Splicing Upregulates Gene Expression.” *Nat. Commun.*,.

Lin, G., L. Li, N. Panwar, J. Wang, S. C. Tjin, X. Wang, and K. T. Yong. (2018). “Non-Viral Gene Therapy Using Multifunctional Nanoparticles: Status, Challenges, and Opportunities.” *Coord. Chem. Rev.*, 374:133–52.

Lister, R. G. (1987). “The Use of a Plus-Maze to Measure Anxiety in the Mouse.” *Psychopharmacology (Berl).*, 92:180–85.

Liu, X., Q. Jiang, S. Mansfield, M. Puttaraju, Y. Zhang, W. Zhou, J. Cohn, ..., and John Engelhardt. (2002). “Partial Correction of Endogenous ΔF508 CFTR in Human Cystic Fibrosis Airway Epithelia by Spliceosome-Mediated RNA Trans-Splicing.” *Nat. Biotechnol.*, 20(1):nbt0102-47.

Llamosas, N., V. Arora, R. Vij, M. Kilinc, L. Bijoch, C. Rojas, A. Reich, ..., and G. Rumbaugh. (2020). “SYNGAP1 Controls the Maturation of Dendrites, Synaptic Function, and Network Activity in Developing Human Neurons.” *J. Neurosci.*, 40(41):7980–94.

Llamosas, N., S. D. Michaelson, T. Vaissiere, C. Rojas, C. A. Miller, and G. Rumbaugh. (2021). “Syngap1 Regulates Experience-Dependent Cortical Ensemble Plasticity by Promoting in Vivo Excitatory Synapse Strengthening.” *Proc. Natl. Acad. Sci. U. S. A.*, 118(34).

Longatti, A., L. Ponzoni, E. Moretto, G. Giansante, N. Lattuada, M. N. Colombo, ..., and Maria Passafaro. (2021). “Arhgap22 Disruption Leads to RAC1 Hyperactivity Affecting Hippocampal Glutamatergic Synapses and Cognition in Mice.” *Mol. Neurobiol.*, 58:6092–6110.

Lord, C., M. Elsabbagh, G. Baird, and J. Veenstra-Vanderweele. (2018). “Autism Spectrum Disorder.” *Lancet*, 392(10146):508–20.

Lorenz, F. K. M., S. Wilde, K. Voigt, E. Kieback, B. Mosetter, D. J. Schendel, and W. Uckert. (2015). “Codon Optimization of the Human Papillomavirus E7 Oncogene Induces a CD8+ T Cell Response to a Cryptic Epitope Not Harbored by Wild-Type E7.” *PLoS One*, 10(3):1–15.

Lugo, J. N., G. D. Smith, E. P. Arbuckle, J. White, A. J. Holley, C. M. Floruta, N. Ahmed, M. C. Gomez, and O. Okonkwo. (2014). “Deletion of PTEN Produces Autism-like Behavioral Deficits and Alterations in Synaptic Proteins.” *Front. Mol. Neurosci.*, 7:1–13.

Markowitz, J. E., W. F. Gillis, C. C. Beron, S. Q. Neufeld, K. Robertson, N. D. Bhagat, R. E. Peterson, ..., and S. R. Datta. (2018). “The Striatum Organizes 3D Behavior via Moment-to-Moment Action Selection.” *Cell*, 174:44-58.e17.

Martín-Jiménez, R., D. Faccenda, E. Allen, H. B. Reichel, L. Arcos, C. Ferraina, D. Strobbe, C. Russell, and M. Campanella. (2018). “Reduction of the ATPase Inhibitory Factor 1 (IF1) Leads to Visual Impairment in Vertebrates.” *Cell Death Dis.*, 9(669).

Massaro, G., M. P. Hughes, S. M. Whaler, K. L. Wallom, D. A. Priestman, F. M. Platt, S. N. Waddington, and A. A. Rahim. (2020). “Systemic AAV9 Gene Therapy Using the Synapsin I Promoter Rescues a Mouse Model of Neuronopathic Gaucher Disease but with Limited Cross-Correction Potential to Astrocytes.” *Hum. Mol. Genet.*, 29(12):1933–49.

Massaro, G., C. N. Z. Mattar, A. M. S. Wong, E. Sirka, S. M. K. Buckley, B. R. Herbert, S. Karlsson, ..., S. N. Waddington, and A. A. Rahim. (2018). “Fetal Gene Therapy for Neurodegenerative Disease of Infants.” *Nat. Med.*, 24:1317–23.

Mastro, T. L., A. Preza, S. Basu, S. Chattarji, S. M. Till, P. C. Kind, and M. B. Kennedy. (2020). “A Sex Difference in the Response of the Rodent Postsynaptic Density to SynGAP Haploinsufficiency.” *Elife*, 9:e52656.

Matsuoka, Y., T. Furuyashiki, K. Yamada, T. Nagai, H. Bito, Y. Tanaka, S. Kitaoka, ..., and S. Narumiya. (2005). “Prostaglandin E Receptor EP1 Controls Impulsive Behavior under Stress.” *PNAS*, 102(44):16066–71.

Mauro, V. P., and S. A. Chappell. (2014). “A Critical Analysis of Codon Optimization in Human Therapeutics.” *Trends Mol. Med.*, 20(11):604–13.

McLean, J. R., G. A. Smith, E. M. Rocha, M. A. Hayes, J. A. Beagan, P. J. Hallett, and O. Isacson. (2014). “Widespread Neuron-Specific Transgene Expression in Brain and Spinal Cord Following Synapsin Promoter-Driven AAV9 Neonatal Intracerebroventricular Injection.” *Neurosci. Lett.*, 576:73–78.

McMahon, A. C., M. W. Barnett, T. S. O’Leary, P. N. Stoney, M. O. Collins, S. Papadia, J. S. Choudhary, ..., D. J. A. Wyllie, and P. C. Kind. (2012). “SynGAP Isoforms Exert Opposing Effects on Synaptic Strength.” *Nat. Commun.*, 3(1):900.

Mendell, J. R., S. Al-Zaidy, R. Shell, W. D. Arnold, L. R. Rodino-Klapac, T. W. Prior, L. Lowes, ..., and Brian K. Kaspar. (2017). “Single-Dose Gene-Replacement Therapy for Spinal Muscular Atrophy.” *N. Engl. J. Med.*, 377(18):1713–22.

Meng, Y., D. Sun, Y. Qin, X. Dong, G. Luo, and Y. Liu. (2021). “Cell-Penetrating Peptides Enhance the Transduction of Adeno-Associated Virus Serotype 9 in the Central Nervous System.” *Mol. Ther. - Methods Clin. Dev.*, 21:28–41.

Michaelson, S. D., E. D. Ozkan, M. Aceti, S. Maity, N. Llamosas, M. Weldon, E. Mizrachi, ..., and G. Rumbaugh. (2018). “SYNGAP1 Heterozygosity Disrupts Sensory Processing by Reducing Touch-Related Activity within Somatosensory Cortex Circuits.” *Nat. Neurosci.*, 21(12):1–13.

Mietzsch, M., V. Casteleyn, S. Weger, S. Zolotukhin, and R. Heilbronn. (2015). “OneBac 2.0: Sf9 Cell Lines for Production of AAV5 Vectors with Enhanced Infectivity and Minimal Encapsidation of Foreign DNA.” *Hum. Gene Ther.*, 26(10):688–97.

Migaud, M., P. Charlesworth, M. Dempster, L. C. Webster, A. M. Watabe, M. Makhinson, Y. He, ..., and S. G. Grant. (1998). “Enhanced Long-Term Potentiation and Impairedlearninginmicewithmutant Postsynaptic Density-95 Protein.” 433–39.

Mignot, C., C. von Stülpnagel, C. Nava, D. Ville, D. Sanlaville, G. Lesca, A. Rastetter, ..., and C. Depienne. (2016). “Genetic and Neurodevelopmental Spectrum of SYNGAP1-Associated Intellectual Disability and Epilepsy.” *J Med Genet*, 53(8):511–22.

Milazzo, C., E. J. Mientjes, I. Wallaard, S. V. Rasmussen, K. D. Erichsen, T. Kakunuri, A. S. E. van der Sman, ..., and Y. Elgersma. (2021). “Antisense Oligonucleotide Treatment Rescues UBE3A Expression and Multiple Phenotypes of an Angelman Syndrome Mouse Model.” *JCI Insight*, 6(15):e145991.

Mizuno, M., S. Hayashi, J. Yoshida, and A. Nakao. (2009). “Effect of Sonoporation on Cationic Liposome-Mediated IFNB Gene Therapy for Metastatic Hepatic Tumors of Murine Colon Cancer.” *Cancer Gene Ther.*, 16(10):806.

Montagutelli, X. (2000). “Effect of the Genetic Background on the Phenotype of Mouse Mutations.” *J. Am. Soc. Nephrol.*, 11(SUPPL. 16):101–5.

Montgomery, Kay C. (1952). “Exploratory Behavior and Its Relation to Spontaneous Alternation in a Series of Maze Exposures.” *J. Comp. Physiol. Psychol.*, 45(1):50–57.

Moon, H. Sakagami, J. Nakayama, and T. Suzuki. (2008). “Differential Distribution of SynGAPα1 and SynGAPβ Isoforms in Rat Neurons.” *Brain Res.*, 1241:62–75.

Moretti, P., J. A. Bouwknecht, R. Teague, R. Paylor, and H. Y. Zoghbi. (2005). “Abnormalities of Social Interactions and Home-Cage Behavior in a Mouse Model of Rett Syndrome.” *Hum. Mol. Genet.*, 14(2):205–20.

Mortimer, N., T. Ganster, A. O’Leary, S. Popp, F. Freudenberg, A. Reif, M. Soler Artigas, ..., and Olga Rivero. (2019). “Dissociation of Impulsivity and Aggression in Mice Deficient for the ADHD Risk Gene Adgrl3: Evidence for Dopamine Transporter Dysregulation.” *Neuropharmacology*, 156(October 2018):107557.

Moy, S. S., N. V. Riddick, V. D. Nikolova, B. L. Teng, K. L. Agster, R. J. Nonneman, N. B. Young, ..., and James W. Bodfish. (2014). “Repetitive Behavior Profile and Supersensitivity to Amphetamine in the C58/J Mouse Model of Autism.” *Behav. Brain Res.*, 259:200–214.

Moyses-Oliveira, M., R. Yadav, S. Erdin, and M. E. Talkowski. (2020). “New Gene Discoveries Highlight Functional Convergence in Autism and Related Neurodevelopmental Disorders.” *Curr. Opin. Genet. Dev.*, 65:195–206.

Muhia, M., J. Feldon, I. Knuesel, and B. K. Yee. (2009). “Appetitively Motivated Instrumental Learning in SynGAP Heterozygous Knockout Mice.” *Behav. Neurosci.*, 123(5):1114–28.

Muhia, M., S. Willadt, B. K. Yee, J. Feldon, J. C. Paterna, S. Schwendener, K. Vogt, M. B. Kennedy, and I. Knuesel. (2012). “Molecular and Behavioral Changes Associated with Adult Hippocampus-Specific SynGAP1 Knockout.” *Learn. Mem.*, 19(7):268–81.

Muhia, M., B. K. Yee, J. Feldon, F. Markopoulos, and I. Knuesel. (2010). “Disruption of

Hippocampus-Regulated Behavioural and Cognitive Processes by Heterozygous Constitutive Deletion of SynGAP." *Eur. J. Neurosci.*, 31(3):529–43.

Mukhopadhyay, A., J. Wright, S. Shirley, D. A. Canton, C. Burkart, R. J. Connolly, J. S. Campbell, and R. H. Pierce. (2019). "Characterization of Abscopal Effects of Intratumoral Electroporation-Mediated IL-12 Gene Therapy." *Gene Ther.*, 26(1–2):1–15.

Munir, K. M. (2018). "The Co-Occurrence of Mental Disorders in Children and Adolescents with Intellectual Disability/Intellectual Developmental Disorder." *Physiol. Behav.*, 176(5):139–48.

Nakai, H., T. A. Storm, and M. A. Kay. (2000). "Recruitment of Single-Stranded Recombinant Adeno-Associated Virus Vector Genomes and Intermolecular Recombination Are Responsible for Stable Transduction of Liver In Vivo." *J. Virol.*, 74(20):9451–63.

Nakajima, R., K. Takao, S. Hattori, H. Shoji, N. Komiyama, S. Grant, and T. Miyakawa. (2019). "Comprehensive Behavioral Analysis of Heterozygous Syngap1 Knockout Mice." *Neuropsychopharmacol Rep.*, 39(3):223–37.

Naso, Michael F., Brian Tomkowicz, William L. Perry, and William R. Strohl. (2017). "Adeno-Associated Virus (AAV) as a Vector for Gene Therapy." *BioDrugs*, 31(4):317–34.

Ni, T., X. Zhou, D. McCarty, I. Zolotukhin, and N. Muzycza. (1992). "In Vitro Replication of Adeno-Associated Virus DNA." *Proc. Natl. Acad. Sci. U. S. A.*, 89(10):4673–77.

Nicola, S. M. (2007). "The Nucleus Accumbens as Part of a Basal Ganglia Action Selection Circuit." *Psychopharmacology (Berl).*, 191:521–50.

Niknam, P., M. R. Raoufy, Y. Fathollahi, and M. Javan. (2019). "Modulating Proteoglycan Receptor PTPσ Using Intracellular Sigma Peptide Improves Remyelination and Functional Recovery in Mice with Demyelinated Optic Chiasm." *Mol. Cell. Neurosci.*, 99:103391.

Nirenberg, M., O. Jones, P. Leder, B. CLark, W. Sly, and S. Pestka. (1963). "On the Coding of Spatial Information." *Cold Spring Harb Symp Quant Biol*, 28:549–57.

Nishizuka, Y. (1988). "The Molecular Heterogeneity of Protein Kinase C and Its Implications for Cellular Regulation." *Nature*, 334(6184):661–65.

Niu, H. M., P. Yang, H. H. Chen, R. H. Hao, S. S. Dong, S. Yao, X. F. Chen, ..., and Y. Guo. (2019). "Comprehensive Functional Annotation of Susceptibility SNPs Prioritized 10 Genes for Schizophrenia." *Transl. Psychiatry*, 9(56).

Njung'e, K., and S. L. Handley. (1991). "Evaluation of Marble-Burying Behavior as a Model of Anxiety." *Pharmacol. Biochem. Behav.*, 38:63–67.

Oh, J. S., P. Manzerra, and M. B. Kennedy. (2004). “Regulation of the Neuron-Specific Ras GTPase-Activating Protein, SynGAP, by Ca2+/Calmodulin-Dependent Protein Kinase II.” *J Biol Chem*, 279(17):17980–88.

Okazaki, Tetsuya, Yoshiaki Saito, Rika Hiraiwa, Shinji Saitoh, Masachika Kai, Kaori Adachi, Yoko Nishimura, Eiji Nanba, and Yoshihiro Maegaki. (2017). “Pharmacoresistant Epileptic Eyelid Twitching in a Child with a Mutation in SYNGAP1.” *Epileptic Disord.*, 19(3):339–44.

Ozkan, E. D., T. K. Creson, E. A. Kramár, C. Rojas, R. R. Seese, A. H. Babyan, Y. Shi, ..., and G. Rumbaugh. (2014). “Reduced Cognition in Syngap1 Mutants Is Caused by Isolated Damage within Developing Forebrain Excitatory Neurons.” *Neuron*, 82(6):1317–33.

Palella, T. D., L. J. Silverman, M. Levine, and W. N. Kelley. (1988). “Herpes Simplex Virus Mediated Human Hypoxanthine-Guanine Phosphoribosyltransferase Gene Transfer Into Neuronal Cells.” *Mol. Cell. Biol.*, 8(1):457–60.

Parker, M. J., A. E. Fryer, D. J. Shears, K. L. Lachlan, S. A. McKee, A. C. Magee, S. Mohammed, ..., DDD Study, and D. R. FitzPatrick. (2015). “De Novo, Heterozygous, Loss-of-Function Mutations in SYNGAP1 Cause a Syndromic Form of Intellectual Disability.” *Am. J. Med. Genet.*, 167A(10):2231–37.

Passini, M. A., J. Bu, A. M. Richards, C. Kinnecom, S. P. Sardi, M. Stanek, Y. Hua, ..., and S. H. Cheng. (2011). “Antisense Oligonucleotides Delivered to the Mouse CNS Ameliorate Symptoms of Severe Spinal Muscular Atrophy Marco.” *Sci. Transl. Med.*, 3(72).

Patel, Dilip R., Roger Apple, Shibani Kanungo, and Ashley Akkal. (2018). “Intellectual Disability: Definitions, Evaluation and Principles of Treatment.” *Pediatr. Med.*, 1.

Peça, J., C. Feliciano, J. T. Ting, W. Wang, M. F. Wells, T. N. Venkatraman, C. D. Lascola, Z. Fu, and G. Feng. (2011). “Shank3 Mutant Mice Display Autistic-like Behaviours and Striatal Dysfunction.” *Nature*, 472:437–42.

Pena, V., M. Hothorn, A. Eberth, N. Kaschau, A. Parret, L. Gremer, F. Bonneau, M. R. Ahmadian, and Klaus Scheffzek. (2008). “The C2 Domain of SynGAP Is Essential for Stimulation of the Rap GTPase Reaction.” *EMBO Rep.*, 9(4):350–55.

Penaud-Budloo, M., A. François, N. Clément, and E. Ayuso. (2018). “Pharmacology of Recombinant Adeno-Associated Virus Production.” *Mol. Ther. - Methods Clin. Dev.*, 8:166–80.

Peranteau, W. H., and A. W. Flake. (2020). “The Future of In Utero Gene Therapy.” *Mol. Diagnosis Ther.*, 24:135–42.

Pierson, E. E., D. Z. Keifer, A. Asokan, and M. F. Jarrold. (2019). “Resolving Adeno-

Associated Viral Particle Diversity With Charge Detection Mass Spectrometry." *Anal. Chem.*, 88(13):6718–25.

Pinto, D., A. T. Pagnamenta, L. Klei, R. Anney, D. Merico, R. Regan, J. Conroy, ..., and C. Betancur. (2010). "Functional Impact of Global Rare Copy Number Variation in Autism Spectrum Disorders." *Nature*, 466(7304):368–72.

Pisanello, F., G. Mandelbaum, M. Pisanello, I. A. Oldenburg, L. Sileo, J. E. Markowitz, R. E. Peterson, ..., and Bernardo L. Sabatini. (2017). "Dynamic Illumination of Spatially Restricted or Large Brain Volumes via a Single Tapered Optical Fiber." *Nat. Neurosci.*, 20(8):1180–88.

Porter, K., N. H. Komiyama, T. Vitalis, P. C. Kind, and S. G. Grant. (2005). "Differential Expression of Two NMDA Receptor Interacting Proteins, PSD-95 and SynGAP during Mouse Development." *Eur. J. Neurosci.*, 21(2):351–62.

Pouzet, B. (1999). "The Effects of NMDA-Induced Retrohippocampal Lesions on Performance of Four Spatial Memory Tasks Known to Be Sensitive to Hippocampal Damage in the Rat." *Eur. J. Neurosci.*, 11(1):123–40.

Powell, S. K., R. Rivera-Soto, and S. J. Gray. (2015). "Viral Expression Cassette Elements to Enhance Transgene Target Specificity and Expression in Gene Therapy." *Discov. Med.*, 19(102):49–57.

Presa, M., R. M. Bailey, C. Davis, T. Murphy, J. Cook, R. Walls, H. Wilpan, ..., and Cathleen Lutz. (2021). "AAV9-Mediated FIG4 Delivery Prolongs Life Span in Charcot-Marie-Tooth Disease Type 4J Mouse Model." *J. Clin. Invest.*, 131(11).

Pritchett, K., and G. B. Mulder. (2003). "The Rotarod." *Contemp. Top. Lab. Anim. Sci.*, 42(6):49.

Purcell, S. M., J. L. Moran, M. Fromer, D. Ruderfer, N. Solovieff, P. Roussos, C. O'Dushlaine, ..., and P. Sklar. (2014). "A Polygenic Burden of Rare Disruptive Mutations in Schizophrenia." *Nature*, 506(7487):185–90.

Raab, D., M. Graf, F. Notka, T. Schödl, and R. Wagner. (2010). "The GeneOptimizer Algorithm: Using a Sliding Window Approach to Cope with the Vast Sequence Space in Multiparameter DNA Sequence Optimization." *Syst. Synth. Biol.*, 4:215–25.

Rashnonejad, A., G. Amini Chermahini, C. Gündüz, H. Onay, A. Aykut, B. Durmaz, M. Baka, ..., and Ferda Özkınay. (2019). "Fetal Gene Therapy Using a Single Injection of Recombinant AAV9 Rescued SMA Phenotype in Mice." *Mol. Ther.*, 27(12):2123–33.

Rauch, A., D. Wieczorek, E. Graf, T. Wieland, S. Endele, T. Schwarzmayr, B. Albrecht, ..., A. Reis, and T. M. Strom. (2012). "Range of Genetic Mutations Associated

with Severe Non-Syndromic Sporadic Intellectual Disability: An Exome Sequencing Study." *Lancet*, 380(9854):1674–82.

Rauch, S., L. M. Shin, and C. I. Wright. (2004). "Neuroimaging Studies of Amygdala Function in Anxiety Disorders." *New York Acad. Sci.*, 389–410.

Rinaldi, L., V. Folliero, L. Palomba, C. Zannella, R. Isticato, R. Di Francia, M. Berretta, ..., and G. Franci. (2018). "Sonoporation by Microbubbles as Gene Therapy Approach against Liver Cancer." *Oncotarget*, 9(85):35600.

Ritter, T., M. Lehmann, and H. Volk. (2002). "Improvements in Gene Therapy: Averting the Immune Response to Adenoviral Vectors." *BioDrugs*, 16(1):3–10.

Robbins, P. D., and S. C. Ghivizzani. (1998). "Viral Vectors for Gene Therapy." *Pharmacol. Ther.*, 80(1):35–47.

Rodgers, R. J., and A. Dalvi. (1997). "Anxiety, Defence and the Elevated plus-Maze." *Neurosci. Biobehav. Rev.*, 21(6):801–10.

Roozendaal, B., B. S. McEwen, and S. Chattarji. (2009). "Stress, Memory and the Amygdala." *Nat. Rev. Neurosci.*, 10(6):423–33.

Roseberry, T. K., A. M. Lee, A. L. Lalive, L. Wilbrecht, A. Bonci, and A. C. Kreitzer. (2016). "Cell-Type-Specific Control of Brainstem Locomotor Circuits by Basal Ganglia." *Cell*, 164(3):526–37.

De Rubeis, S., X. He, A. P. Goldberg, C. S. Poultney, K. Samocha, A. E. Cicek, Y. Kou, ..., and J. D. Buxbaum. (2014). "Synaptic, Transcriptional and Chromatin Genes Disrupted in Autism." *Nature*, 515(7526):209.

Rudolph, S., C. Guo, S. L. Pashkovski, T. Osorno, W. F. Gillis, J. M. Krauss, H. Nyitrai, ..., and Wade G. Regehr. (2020). "Cerebellum-Specific Deletion of the GABAA Receptor δ Subunit Leads to Sex-Specific Disruption of Behavior." *Cell Rep.*, 33:108338.

Rumbaugh, G., J. P. Adams, J. H. Kim, and R. L. Huganir. (2006). "SynGAP Regulates Synaptic Strength and Mitogen-Activated Protein Kinases in Cultured Neurons." *PNAS*, 103(12):4344–51.

Sakuma, T., M. A. Barry, and Y. Ikeda. (2012). "Lentiviral Vectors: Basic to Translational." *Biochem. J.*, 443(3):603–18.

Schnödt, M., and H. Büning. (2017). "Improving the Quality of Adeno-Associated Viral Vector Preparations: The Challenge of Product-Related Impurities." *Hum. Gene Ther. Methods*, 28(3):101–8.

Shahryari, A., M. S. Jazi, S. Mohammadi, H. R. Nikoo, Z. Nazari, E. S. Hosseini, I. Burtscher, S. J. Mowla, and H. Lickert. (2019). "Development and Clinical

Translation of Approved Gene Therapy Products for Genetic Disorders." *Front. Genet.*, 10:868.

Sharp, P. M., and L. Wen-Hsiung. (1986). "The Codon Adaptation Index - a Measure of Directional Synonymous Codon Usage Bias, and Its Potential Applications." *Nucleic Acids Res.*, 14(3):4683–90.

Sheikha, T. I., A. M. de Pazc, S. Akhtard, J. Ausióc, and J. B. Vincent. (2017). "The Role of N-Terminal Modification of MeCP2 in the Pathophysiology of Rett Syndrome." *BioRxiv*, 1–24.

Shirley, J., Y. Jong, C. Terhorst, and R. Herzog. (2020). "Immune Responses to Viral Gene Therapy Vectors." *Mol Ther*, 28(3):709–22.

Silachev, D., A. Koval, M. Savitsky, G. Padmasola, C. Quairiaux, F. Thorel, and V. L. Katanaev. (2022). "Mouse Models Characterize GNAO1 Encephalopathy as a Neurodevelopmental Disorder Leading to Motor Anomalies: From a Severe G203R to a Milder C215Y Mutation." *Acta Neuropathol. Commun.*, 10:9.

Silverman, J. L., M. Yang, C. Lord, and J. N. Crawley. (2010). "Behavioural Phenotyping Assays for Mouse Models of Autism." *Nat. Rev. Neurosci.*, 11:490–502.

Simonato, M., R. Manservigi, P. Marconi, and J. Glorioso. (2000). "Gene Transfer into Neurones for the Molecular Analysis of Behaviour: Focus on Herpes Simplex Vectors." *Trends. Neurosci.*, 23:183–90.

Simonoff, E., A. Pickles, T. Charman, S. Chandler, T. Loucas, and G. Baird. (2008). "Psychiatric Disorders in Children with Autism Spectrum Disorders: Prevalence, Comorbidity, and Associated Factors in a Population-Derived Sample." *J. Am. Acad. Child Adolesc. Psychiatry*, 47(8):921–29.

Sinnett, S. E., R. D. Hector, K. K. E. Gadalla, C. Heindel, D. Chen, V. Zaric, M. E. S. Bailey, S. R. Cobb, and S. J. Gray. (2017). "Improved MECP2 Gene Therapy Extends the Survival of MeCP2-Null Mice without Apparent Toxicity after Intracisternal Delivery." *Mol. Ther. - Methods Clin. Dev.*, 5:106–15.

Sirivelu, M. P., L. Newman, X. Palazzi, I. D. Pardo, S. W. Kumpf, J. Qian, T. Franks, ..., and Joseph Brady. (2021). "Biodistribution and Tolerability of AAV-PHP.B-CBh-SMN1 in Wistar Han Rats and Cynomolgus Macaques Reveal Different Toxicologic Profiles." 33.

Smith-Hicks, C., D. Wright, A. Kenny, R. C. Stowe, M. Mccormack, A. C. Stanfield, and J. L. Holder. (2021). "Sleep Abnormalities in the Synaptopathies — SYNGAP1 - Related Intellectual Disability and Phelan – McDermid Syndrome." *Brain Sci.*, 11:1229.

Song, S. H., and G. J. Augustine. (2016). "Synapsin Isoforms Regulating GABA Release

from Hippocampal Interneurons." *J. Neurosci.*, 36(25):6742–57.

Spencer, P. S., E. Siller, J. F. Anderson, and J. M. Barral. (2012). "Silent Substitutions Predictably Alter Translation Elongation Rates and Protein Folding Efficiencies." *J. Mol. Biol.*, 422:328–35.

Srivastava, A., E. W. Lusby, and K. I. Berns. (1983). "Nucleotide Sequence and Organization of the Adeno-Associated Virus 2 Genome." *J. Virol.*, 45(2):555–64.

Stohn, J. P., M. E. Martinez, and A. Hernandez. (2016). "Decreased Anxiety- and Depression-like Behaviors and Hyperactivity in a Type 3 Deiodinase-Deficient Mouse Showing Brain Thyrotoxicosis and Peripheral Hypothyroidism." *Psychoneuroendocrinology*, 74:46–56.

Stülpnagel, C., T. Hartlieb, I. Borggräfe, A. Coppola, E. Gennaro, K. Eschermann, L. Kiwull, ..., and Gerhard Kluger. (2018). "Chewing Induced Reflex Seizures („eating Epilepsy") and Eye Closure Sensitivity as a Common Feature in Pediatric Patients with SYNGAP1 Mutations: Review of Literature and Report of 8 Cases." *Seizure*, 65:131–37.

Sullivan, B. J., S. Ammanuel, P. A. Kipnis, Y. Araki, R. L. Huganir, and S. D. Kadam. (2020). "Low-Dose Perampanel Rescues Cortical Gamma Dysregulation Associated With Parvalbumin Interneuron GluA2 Upregulation in Epileptic Syngap1+/- Mice." *Biol. Psychiatry*, 87:829–42.

Swiech, L., M. Heidenreich, A. Banerjee, N. Habib, Y. Li, J. Trombetta, M. Sur, and F. Zhang. (2015). "In Vivo Interrogation of Gene Function in the Mammalian Brain Using CRISPR-Cas9." *Nat. Biotechnol.*, 33(1):102–6.

Takeuchi, H., S. I. Yatsugi, and T. Yamaguchi. (2002). "Effect of YM992, a Novel Antidepressant with Selective Serotonin Re-Uptake Inhibitory and 5-HT2A Receptor Antagonistic Activity, on a Marble-Burying Behavior Test as an Obsessive-Compulsive Disorder Model." *Jpn. J. Pharmacol.*, 90:197–200.

Tanenhaus, A., T. Stowe, A. Young, J. McLaughlin, R. Aeran, I. W. Lin, J. Li, ..., and S. Tagliatela. (2022). "Cell-Selective Adeno-Associated Virus-Mediated SCN1A Gene Regulation Therapy Rescues Mortality and Seizure Phenotypes in a Dravet Syndrome Mouse Model and Is Well Tolerated in Nonhuman Primates." *Hum. Gene Ther.*, 33(11–12):579–97.

Teng, S., T. Madej, A. Panchenko, and E. Alexov. (2009). "Modeling Effects of Human Single Nucleotide Polymorphisms on Protein-Protein Interactions." *Biophys. J.*, 96(6):2178–88.

Terpe, K. (2003). "Overview of Tag Protein Fusions: From Molecular and Biochemical Fundamentals to Commercial Systems." *Appl. Microbiol. Biotechnol.*, 60(5):523–33.

Thomas, A., A. Burant, N. Bui, D. Graham, L. A. Yuva-Paylor, and R. Paylor. (2009). “Marble Burying Reflects a Repetitive and Perseverative Behavior More than Novelty-Induced Anxiety.” *Psychopharmacology (Berl).*, 204(2):361–73.

Thomas, P., and T. G. Smart. (2005). “HEK293 Cell Line : A Vehicle for the Expression of Recombinant Proteins.” *J. Pharmacol. Toxicol. Methods*, 51:187–200.

Thusberg, J., and M. Vihinen. (2009). “Pathogenic or Not? And If so, Then How? Studying the Effects of Missense Mutations Using Bioinformatics Methods.” *Hum. Mutat.*, 30(5):703–14.

Tian, Q., S. B. Stepaniants, M. Mao, L. Weng, M. C. Feetham, M. J. Doyle, E. C. Yi, H. Dai, ..., and Leroy E. Hood. (2004). “Integrated Genomic and Proteomic Analyses of Gene Expression in Mammalian Cells.” *Mol. Cell. Proteomics*, 3(10):960–69.

Tomoda, T., J. Kim, C. Zhan, and M. Hatten. (2004). “Role of Unc51.1 and Its Binding Partners in CNS Axon Outgrowth.” *Gene Dev.*, 18(5):541–58.

Tornoe, J., P. Kusk, T. E. Johansen, and P. R. Jensen. (2002). “Generation of a Synthetic Mammalian Promoter Library by Modification of Sequences Spacing Transcription Factor Binding Sites.” *Gene*, 297:21–32.

Tsai, C. J., Z. E. Sauna, C. Kimchi-Sarfaty, S. V. Ambudkar, M. M. Gottesman, and R. Nussinov. (2008). “Synonymous Mutations and Ribosome Stalling Can Lead to Altered Folding Pathways and Distinct Minima.” *J. Mol. Biol.*, 383(2):281–91.

Tye, K. M., R. Prakash, S. Y. Kim, Lief E. Fenno, L. Grosenick, H. Zarabi, K. R. Thompson, ..., and K. Deisseroth. (2011). “Amygdala Circuitry Mediating Reversible and Bidirectional Control of Anxiety.” *Nature*, 471(7338):358–62.

Vazquez, L. E., H. J. Chen, I. Sokolova, I. Knuesel, and M. B. Kennedy. (2004). “SynGAP Regulates Spine Formation.” *J. Neurosci.*, 24(40):8862–72.

Verma, V., M. J. V. Kumar, K. Sharma, S. Rajaram, R. Muddashetty, R. Manjithaya, T. Behnisch, and J. P. Clement. (2022). “Pharmacological Intervention in Young Adolescents Rescues Synaptic Physiology and Behavioural Deficits in Syngap1 +/− Mice.” *Exp. Brain Res.*, 240:289–309.

Verma, V., A. Paul, A. A. Vishwanath, B. Vaidya, and J. P. Clement. (2019). “Understanding Intellectual Disability and Autism Spectrum Disorders from Common Mouse Models: Synapses to Behaviour.” *Open Biol.*, 9:180265.

Vissers, L. E. L. M., J. De Ligt, C. Gilissen, I. Janssen, M. Steehouwer, P. de Vries, B. van Lier, ..., H. G. Brunner, and J. A. Veltman. (2010). “A de Novo Paradigm for Mental Retardation.” *Nat. Genet.*, 42(12):1109–12.

Vissers, L. E. L. M., K. J. M. V. Nimwegen, J. H. Schieving, E. Kamsteeg, T. Kleefstra, H. G. Yntema, R. Pfundt, ..., and M. A. A. P. Willemsen. (2017). “A Clinical Utility

Study of Exome Sequencing versus Conventional Genetic Testing in Pediatric Neurology." *Nat. Publ. Gr.*, 19(9):1055–63.

Vlaskamp, D., B. Shaw, R. Burgess, D. Mei, M. Montomoli, H. Xie, C. T. Myers, ..., and I. E. Scheffer. (2019). "SYNGAP1 Encephalopathy: A Distinctive Generalized Developmental and Epileptic Encephalopathy." *Neurology*, 92:96–107.

Walkup, W. G., T. L. Mastro, L. T. Schenker, J. Vielmetter, R. Hu, A. Iancu, ..., and M. B. Kennedy. (2016). "A Model for Regulation by SynGAP-A1 of Binding of Synaptic Proteins to PDZ-Domain 'Slots' in the Postsynaptic Density." *Elife*, 5:1–31.

Walkup, W. G., M. J. Sweredoski, R. L. Graham, S. Hess, and M. B. Kennedy. (2018). "Phosphorylation of Synaptic GTPase-Activating Protein (SynGAP) by Polo-like Kinase (Plk2) Alters the Ratio of Its GAP Activity toward HRas, Rap1 and Rap2 GTPases." *Biochem. Biophys. Res. Commun.*, 503:1599–1604.

Walkup, W. G., L. Washburn, M. J. Sweredoski, H. J. Carlisle, R. L. Graham, S. Hess, and M. B. Kennedy. (2015). "Phosphorylation of Synaptic GTPase-Activating Protein (SynGAP) by Ca2+/Calmodulin-Dependent Protein Kinase II (CaMKII) and Cyclin-Dependent Kinase 5 (CDK5) Alters the Ratio of Its GAP Activity toward Ras and Rap GTPases." *J. Biol. Chem.*, 290(8):4908–27.

Wang, C. C., R. G. Held, and B. J. Hall. (2013). "SynGAP Regulates Protein Synthesis and Homeostatic Synaptic Plasticity in Developing Cortical Networks." *PLoS One*, 8(12):e83941.

Wang, D., P. W. L. Tai, G. Gao, P. Systems, and P. W. L. Tai. (2019). "Adeno-Associated Virus Vector as a Platform for Gene Therapy Delivery." *Nat. Rev. Drug. Discov.*, 18(5):358–78.

Wang, S., and R. Huang. (2019). "Non-Viral Nucleic Acid Delivery to the Central Nervous System and Brain Tumors." *J. Gene Med.*, 21(7):5–13.

Wang, W., W. Duan, Y. Wang, D. Wen, Y. Liu, Z. Li, H. Hu, ..., and C. Li. (2017). "Intrathecal Delivery of SsAAV9-DAO Extends Survival in SOD1G93A ALS Mice." *Neurochem. Res.*, 42(4):986–96.

Ward, N. J., S. M. K. Buckley, S. N. Waddington, T. VandenDriessche, M. K. L. Chuah, A. C. Nathwani, J. McIntosh, ..., and John H. McVey. (2011). "Codon Optimization of Human Factor VIII CDNAs Leads to High-Level Expression." *Blood*, 117(3):798–807.

Weldon, M., M. Kilinc, J. Holder, and G. Rumbaugh. (2018). "The First International Conference on SYNGAP1-Related Brain Disorders: A Stakeholder Meeting of Families, Researchers, Clinicians, and Regulators." *J. Neurodev. Disord.*, 10:6.

Wengert, E. R., P. K. Wagley, S. M. Strohm, N. Reza, I. C. Wenker, R. P. Gaykema, A. Christiansen, G. Liau, and M. K. Patel. (2022). “Targeted Augmentation of Nuclear Gene Output (TANGO) of Scn1a Rescues Parvalbumin Interneuron Excitability and Reduces Seizures in a Mouse Model of Dravet Syndrome.” *Brain Res.*, 1775:147743.

Wiley, J. L., A. F. Cristello, and R. L. Balster. (1995). “Effects of Site-Selective NMDA Receptor Antagonists in an Elevated plus-Maze Model of Anxiety in Mice.” *Eur. J. Pharmacol.*, 294:101–7.

Willsey, H. R., A. J. Willsey, B. Wang, and M. W. State. (2022). “Genomics, Convergent Neuroscience and Progress in Understanding Autism Spectrum Disorder.” *Nat. Rev. Neurosci.*, 23:323–41.

Wiltschko, A. B., M. J. Johnson, G. Iurilli, R. E. Peterson, J. M. Katon, S. L. Pashkovski, V. E. Abraira, R. P. Adams, and S. R. Datta. (2015). “Mapping Sub-Second Structure in Mouse Behavior.” *Neuron*, 88(6):1121–35.

Wiltschko, Al. B., T. Tsukahara, A. Zeine, R. Anyoha, W. F. Gillis, J. E. Markowitz, R. E. Peterson, ..., and S. R. Datta. (2021). “Revealing the Structure of Pharmacobehavioral Space through Motion Sequencing.” *Nat. Neurosci.*, 23(11):1433–43.

Wolfer, D. P., W. E. Crusio, and H. P. Lipp. (2002). “Knockout Mice: Simple Solutions to the Problems of Genetic Background and Flanking Genes.” *Trends Neurosci.*, 25(7):336–40.

Won, H., W. Mah, E. Kim, J. W. Kim, E. K. Hahm, M. H. Kim, S. Cho, ..., and Eunjoon Kim. (2011). “GIT1 Is Associated with ADHD in Humans and ADHD-like Behaviors in Mice.” *Nat. Med.*, 17(5):566–72.

Wörner, T. P., A. Bennett, S. Habka, J. Snijder, O. Friese, T. Powers, M. Agbandje-McKenna, and A. J. R. Heck. (2021). “Adeno-Associated Virus Capsid Assembly Is Divergent and Stochastic.” *Nat. Commun.*, 12(1):1–9.

Writzl, K., and A. C. Knegt. (2013). “6p21.3 Microdeletion Involving the SYNGAP1 Gene in a Patient with Intellectual Disability, Seizures, and Severe Speech Impairment.” *Am. J. Med. Genet. Part A*, 161A:1682–85.

Wu, Y., T. Mei, L. Jiang, Z. Han, R. Dong, T. Yang, and F. Xu. (2019). “Development of Versatile and Flexible Sf9 Packaging Cell Line-Dependent Onebac System for Large-Scale Recombinant Adeno-Associated Virus Production.” *Hum. Gene Ther. Methods*, 30(5):172–83.

Wu, Z., A. Asokan, and R. Samulski. (2006). “Adeno-Associated Virus Serotypes: Vector Toolkit for Human Gene Therapy.” *Mol Ther*, 14(3):316–27.

Wu, Z., H. Yang, and P. Colosi. (2010). “Effect of Genome Size on AAV Vector Packaging.” *Mol. Ther.*, 18(1):80–86.

Yamaguchi, T., H. Shirataki, S. Kishida, M. Miyazaki, J. Nishikawa, K. Wada, S. Numata, K. Kaibuchi, and Y. Takai. (1993). “Two Functionally Different Domains of Rabphilin-3A, Rab3A P25/Smg P25A-Binding and Phospholipid- and Ca(2+)-Binding Domains.” *J. Biol. Chem.*, 268(36):27164–70.

Yang, Y., J. H. Tao-Cheng, K. U. Bayer, T. S. Reese, and A. Dosemeci. (2013). “Camkii-Mediated Phosphorylation Regulates Distributions of Syngap-A1 and -A2 at the Postsynaptic Density.” *PLoS One*, 8(8):e71795.

Yao, Y., J. Wang, Y. Liu, Y. Qu, K. Wang, Y. Zhang, Y. Chang, ..., and Fengfeng Bei. (2022). “Variants of the Adeno-Associated Virus Serotype 9 with Enhanced Penetration of the Blood–Brain Barrier in Rodents and Primates.” *Nat. Biomed. Eng.*, 6:1257–71.

Yin, W., P. Xiang, and Q. Li. (2005). “Investigations of the Effect of DNA Size in Transient Transfection Assay Using Dual Luciferase System.” *Anal. Biochem.*, 346:289–94.

Zeng, M., G. Bai, and M. Zhang. (2019). “Anchoring High Concentrations of SynGAP at Postsynaptic Densities via Liquid-Liquid Phase Separation.” *Small GTPases*, 10(4):296–304.

Zeng, M., Y. Shang, Y. Araki, T. Guo, R. L. Huganir, and M. Zhang. (2016). “Phase Transition in Postsynaptic Densities Underlies Formation of Synaptic Complexes and Synaptic Plasticity.” *Cell*, 166:1163-1175.e12.

Zhang, Z., M. A. Miteva, L. Wang, and E. Alexov. (2012). “Analyzing Effects of Naturally Occurring Missense Mutations.” *Comput. Math. Methods Med.*, 2012.

Zhang, Z., S. Teng, L. Wang, C. E. Schwartz, and E. Alexov. (2010). “Computational Analysis of Missense Mutations Causing Snyder-Robinson Syndrome.” *Hum. Mutat.*, 31(9):1043–49.

Zhu, J. J., Y. Qin, M. Zhao, L. Van Aelst, and R. Malinow. (2002). “Ras and Rap Control AMPA Receptor Trafficking during Synaptic Plasticity.” *Cell*, 110(4):443–55.

Zincarelli, C., S. Soltys, G. Rengo, and J. E. Rabinowitz. (2008). “Analysis of AAV Serotypes 1-9 Mediated Gene Expression and Tropism in Mice after Systemic Injection.” *Mol. Ther.*, 16(6):1073–80.

Zoghbi, H. Y., and M. F. Bear. (2012). “Synaptic Dysfunction in Neurodevelopmental Disorders Associated with Autism and Intellectual Disabilities.” *Cold Spring Harb. Perspect. Biol.*, 4(3).

Zollino, M., F. Gurrieri, D. Orteschi, G. Marangi, V. Leuzzi, and G. Neri. (2011).

"Integrated Analysis of Clinical Signs and Literature Data for the Diagnosis and Therapy of a Previously Undescribed 6p21.3 Deletion Syndrome." *Eur. J. Hum. Genet.*, 19:239–42.